SID 67-542-2

INFLUENCE OF STRUCTURE AND MATERIAL RESEARCH ON ADVANCED LAUNCH SYSTEMS' WEIGHT, PERFORMANCE, AND COST

VOLUME II

PHASE II INTERIM REPORT

By J. A. Boddy and J. C. Mitchell

Space Division
North American Aviation, Inc.

AUGUST 1967

Prepared under Contract NAS7-368 by
NORTH AMERICAN AVIATION, INC.
SPACE DIVISION
Downey, California

for

Headquarters, Office of Advanced Research and Technology
NATIONAL AERONAUTICS AND SPACE ADMINISTRATION

FOREWORD

This report documents the Phase II study effort completed under Contract NAS7-368, Development of Programmed Assistance in Directing Structures Research. The report covers the contract period from June 30, 1966 through June 30, 1967.

Phase II of this program is involved with extending the structural design synthesis analyses initiated during Phase I to include advanced types of structural concepts. These advanced structural concepts were applied to the series of base line expendable launch systems of Phase I to determine beneficial structures and materials research areas. This current study was also devoted to the development of a technique for the parametric synthesis of expendable first stages (winged body) and the definition of six representative vehicle systems for future study of areas for fruitful structures and materials research. A plan was developed for turnover of the Phase I programs to NASA and the feasibility of the parametric synthesis of re-entry vehicles was studied.

This study is being funded by the National Aeronautics and Space Administration, Office of Advanced Research and Technology, under the direction of Mr. M.G. Rosche, Chief of Structures, assisted by Mr. D.A. Gilstad, Chief, Structural Loads and Cryogenic Structures.

Study effort was accomplished at the Space Division of North American Aviation, Inc., Downey, by the Structures and Materials Department, Research and Engineering Division, under the direction of Dr. L.A. Harris. Principal investigators included Messrs. J.C. Mitchell, L.A. Moss, and C.W. Martindale, with additional contributions by Messrs. D. Jones (Propulsion), and L.B. Norwood (Manufacturing). All work was under the supervision of Mr. W.D. McKaig, Program Manager, and J.A. Boddy, Project Engineer.

PRECEDING PAGE BLANK NOT FILMED.

CONTENTS

ILLUSTRATIONS

Figure Page

TABLES

Table Page

INFLUENCE OF STRUCTURE AND MATERIAL RESEARCH ON ADVANCED LAUNCH SYSTEMS' WEIGHT, PERFORMANCE, AND COST

VOLUME II - PHASE II INTERIM REPORT

By J.A. Boddy and J.C. Mitchell
Space Division
North American Aviation, Inc.

SUMMARY

The second phase of this contract used information from the base line vehicle systems developed in Phase I to assess the relative benefits to be derived from advancements in structures and materials. The North American Aviation, Inc. Space Division Launch Vehicle Synthesis programs were modified and used to synthesize families of vertically launched, tandem-staged booster vehicles.

Base point vehicles of Phase I were derived for predicted improvements in propulsion and propellant characteristics considering advances through three periods; i.e., 1966 to 1970, 1970 to 1980, and the post-1980 period. For each of the periods, the equivalent 100-nautical-mile earth orbital payloads were classified into the following ranges:

30 000 to 100 000 pounds—medium range payload class
225 000 to 500 000 pounds—Saturn payload class
1 000 000 to 2 000 000 pounds—post-Saturn payload class

These payload ranges were assumed to encompass anticipated future missions for the periods under consideration and resulted in the identification and definition, in sufficient detail, of typical vehicle systems on which to operate in order to assess the effects of structures and materials advances and to identify areas where research in structures and materials will be most effective from a technological and systems aspect.

During this Phase (II), structural analyses were conducted on a spectrum of stage diameters-(260 to 540 inches) and a range of loading intensities

(2 000 to 20 000 pounds per inch), and included shell analyses to obtain optimum weight for corrugated sandwich, multiwall corrugated, and double-wall skin stringer stiffeners using sine-wave substructure. Materials investigated for the three periods included aluminum, titanium, and beryllium. Manufacturing limitations and improvements were considered in the structural investigation.

The method of evaluation involved a component-by-component substitution in the base point vehicle systems. Estimated manufacturing complexity factors, material costs with year, and manhour requirements were included in the cost assessment. Cost assessment was accomplished by isolating each structural component and performing a comparative evaluation of the new component to the base point component, which was considered to be aluminum integral skin-stringer construction. Final assessment is made in terms of component weight reduction, equivalent payload gained from this reduction, and cost ratio for the new component which is identified as additional dollars cost per pound of payload gained. The three merit functions are then organized in arrays to order their importance.

It is recognized that other merit functions exist, e.g., effect of design on production schedule, but these indices are not readily analyzed numerically and not treated further herein. Based upon the study merit functions, the study results have indicated the following: Multiwall and double-wall shell concepts for tanks and unpressurized structures offer distinct structural advantage; research is required in design application, manufacturing techniques, and in core stiffness requirements and general instability analysis and test verification. Honeycomb sandwich is beneficial for most booster stage applications; for large systems, deep core is required, and related research in design application and manufacturing technology is indicated. Beryllium structures offer the most weight advantage although most costly; moderate cost improvements resulting from materials and manufacturing research (and design experience) will make beryllium structures highly competitive. Presently, the most attractive weight-to-cost design is aluminum skin-stiffened using Z- or hat-section stringers. Simplified construction (ring-stiffened only), if used for first stages when cost and/or schedule considerations are paramount, results in moderate payload decreases. Improvements in properties of a given material should be directed to multiwall and honeycomb sandwich concepts only. Externally positioned longitudinal stiffeners are most effective for beryllium designs; aluminum and titanium designs require individual evaluation for small improvements, if any; eccentricity effects diminish with increased shell diameter. Recoverable vehicle systems with their small payload-to-launch-weight ratio will benefit more markedly from structural weight reductions, particularly in the upper stages.

Generally, research would be more beneficial when devoted to manufacturing and design development for new and advanced structural concepts and for developing materials with markedly improved mechanical and physical properties rather than by forcing improvement of current material ultimate strength properties.

Parametric synthesis approaches initiated in Phase I were extended to include recoverable first stages with winged body shapes and flyback propulsion system and landing provisions. A series of baseline partially recoverable vehicles was generated for a range of payload capabilities. Sizing and associated design loading environments for the partially recoverable vehicles are covered in this report. Structural and material trade-offs on these baseline vehicles will be conducted in planned future study effort.

A plan was established to provide for the turnover to NASA in a future phase of the automated subroutines developed during the Phase I study. The feasibility for the development of a parametric synthesis program for re-entry vehicles was investigated.

INTRODUCTION

The structural and material sciences have contributed significantly to the development of launch-vehicle and space-vehicle technology and to the achievement of the present state of the art. Efficient development of future launch vehicle systems depends upon identifying appropriate research required in the structures and materials disciplines. Effective research can only result from proper interplay among various advances in such disciplines as structural sciences, propulsion technology, and flight technology. Determination of the desirable directions for structural and materials research requires a method that permits evaluation of predicted advances in terms of weight, performance, and cost benefits for the various classes or types of vehicles foreseen to fulfill the requirements of future space systems.

In order that decisions be sensible and timely, the spectrum of future vehicle systems, which result from predicted advances in all the technological disciplines, must be understood. Any technique used to provide the necessary data for research and development planning must have the capability to synthesize these future vehicle systems and to measure the interactions of the basic launch vehicle parameters with the structural system as they affect vehicle weight, performance, and cost. This technique must of necessity, due to the complex systems being studied, be capable of starting with basic mission requirements and efficiently synthesize realistic vehicle systems to meet these requirements, evaluate the effects of suggested structures and materials advances, and identify the most useful application of an advancement. This application then must be identified by specific vehicle system and type of component in terms of weight improvement, performance improvement, and cost improvement.

This report covers the second phase of contract NAS7-368 in which the Space Division of North American Aviation, Inc., has been involved in modifying, extending, and utilizing automated analytical techniques to determine significant structures and materials research areas in current and predicted launch vehicle systems. The Phase I study (ref. 1) covered the parametric synthesis[1] of expendable launch systems vehicles, followed by a preliminary

---

[1] Parametric Synthesis: An automated technique in which numerous vehicle systems are synthesized using limited input parameters and resulting in lumped-mass definitions of vehicle stages and their primary subsystems, stage performance ratios, and gross size characteristics.

design synthesis[1] of most of the major structural components of these vehicle systems. The major portion of the work accomplished during the second phase extended the design synthesis to cover other constructional concepts and the development of a program for the parametric synthesis of launch vehicles having a recoverable, winged first stage with flyback capabilities, and the definition of a series of basepoint vehicles which can be used for future preliminary design synthesis studies to identify profitable areas for structures and materials research in such systems.

During Phase I of this study, a series of current, near-term, and future basepoint expendable launch vehicles were synthesized. Aluminum, titanium and beryllium materials were utilized in monocoque, waffle, skin-stringer, and honeycomb sandwich shells, and their performance and cost merits were assessed within the basepoint vehicle families. The extension of this study task, reported herein, covers corrugated, corrugated sandwich, and several multiwall shell concepts, as well as several bulkhead concepts, with merit functions assessed using the same basepoint expendable vehicles and the same material types and property predictions as utilized during Phase I. Improvements in the costing assessment have been incorporated herein.

Future mission and economic considerations indicate the need for serious evaluation of launch vehicle recovery and reusability. Booster recovery with such devices as parachutes and retrosystems has been considered by NASA and the industry as an interim step before more sophisticated winged and powered recovery systems are developed. Parachute and retrorocket recovery involve complex detail design problems, rather than the basic structures and materials trade-offs being considered in this study. Other NASA studies, such as the Reusable Orbital Transport Study, have considered entirely new vehicle concepts with special body shape characteristics, and employing not only horizontal recovery but horizontal take-off as well. A reasonable vehicle evolution is to first modify the lower stages of the expendable system to a winged body system with powered fly-back and horizontal landing while still retaining the expendable upper stage. The next step could include rendering the upper stage as recoverable, using both winged body and lifting body shapes for the upper stage. The first step of modifying a lower stage is covered in the present Phase II and reported herein.

Recoverable launch vehicle systems emphasize and amplify the need for structures and materials research. In an expendable system, the payload-to-liftoff weight ratio is around 5 percent, whereas in a recoverable system this

[1] Preliminary Design Synthesis: An automated technique in which a few vehicle systems are subjected to preliminary design analysis considering component design constraints and resulting in identification of optimum component design within the input constraints - in this study, considering only the structural subsystem.

ratio is decreased to 1 to 2 percent. Weights saved in the structural system have a 200- to 300-percent greater impact in performance and cost in the recoverable system than in the expendable vehicle. It therefore becomes most important that the synthesis of the recoverable base point vehicles be as realistic and practical as possible. If a recoverable system is to become a reality, it could well owe its existence to the proper structures and materials application and the proper a priori application of research funds in the structural sciences.

This report also includes a detailed discussion of the plan to be followed in a future phase in turning over to NASA of the computer programs developed during Phase I. Finally, this report includes the results of a brief study conducted to evaluate the feasibility of the parametric synthesis of reentry vehicles.

The effort documented in this report utilizes the North American Aviation, Inc., Space Division background in vehicle synthesis and computer-aided design by modifying and extending digital computer subroutines from these programs. It also draws considerably on work in recoverable launch vehicle systems studies performed by NAA/SD and others. Obviously, the background developed in Phase I of this contract is used extensively wherever possible and appropriate.

STUDY APPROACH

Overall study tasks include the modification, extension, and application of computer programs to synthesize vehicle systems, perform preliminary structural design analysis, and conduct trade-off studies. The primary study objective is to identify systems-oriented functional research in the structural sciences which will result in maximum weight, performance and cost dividends.

During Phase I of this program, a method was evolved which used predicted future vehicle and mission requirements to synthesize expendable vehicle generic families to satisfy these requirements. Then, operating within a generic family, component weight reductions were assessed for various structures and material improvements to determine weight, performance, and economic benefits of the predicted improvements.

The vehicles families synthesized for basepoints were limited in the study to two-stage, expendable, tandem-staged, integral tank, vehicles covering three orbital payload range capabilities: 30 000 to 100 000 pounds, 240 000 to 445 000 pounds, and 1 000 000 to 2 000 000 pounds. Propellants were LO_2/RP-1 on the first stage and LO_2/LH_2 on the upper stage. Propulsion systems were synthesized using "rubberized" clusters of the F-1 and J-2 engines. The structural design environment resulted from a typical AMR launch condition and trajectory. Stage diameters and mass proportioning were identified by the Parametric Synthesis Program. Aluminum, titanium, and beryllium materials with: (A) current properties, (B) a 10-percent improvement, and (C) a 20-percent improvement were considered in monocoque, skin-stringer, waffle, and honeycomb sandwich constructions.

The first task in the second phase of this study (covered in this report) uses the same material property predictions to assess the weight, performance, and cost benefits of advanced construction types. The construction types considered in this phase include the following:

Shells

Multiwall concepts with skin-stringer facings

Multiwall concepts with corrugated sandwich facings

Corrugated core sandwich

Ring-stiffened

Longitudinally stiffened, eccentricity effects (stiffeners on one side)

Bulkheads

Elliptical

Oblate spheroid

Low profile

Special consideration was given to the application of both the Phase I and Phase II shell constructions to unpressurized frustums. Analysis was extended to account for discontinuity stresses at bulkhead-and-cylinder joints. As in the first study phase, per references 1 and 2 , structural design synthesis procedures were developed and run for the various internal pressures and load environments for a series of tank diameters that had been established for the basepoint expendable vehicles. After synthesizing the proper structural components, weight reductions were then calculated within the vehicle families and the effectiveness of the predicted improvements assessed.

The second major task of the Phase II study reported herein concerned the parametric synthesis of winged body recoverable first stages using a horizontally-powered flyback and landing mode. The approach was to use minimum modifications to the Phase I expendable stage to affect the conditions. The modifications basically consisted of sizing flyback engines, flyback fuel requirements, wings and control surfaces for recovery, and of adding a manned or unmanned equipment section to fly and land the vehicle. Other provisions were included to make allowance in the design for the new thermal and load environments encountered during launch and recovery. Figure 1 illustrates the recovery penalties that were included and identifies six basic areas where new synthesis techniques were required. Weight scaling equations were written in the program to account for such items as surfaces (wings, controls), landing gear, pilots compartment and ejection, flyback propulsion and fixed equipment. Wing sizing parameters such as wing loading, aspect ratio, taper ratio, sweepback angle, and thickness-to-chord ratio were handled as input variables.

Vehicle design concepts used in this study were two-stage launch vehicles in a tandem arrangement. Basepoint vehicles synthesized with this program

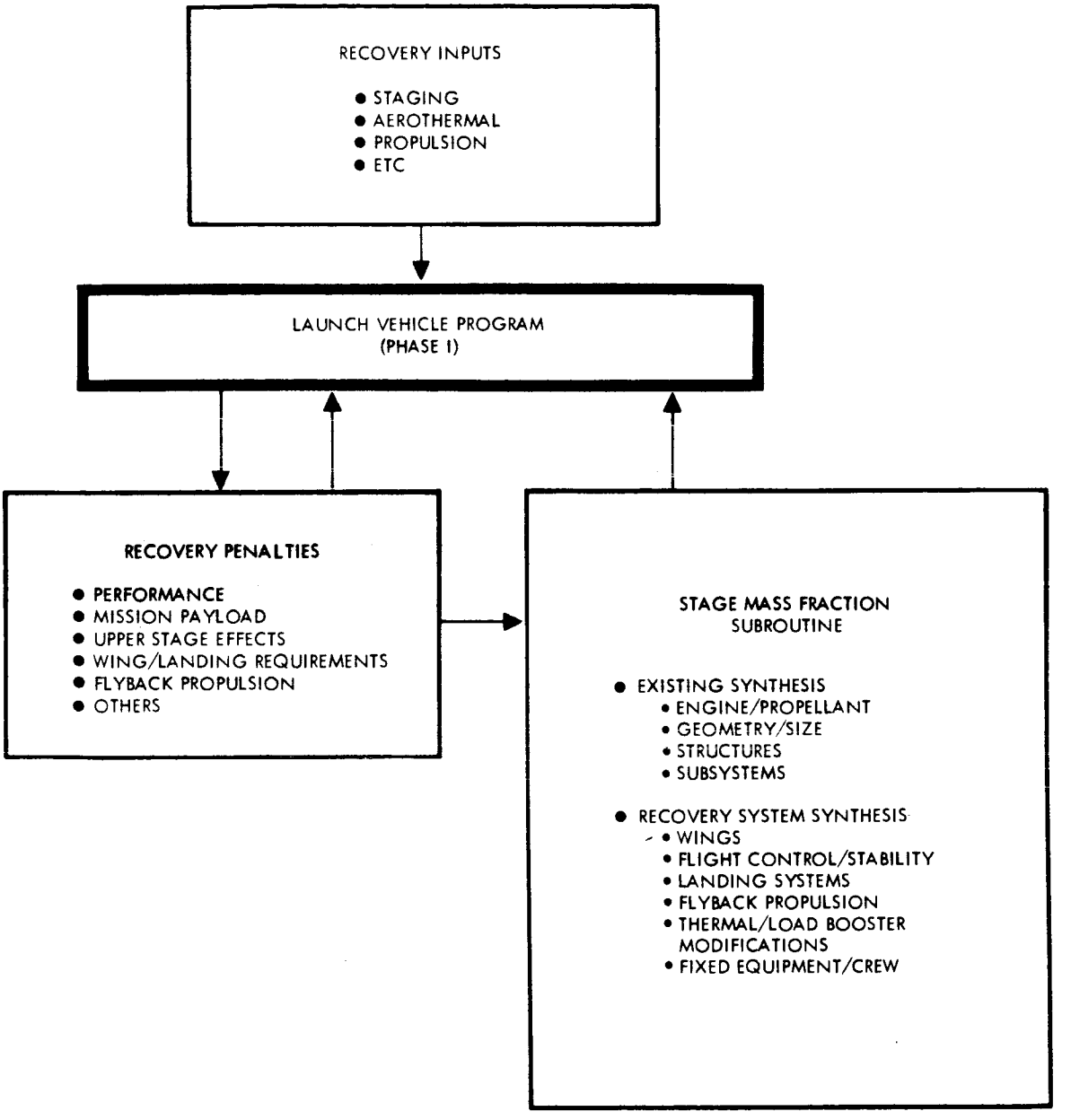

Figure 1. - Booster Recovery System Synthesis

primarily emphasized an orbital payload range of 20 000 to 60 000 pounds, this being the primary range of interest for the reusable orbital transport studies per references 2 through 5. However, other payload configurations were synthesized, to provide reference points to compare with the Phase I expendable vehicles.

The recoverable vehicle synthesis was accomplished to provide base-point families in which to conduct structural assessments during a future phase of study. These vehicles, being more complex in their design interfaces, are several times more difficult to synthesize than their expendable counterparts. Therefore, this task represented a major portion of the Phase II effort.

Two other smaller tasks are covered in this report. The first, covers the result of an investigation of some of the problems associated with extending the parametric synthesis program to handle recoverable upper stages (reentry vehicles); and the second, presents a plan for turning over the Phase I computer programs to NASA for use in their agencies.

All of the data, assessments, and conclusions presented in reference 1 and in this report are predicated on specific input constraints to the digital computer programs. NASA, in exercising these programs with other input criteria, will find them useful in establishing checkpoints for future vehicle studies and for channeling the right research funds into the proper areas to produce results timely to future vehicle development.

STRUCTURAL DESIGN SYNTHESIS

During Phase I of this contract, the portion of the program that describes the structural components was separated from the parametric synthesis section. This permitted the structural components to be analyzed individually without associating any of the structural components with a particular launch vehicle. In addition, the assessment of the effects of the substitution of different types of materials, constructions, manufacturing limitations, or analytical methods on the structural components could be obtained by an independent exercise of the design synthesis subroutines. The structural components considered were defined by a range of diameters, lengths, mechanical loads, and thermal environments representative of those associated with the medium range payload class, the Saturn class, and the post-Saturn class vehicles. The design synthesis determines the resultant unit shell weights for the entire spectrum of radii, mechanical loads, and thermal environments.

In the final assessment of the program the unit shell weights obtained by the design synthesis subroutines were correlated with various components of specific launch vehicles. A design envelope was specified for each of these components as a function of the vehicle's flight trajectory. One element of the design envelope for an unpressurized shell may be a temperature spectrum which varies from room temperature during prelaunch conditions to a maximum of approximately 400°F. In addition, various components of the vehicle's stage may be subjected to maximum loading conditions at prelaunch, at the max $q\alpha$ condition, or at end boost. In order to evaluate the complete design spectrum, the structural design synthesis was conducted for a range of loading intensities, cylindrical diameters, and thermal environments. The primary temperatures considered were room temperature (prelaunch), cryogenic temperature, and the maximum external temperature associated with the end boost condition.

The tensile loading intensity to which a structural component is subjected results from a combination of requirements. The maximum tensile loads for some portions of the propellant tanks result from the ullage requirements for the engine system and the associated bending moment of a particular flight condition. This pressure determines the minimum required skin thickness for the structural component. The maximum compressive loading intensity

dictates the required stiffness of the structural component. The maximum compressive stress is determined by the axial acceleration and the maximum bending moment if the shell is unpressurized. A nominal relief pressure reduces the compressive loading intensities for pressurized components. The relief pressure consists of the ground atmospheric pressure and a nominal differential pressure which is sufficient to prevent propellant boiloff.

Various safety factors are applied to all of these loading conditions. For convenience, the relative magnitudes of these safety factors are established external to the subroutines. This permits consideration in the design synthesis subroutines of only an ultimate tensile or compressive loading intensity. In this study, the ultimate and limit factors of safety are 1.4 and 1.1 respectively.

Numerous alterations of the structural design of a component must be considered to evaluate effectively the significance of technological advances. These include replacing materials to evaluate increases in material allowables; for example, making replacements to increase the compressive yield strength and the ultimate tensile strength of the various base-line materials. In addition, significant weight reductions may be obtained by replacing base point configuration and material with a different type of construction, material, or both.

A third approach which may result in significant weight reductions lies in the relaxation of the manufacturing restrictions presently placed on all structural components. In addition, the structural weight of the component may be reduced by improving the analytical methods that are used to perform the structural analysis in the design synthesis subroutines. In Phase II, the stability analysis for the various structural configurations are based on the Small Deflection Theory. The results obtained by applying this theory are modified by correction factors based on experimental data obtained from tests of isotropic monocoque shells.

The various design synthesis subroutines which were developed during Phase II of this program were exercised for various types and magnitudes of improvements for material and construction, types of analysis, etc., to cover the design spectrum for the Phase I base-point vehicles. The results of all these improvements are summarized in this section to provide a description of the pertinent data obtained from the synthesis study. These advances and the associated unit shell weight reductions are discussed for the various vehicle systems in the "Assessment" section of this report. Each type of advance and improvement is evaluated and treated separately for the range of construction and materials under consideration in Phase I and II of this study.

During Phase II of this study, the primary types of construction considered for cylindrical and conical segments of the launch vehicles were multiwall skin stringer, longitudinally corrugated core sandwich, ring-stiffened monocoque, and skin stringer with eccentricity effects considered. In addition, synthesis programs for bulkheads with elliptical, oblate spheroidal, or modified semitoroidal curvature were developed. The continuous linking of these subroutines with those developed during Phase I, i. e., waffle, honeycomb sandwich, skin stringer, and monocoque, permits an extensive parametric study using all types of construction simultaneously and resulting in a convenient display of data.

The unit shell weights for the various concepts and materials for a range of design parameters have been summarized in this section. Printouts from the computer programs for the test cases contain significantly more data than shell weights. In fact, the print formats spell out in detail a complete description of the individual structural elements with their thicknesses, lengths, and pitches, sufficient information for the preliminary design. An indication of the elemental detail for the various structural concepts is shown in Table A-3 in Appendix A. The carpet plots show results for, at most, five loading intensities, while in fact the program was run in steps of 2000 pounds per inch, ranging from 2000 to 40 000 pounds per inch in intensity; i. e., 20 design conditions per case. The number of test cases that were synthesized is indicated by Table 1, compiled for one type of material and construction.

TABLE 1 . - TEST CASES SYNTHESIZED FOR MULTIWALL STIFFENED CONCEPT USING TITANIUM

Parameter	Range	Number
Loading	2 000 to 40 000 lb/in	20
Titanium Material	Grades A and C	2
Stiffeners	Integral, Z, top hat "I"	4
Stiffener pitch	3 to 5 in.	3
Substructure depth	4 to 8 in.	3
Temperature	± 300° F	2
Radius	130 to 270 in.	3

Although this parameter matrix of combinations and permutations was not completed, there were 2160 cases synthesized. This process was repeated for aluminum and then for the other structural concepts. The total design synthesized for the cylindrical shells and their detail data amounted to approximately 8000 design conditions.

The material properties considered for the design synthesis study were selected in Phase I. Table 2 shows these properties for a range of temperatures for current materials such as aluminum, titanium, and beryllium. These values formed the basis for the design evaluation of current materials, which was used in considering a series of material properties improvements. This series of upgraded values was based on the material predictions discussed in the "Parametric Synthesis" section. Table 3 shows the current material properties (Material A) and two steps of upgrading designated Material B and Material C. These improvements amounted to approximately 10 percent and 20 percent for aluminum, 5 percent and 10 percent for titanium, and, optimistically, 15 and 25 percent for beryllium. These percentage improvements in material properties were used to exercise the preliminary design synthesis routines and the range of improvements covering the predicted material advances discussed under "Parametric Synthesis" (Phase 1).

The material property improvements involved the consideration that the magnitudes of both the compressive yield and tensile stress levels were correspondingly increased, but the shape of the stress strain curve was invariant with only a shift in magnitude. Since no detailed knowledge of these advanced materials is obtainable and, at best, most of these advances are postulated, the plasticity factor is assumed to be identical to that for the parent material. When these new materials have been developed and their properties sufficiently defined, they can again be exercised through the design synthesis programs to obtain further detailed information for design concepts that utilize all the additional, more exact values of the new material properties.

One effective method of reducing the weight of structural components is to improve the material properties by alloying current materials. Present-day alloy systems which have performed well in space structures are expected to be used for the next fifteen years, or more. During this period, their design properties are expected to improve significantly. The types of materials that were considered during Phase I of this study were aluminum, titanium, magnesium, beryllium, and high-strength stainless steel. The design synthesis of magnesium and stainless steel components did not appear to be sufficiently attractive to warrant detailed consideration. In addition, the refractory alloys and superalloys were not included in Phases I or II of this

TABLE 2. - CURRENT MATERIAL PROPERTIES - ALUMINUM, TITANIUM, AND BERYLLIUM

Temperature (Degrees F)	Aluminum 2014-T6				Aluminum 7075				Titanium 5A1-2.5 (ELI)			
	Fcy ($psix10^{-3}$)	Ftu ($psix10^{-3}$)	Fty ($psix10^{-3}$)	E ($psix10^{-6}$)	Fcy ($psix10^{-3}$)	Ftu ($psix10^{-3}$)	Fty ($psix10^{-3}$)	E ($psix10^{-6}$)	Fcy ($psix10^{-3}$)	Ftu ($psix10^{-3}$)	Fty ($psix10^{-3}$)	E ($psix10^{-6}$)
-423	75.3	90.4	73.7	11.90					190	210	190	17.05
-300	68.2	76.5	65.6	11.45	89	87	75	11.1	149	166	149	16.88
-100	62.7	69.1	60.0	10.95	76	80	70	10.7	113	125	113	16.30
78	60.4	66.6	59.0	10.60	71	77	66	10.5	94	104	94	15.52
200	57.2	62.5	56.0	10.40	67	72	62	9.9	84	93	84	15.26
400	33.5	37.1	29.3	9.56	38	34	31	8.6	72	80	72	15.12

Temperature (Degrees F)	Titanium 6AL-4V				Beryllium			
	Fcy ($psix10^{-3}$)	Ftu ($psix10^{-3}$)	Fty ($psix10^{-3}$)	E ($psix10^{-6}$)	Fcy ($psix10^{-3}$)	Ftu ($psix10^{-3}$)	Fty ($psix10^{-3}$)	E ($psix10^{-6}$)
-423	210	223	210	19.4				
-300	190	195	190	16.7				
-100	140	152	140	15.9				
78	126	130	120	15.8	50	70	55	42
200	113	117	107	15.1	49	67	54	42
400	97	104	89	13.9	47	62	53	41

TABLE 3. - REPRESENTATIVE MATERIAL PROPERTIES AND ADVANCEMENTS

Temperature (Degrees F)	Aluminum A			Aluminum B			Aluminum C		
	Fcy ($psix10^{-3}$)	Ftu ($psix10^{-3}$)	E ($psix10^{-6}$)	Fcy ($psix10^{-3}$)	Ftu ($psix10^{-3}$)	E ($psix10^{-6}$)	Fcy ($psix10^{-3}$)	Ftu ($psix10^{-3}$)	E ($psix10^{-6}$)
-300	65	75	10.6	70	80	10.6	75	85	10.6
300	50	55	10.0	55	60	10.0	60	65	10.0
	Titanium A			Titanium B			Titanium C		
-300	120	135	15.8	125	140	15.8	135	150	15.8
300	100	115	14.0	105	120	14.0	110	125	14.0
	Beryllium A			Beryllium B			Beryllium C		
-300	48	63	43	55	70	43	60	75	43
300	48	63	43	55	70	43	60	75	43

study, because the structural components being evaluated are not subjected to severe environments. Hence, in Phase II, aluminum, titanium, and beryllium are the only materials considered.

For the design synthesis portion, only improvements in the physical strength and stiffness properties of the material are considered. The effect of the manufacturing difficulties, fabrication limitations, cost considerations, etc., are considered and discussed in other sections of this report where the various structural components and types of materials are associated with specific vehicles in the assessment evaluation. The design synthesis assumes that any of the materials discussed and used in the structural evaluation will be readily attainable and have the desired and required fabrication properties from which to produce the components. Also, it is assumed that these materials can be welded and joined to form the structural components under discussion. Manufacturing difficulties are discussed in the assessment portion of this study where the relative manufacturing complexity factors are covered.

The material improvements are expressed as a percentage increase of a nominal compression yield and in tensile ultimate strength of current materials. The shape of the stress-strain diagram for the plasticity considerations for advanced alloy materials is assumed to be identical to that of the current material. The plasticity curve of the material is expressed mathematically for inclusion in the computer subroutines to provide access to the plasticity correction factors for the various materials. Design synthesis analyses to evaluate minimum weight for the structural components must consider materials in the elastic and plastic ranges.

Double-Wall Skin Stringer

The prime class of double-wall construction evaluated was double-wall skin stringer. This composite shell structure (fig. 2) consists of two face panels separated by a sine-wave substructure. Each face panel is a single face skin stiffened with an integral, Z, hat, or I section stringer attached to the outer face. This type of advanced concept has been considered as a lightweight design for unpressurized shells for cylinders of the Saturn V diameter, reference 6 . The synthesis of these design concepts was investigated using aluminum and titanium with both current and future (postulated) properties. Beryllium, which is difficult to form, machine, and bond, was considered as an advanced material and as such was not combined with the advanced design

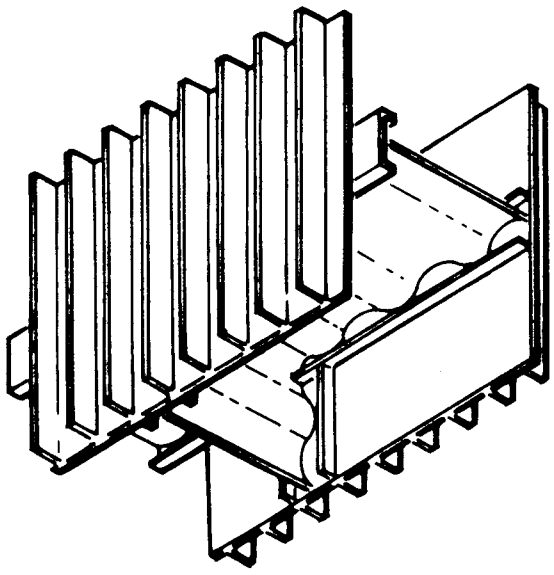

INTEGRAL STIFFENERS

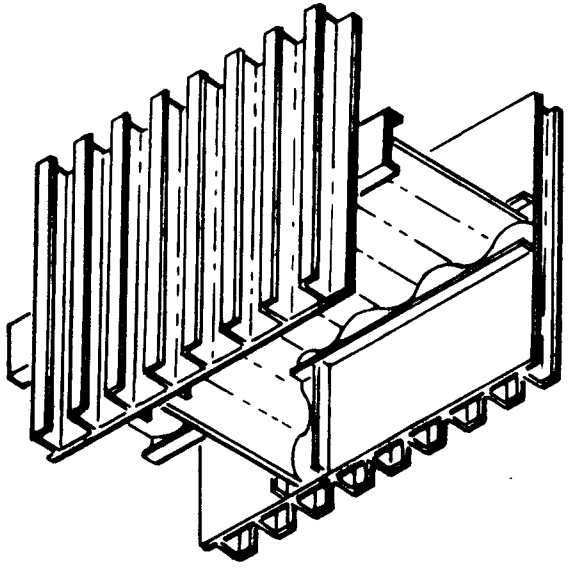

Z SECTION STIFFENERS

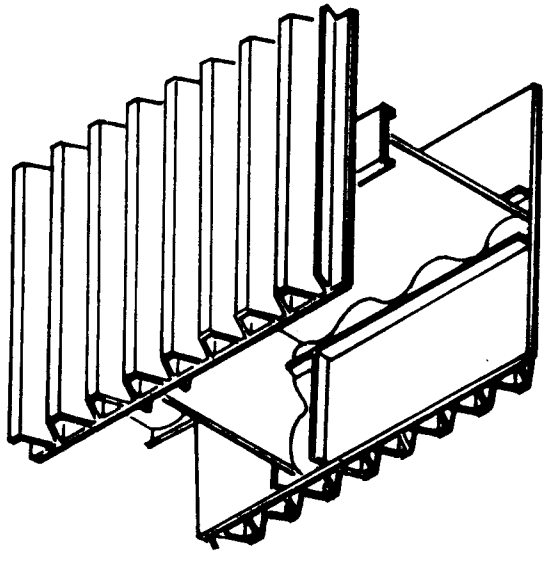

TOP-HAT STIFFENERS

Figure 2. - Double-Wall Skin-Stringer Concepts

concept. The double-wall skin stringer design consists of many elements and the attaching of the facing sheets to the substructure could present extreme difficulties when beryllium is employed.

Combinations of materials were not investigated in detail during this study. The designs considered were all-aluminum or all-titanium. A concept with titanium facing sheets and an aluminum substructure could result in a slightly lighter design. A combined material sandwich, titanium with aluminum core, is best but this results from a minimum foil thickness requirement for the core. With the double wall, the substructure pitch is sufficiently large to allow the substructure webs to be thin sheets and its design criteria is a shear rigidity. Therefore, the stiffness-to-density ratio (E/ρ) is about the same for titanium as for aluminum and could not result in significant weight wavings.

Due to the rather deep overall sections (6 inches) this facet could decrease the usable volume inside a given external mould line for the vehicle. This penalty should not be too significant in the unpressurized regions, skirts, interstages, center section, where volume is not at a premium. For a tank shell these design concepts could present a loss of 3 percent in volume for a 400-inch diameter tank, which is quite significant and would negate any weight savings. Another problem could be the sealing of the inner facing to prevent propellant being trapped between the walls. If propellant is allowed between walls, using the walls opening as a longitudinal ducting, then the outer facing only restrains the pressure in hoop tension. For a sealed concept, the space between the facing sheets would require purging or evacuating for the insulation requirements. Any collapsing pressure differential across the walls might result in an external pressure design condition on the outer facing sheet during ground hold. In light of these restraints the test case data generated did not include specific burst pressure or estimate collapse pressure design criteria. The only consideration was with the temperature and material properties at -300° F. Later design checks were made and it was found that the multi-wall combined skin thicknesses were sufficient to withstand the hoop stresses due to anticipated tank pressures.

There are many design parameters and variations to consider when considering the optimum design conditions. If the synthesis is not constrained it would sometimes generate design sections which, although extremely light in weight, are not esthetically pleasing and in fact are difficult if not impossible to fabricate. Therefore, several of the design parameters were initially investigated to determine their "minimum" weight configuration and its associated feasibility of fabrication. In this fashion several of the optimum

design parameters can be effectively controlled by a preselected minimum design constraint. A testing of the primary design parameters comprised the following:

1. Stiffener pitch
2. Stiffened height
3. Stiffened shape
4. Material selection
5. Substructure height

The influence of the stringer pitch on the unit shell weight of the double-wall skin stringer cylinder was first evaluated. This evaluation indicated that (fig. 3 and fig. 4) for compressive loading intensities (12 000 lb/in. and less), the minimum structural weight is obtained when the stringers are spaced as closely as possible. For this study, as a practical manufacturing consideration, the minimum stringer spacing was 3.0 inches and the remainder of the data was generated at this 3.0-inch pitch. At higher loading intensities, the influence of stringer pitch becomes negligible. For the 130-inch radius aluminum integral, multiwall skin stringer cylinder, figure 3, a 4.0-inch stringer spacing results in a unit shell weight increase of approximately 0.4 lb/ft^2 for loading intensities of less than 12 000 lb/in. The unit shell weight differential associated with the 3.0- and 4.0-inch stringer pitches diminishes rapidly in the 12 000 to 16 000 lb/in. loading regime, and the unit shell weights are approximately equal for the 16 000 to 20 000 lb/in. range of loads. For 198-inch radius components with aluminum integral stringers (fig. 4), a unit shell weight increase of approximately 0.5 lb/ft^2 is associated with a 4.0-inch stringer pitch as compared to the 3.0 inch stringer pitch, for compressive loading intensities of less than 12 000 lb/in. In the loading regime of 16 000 to 20 000 lb/in., unit shell weight penalty associated with 4.0-inch stringer pitch is approximately 0.2 to 0.1 lb/ft^2. The identical weight penalty trends with the stiffener spacing was observed for the titanium designs.

Various stiffener shapes were considered to determine their ordering in terms of their weight index. The shapes included:

1. Integral
2. Top hat section
3. Z section
4. I section

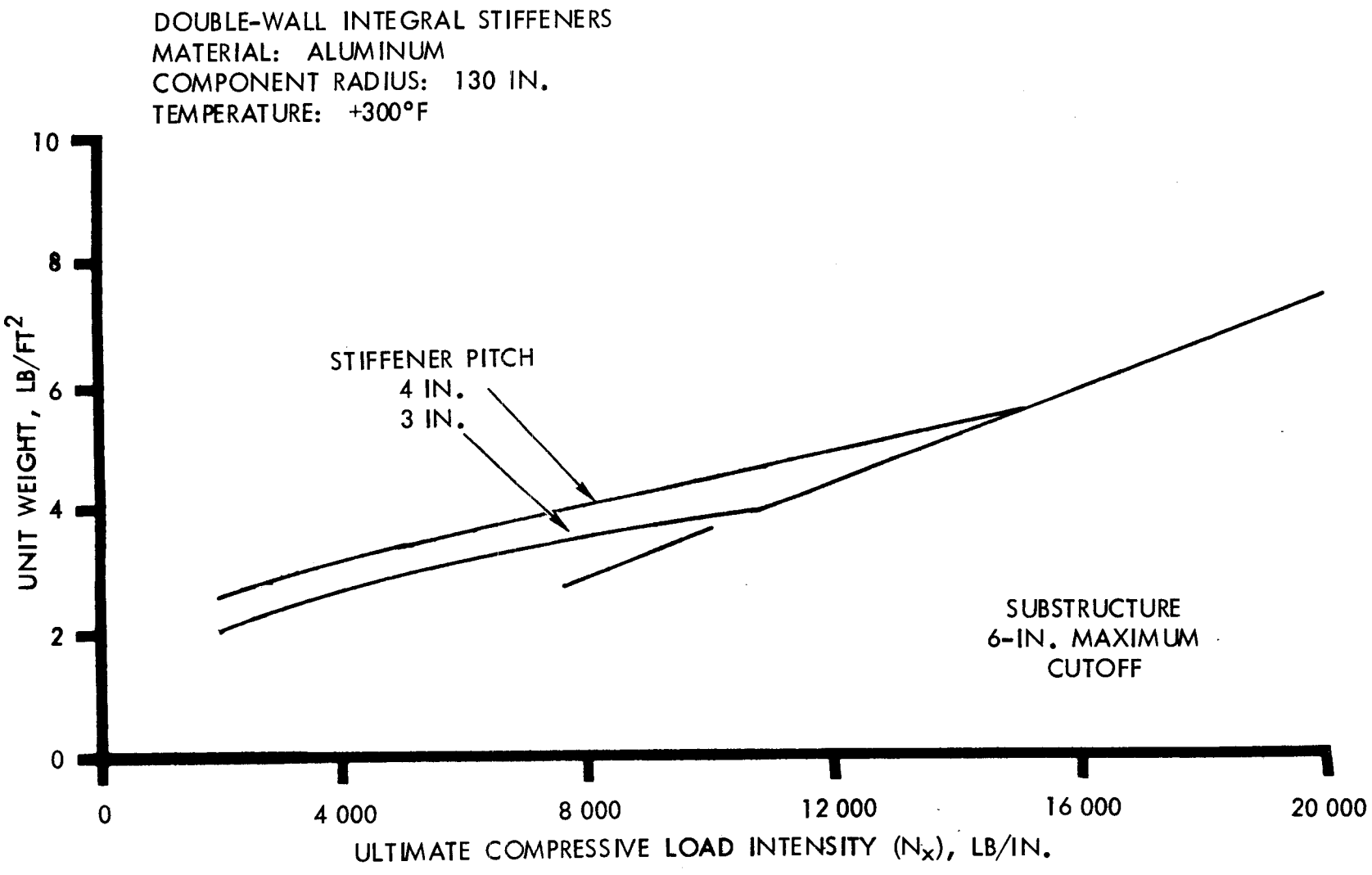

Figure 3. - Stiffener Pitch Variation at 130-Inch Radius

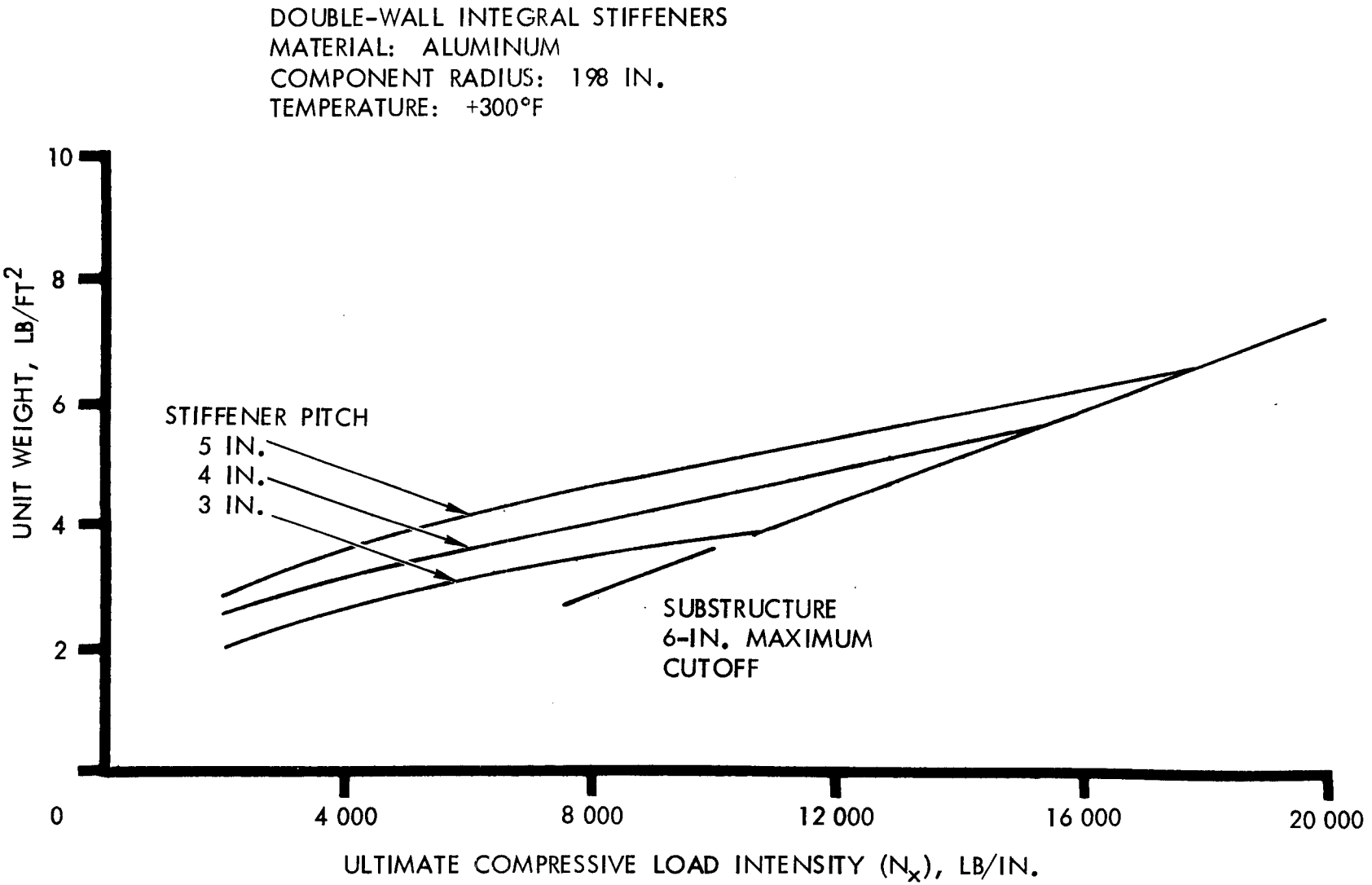

Figure 4. - Stiffener Pitch Variation at 198-Inch Radius

Figures 5 , 6 , and 7 indicate the weights ordering for aluminum and titanium respectively. These curves also reflected the relative change, if any, resulting from the radius variation 130 to 270 inches. It was seen that in all cases, the I section shape resulted in the heaviest design while the top hat section produced the lightest. The unit shell weight of the I section multi-wall skin stringer cylinder was approximately 0.5 lb/ft^2 greater than the unit shell weight of the hat section multi-wall skin stringer cylinder over the entire loading spectrum (2 000 to 20 000 lb/in.). Therefore, the remainder of the test results shown in this section are for integral or top hat section and will reflect the two lightest in the unit weight spread.

Stiffener heights for the facing sheets of a light-weight design with a 3-inch stiffener pitch were not excessively long; for most designs with loading intensity less than 20 000 lb/in., the length was less than 1.0 inch. Therefore, the synthesis program was allowed to search for itself the optimum stiffener height and there were no imposed manufacturing restrictions.

The influence of limiting the maximum substructure depth to 4 to 8 inches was also evaluated. For aluminum and a 270-inch radius component (fig. 8 and fig. 9) the unit shell weight was independent of the maximum substructure height for compressive loading intensities of 12 000 lb/in., or less. At a compressive loading intensity of 20 000 lb/in, the 4.0-inch substructure height restriction resulted in a unit shell weight 10-percent greater than that associated with a maximum substructure height of 8.0 inches. A 3-percent weight penalty resulted from imposing a 6-inch substructure height restriction. The weight penalty associated with the 4.0 inch substructure height restriction was less than 2 percent for the 130-inch radius component for the entire loading spectrum (fig. 10). This effect of weight penalties for restricting the substructure height using titanium was even less noticeable than with aluminum over the range of substructure height considered.

Another parameter variation is in the grade of material and its strength properties. A 20-percent improvement in the compressive yield strength of the aluminum hat section double-wall skin stringer component with a 270-inch radius (fig. 11) resulted in a unit shell weight reduction of 6 to 10 percent in the 16 000 to 20 000 lb/in loading range. Improving the titanium material properties by 10 percent had little effect on the unit shell weight of the components over the entire loading and radii spectrum.

Figures 12 and 13 illustrate the influence of changes in the component radius (130 to 270 inches) and of the applied loading intensities (2000 to 20 000 lb/in.) on the unit shell weight for construction with integral and top hat stiffeners. This figure indicates that for compressive loading intensities of less than 12 000 lb/in., the unit shell weight is relatively independent of the

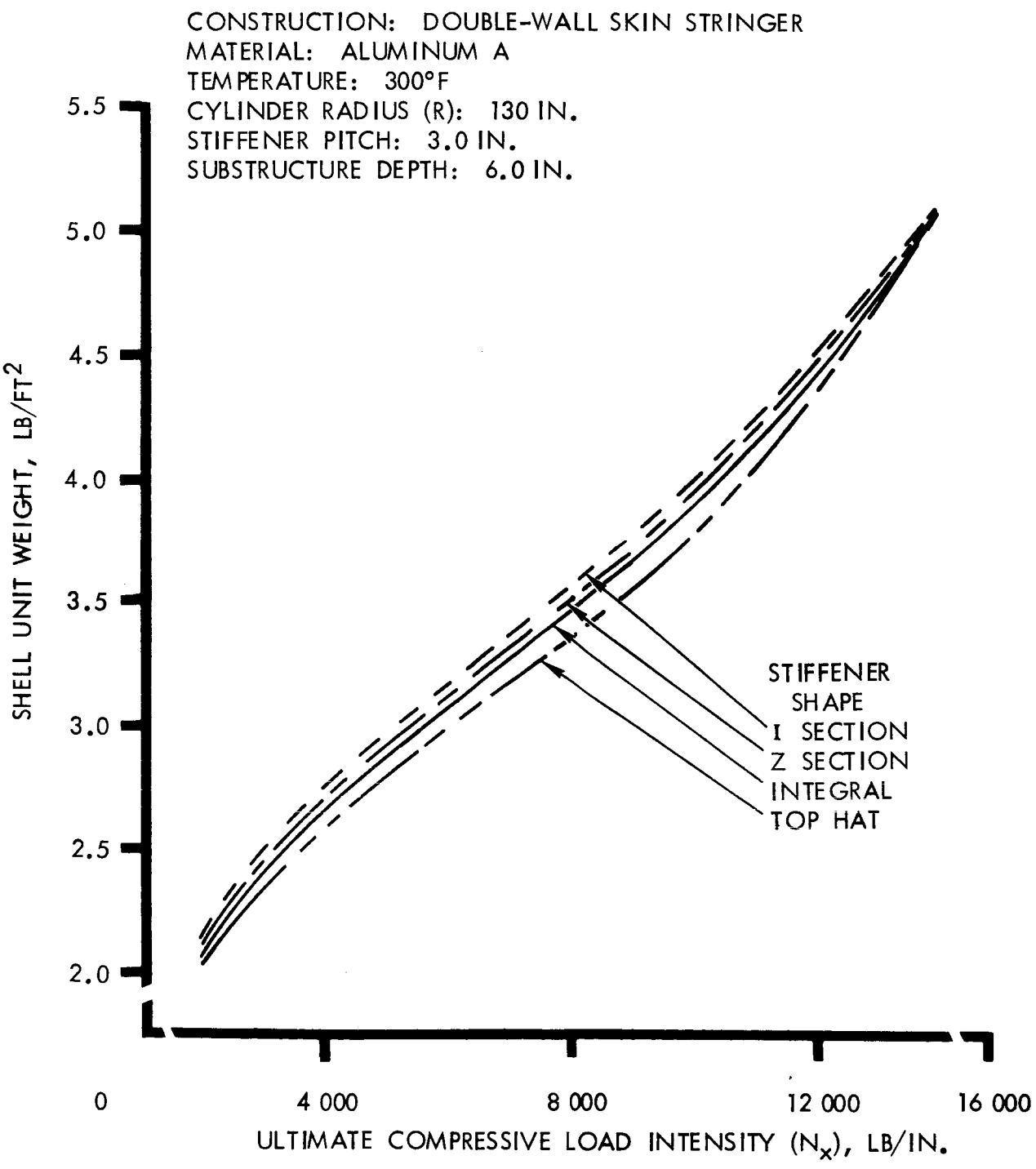

Figure 5. - Effect of Stiffener Shape at 130-Inch Radius in Aluminum

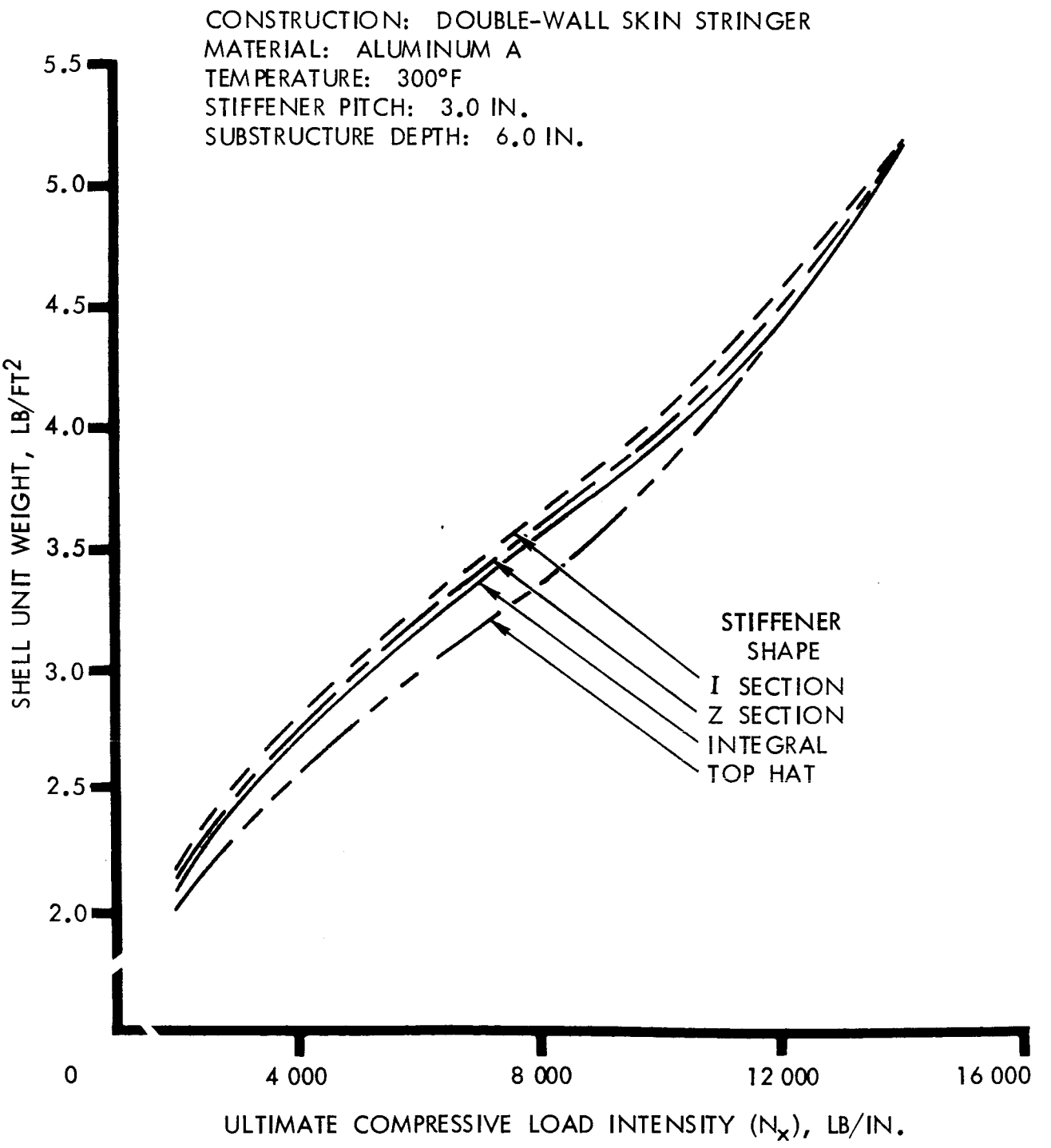

Figure 6. - Effect of Stiffener Shape at 270-Inch Radius in Aluminum

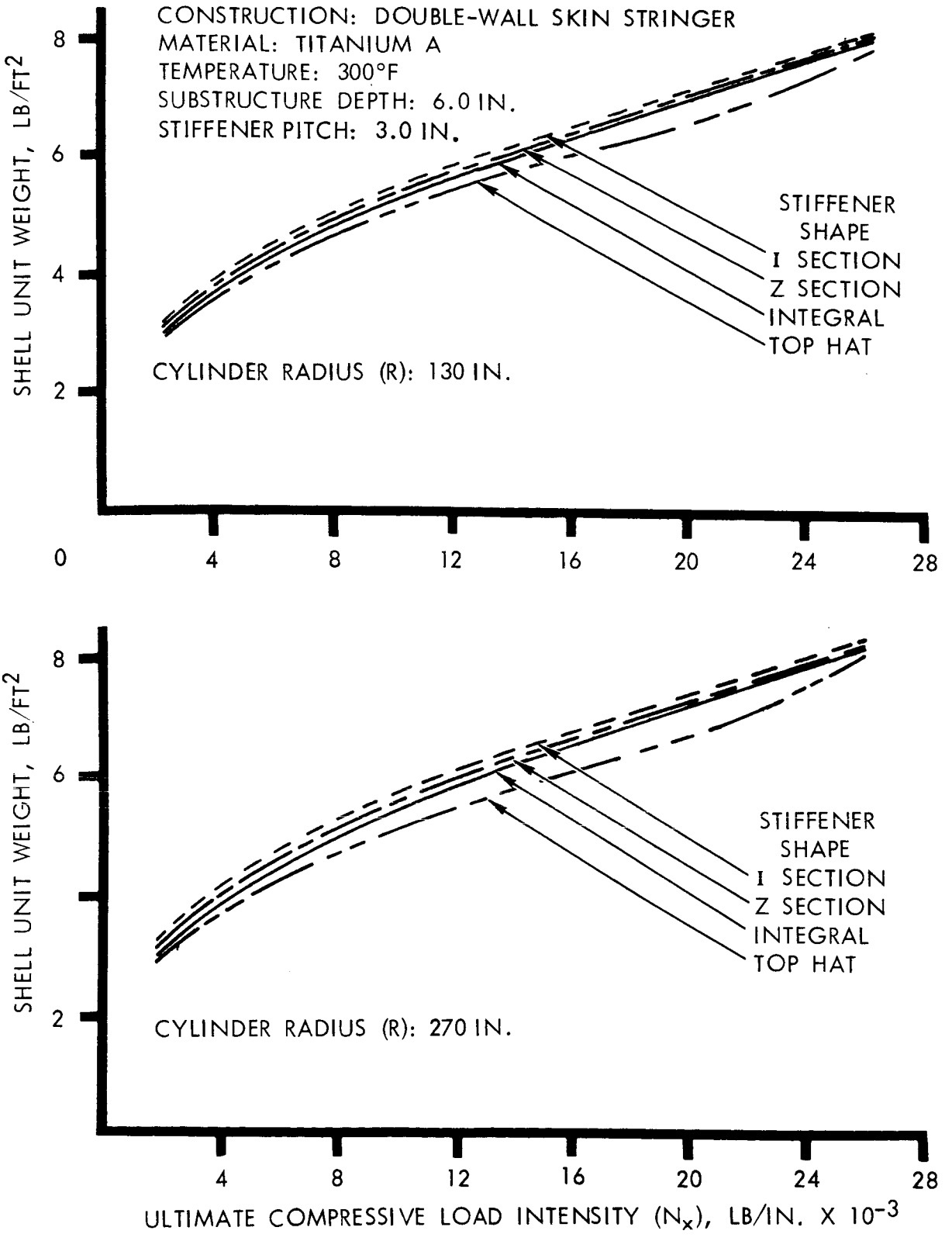

Figure 7. - Effect of Stiffener Shape in Titanium

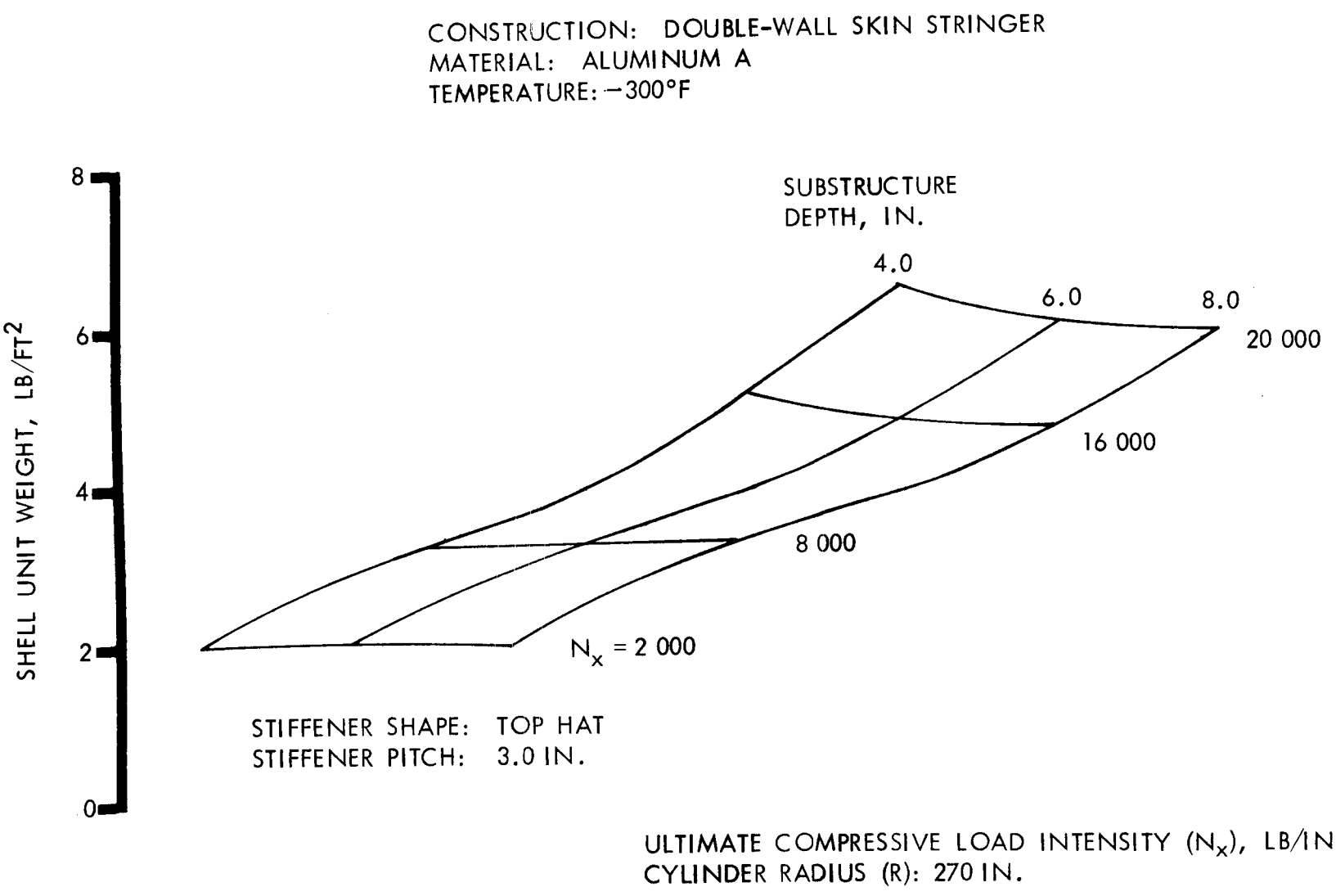

Figure 8. - Effect of Substructure Depth at 270-Inch Radius, Top-Hat Section

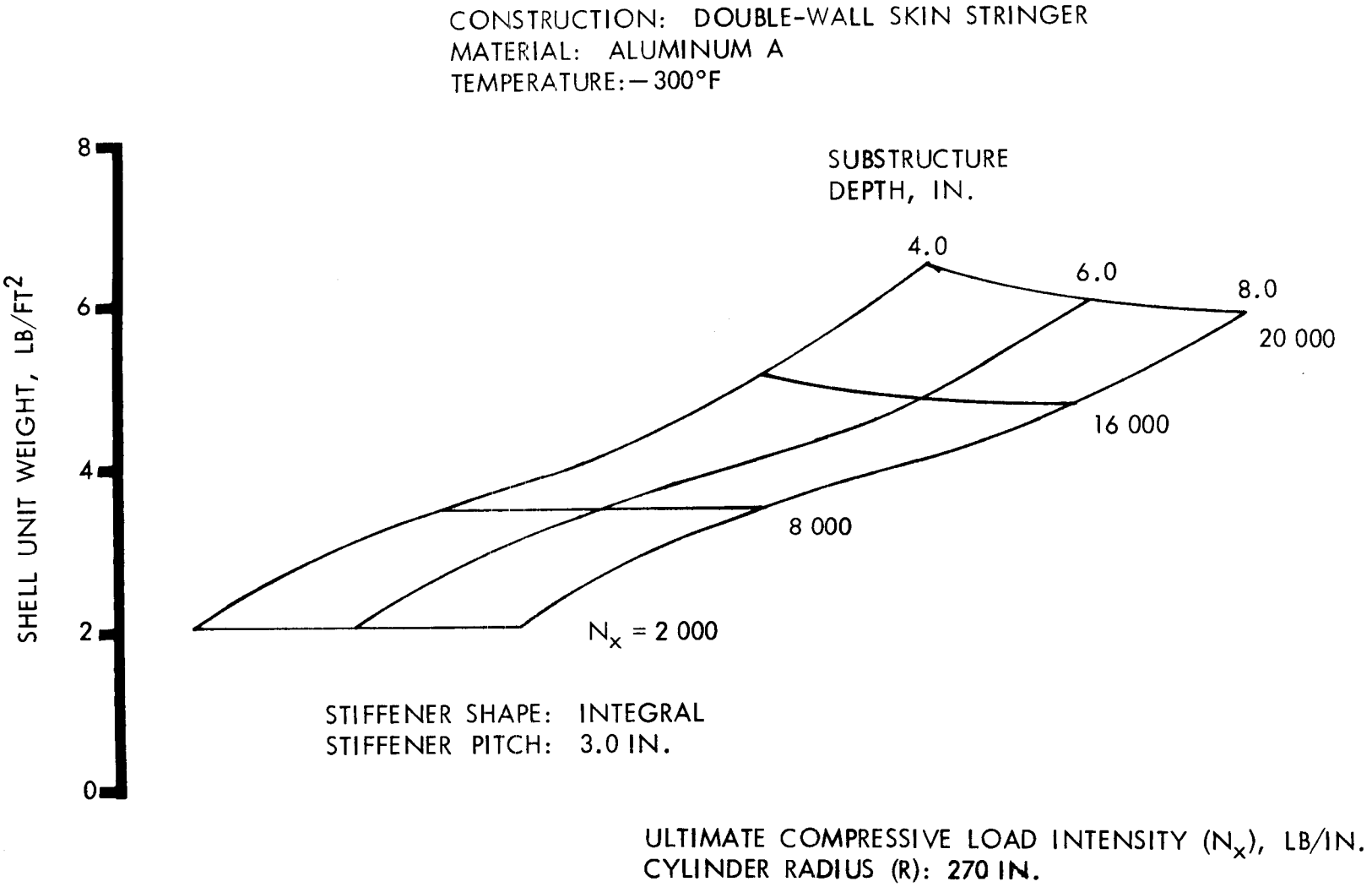

Figure 9 . - Effect of Substructure Depth at 270-Inch Radius, Integral Section

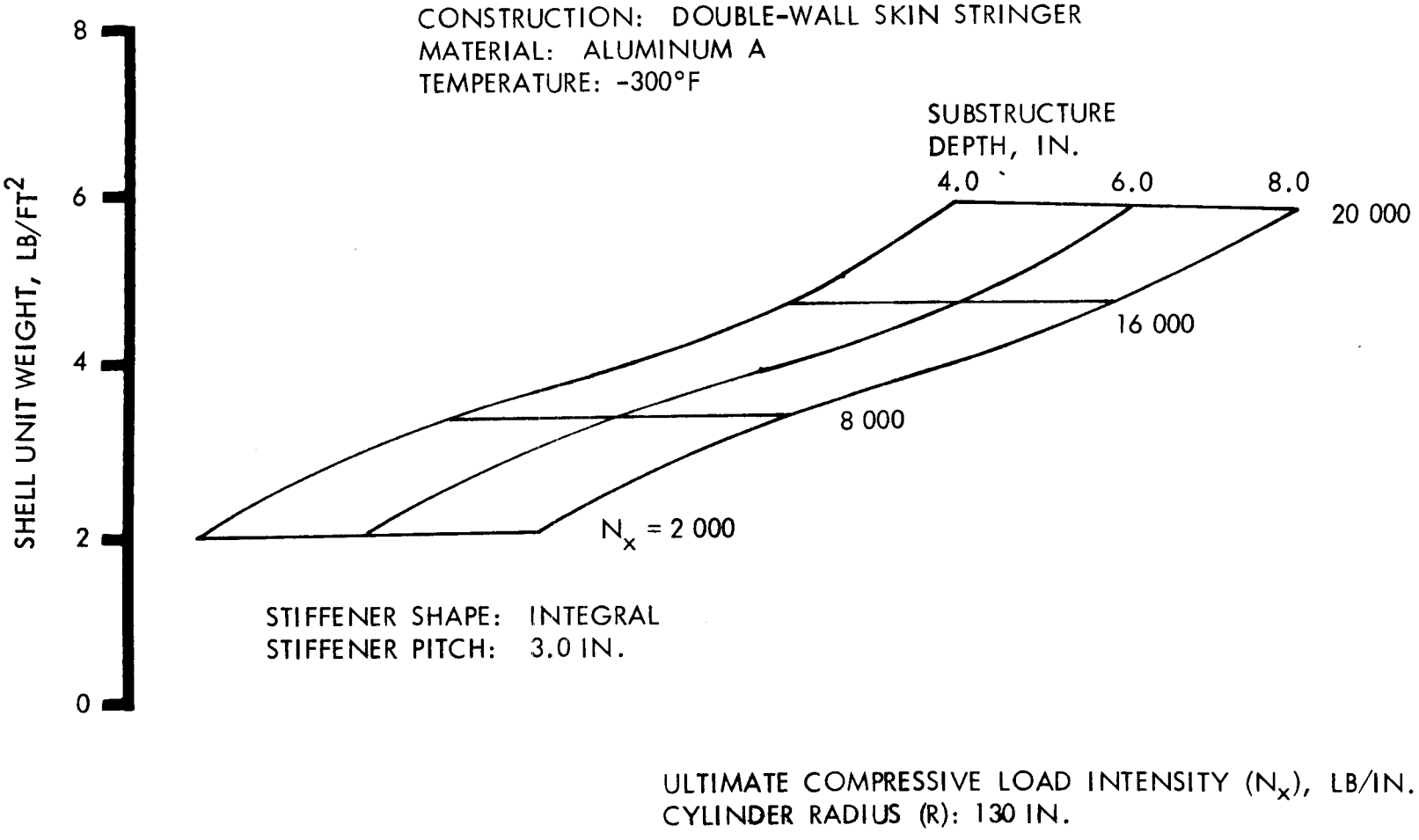

Figure 10. - Effect of Substructure Depth at 130-Inch Radius, Integral Section

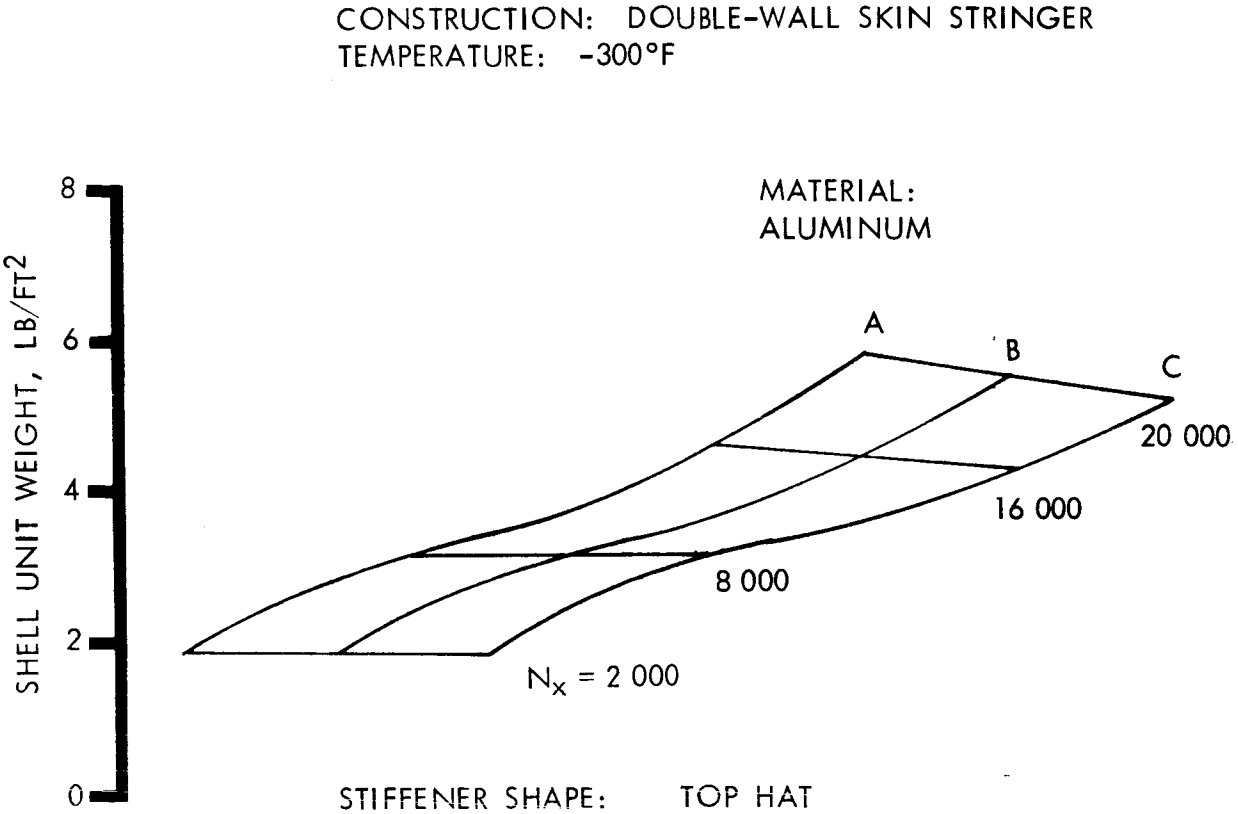

Figure 11. - Variation of Material Grade at 270-Inch Radius, Top-Hat Section

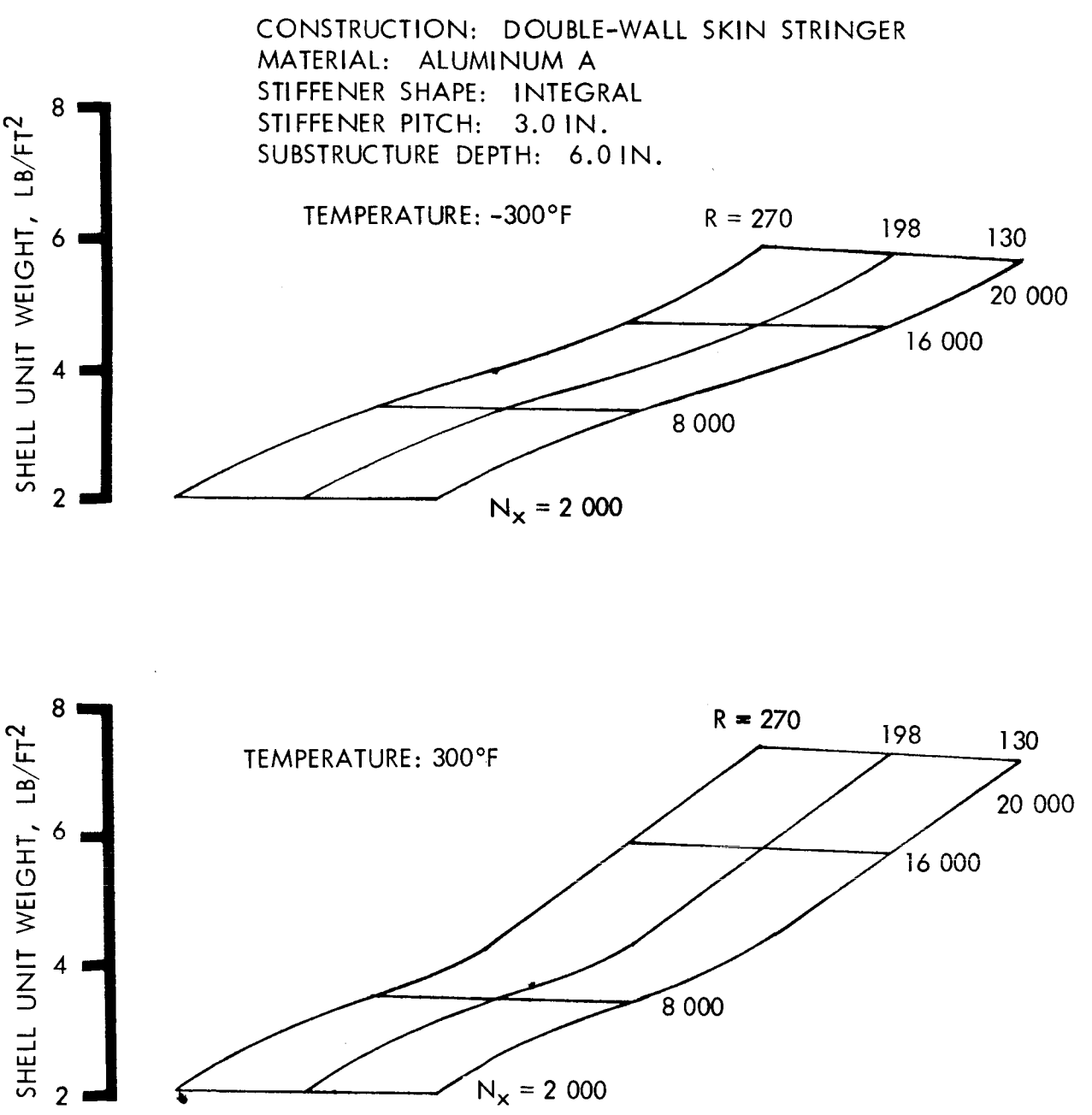

Figure 12. - Unit Shell Weight for Integral Section With Aluminum

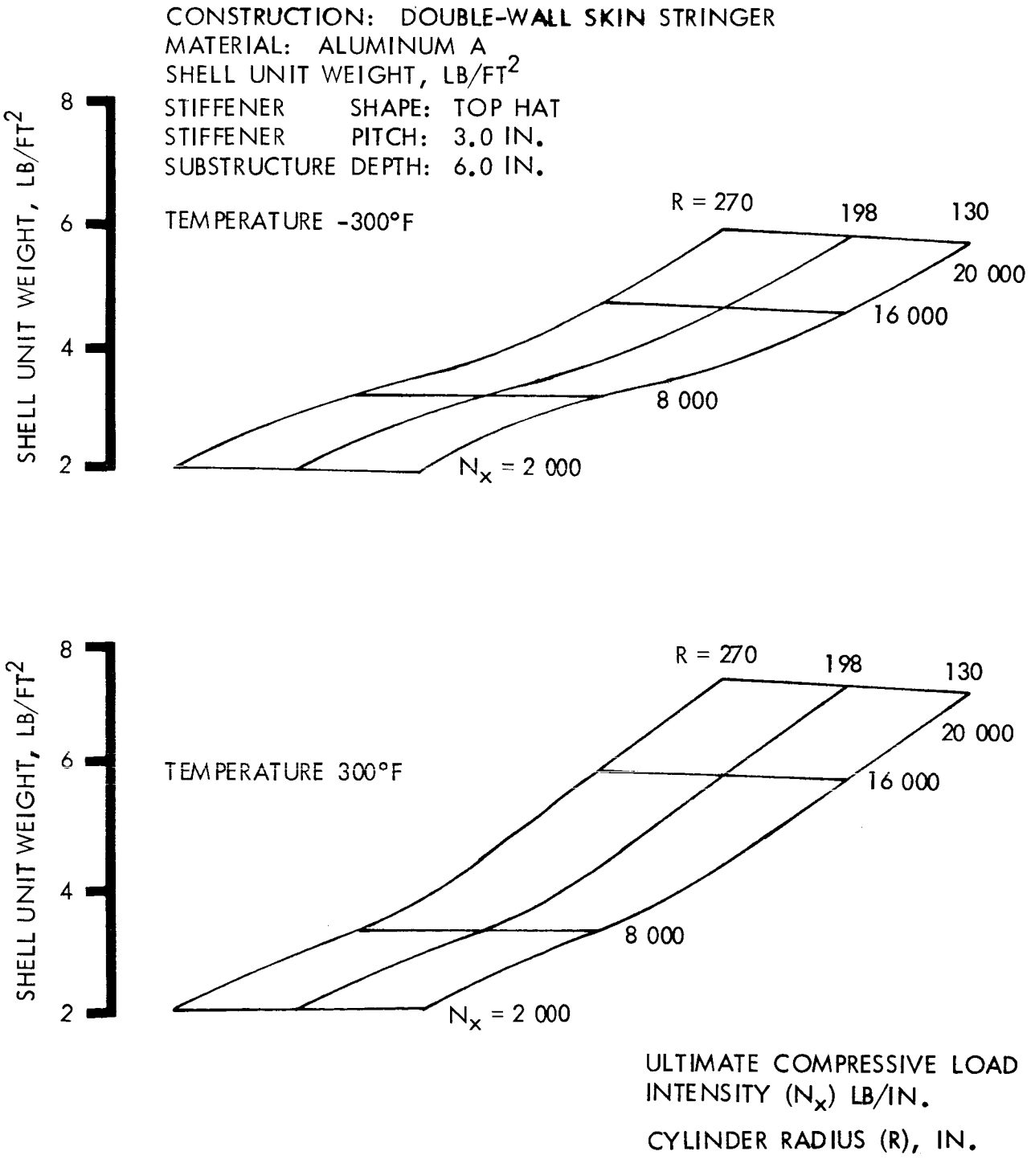

Figure 13. - Unit Shell Weight for Top-Hat Section With Aluminum

component's radius. In addition, it indicates that at a compressive loading intensity of 20 000 lb/in., the 270-inch radius component has a unit shell weight that is about 4 percent greater than the unit shell weight of the 130-inch radius component.

The unit shell weights for the titanium are shown in the next several figures for the four different stringer shapes with a 3-inch stiffener pitch and a 6-inch substructure height for titanium A and titanium C. The integral stringers are shown in figures 14, 15; I section in figures 16 and 17; Z section in figures 18 and 19; and top hat section in figures 20 and 21. Figure 22 shows that the substructure reduction to 4 inches for the titanium A with an integral stiffener does not significantly affect the shell unit weight.

The results of these unit weight plots indicate that the design with titanium was always lighter than with aluminum, and that therefore the **stiffener pitch should be as close as possible, the substructure height as large as possible, and the ordering of stiffener shapes from lightest weight** to heaviest is

1. **Top hat section**
2. **Integral**
3. Z section
4. I section

It should be remembered that although titanium top hat sections closely pitched resulted in the lightest configuration, when cost of material and construction is considered, the additional cost involved might not make it economically attractive. These implications are discussed in the cost assessment section of this report.

Multiwall Corrugated Cylinders

Another type of multiwall construction considered was multi-wall corrugated sandwich cylinders. In this construction (fig. A 1), the longitudinally corrugated core sandwich face panels are separated by a light-weight sine-wave substructure. The corrugated core thickness, spacing, and the angle of the core sheets to the facing covers was automatically determined by the synthesis programs. The analysis for the local stability of the discrete structural

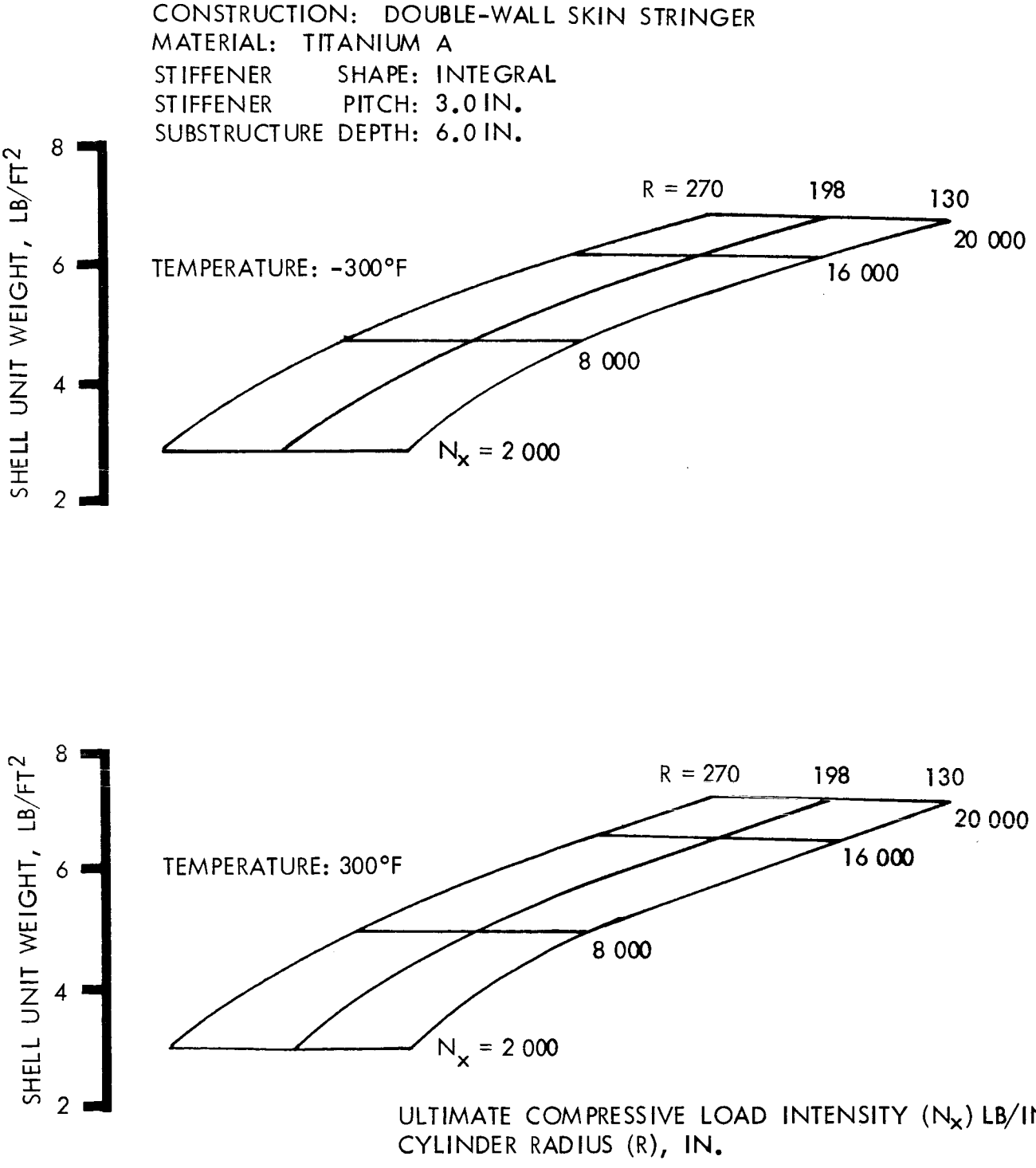

Figure 14. - Unit Shell Weight for Integral Section With Titanium A

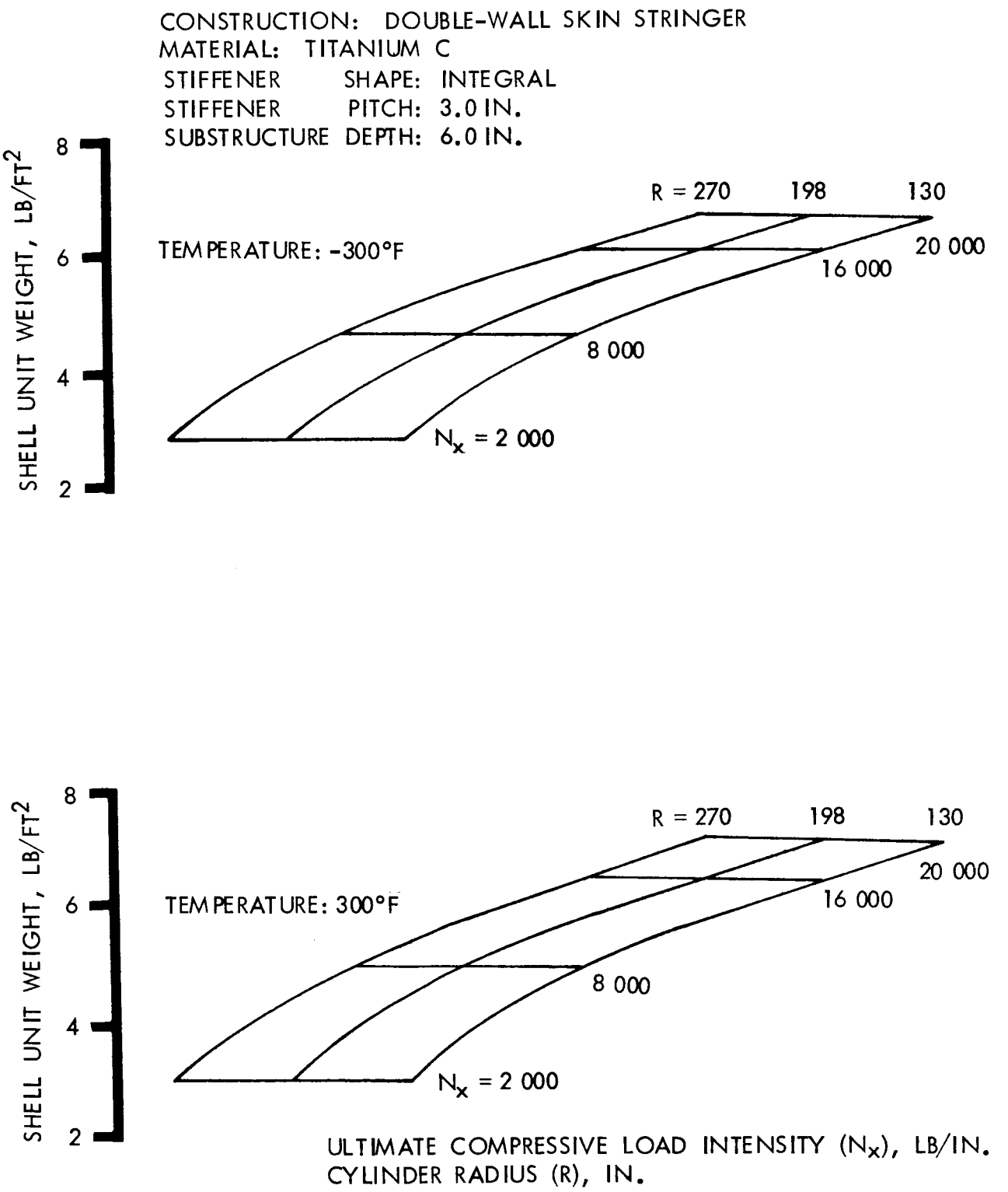

Figure 15. - Unit Shell Weight for Integral Section With Titanium C

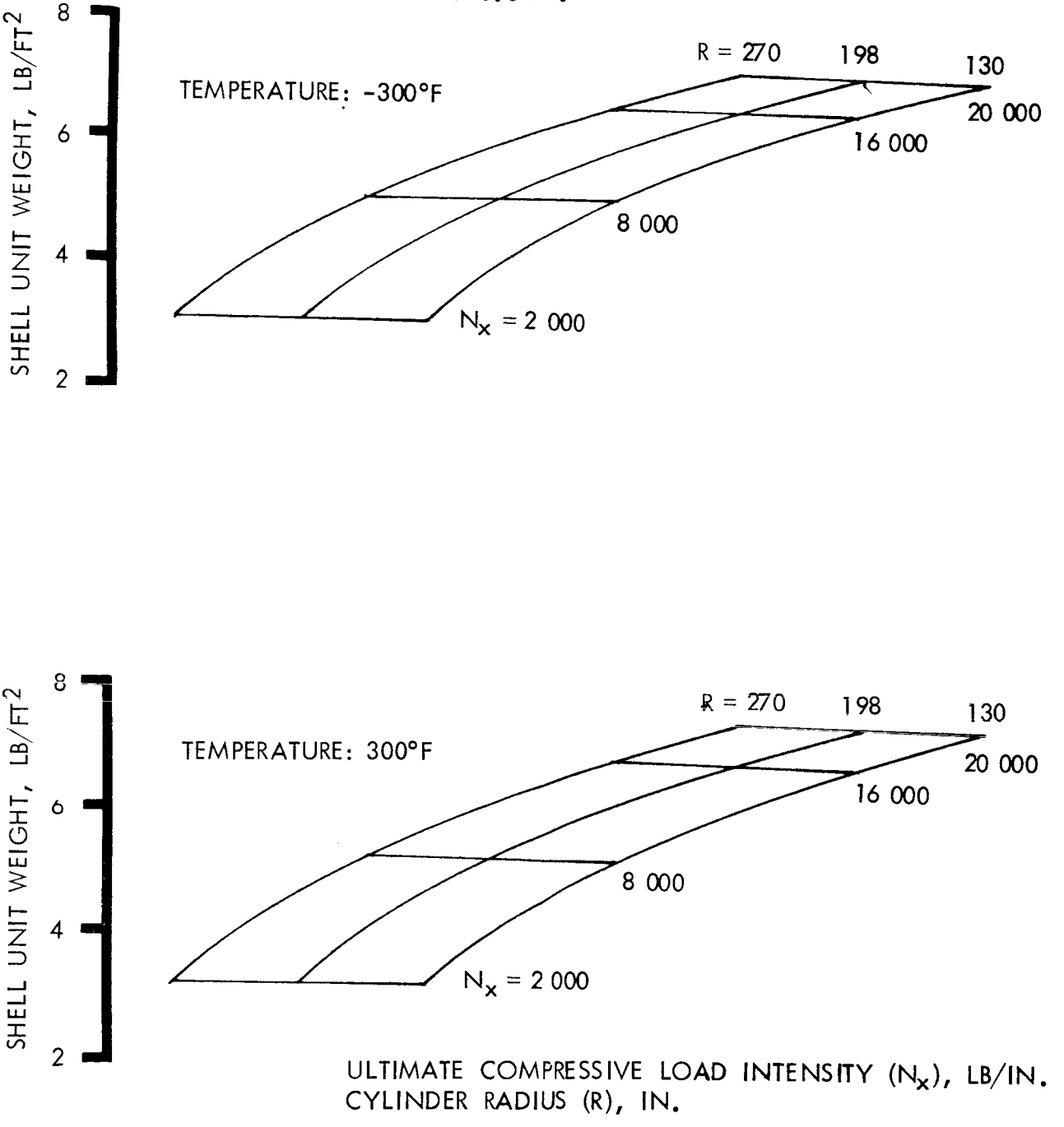

Figure 16. - Unit Shell Weight for I Section With Titanium A

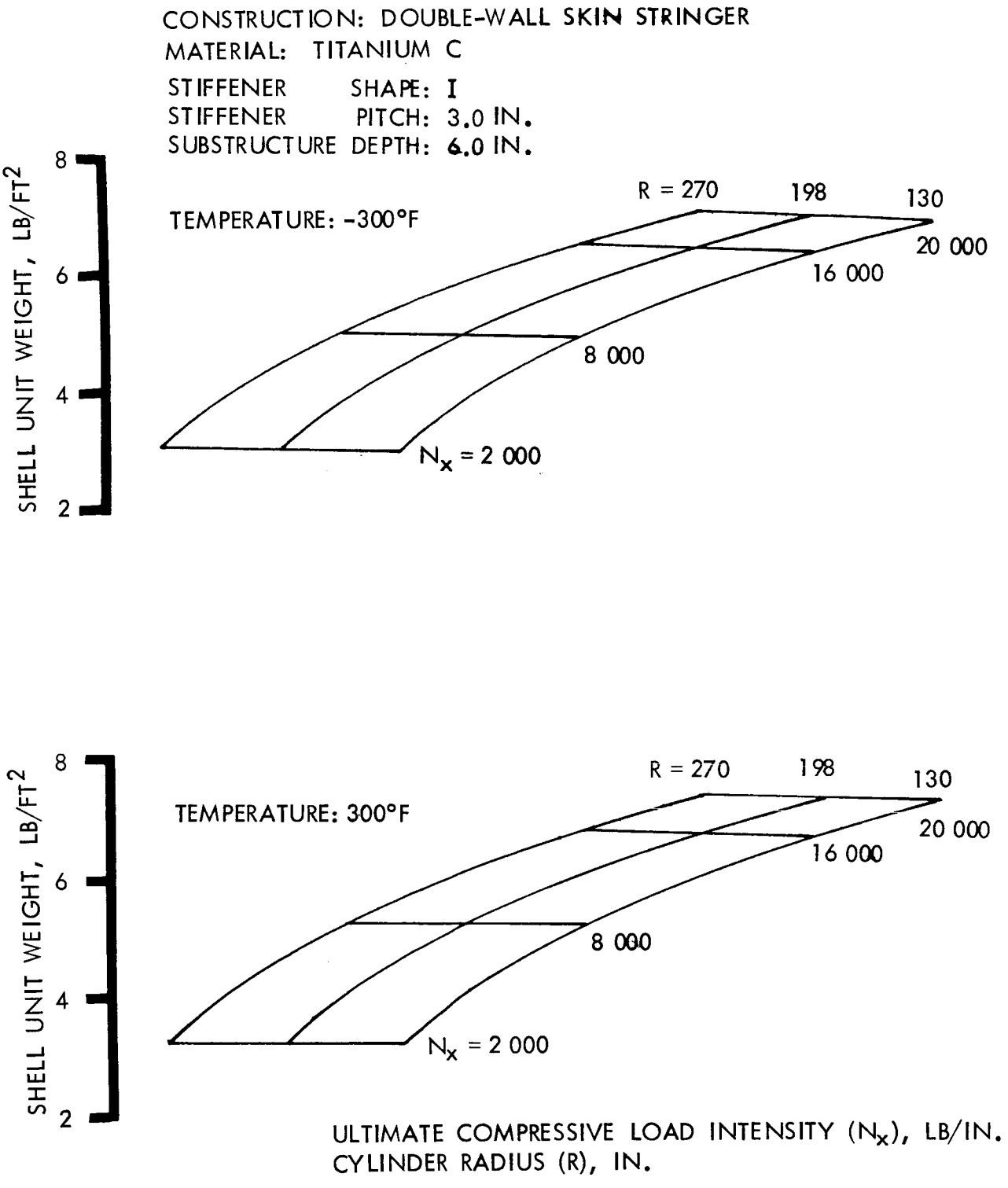

Figure 17. - Unit Shell Weight for I Section With Titanium C

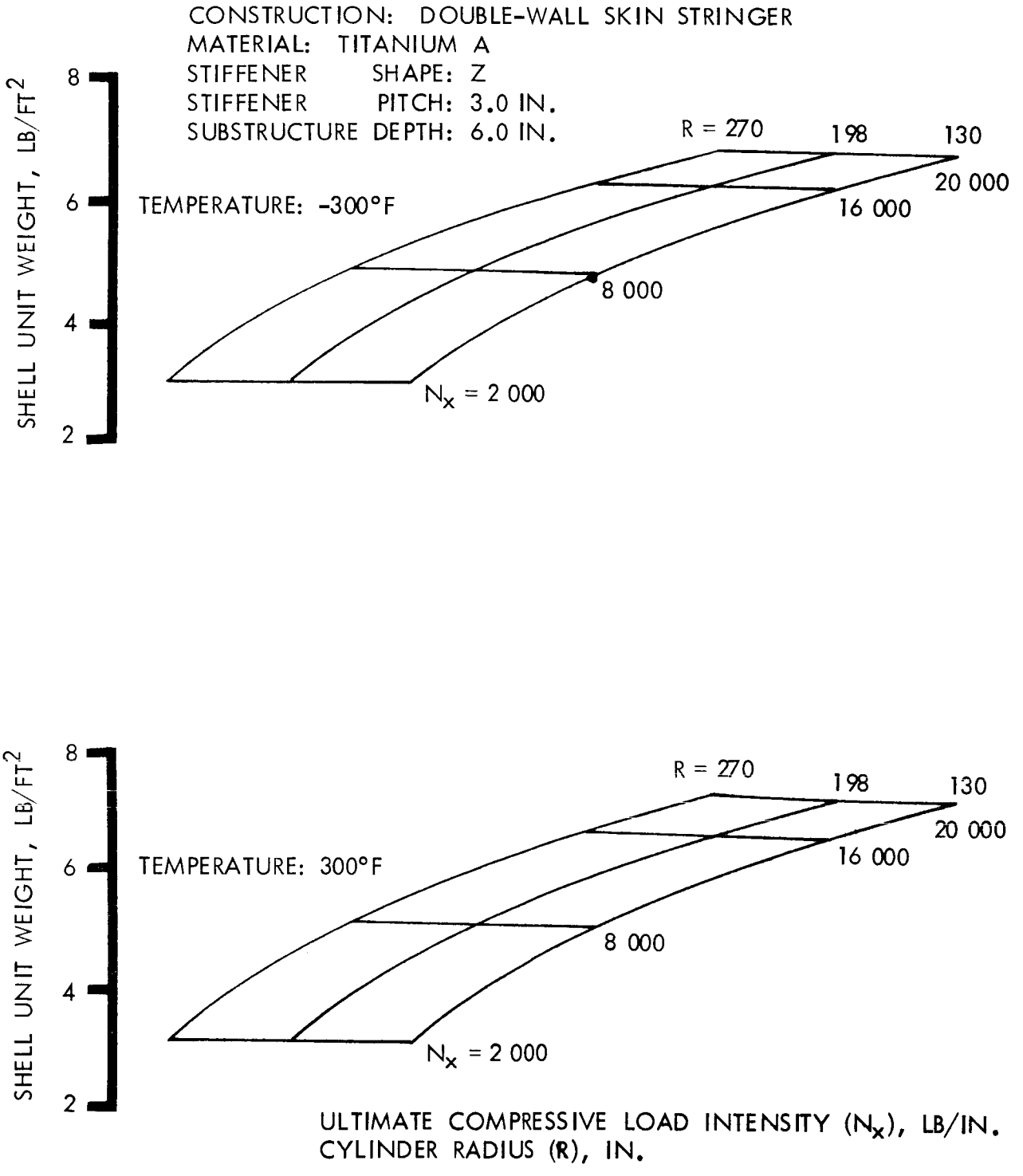

Figure 18. - Unit Shell Weight for Z Section With Titanium A

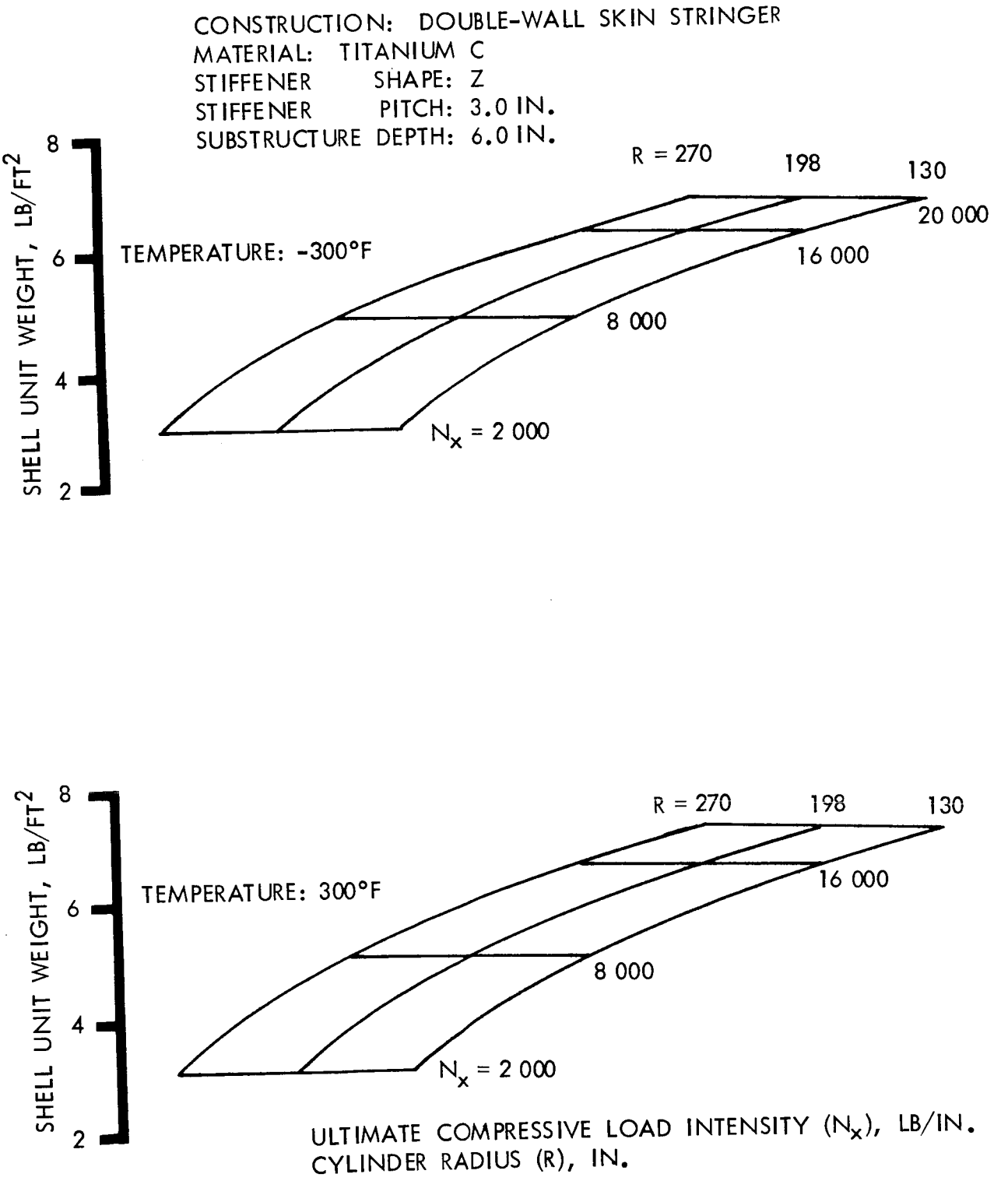

Figure 19. - Unit Shell Weight for Z Section With Titanium C

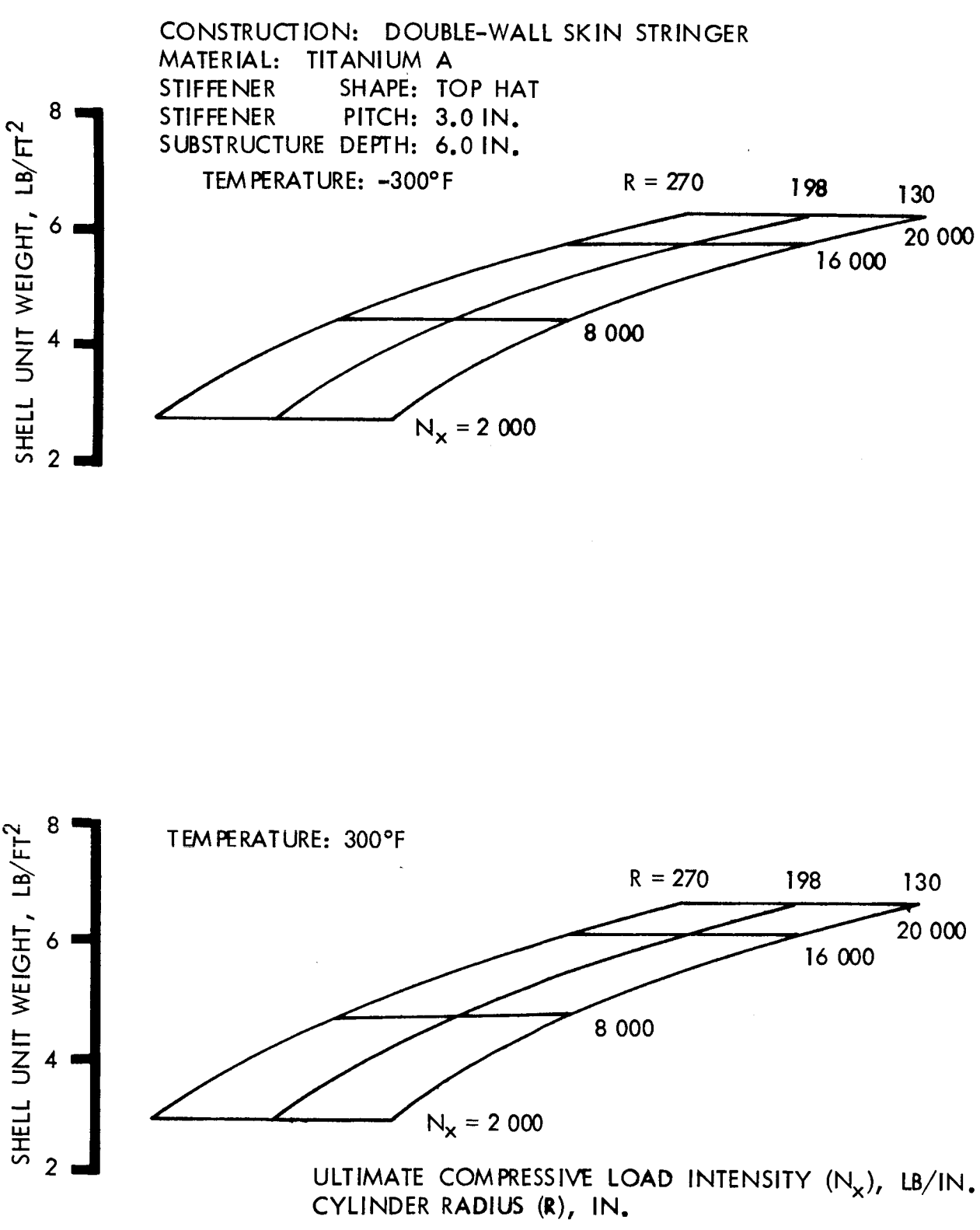

Figure 20. - Unit Shell Weight for Top-Hat Section With Titanium A

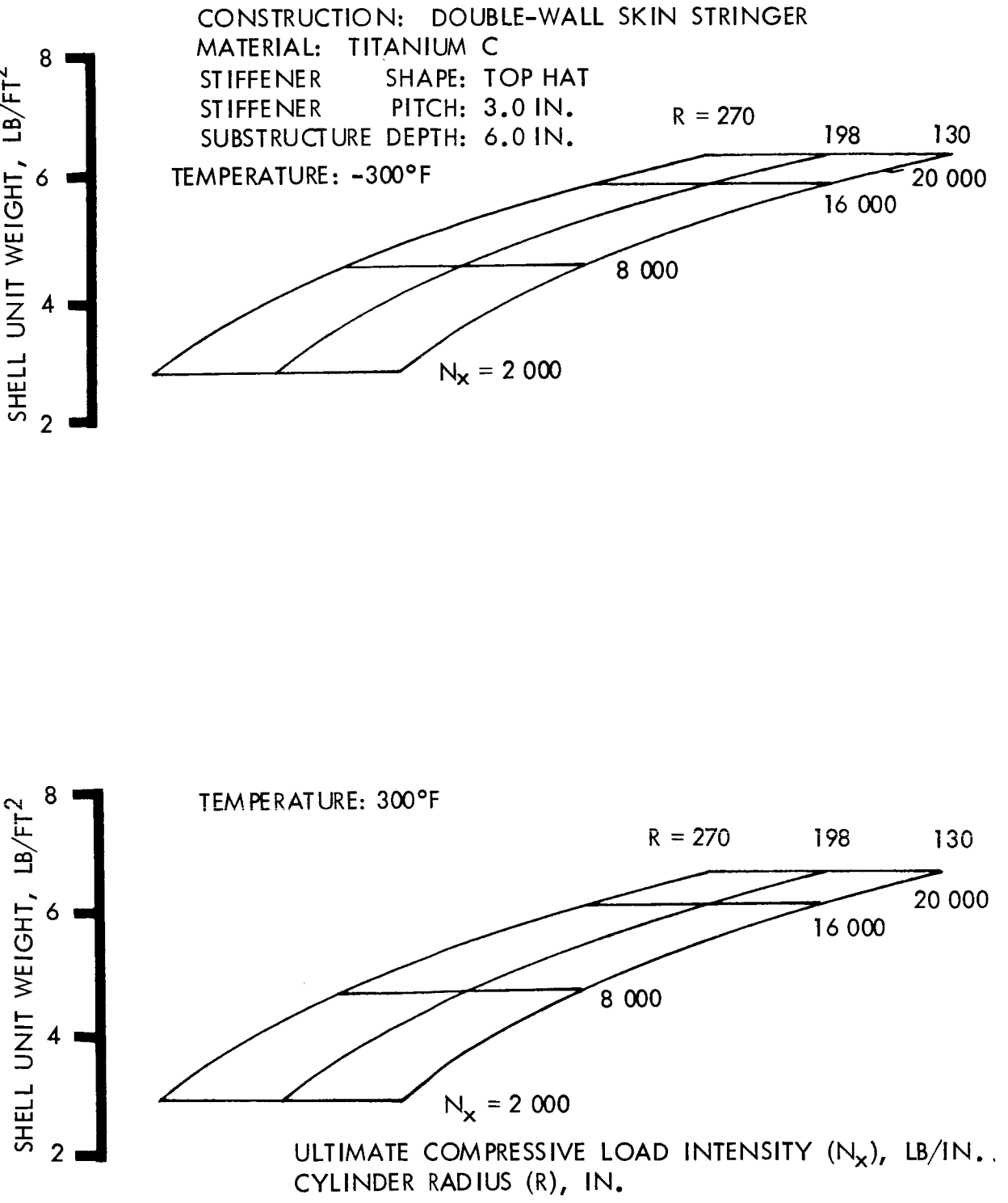

Figure 21. - Unit Shell Weight for Top-Hat Section With Titanium C

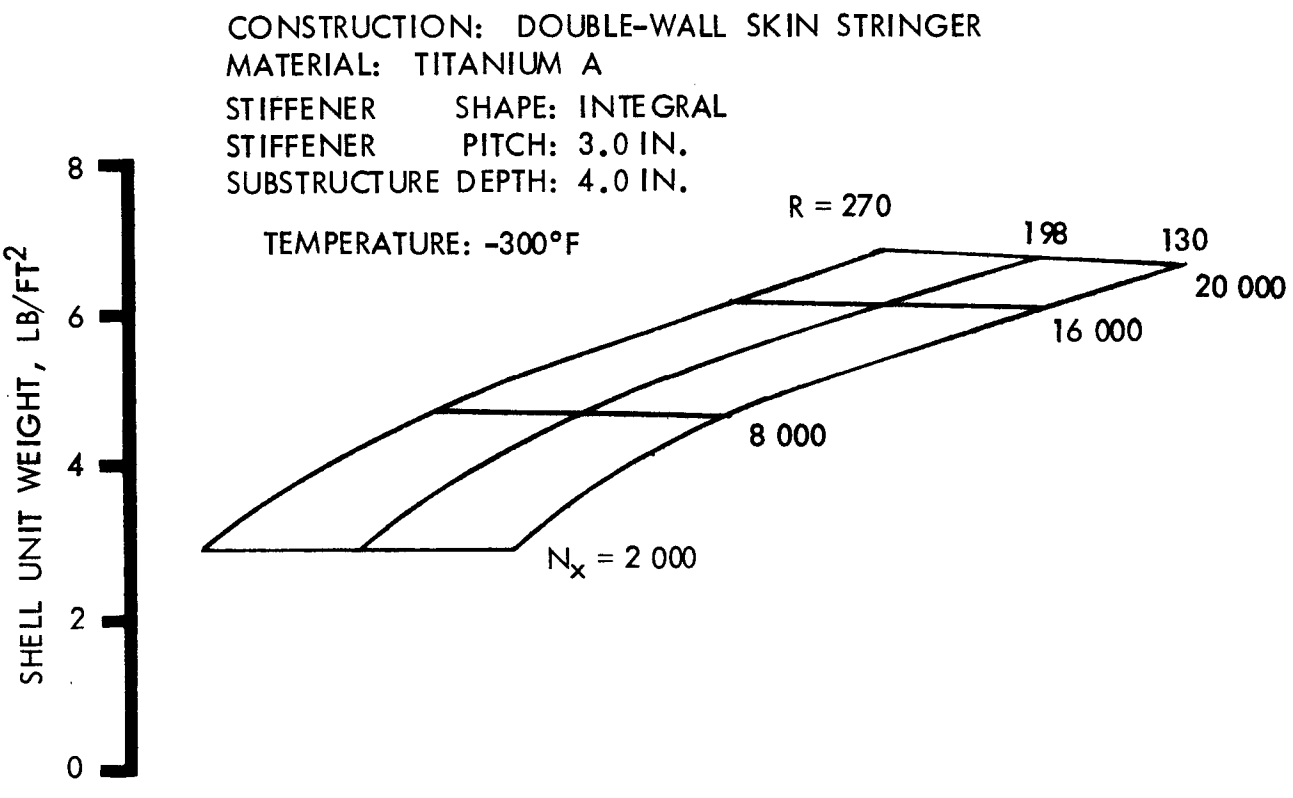

Figure 22. - Unit Shell Weight for Integral Section With Titanium A at 4-Inch Depth

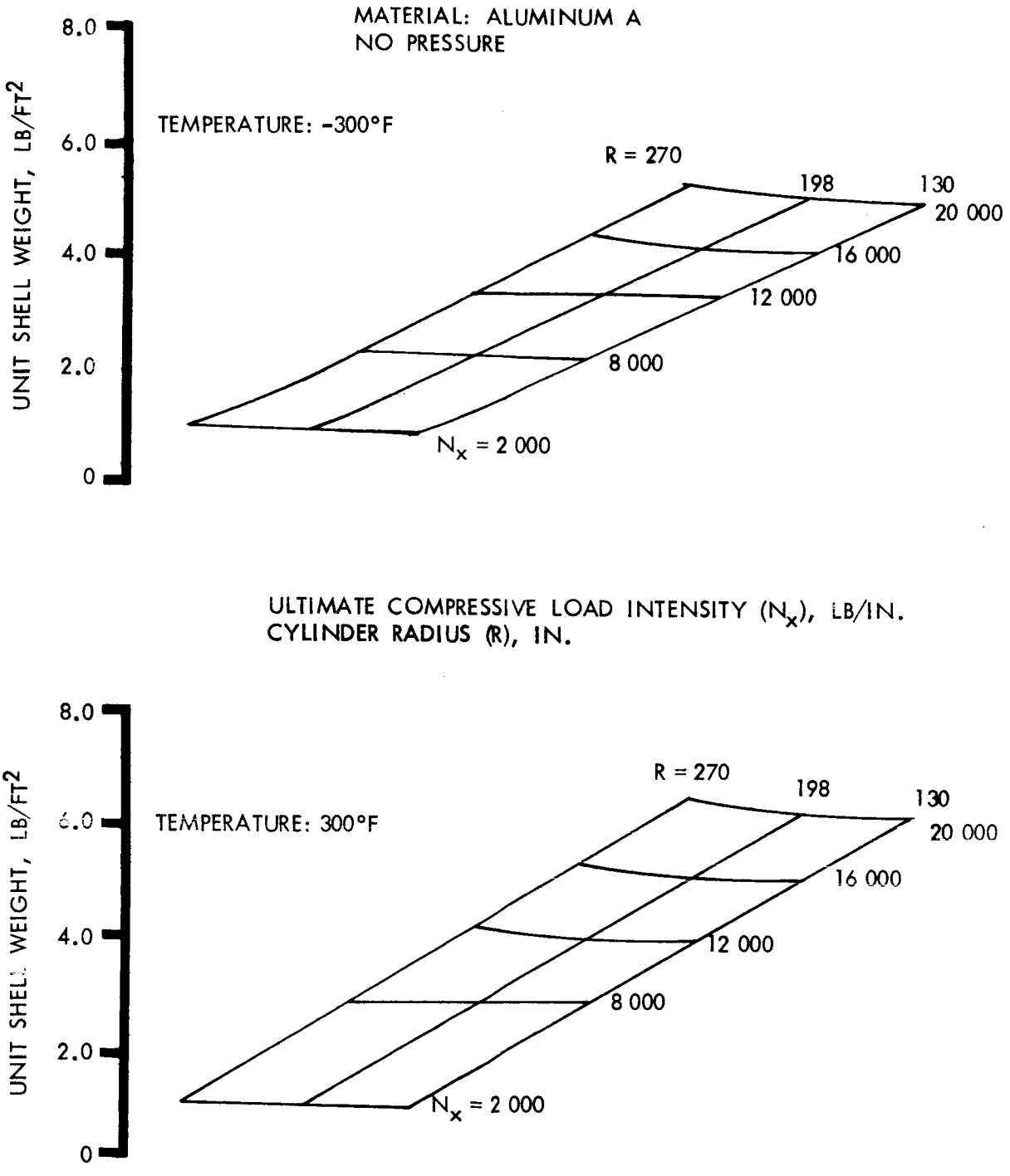

Figure 23. - Multiwall Corrugated Cylinder, Aluminum A

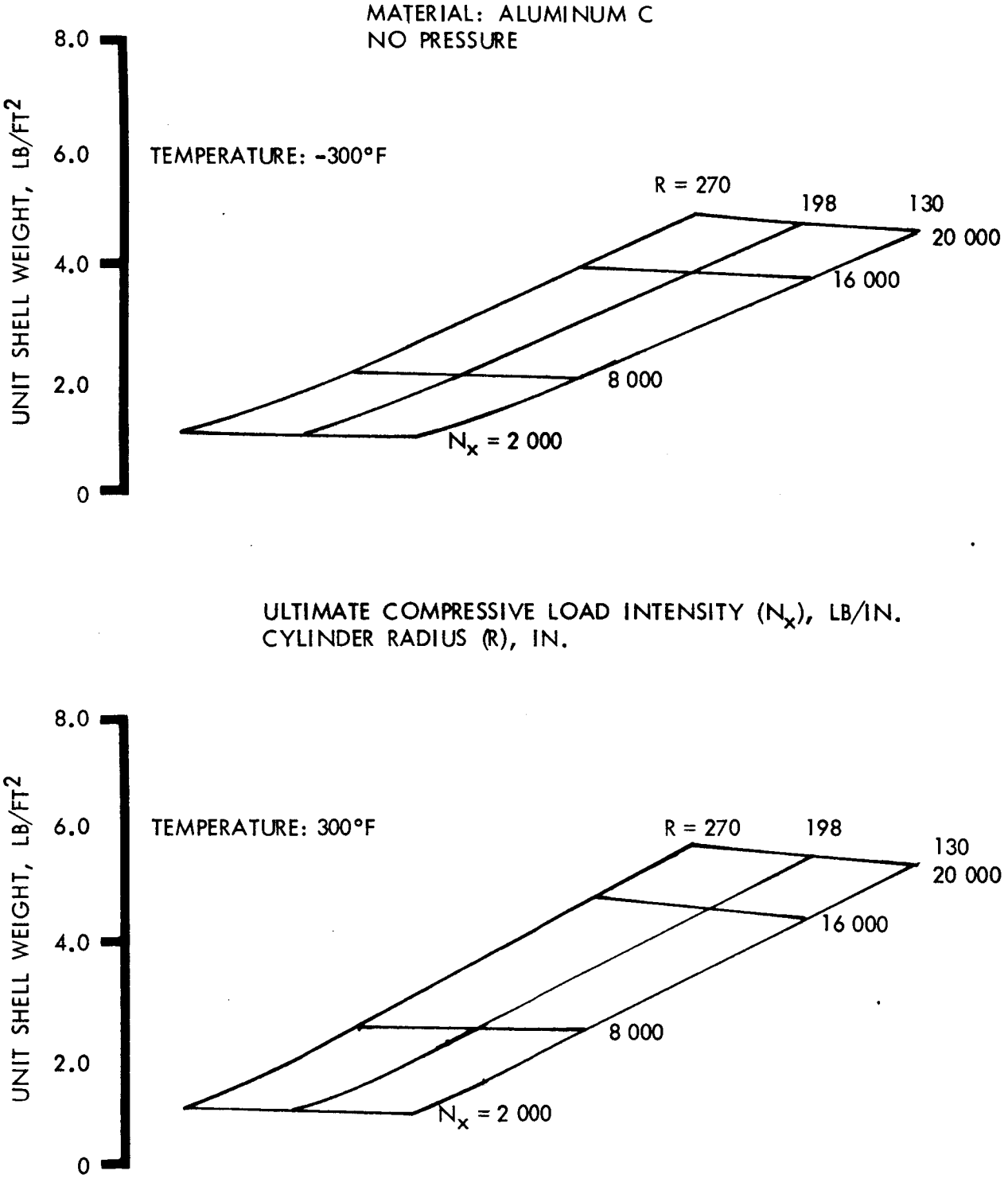

Figure 24.- Multiwall Corrugated Cylinder, Aluminum C

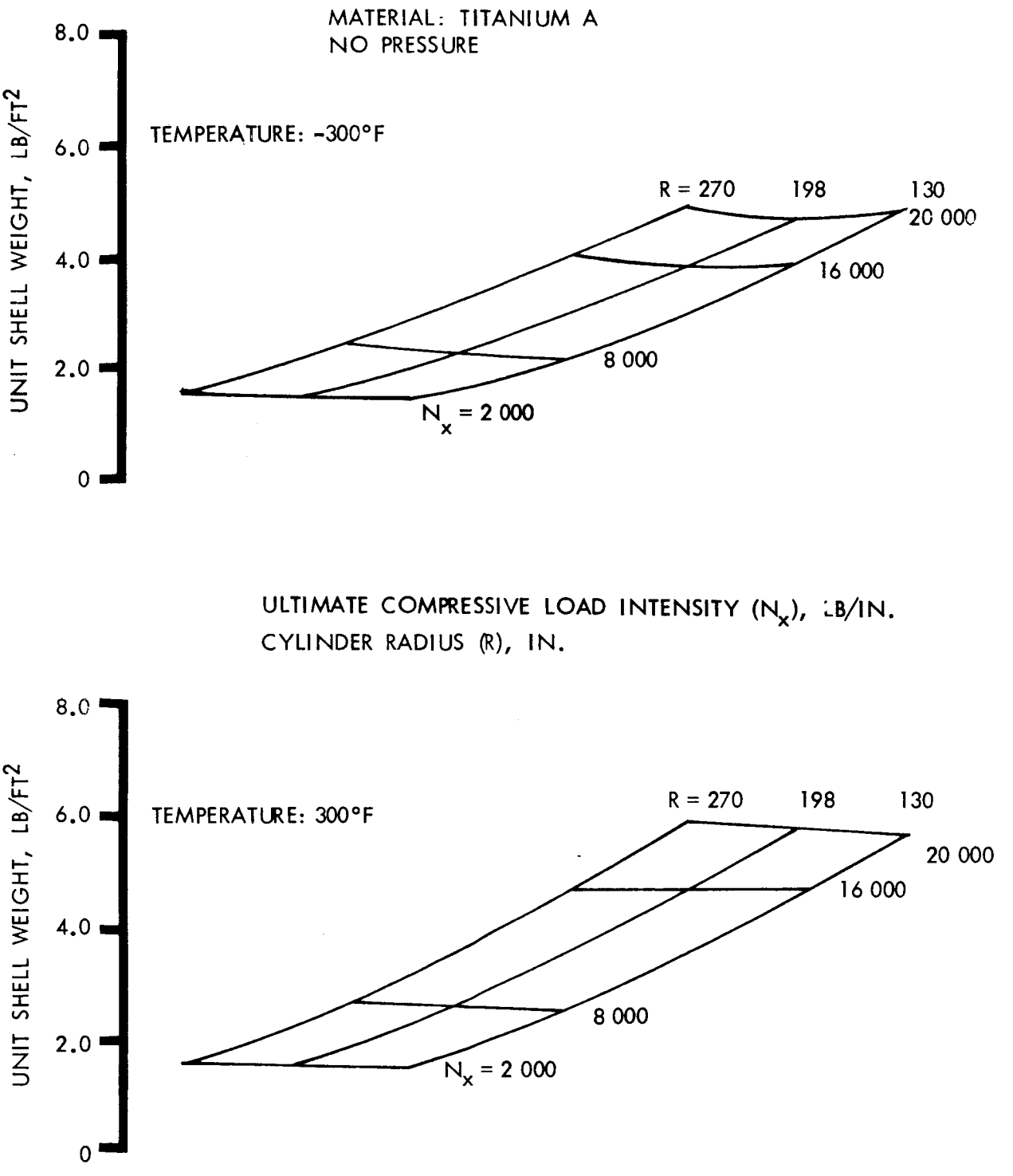

Figure 25.- Multiwall Corrugated Cylinder, Titanium A

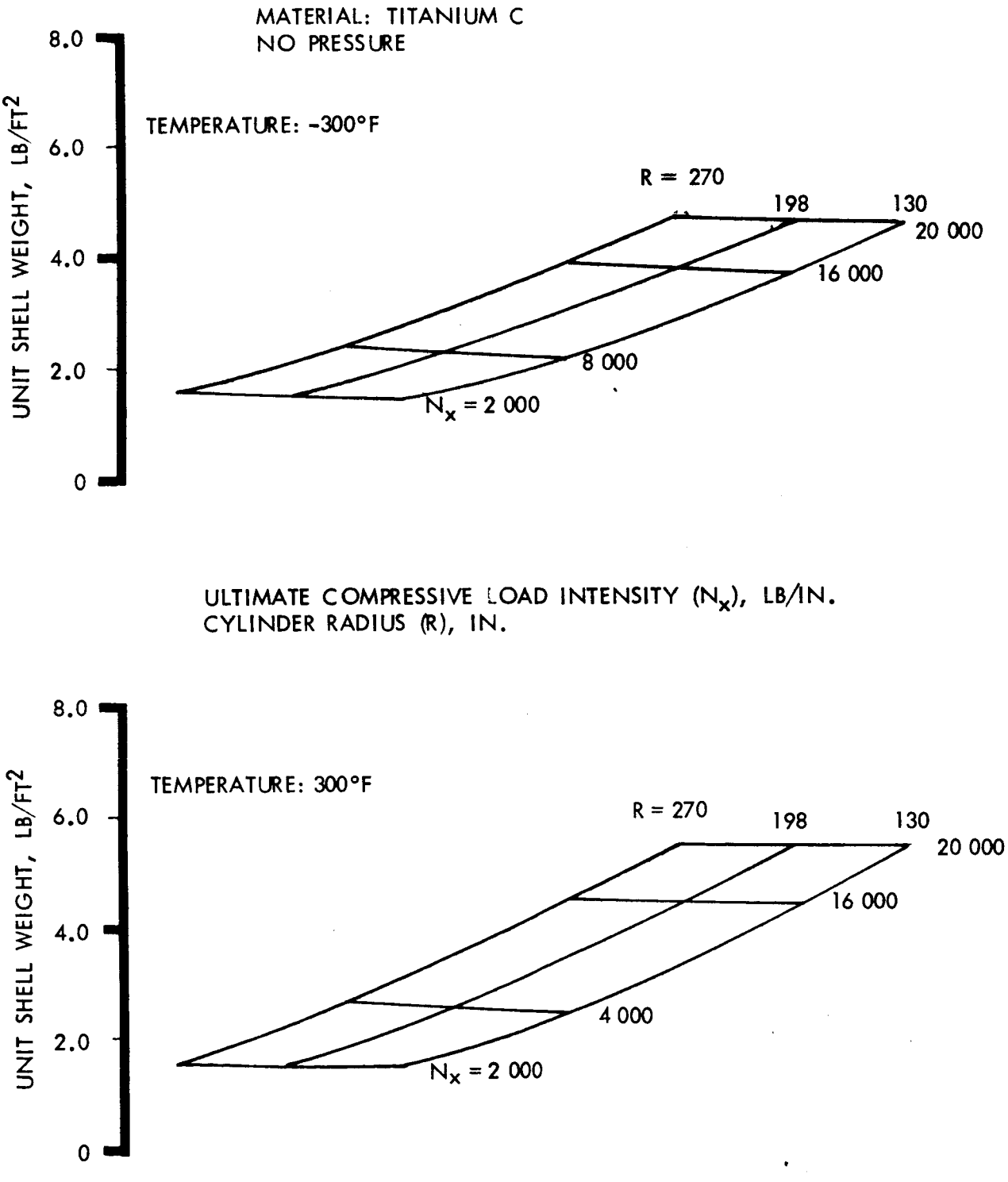

Figure 26. - Multiwall Corrugated Cylinder, Titanium C

elements and general instability of the overall cylinder is discussed in Appendix A. The unit weights shown in figures 23 through 26 are for the metallic elements only and do not include any allowances for bonding of skins and/or substructure or edge and close-out fittings.

Components associated with the medium-range payload class (130-in. radius), the Saturn class (198-in. radius), and the post-Saturn class (270-in. radius) vehicles were synthesized for compressive loading intensities ranging from 2 000 to 20 000 lb/in. The material properties used in the synthesis of aluminum (titanium) components ranged from a compressive yield strength of 50 000 psi (100 000 psi) with an ultimate tensile strength of 55 000 psi (115 000 psi), which typifies the properties associated with present aluminum alloys at 300°F, to a compressive yield stress of 60 000 psi (120 000 psi), and an ultimate tensile strength of 65 000 psi (125 000 psi). The latter properties are considered to represent those obtainable in the 1980 time period. Figure 23 illustrates the influence of the applied loading intensity and the component's radius on the resultant unit shell weight for the -300°F to +300°F temperature regime. This figure shows that the influence of component radius (130 in. to 270 in.) is negligible for loading intensities less than 12 000 lb/in. For a loading intensity of 20 000 lb/in, the 270-inch radius component's unit shell weight is approximately 8 percent greater than the unit shell weight of the 130-inch radius component.

In addition, figures 23 and 24 illustrate that at the high loading intensity (20 000 lb/in.), a 20 percent improvement in the material properties of aluminum results in a unit shell weight reduction at 8 to 13 percent in the ±300°F temperature regime. A ten percent improvement of the material properties of titanium, figures 25 and 26, results in a decrease in the unit shell weight of approximately 5 to 10 percent at the 20 000 lb/in. loading intensity. In general, the greatest reduction in weight for both aluminum and titanium is achieved when the temperature is +300°F.

It appears that this construction concept was slightly lighter in general than the double-wall skin stringer. But the weight differences are so small that the added complexities associated with fabrication of the facing panels and their attachment to the substructure would not warrant the use of this concept. This is discussed further in the section on cost assessment.

Longitudinally Corrugated Core Sandwich Cylinders

The influence of the compressive loading intensity and the component radius on the resultant unit shell weight for longitudinally corrugated core sandwich cylinders is presented in figure 27. This figure indicates that the

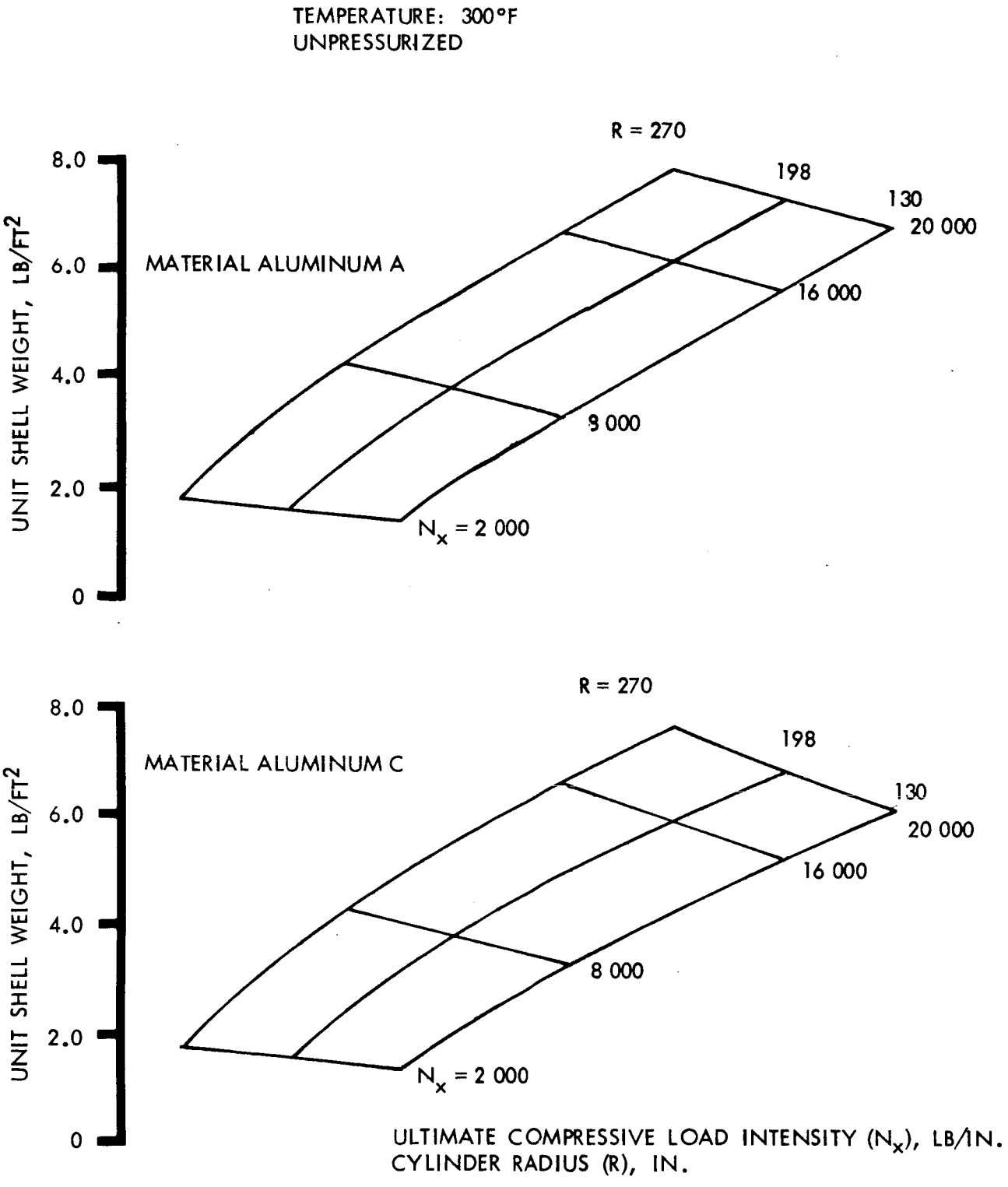

Figure 27. - Corrugated Sandwich - Material Improvement

unit shell weight is proportional to the radius of the components for components with a radius in the 130- to 270-inch range. It also shows that non-pressurized aluminum corrugated sandwich cylinders with compressive loading intensities of 12 000 lb/in. or less are relatively insensitive to improvements of 20 percent or less in the material's properties. In the 12 000 to 20 000 lb/in. loading range, the unit shell weight of the 130-inch radius component may be reduced 4 to 10 percent by improving the material properties by 20 percent. The larger weight reductions occur at the higher loading intensities. If the compressive loading intensity is greater than 16 000 lb/in., a 20-percent improvement of material properties will result in the unit shell weight, decreasing 3 to 6 percent for the 198-inch radius components. The 270-inch radius aluminum corrugated core sandwich cylinder is insensitive to improvements in material properties of 20 percent or less.

A 20-percent improvement in the pressurized aluminum material properties for longitudinally corrugated core sandwich cylinders results in a unit shell weight decrease of approximately 10 percent at the small loading intensities (N_x = 4000 lb/in.). This potential weight reduction is inversely proportional to the compressive loading intensity and decreases rapidly with increasing loading intensity. At a compressive loading intensity of 10 000 lb/in., the potential weight reduction is approximately one percent.

The unit shell weight of titanium components is rather insensitive to material property improvements of 10 percent or less. This is because the component stress levels are considerably less than the compressive yield strength of the material. For pressurized titanium longitudinally corrugated sandwich cylinders with a compressive loading intensity of less than 8000 lb/in., a small weight reduction (3.5 percent) is obtainable by improving the material allowables by 10 percent.

Ring-Stiffened Cylindrical Shells

An interest has been expressed in the design of inexpensive and easily fabricated shells for booster systems, either to solve the economic or development scheduling problems. The simplest concept would be a monocoque concept of rolled and single curvature skins welded together for the booster tanks and unpressurized shells. An obvious refinement to this grossly over-weight concept would be to attach simple ring frames to assist in stabilizing the skins. These rings allow the shell to be considered as a short column between rings of a monocoque construction. For this condition, involving the forcing of buckling modes between rings, the rings are designed

by Shanley's equation. If the rings participate in the buckling mode, the resulting design is lighter. The analysis and synthesis approach for this design concept is explained in Appendix A.

The influence of ring-frames spacing on the unit shell weight of ring-stiffened cylindrical shells subjected to compressive loading intensities in the 2000 lb/in. to 20 000 lb/in. range is illustrated in figure 28. This figure shows that for unpressurized 130-inch radius components, the unit shell weight of monocoque cylindrical shells can be reduced 25 to 35 percent by adding ring frames with 16-inch spacing. This weight reduction is achievable in aluminum (fig. 28) and titanium (fig. 29) specimens for the entire loading spectrum. When compared with integral skin stringer construction, however, the unit shell weight of the 16-inch ring spacing ring-stiffened cylinder is approximately 40-percent greater. Improving the material properties of aluminum or titanium does not influence the unit shell weights because the components stress levels are a small percentage of the material proportional limit for the entire range.

The unit shell weight of the pressurized (tank pressure, 50 psi), 130-inch radius monocoque cylindrical shell (figs. 30 and 31) can be reduced 20 to 34 percent by adding ring frame at 16.0-inch intervals. Smaller weight reductions are obtainable at the low loading intensities (~2000 lb/in.). As the loading intensity increases, the potential weight reduction increases until a maximum of 34 percent is obtainable at 20 000 lb/in. compressive loading intensity. This weight reduction is achievable for both titanium (fig. 31) and aluminum (fig. 30) cylinders. Improving the material properties of aluminum or titanium does not affect the unit shell weight.

The influence of ring-frame spacing on the unit shell weight of 198 radius ring-stiffened cylindrical shells followed the general trend observed for 130-inch spacing. That is, 25.0-inch ring frame spacing reduced the unit shell weight of an unpressurized cylinder from 25 to 35 percent (figs. 32 and 33), and of pressurized cylinders from 20 to 30 percent (figs. 34 and 35). These potential weight reductions are proportional to the magnitude of the compressive loading intensity, the smallest weight reduction occurring when the compressive loading intensity is approximately 2000 lb/in. The material property improvements did not reduce the unit shell weight because the component stress levels are considerably less than the proportional limit of the base-line materials.

The weight penalties for a Saturn-class vehicle are discussed in the cost assessment section.

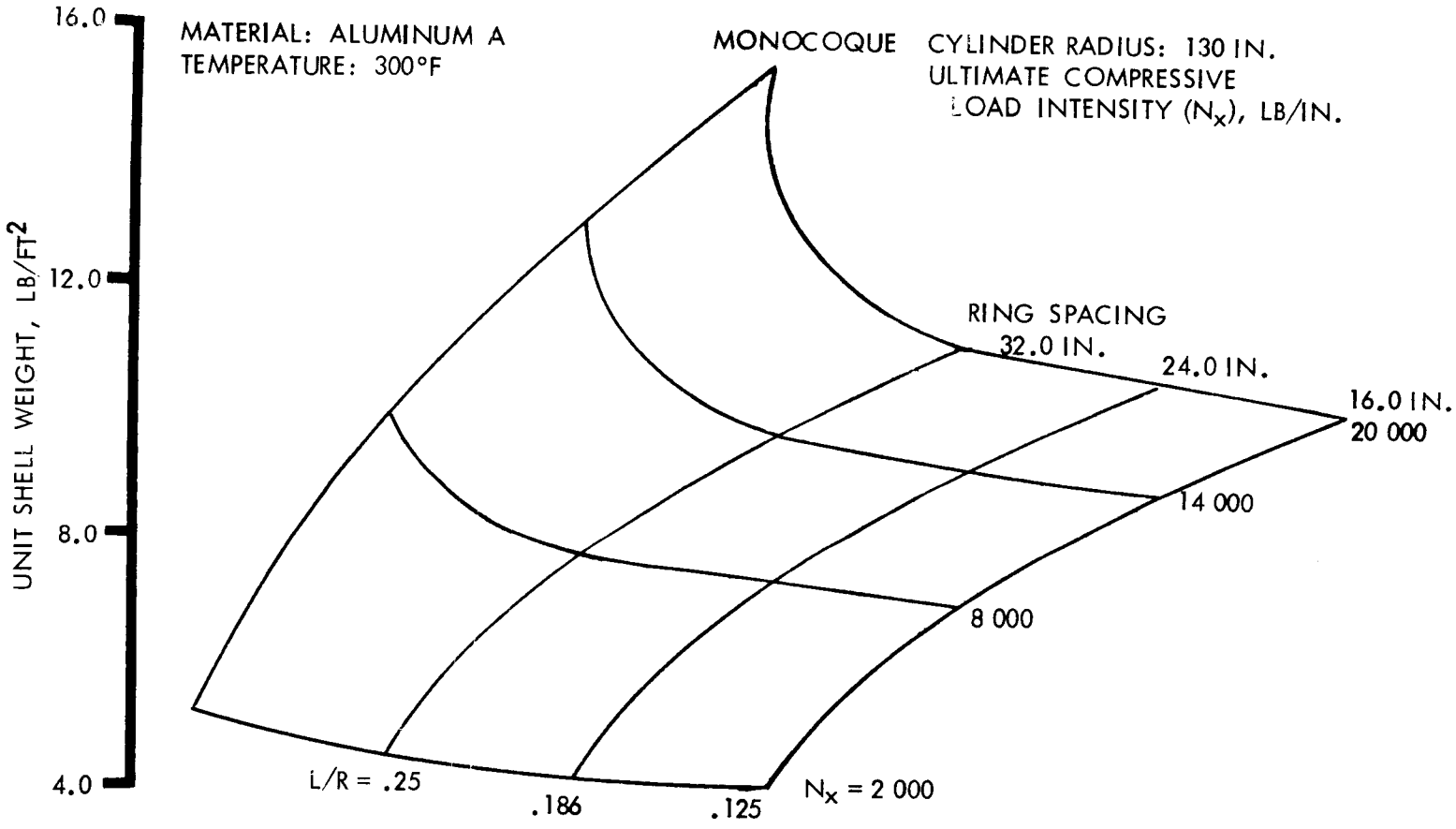

Figure 28. - Ring-Stiffened Unpressurized Cylinder, Aluminum A, Cylinder Radius 130 Inches

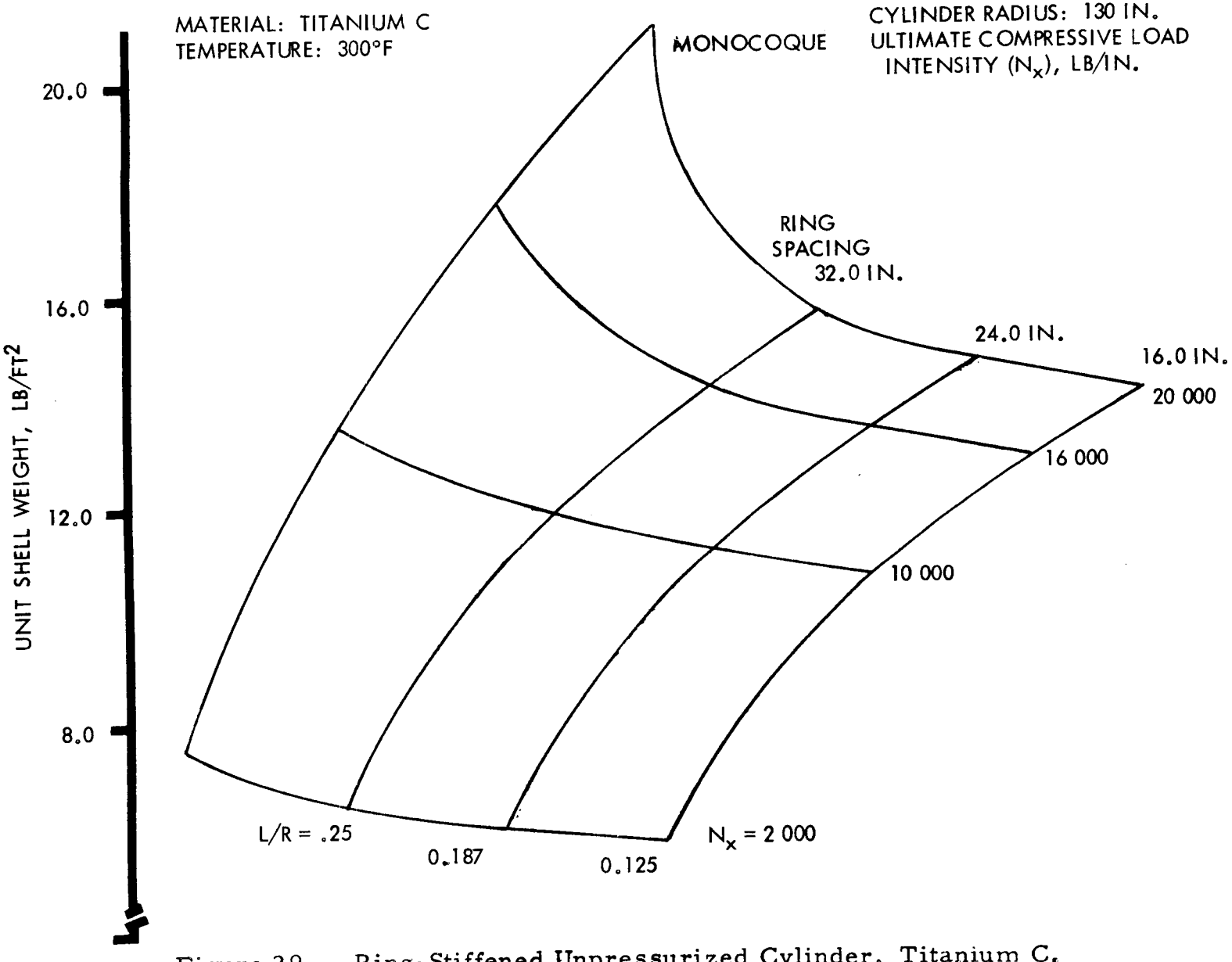

Figure 29. - Ring-Stiffened Unpressurized Cylinder, Titanium C, Cylinder Radius 130 Inches

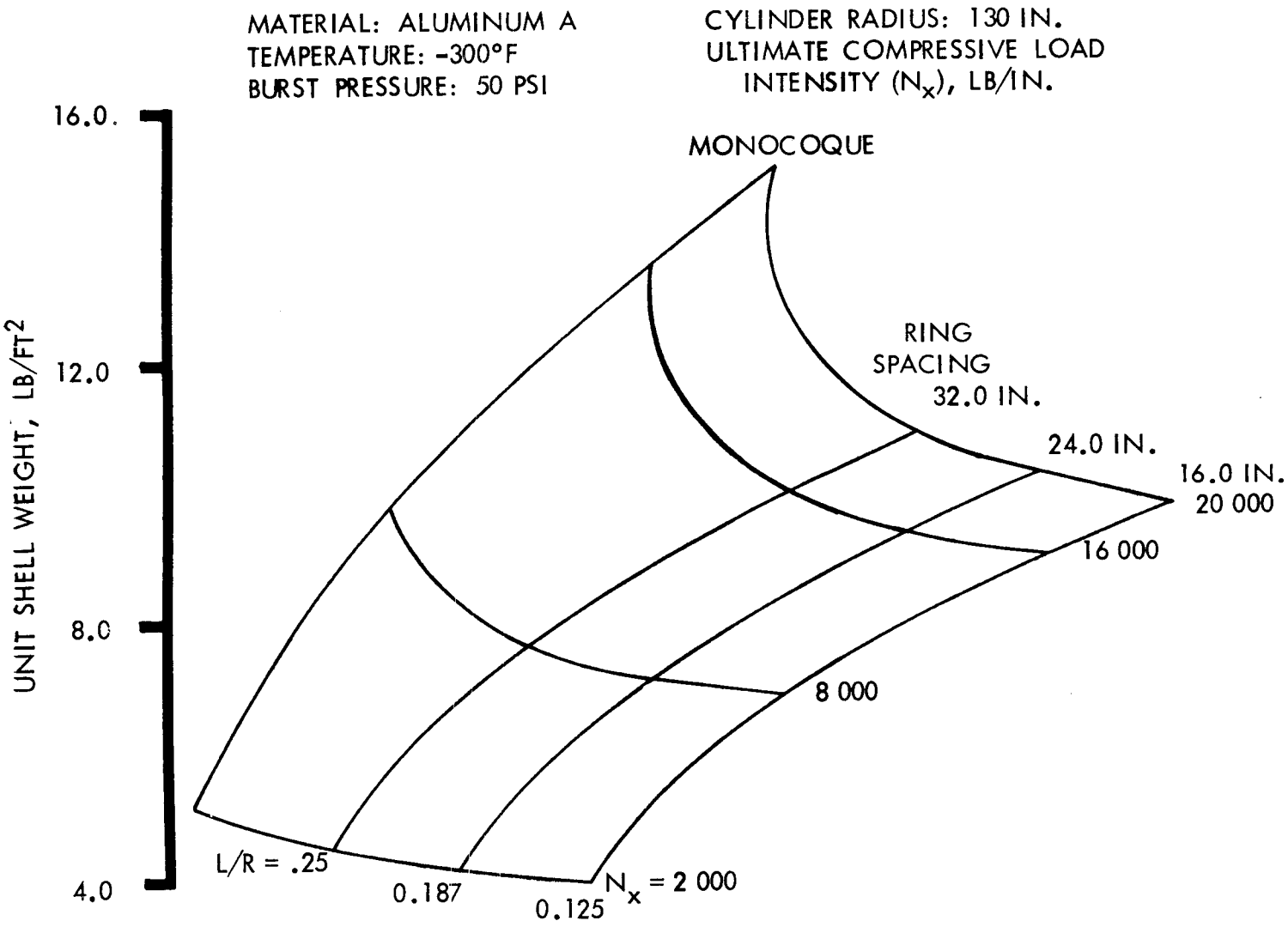

Figure 30. - Ring-Stiffened Pressurized Cylinder, Aluminum A, Cylinder Radius 130 Inches

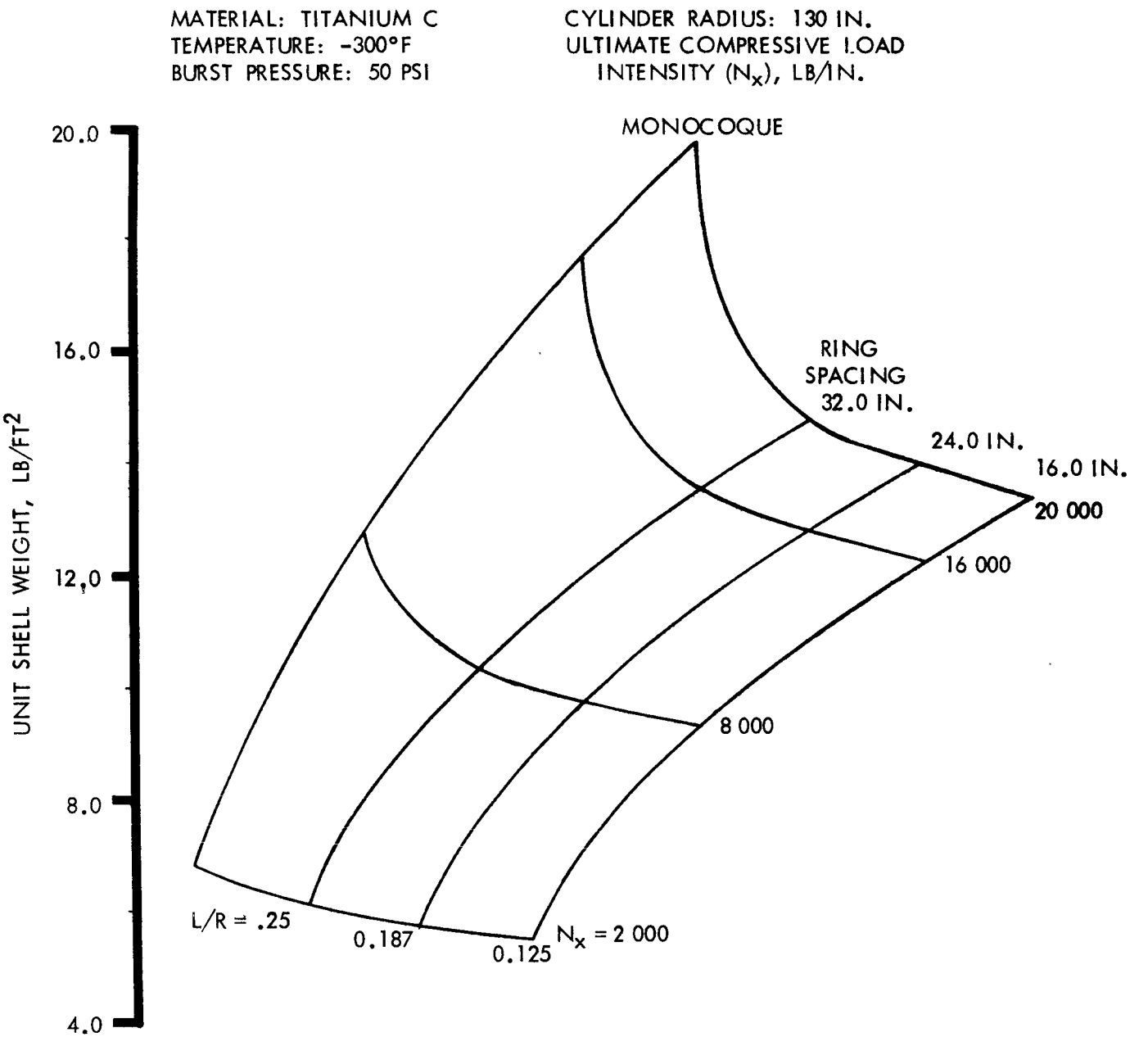

Figure 31. - Ring-Stiffened Pressurized Cylinder, Titianium C, Cylinder Radius 130 Inches

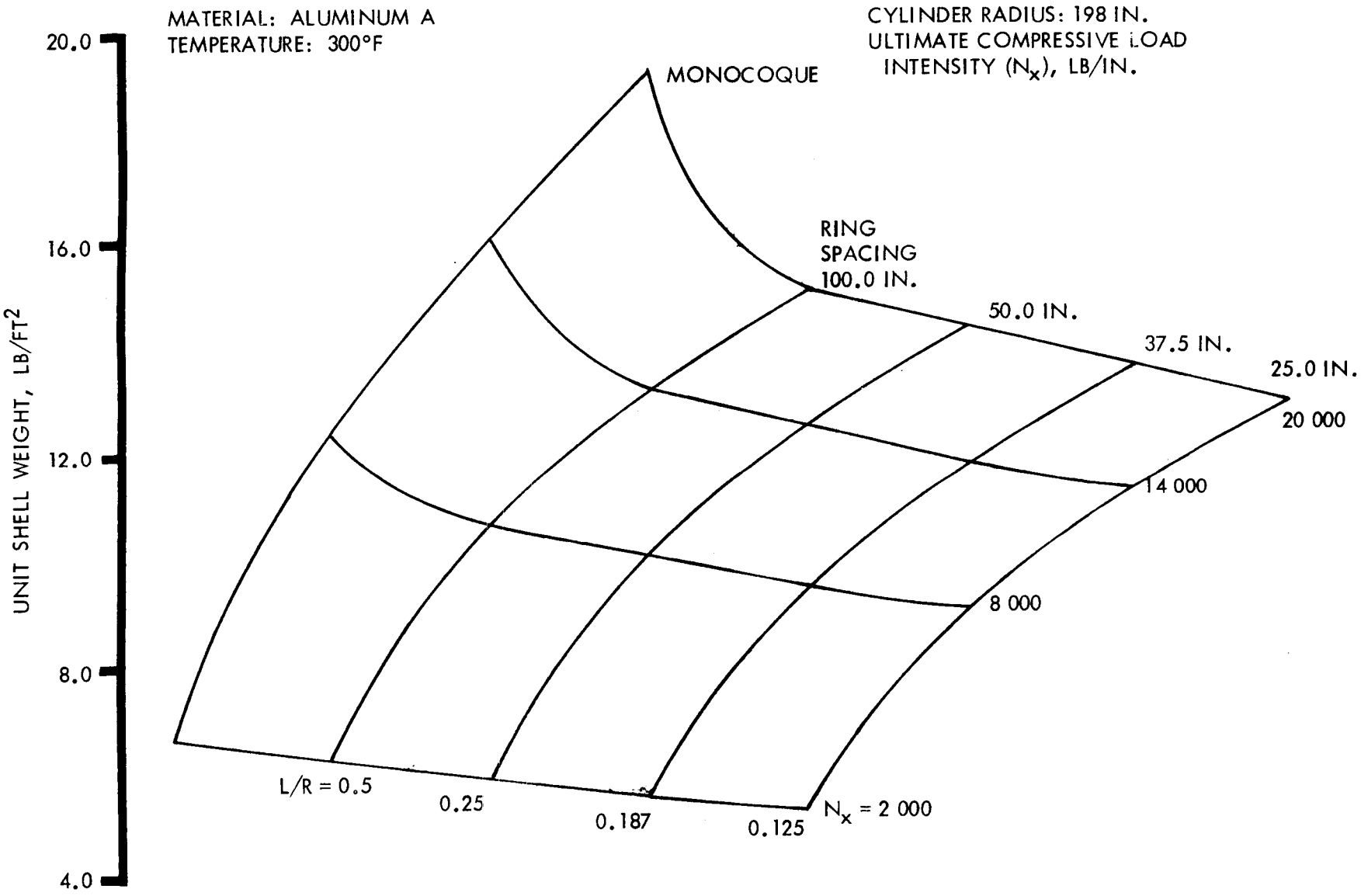

Figure 32. - Ring-Stiffened Unpressurized Cylinder, Aluminum A, Cylinder Radius 198 Inches

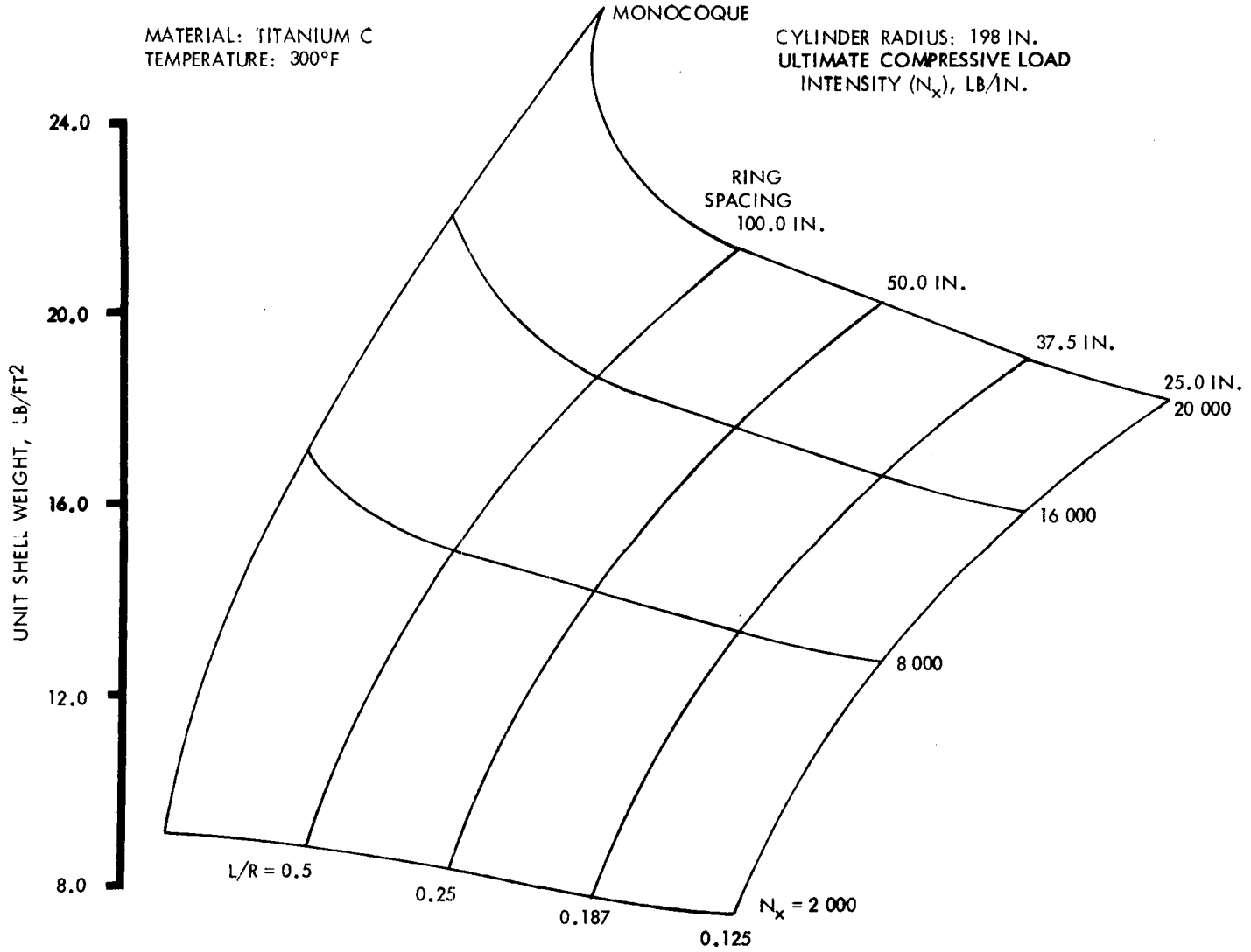

Figure 33. - Ring-Stiffened Unpressurized Cylinder, Titanium C, Cylinder Radius 198 Inches

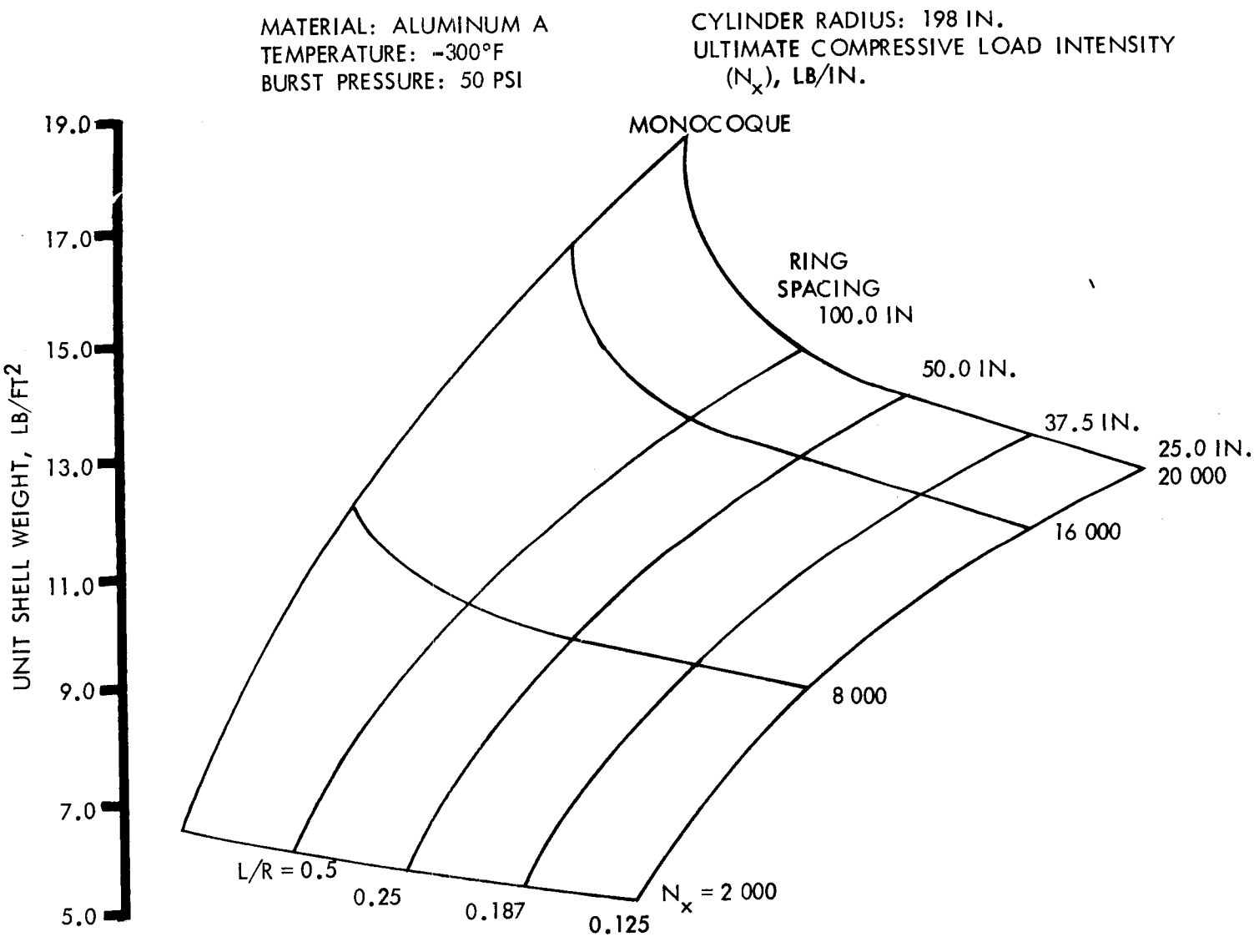

Figure 34. - Ring-Stiffened Pressurized Cylinder, Aluminum A, Cylinder Radius 198 Inches

MATERIAL: TITANIUM C
TEMPERATURE: -300°F
BURST PRESSURE: 50 PSI

CYLINDER RADIUS: 198 IN.
ULTIMATE COMPRESSIVE LOAD INTENSITY (N_x), LB/IN.

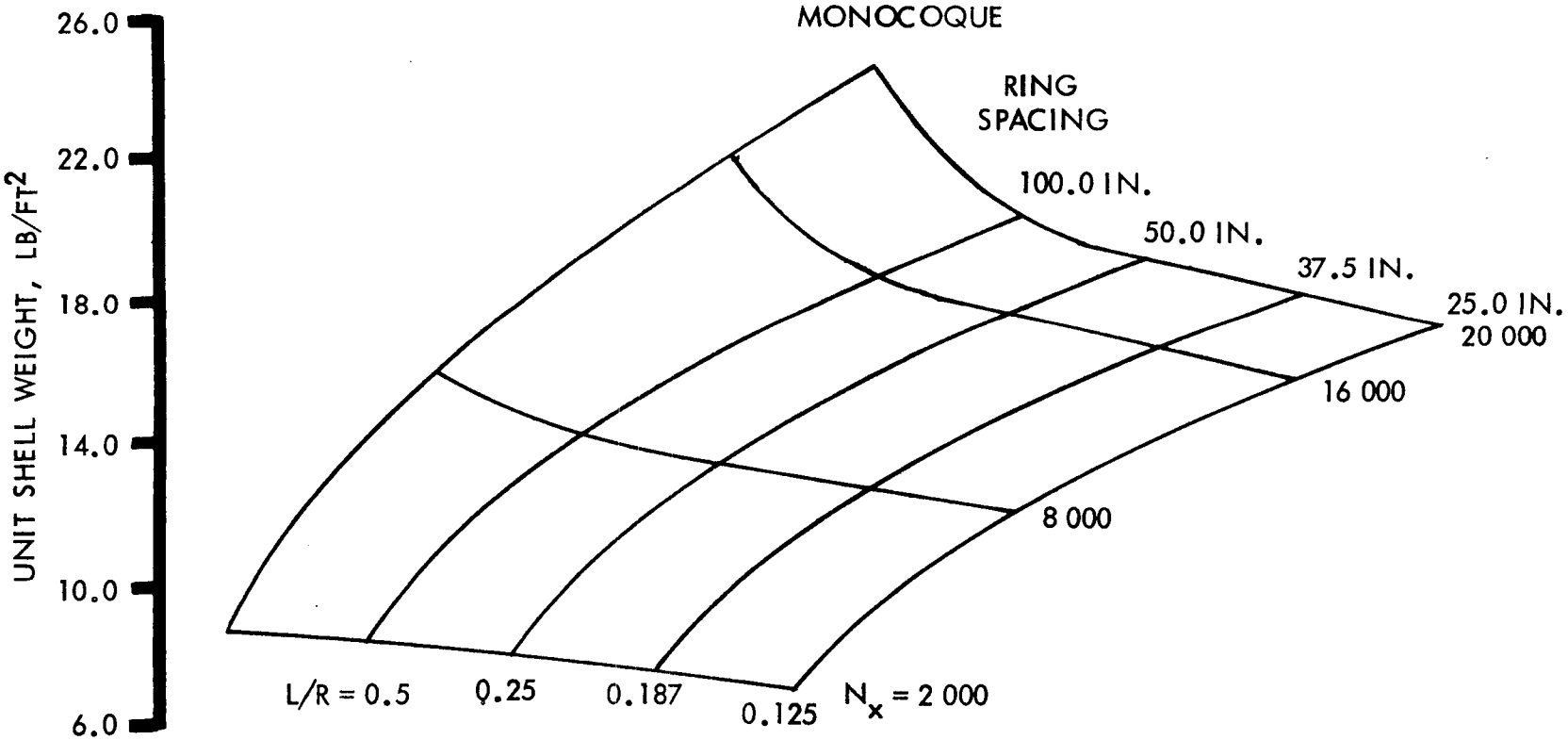

Figure 35. - Ring-Stiffened Pressurized Cylinder, Titanium C, Cylinder Radius 198 Inches

Buckling of Eccentrically Stiffened Cylinders

The importance of the eccentricity or one-sidedness of the cylindrical shell's stiffening elements in determining the allowable buckling strength has been discussed in several analytical studies (refs. 7 through 14). These studies have tended to indicate the distinct improvement in a cylinder's buckling strength when the stiffeners are placed externally. Reference 8 indicates that the eccentricity effects are large even with very large diameter cylinders of "practical proportion" and therefore should be accounted for in any buckling analysis.

Results from an experimental and theoretical study (ref. 11) of the effect of stiffener eccentricity (one-sidedness) on buckling have been reported. In the experimental investigation, axial-compression tests were conducted on twelve longitudinally stiffened cylinders which represent six configurations with internal or external, integral or Z-stiffeners. For certain configurations, externally stiffened cylinders were found to carry over twice the load sustained by their internally stiffened counterparts. The experimental results for axially loaded cylinders range from 70 to 95 percent of the corresponding theoretical predictions. Furthermore, the comparison in reference 11 of results for clamped and simply supported cylinders with the test data revealed that edge clamping has a significant effect.

Figure 36 (reproduced from ref. 11) shows the correlation between theory and a series of experimental test data. These comparisons were made with test specimens for small-radius cylinders (9.55 and 15.92 inches) fabricated under ideal conditions. The tests were carefully controlled, and boundary conditions were explicitly defined. How well theory will compare with test data for a large cylinder with a practical light-weight design is a matter of conjecture. Most of the theoretical weight comparisons have been made either with a small radius cylinder or with a poorly proportioned one; i.e., the design is not efficient in regard to weight. Reference 12 states that test values compared 70 to 95 percent of the classical values from reference 11 test data since each cylinder test was associated with large values of "Z" where the post-buckling coefficient is most negative and out of the range in which an outside stiffened cylinder should be more imperfection-sensitive than one with inside stiffening. Reference 12 indicates there are ranges of outside stiffened cylinders which are critically imperfection-sensitive and little test data, if any, is available for correlation.

Figure 36 indicates the buckling mode patterns associated with the respective inside or outside stiffened cylinders tested in reference 11. Reference 13 evaluated the buckling modes by an approach suggested by

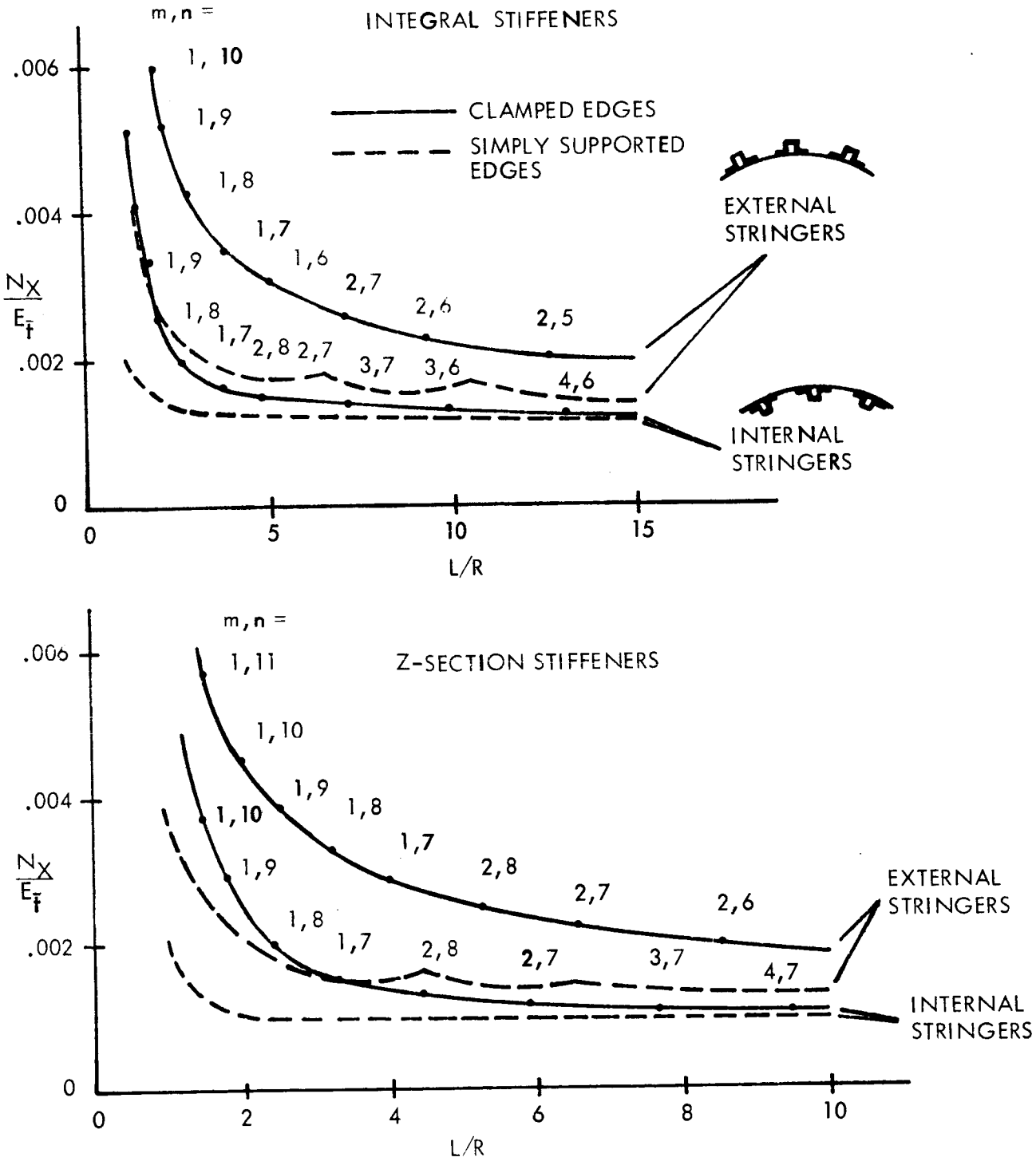

Figure 36. - Buckling of Axially Compressed Cylinders

Becker and does not reflect any mode changes whether stiffeners are inside or outside. Figure 36 clearly showed that the mode pattern can be displaced by at least one buckle in each direction. The synthesis program that was developed for this study was based upon reference 8 analysis and searched for the minimum buckling mode. This approach is described in detail in Appendix A.

The approach adapted for this study was not to optimize a given skin-stringer arrangement using an analysis of an isotopic cylinder and its eccentricity effects, but instead, the section was optimized by the synthesis methods employed during Phase I of the study. The optimized design was then analyzed to determine the relative merits of the positioning of the stiffeners. Since the shells make up the outer surface of the boost vehicle it was considered undesirable to place the circumferential rings outside the shell due to their pronounced effect on vehicle drag. Outside longitudinal stiffeners would not greatly effect drag performance, and therefore these results only deal with the positioning of the stringers, while the rings are always considered inside.

Many designs, practical and fairly light in weight, with an extensive range of loading intensities, component size, and material were considered. Figures 37 through 39 show effectiveness ratio results for designs using aluminum, titanium and beryllium. The stringer shapes for these three figures were an integral section and their pitch varied from 5 to 13 inches. It can be seen that for the designs considered there was a fair scattering of results; sometimes it was preferable to position the stiffeners inside in figure 37 (aluminum) and in figure 38 (titanium).

The positioning effect decreases as the shell radius increases; i. e., the individual elements are approaching a flat sheet which does not discriminate between inside and outside. With the aluminum and titanium designs investigated the best improvement in load-carrying capability was found to be at most 20 percent for the lightly loaded regions. As the load intensity increases, up to the 20 000 lb/in. limit this one-sidedness effect decreases. With beryllium designs there appears to be a significant effectiveness of the outside stringers for the high-loading intensity range; up to 80 percent at the 130-inch radius and 30 percent at the 270-inch radius.

The previous results were concerned with integrally stiffened designs. Figures 40 and 41 demonstrate the effect of stiffening with Z and top hat section stringers for aluminum and beryllium for a series of loading intensities: 2 000, 5 000 and 10 000 lb/in. at three different pitches. It appeared that the top hat section stiffener was able to take more advantage of an outside eccentricity to increase the load-carrying capability.

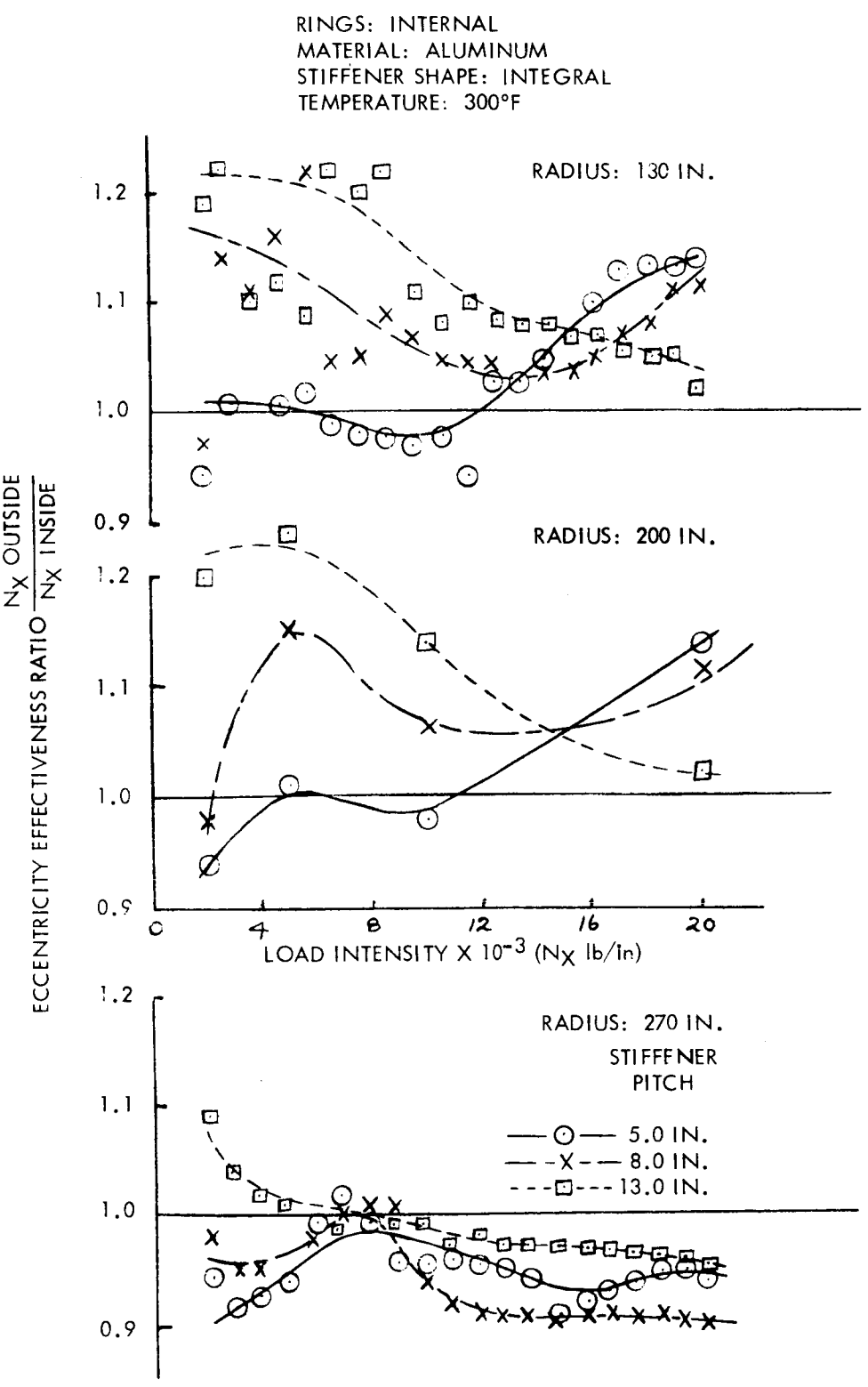

Figure 37. - Relative Merit of Externally Stiffened Aluminum Shells

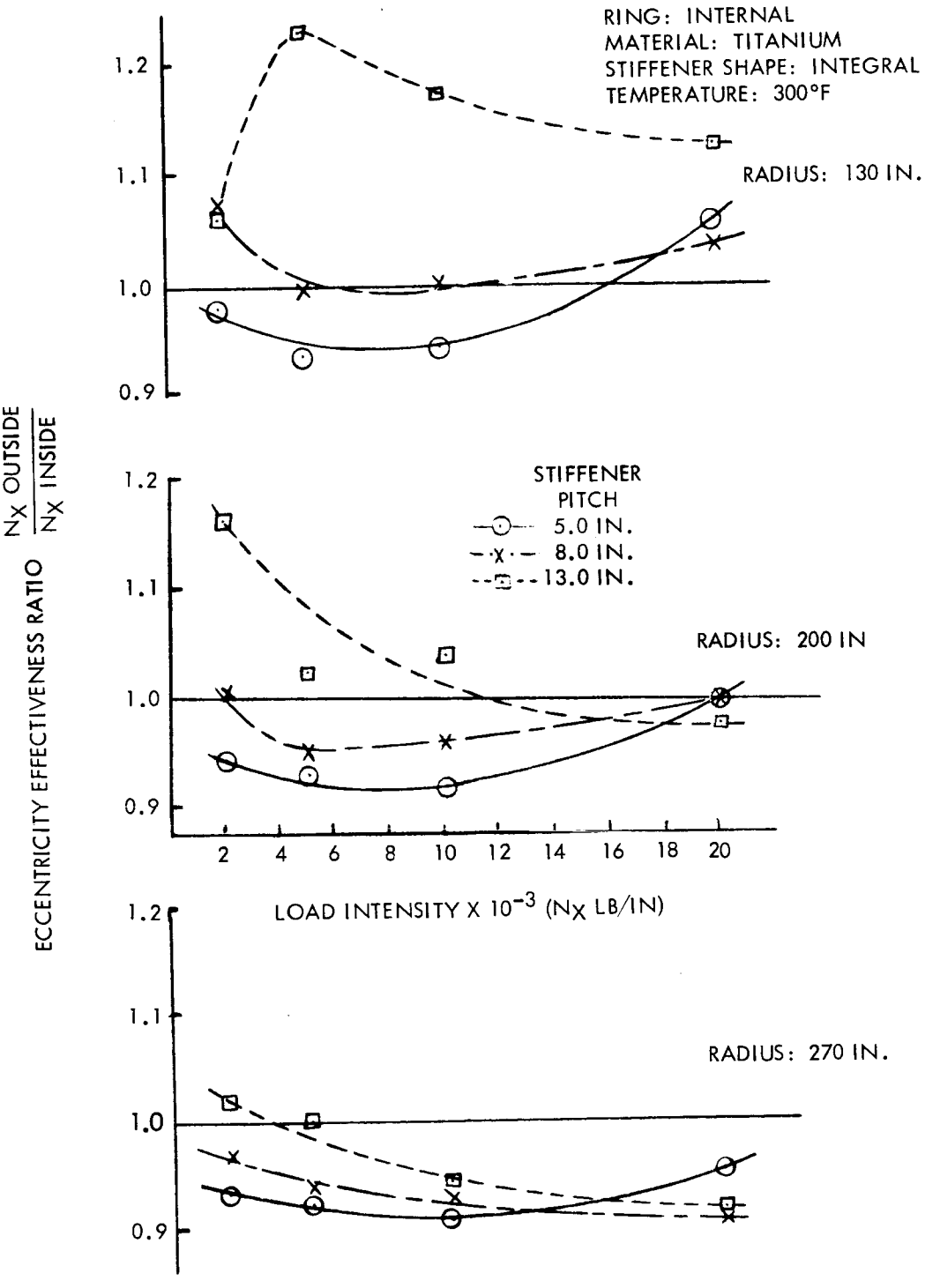

Figure 38. - Relative Merit of Externally Stiffened Titanium Shells

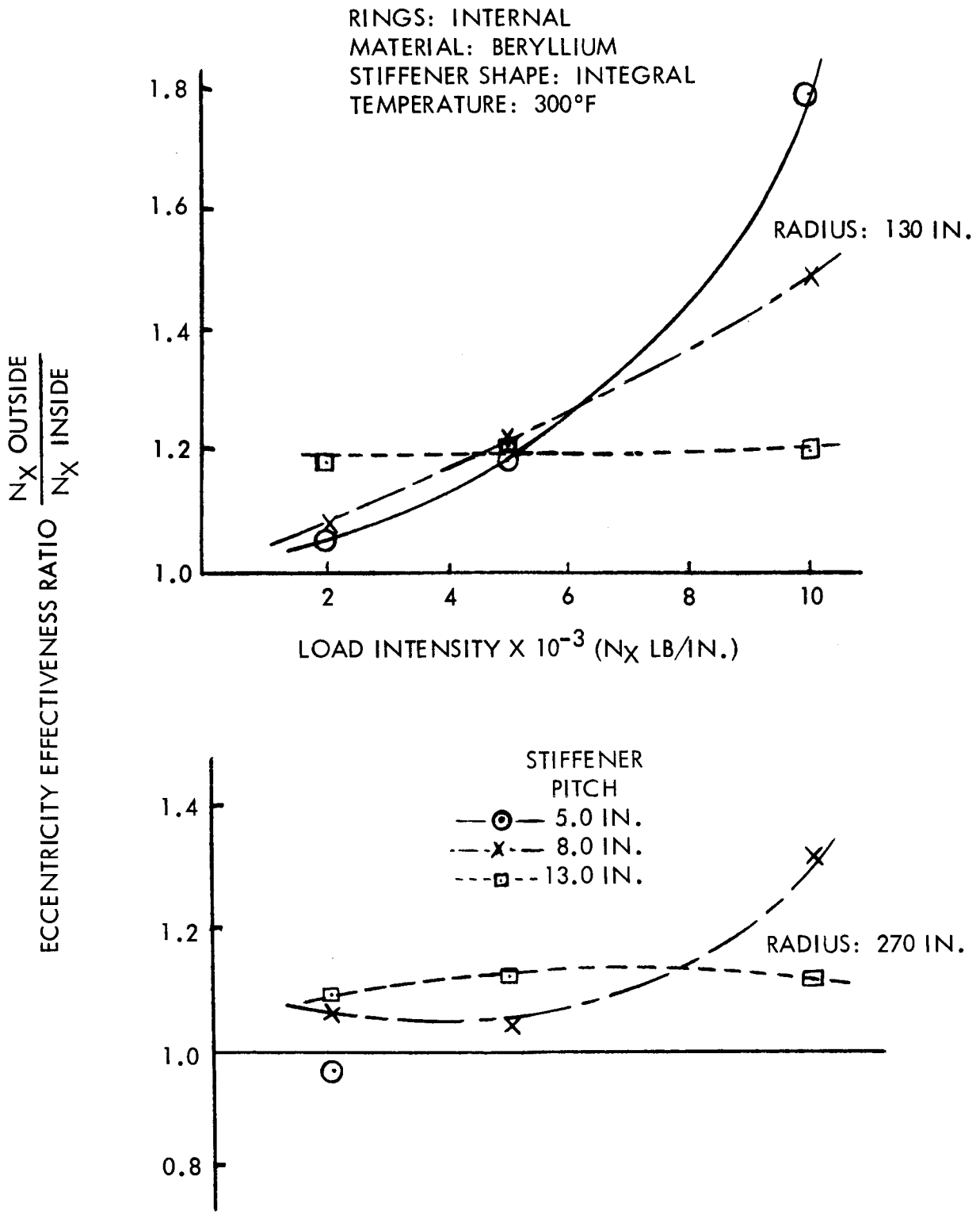

Figure 39. - Relative Merit of Externally Stiffened Beryllium Shells

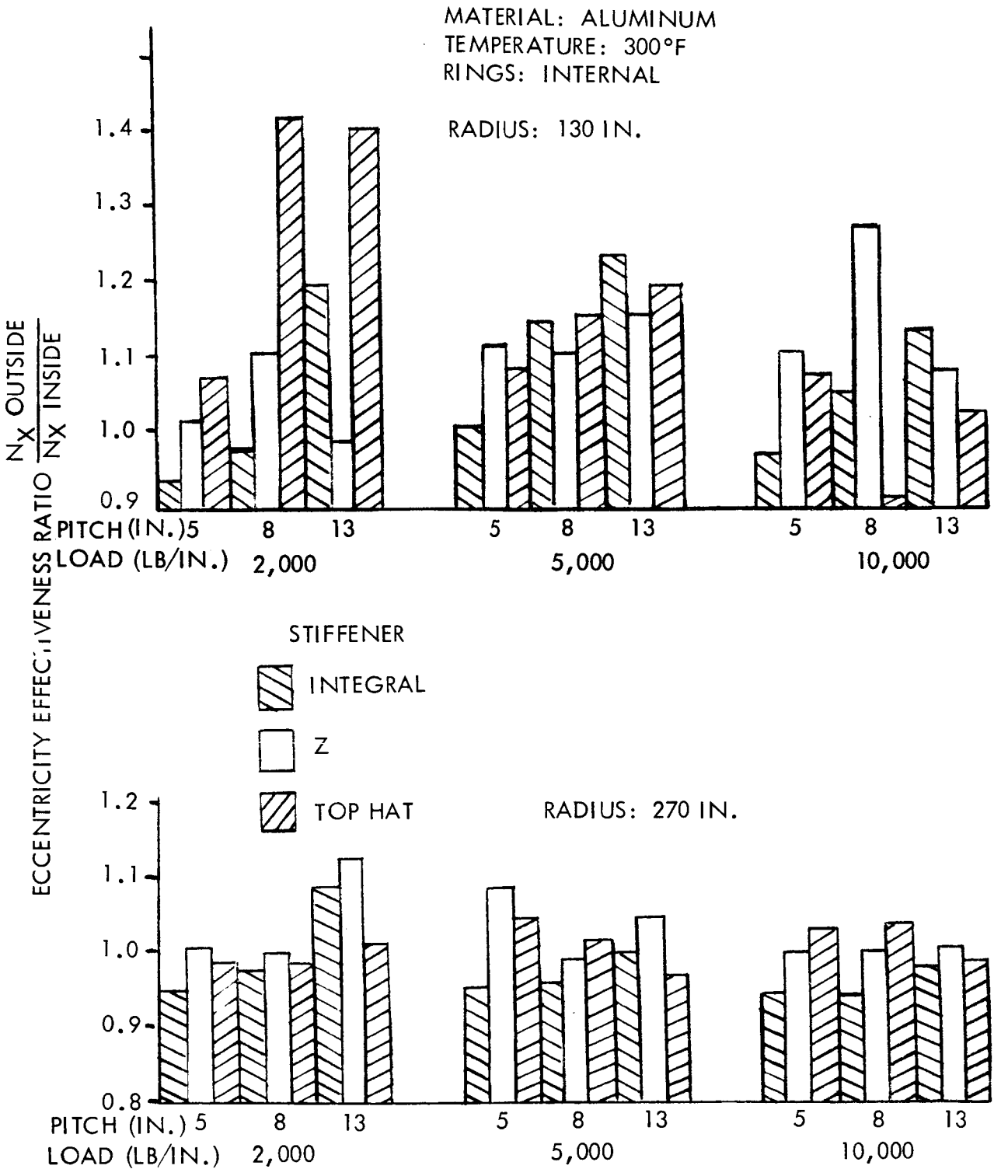

Figure 40. - Effect of Stiffener Shape on Eccentricity Effectiveness, Aluminum

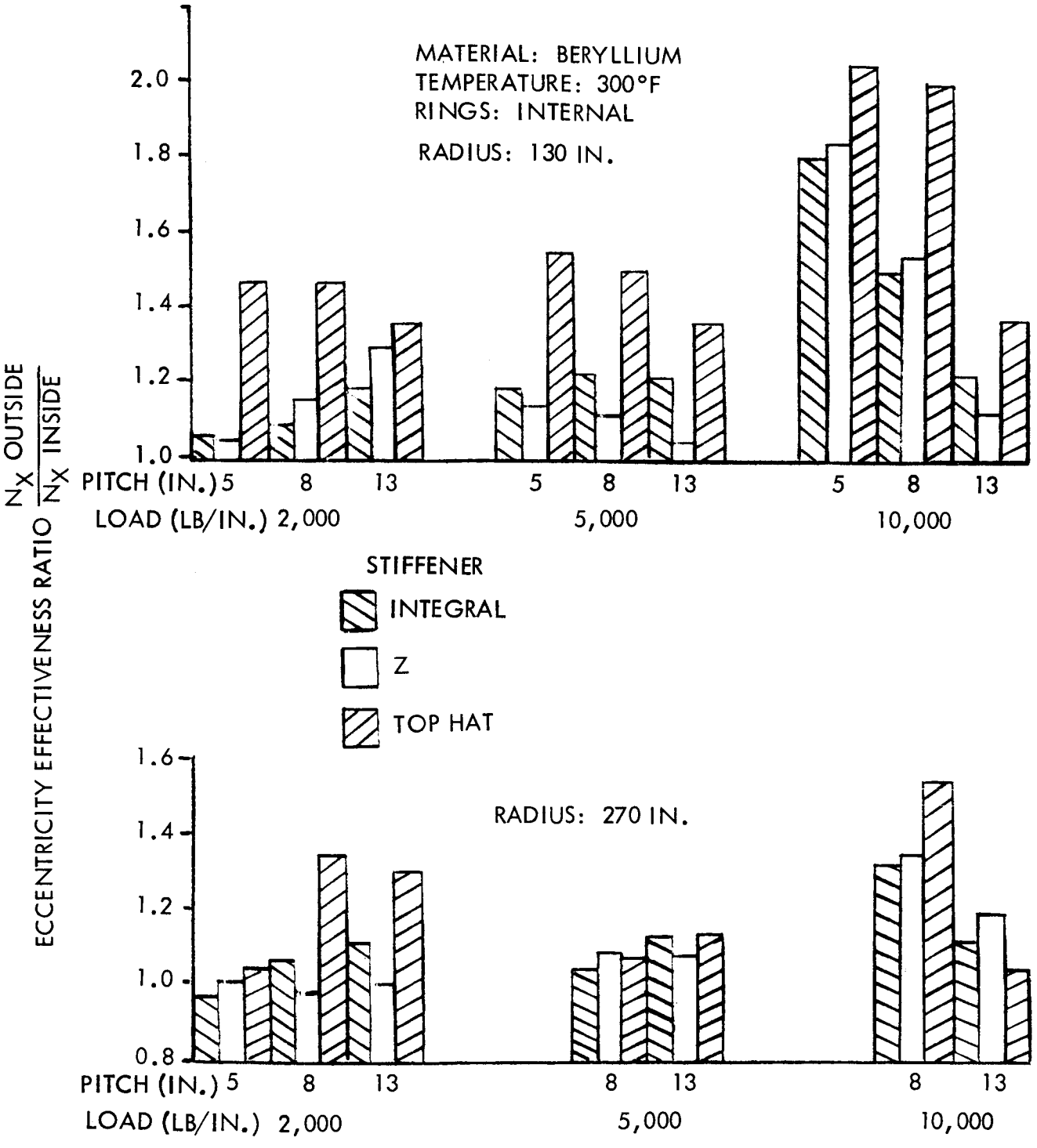

Figure 41. - Effect of Stiffener Shape on Eccentricity Effectiveness, Beryllium

The computer printouts in Appendix A show the theoretical loading capability and the buckling mode shapes associated with this minimum capability. The theoretical N_x are currently quoted by the synthesis program, since only the difference between inside and outside stiffeners was of interest. This difference is essentially the same whether the values compared are theoretical or adjusted experimental. The theoretical buckling coefficient is 0.6, to which should be applied a knockdown factor (ref. 14) based on the designs relative flexural and bending stiffness parameters. Table 4 shows the correct N_x for a few selected cases that had been synthesized by the program, and their corrected N_x values were in good agreement with the

TABLE 4. - ECCENTRICALLY STIFFENED CYLINDERS
EXPERIMENT - THEORY CORRELATION FACTOR

Material	Applied Load Intensity	Pitch (in.)	Equiv. R/t	Correct Factor (Cc)	Corrected $N_{x\,crit}$	
					Outside	Inside
Aluminum	2 000	5	203	0.214	2 110	2 260
		8	245	0.207	2 530	2 260
		13	277	0.199	3 860	3 220
Aluminum	5 000	5	229	0.210	5 100	5 040
		8	276	0.204	6 730	5 830
		13	351	0.194	7 250	5 850
Beryllium	5 000	5	245	0.209	8 600	7 250
		8	264	0.206	11 000	8 800
		13	353	0.194	11 400	9 300
Aluminum	10 000	8	115	0.225	11 300	10 600
		13	129	0.224	15 500	13 600
Beryllium	10 000	8	220	0.213	14 400	10 000
		13	248	0.207	20 500	16 900

Shell Radius 130 ins.
Stringer Shape - Integral
Temperature 300° F
N_x Ultimate compressive load intensity lb/ins.

design requirement conditions. Table 5 shows the buckling patterns associated with the minimum load-carrying capability for both the orthotropic synthesis and isotropic, inside and outside, synthesis. It can be clearly seen that since these buckling patterns change appreciably, if any comparison is to be made between inside and outside merits then the appropriate mode for each condition must be used; otherwise the errors involved in using an assumed constant value could produce erroneous differences.

The cases that were considered indicated a general pattern of outside stiffener efficiency and the specific loading capability increase. Figure 42 is a simplified pictorial map of the aluminum data summarized. Cross-hatching indicates those areas where outside stiffeners are most efficient, while the numbered contours indicate the magnitude of improvement. Figure 43 shows the same effect with titanium.

Bulkheads

For the synthesis of membrane bulkheads during Phase I design studies, a simplified weight-scaling relationship was employed. Phase II involved the development of a series of synthesis programs to define required monocoque skin thickness and component weights for a series of bulkhead shapes. Shape-synthesis programs were written for each of the following:

ellipsoidal
oblate spheroid
semitoroidal

The program output formats supply sufficient information to size and determine component weight for bulkheads of monocoque construction. Other types of construction are discussed later in this section.

The buckling analysis for the ellipsoidal and oblate spheroidal bulkheads was based upon an equivalent spherical shell analysis using the classic von Karmen-Tsien formula to predict the buckling of monocoque spherical shells. The classical equation is

$$\sigma_{CR} = 0.606\ CE\ \frac{t}{R\ (\sin\ \beta)^{1/3}}$$

where C = 25 percent, the buckling correction factor required to correlate theoretical with experimental results, and for the ellipsoidal bulkhead

TABLE 5. - BUCKLING PATTERN FOR ECCENTRICALLY STIFFENED ALUMINUM CYLINDERS WITH INTEGRALLY SHAPED STRINGERS

Load Intensity N_x (lb/ins.)		2 000		5 000		10 000		20 000	
Buckle wave pattern		M	N	M	N	M	N	M	N
Stiffener pitch (in.)*		SHELL RADIUS—130 IN.							
5 in.	Ortho	10	7	6	6	6	5	4	5
	Out	10	8	7	7	6	6	4	6
	In	9	8	6	7	5	6	4	6
	Wt	2.23		3.53		4.77		7.28	
8 in.	Ortho	9	8	5	7	5	6	4	5
	Out	10	9	5	8	6	7	5	6
	In	9	9	5	8	5	7	4	6
	Wt	2.70		3.96		5.40		7.48	
13 in.	Ortho	4	9	4	8	4	6	5	6
	Out	5	11	4	9	5	7	6	6
	In	5	11	4	9	4	7	5	7
	Wt	3.47		4.86		6.56		8.63	
Stiffener pitch (in.)		SHELL RADIUS—200 IN.							
5 in.	Ortho	9	7	6	6	7	5	5	5
	Out	9	8	6	7	7	6	5	6
	In	8	8	5	7	6	6	5	6
	Wt	2.61		3.99		5.76		8.23	
8 in.	Ortho	10	7	6	7	6	6	6	5
	Out	10	8	7	8	6	6	6	6
	In	9	9	6	8	5	7	5	6
	Wt	2.95		4.30		6.15		8.45	
13 in.	Ortho	9	9	7	8	7	6	8	5
	Out	10	10	8	8	8	7	8	6
	In	9	10	7	9	7	7	7	6
	Wt	3.63		5.12		7.27		9.90	

*Ortho - Orthotropic analysis
Out - Isotropic analysis with stiffeners outside, rings inside
In - Isotropic analysis with stiffeners inside, rings inside
Wt - Unit shell weights lb/ft^2

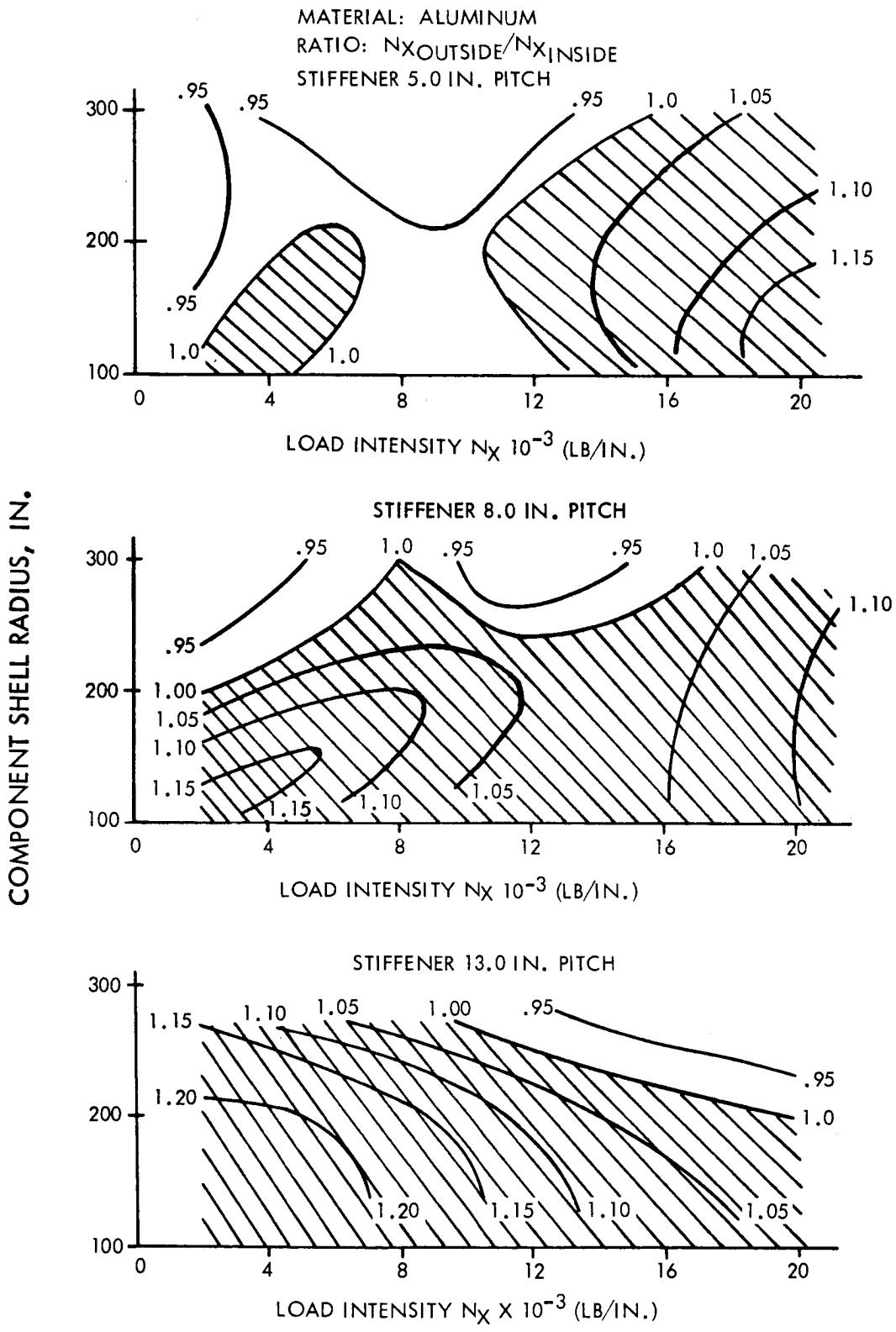

Figure 42. - Stiffener Positioning Effectiveness Ratio

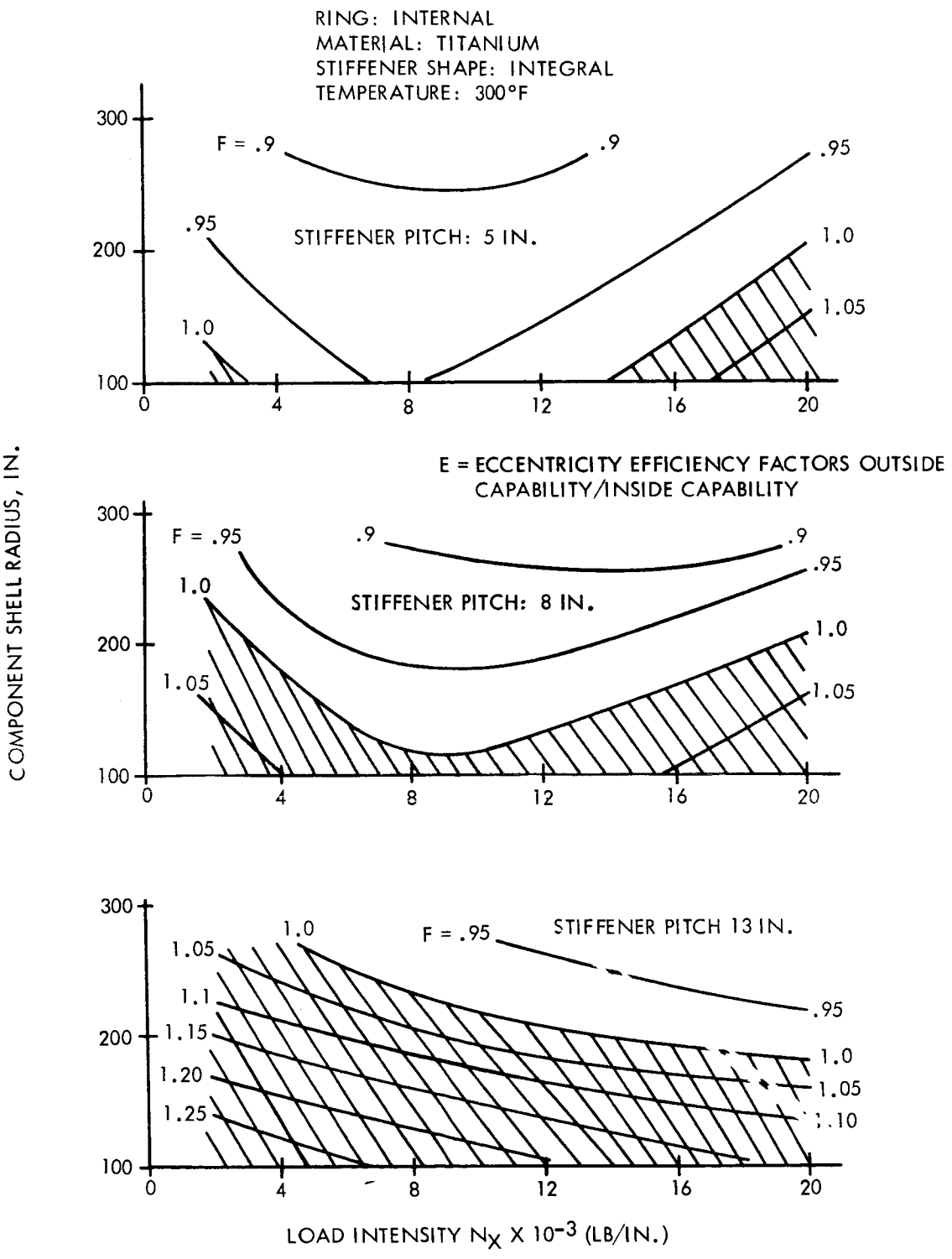

Figure 43. - Relative Merit of Externally Stiffened Titanium Shells, Component Shell Radius Versus Load Intensity

$$\beta = \pi - 2 \arctan\left(\frac{a}{b}\right)$$

$$R = \frac{a}{\sin \beta}$$

a = semi-major axis

b = semi-minor axis

The program allows any size and aspect ratio of bulkhead to be synthesized and furnishes outputs on the component weight and/or the required skin thickness at the equator, midpoint, and apex of the bulkhead. Table A 8 is a printout for a series of elliptical dome bulkheads with aspect ratios of $\sqrt{2}$ subject to an internal pressure. These skin thicknesses are either based on strength or stiffness requirements. The program has the ability to use the external collapsing pressure to assess the required monocoque skin thickness for prevention of buckling. Figure 44 shows the component weight variation with matching cylinder radius using aluminum with a yield stress of 65 000 lb/in.^{2} and ultimate stress of 75 000 lb/in.^{2} at a temperature of -300° F. The curves of $\sqrt{2}$ ellipsoidal bulkhead have been drawn for a series of internal pressures ranging from 35 to 80 psi.

Table A 8 shows a typical output format for the oblate spheroidal bulkhead with a dome shape index, n = 1. Figure 45 shows the weight results for aluminum bulkheads with a range of diameters and internal pressures.

The semitoroidal bulkhead concept is a low profile design, and although the bulkhead component weight is more than for a simple ellipsoidal dome, the advantage gained in dome height reduction and, hence, shortening of the vehicle could offset the component weight penalty and result in overall system weight reduction and performance improvement.

The stability analysis for the complex shape of the outer toroidal membrane coupled to an inner ellipsoidal membrane is beyond the current synthesis capability of the program. Therefore, the stability of the total membrane was considered as two separate membrane shapes, and their load interaction at the intersection was not considered. The inner dome, ellipsoidal, was converted to an equivalent spherical cross section, and its stability analysis was identical to that given for monocoque ellipsoidal bulkheads in Appendix A. The outer membrane was analyzed as a toroidal shell under uniform external pressure. The stability analysis followed the method used by Sobel and Flügge (ref. A-15), and a copy of their buckling curve used for the synthesis program was reproduced in figure A-16.

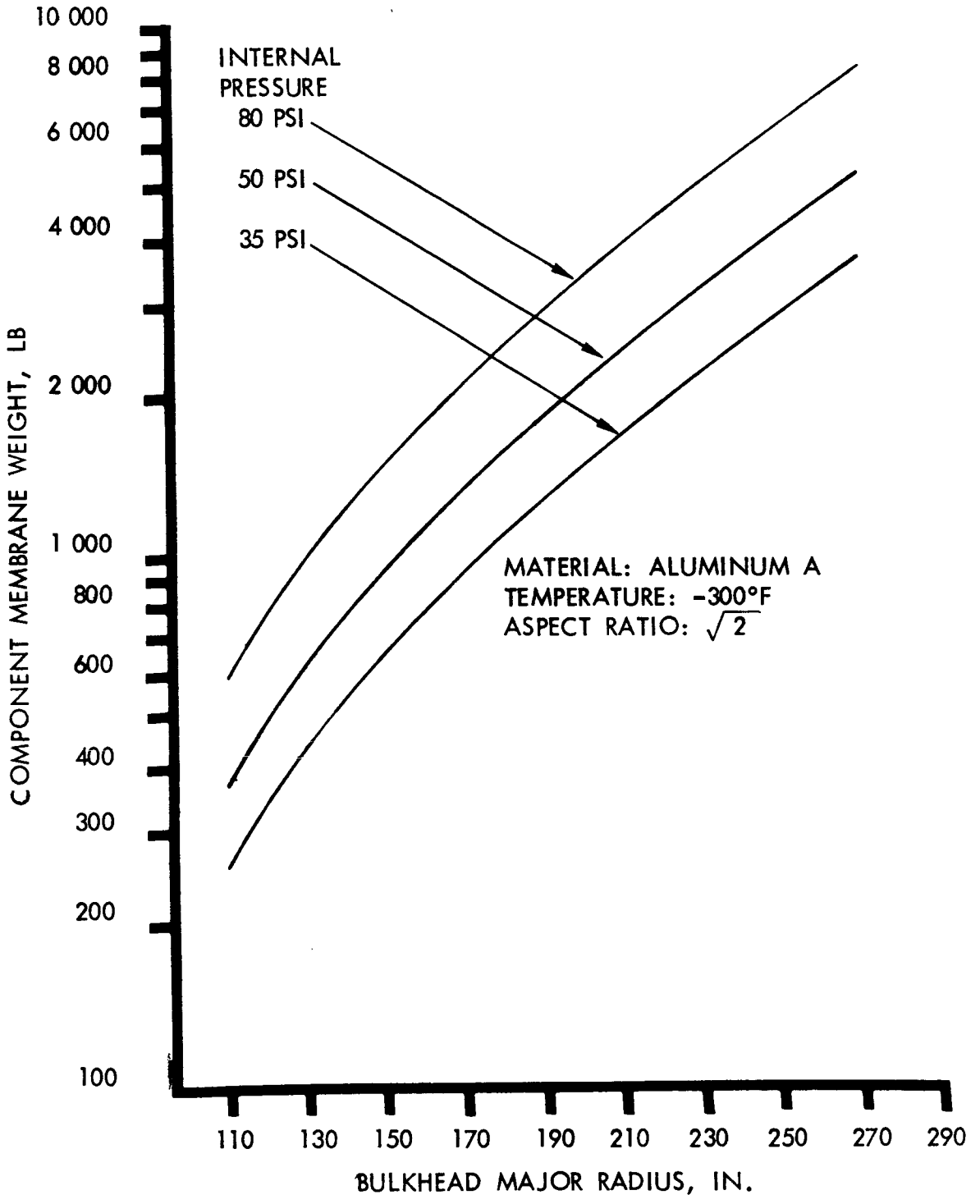

Figure 44. - Ellipsoidal Bulkhead Component Weight

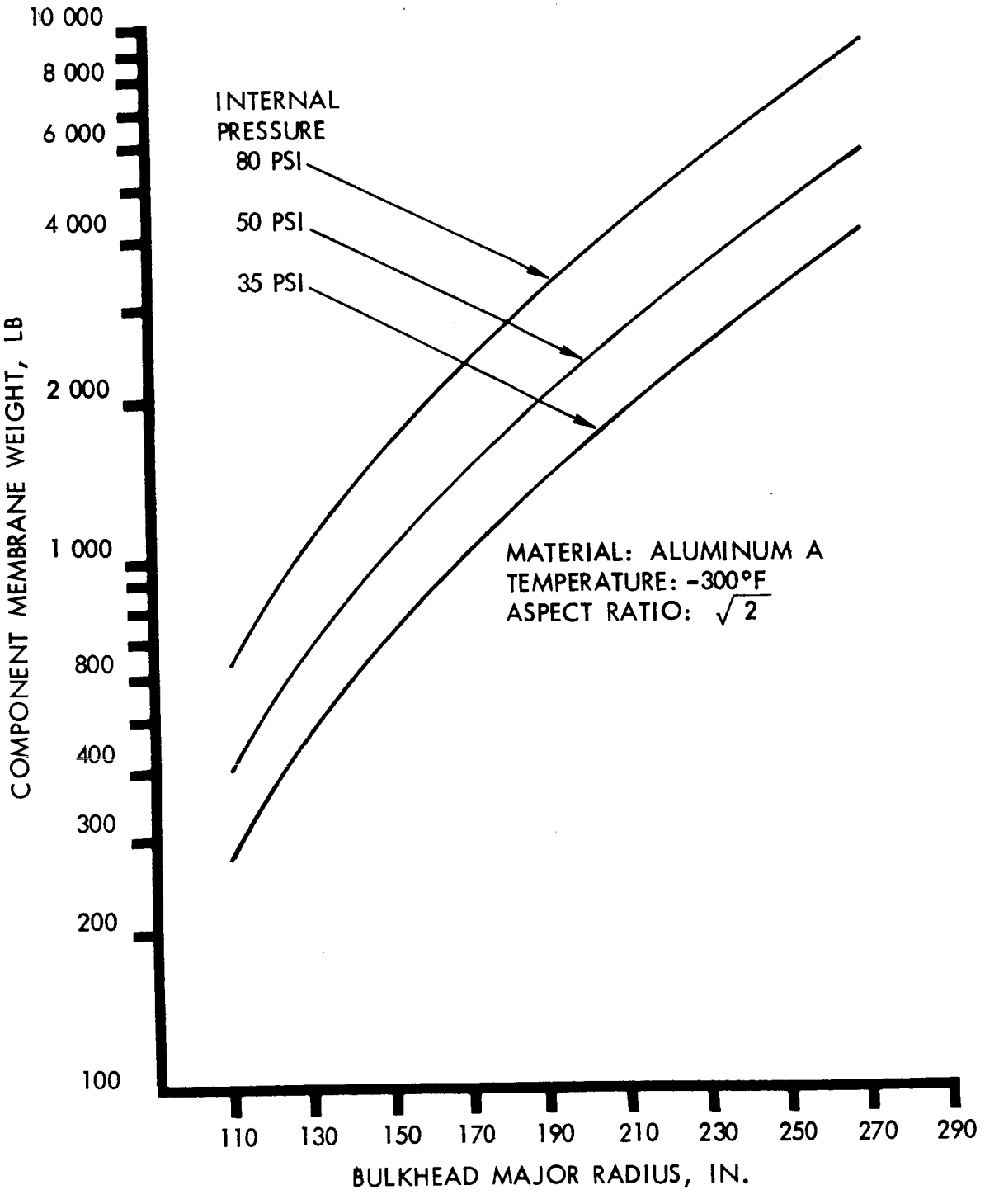

Figure 45. - Oblate Spheroidal Bulkhead Component Weight

An example of the program output is shown in table A-8. It defines the required thicknesses for points on the toroidal and ellipsoidal segments of the bulkheads and the tension thickness of the web of the center tension cylinder joining the two bulkheads. This cylinder diameter is identical to the junction surface of the center ellipsoidal dome and the outer toroidal membrane. The weight of this center cylinder is not quoted in the component weight since its weight is strictly a function of propellant tank length. The weights quoted in tableA8 and figure 46 are only for the outer toroidal membrane. Additional weights for this design concept are required for the center cylinder and the inner ellipsoidal membrane; these are obtainable from the ellipsoidal synthesis program.

Although these bulkhead shapes have been considered monocoque construction, the program computer output results indicate the required thicknesses for either strength or stability. These thicknesses can be considered as the required equivalent thickness, and other types of construction, honeycomb or waffle, can be used if an equivalent thickness conversion effect is taken into account. The tension requirements due to the internal pressure will dictate the skin thickness, and any compressive load intensities present will determine the stiffness requirement; i. e., sandwich core thickness or waffle grid pattern.

Acoustic Problems in Large Booster Systems

One of the potentially critical contributions to the environment experienced by a large rocket vehicle, particularly during the launch phase, is the randomly fluctuating pressure field resulting from the acoustic energy generated by the rocket engines. In addition, the turbulent boundary layer along the vehicle during transonic and supersonic flight causes high, external, fluctuating loads. The vehicle structure response to these loads results in vibrational inputs to components and equipment mounted on the primary structure. The equipment may fail in service, due to experiencing excessive acceleration or displacement, or by fatigue. A cursory investigation was conducted to define the magnitude of sound pressure levels for large boost systems to ascertain whether they were more severe than the levels encountered in the current Saturn class structures experience.

The available methods for predicting such an acoustic environment and the resulting vibration response cannot lead to exact values; however, gross estimates based on extrapolation of test data would enable an adequate test

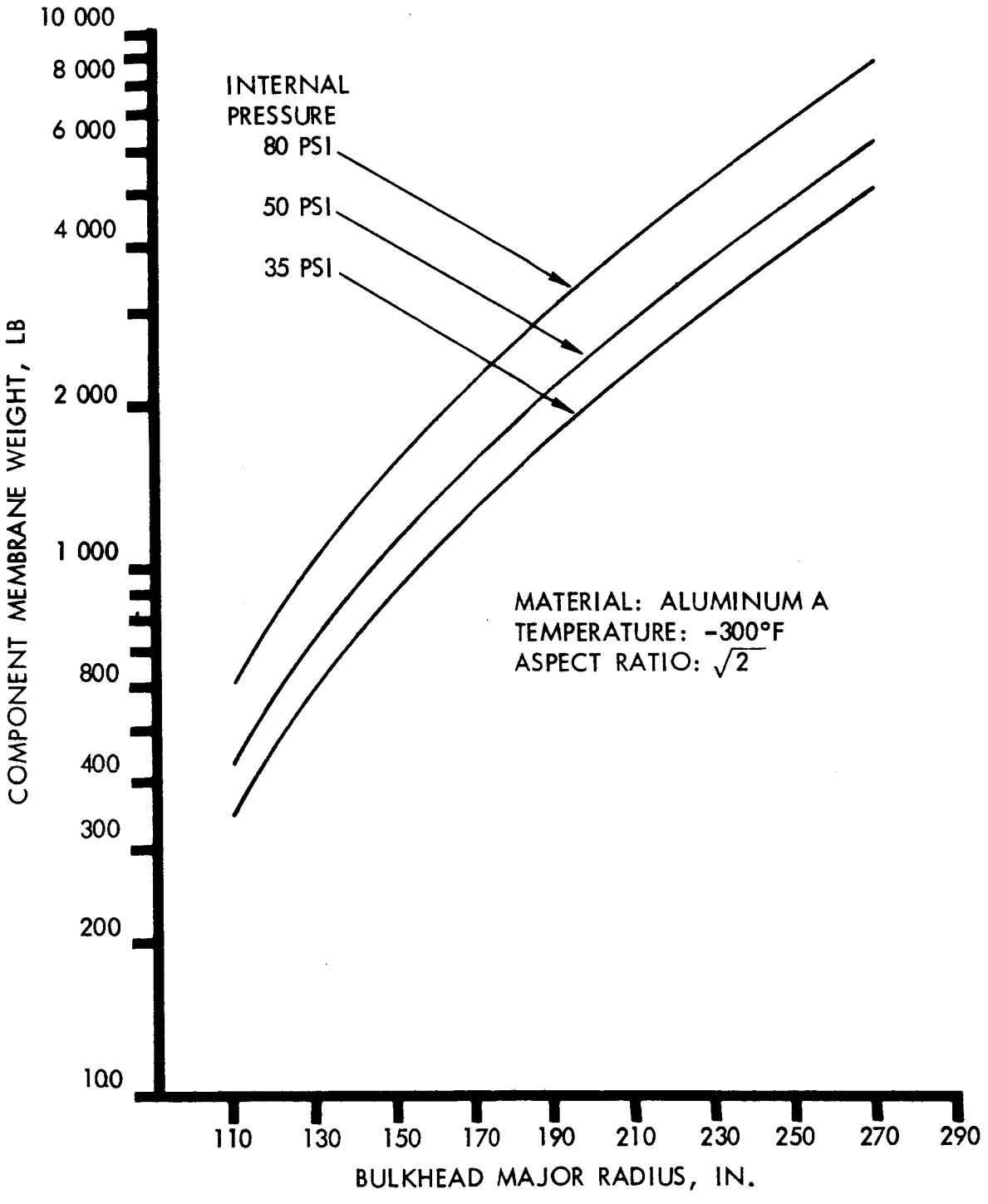

Figure 46. - Semitoroidal Bulkhead Component Weight

program to be defined when detailed information on the design becomes available. With the present technology it is not possible to establish acoustical boundaries for use as input to the design of the vehicle structure.

In the following sections the acoustical levels which can be expected on large booster systems are predicted, and the associated problems discussed. The method used to calculate engine noise sound pressure level (SPL) generally leads to conservative estimates, somewhat higher than actual measured values. By extrapolating measured acoustic data, obtained during J-2 static firing tests, an approximate estimate of the engine noise environment along the new vehicle structure can be made. These predictions are based on the following assumptions:

The sound power level (SPL) is proportional to the mechanical power in the exhaust jet, and the efficiency of conversion from mechanical to acoustical energy is equal for all cases being considered.

Acoustical energy is dissipated in an inverse-square manner with distance from the noise source.

The noise source is located in the nozzle exit plane, at the centroid of the nozzle cluster.

Effects of jet-deflectors at the test-site or launch pad are the same for all cases.

Engine clustering effects can be ignored.

For a cluster of five J-2 engines, with a total thrust T_o of 805 000 lb and effective exhaust velocity V_o of 10 465 ft/sec, the overall SPL measured at a point approximately 25 feet from the nozzle exit plane was 161 db (re 0.0002 dynes/sq cm). The difference in SPL caused by the increased mechanical power of the new booster is

$$\Delta \text{ SPL} = 10 \log_{10} \frac{W_1}{W_o}$$

where

W_o = mechanical power of five J-2 engines

$= 1/2 \; T_o \; V_o$

and

W_1 = mechanical power of the engines in the new booster

$= 1/2\ T_1\ V_1$

Thrust T_1 of the new booster is 30×10^6 pounds; under the assumption that a specific impulse of 350 seconds will be possible, the effective exhaust velocity V_1 will be approximately 11 250 ft/sec.

The resulting overall SPL at a point 25 feet from the noise source is thus

$$SPL_1 = 161 + \Delta SPL$$

$$SP = 161 + 10 \log_{10} \left[\frac{1/2\ T_1\ V_1}{1/2\ T_o\ V_o} \right]$$

$$= 161 + 10 \log_{10} \left[\frac{30 \times 10^6 \times 11\ 250}{805\ 000 \times 10\ 465} \right]$$

$$= 177 \text{ db}$$

The variation of SPL_1 along the structure is given by

$$SPL_1(R) = 177 - 10 \log_{10} \left[\frac{R}{25} \right]^2$$

where R is the distance in feet forward of the nozzle exit plane. Values of SPL_1 are shown in table 6 and plotted in figure 47.

Despite the considerable research being performed in the field of aero-acoustics, there still exists no analytical method by which to predict accurately the aerodynamic noise experienced by the flight vehicle. The best approach is to use existing wind tunnel data derived from tests on appropriate models together with flight test data on similar vehicles.

The total aerodynamic noise derives from the turbulent boundary layer and its interaction with shock waves, separated flow caused by abrupt changes in vehicle shape, base pressure fluctuation, and protuberance and wake noise. Obviously, the noise level is strongly affected by vehicle geometry and is highly dependent on the flight profile, changing with altitude, dynamic pressure, Mach number, and angle of attack.

TABLE 6. - PREDICTED OVERALL SOUND PRESSURE LEVEL DUE TO ENGINE NOISE, AT SEA-LEVEL

Station (inches)	Overall SPL (dB re 0.0002 dynes/sq cm)
300	175
600	171
900	167.4
1200	165
1500	163
1800	161.4
2400	159
3600	155.4
4800	153
6000	150.8
7200	149.4
7900	148.6

From these considerations, it is clear that an accurate prediction of the aero-acoustical environment requires an extensive wind-tunnel test program, using models which have the characteristics of the launch vehicles being designed, and performed under conditions simulating the trajectory parameters of interest. In the absence of such ideal conditions, it is possible to estimate the environment with a fair degree of confidence through the use of test data accumulated on the S-II and Apollo programs by assuming that the same maximum levels will be reached along the new vehicle at interstage changes of diameter. Such an estimate was made, and is plotted in figure 47.

The envelope of sound pressure levels in figure 47 shows that engine noise at launch is most critical for the large vehicle considered (1×10^6 lb payload) at vehicle stations up to about 2300 inches, while the structure forward of this point receives its worst acoustical input from noise originating in the turbulent boundary layer. High acoustical pressures will also be experienced during static firing tests; however, these will probably be less severe than the launch environment, since more effective noise-reduction techniques can generally be employed in a static-test installation.

The curve of aerodynamic noise is scaled from a similar curve predicting acoustic levels on the Saturn V vehicles. It represents an envelope covering a wide range of angles of attack and Mach numbers. Peaks at Stations 3000 and 7350 correspond to local high levels which would be expected to occur just aft of the shoulders at the stage intersections and on the payload.

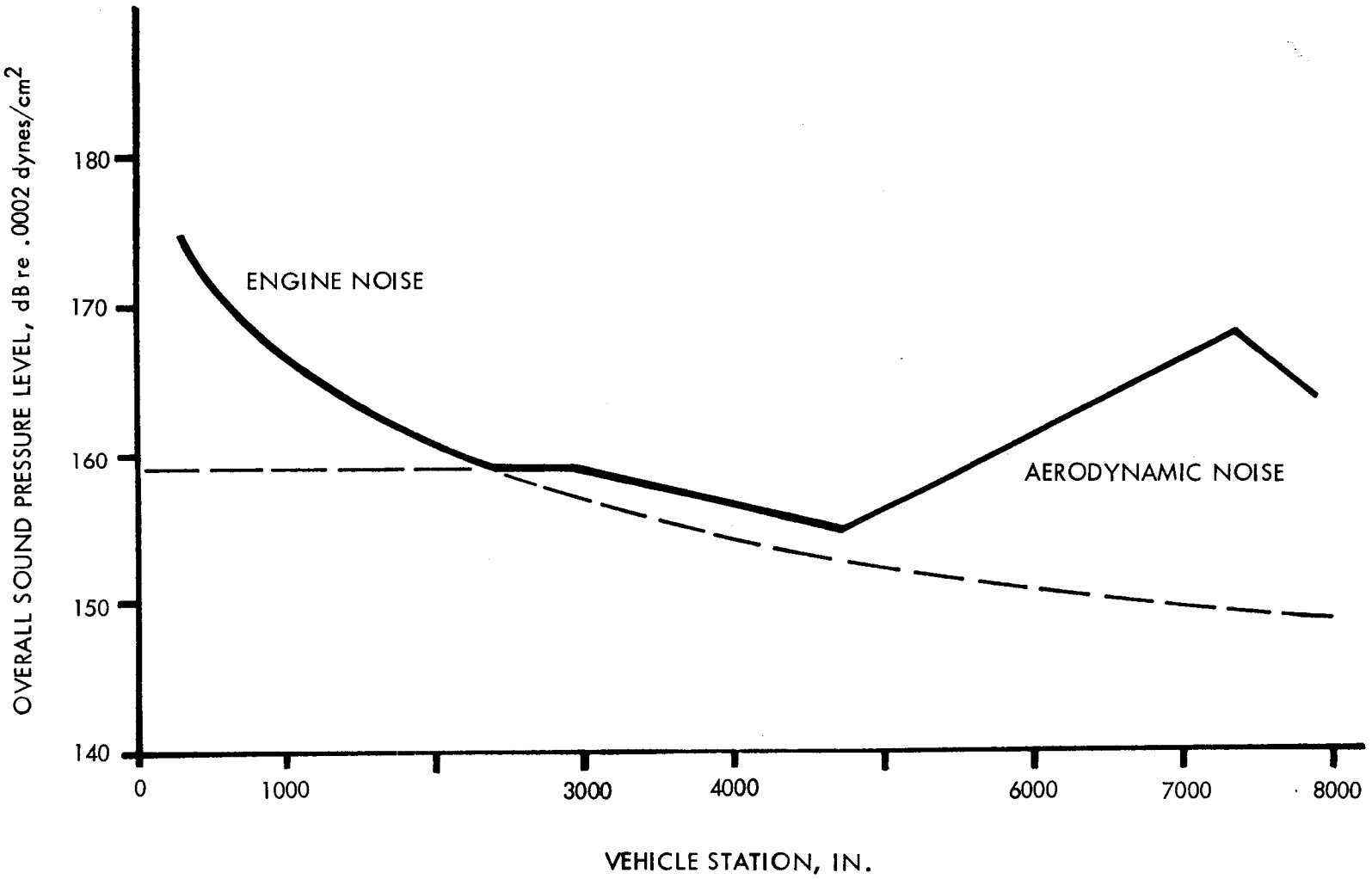

Figure 47. - Predicted Maximum Acoustic Levels on Post-Saturn-Payload-Class Vehicle, Two-Stage, 1985 I_{sp}, 2 000 000-Pound Orbital Payload

This acoustical information could be used to estimate local vibration levels on the vehicle, which would customarily be the basis for vibration test levels. At the present time, there is no established method by which the information can be used as quantitative design parameters. On the other hand, an experienced dynamicist can employ the curves to decide where, for example, special attention should be paid to the possibility of experiencing fatigue failures due to high local vibratory stresses. The external acoustical environment will also affect the selection of sound insulation material used to protect spacecraft crew members.

ASSESSMENT

To obtain a better insight into where and when it is advantageous to achieve a particular material property and/or construction improvement, the relative assessment must be directed towards a specific structural component of a particular vehicle system. General conclusions as to the benefits for all vehicle systems of a particular material and concept cannot be rigidly stated. It has been found that for some vehicle systems, the lightest concept is not the most efficient approach because of the additional construction costs involved and also because the performance improvements are incompatible. The ground rules and design criteria which are used in the derivation of merit indices must be clearly stated before decisions can be based on the merit functions.

If component weight reduction, per se, is the only merit function used, a true indication of the significance of the weight reduction may not result. Weight reduction effects upon overall system payload performance, schedule, and cost are the governing criteria in the aerospace industry. Component weight reduced and payload (pounds) gained can be translated into a structural cost index which can assist in the economic justification of a specific material and design for a particular component. The merit functions used during Phase 1: component weight reductions, equivalent payload performance changes, and effective cost ratios, are considered applicable for this phase of the study. An ordering of these merit functions can indicate the relative worth.

Depending upon the circumstances, management decisions can be based on each of these merit functions by themselves; however, the objective of this study is to indicate and demonstrate a method wherein these decisions will be less limited and, possibly, misleading. (Weight reduction, payload gain, and cost index are considered as a set of indices unique to a component change in a particular vehicle base point.) Typical results are indicated, which are limited to six vehicles with expendable stages as synthesized during Phase 1 and defined in Volume 1 of this report. The types of structural concepts investigated herein are classed as advanced designs—double-walled and multiwalled construction.

The vehicle geometry for these six expendable base point vehicles is summarized in figure 48. Compressive loading, N_x, intensities for the shell

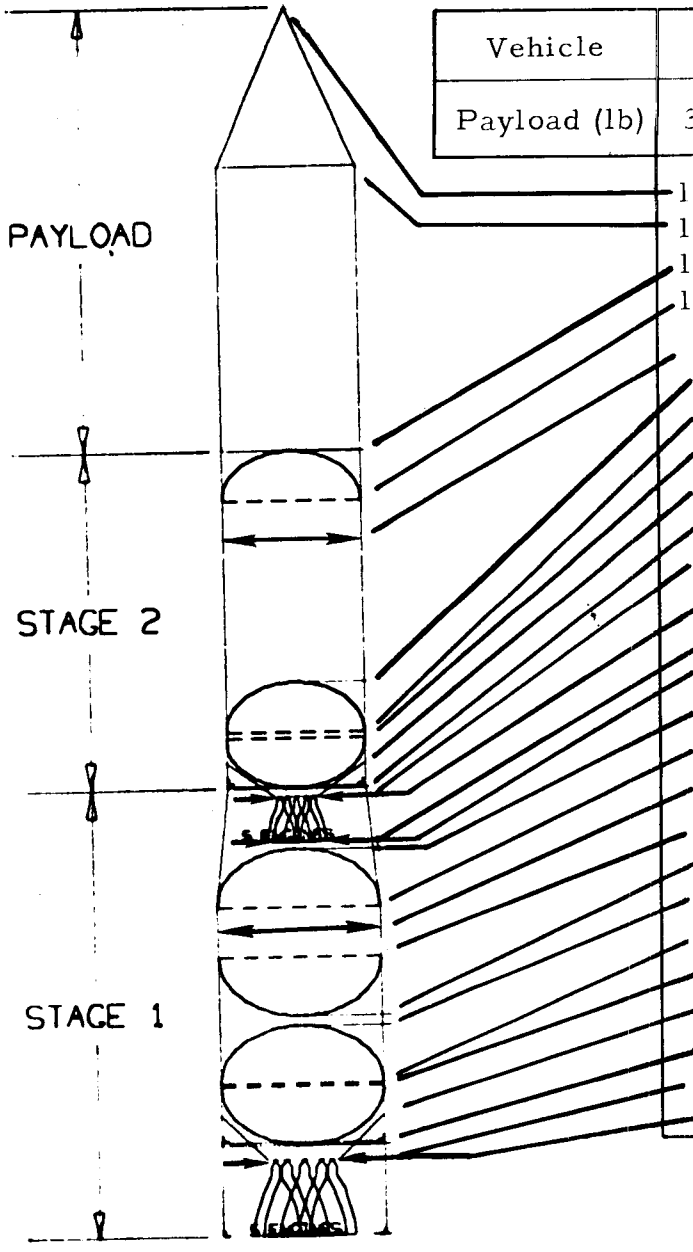

Vehicle	Medium Range		Saturn Class		Post-Saturn		
Payload (lb)	30 000	100 000	240 000	445 000	1 000 000	2 000 000	
	1914.9	2444.3	3986.8	4384.8	6549.9	7902.3	
	1672.9	2158.3	3551.2	3949.2	5955.9	7308.3	
	1232.9	1638.3	2759.2	3157.2	4875.9	6228.3	
	1155.1	1546.3	2619.2	3017.2	4684.9	6037.3	*
	220.0	260.0	396.0	396.0	540.0	540.0	*
	868.8	1119.7	2086.4	2357.9	3444.8	4182.7	
	791.0	1027.8	1946.3	2217.8	3253.9	3991.8	
	781.8	969.6	1924.4	2156.6	3064.7	3612.2	
	742.9	943.6	1854.3	2086.6	2969.3	3516.7	
	704.0	897.6	1784.3	2016.6	2873.8	3421.2	
	689.9	877.0	1750.4	1977.8	2807.5	3339.1	
	64.4	94.3	159.6	181.9	317.5	393.0	*
	97.1	142.2	240.7	274.3	478.8	592.6	*
	619.3	774.2	1580.6	1783.6	2475.7	2928.1	
	608.3	761.2	1560.8	1763.8	2448.7	2901.1	
	516.4	647.6	1420.9	1623.8	2222.4	2672.0	
	260.0	321.1	396.0	396.0	640.0	648.0	*
	438.5	557.9	1000.8	1101.0	1656.5	1901.9	
	346.5	444.3	860.8	961.0	1430.2	1672.8	
	330.9	425.1	837.0	937.2	1391.8	1633.9	
	239.0	311.5	697.0	797.2	1165.5	1404.8	
	235.5	311.3	502.3	537.9	921.7	1034.1	
	189.5	254.5	432.3	467.9	808.5	919.5	
	143.6	197.7	362.2	397.9	606.4	805.0	
	119.6	164.8	301.9	331.6	579.5	670.8	
	112.1	154.9	289.9	317.5	563.9	652.0	*

*DIAMETERS

Figure 48. - Vehicle Stations and Diameters for the Base-Point Designs (in.)

structural components for these vehicles was from 2000 pounds per inch to in excess of 20 000 pounds per inch (see table 7). Figures 49 and 50 illustrate the basic unpressurized shell weight comparisons, and present an ordering of the weight merit function for a range of applied load, for the conventional structures considered in Phase I. Trends for the 270-inch radius vehicle, post-Saturn vehicle in figure 48, were similar to those illustrated in figure 50, but of a larger unit weight.

Figures 49 and 50, show that aluminum and titanium honeycomb sandwich offer the best weight advantage throughout the loading range and stage diameters considered, when compared to waffle, integral skin-stringer and hat section skin-stringer constructions. Aluminum hat-section skin stringer is lighter than the basepoint integral skin stringer. The aluminum waffle construction for the small radius vehicles and a loading intensity less than 4000 pounds/inch is indicated in figure 49 as being lighter than integral skin-stringer, and comparable to an efficiently designed low weight hat-section stiffened shell. Application of this waffle construction may be considered as a competitive in lightly loaded shells such as small-diameter upper stages for both unpressurized and pressurized shells. When conventional beryllium structures are compared to the basepoint material and construction (figure 51) the distinct weight advantage of using beryllium is evident for all types of construction when compared to the basepoint concept.

The advanced aluminum structures, which are more thoroughly discussed in Appendix A, are compared to the basepoint construction in figure 52. These constructions (corrugated sandwich, multiwall construction with hat-section face sheets, and multiwall construction with corrugated sandwich face sheets) offer a distinct weight advantage over the base point design, but certainly not as pronounced as the beryllium structures in figure 51. Other types of stiffener elements were investigated during the study; these were Z, I section and integral stiffeners. It was found that the best performance, weightwise, was obtained using hat-section stiffeners. As two facings panels are required to withstand the compressive loads, the stiffener elements for each panel to meet general instability requirements are correspondingly smaller than the optimum design of single sheet concepts. The trend for the multiwall skin-stringer design with the sine-wave substructure is towards thin-gauge facing sheets, closely spaced longitudinal stiffener elements of small dimensions. The closer the pitch, the lighter the construction, but the fabrication costs for machining, fastening, riveting, welding or bonding increase for the additional operations. Diffusion bonding of the individual facing sheets composed of the small, closely pitched elements might offer an acceptable solution, both with regard to the lightest weight design and retention of comparable fabrication costs. The advanced design concepts fabricated in titanium are indicated in figure 53.

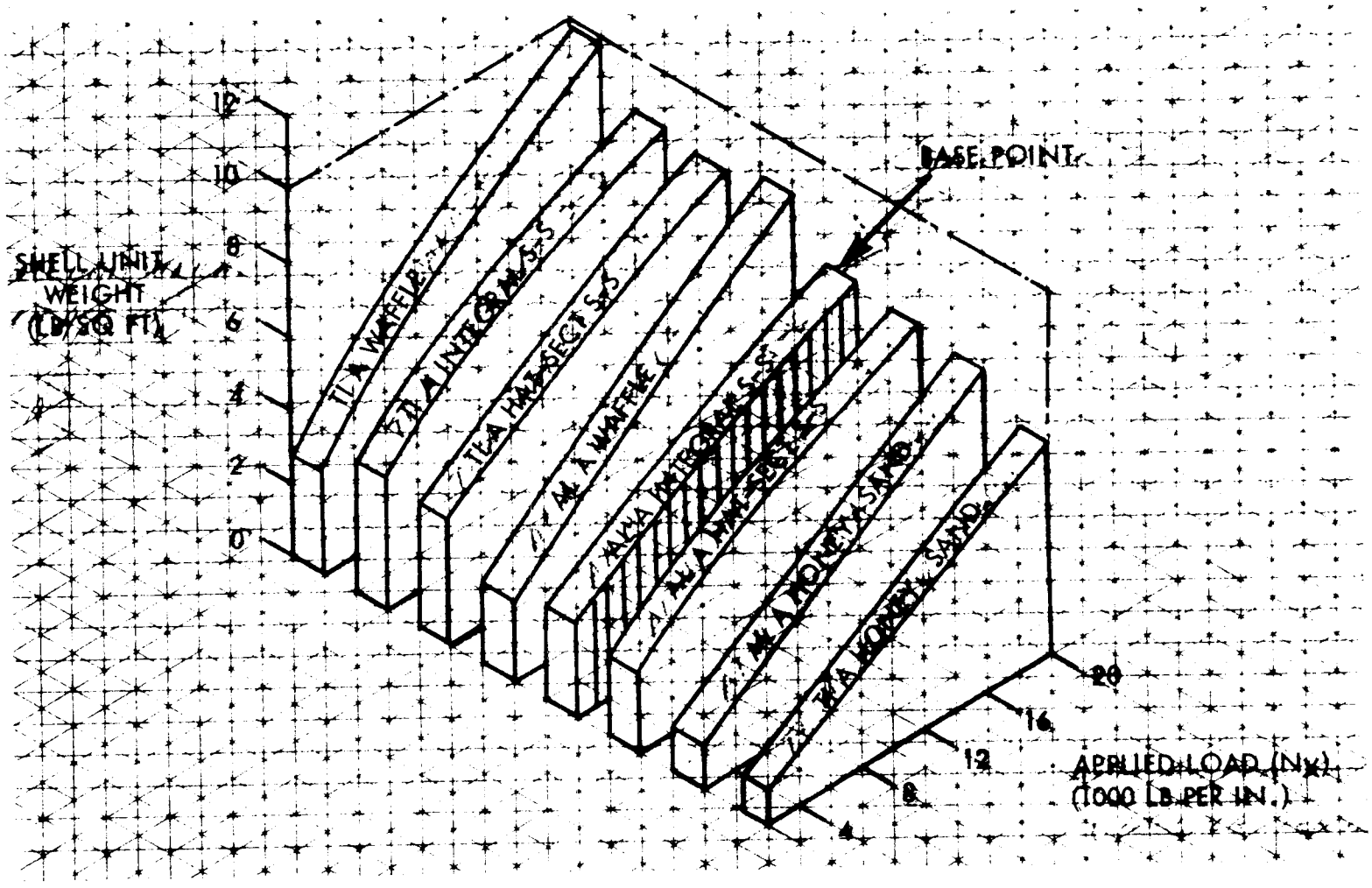

Figure 49. - Shell Unit Weights for Conventional Titanium and Aluminum Structures—130-Inch Radius, 300°F, No Pressure

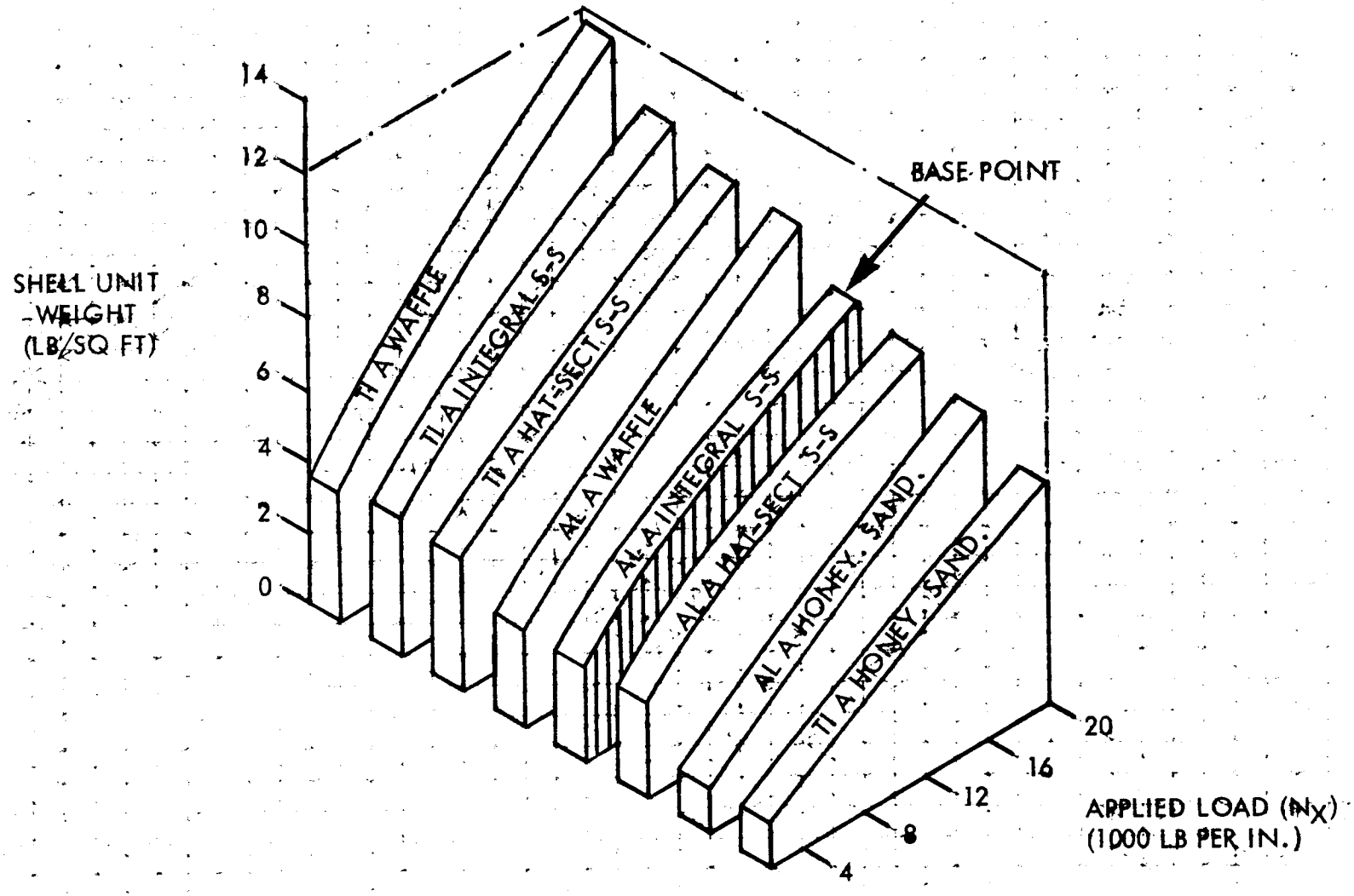

Figure 50. - Shell Unit Weights for Conventional Titanium and Aluminum Structures — 198-Inch Radius, 300°F, No Pressure

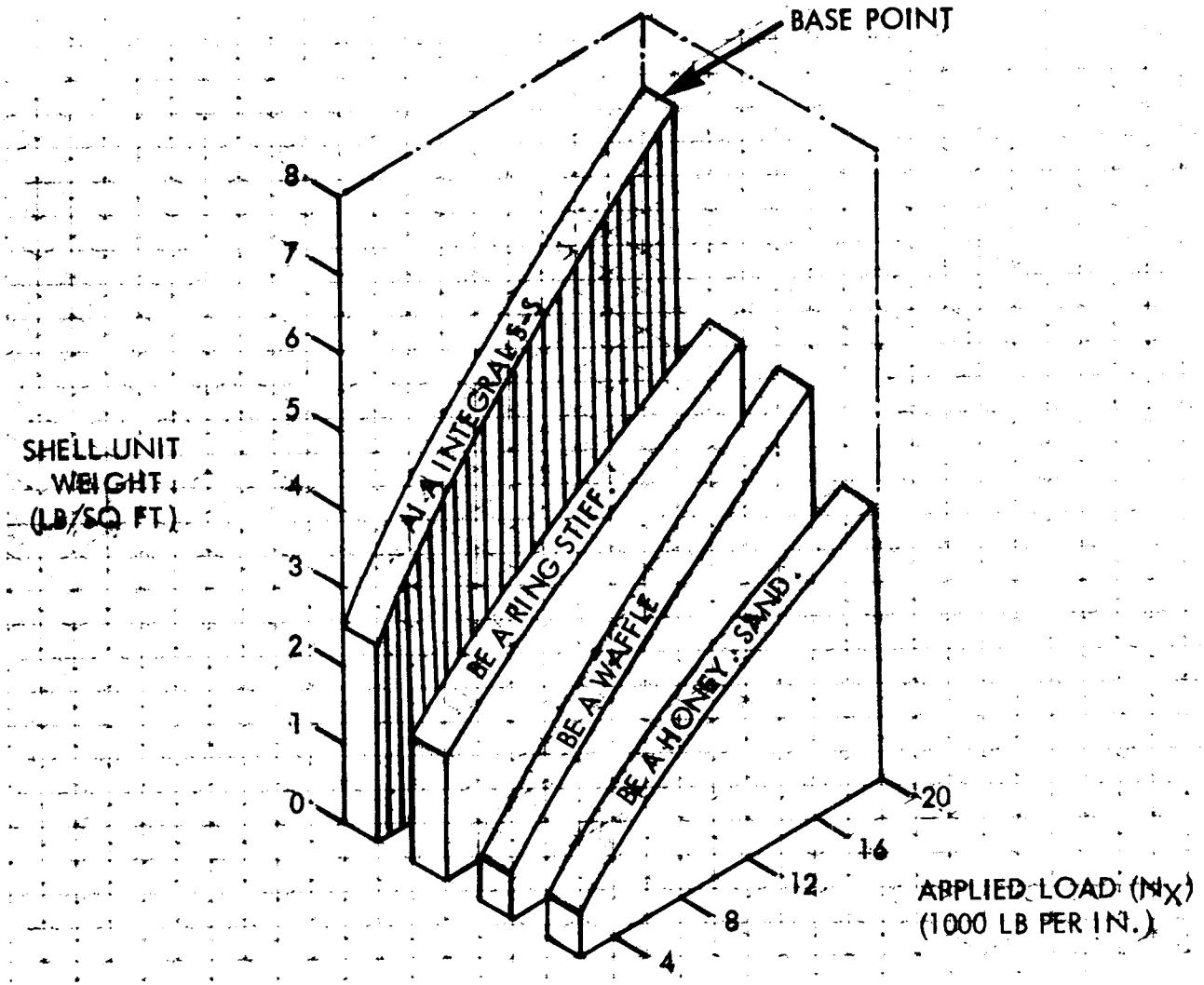

Figure 51. - Shell Unit Weights for Conventional Beryllium Structures — 130-Inch Radius, 300°F, No Pressure

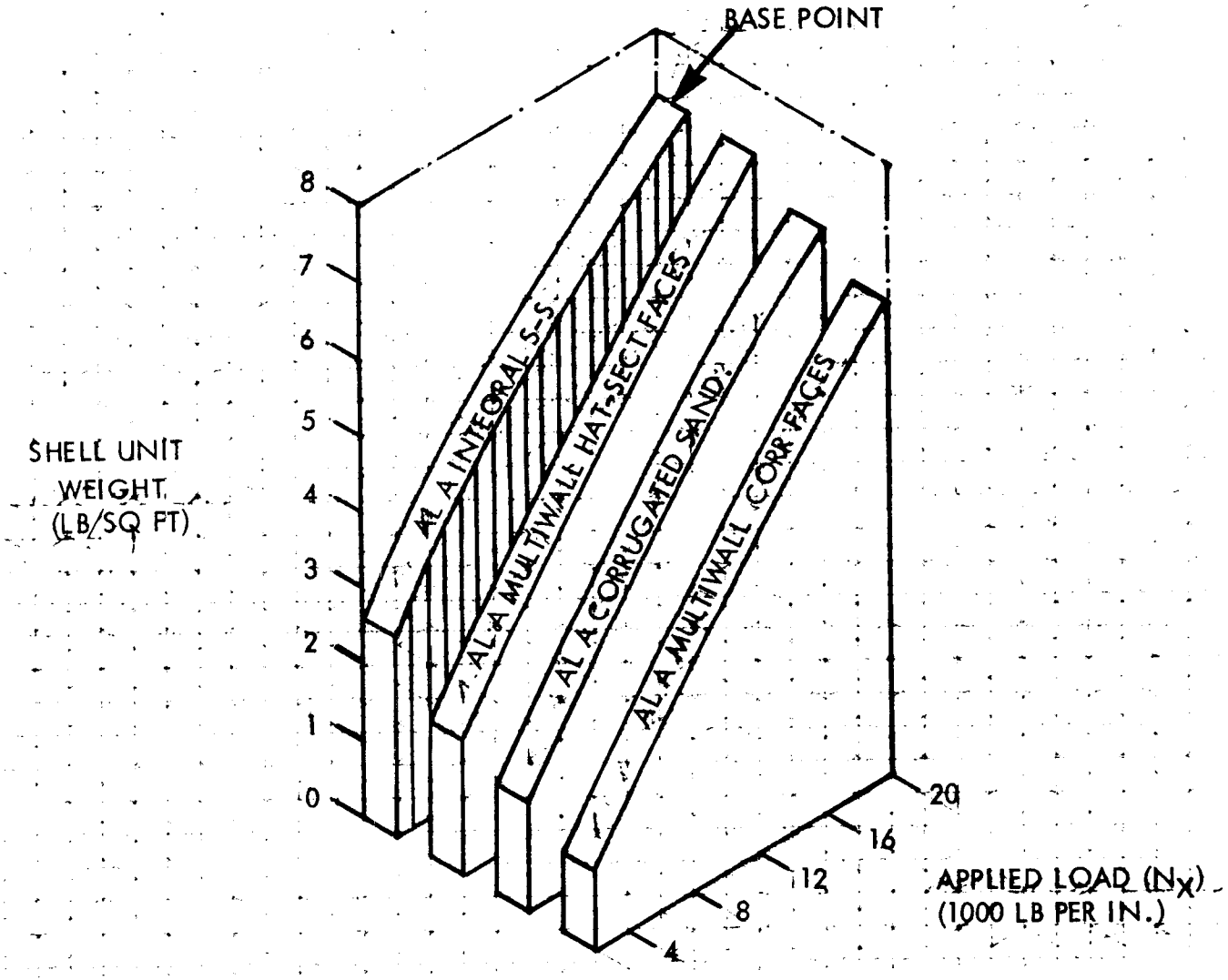

Figure 52. - Shell Unit Weights for Advanced Aluminum Structures—
130-Inch Radius, 300°F, No Pressure

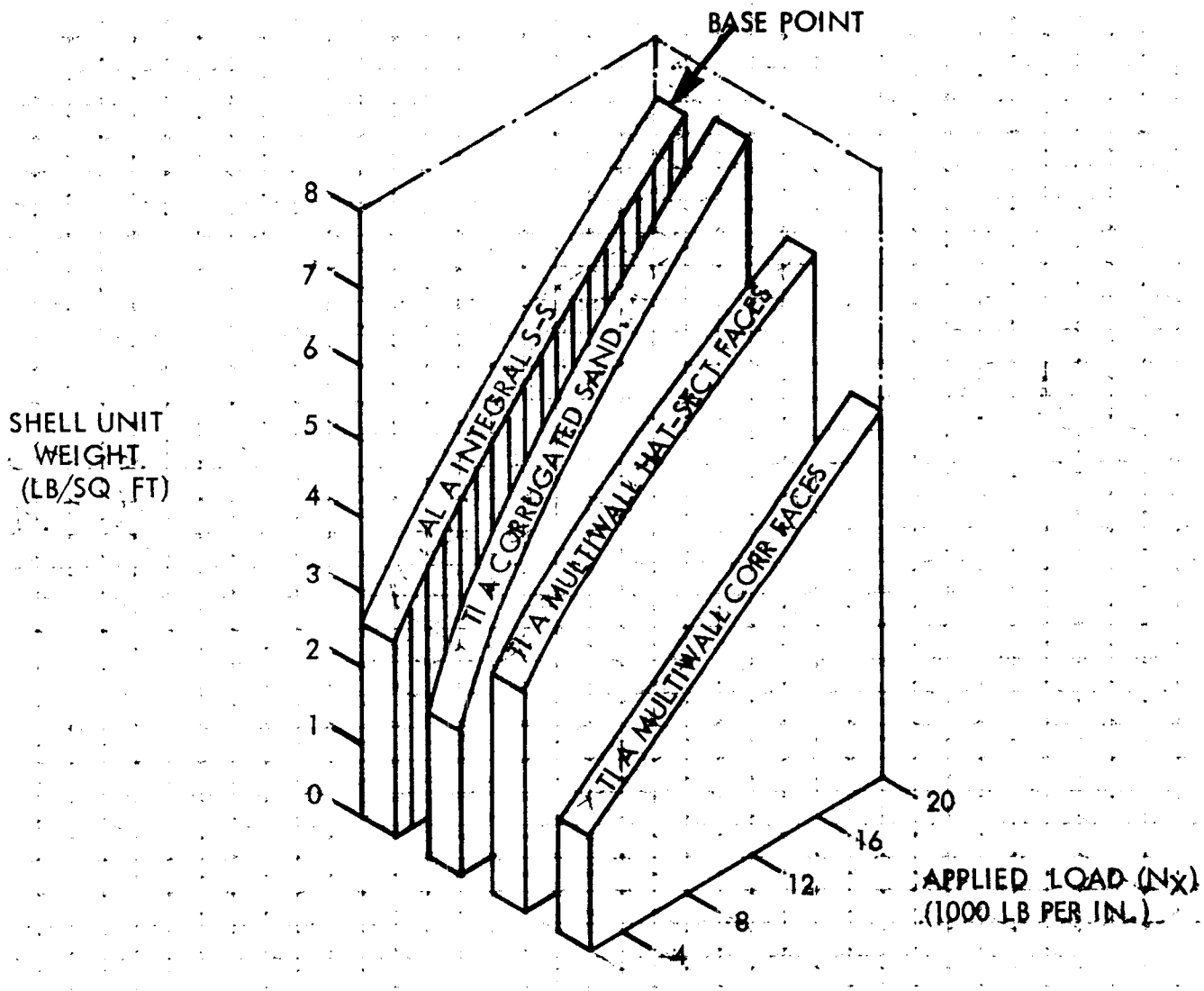

Figure 53. - Shell Unit Weights for Advanced Titanium Structures— 130-Inch Radius, 300°F, No Pressure

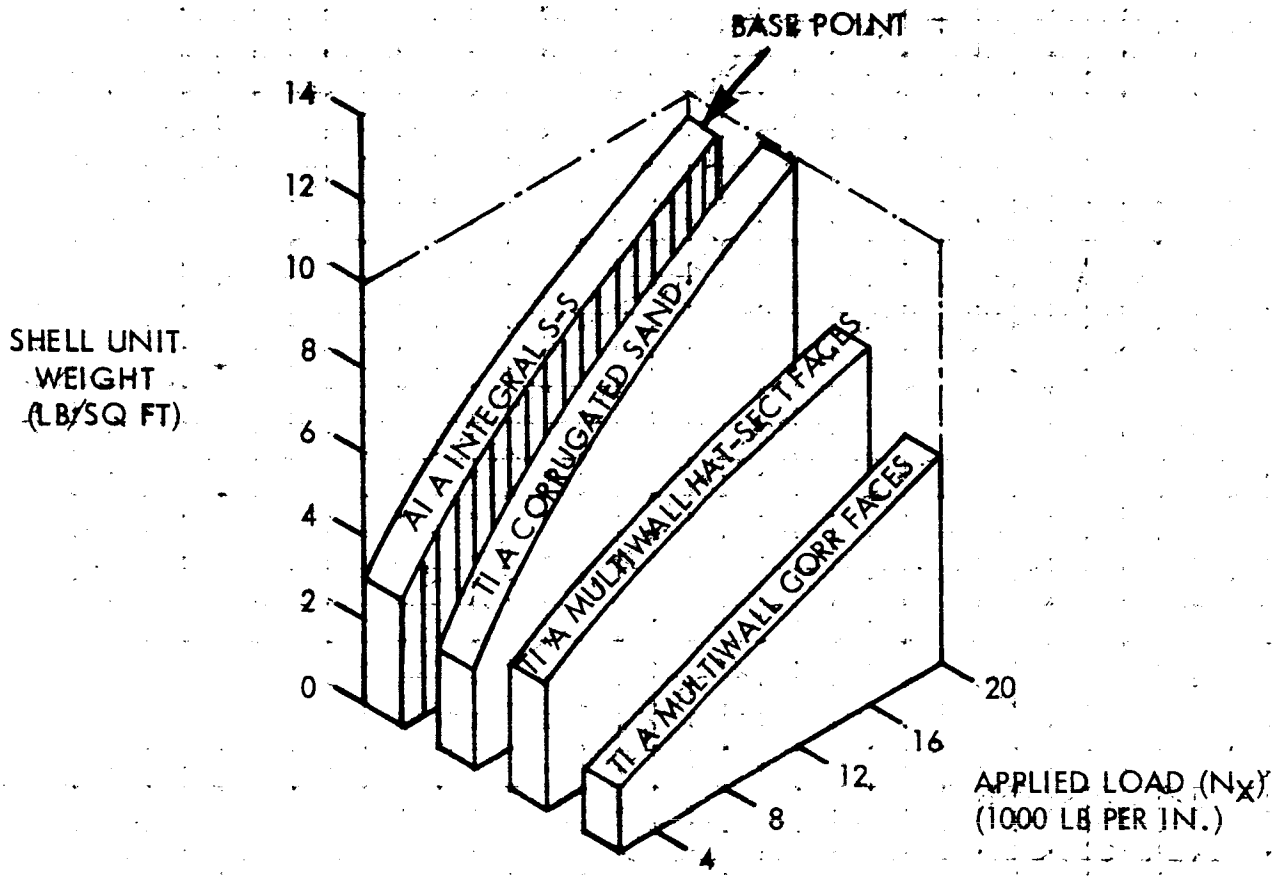

Figure 54. - Shell Unit Weight for Advanced Titanium Structures — 270-Inch Radius, 300°F, No Pressure

TABLE 7. - STRUCTURAL COMPONENTS AND THEIR DESIGN APPLIED LOAD, N_x

Structural Component / Vehicle Payload Class / Sizing Parameter (I_{sp}, thrust)	Medium Range		Saturn		Post-Saturn	
	Current	1985	Current	1985	Current	1985
Stage I						
Interstage	2 885	3 273	7 965	8 685	20 120	23 100
Forward skirt	2 905	3 340	8 005	8 730	20 210	26 000
Forward tank wall	1 950	2 700	7 400	8 100	17 180	22 160
Center section	2 100	2 950	8 365	9 115	17 500	23 500
Aft tank wall			9 760	9 745	18 500	22 500
Aft skirt	1 800	2 285	6 965	7 535	9 300	17 500
Stage II						
Forward skirt	1 245	1 530	2 750	2 895	4 355	6 510
Forward tank wall	1 295	1 650	3 070	3 255	5 535	7 240
Aft tank wall	1 650	1 950	6 300	6 780	8 640	9 635
Aft skirt	2 180	3 170	6 765	8 650	18 150	22 800

Note: Values in right-hand columns give component ultimate design loads, N_x, in pounds per inch.

The multiwall construction with corrugated face sheets offers the lightest weight advantage in aluminum (fig. 52), rather than titanium (fig. 53). Figures 51, 52 and 53 are for the 130-inch radius vehicle. Comparing figure 54 (270 in radius) with figure 53, it can be seen that, although the magnitude of the weight values are altered, no relative change is made in position of the constructions. From a purely weight-loading standpoint, the advanced structures appear desirable, but they are not competitive, weightwise, with the more conventional types of construction utilizing beryllium.

The structural designs, vehicle geometry, and design loads are reflected in the component weight summaries shown in tables 8 through 13 for the six basepoint vehicles. Computer printouts for these weights, along with payload and weight changes and cost ratios are contained in Appendix D to this report. The multiwall corrugated unpressurized shells offer a distinct weight advantage in all but the lightly loaded upper stage of the 30 000-pound payload vehicle. Honeycomb sandwich offers a weight advantage when used for pressurized structure; for the smaller stages (tables 8 and 9), this is not so pronounced. The bulkhead weights illustrated in tables 8 through 13 reflect change of material for an ellipsoidal bulkhead configuration.

In the small payload vehicles (tables 8 and 9) with lightly loaded shells, the waffle constructions appear lighter than the integral skin-stringer constructions. This will not always be the case, and it resulted from the assumed manufacturing constraints and limitations imposed on both the basepoint construction and the waffle construction. The eight-inch and five-inch stringer pitches for the basepoint stages one and two, respectively, and the integral skin-stringer height restriction of two inches tended to favor the waffle construction. This situation would change if these constraints were removed. Tables 8 through 13 provide a means of comparing the relative weights of the major structural components for the six baseline vehicles with various representative structural concepts and materials. These comparisons can be made relative to the basepoint design or with all the other designs shown to define their relative weight ordering as applied to each structural component.

Table 14 summarizes some weight reductions with an improvement of ten percent in material properties for the loading indices covering the base point vehicles. Weight reductions quoted in table 14 are percentages from base point materials with current strength properties. The concepts shown appear to be the only construction that can benefit from improvement in the material properties. Other designs—waffle, integral stringer, etc., are designed by instability modes that do not allow the structural elements to work up to their strength capabilities.

TABLE 8. - COMPONENT WEIGHT SUMMARY (LB), 30 000-LB PAYLOAD EXPENDABLE VEHICLE, CURRENT I_{sp}

Component	Aluminum A										Honeycomb Sandwich			
	Integral Skin Stringer	Waffle	Hat-Sect. Skin Stringer	Monocoque	Ring Stiffened	Honeycomb Sandwich	Corrugated Sandwich	Multiwall Corrugated	Double-Wall Hat Section	Double-Wall Z Section	Aluminum B	Aluminum C	Titanium A	Beryllium A
Stage I														
Interstage	1 505	1 231	1 480	3 012	2 442	621	852	603	1 166	1 278	621	580	598	301
Forward skirt	1 458	1 169	1 428	2 869	2 341	593	811	570	1 116	1 220	558	535	570	293
Forward tankwall	1 395	1 159	1 287	2 708	2 097	1 260	1 158	1 380	1 136	1 251	1 235	1 158	1 054	283
Center section	3 116	2 646	3 023	6 718	5 099	1 272	1 745	1 322	2 432	2 670	1 243	1 190	1 243	700
Aft tankwall	63	53	57	128	92	57	47	50	47	53	55	52	47	18
Aft skirt	1 434	1 220	1 374	2 965	2 251	693	757	613	1 130	1 242	586	522	538	298
Forward bulkhead	700	–	–	–	–	–	–	–	–	–	657	617	628	573
Internal bulkhead	1 595	–	–	–	–	–	–	–	–	–	1 495	1 405	1 429	1 304
Internal aft bulkhead	700	–	–	–	–	–	–	–	–	–	657	617	628	573
Aft bulkhead	1 598	–	–	–	–	–	–	–	–	–	1 499	1 410	1 434	1 307
Stage II														
Forward skirt	752	732	701	1 810	1 315	370	582	396	791	868	365	360	383	229
Forward tankwall	3 882	2 994	1 876	6 832	4 690	3 212	2 660	4 182	2 530	3 390	3 407	3 006	2 765	786
Aft tankwall	103	86	78	193	139	89	76	111	74	89	89	89	82	22
Aft skirt	808	790	728	1 947	1 521	400	544	408	732	796	397	348	329	160
Forward bulkhead	424	–	–	–	–	–	–	–	–	–	397	374	385	351
Internal bulkhead	764	–	–	–	–	–	–	–	–	–	716	674	692	632
Aft bulkhead	1 315	–	–	–	–	–	–	–	–	–	1 232	1 160	1 190	1 085

TABLE 9. - COMPONENT WEIGHT SUMMARY (LB), 100 000-LB PAYLOAD EXPENDABLE VEHICLE, 1985 I_{sp}

Component	Aluminum A										Honeycomb Sandwich			
	Integral Skin Stringer	Waffle	Hat-Sect. Skin Stringer	Monocoque	Ring Stiffened	Honeycomb Sandwich	Corrugated Sandwich	Multiwall Corrugated	Double-Wall Hat Section	Double-Wall Z Section	Aluminum B	Aluminum C	Titanium A	Beryllium A
Stage I														
Interstage	3 431	2 799	3 048	6 727	5 191	1 720	2 071	1 380	2 655	2 708	1 540	1 465	1 529	811
Forward skirt	2 840	2 361	1 262	5 530	4 317	1 297	1 681	1 076	2 267	2 306	1 201	1 124	1 201	665
Forward tankwall	2 476	1 937	2 106	4 293	3 329	1 559	1 776	1 908	2 420	2 498	1 466	1 396	1 458	1 152
Center section	6 079	5 078	5 525	11 858	9 368	2 828	3 689	2 398	4 878	4 960	2 644	2 480	2 623	1 502
Aft tankwall	–	–	–	–	–	–	–	–	–	–	–	–	–	–
Aft skirt	2 810	2 274	2 539	5 440	4 225	1 269	1 664	1 125	2 159	2 195	1 215	1 143	1 206	714
Forward bulkhead	1 319	–	–	–	–	–	–	–	–	–	1 237	1 164	1 183	1 078
Internal bulkhead	3 109	–	–	–	–	–	–	–	–	–	2 916	2 742	2 790	2 542
Internal aft bulkhead	1 319	–	–	–	–	–	–	–	–	–	1 237	1 164	1 183	1 078
Aft bulkhead	3 119	–	–	–	–	–	–	–	–	–	2 925	2 752	2 798	2 551
Stage II														
Forward skirt	1 302	1 383	543	3 510	2 580	558	824	690	1 317	1 352	614	565	607	384
Forward tankwall	7 793	6 449	6 300	15 380	11 550	5 842	6 664	6 792	8 394	8 650	5 651	5 461	5 588	3 230
Aft tankwall	618	528	518	1 244	968	460	532	608	766	791	445	430	440	369
Aft skirt	1 427	1 349	1 199	3 232	2 518	781	943	684	1 254	1 285	709	668	698	418
Forward bulkhead	700	–	–	–	–	–	–	–	–	–	657	617	628	573
Internal bulkhead	1 260	–	–	–	–	–	–	–	–	–	1 183	1 111	1 140	1 040
Aft bulkhead	2 387	–	–	–	–	–	–	–	–	–	2 239	2 106	2 142	1 953

TABLE 10. - COMPONENT WEIGHT SUMMARY (LB), 240 000-LB PAYLOAD EXPENDABLE VEHICLE, CURRENT I_{sp}

Component	Aluminum A										Honeycomb Sandwich			
	Integral Skin Stringer	Waffle	Hat-Sect. Skin Stringer	Monocoque	Ring Stiffened	Honeycomb Sandwich	Corrugated Sandwich	Multiwall Corrugated	Double-Wall Hat Section	Double-Wall Z Section	Aluminum B	Aluminum C	Titanium A	Beryllium A
Stage I														
Interstage	10 688	10 665	9 370	24 234	17 711	6 372	7 605	5 785	8 091	8 131	5 987	5 664	5 886	3 665
Forward skirt	6 638	6 760	5 801	15 031	11 002	3 940	4 714	3 566	5 088	5 113	3 704	3 504	3 641	2 018
Forward tankwall	19 625	19 652	17 257	43 574	32 285	11 287	15 063	15 406	13 919	14 109	10 487	9 838	12 279	8 811
Center section	14 384	14 619	12 613	32 207	23 343	8 640	10 273	7 586	11 116	11 274	8 113	7 665	7 955	4 424
Aft tankwall	9 029	9 370	8 004	19 538	13 179	4 873	6 687	6 288	6 472	6 534	4 550	4 274	5 258	3 615
Aft skirt	6 668	6 662	5 835	15 012	12 316	3 778	4 679	3 374	4 974	5 042	3 563	3 388	3 536	1 136
Forward bulkhead	2 474	–	–	–	–	–	–	–	–	–	2 320	2 183	1 181	2 041
Internal bulkhead	7 473	–	–	–	–	–	–	–	–	–	7 004	6 595	6 765	6 166
Internal aft bulkhead	2 474	–	–	–	–	–	–	–	–	–	2 320	2 183	1 181	2 041
Aft bulkhead	7 355	–	–	–	–	–	–	–	–	–	6 907	6 490	6 658	6 069
Stage II														
Forward skirt	5 017	5 530	4 326	12 978	11 570	2 372	3 344	3 147	4 840	4 928	2 285	2 197	2 337	1 261
Forward tankwall	24 041	26 738	20 998	61 896	48 029	22 795	26 172	32 512	22 758	23 165	21 023	19 492	23 922	17 878
Aft tankwall	874	951	794	2 131	1 599	626	777	813	727	737	578	544	630	460
Aft skirt	5 703	6 065	5 128	13 791	11 483	3 435	4 324	3 038	4 727	4 790	3 235	3 073	3 210	1 768
Forward bulkhead	2 474	–	–	–	–	–	–	–	–	–	2 320	2 183	1 181	2 041
Internal bulkhead	4 453	–	–	–	–	–	–	–	–	–	4 176	3 929	2 125	3 670
Aft bulkhead	10 887	–	–	–	–	–	–	–	–	–	10 224	9 606	9 855	8 983

TABLE 11. - COMPONENT WEIGHT SUMMARY (LB), 445 000-LB PAYLOAD EXPENDABLE VEHICLE, 1985 I_{sp}

Component	Aluminum A										Honeycomb Sandwich			
	Integral Skin Stringer	Waffle	Hat-Sect. Skin Stringer	Monocoque	Ring Stiffened	Honeycomb Sandwich	Corrugated Sandwich	Multiwall Corrugated	Double-Wall Hat Section	Double-Wall Z Section	Aluminum B	Aluminum C	Titanium A	Beryllium A
Stage I														
Interstage	12 975	13 512	11 472	28 952	20 374	8 096	9 430	7 562	10 008	10 119	7 606	7 184	7 451	4 709
Forward skirt	7 187	7 594	6 414	16 251	11 357	4 497	5 236	4 189	5 605	5 667	4 226	3 991	4 139	2 320
Forward tankwall	24 983	25 695	22 289	55 962	39 452	13 830	18 678	18 144	18 678	19 345	12 541	11 785	14 809	10 411
Center section	15 384	15 964	13 720	34 614	24 167	9 764	11 278	9 033	11 904	12 009	9 137	8 615	8 928	4 996
Aft tankwall	12 283	13 795	10 958	27 645	18 831	6 606	9 141	8 497	8 829	8 933	6 170	5 962	7 063	4 906
Aft skirt	7 142	7 747	6 275	16 216	12 050	4 228	5 078	4 613	5 783	5 849	4 015	3 802	3 948	2 192
Forward bulkhead	2 474	–	–	–	–	–	–	–	–	–	2 320	2 183	1 181	2 041
Internal bulkhead	7 852	–	–	–	–	–	–	–	–	–	7 359	6 929	7 108	6 479
Internal aft bulkhead	2 474	–	–	–	–	–	–	–	–	–	2 320	2 183	1 181	2 041
Aft bulkhead	7 690	–	–	–	–	–	–	–	–	–	7 222	6 785	6 961	6 345
Stage II														
Forward skirt	5 197	5 761	4 558	13 421	11 817	2 516	3 538	2 224	4 991	5 166	2 447	2 360	2 499	1 166
Forward tankwall	28 726	34 077	25 570	72 858	56 044	25 567	32 703	36 337	27 707	28 343	23 586	21 966	26 917	20 165
Aft tankwall	2 481	2 674	2 265	5 990	4 409	1 563	2 050	2 129	1 998	2 035	1 532	1 386	1 672	1 204
Aft skirt	5 973	6 181	5 502	14 505	11 327	3 767	4 568	3 441	5 096	5 156	3 576	3 386	3 517	1 948
Forward bulkhead	2 474	–	–	–	–	–	–	–	–	–	2 320	2 183	1 181	2 041
Internal bulkhead	4 453	–	–	–	–	–	–	–	–	–	4 176	3 929	2 125	3 670
Aft bulkhead	11 296	–	–	–	–	–	–	–	–	–	10 608	9 967	10 226	9 320

TABLE 12. - COMPONENT WEIGHT SUMMARY (LB), 1 000 000-LB PAYLOAD EXPENDABLE VEHICLE, CURRENT I_{sp}

	Aluminum A										Honeycomb Sandwich			
											Aluminum			
Component	Integral Skin Stringer	Waffle	Hat-Sect. Skin Stringer	Monocoque	Ring Stiffened	Honeycomb Sandwich	Corrugated Sandwich	Multiwall Corrugated	Double-Wall Hat Section	Double-Wall Z Section	B	C	Titanium A	Beryllium A
Stage I														
Interstage	67 608	58 202	55 975	132 057	85 177	44 741	47 950	33 117	45 589	45 891	41 835	38 808	40 019	23 335
Forward skirt	33 230	29 003	27 110	64 980	43 944	21 033	22 786	16 119	21 252	21 440	20 876	19 437	19 718	10 991
Forward tankwall	74 156	64 014	58 251	145 814	86 310	37 478	46 813	41 459	37 684	37 821	35 762	34 114	40 635	25 920
Center section	71 023	62 609	56 435	139 990	92 427	45 026	49 051	33 633	45 299	45 766	41 888	39 432	41 478	21 665
Aft tankwall	31 714	28 358	24 829	61 812	39 523	16 593	20 909	18 607	16 145	16 273	15 634	14 771	18 671	11 780
Aft skirt	33 555	34 092	41 039	68 643	44 769	18 674	22 558	13 104	15 304	15 491	17 176	15 023	16 755	9 194
Forward bulkhead	10 444	–	–	–	–	–	–	–	–	–	9 792	9 216	9 454	8 618
Internal bulkhead	36 978	–	–	–	–	–	–	–	–	–	34 662	32 626	33 466	30 505
Internal aft bulkhead	10 444	–	–	–	–	–	–	–	–	–	9 792	9 216	9 454	8 618
Aft bulkhead	36 396	–	–	–	–	–	–	–	–	–	34 123	32 114	32 942	30 029
Stage II														
Forward skirt	15 286	20 093	13 702	26 431	27 332	10 342	10 960	5 648	10 025	10 212	7 933	7 303	7 822	3 850
Forward tankwall	102 531	66 641	66 367	155 759	107 270	54 303	64 773	77 418	34 845	35 548	44 557	37 595	47 759	42 957
Aft tankwall	16 703	12 232	10 050	33 056	19 858	8 340	10 740	11 493	6 971	7 076	7 676	7 282	7 842	6 633
Aft skirt	19 979	20 655	18 537	47 170	29 429	15 698	17 057	11 712	16 145	16 384	14 815	13 717	14 147	8 112
Forward bulkhead	6 274	–	–	–	–	–	–	–	–	–	5 882	5 536	5 680	5 177
Internal bulkhead	11 292	–	–	–	–	–	–	–	–	–	10 586	9 964	10 214	9 311
Aft bulkhead	40 930	–	–	–	–	–	–	–	–	–	38 370	36 117	37 043	33 767

TABLE 13. - COMPONENT WEIGHT SUMMARY (LB), 2 000 000-LB PAYLOAD EXPENDABLE VEHICLE, 1985 I_{sp}

	Aluminum A										Honeycomb Sandwich			
											Aluminum			
Component	Integral Skin Stringer	Waffle	Hat-Sect. Skin Stringer	Monocoque	Ring Stiffened	Honeycomb Sandwich	Corrugated Sandwich	Multiwall Corrugated	Double-Wall Hat Section	Double-Wall Z Section	B	C	Titanium A	Beryllium A
Stage I														
Interstage	100 241	81 921	84 941	198 538	121 028	70 142	72 663	50 990	58 298	70 730	65 354	61 490	62 162	40 956
Forward skirt	40 906	33 517	34 644	82 237	49 197	28 742	29 818	20 859	23 971	29 476	27 732	26 057	26 262	16 776
Forward tankwall	107 677	90 390	85 542	209 616	119 572	63 607	75 043	59 070	62 284	66 820	61 433	58 692	69 089	45 022
Center section	83 816	68 854	71 422	168 763	97 119	59 829	61 576	43 474	49 485	61 576	57 243	54 167	54 587	34 931
Aft tankwall	51 158	43 182	40 703	99 505	58 354	30 347	35 727	28 151	30 123	33 082	29 496	28 241	33 306	23 361
Aft skirt	39 350	31 662	32 761	78 669	45 381	28 864	27 920	19 703	22 046	27 095	23 828	23 696	23 828	15 150
Forward bulkhead	10 841	–	–	–	–	–	–	–	–	–	10 163	9 567	9 813	8 947
Internal bulkhead	41 586	–	–	–	–	–	–	–	–	–	38 986	36 693	37 636	34 311
Internal aft bulkhead	10 841	–	–	–	–	–	–	–	–	–	10 163	9 567	9 813	8 947
Aft bulkhead	39 350	–	–	–	–	–	–	–	–	–	36 890	34 722	35 613	32 463
Stage II														
Forward skirt	16 604	16 662	14 727	41 110	25 098	9 213	12 287	6 469	9 817	10 889	8 762	8 536	8 794	4 985
Forward tankwall	176 547	123 599	117 346	316 835	186 647	90 363	112 546	126 556	68 676	72 351	74 430	62 822	80 348	71 612
Aft tankwall	39 380	29 761	26 939	69 020	44 171	19 386	25 682	26 549	16 479	18 454	17 954	17 046	18 336	15 558
Aft skirt	23 750	22 685	20 927	50 144	30 459	19 249	20 317	14 708	16 931	20 380	19 022	17 890	17 931	11 508
Forward bulkhead	6 274	–	–	–	–	–	–	–	–	–	5 882	5 536	5 680	5 177
Internal bulkhead	11 292	–	–	–	–	–	–	–	–	–	10 586	9 964	10 214	9 311
Aft bulkhead	23 750	–	–	–	–	–	–	–	–	–	22 264	20 957	21 494	19 594

TABLE 14. - WEIGHT REDUCTION WITH MATERIAL IMPROVEMENT

	Cylinder Radius, In.	130			198			270		
	Load Intensity, 10^{-3} lb/in.	5	10	20	5	10	20	5	10	20
Aluminum										
Pressure										
Honeycomb		7.3	6.9	6.9	8.1	7.4	7.4	8.1	7.6	7.5
Multiwall corrugated		6.0	5.6	5.1	6.2	5.6	5.5	6.5	6.3	5.4
Sandwich corrugated		4.2	.7	0	3.4	2.2	1.0	3.8	2.5	1.0
Skin stringer Z		6.6	8.1	.7	6.3	2.5	2.0	6.2	6.0	3.2
No pressure										
Honeycomb		6.9	7.4	7.9	5.8	7.0	7.6	5.6	6.4	7.3
Multiwall corrugated		7.9	7.1	7.5	6.3	5.7	5.8	6.7	7.1	7.0
Sandwich corrugated		.5	1.0	1.5	0	.5	1.4	0	0	1.0
Titanium										
Pressure										
Honeycomb		5.7	6.2	6.0	6.5	6.5	6.7	6.9	6.5	6.2
Multiwall corrugated		3.5	3.0	3.3	5.9	6.0	6.0	8.0	4.9	3.9
Sandwich corrugated		1.0	0.5	0	5.0	1.0	0	2.5	1.5	0
Skin stringer Z		0	0	0	0	0	0	6.9	4.5	0
No pressure										
Honeycomb		5.8	6.9	7.6	4.3	5.8	7.1	3.9	3.9	6.7
Multiwall corrugated		1.9	4.2	5.5	1.8	5.3	8.2	1.3	4.5	8.2
Sandwich corrugated		0	0	0	0	0	0	0	0	0
Skin stringer Z		0	0	1.6	0	0	2.0	0	0	2.8
Beryllium										
Pressure										
Honeycomb		5.6	8.0	9.4	6.8	6.8	7.1	6.8	6.3	7.1
Multiwall corrugated		6.8	3.8	0	6.4	4.3	0	7.0	5.5	5.9
Skin stringer Z		6.2	3.0	8.6	6.3	6.0	3.9	6.4	6.2	3.0
No pressure										
Honeycomb		7.8	8.2	8.4	6.8	8.0	8.0	6.5	6.7	8.3
Multiwall corrugated		6.4	6.8	7.6	6.3	7.5	8.5	7.2	7.4	7.8
Skin stringer Z		0	5.1	6.8	0	3.7	8.2	0	4.0	7.5

Note: Material improvement is 10 percent.
Values quoted are in percent of weight reduction.
Pressure = 50 psi burst pressure.

Table 14 constructions employ skins which are worked to a high stress level thereby taking advantage of material improvements. Here again, honeycomb sandwich offers the greatest weight saving potential with material improvement in the smaller radii, lower loaded vehicles. The multiwall corrugated sandwich with improved material appears desirable in the large-radius low-load components, this being more pronounced where the structure is not pressure-relieved.

Tables 15 through 21 present summaries of the payload changes resulting from substitution of materials and constructions in the six basepoint vehicles. These data are summarized from the assessment computer printouts contained in Appendix D. Lower stages reflect weight-change trends as modified by the payload exchange ratios as shown in table 22. Payload weight changes for the upper stages follow the same pattern as the component weight changes illustrated in tables 8 through 13, since the upper stage payload exchange ratio is 1.0.

For the 30 000-pound payload vehicle, nine percent of the affected weight saving in a component can be added as an equivalent payload gain. The payload exchange ratio, as described in reference 16, results from the stage proportions in the total vehicle stack and their velocity characteristics, so that each case must be treated separately.

First-stage payload weight changes substantiate the findings previously mentioned. In the current material and conventional constructions, the use of monocoque or ring-stiffened construction appears to be quite inefficient; waffle construction looks interesting in the small payload vehicles (tables 15 and 16), hat-section skin-stringer, is more efficient than the integral skin-stringer, and honeycomb sandwich offers a good payload advantage in most components. The advanced constructions appear to offer some advantages in specific components with high loading environments.

A more obvious effect can be traced in tables 15 through 20 concerning the second stage because of the much more significant payload exchange ratio. In the 240 000-pound payload vehicle, for example (table 17), multiwall corrugated sandwich looks attractive for unpressurized shells, but poor for use in pressurized structures. This application should be investigated further, especially for space-vehicle applications. The monocoque and ring-stiffened constructions were included in the design synthesis considerations to investigate the anticipated weight penalties and performance degradation for a range of vehicles. Although these latter concepts are obviously heavier, the attractive features are ease of fabrication and, possibly, lower cost. Furthermore, in special situations where an extremely "tight" schedule exists and where the weight penalty is acceptable from a performance standpoint, these simple constructions may warrant serious consideration. The tables 15

TABLE 15. - PAYLOAD WEIGHT CHANGE SUMMARY (CHANGE FROM ALUMINUM A INTEGRAL SKIN STRINGER BASEPOINT) 30 000-POUND PAYLOAD, EXPENDABLE VEHICLE, CURRENT I_{sp}

Component	Aluminum A									Honeycomb Sandwich			
	Waffle	Hat-Section Skin Stringer	Monocoque	Ring Stiffened	Honeycomb Sandwich	Corrugated Sandwich	Multi-Wall Corrugated	Double-Wall Hat-Sect. Skin-Stringer Faces	Double-Wall Z-Sect. Skin-Stringer Faces	Aluminum B	Aluminum C	Titanium A	Beryllium A
Stage I													
Interstage	25	2	-136	-84	80	59	81	31	20	80	83	82	108
Forward skirt	26	3	-127	-80	78	58	80	31	21	81	83	80	105
Forward tankwall	21	10	-118	-63	12	21	1	23	13	14	21	31	100
Center section	42	8	-324	-178	166	123	161	62	40	169	173	169	217
Aft tankwall	1	1	-6	-3	1	1	2	1	1	1	1	1	4
Aft skirt	19	5	-138	-73	67	61	74	27	17	76	82	81	102
Forward bulkhead	—	—	—	—	—	—	—	—	—	4	7	6	11
Internal bulkhead	—	—	—	—	—	—	—	—	—	9	17	15	26
Internal aft bulkhead	—	—	—	—	—	—	—	—	—	4	7	6	11
Aft bulkhead	—	—	—	—	—	—	—	—	—	9	17	15	26
Stage II													
Forward skirt	20	51	-1058	-563	382	170	356	—	—	392	387	369	523
Forward tankwall	888	2006	-2950	-808	670	1222	-300	1352	492	475	876	1117	3096
Aft tankwall	17	25	-90	-36	14	27	-8	29	14	14	14	21	81
Aft skirt	18	80	-1139	-713	408	264	400	76	12	411	460	479	648
Forward bulkhead	—	—	—	—	—	—	—	—	—	27	50	39	73
Internal bulkhead	—	—	—	—	—	—	—	—	—	48	90	72	132
Aft bulkhead	—	—	—	—	—	—	—	—	—	83	155	125	230

TABLE 16. - PAYLOAD WEIGHT CHANGE SUMMARY
(CHANGE FROM ALUMINUM A INTEGRAL SKIN STRINGER BASEPOINT)
100 000-POUND PAYLOAD, EXPENDABLE VEHICLE, 1985 I_{sp}

Component	Aluminum A									Honeycomb Sandwich			
	Waffle	Hat-Section Skin Stringer	Mono-coque	Ring-Stiffened	Honey-comb Sand-wich	Corru-gated Sand-wich	Multi-Wall Corru-gated	Double-Wall Hat-Sect. Skin-Stringer Faces	Double-Wall Z-Sect. Skin-Stringer Faces	Aluminum B	Aluminum C	Tita-nium A	Beryl-lium A
Stage I													
Interstage	76	46	-396	-211	205	163	246	93	87	227	236	228	314
Forward skirt	57	189	-323	-177	185	139	212	69	64	197	206	197	261
Forward tank wall	65	44	-218	-102	110	84	68	7	-3	121	130	122	159
Center section	120	66	-693	-395	390	287	442	144	134	412	432	415	549
Aft tank wall	—	—	—	—	—	—	—	—	—	—	—	—	—
Aft skirt	64	32	-316	-170	185	137	202	78	74	191	200	193	251
Forward bulkhead	—	—	—	—	—	—	—	—	—	10	19	16	29
Internal bulkhead	—	—	—	—	—	—	—	—	—	23	44	38	68
Internal aft bulkhead	—	—	—	—	—	—	—	—	—	10	19	16	29
Aft bulkhead	—	—	—	—	—	—	—	—	—	23	44	38	68
Stage II													
Forward skirt	-81	759	-2208	-1278	744	478	612	-15	-50	688	737	695	918
Forward tank wall	1344	1493	-7587	-3757	1951	1129	1001	-601	-857	2142	2332	2205	4563
Aft tank wall	90	100	-626	-350	158	86	10	-148	-173	173	188	178	249
Aft skirt	78	228	-1805	-1091	646	484	743	173	142	718	759	729	1009
Forward bulkhead	—	—	—	—	—	—	—	—	—	43	83	72	127
Internal bulkhead	—	—	—	—	—	—	—	—	—	77	149	120	220
Aft bulkhead	—	—	—	—	—	—	—	—	—	148	281	245	434

TABLE 17. - PAYLOAD WEIGHT CHANGE SUMMARY (CHANGE FROM ALUMINUM A INTEGRAL SKIN STRINGER BASEPOINT) 240 000-POUND PAYLOAD, EXPENDABLE VEHICLE, CURRENT I_{sp}

Component	Aluminum A									Honeycomb Sandwich			
	Waffle	Hat-Section Skin Stringer	Monocoque	Ring-Stiffened	Honeycomb Sandwich	Corrugated Sandwich	Multi-Wall Corrugated	Double-Wall Hat-Sect. Skin-Stringer Faces	Double-Wall Z-Sect. Skin Stringer Faces	Aluminum B	Aluminum C	Titanium A	Beryllium A
Stage I													
Interstage	3	145	-1 496	-772	475	339	539	286	281	517	553	528	773
Forward skirt	-13	92	-923	-480	297	212	338	171	168	323	345	330	508
Forward tank wall	-3	260	-2 634	-1 393	917	502	464	628	607	1 005	1 077	808	1 190
Center section	-26	195	-1 961	-985	632	452	748	359	342	690	739	707	1 096
Aft tank wall	-38	113	-1 156	-456	457	258	302	281	274	493	523	415	596
Aft skirt	1	92	-918	-621	318	219	362	186	179	342	361	345	609
Forward bulkhead	—	—	—	—	—	—	—	—	—	17	32	142	48
Internal bulkhead	—	—	—	—	—	—	—	—	—	52	97	78	144
Internal aft bulkhead	—	—	—	—	—	—	—	—	—	17	32	142	48
Aft bulkhead	—	—	—	—	—	—	—	—	—	49	95	77	142
Stage II													
Forward skirt	-513	691	-7 961	-6 553	2 645	1 673	2 870	177	89	2 732	2 820	2 680	3 756
Forward tank wall	-2 697	3 043	-37 855	-23 988	1 246	-2 131	-8 470	1 283	876	3 018	4 549	119	6 163
Aft tank wall	-77	80	-1 257	-725	248	97	61	147	137	296	330	244	414
Aft skirt	-362	575	-8 088	-5 780	2 268	1 379	2 665	976	913	2 468	2 630	2 493	3 935
Forward bulkhead	—	—	—	—	—	—	—	—	—	154	291	1 294	433
Internal bulkhead	—	—	—	—	—	—	—	—	—	277	524	2 328	783
Aft bulkhead	—	—	—	—	—	—	—	—	—	663	1 281	1 032	1 904

TABLE 18. - PAYLOAD WEIGHT CHANGE SUMMARY
(CHANGE FROM ALUMINUM A INTEGRAL SKIN STRINGER BASEPOINT)
445 000-POUND PAYLOAD, EXPENDABLE VEHICLE, 1985 I_{sp}

Component	Aluminum A									Honeycomb Sandwich			
	Waffle	Hat-Section Skin Stringer	Mono-coque	Ring-Stiffened	Honey-comb Sand-wich	Corru-gated Sand-wich	Multi-Wall Corru-gated	Double-Wall Hat-Sect. Skin-Stringer Faces	Double-Wall Z-Sect. Skin-Stringer Faces	Aluminum		Tita-nium	Beryl-lium
										B	C	A	A
Stage I													
Interstage	-81	225	-2 397	-1 110	732	532	812	445	428	805	869	829	1 240
Forward skirt	-61	116	-1 360	-625	404	293	450	237	228	444	479	457	730
Forward tank wall	-107	404	-4 647	-2 170	1 673	946	1 026	946	846	1 866	1 980	1 526	2 186
Center section	-87	250	-2 884	-1 317	843	616	953	522	506	937	1 015	968	1 558
Aft tank wall	-227	199	-2 304	-982	852	471	568	518	502	917	948	783	1 107
Aft skirt	-91	130	-1 361	-736	437	310	379	204	194	469	501	479	742
Forward bulkhead	—	—	—	—	—	—	—	—	—	23	44	194	65
Internal bulkhead	—	—	—	—	—	—	—	—	—	74	138	112	206
Internal aft bulkhead	—	—	—	—	—	—	—	—	—	23	44	194	65
Aft bulkhead	—	—	—	—	—	—	—	—	—	70	136	109	202
Stage II													
Forward skirt	-564	639	-8 224	-6 620	2 681	1 659	2 973	206	31	2 750	2 837	2 698	4 031
Forward tank wall	-5 351	3 156	-44 132	-27 318	3 159	-3 977	-7 611	1 019	383	5 140	6 760	1 809	8 561
Aft tank wall	-193	216	-3 509	-1 928	918	431	352	483	446	949	1 095	809	1 277
Aft skirt	-208	471	-8 532	-5 354	2 206	1 405	2 532	877	817	2 397	2 587	2 456	4 025
Forward bulkhead	—	—	—	—	—	—	—	—	—	154	291	1 293	433
Internal bulkhead	—	—	—	—	—	—	—	—	—	277	524	2 328	783
Aft bulkhead	—	—	—	—	—	—	—	—	—	688	1 329	1 070	1 976

TABLE 19. - PAYLOAD WEIGHT CHANGE SUMMARY
(CHANGE FROM ALUMINUM A INTEGRAL SKIN STRINGER BASEPOINT)
1 000 000-POUND PAYLOAD, EXPENDABLE VEHICLE, CURRENT I_{sp}

Component	Aluminum A									Honeycomb Sandwich			
	Waffle	Hat-Section Skin Stringer	Monocoque	Ring-Stiffened	Honeycomb Sandwich	Corrugated Sandwich	Multi-Wall Corrugated	Double-Wall Hat-Sect. Skin-Stringer Faces	Double-Wall Z-Sect. Skin-Stringer Faces	Aluminum B	Aluminum C	Titanium A	Beryllium A
Stage I													
Interstage	1 035	1 280	-7 089	-1 933	2 515	2 162	3 794	2 422	2 389	2 835	3 168	3 035	4 868
Forward skirt	465	673	-3 493	-1 179	1 342	1 149	1 882	1 318	1 297	1 359	1 517	1 486	2 446
Forward tank wall	1 116	1 750	-7 882	-1 337	4 035	3 008	3 597	4 012	3 997	4 223	4 405	3 687	5 306
Center section	926	1 605	-7 586	-2 354	2 860	2 417	4 113	2 830	2 777	3 205	3 475	3 250	5 429
Aft tank wall	369	757	-3 311	-859	1 663	1 189	1 442	1 713	1 698	1 769	1 864	1 435	2 193
Aft skirt	-59	-823	-3 860	-1 234	1 637	1 210	2 250	2 008	1 987	1 802	2 038	1 848	2 680
Forward bulkhead	—	—	—	—	—	—	—	—	—	72	135	109	201
Internal bulkhead	—	—	—	—	—	—	—	—	—	254	479	386	712
Internal aft bulkhead	—	—	—	—	—	—	—	—	—	72	135	109	201
Aft bulkhead	—	—	—	—	—	—	—	—	—	250	471	380	700
Stage II													
Forward skirt	-4 807	1 584	-11 145	-12 046	4 944	4 326	9 638	5 261	5 074	7 353	7 983	7 464	11 436
Forward tank wall	35 890	36 164	-53 228	-4 739	48 228	37 758	25 113	67 686	66 983	57 974	64 936	54 772	59 574
Aft tank wall	4 471	6 653	-16 353	-3 155	8 363	5 963	5 210	9 732	9 627	9 027	9 421	8 861	10 070
Aft skirt	-676	1 442	-27 191	-9 450	4 281	2 922	8 267	3 834	3 595	5 164	6 262	5 832	11 867
Forward bulkhead	—	—	—	—	—	—	—	—	—	392	738	594	1 097
Internal bulkhead	—	—	—	—	—	—	—	—	—	706	1 328	1 078	1 981
Aft bulkhead	—	—	—	—	—	—	—	—	—	2 560	4 813	3 887	7 163

TABLE 20. - PAYLOAD WEIGHT CHANGE SUMMARY
(CHANGE FROM ALUMINUM A INTEGRAL SKIN STRINGER BASEPOINT)
2 000 000-POUND PAYLOAD, EXPENDABLE VEHICLE, 1985 I_{sp}

Component	Aluminum A									Honeycomb Sandwich			
	Waffle	Hat-Section Skin Stringer	Monocoque	Ring-Stiffened	Honeycomb Sandwich	Corrugated Sandwich	Multi-Wall Corrugated	Double-Wall Hat-Sect. Skin-Stringer Faces	Double-Wall -Sect. Skin-Stringer Faces	Aluminum B	Aluminum C	Titanium A	Beryllium A
Stage I													
Interstage	2 382	1 989	-12 779	-2 701	3 913	3 585	6 403	5 453	3 836	4 535	5 038	4 950	7 707
Forward skirt	961	814	-5 373	1 078	1 584	1 441	2 606	2 202	1 486	1 713	1 930	1 904	3 137
Forward tank wall	2 247	2 877	-13 252	-1 546	5 729	4 242	6 319	5 901	5 311	6 012	6 368	5 016	8 145
Center section	1 945	1 611	-11 043	-1 729	3 118	2 891	5 244	4 463	2 891	3 455	3 854	3 800	6 355
Aft tank wall	1 037	1 359	-6 285	-936	2 705	2 006	2 991	2 735	2 350	2 816	2 979	2 321	3 614
Aft skirt	1 000	857	-5 112	-784	1 623	1 486	2 554	2 250	1 593	2 018	2 035	2 018	3 140
Forward bulkhead	—	—	—	—	—	—	—	—	—	88	166	134	246
Internal bulkhead	—	—	—	—	—	—	—	—	—	338	636	513	946
Internal aft bulkhead	—	—	—	—	—	—	—	—	—	88	166	134	246
Aft bulkhead	—	—	—	—	—	—	—	—	—	320	602	486	895
Stage II													
Forward skirt	-58	1 877	-24 506	-8 494	7 391	4 317	10 135	6 787	5 715	7 842	8 068	7 810	11 619
Forward tank wall	52 948	59 201	-140 288	-10 100	86 184	64 001	49 991	107 871	104 196	102 117	113 725	96 199	104 935
Aft tank wall	9 619	12 441	-29 640	-4 791	19 994	13 698	12 831	22 901	20 926	21 426	22 334	21 044	23 822
Aft skirt	1 065	2 823	-26 394	-6 709	4 501	3 433	9 042	6 819	3 370	4 728	5 860	5 819	12 242
Forward bulkhead	—	—	—	—	—	—	—	—	—	392	738	594	1 097
Internal bulkhead	—	—	—	—	—	—	—	—	—	706	1 328	1 078	1 981
Aft bulkhead	—	—	—	—	—	—	—	—	—	1 486	2 793	2 256	4 156

TABLE 21. - COST RATIO SUMMARY (DOLLARS PER POUND OF PAYLOAD GAINED) VALUES NORMALIZED BETWEEN PRESSURIZED AND UNPRESSURIZED SHELLS

		Aluminum A										Honeycomb Sandwich			
Vehicle / Payload	Stage	Integral Skin Stringer	Waffle	Hat-Section Skin Stringer	Monocoque	Ring Stiffened	Honeycomb Sandwich	Corrugated Sandwich	Multi-Wall Corrugated	Double-Wall Hat-Sect. Skin-Stringer Faces	Double-Wall Z-Sect. Skin-Stringer Faces	Aluminum B	Aluminum C	Titanium A	Beryllium A
30 000-pound payload	1	0	120	-4100	120*	220*	-15	25	45	160	234	-15	-13	900	900
	2	0	90	-170	12*	30*	-7	-12	-3	20	40	-8	-7	90	90
100 000-pound payload	1	0	80	-550	90*	170*	20	60	55	170	165	20	20	620	830
	2	0	20	-50	8*	20*	-6	3	10	40	27	-6	-6	90	120
240 000-pound payload	1	0	-1200**	-380	36*	75*	100	185	185	290	300	90	85	910	1120
	2	0	-25**	-65	5*	7*	10	0	3	80	100	7	5	135	250
445 000-pound payload	1	0	390*	-280	25*	60*	80	150	150	250	260	75	70	710	910
	2	0	-40**	-70	5*	7*	9	3	2	100	400	7	6	310	220
1 000 000-pound payload	1	0	-230**	-130	30*	130*	160	240	180	240	240	160	140	970	1180
	2	0	-55**	-40	6*	40*	20	30	25	30	30	14	12	110	140
2 000 000-pound payload	1	0	140	-120	20*	170*	180	240	170	200	280	160	150	1000	1300
	2	0	20	-25	3*	30*	30	30	24	24	35	20	16	125	165

Note: See Appendix D for additional details and for bulkhead ratios.
*Ratio results from dollar reduction, additional weight and payload loss.
**Ratio results from additional dollars, additional weight and payload loss.

TABLE 22. - FIRST STAGE WEIGHT CHANGE TRENDS

Vehicle Payload (lb)	Term	First-Stage Exchange Ratio
30 000	Current	0.09
100 000	1985	0.12
240 000	Current	0.11
445 000	1985	0.15
1 000 000	Current	0.11
2 000 000	1985	0.13

through 20 show the magnitude of payload reductions that could be anticipated for typical vehicle systems with these simple concepts.

From the standpoint of improved payload weight, it appears that a substitution of construction type is more beneficial than an improvement in a particular material property while keeping the same construction. For example, in the stage-one interstage (table 18) substituting honeycomb sandwich for integral skin-stringer adds 475 pounds to the payload. A 20 percent improvement in material property, for honeycomb sandwich, adds only 45 pounds, while a change to beryllium material, again for honeycomb sandwich, adds about 300 pounds. Comparing these changes to the overall payload weight, the 475-pound change is only 0.2 percent; the 45-pound change, 0.02 percent; and the 300-pound change, 0.12 percent. All of these changes can easily be lost within the accuracy of any analytical procedure. Consideration of these facts shows that, though meaningful, payload changes cannot be used as a final guide to deciding what improvement to put research dollars into.

Appendix D includes a series of computer printouts which contain a cost ratio. This cost ratio is in terms of dollars paid per pound of payload gained, and is relative to, and only to, the base point component. The cost ratios in the printouts can be ordered to select most likely candidates. But, since this ratio is a function of change in dollar cost, change in component weight, and change in payload, care must be exercised to recognize the sign convention of each parameter and the sign convention of the cost ratio itself. For example, a plus ratio is generally better than a negative ratio, unless it results from a combination of a dollar reduction, added component weight and a reduction in payload weight. A negative ratio should be discounted if it results from a combination of added cost, added weight, and payload loss.

Table 21 presents a summary of the cost ratio information shown in Appendix D. The cost ratio has been "normalized" for each stage by averaging values for components which display typical trends and does not include ratios for components where the component is extremely small and prejudices the ratio. Except for those values indicated (monocoque, ring-stiffened and some waffle cases) by asterisks on the table, all values may be scanned for the maximized negative value. From the ground rules considered in this study (material properties, design constraints, weight complexity factors, cost complexity factors, material costs, number of units manufactured, and time schedule), no material and construction combination appears to be more beneficial, cost-wise, than the aluminum hat-section skin-stringer. Also, if honeycomb sandwich is used, it appears to be more cost effective in the small vehicle class (30 000- and 100 000-pound payloads). Table 21 substantiates some previous decisions made for the Saturn V vehicle by NASA. Ratios displayed in table 21 for beryllium and titanium indicate that present manufacturing technology, again based upon the input ground rules clearly spelled out in this report, is not far enough advanced to make the use of either material cost effective from a general application viewpoint.

In order to provide a clearer understanding of the present problem and what must be done, the cost data from Appendix D are displayed in figures through in a slightly different fashion. In these figures weight, payload, and cost values are plotted for the following partials:

Alternate component weight versus base point component weight

Alternate component cost versus base point component cost

Payload weight gained versus base point component weight

The figures 55 through 58 are separated into four quadrants. Quadrant I is the most desirable, representing a weight decrease, payload gain, and reduced cost. Quadrant II is next in desirability, resulting from a weight decrease and a payload gain, but costing dollars to achieve. Quadrant III represents a reduced cost but with a gain in component weight and a decrease in payload. Quadrant IV represents weight increase, payload loss, and cost increase. Any partials falling within quadrant IV need no further justification. Values that fall in quadrants II and III have to be assessed individually to determine their relative effectiveness. This will be based upon the economic justification, i. e., How much is the payload worth? With this "worth index," the most beneficial material and construction arrangement can be ontained from these partials. The partials illustrated in figures 55 through 58 are limited to a particular stage of a base point vehicle to simplify presentation and to illustrate the basic conclusions that can be drawn from these base-points. In all figures the locus of 1.0, 1.0, 0.0 for weight, cost and payload

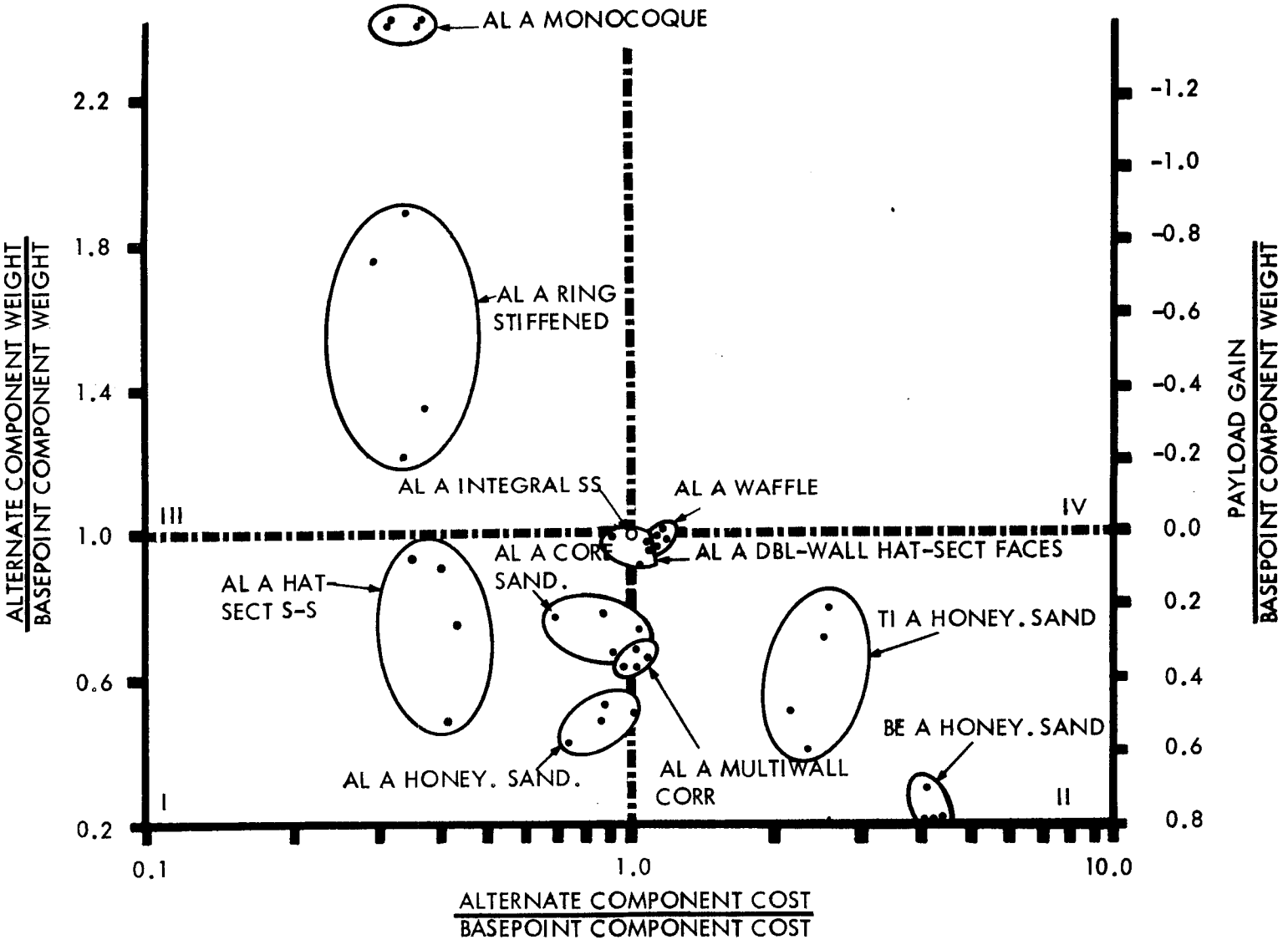

Figure 55. Merit Partials for 30 000-Pound-Payload Vehicle (Second Stage)

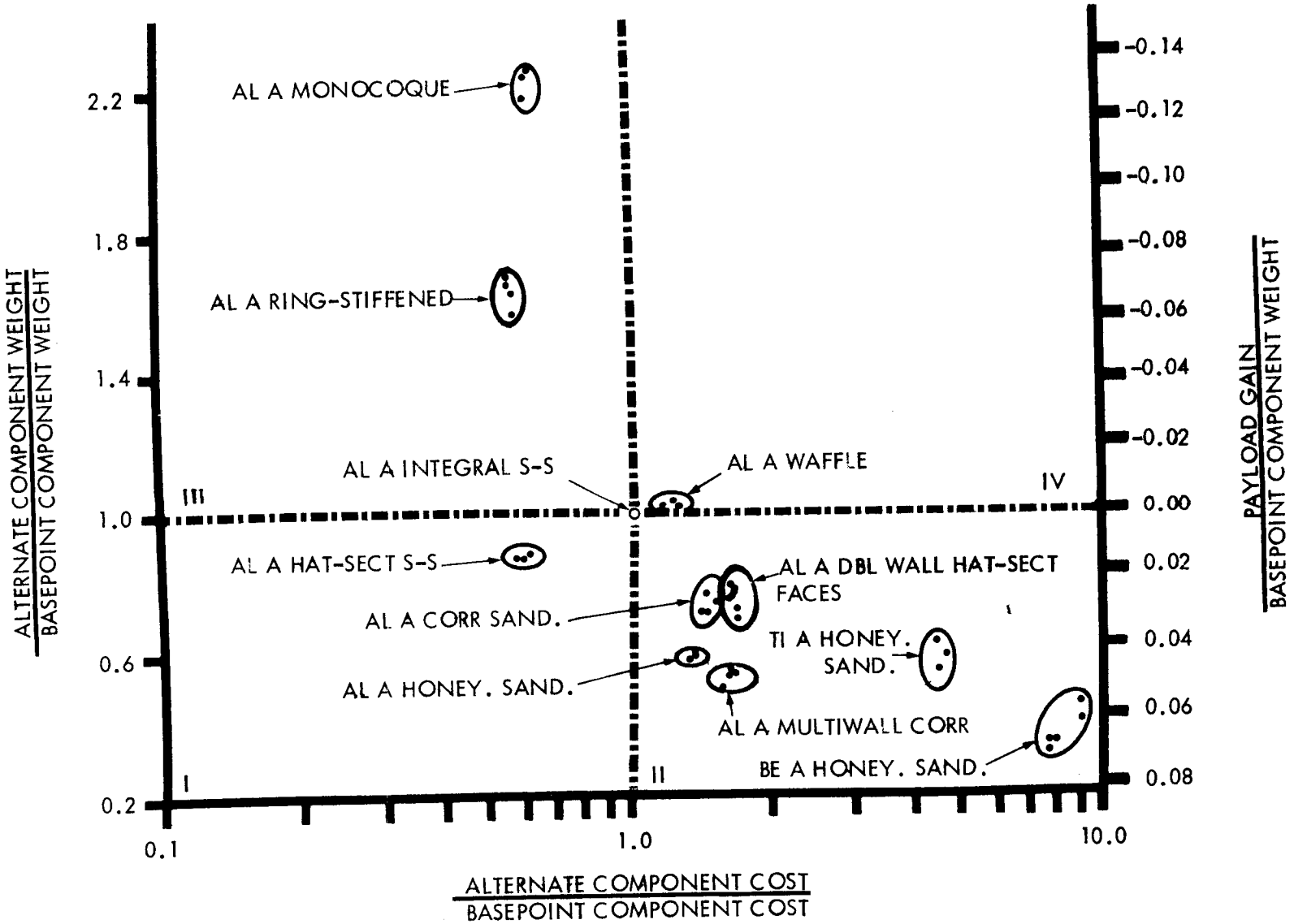

Figure 56. Merit Partials for 240 000-Pound-Payload Vehicle (First Stage)

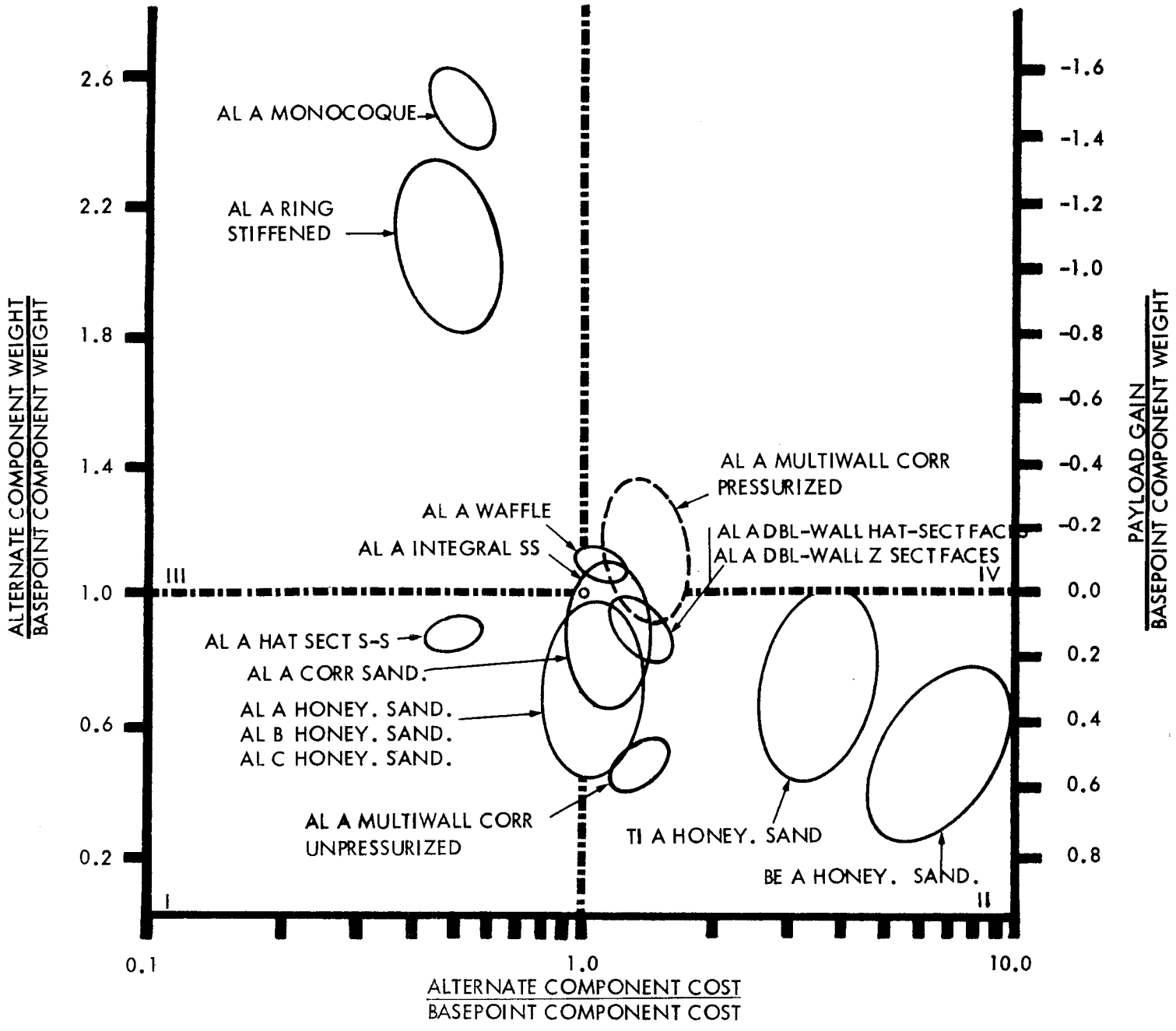

Figure 57. Merit Partials for 240 000-Pound-Payload Vehicle (Second Stage)

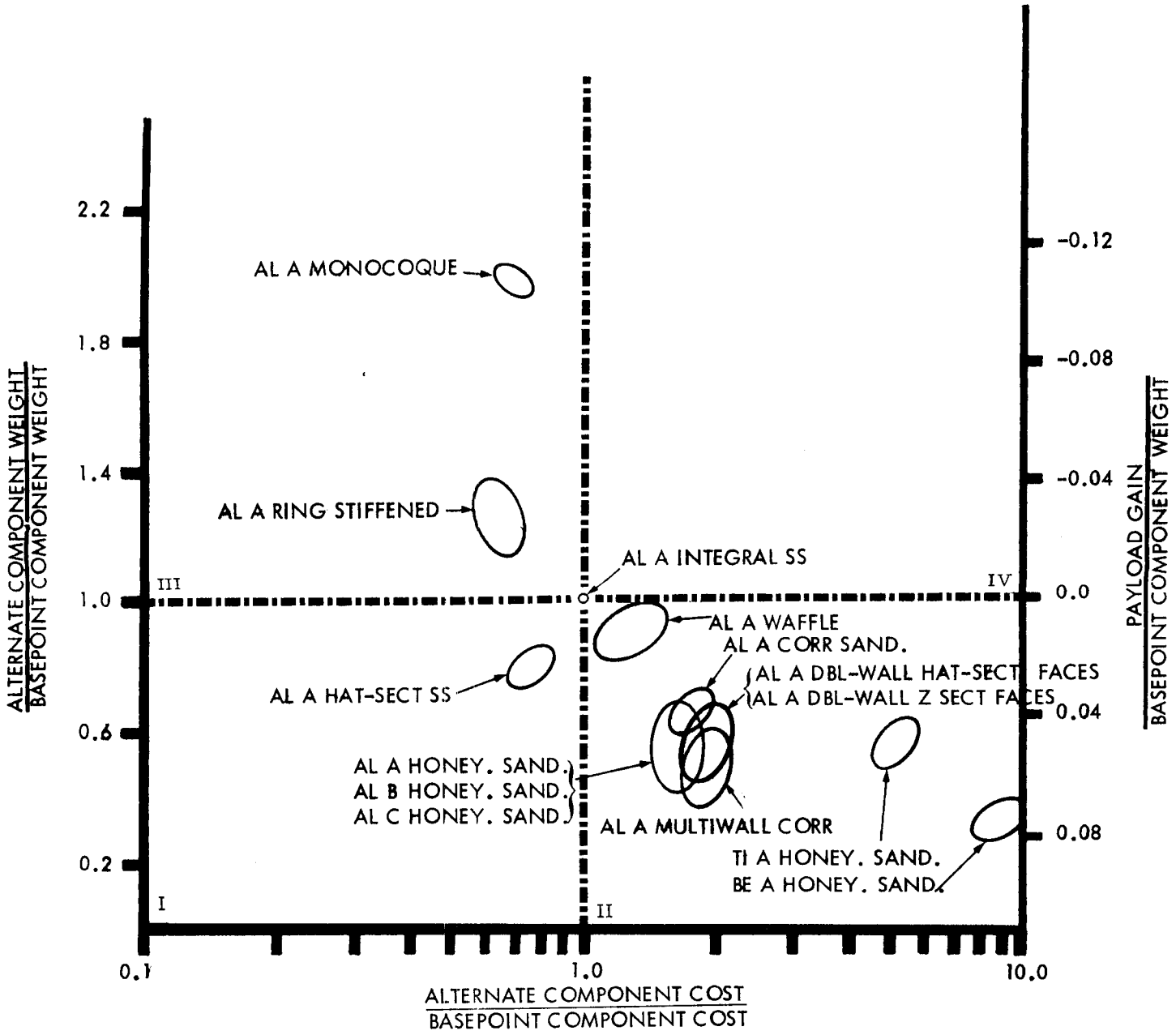

Figure 58. Merit Partials for 1 000 000-Pound-Payload Vehicle (First Stage)

partials, respectively, is the synthesized referenced basepoint. This does not mean that two material and constructions types other than the basepoint cannot be considered without the referenced basepoint, since all positions are relative and therefore comparitive.

Figure 55 shows partials for the upper stage of the 30 000-pound-payload vehicle. Structural components of this stage are lightly loaded, many of the skins being dictated by minimum-gauge criteria. Where the small compressive loading is coupled with internal pressure, data points for the partials tend to move toward quadrants III and IV. Actual partials are spotted within the zones of interest for each material and construction type considered. Aluminum concepts which offer greatest potential are honeycomb sandwich, corrugated sandwich and multiwall construction with corrugated sandwich facings. Improved manufacturing learning in these concepts would shift these partials benefically to the left of quadrant I. The position of beryllium sandwich at the most favorable position weight-wise should be noted. A tremendous potential exists if the cost of these structures, this being a fabricating problem coupled with a new material concept, can be reduced. If the cost complexity of beryllium structures could be halved, they would be competitive with any known material.

Figure 56 presents partials for the first stage of the 240 000-pound-payload vehicle. Actual data points for the partials, which have been spotted within the egg-shaped zones of interest, tend to merge more closely than in the prior figure. This is due to a higher loading environment and the less significant effects of the pressure relief. Also, the loading values tend to be closer together, and many of the partials in a zone are identical in value. In figure 56, the zones of interest have shifted to the right of the figure in an adverse manner. This phenomenon is due to the size characteristics of the components coupled with a smaller reaction between pounds saved and payload gained due to the payload exchange ratios. The only competitive material and construction type displayed in quadrant I is aluminum hat-section skin-stringer. This does not rule out quadrant II constructions.

Figure 56 further verifies the assumption that, when consideration is restricted to a particular stage, the percent of change in weight (and cost or payload) associated with substituting one component type with another is relatively independent of the stage component selected. Considering figure 56, the only restrictions to this generalization results when the compressive loading intensities coupled with internal pressures are sufficiently small that the skin thicknesses required are determined by minimum guages, or by the pressure requirements. To survey the range of base points investigated in this study zones of material and construction partials are displayed in figure 57 for the upper stage of the 240 000-pound-payload vehicle and in

figure 58 for the first stage of the large 1 000 000-pound-payload vehicle. Figures 55 through 58 show partials for the vehicles sized to current propulsion characteristics.

At this point, it is relatively easy to ascertain what must be done to make a material and construction type weight- or cost-effective (i. e., improve properties, remove design constraints, reduce cost complexity). What is difficult is isolating why and to what this should be done. In order to arrive at these conclusions, a decision must be made as to the relative value of placing a pound of payload in orbit. In other words, only study-limited conclusions can be drawn from the data herein presented. Specific problems require specific runs through the synthesis program.

Figure 57 illustrates the comparitive partials for the upper stage of the 240 000-pound-payload vehicle (see figure 56 for the first stage). Trends follow the same general pattern as for the upper stage of the small vehicle (fig. 56). Again, the egg-shaped zones are broadened by the influence of the more lightly loaded pressurized shells. Cost partials are not as good here as in the vehicle treated in figure 55. This is due to the larger size of the upper stage coupled with the lower loading. It is interesting to note that the A, B, and C aluminums (0, 10, 20 percent improvement) for honeycomb sandwich fall into the same general area, indicating that material improvement is not as significant as a change in basic construction.

In figure 58, which illustrates partials for the first stage of a large vehicle (1 000 000-pound-payload), the distribution of partials is similar to the smaller first stage treated in figure 56. The only significant change is that waffle structures become a little more performance competitive, again due to the integral skin-stringer and waffle constraints input to the program.

RECOVERABLE VEHICLE SYNTHESIS

Introduction

In order to investigate the effects and benefits from material and structural research as applied to vehicle systems, a realistic series of basepoint vehicle systems is required. This requirement is more applicable when structural improvements are assessed against a vehicle system which possesses a recoverable stage. For such a system, the ratio of payload weight to vehicle lift-off weight can be about 3 to 4 percent, and any weight reductions will have a noticeable effect on payload improvement.

Sizing a realistic vehicle has to consider the development period in order to include not only predicted advancements in material and structures, but also those advancements that would probably occur in the other disciplines that primarily influence the vehicle design. For example, the vehicle propulsion system must be representative of the period considered—items such as changes in thrust, specific impulse, propellant density, and the basic engine accesories must be unique to that particular period. The complicated interplay of these parameters is difficult to measure manually and, therefore, requires this automated procedure to make these interactions fully understood.

The automated technique must be flexible enough that parameter inputs can be readily altered. Efficient running time and readily discernible displays must be used to output the large quantities of data in order that important parameters can be selected. This technique must also be flexible enough that it can easily be used to analyze other vehicle configurations and structural arrangements at some future date without requiring a completely new program approach or extensive modification.

From a structural standpoint, the size, design loading, and thermal environment of a structural component have considerable influence upon the choice of materials, types of constructions, and fabrication method employed. In order to realistically determine what these advanced launch vehicles and their structural design environments might represent, it is necessary to begin with a mission definition and to establish payload, vehicle size, and performance characteristics. Vehicle system parameters strongly interact, and the vehicle structural system is greatly influenced by each of them. With its strong dependency on other subsystems, structural sciences research cannot be evolved in a vacuum. It must reflect the basic mission

requirement and its interaction between the structural system and the other functional systems. Economic measurements must also be included to determine the worth of conducting research in a particular structural area.

The major objectives of the parametric synthesis during this second study phase were to synthesize recoverable first stages for a series of base-point vehicle systems. The vehicles considered were vertical-launched, tandem staged, bipropellant systems. Major elements of the study were the evaluation of comparative configurations and their performance for several orbital transport systems having recoverable first stages with a typical range of payload capability (20 000 to 60 000 pounds).

In order to enhance the comparison with expendable vehicle systems, identical system design philosophy was maintained, where possible. Consequently, both systems utilized the same tandem stage and tankage arrangement, vertical take-off mode, boost trajectory profile, and design and load criteria. Sensitivity to some of these parameters was monitored during the study to investigate their effects on the complete base point vehicles.

Sensitivity of gross weight of the major subsystems to parameter variations were established to indicate the system feasibility to several of the basic assumptions. Parametric trade-off exercises were conducted for staging conditions, trajectory profile, flyback range, mixture ratio, vehicle geometry, design criteria, safety factors, materials, etc.

Vehicle Synthesis

This phase of the study was limited to the parametric synthesis of vertical-launched, tandem-staged, bipropellant vehicles with the first stage having a fully recoverable capability, and with an expendable upper stage. The recovery mode for the first stage vehicle was to perform various flight maneuvers to reduce apogee and entry heating and loading, and to provide subsonic cruise capability for a specified range and a final horizontal landing.

In order to make the parametric synthesis program compatible with Phase I expendable vehicle studies and any future requirements for synthesis of recoverable upper stages, the synthesis program used many of the basic Phase I subroutines along with several additional routines to account for the required recovery features. The synthesis of the recovery features was enclosed in a stage iteration loop for convergence to a stage system weight definition consistent with the proposed performance of the stages. These convergence loops are identical for every stage of a vehicle system (fig. 59). This

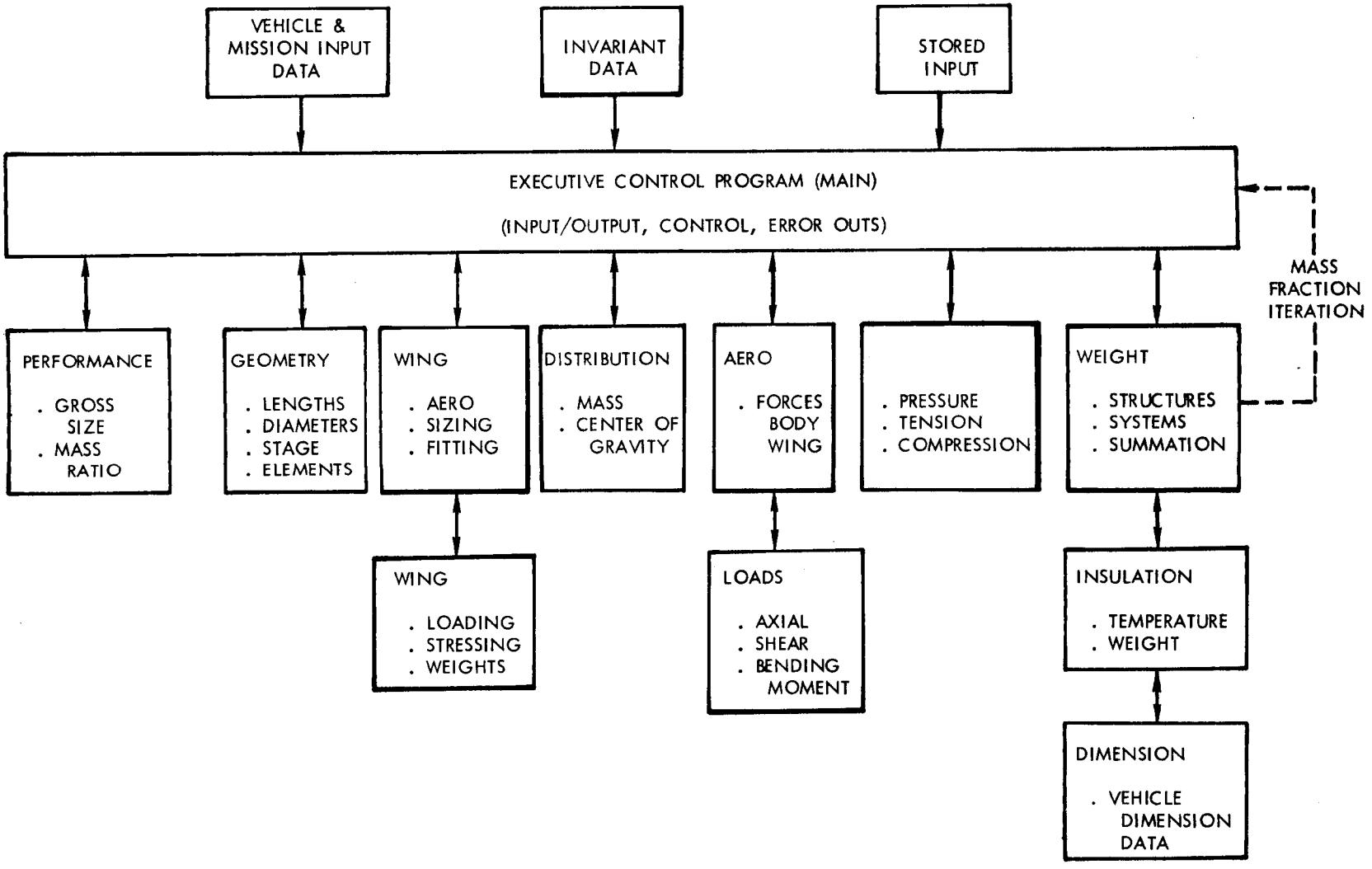

Figure 59. - Parametric Synthesis Logic for Recoverable Vehicles

figure shows the 11 major subroutines and the master executive program (MAIN) which perform the entire vehicle synthesis. Each subroutine requires input information to perform its synthesis function. Most of this information is generated and synthesized from previously executed subroutines in the program. The flow chart in figure 59 reflects the primary sequencing of subroutines; there may be a few jump-back iteration loops between individual subroutines to achieve proper proportioning, fitting, convergence, etc. The large amount of data interflow between subroutines required a close control of the stagewise synthesis logic. For the structural weight sizing, a loading description is required, this being obtained indirectly from the flight loads (LOADS) subroutine. This routine calculates axial, shear and bending moments arising from all the major structural elements of the entire vehicle system.

During the program development, space and instructions were reserved for some of the recovery features of stages other than the first stage, thereby providing a program logic which can easily be extended to upper recoverable stages. Some elements have already been incorporated which will systematically size and proportion a recoverable upper stage. At present, the weight synthesis of the individual structural and insulation upper stage elements do not reflect true entry temperatures. Therefore, at the present time, the recoverable upper stage is only effectively sized when a predetermined mass fraction (ν_B) is supplied to the program. This fixed mass fraction permits assignment of a size and shape definition to the recoverable upper stage, and assessment of its loading and aerodynamic effects during flight on the total vehicle system.

The parametric vehicle synthesis shown in figure 59 involves greater depth of analysis than is usually considered in parametric vehicle sizing and is in fact more of a "preliminary design" nature. This requirement resulted from the fact that in order to perform an intelligent structural evaluation and trade-off studies, the vehicle definition has to be fairly detailed. The major structural elements size and weight have to be defined, and more important, the realistic loading environment must be described and the interaction of the structural changes on the total vehicle system must be defined. This was demonstrated for the expendable vehicles in reference 11.

The area of interest for a fully recoverable vehicle system appears to be for an orbital payload range from 20 000 to 60 000 pounds. In order to achieve these payloads with a practical size and cost effective system, it would require at least an uprated propulsion and propellant system. For a fully recoverable vehicle, the payload is less than 1 percent of the total vehicle system, using current propulsion systems. Previous in-house parametric studies of optimum performance mass ratios for vertical take-off rocket vehicles have indicated the magnitude of anticipated payload capability

for various systems. Figure 60 shows the payload ratio for a range of efficiently allotted stage structural mass fractions for a range of staging velocities. Indicated on this figure are the mass fractions associated with both expendable and recoverable stages. Figure 61 shows the same effects for an advanced propulsive system. Both of these figures indicate the marginal payload performance that must be associated with these vehicle systems. Therefore, the Phase II study deals with only advanced propulsive systems to evaluate the vehicle size for the 20 000 to 60 000 pound payloads. The launch weight associated with this payload range is defined for a series of basepoint vehicle systems having a recoverable first stage and an expendable second stage. Naturally these vehicles have payloads larger than the 20-to-60 K region of the fully recoverable systems. These recoverable first stage, expendable second stage vehicles have been subjected to a comprehensive study to assess their relative sizes and design loading environments. Also, a series of parameter sensitivities for these base points was investigated.

The problem therefore is to define the basic requirements, criteria and system characteristics and then synthesize the resulting vehicle system. Areas requiring definition include:

Mission requirements
- Altitudes
- Payloads
- Range
- Velocity required

Trajectory
- Trajectory profile
- Velocity losses
- Staging conditions
- Abort provisions
- Entry mode

Propulsion
- Engine systems
- Propellant characteristics
- Flyback engine systems

Structural design
- Design criteria and philosophy
- Construction concepts
- Material selection
- Thermal protection

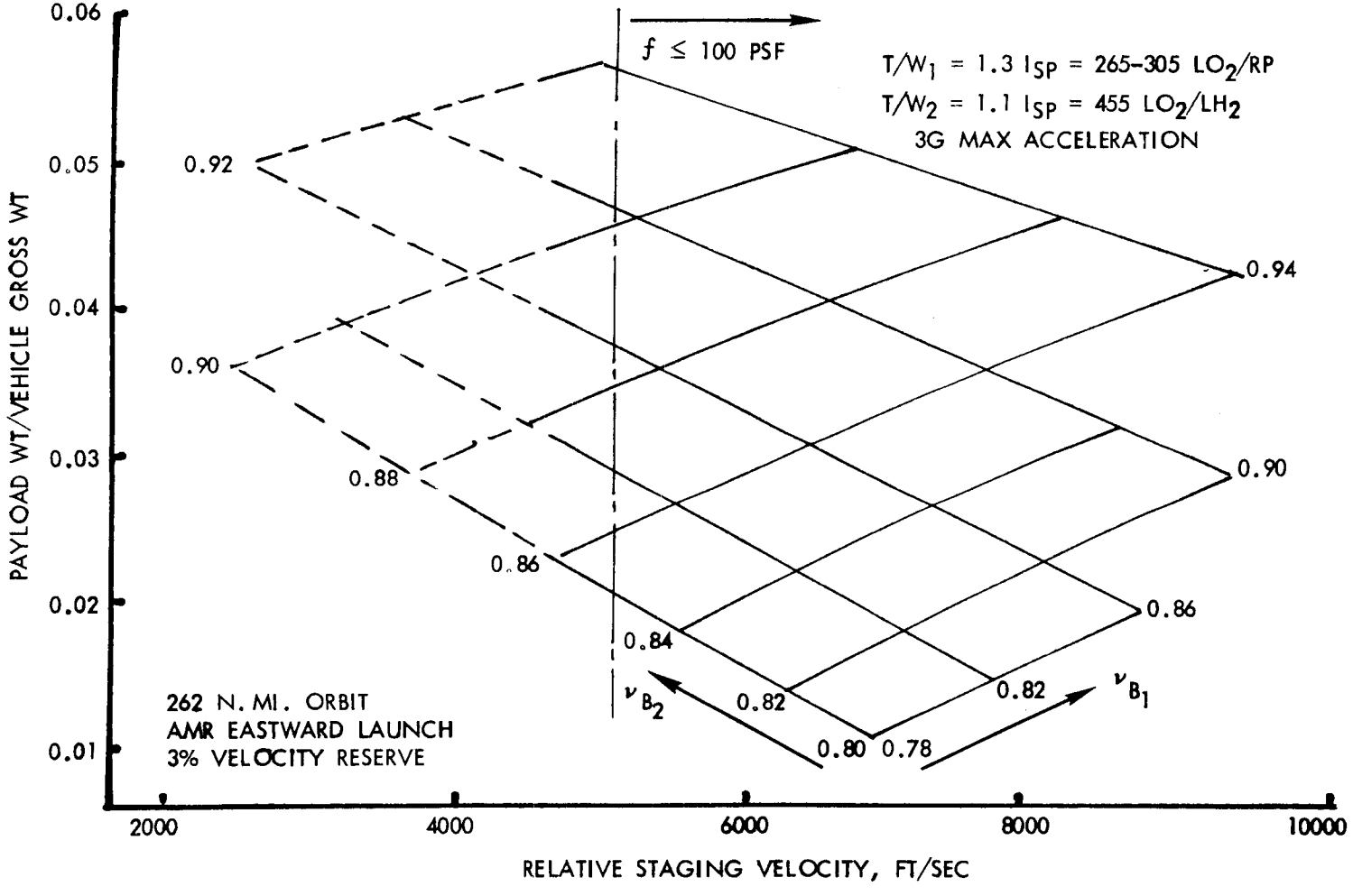

Figure 60. - VTO Rocket Vehicle Performance, LO_2-RP/LO_2-LH_2

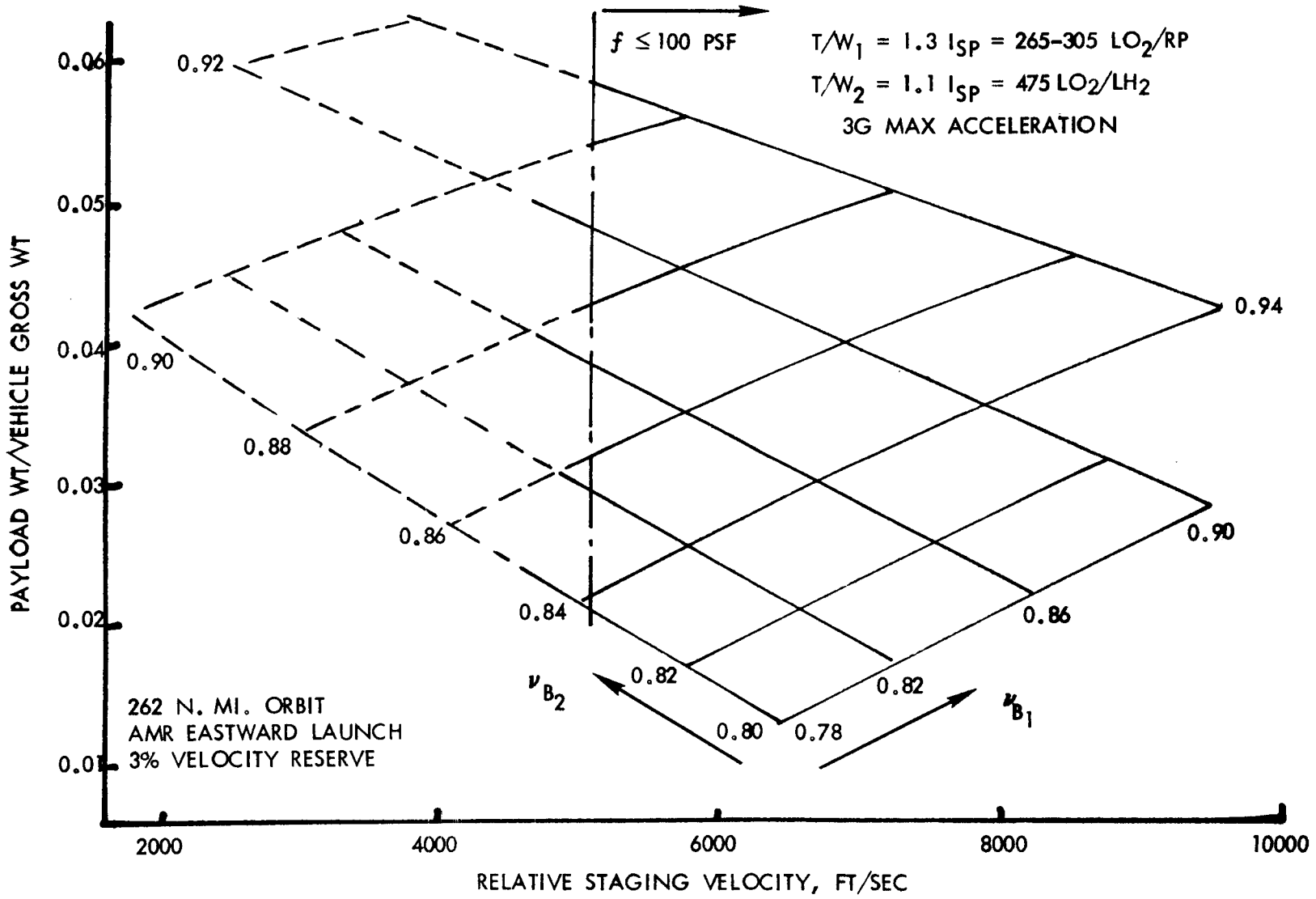

Figure 61. - VTO Rocket Vehicle Performance, LO_2-RP/LF_2-LH_2

Aerodynamics
- Wing shape and characteristics
- Aerothermal details

Vehicle stage proportioning
- Structure and subsystem weights
- Performance data
- Sensitivities

Mission Requirements and Ground Rules

Initiation of the parametric vehicle synthesis task is dependent upon a definition of the missions to be investigated and technological predictions concerning the advances that might be expected in material properties, manufacturing techniques, and propulsion and propellant systems. For Phase I of the study, three basic periods were selected for investigation:

Current period	1966 to 1970
Near-term period	1970 to 1980 (1975)
Future	1980+ (1985)

The test cases in the Phase I report (ref. 1) covered two- and three-stage launch vehicles capable of injecting payloads into near-earth orbit. However, the program and technique that was developed could be used to operate on various equivalent payload concepts, such as escape payload from Earth orbit, by including velocity calculations for injection, ejection, and transfer modes.

The Phase II study is concerned with recoverable first stage vehicles and their typical mission flight mode and system requirements. The recovery of the first stage could be the intermediate step from the current expendable vehicle system to future fully recovery mission vehicles. Several studies have been conducted with a fully recoverable system (ref. 4 and ref. 17). In this study, parametric synthesis of the first stage recoverable basepoint vehicles was influenced by the previously defined mission and payload requirements for a spectrum of fully recoverable vehicle systems. The payload range for these latter vehicles was considered to be 20 000 to 60 000 pounds in earth orbit, and the vehicles were considered to have optimal staging condtions for injection of this payload range. The upper recoverable stage was replaced with an expendable system; liftoff weight remaining invariant, and the resulting recoverable and expendable vehicle capabilities and design criteria were redefined for the basepoint design conditions. The propulsion

and propellant systems associated with the recoverable-expendable systems were identical to those used in Phase I of the study in order to retain common ground rules between the study's two phases.

A survey of current and past studies was conducted to identify a reasonable spectrum of equivalent payloads in Earth orbit (ref. 17, 18, and 19). A fully recoverable vehicle system can be made to fulfill a variety of mission programs, some of which are discussed in the following paragraphs. The basic function of such a system is considered to be logistic support of manned orbital space stations, (ref. 19), and these are subdivided into:

Space station support
- Orbital laboratory support
- Planetary mission support
- Lunar base support

Unmanned payload delivery
Manned military mission
Global range transport

Each one of these missions is concerned with the delivery of cargo and passengers to a near-Earth orbit and the operation of ferrying passengers for space station crew rotation. Typical mission requirements for these missions were quoted in reference 19 and a summary is shown in table 23.

TABLE 23. - MISSION REQUIREMENTS SUMMARY

Mission	Orbit		Mission Crew	Mission Duration (Days)	Crew Stay Time (Mos.)	Cargo and Passengers (lb)
	Alt. (n. mi.)	Incl. (deg)				
Space station support	262	30	24-50	Continuous	1 to 3	215 to 870
Planetary support	262	30	16-50	90 to 120	1 to 2	570 to 1650
Lunar base support	262	30	21-24	Continuous	3 to 6	700 to 1030
Payload delivery	2-500	30-90	2	1	-	-
Manned military	1-300	25-90	8	Continuous	0.5 to 1	289 to 578

These missions are representative of support requirements of all planetary missions. Cargo-to-passenger ratios for such missions are shown as of function of the orbital operations duty period in figure 62. Similar payload and passenger requirements could be associated with a lunar base support. Figure 63 shows typical annual cargo requirements for such an operation, and figure 64 indicates the passenger trips necessary for personnel rotation.

With all the different types of missions, certain requirements apply generally to all the orbital missions. Two such requirements are the vehicle velocity to provide for launch windows - lateral range for convenient return opportunities — and velocities to establish circular orbits at various altitudes and inclinations. The velocity requirements for a two-stage recoverable system (ref. 17 and 19) are used for this study and are summarized in table 24. In addition to the velocity requirements shown on the table are percentage velocity reserves and stage losses associated with drag, gravity and thrust misalignment, and vectoring. A discussion of these losses is given in the section on trajectories.

TABLE 24. - VELOCITY REQUIREMENT

Velocity Increment	Requirement (fps)
Circular velocity at 50 n. mi.	25 740
Less Earth rotation	1 246
Net velocity	24 494
First stage net boost	5 750
Second stage boost	18 744
Hohmann transfer perigee at 50 to 100 n. mi.	91
Launch window	100
Hohmann transfer to 100 n. mi. - Apogee $\angle V$	91
Hohmann transfer to 262 n. mi.	529
Deorbit impulse	430
Attitude control	173
Second stage velocity net	20 158

From the types of missions already discussed, and from typical velocity and mission requirements, a series of mission and design ground rules which

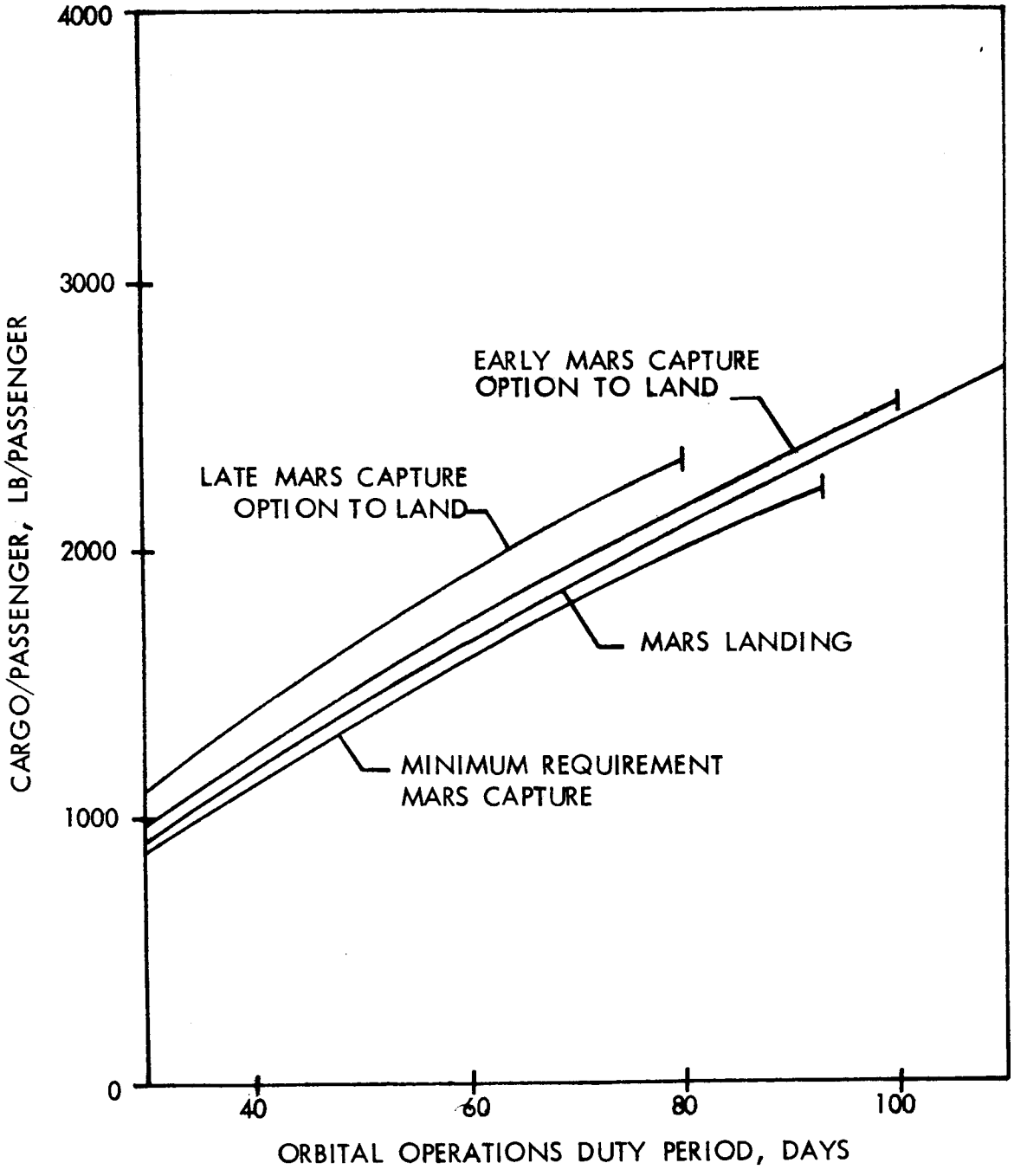

Figure 62. - Cargo/Passenger Mix for Planetary Support Missions

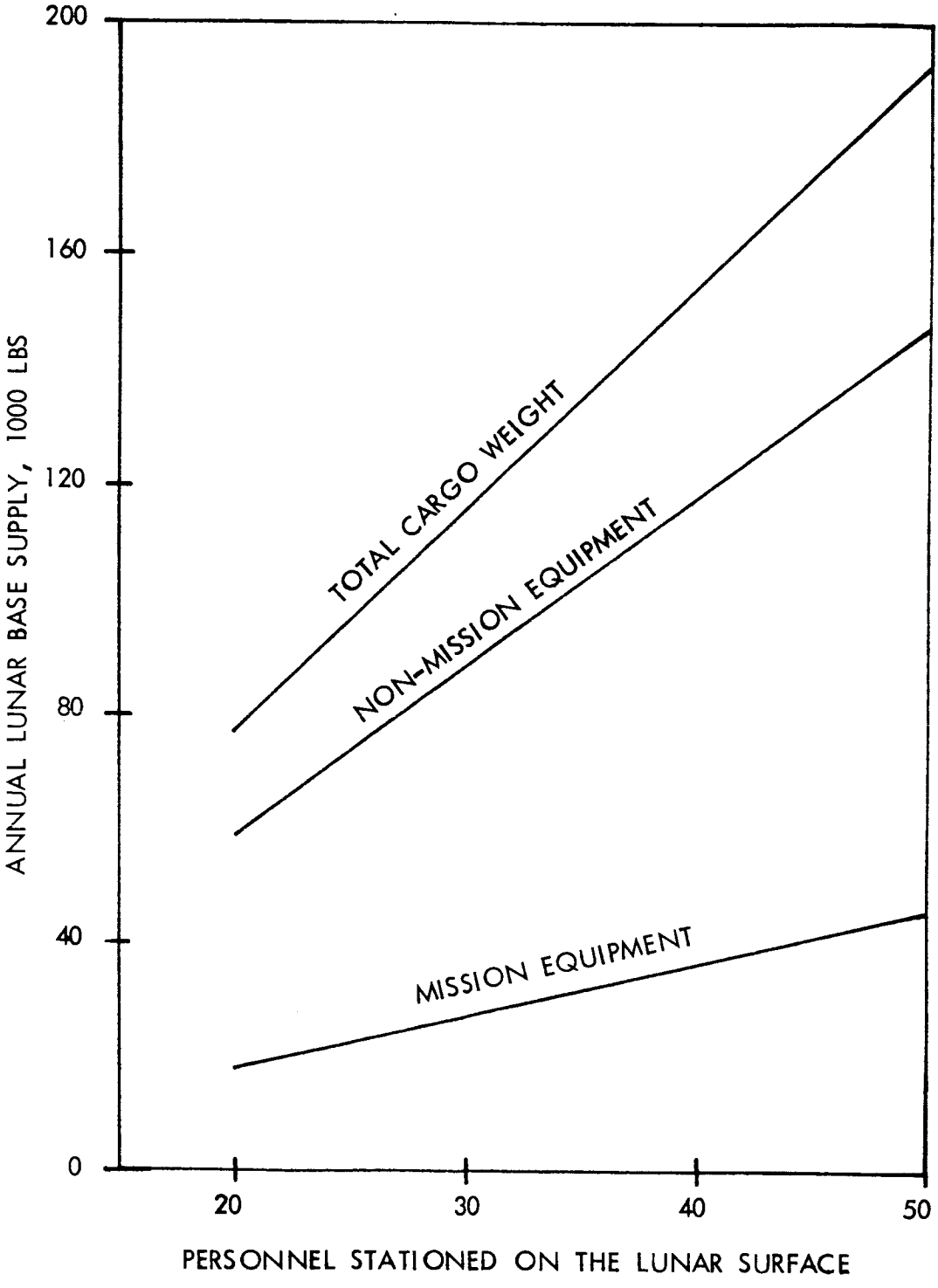

Figure 63.- Annual Lunar Base Cargo Requirement

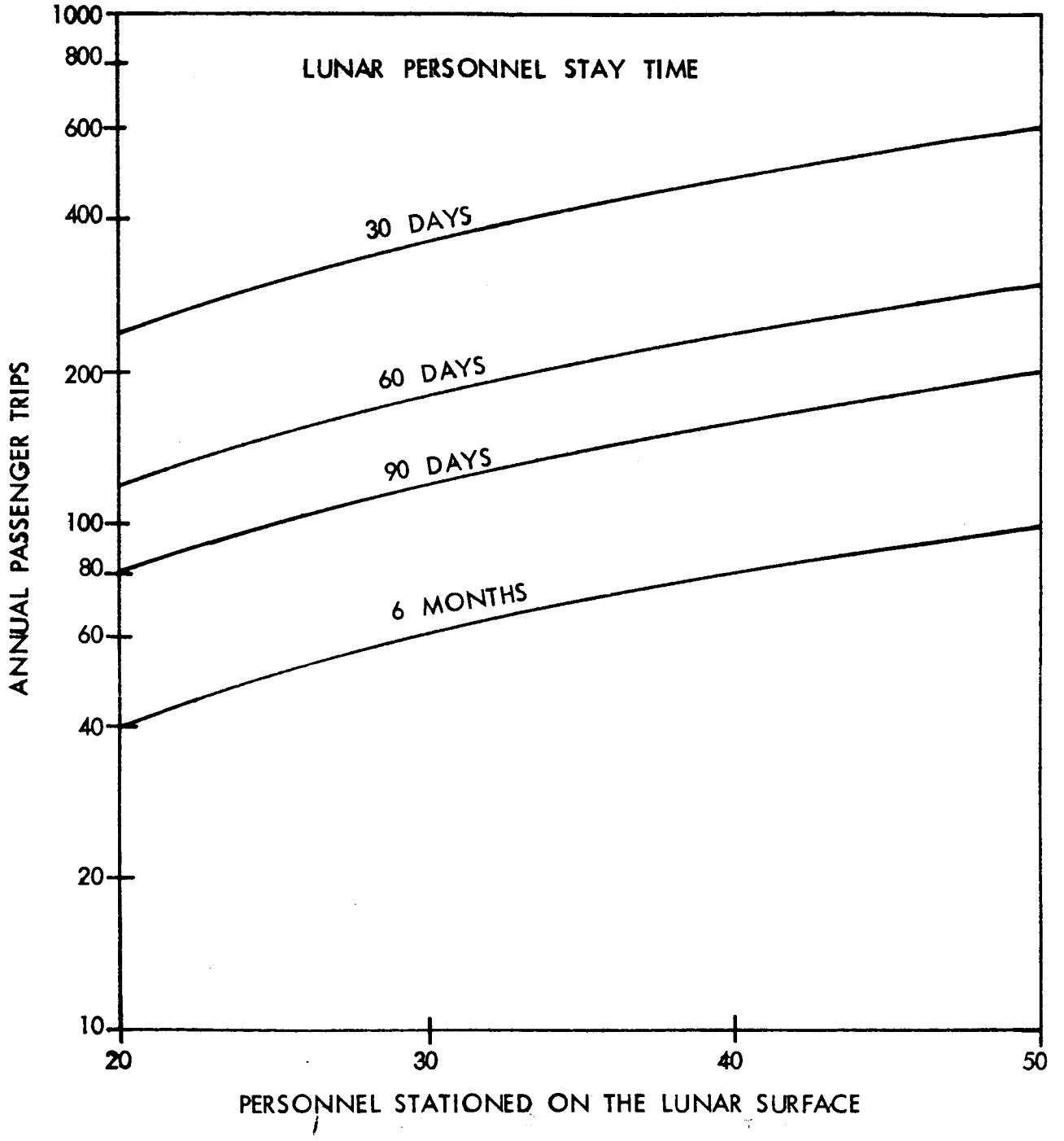

Figure 64. - Annual Passenger Trips to Lunar Base

emerge for the recoverable vehicle systems synthesized in this study are given as follows:

1. Vertical launched, horizontal recovery

2. Two-stage (first stage recoverable, second stage expendable), tandem-staging arrangement.

3. Designed with near-term (1970 to 1980) and future (post-1980) system characteristics.

4. Payload spectrum associated with 20 000 to 60 000 pounds for a fully recoverable system.

5. Eastward launch from AMR and mission orbit attitude of 262 nautical miles

6. Maximum boost acceleration: 3 g

7. Boost phase terminates with circular injection at 50 nautical miles

8. Staging velocity of 6500 fps (relative)

9. Propellant: O_2 - RP first stage
   O_2 - H_2 second stage

10. Thrust-to-weight ratios of 1.25 first stage and 1.0 second stage

Whereas these were the ground rules and design criteria used for the study results, the parametric vehicle synthesis program is not limited to these specific rules but has the ability to handle a wide variation of design parameter values and is easily modified for additional parameters.

Vehicle Description

The base-line vehicle systems considered for this study were defined by NASA and reference 20 to comprise a vertically launched, horizontally landed, recoverable first stage and an expendable upper stage. The various vehicle shape contenders for the role of recoverable vehicle systems include

Lifting body
Winged body
High lift-to-drag ratio body

Each vehicle shape has its own relative merit when considered as a recoverable system. For a gradual evolution sequence from an expendable system to a fully recoverable system, the first step could be to use an existing expendable stage and simply add recovery features as required. An evolution such as this would tend to consider a tandem stage system with a winged body recoverable first stage. Such recovery systems using state-of-the-art designs, tankage, etc., have been evaluated in this study to define a series of base line vehicle systems representative of a size spectrum of future recoverable vehicle system.

The base line vehicle system represents the base to which tradeoff, optimization and sensitivity studies can be progressively applied. With the basic mission and operational profile established, broad propulsion, structures, design criteria, trajectory and aerodynamic characteristics can be investigated to determine their relative sensitivities. A description of the base line vehicle size, weight and design loading environment permits subsequent efforts to be directed toward assessing tradeoffs, effects and benefits arising from structural and material advancements when applied to such vehicle systems.

The basic load-carrying structure which comprises the backbone of the vehicle is the integral tanks, interstages, and skirts of both the first and second tandem stages. In the forward end of the nose section of stage one are the crew and recovery control capsule and the nose landing gear. The main lifting surfaces are considered attached to the rear section of stage one with the main landing gear loads fed into the wing structure. Engine thrust loads are transmitted via the thrust structure into the integral tanks and outer shell. Engine systems required for flyback range requirements are assumed to be mounted on the first stage wings. Such a recoverable-expendable vehicle system is shown in figure 65, and the major structural components of the first stage are indicated in figure 66.

The crew compartment for the first stage recoverable vehicle was considered as a hemispherical nose and, if required, a cylindrical section aft of the nose as the crew volume requirements dictate. This shape was assigned to allocate a specific volume between stages and is not intended to constitute the final design shape for the entry vehicle. Specific weight allotment for the crew capsule was provided with the input data. An unpressurized shroud around this nose section to connect the two stages together was designed by the compressive loading intensity experienced by the outer shell.

The tankage arrangement for both stages was considered to be tandem cylindrical tanks with $\sqrt{2}$ ellipsoidal bulkheads. Tanks for the first stage were separated by a short unpressurized center section, while the second stage tanks were considered to have a common bulkhead. The bulkhead

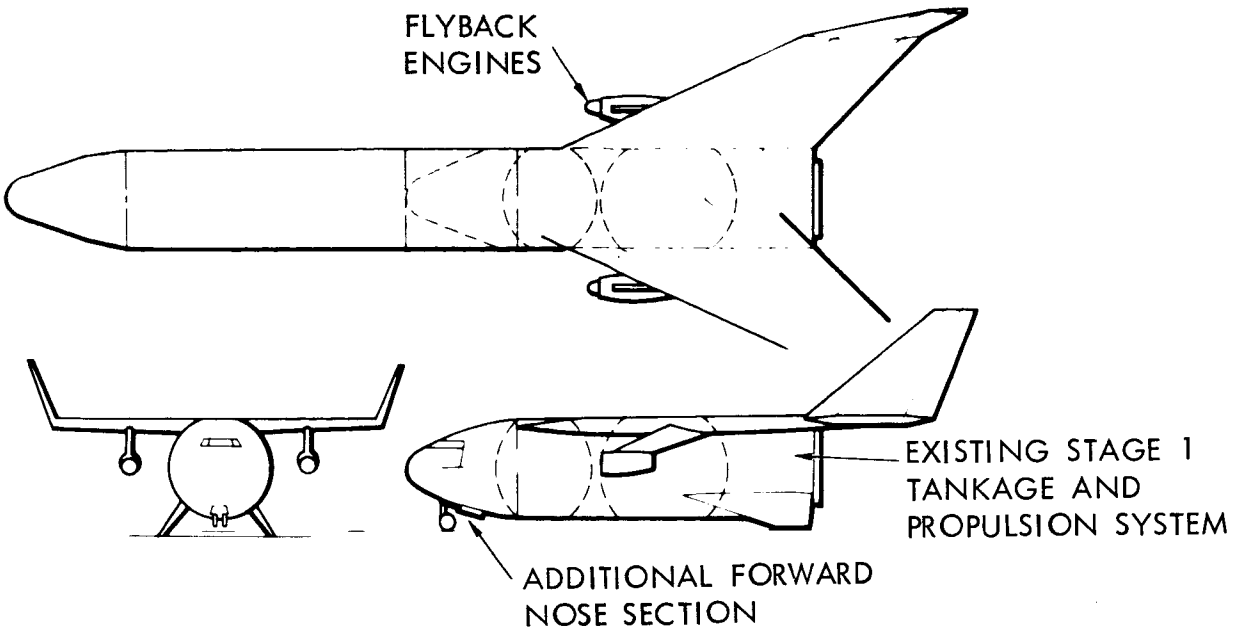

Figure 65. - Typical Recoverable First-Stage Vehicle

arrangement for the various stages can be preselected for the program synthesis by the use of the bulkhead indicator input information. The design loading conditions for the tank walls and bulkhead domes were automatically assessed by the synthesis program. Ullage pressures plus the maximum hydrostatic heads designed the required skin thicknesses, while the axial loads, bending moments and pressure relief, if any, throughout the flight profile produced a compressive loading intensity for the shell's stability requirements. The actual design loading intensity was identified in the computer printouts together with the shell weight assessment.

Unpressurized shells, such as skirts, interstage and center sections, were considered to be cylindrical shells of a typical aluminum skin-stringer-ring construction. Their design loading environment was a compressive loading intensity due to the axial acceleration, and bending moments from airloads, control moments, and inertia relief loads.

The wing structural design was a multispar load carrying main wing box with cantilevered leading and trailing edges. Design loading envelope for the wing was either due to the entry loads and maneuvers or the dynamic pressure plus wind gusts during the ascent boost phase. Airloads were considered to impose shear and bending in the main structural box, the bending

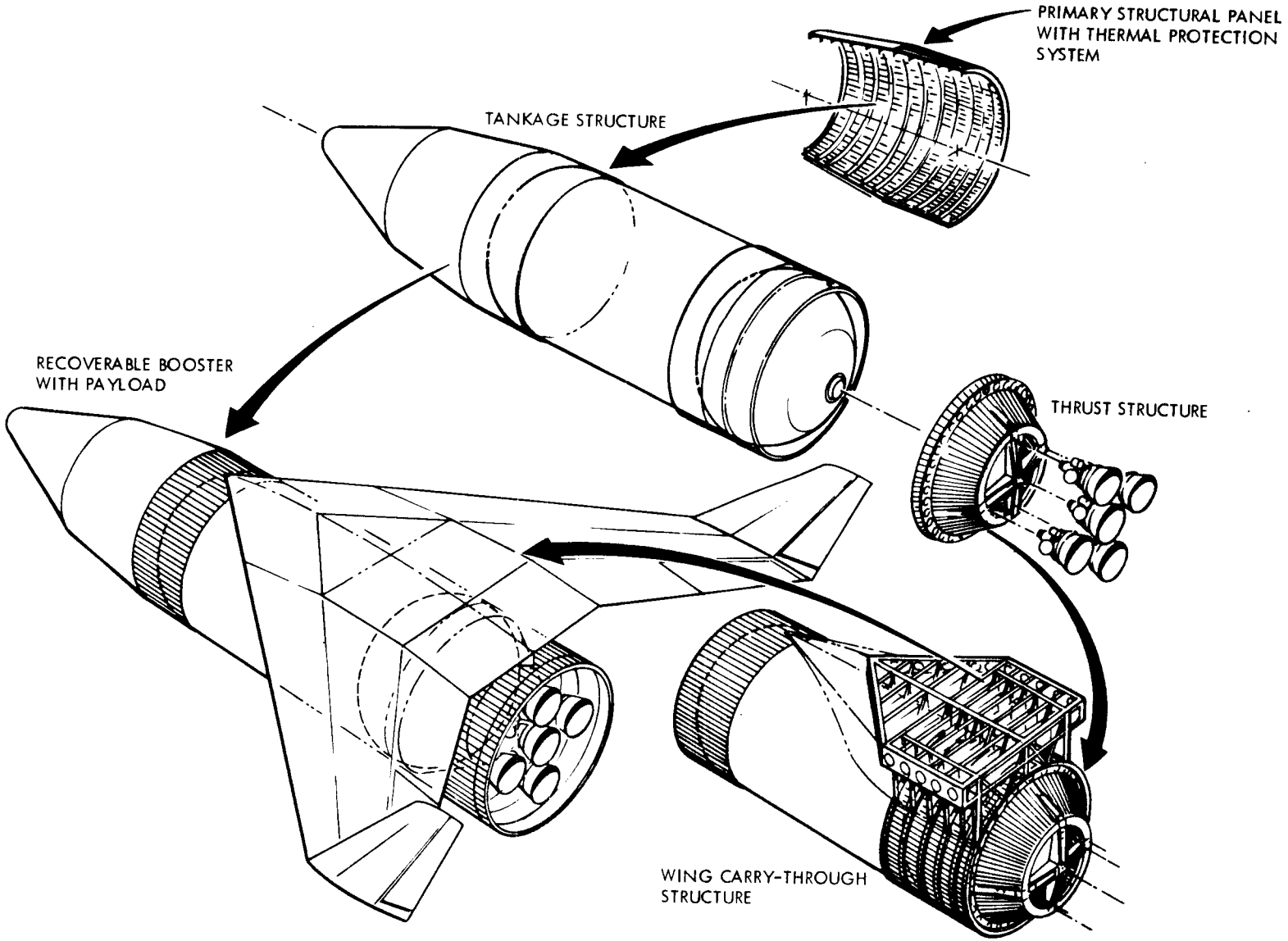

Figure 66. - Recoverable Upper-Stage Booster Concept

was taken as differential end loads in the cover panels and spar caps and the shear reacted by the spar webs. A more detailed description of the load paths and analysis for the weight estimation is supplied in Appendix B. It should be realized that the parametric synthesis is more concerned with the over-all system size and weight description than with the minor structural details. Therefore, the total weight assessment for the wings is realistic without defining the structural elements and its attachment to the main fuselage. The wing carry-through was considered to be a beam structure to handle the wing bending and circular ring frames to transmit the shear into the fuselage. Positioning of the wing structure was placed as far aft on the stage shell as possible to achieve the most stable arrangement. The near spar is attached to an existing heavy kick frame at the aft bulkhead thrust structure junction. The forward spar tries to position itself to preserve a structural box at least 50 percent of the root chord and at the same time search for a likely tie-in station, i.e., a bulkhead-unpressurized shell junction where a frame already exists. For some designs, this will not be possible as is the case of a LO_2/LH_2 second stage with a stage fineness ratio that allows the LO_2 tank to have a short-wall length. With this design, the forward spar will be positioned to a ring frame within the forward tank structure. For the base line vehicle systems with an expendable upper stage, this position problem of the forward spar does not exist.

A parametric weight synthesis estimation for the thermal protection requirements for the wing and fuselage of the recoverable stages is dependent upon the staging conditions, velocity, and altitude. Figure B-28 (Appendix B) indicates typical equilibrium temperatures that are encountered during the entry mode. The initial parametric synthesis of a vehicle system has to rely upon stored temperature data for the initial input information. Once a vehicle system's size and weight have been defined, a detailed trajectory, aerothermal, and thermal analysis can be conducted to check the original thermal and insulation assumptions that were supplied to the synthesis program. As more detailed and reliable information is obtained, it can be systematically exercised through the synthesis program. For the base vehicle studies, an equilibrium temperature of 2000°R was used, and the thermal map over the vehicle was evaluated by a simplified empirical relationship as discussed in Appendix B. The equilibrium temperature and heat flux were considered to be acting for 600 seconds, which is representative of the entry flight times. Insulation requirements for this thermal history to produce a back-face temperature of the load-carrying structure (aluminum at 300°F) were developed external to the vehicle synthesis program. The insulation example used was microquartz with a three-pound-per-cubic foot density and an additional weight assignment of one-half pound per square foot for the external metal heatshield attachment and support structure for the insulation material. This thermal protection system was applied to the wing and the fuselage shells. Unit weight-temperature variation curves that were used

for the synthesis evaluation are shown in figure B-33 and the total insulation weight for the vehicle system is detailed by the program output.

Design Criteria

The vehicle design load factors are based on the mission trajectory profile. Distribution of air loads during various discrete points along both the boost and reentry trajectories are considered in the critical design conditions for the various structural elements of the vehicle system. Most of the pertinent load evaluation, distribution and weight assignment is synthesized automatically by the parametric vehicle synthesis program.

Several conditions were considered in evaluating the structural components, including

Prelaunch
Maximum dynamic pressure
Maximum acceleration near end boost of Stage 1
Reentry and maneuver
Landing

The axial loads and pressure heads arising from accelerations and the bending moments due to maneuvers and airloads were converted to equivalent compressive or tensile load intensities for the structural weight assessments for the fuselage shells and wing structures.

In the prelaunch conditions, it was assumed that the ground-handling loads were within the strength capabilities as determined by flight loads and, thus, did not incur extra-weight penalties. In the vertical launch portion, the vehicle is subjected to 99.9 percent wind profile on the launch pad. AMR (ref. 21) steady-state and peak wind velocities were considered and are shown in table 25. For the synthesis program, a linear approximation was used for relative simplicity.

In the launch position, the peak winds are applied in the direction resulting in the maximum loading. The analysis considers the loads from steady-state winds and applies a dynamic magnification factor of 1.54 and a normal vortex shedding factor of 1.25, as considered for the design conditions for the Saturn V vehicle system (ref. 22). These factors, which are variable inputs to the program, result in a design condition that is equivalent to 2.83 times the steady-state wind loads. The vehicle may contain any amount

TABLE 25. - PRELAUNCH WIND PROFILE AT AMR

Height (feet)	Steady State (knots)	Peak (knots)
10	23.0	32.2
30	28.7	40.2
60	32.9	46.1
100	36.5	51.1
200	41.9	58.7
300	45.4	63.6
400	48.1	67.3

of fuel from empty to full when subject to these wind loads, and the propellant tanks are considered to be unpressurized. This condition is regarded as the most severe design condition to be encountered at prelaunch and is automatically considered by the program in the structural design load evaluation.

Design load environments during the maximum dynamic pressure are considered as the result of the vehicle system encountering a sharp edge gust. The vehicle is assumed to be programmed for a minimum load flight profile to alleviate severe wing loading prior to encountering a gust. This requirement supposes that the vehicle control system will respond to the gradual build-up of the winds and is only required to design for the additional wind gust of 9 meters/second, maximum. The effect of this assumption is considered in the sensitivity studies. The gust velocities, vehicle velocity of $M \approx 1.2$ at 35 000 feet altitude, and the relative attitude of the flight profile to the local wind stream are considered to introduce a relative angle of attack of about 3 degrees. If a control delay lag of 1 degree is assumed, the total angle of attack for the synthesis program was taken as 4 degrees. The maximum dynamic pressure is dependent upon the flight profile and the rocket performance. A typical dynamic pressure and velocity variation with initial thrust-to-weight ratio and a typical gravity turn trajectory is shown in figure 67. For the design condition of $T/W = 1.25$, a dynamic pressure of 720 pounds/foot^2 was used for a mach number of 1.2. The design loadings resulting from this environment were evaluated during the vehicle synthesis. A restoring moment to the aerodynamic disturbance was supplied by gimballing of the main rocket engines whose maximum gimbal angle for the design structural envelope was considered to be 8 degrees (again a program input). Due to engine-system inertia and control-delay lag, full advantage should not be taken of the maximum engine gimbal allowance. The design loads associated with the maximum dynamic pressure for the Saturn V vehicle (ref. 23) show that the dynamic analysis considered the engine system to be at +30 percent of full gimbal position. A similar control setting of about 2.5 degrees is used for the vehicle synthesis input data.

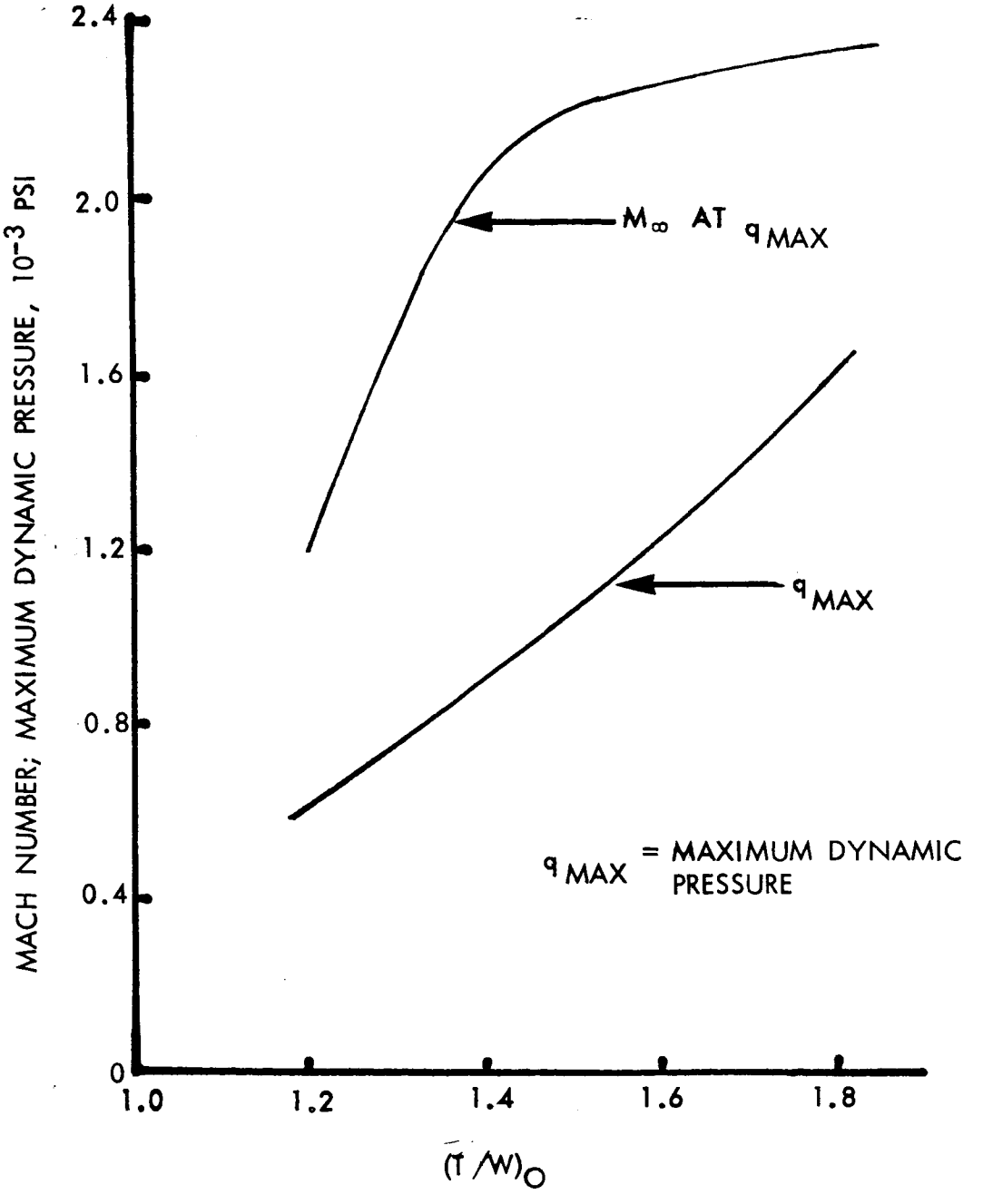

Figure 67. - Typical Dynamic Pressure and Velocity Variation With Initial Thrust-to-Weight Ratio and Typical Gravity-Turn Trajectory

The maximum acceleration experienced by the vehicle system was assumed not to exceed 3 g normal acceleration, or to be equivalent to the acceleration due to maximum thrust at end boost, whichever is minimum. Separation of the first stage was assumed to occur in a relatively low dynamic pressure regime, and the air loading was not considered in the machine analysis. An engine-thrust misalignment at end boost was assessed for its contribution to the design load bending envelope. The magnitude of engine misalignment was based upon the Saturn V criteria (ref. 22) and is quoted as:

$$T_{LAT} = \text{THRUST} \times \sin\left(\frac{1^\circ}{\sqrt{n}}\right)$$

where n is the number of engines.

Thermal loads incurred during the atmospheric boost flight were combined with the mechanical loads to arrive at the design condition. A typical reference temperature of 300°F for the entire vehicle structure was considered at end boost for the weight-load design curve evaluation.

Atmospheric entry for the first stage is a load-factor modulated entry after a coast to apogee. Nominally, the vehicle will initially use its wings to reduce the apogee altitude and enter at an angle of attack corresponding to $C_{L_{max}}$ and remain at this altitude until a resultant limit load factor is attained (ref.18). A reduction in angle of attack will be introduced to maintain the limit load factor (4.0). For structural design considerations, this load factor will be associated with a first-stage vehicle without the boost propellant mass. Maximum entry heating reference temperature considered was 2000°R for the equilibrium wall temperature 5 feet aft of the stagnation point. For these design environments during entry, the first-stage vehicle was considered to have a hypersonic wing loading of 50 pounds/foot^2 and (L/D) max = 3.0. The equilibrium temperatures variation of such a vehicle for a range of staging velocities and altitudes is shown in Appendix B, figure B-30.

The factors of safety associated with the base line vehicle systems for the structural design evaluation were:

Yield factor of safety = 1.10
Ultimate factor of safety = 1.40
Propellant tanks
- Proof pressure = 1.05 x limit pressure
- Yield pressure = 1.1 x limit pressure
- Burst pressure = 1.4 x limit pressure

The tankage structural shell was evaluated to ultimate loads combined with minimum relief pressure for compressive loading intensities and combined with burst pressures for tensile hoop stresses.

Mission Profile

The total mission profile and its associated velocity requirements were considered for a two-stage recoverable vehicle system. Preliminary parametric sizing of the vehicle indicated that with regard to minimization of launch weight for the design conditions considered, an efficient staging velocity would be around 6500 fps. Therefore, the total mission profile, particularly the ascent phase, was similar to that of the vertically launched Reusable Orbital Transport (ref. 19). A schematic of the ascent profile is shown in figure 68 with first-stage boost to 6800 fps at an altitude of 175 000 feet and a flight path angle of 20 degrees. At this point, stage separation is commanded, and the second stage proceeds to a phasing orbit and thence, via Hohmann transfer, to its rendezvous orbit. The velocity requirement associated with the second-stage ascent, rendezvous, and deorbit were defined in the mission requirement section of this report.

With the vertical launch mode, the vehicle is given a slight kick angle several seconds after the initial lift-off and it performs a modified gravity turn. In the region of maximum dynamic pressure, lift generated in a simple gravity turn profile is of considerable magnitude, resulting in excessively large wing design load factors. In order to effectively reduce wing design requirements, the wing lift is minimized by flying into the gradual wind build-up, i.e., $\alpha = 0$ in the maximum dynamic pressure region. At the higher altitude and some reasonable pressure level, trajectory is switched to a vehicle altitude that corresponds to the thrust parallel with the velocity vector. Therefore, altitude controls are required for the boost phase, with thrust vector control during the immediate post-launch period and then aerodynamic control when available. Dynamic pressures and velocity that are encountered for typical vertical ascent trajectory were correlated and are shown in figure 67 for a range of thrust-to-weight ratios. For the base line vehicle system, these were set at 720 pounds/foot^2 dynamic pressure and Mach number ≈ 1.2.

For reasons of passenger comfort, a maximum acceleration constraint should be imposed on the flight path. With the vehicles developed, the unconstrained thrust of the first stage will result in maximum acceleration of around 3.5 g. When thrust modulation is applied during the latter portion of first-stage boost to reduce the maximum acceleration, a performance

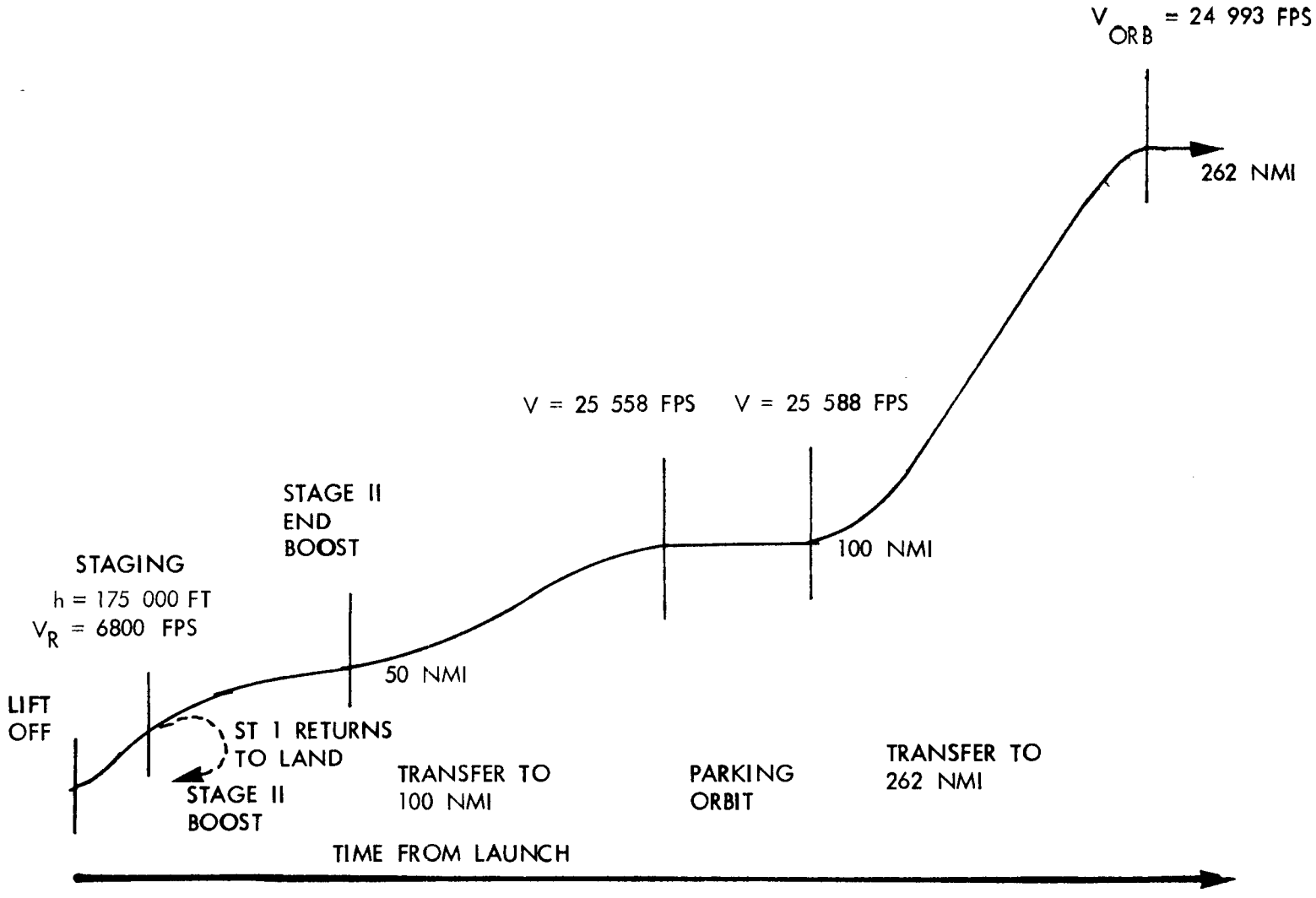

Figure 68. - Ascent Profile

penalty in the form of longer burning and perhaps additional velocity losses is incurred. Velocity losses used for this study were based upon available 3 g limit trajectory information.

In order to account for variations in performance etc., propulsion reserves were included for thrust vector control losses and mixture ratio shift. Velocity reserves, in addition, were taken to account for variations in aerodynamic coefficients, atmospheric density, maneuvering requirements in atmospheric flight. A value of 1000 feet/second was taken; this is in agreement with the Reusable Orbital Transport design conditions (ref. 19).

The system's ideal velocity requirement and their apportionment to the various stages are strongly dependent upon the type of trajectory flown and the aerodynamic characteristics of the vehicle system. Ideal velocity requirements for each stage consist of the velocity increment to achieve a required staging condition. This includes drag, gravity, and thrust-line losses and is a function of vehicle aerodynamic characteristics, flight path profile, thrust-to-weight ratio of the stage, staging velocity, and acceleration limit. In order to account for the velocity losses that each stage experiences, a detailed trajectory of a complete vehicle system has to be considered and evaluated. For the parametric synthesis routine, extensive use has been made of existing study data and the NAA Space Division parametric data bank.

The first-stage performance mass ratios were actually determined by simulating the trajectories of a family of typical vehicles on the IBM 7094 digital computer with the aid of the NAA AP-188 computer program. These typical vehicles had a constant gross weight at launch and were flown to various staging velocities with different thrust-to-weight ratios. The resulting simulated trajectories consisted of a vertical boost period followed by a ballistic path until the vehicles either reached the staging velocity or left the sensible atmosphere. Upon attaining the staging velocity, the mass ratio of the stage was evaluated from the burnout weight as follows:

$$\mu = \frac{W_o}{W_{B.O.}} \tag{1}$$

where

W_o = initial weight

$W_{B.O.}$ = burnout weight

μ = performance mass ratio

During the first stage flight profile, there are two possible flight programs:

Zero lift: The lift on the wing is zero and the wing design load factor is established by the critical gust during the maximum dynamic pressure regime. However, there is a thrust component normal to the velocity vector. This results in a performance loss, especially toward the end-boost condition of stage one.

Thrust along velocity vector: This involves a negative wing angle of attack, and in the region of maximum dynamic pressure the lift generated is of considerable magnitude, causing large wing design load factors.

For the cause of wing lightness and an overall efficient vehicle system, a combination of the two flight programs is most promising; i.e., minimize wing lift and hence wing weight ($\alpha = 0$ during gust periods), and above maximum dynamic pressure switch to thrust parallel with velocity vector. Therefore, the vehicles were flown along a ballistic path within the atmosphere, the only aerodynamic parameter necessary for the trajectory simulation is the zero-lift-to-drag coefficient. Figure 69 shows the zero-lift-to-drag coefficients as a function of Mach number which were used for this investigation. These drag coefficients were held constant for the entire family of launch vehicles investigated.

The second-stage performance mass ratios were also determined from IBM simulated trajectories using the same AP-188 program. These stages were flown from the first-stage staging conditions to the burnout condition. The burnout velocity for all the vehicles was held constant at 26 053 feet per second at an altitude of 400 000 feet and a flight path angle of zero degrees. This burnout velocity of 26 053 fps represents the supercircular velocity at the perigee altitude of 400 000 feet required to coast to 262 nautical miles. Upon attaining the 262-nautical-mile altitude, the vehicles were injected into a circular orbit. The required injection velocity for the 262-nautical-mile orbit of 342 feet per second was also added by mass ratio to the burnout velocity by the following relationships

$$\mu = \frac{W_o}{W_{BO}} \ln^{-1} \left(\frac{\Delta V_i}{I_{sp}\, g}\right) \tag{2}$$

$$V_i = V_c - V_e \tag{3}$$

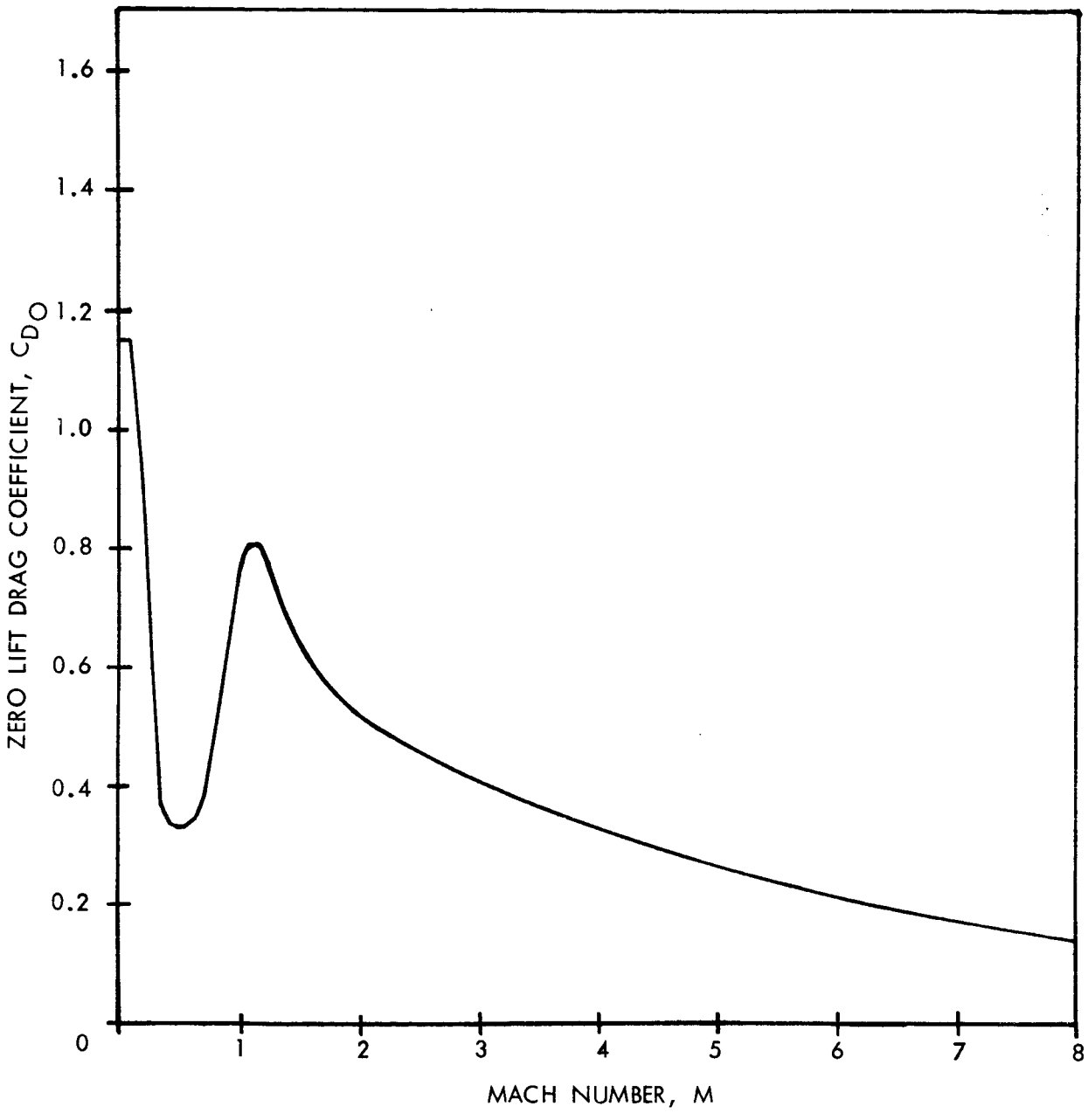

Figure 69.- Zero-Lift Drag Coefficient

where

I_{sp} = specific impulse

g = gravitational acceleration

V_c = circular velocity

V_e = elliptical velocity

The second stages were controlled during boost by vectoring the thrust to achieve the optimum path from the staging conditions to the burnout conditions. In addition, the AP-188 program also determined the optimum first-stage ballistic path through the atmosphere by varying both the time of the vertical boost phase and the initial kick angle after vertical boost.

All the simulated trajectories were obtained from a 90-degree launch azimuth at Cape Kennedy. The performance mass ratios include propellant sufficient to provide the specified reserve.

These velocity reserves were added to the performance mass ratios by the following equation

$$\mu = \ln^{-1} (K_V \ln \frac{W_o}{W_{BO}})$$

where

K_V = velocity reserve ratio, $\frac{\Delta V_R}{V}$

ΔV_R = velocity with reserve

V = velocity without reserve

In general, the maximum acceleration during boost on the vehicles was limited to the specified 3 g's. This acceleration limit was imposed to simulate a man-carrying system. The results of the computer-program-optimized trajectory are shown in table 26 for a series of vehicle systems. Table 26 and figure 70 indicate the required mass ratios for the two-stage vehicle flying an optimum trajectory. Other results had the 3 g maximum acceleration limit removed but the percentage changes in the mass ratios were within the accuracy of our parametric study; therefore, it was not included. The results of table 25 were rearranged to extract the velocity losses associated with each stage. It was found that the velocity losses of the first stage were

TABLE 26. - PERFORMANCE MASS RATIOS (μ)

Launch mode: VTO
Stage I propellant: $LO_2/RP\text{-}1$
Stage II propellant: LF_2/LH_2
Stage I I_{sp} altitude variation: 265-305

Burnout velocity: 26 053 ft/sec (inertial)
Maximum acceleration limit: 3 g's
Reserve propellant: 3 percent
Burnout altitude: 400 000 ft
Hohmann transfer to: 262 n. mi.

			$I_{sp}(2) = 455$		$I_{sp}(2) = 475$					$I_{sp}(2) = 455$		$I_{sp}(2) = 475$	
$(T/w)_0$	$(T/w)_2$	V_s	1	2	1	2	$(T/w)_0$	$(T/w)_2$	V_s	1	2	1	2
1.3	.8	4470	2.3565	5.1737	2.3565	4.8184	1.5	1.3	4 880	2.3008	4.5316	2.3008	4.2515
		6640	3.0582	4.1069	3.0582	3.8619			7 180	3.0122	3.7307	3.0122	3.5401
		7840	3.4821	3.6870	3.4821	3.4900			8 600	3.5500	3.3490	3.55	3.1800
		9380	4.1223	3.2271	4.1223	3.0716			9 895	4.0808	3.0104	4.0808	2.8743
1.3	1.1	4570	2.3565	4.7381	2.3565	4.4373	1.7	.8	4 300	2.1058	5.2524	2.1058	4.8990
		6640	3.0122	3.9300	3.0122	3.6047			6 045	2.601	4.3587	2.6010	4.0966
		7820	3.4522	3.5585	3.4522	3.3152			8 560	3.4522	3.4622	3.4522	3.2855
		9350	4.0808	3.1530	4.0808	2.9869			10 000	3.9950	3.0150	3.995	2.864
1.3	1.3	4620	2.3565	4.6366	2.3565	4.3471	1.7	1.1	4 400	2.1058	4.8237	2.1058	4.5143
		6410	2.9676	3.9500	2.9676	3.7261			6 095	2.6010	4.1174	2.6010	3.8789
		7810	3.4229	3.5403	3.4229	3.3468			8 660	3.4522	3.3394	3.4522	3.1746
		9260	4.0400	3.1528	4.0400	3.0042			10 000	3.9470	3.000	3.947	2.8400
1.5	.8	4720	2.3008	5.0017	2.3008	4.6740	1.7	1.3	4 430	2.1058	4.7224	2.1058	4.4439
		6085	2.7068	4.3419	2.7068	4.1427			6 110	2.6010	4.0618	2.6010	3.8290
		7160	3.0582	3.9193	3.0582	3.7009			8 680	3.4522	3.3107	3.4522	3.1481
		9890	4.1223	3.0935	4.1223	2.9503			10 000	3.9350	2.9700	3.935	2.8200
1.5	1.1	4840	2.3008	4.6231	2.3008	4.3339							
		6085	2.6706	4.1316	2.6706	3.8920							
		7140	3.0122	3.7779	3.0122	3.5729							
		9840	4.0808	3.0410	4.0808	2.8851							

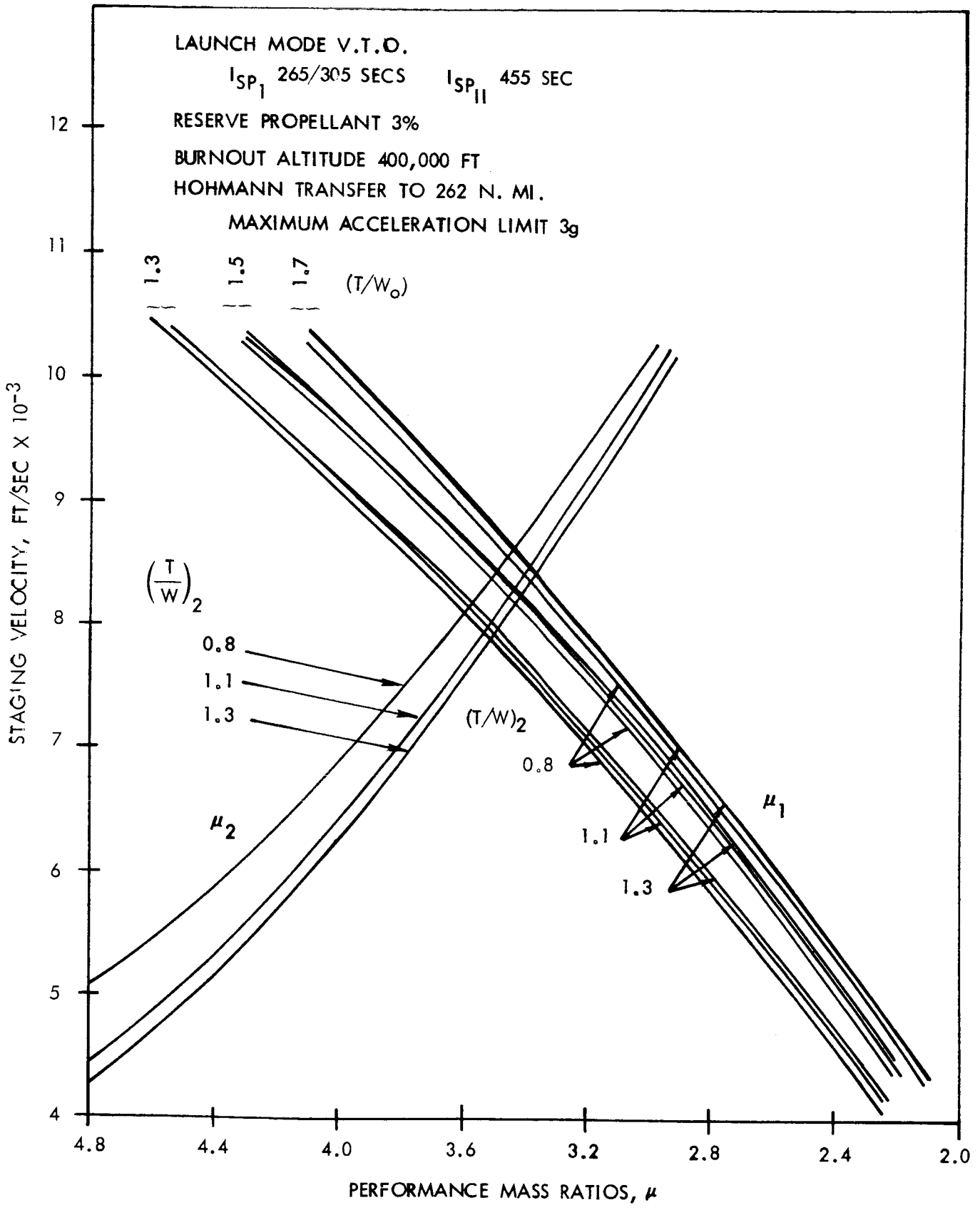

Figure 70. - Performance Mass Ratios

insensitive to the thrust-to-weight ratio of the second stage and vice-versa; the error of this assumption was less than 3 percent for the velocity losses. Resulting maps of first- and second-stage losses as a function of thrust-to-weight of the stage and staging velocity are shown in figures 71 and 72. These carpet plots were for I_{sp}'s 265/305 and 455 for the first and second stage, respectively. It was found that an increased I_{sp} of the second stage (I_{sp} = 475 seconds) did not significantly affect the velocity losses of the second stage. Therefore, figure 72 is used for the second stages with current and advanced engine systems.

Propulsion Considerations

Recoverable launch stages involve two primary propulsion systems: for the launch phase, and for the powered flyback phase of recovery. During Phase I of this study (ref. 1) liquid-propellant rocket engines were investigated on the basis of past developments, scheduled future developments, and projected capabilities during the 1975 to 1985 time period.

Figure 73 shows a trend of rocket engine thrust as a function of the year of initial flight. These data resulted from current investigations as well as numerous past NAA investigations aimed at projecting rocket engine developments. These investigations again have indicated that the prime governor on rocket engine thrust level is the national goal, whether it be space exploration or the result of military requirements. Past developments have tended to conform to the following pattern. A liquid oxygen/RP-1 engine is developed first at a given thrust level. After the development and successful operation of such engines, there follows the development of a new higher performance engine employing high-energy (or storable) propellants. This engine development format has occurred on several occasions in the past and is expected to continue in the future, due to the desire for high confidence in engine development programs. In figure 73, it can be seen that it requires approximately 10 years to achieve an order-of-magnitude increase in engine thrust level. It can also be seen that, approximately five years following the basic engine development at a given thrust level, a high-energy engine is produced. Typically, each step requires a substantial increase in the then-current technology.

Engine performance predictions during the desired time period are shown in figure 74. These data were based on past and current rocket engines performance, with the addition of the performance predicted for advanced engines now in the early stages of development. The extrapolation of this data into the post-1975 period was made by considering advanced propellant

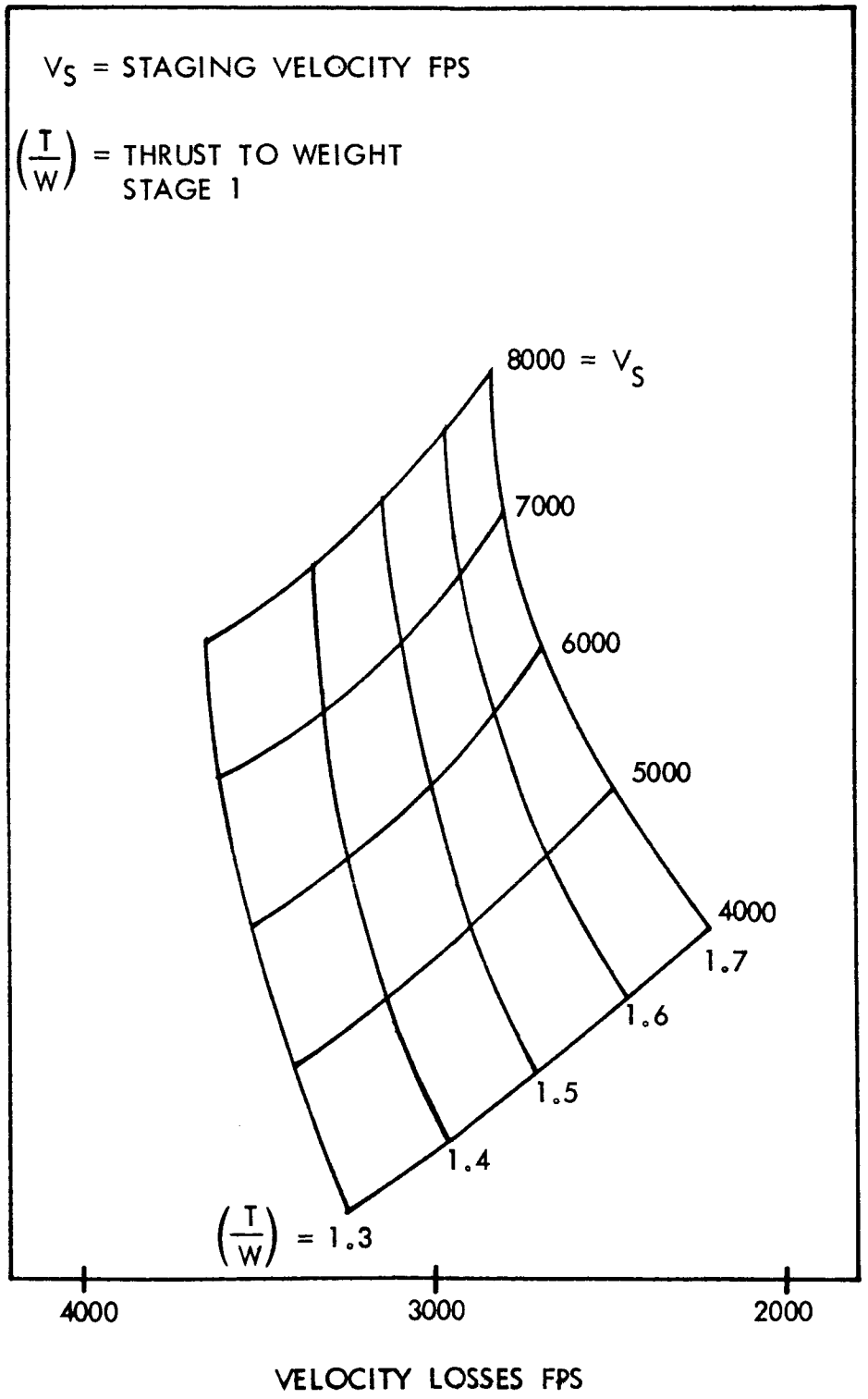

Figure 71. - Velocity Losses for First Stage

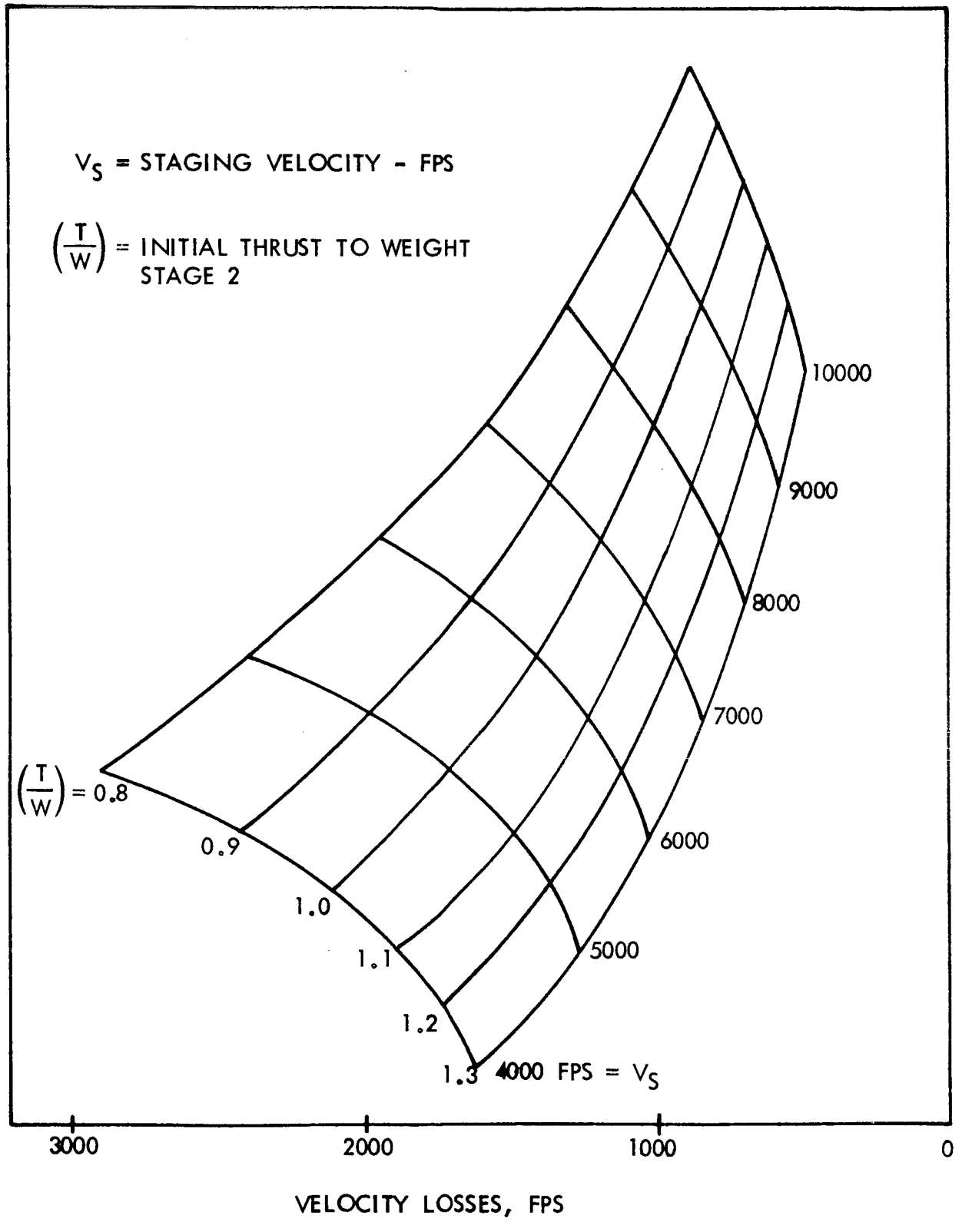

Figure 72. - Velocity Losses for Second Stage

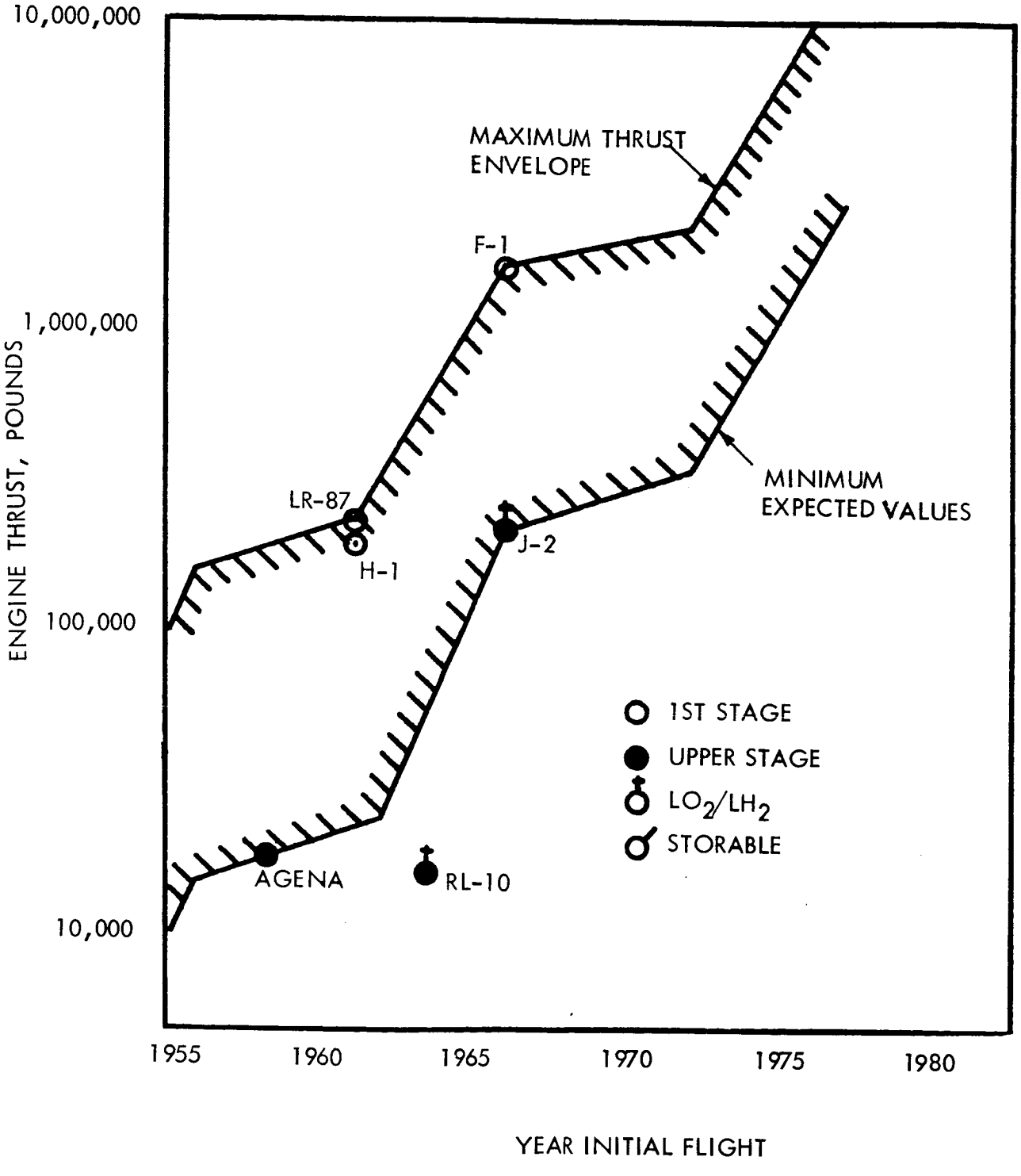

Figure 73. - Liquid-Propellant Rocket Engine Thrust Trends

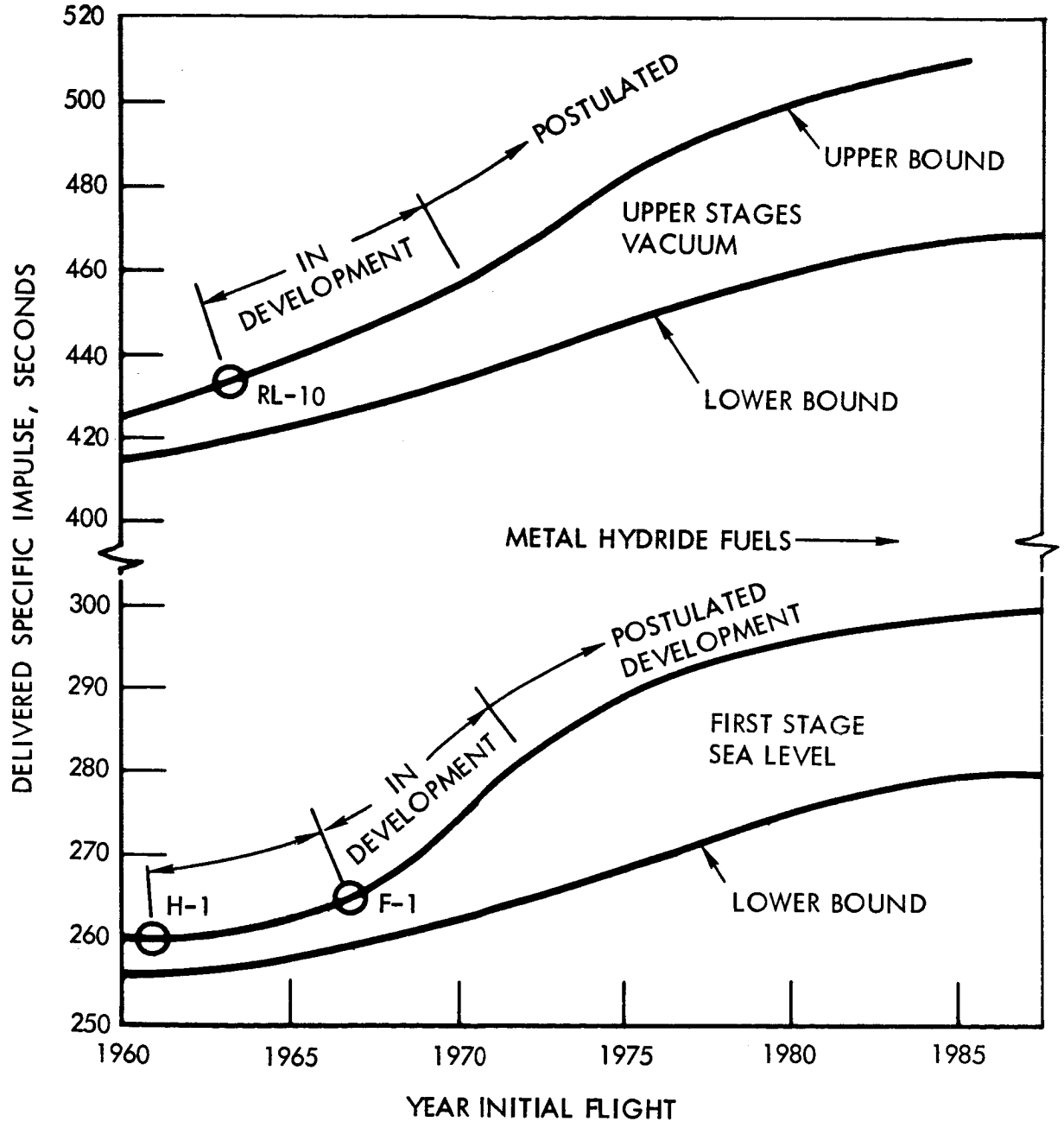

Figure 74.- Estimated Future Performance Trends for Liquid-Propellant Rocket Engines

combinations that are now undergoing basic performance feasibility tests. Figure 74 shows predicted performance of first-stage engines in which dense propellant combinations are utilized to minimize first-stage volume and cost. Such propellants are liquid oxygen/RP-1, the storable combination of nitrogen/tetroxide and Aerozine-50, and advanced storable formulations containing light metals. The upper-stage rocket engine performance predictions shown in figure 74 are based on the utilization of high-energy propellant combinations typified by liquid oxygen/hydrogen, fluorine/hydrogen, and later additions of the light metals and light metal hydrides.

Figure 75 presents predicted engine-thrust to engine-weight ratio trends. It will be noted that there is a distinct difference in engine weight between engines employing cryogenic propellants and those employing the storable propellants. This is due to the relatively high density exhibited by the storable propellants and the resulting reduction in turbomachinery and thrust-chamber weight. Figure 76 presents 1965 engine-thrust to engine-weight ratio as a function of thrust level for various engines ranging in size from 15 000 to 1 500 000 pounds of thrust. These data may be modified to reflect weight characteristics during any year by ratioing according to the trends presented in figure 76.

The trends shown in figures 73 through 76 are based upon data derived from rocket engines developed for expendable stages. Recoverable stages imply reusability and extended life in the rocket engine system. Rocket engines used on the Saturn S-IB and S-V have been considered in studies of recoverable stages (ref. 2 through ref. 5). These studies have considered the F-1 and H-1 engines for first-stage applications and the J-2, LR-87, and RL-10 for upper-stage use (fig. 75). Included in these studies were changes in engine sizing parameters such as expansion ratio and chamber pressure to provide higher delivered specific impulse. Various weight additions were considered in adapting these engines to recovery such as changes in exhaust aspirators, heat exchangers, nozzle insulation protection, and nozzle coolants. Per reference 2, the major problem component in adapting rocket engines to recovery and reusability is the combustion chamber. Components such as turbopumps can be replaced when required, but the shielding-acoustic-protection requirements may result in redesign of the thrust chamber. No problem is anticipated in throttling these engines to ±20 percent. Reference 2 indicates that, from a cost standpoint, the F-1 engine should be considered for first-stage applications.

The propulsion system has caused 9 out of 11 of the catastrophic failures that have historically occurred (ref. 2). A multiengine configuration appears to be more reliable, including uprated configurations. Application of current technology has improved this reliability. The parametric synthesis program uses "rubberized" engines based upon H-1, F-1, and J-2 designs.

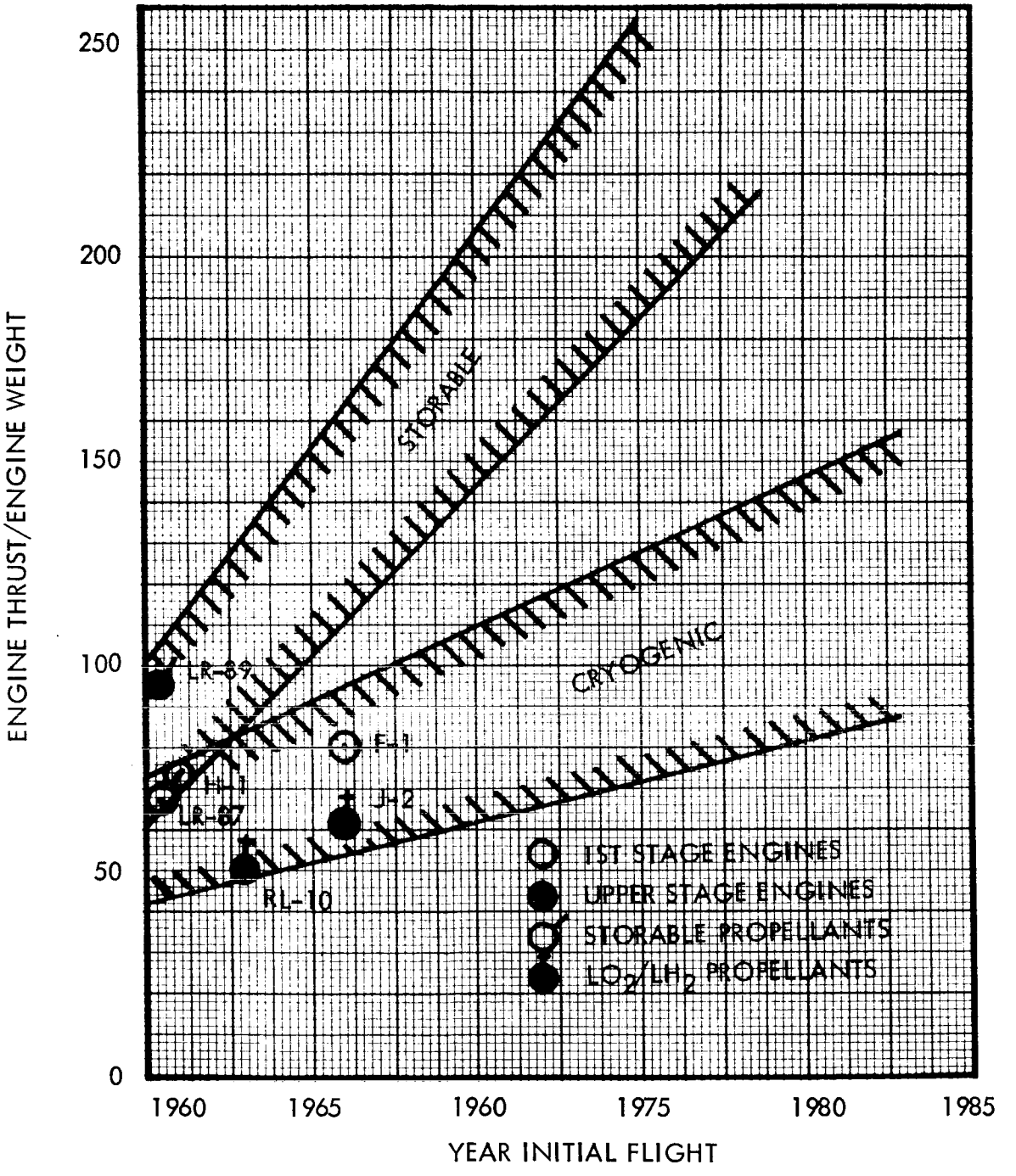

Figure 75. - Current and Predicted Future Engine Thrust-To-Weight Ratio Trends

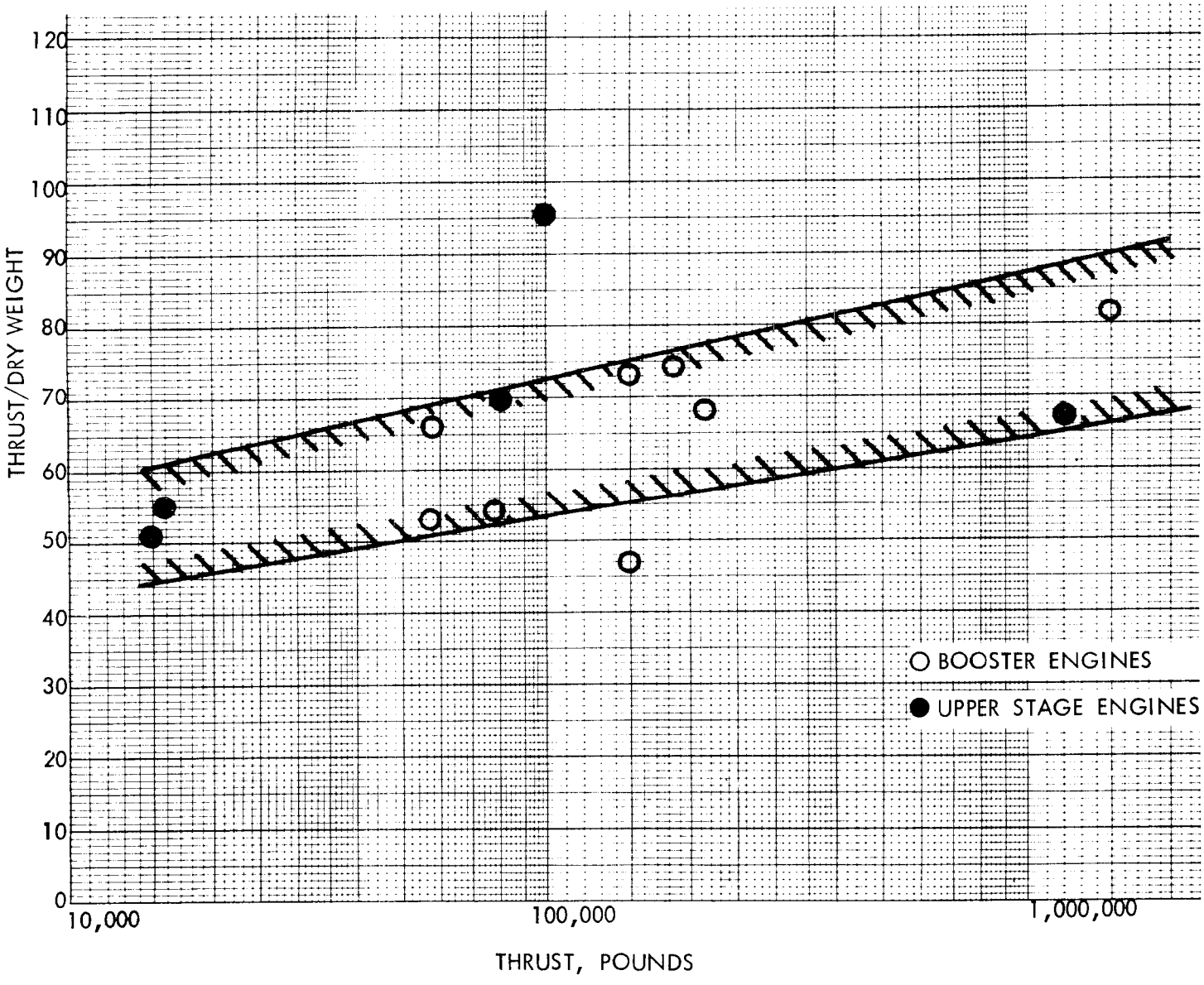

Figure 76. - Liquid Propellant Engine Thrust-to-Weight Ratio - Regenerative Cooled

The effects of mixture ratio, expansion ratio, and chamber pressure can be assessed in terms of effect upon stage mass fraction and booster geometry. For the basepoint recoverable vehicles considered in this phase of the study, a 2.25:1 propellant mixture ratio (LO_2/RP-1) was used on the first stage with an expansion ratio of 25 and a chamber pressure of 1000. Five first-stage engines were used with four gimballed and one fixed. Upper-stage engines were "rubberized" J-2's, using a propellant mixture ratio of 5:1 (LO_2/LH_2), an expansion ratio of 35, and a chamber pressure of 632 psi. Any of these parameters can be changed merely by altering program inputs.

Staging rockets (separation and ullage) parametrically sized in the program are based upon solid motors employing a specific impulse of 260 seconds. This concept is in agreement with current hardware concepts and with other recoverable vehicle studies (ref. 2).

The flyback propulsion system uses a turbojet, high-bypass-ratio turbofan engine similar to the Pratt and Whitney STF 200. These engines were used because of their low specific fuel consumption resulting in lowest total system weight. This system is a significant portion of the inert vehicle weight, and the program provides sensitivity measurements to parametrically optimize flyback propulsion system inputs for Mach number and flyback range. These inputs and their effects are discussed further in Appendix B.

Vehicle Proportioning

The synthesis program was initially used to assist in defining the optimum staging velocity for a fully recoverable wing-body vehicle. The selection of the optimum staging velocity was to be on the basis of minimum weight and, therefore, has to consider the fully recoverable vehicle. A fully recoverable vehicle with three different size payloads into orbit of 20 000, 40 000, and 60 000 pounds was considered. A recoverable first-stage, expendable upper-stage vehicle does not possess a reasonable optimum staging velocity weightwise, since it tries to reduce the size of the recoverable first stage with the degraded performance. Because the synthesis program was not able to evaluate the thermal requirements and weights for the severe temperatures during entry from circular velocity, use was made of existing mass fraction data. Figure 77 shows such a range of mass fractions for a series of propellant loadings for two propellant mixture ratios. These values were obtained from detail studies conducted on winged-body vehicle systems

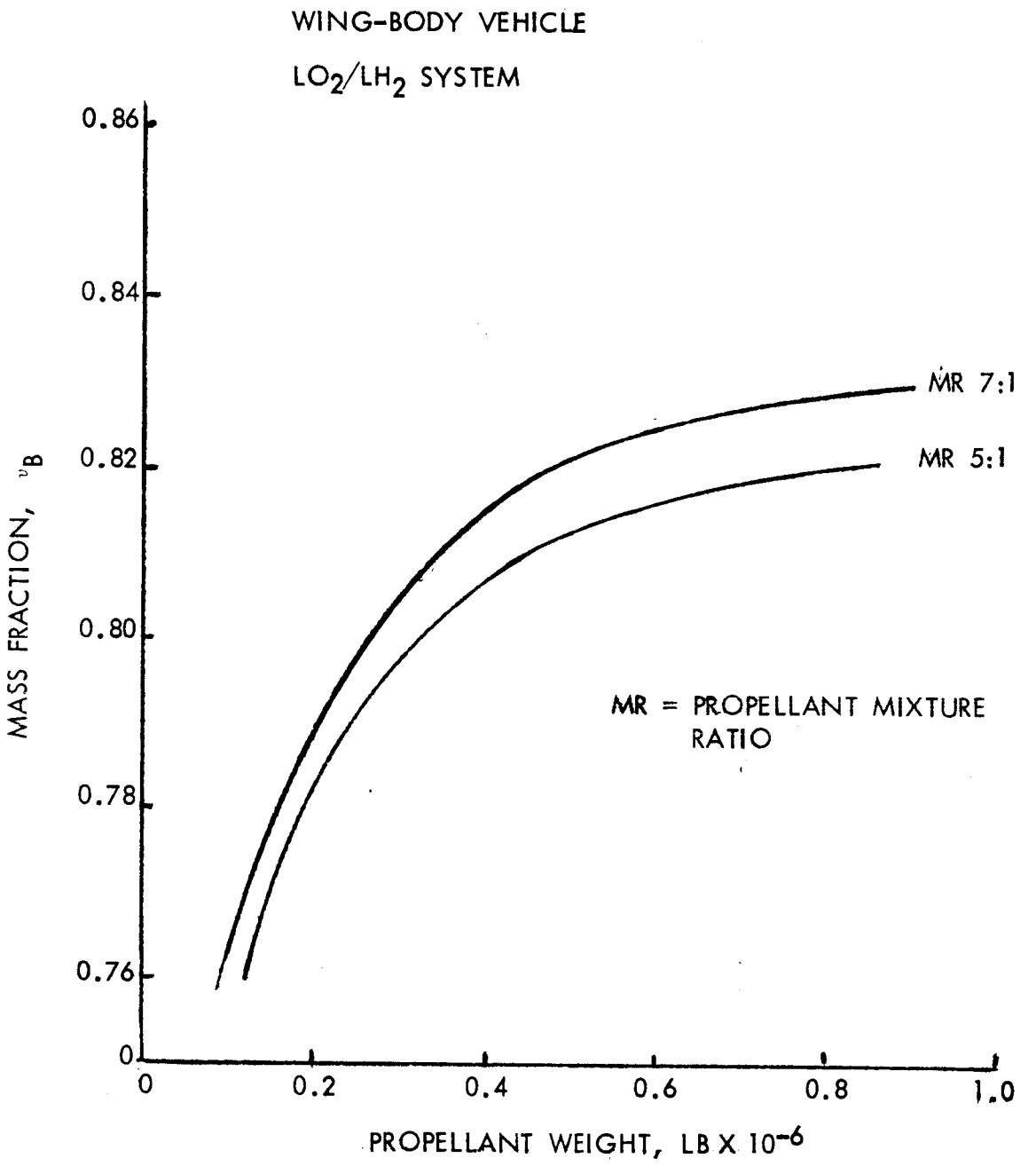

Figure 77. - Stage Mass Fraction for Recoverable Vehicle

with an LO_2/LH_2 propulsion system and obtained from reference 24. The mass fraction ratio v_B is expressed as

$$v_B = \frac{\text{Weight of propellant}}{\text{Weight of propellant + weight of stage}}$$

The weight of stage included in this assessment was for the engines, structure and recovery systems of two crews, controls, wings, and landing gear. There are no flyback cruise capabilities nor passengers and cargo returned from orbit. Payload weight of 20 000 to 60 000 pounds was placed in orbit and left there; return consideration is discussed later.

The parametric vehicle synthesis was exercised with the appropriate mass fraction relationships of figure 77 to synthesize the total vehicle system. Initially current propulsion systems and characteristics were considered; mixture ratio of 5:1 and specific impulse I_{sp} = 425 seconds for the upper stage with the lower stage possessing I_{sp} = 290 seconds average values for sea level and vacuum and a mixture ratio of 2.25:1. The resulting vehicles were marginal, performance-wise, with staging velocity requirements imposing performance mass ratios that were incompatible with the mass fraction criteria of figure 77. Therefore, current propulsion system and specific impulses were not considered as practical systems for the recoverable-expendable vehicle systems.

Advanced propulsion systems investigated during Phase 1 of the study were taken to be applicable for the recoverable vehicle systems. In order to preserve consistency between the two phases of this study, identical characteristics were used, as follows:

Near-term: Post-1975

First stage	LO_2/RP_1 system	308 seconds average
Second stage	LO_2/LH_2 system	460 seconds

Future: Post-1985

First stage	LO_2/RP_1 system	340 seconds average
Second stage	LO_2/LH_2 system	500 seconds

Further details of these propulsion systems are discussed in the preceding section of propulsion performance.

Recoverable vehicles were synthesized with the near-term propulsion system for a range of payloads injected into Earth orbit. The program was allowed to systematically size the vehicle stages with no tank-diameter-requirements input data. The program performed a search procedure to

define an acceptable diameter for each of the various stages that do not result in a hammerhead configuration (lower-stage diameter smaller than stages above). The smaller propellant tank was prescribed, as a minimum, to be an ellipsoidal tank equal to the stage diameter. Then an acceptable wing was fitted within prescribed aspect-ratio and taper-ratio limits. It was found by inspection of the computer results that, for a LO_2/RP1 stage with short tanks, the wing root chord required was longer than practical, i.e., its position resulted in the leading edge being too close to the nose portion of the first stage. Built into the synthesis program was sizing logic that would progressively reduce the stage diameter, i.e., increase the stage fineness ratio until an acceptable wing planform could be fitted. The preliminary results were with the stage diameter dictated internally by the program. The initial diameters were rounded off to likely size, and the program was rerun to find the weight effects of these modified diameters. The resulting vehicle shapes produced appear to be practical design configurations. Stage diameters used for the three payload weights are as follows:

Payload (lb)	Stage	Diameter (in.)
20 000	1	260
	2	220
40 000	1	300
	2	260
60 000	1	320
	2	300

A breakdown of stage gross and burnout weights is shown for 20 000-, 40 000-, and 60 000-pound payloads in figure 78, 79, and 80, respectively. These results indicate that, with the vehicle systems used and the mass-fraction, propellant-size relationships for the upper stage as per figure 81, a minimum liftoff system weight appears to exist at a staging velocity of 6800 feet/second. The total velocity requirements to attain orbit, rendezvous, and deorbit are quoted in table 24, and the velocity losses for each stage are shown in figures 71 and 72 for thrust-to-weight ratios of 1.25 for the first stage and 1.0 for the upper stage. Although preselected mass fractions were used for the upper stage, the synthesis program sized and proportioned the winged upper stage correctly and determined its effect on the design requirements and loading for the bottom stage. With the velocity requirements for the recoverable first stage and the flight and prelaunch loads identified, the first stage was systematically sized and component weight evolved. The weight summary from the program outputs are shown in figures 78, 79, and 80. The baseline vehicle systems were now assumed to be optimally proportioned at the 6800 feet/second staging velocity.

STAGE 1: RECOVERABLE
STAGE 2: RECOVERABLE

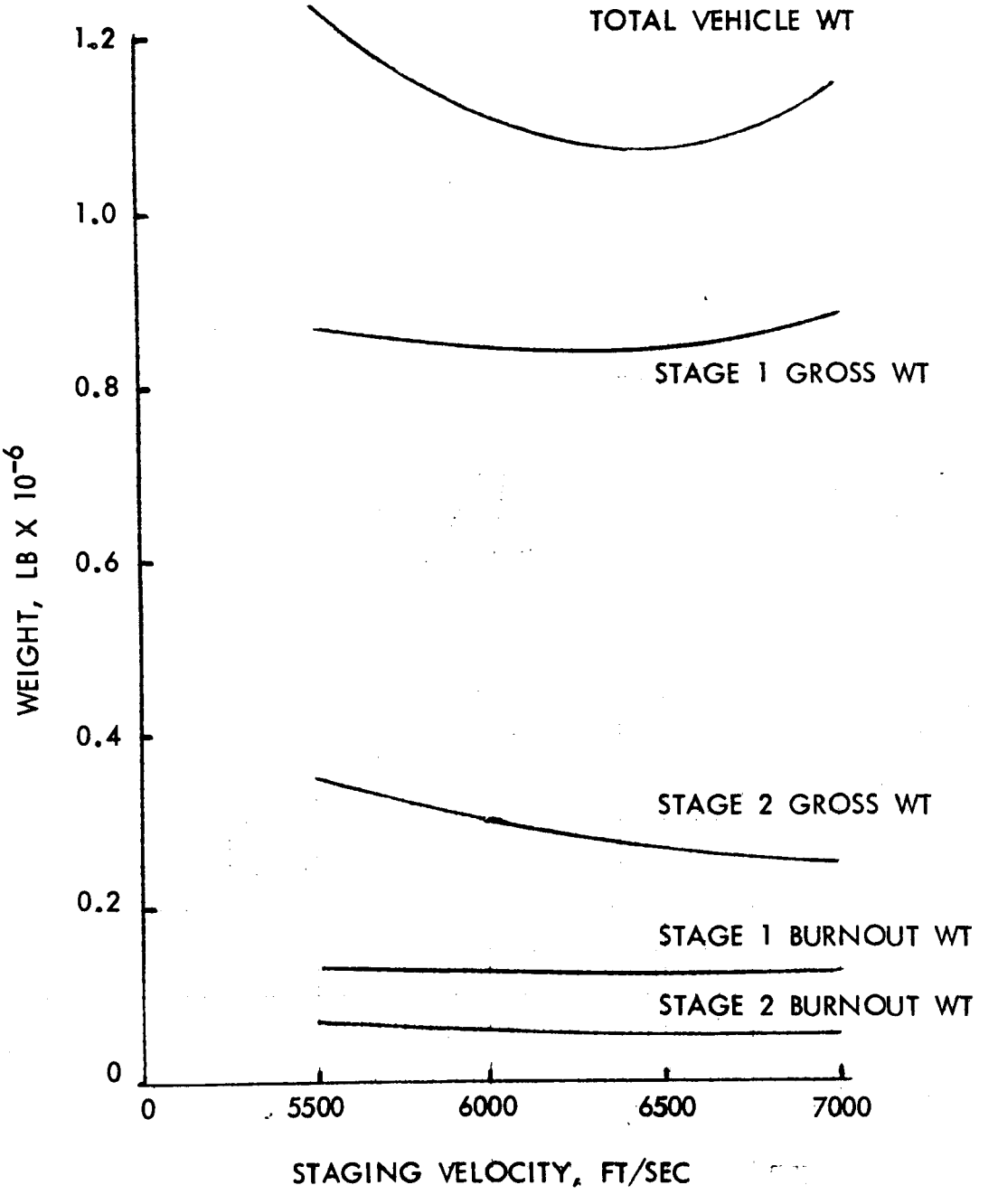

Figure 78. - Staging Velocity Effects—20 000-Pound Payload

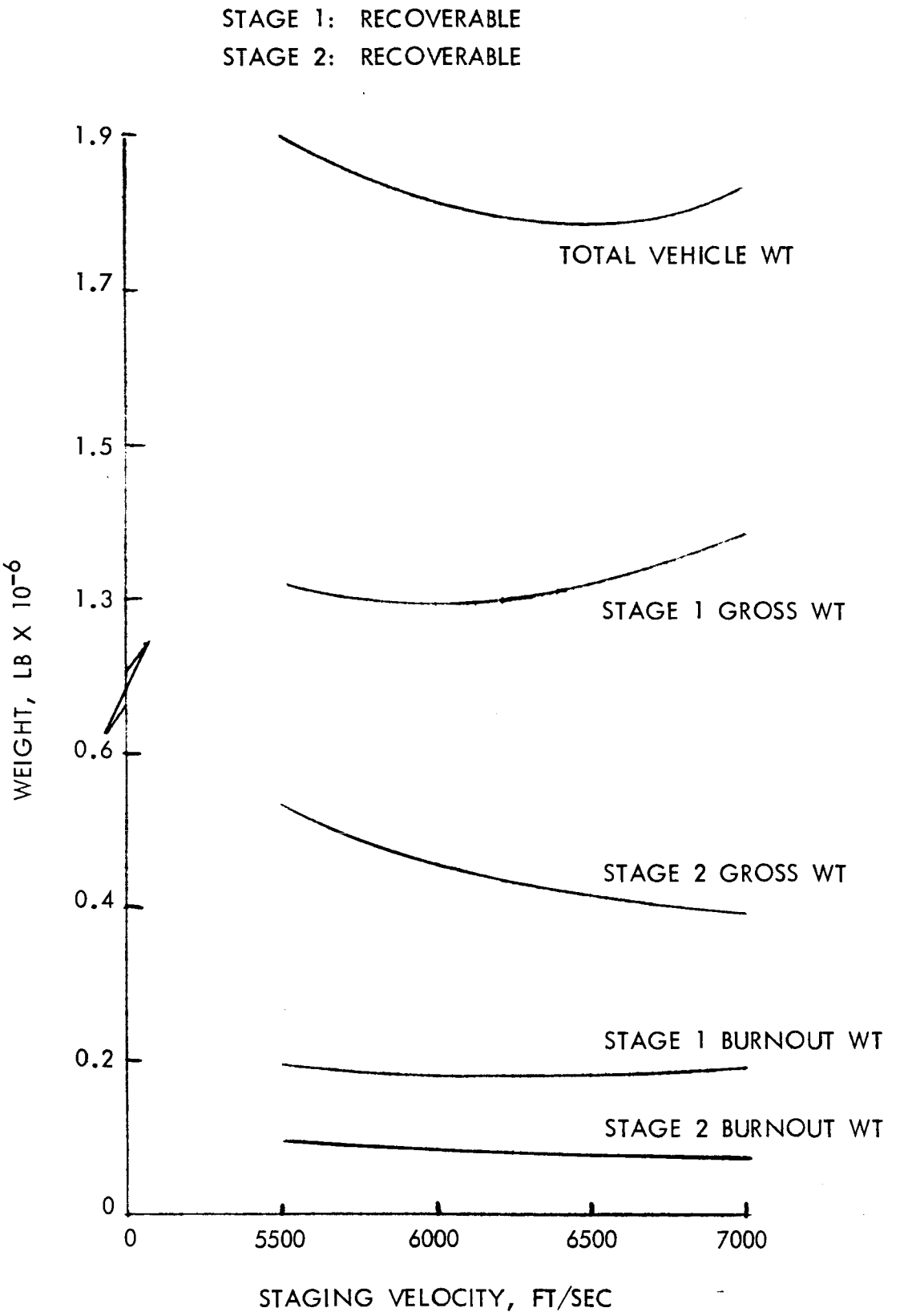

Figure 79. - Staging Velocity Effects—40 000-Pound Payload

STAGE 1: RECOVERABLE
STAGE 2: RECOVERABLE

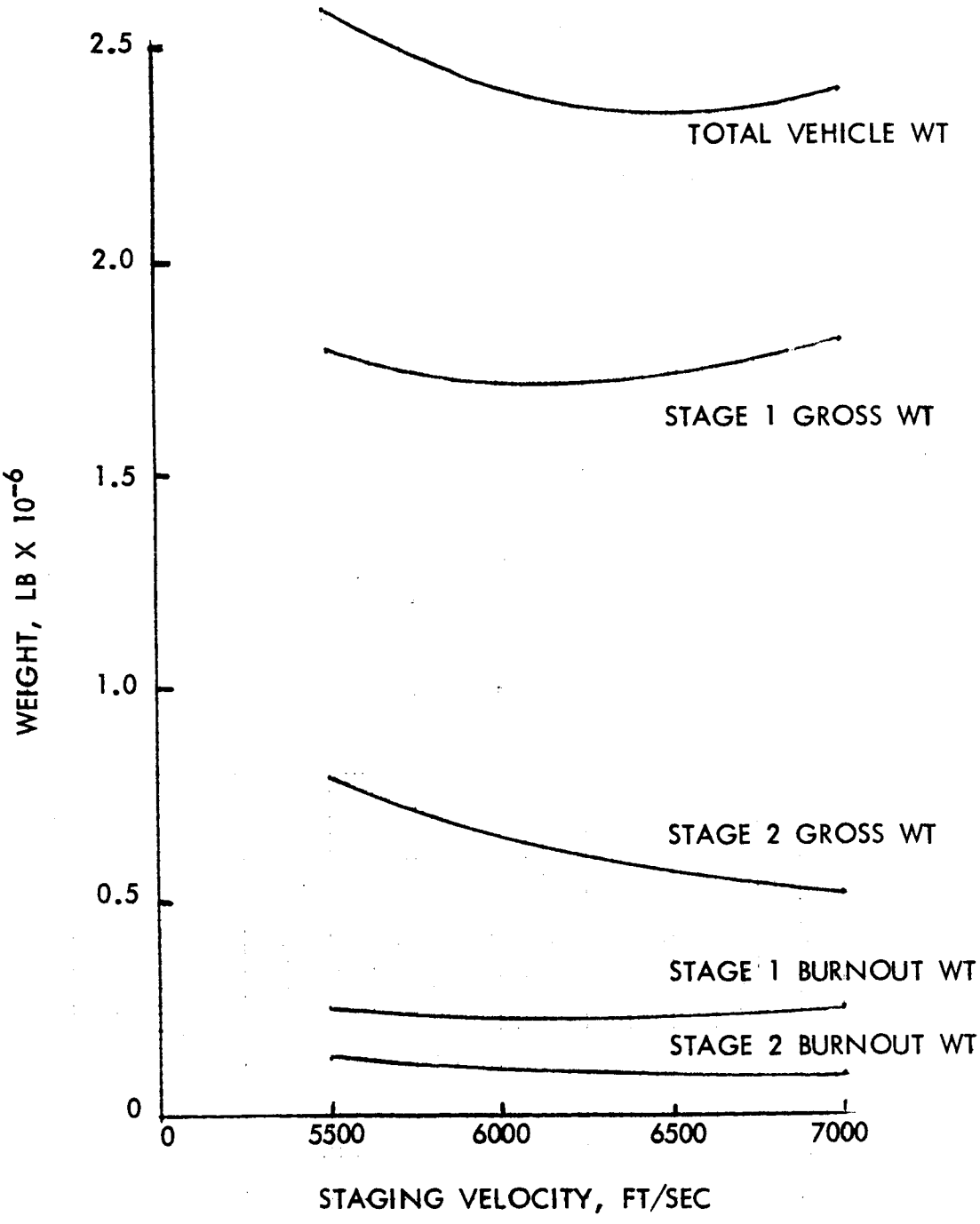

Figure 80. - Staging Velocity Effects—60 000-Pound Payload

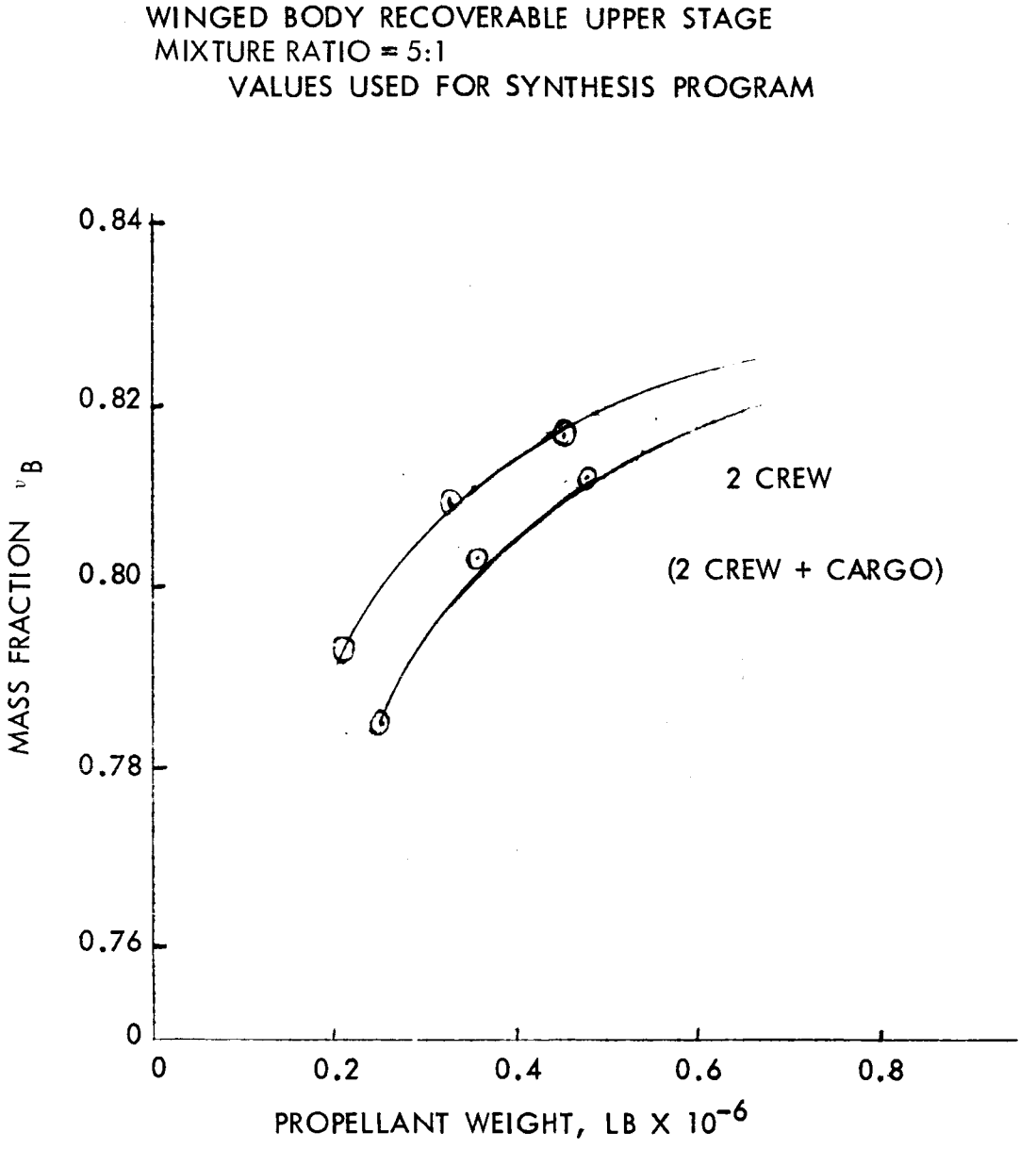

Figure 81. - Mass Fractions for Recoverable Upper Stage

The Reusable Orbital Transport concept (ref. 18) was concerned with the delivery of payload into orbit and the subsequent return of passengers; i.e., cargo onboard during the reentry and return-flight phase. Therefore, the mass fraction ratios of figure 77 were reestimated to consider the inclusion of 3000 pounds of return weight, either cargo or passengers plus equipment. These changes to the mass fraction are shown in figure 81, and the actual value points for the 20 000-, 40 000-, and 60 000-pound vehicles are shown for the entry conditions of two crew members plus cargo. The modified mass fractions were used for the program inputs, and the vehicles were resized. Variations in the required launch weight and individual stage weights are seen in figure 82 for the complete range of payload weights. The launch weights for the baseline recoverable-expendable vehicle systems were selected from the results of figure 82, and are as follows:

Orbital Payload Weight (lb)	Launch Weight ($\times 10^6$ lb)
20 000	1.3
40 000	1.9
60 000	2.5

Since these launch weights are required to inject 20 000 to 60 000 pounds of payload into orbit in a fully recoverable mode, the launch weights were used to determine payload capability for the mode with an expendable upper stage. This could be considered in the building-block approach of gradually evolving from an expendable vehicle system, initially adding wings to a first stage for its recovery, and performing the same approach to the upper stage. The improvement in payload capability with the expendable upper-stage vehicle system is shown in figure 83. Replacement of the winged body upper stage with the expendable configuration completely altered the prelaunch and in-flight loading environment of the vehicle system. Additional cases were investigated with future (post-1985) propulsion characteristic for the same lift-off vehicle weights. These changes are reflected in figure 83 and show the marked improvement in payload capabilities.

Base Line Vehicle Systems

This section defines in detail the design characteristics and performance for the series of base-line recoverable-expendable vehicle systems. Velocity requirements to achieve orbit, losses, control and reserves are broken down

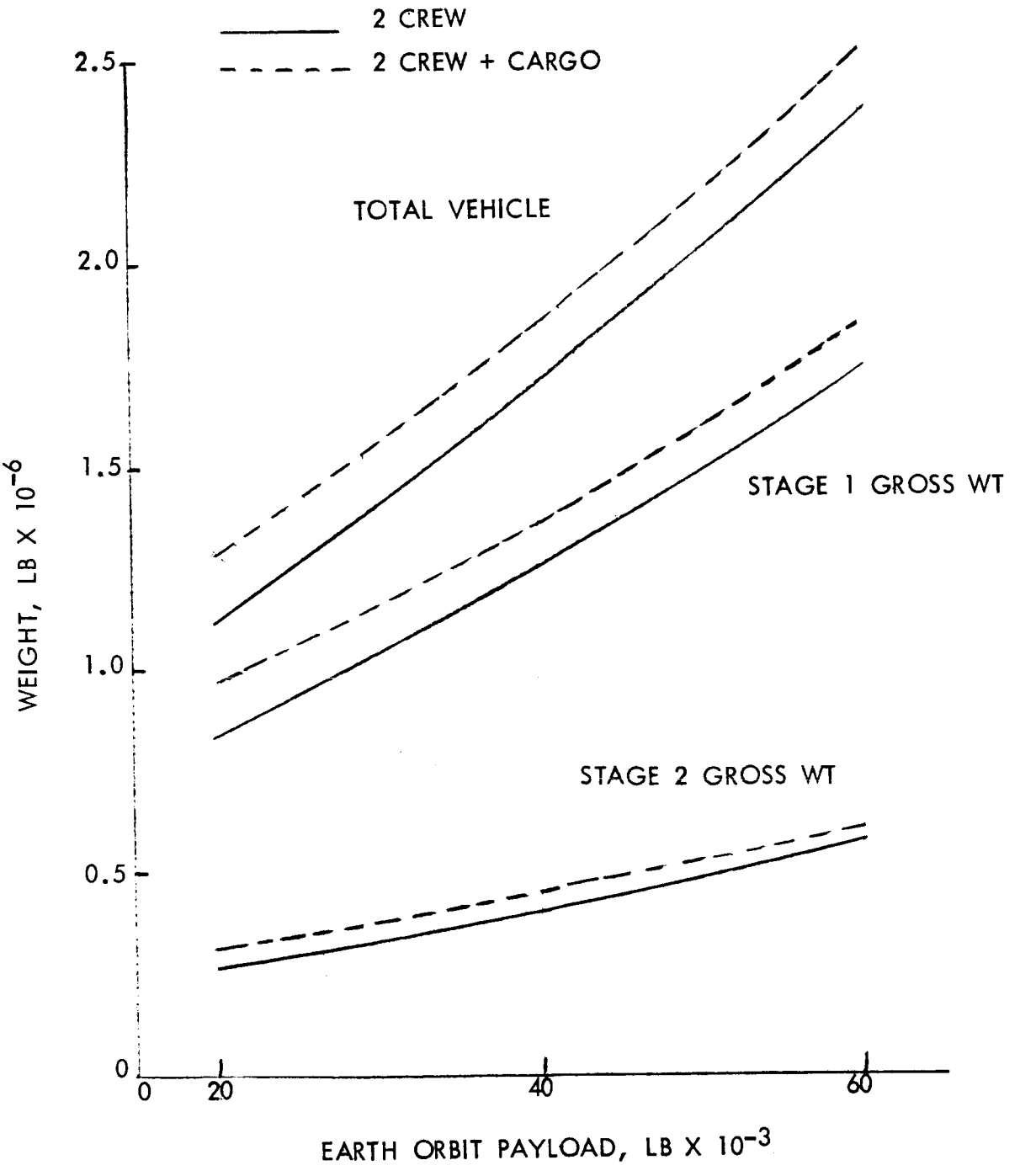

Figure 82. - Recoverable-Recoverable Vehicle Sizing

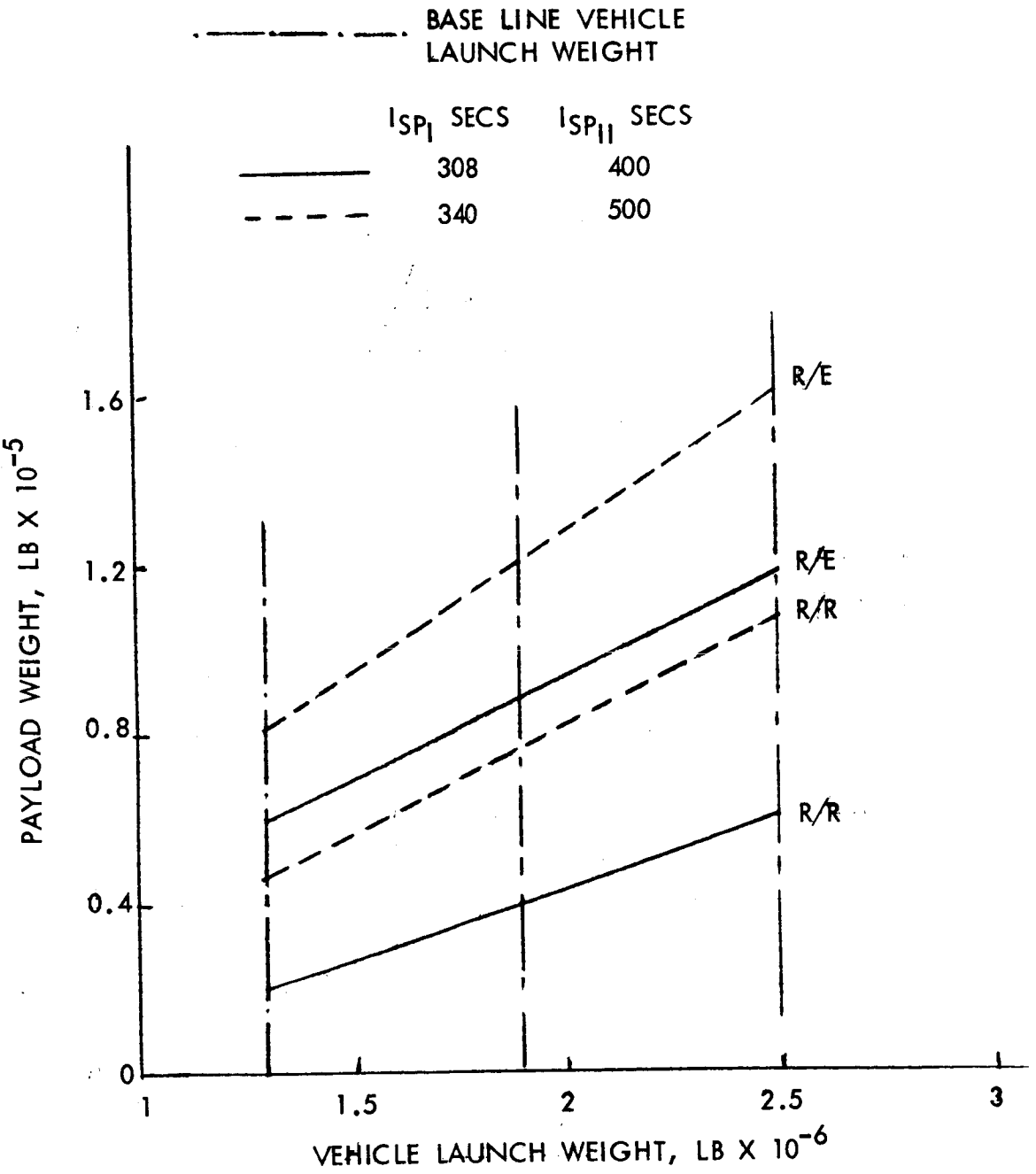

Figure 83. - Effect of Expendable Upper Stages

in detail for each stage in table 27. All the base-line systems were sized to these stage velocities. Vehicle design characteristics, table 28 show the geometrical size parameters used; some of these parameters were varied for the sensitivity studies. Flyback requirements and systems were assumed to be subsonic turbofan engines, these engines being assumed to be adequately protected against high temperatures during entry. Cruise range for the flyback condition was not investigated by determination of staging and entry position down-range and the distance required to flyback to base; instead, a typical range of 300 nautical miles was taken to evaluate the additional fuel requirements.

TABLE 27. - STAGE VELOCITY REQUIREMENTS FOR RECOVERABLE-EXPENDABLE VEHICLES

Velocity Factor	Requirement, fps
Circular velocity at 50 n. mi.	25 740
Less earth rotation	1 246
Net velocity to be gained	24 494
First-stage velocity at end boost	6 800
First-stage velocity losses	3 260
Total velocity requirement for first stage	10 060
Second-stage boost requirements	17 694
Hohmann transfer at 50 to 100 n. mi.	91
Launch window	100
Hohmann transfer to 100 n. mi. apogee ' V	91
Hohmann transfer to 262 n. mi.	529
1. 5% reserve for deviation from normal operating procedure	300
Second-stage velocity losses	1 010
Total velocity requirement for second stage	19 815

Propulsion and propellant characteristics shown in table 29 were taken to represent the engine systems for the two stages. Near-term engine systems have specific impulses of 308 seconds average for the first stage and 460 seconds for the upper stages. When future systems (post-1985) are discussed, these impulses are increased to 340 seconds average and 500 seconds vacuum. Ullage factors of 10 percent and 15 percent are quoted, but these values are for the total volume of fuel and oxidizer to allow adequate sizing of the LO_2 tanks. Ullage pressures are 39. 0 and 36. 0 psi, respectively,

TABLE 28. - VEHICLE DESIGN CHARACTERISTICS

Characteristic	Value
Bulkhead Aspect Ratio	
Stage 1	$\sqrt{2}$
Stage 2	$\sqrt{2}$
Separate bulkheads Stage 1	
Common bulkheads Stage 2	
Payload fineness ratio for cylinder	0.5
Payload cone half-angle	35°
Crew equipment weight	3000 lb
Wing aspect ratio, minimum	2.25
Wing aspect ratio, maximum	2.5
Wing taper ratio	0.45
Maximum allowable leading edge sweep	60°
Thickness-to-chord ratio, percent	8
Fin area to wing area, percent	8
Hypersonic wing loading during entry	50 lb/ft^2
Flyback range	300 n. mi.
Flyback (L/D) maximum	5.0
Flyback cruise Mach number	0.6
Specific fuel consumption	0.7 lb/hp/hr
Thrust to installed engine weight ratio	3.0

which, coupled with the flight hydrostatic pressure head, will meet engine net-positive-suction-head requirements and result in the design loading for the tanks and bulkheads. Aerodynamic conditions and trajectory data were not synthesized by the program but were supplied as input data. A summary of this data is given in table 30. Ground wind profiles, gust magnification, and vortex shedding factors are taken similar to the Saturn design conditions (ref. 22). Maximum dynamic pressure conditions for vertically launched vehicles occur between 30 000 to 35 000 feet altitude, and typical trajectory flight profiles assisted in defining applicable dynamic pressures and Mach numbers, figure 68. For the baseline vehicles, 720 pounds/square feet was the maximum dynamic pressure, and the relative flight angle of attack due to a sharp-edge wind spike of 9 meters/second was 4 degrees; this presupposed that the vehicle was being flown with a minimum-lift trajectory prior to the gust. As the payload envelope shape and aerodynamic characteristics are not explicitly defined, the total normal force from the payload envelope was taken

TABLE 29. - PROPULSION AND PROPELLANT CHARACTERISTICS

Characteristic	Value	
	Stage 1	Stage 2
Engine system propellants	LO_2/RP_1	LO_2/LH_2
Thrust-to-weight at liftoff	1.25	1.0
Number of engines	5	1
Number of movable engines	4	—
Engine specific impulse, sec	308	460
Chamber pressure, psi	1000	632
Engine expansion ratio	25	35
Gimbal angle at max q	4.0°	—
Mixture ratio oxid/fuel	2.25	5.0
Oxidizer density, lb/in^3	0.0413	0.0413
Fuel density, lb/in^3	0.0292	0.00256
Ullage factor, percent	10	15
Ullage pressure, lb/in^2	39.0	36.0

as 80 000 pounds and the drag as 50 000 pounds for the maximum-dynamic-pressure condition. With these loads and the aerodynamic coefficients for the basic elements of the vehicle, the overall axial load, shear, and bending moments experienced by the fuselage were developed systematically. Although 5 g maximum acceleration allowable is quoted in table 30, this was only a maximum stop for the program logic. In fact, the actual acceleration of the vehicle at end boost was defined by the vehicle thrust and burnout weight conditions.

Structural material properties shown in table 31 were considered for the all-aluminum base line vehicles. Cryogenic insulation unit weights for ground-hold criteria were taken similar to current insulation systems used on SII and SIVB stages. Additional insulation weights and an outer metal heat-shield were assessed for the entry phase; these insulation unit weights are shown in figures 84 and 85.

Results of the synthesized base line vehicles are given in tables 32 through 60 for both near-term and future I_{sp} with 1.3×10^6 to 2.5×10^6 pounds lift-off vehicles. The future I_{sp} systems were sized independently of the near-term systems, but many of the design parameters for the former were evolved by the vehicles sized with near-term specific impulses. Parameters that remained invarient included liftoff weight, stage thrust-to-weight ratio, staging velocity, and stage diameter. Each vehicle system is defined with five tables and their contents can be broken down as follows:

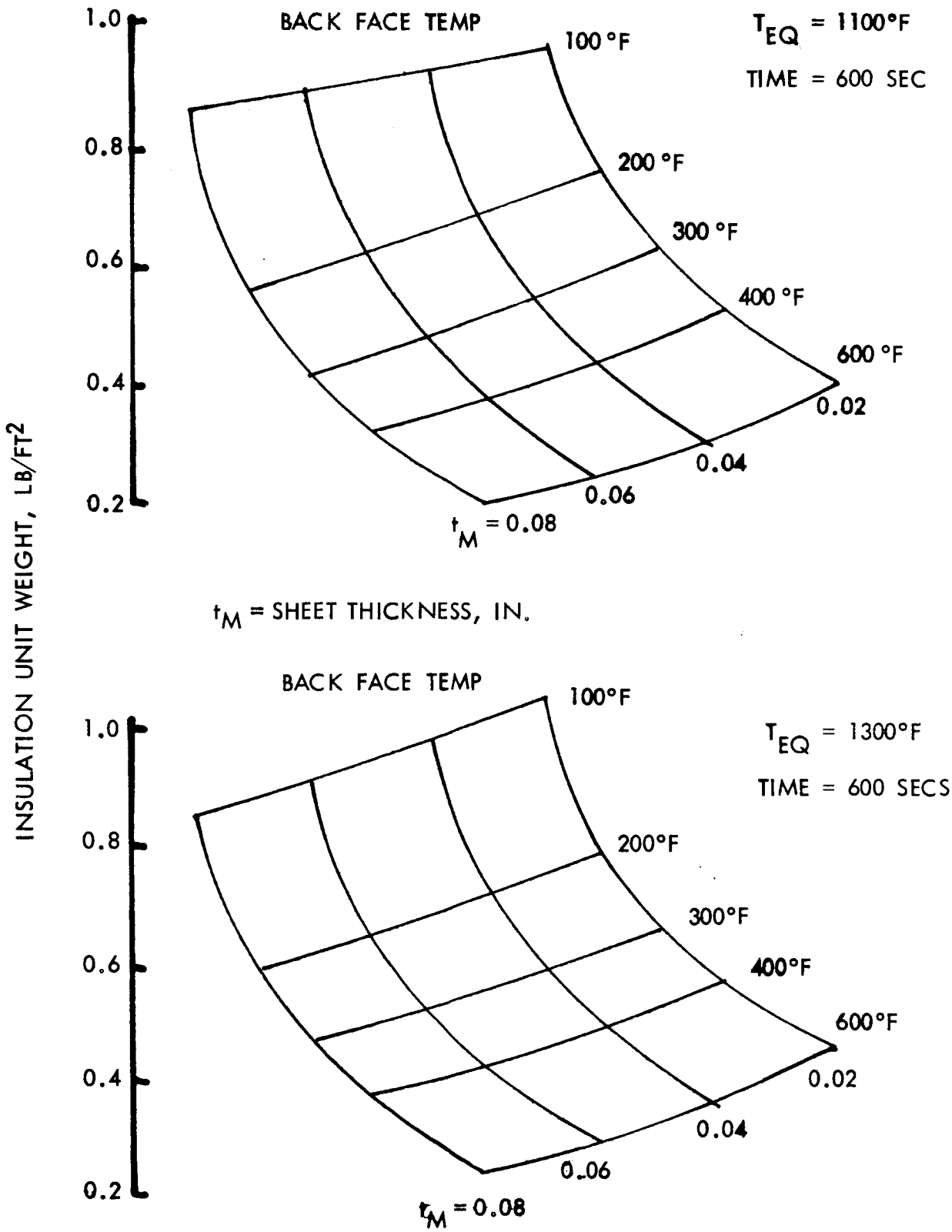

Figure 84. Insulation Weights for 1100 and 1300°F

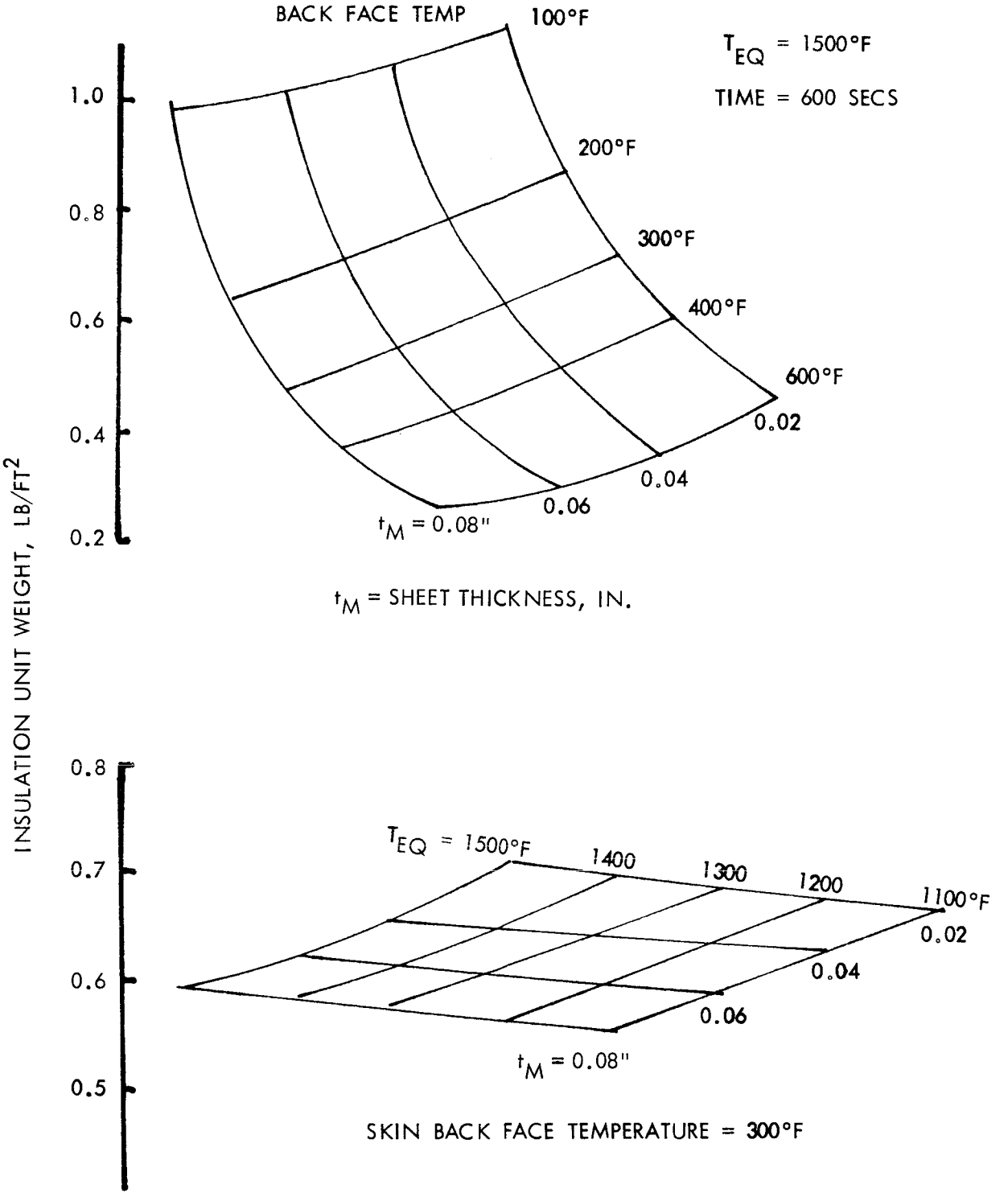

Figure 85. - Insulation Weights for 1500°F

TABLE 30. - AERODYNAMIC TRAJECTORY DATA

Parameter	Value
Wind velocity at reference altitude	90 ft/sec
Wind velocity at ground	50 ft/sec
Reference altitude	500 ft
Gust factor	1.54
Vortex shedding factor	1.25
Normal coefficient on body element	0.7
Normal coefficient on wing element	1.2
Normal coefficient on payload	0.7
Maximum dynamic pressure (q_{max})	720 lb/ft^2
Angle of attack at q_{max}	4°
Lift curve slope for wing at q_{max}	0.04
Wing incidence at q_{max}	4°
Lift curve slope for frustum at q_{max}	0.025
Lift force from payload envelope at q_{max}	80 000 lb
Total payload drag at q_{max}	50 000 lb
Drag coefficient for wing at q_{max}	0.2
Drag coefficient for frustum at q_{max}	0.1
Maximum acceleration allowable	5 g
Stall velocity prior to landing	150 knots
Touchdown angle	15°
Lift curve slope at landing	0.04

Tables 32 through 37

Weight - payload, burnout, propellant, stage, and structure and subsystems

Performance - mass ratio, mass fraction, delta velocity and specific impulse

Dimensional data - size description of complete vehicle system

Tables 38 through 43

Weight distribution - prelaunch, max $q\alpha$, end boost

TABLE 31. - STRUCTURAL MATERIAL DATA

Material Property	Value
Fuselage shell-aluminum	
Young's modulus at room temperature	10.5×10^6 lb/in^2
Young's modulus at end boost temperature	9.6×10^6 lb/in^2
Material density	0.1 lb/in^3
Ultimate stress level, ftu, ave. value, R. T.	65 000 lb/in^2
Wing and fin-aluminum	
Young's modulus at room temperature	10.5×10^6 lb/in^2
Young's modulus during entry (760°R backface)	9.6×10^6 lb/in^2
Working stress level wing cover plate (R. T.)	65 000 lb/in^2
Stress level for cover plates during entry	60 000 lb/in^2
Shear stress for spar webs (R. T.)	30 000 lb/in^2
Shear stress for L. E. & T. E. (R. T.)	30 000 lb/in^2
Density of wing material	0.1 lb/in^3
Stagnation equilibrium temperature	2000°R
Back-face temperature for fuselage	760°R
Back-face temperature for wing	760°R
Ultimate safety factor (mech loads)	1.4

Loads matrix - axial shear and bending moment at prelaunch, max qα, end boost

Tables 44 through 49

Pressure matrix - prelaunch, max qα, end boost

Applied loads - design compressive loading intensity at prelaunch, max qα, end boost and maximum envelope

Tables 50 through 55

Recovery features - wing weights and insulation weights

Tables 56 through 61

Weight statement - component and subsystem weight descriptions.

TABLE 32. - PERFORMANCE CHARACTERISTICS FOR 1.3 X 10^6-POUND VEHICLE, NEAR-TERM I_{sp}

WEIGHT PERFORMANCE CHARACTERISTICS

STAGE	1	2
WEIGHT (LB)		
PAYLOAD	339212.	58528.
BURN-OUT	133664.	30492.
STRUCTURE/SUBSYSTEMS	111764.	23296.
ENGINES	21900.	7196.
PROPELLANT	831124.	250192.
STAGE	964788.	280684.
RATIOS		
PERFORMANCE	0.63736	0.73757
MASS FRACTION	0.86146	0.89137
DELTA VELOCITY (FPS)	10060.	19815.
SPECIFIC IMPULSE (SEC)	308.	460.

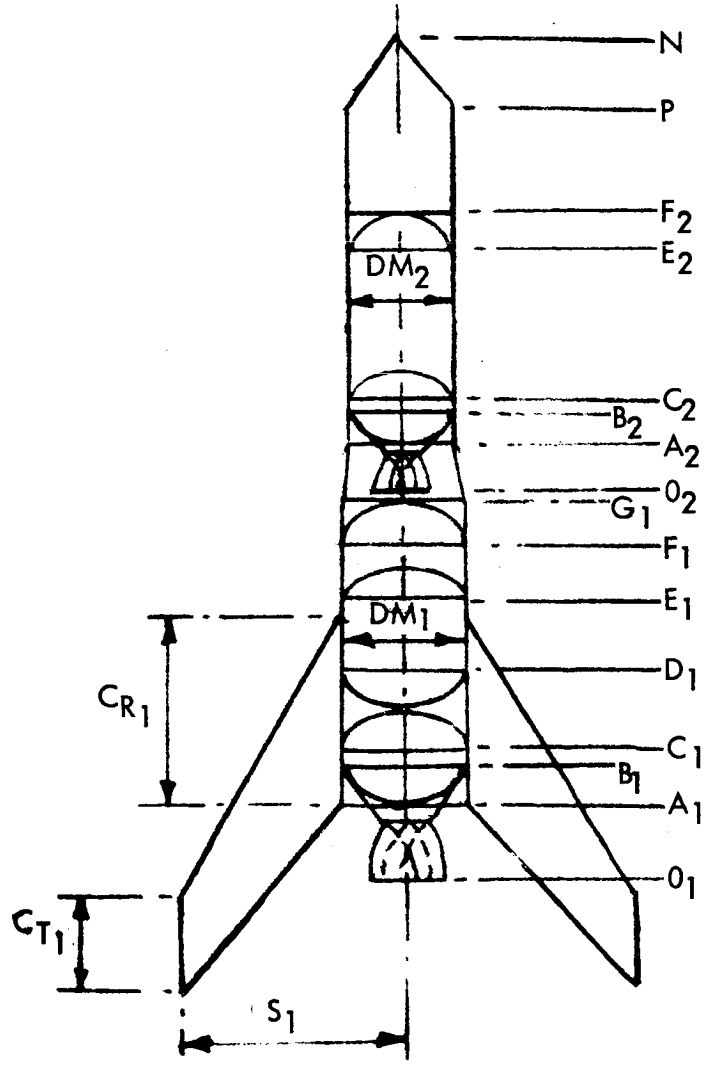

Station	Stage 1*	Stage 2*
N	—	2025.9
P	—	1868.8
C_T	216.0	—
C_R	479.0	—
S	521.0	—
DM	260.0	220.0
G	915.8	—
F	785.8	1758.8
E	693.9	1681.0
D	524.8	—
C	325.3	1254.7
B	264.5	1124.3
A	172.6	1046.5
0	0	1026.5

*Dimensions in inches

TABLE 33. - PERFORMANCE CHARACTERISTICS FOR 1.3 X 10^6-POUND VEHICLE, FUTURE I_{sp}

WEIGHT PERFORMANCE CHARACTERISTICS

STAGE	1	2
WEIGHT (LB)		
PAYLOAD	389469.	80351.
BURN-OUT	130778.	33403.
STRUCTURE/SUBSYSTEMS	108878.	25417.
ENGINES	21900.	7986.
PROPELLANT	783754.	275715.
STAGE	914531.	309117.
RATIOS		
PERFORMANCE	0.60104	0.70793
MASS FRACTION	0.85700	0.89194
DELTA VELOCITY (FPS)	10060.	19815.
SPECIFIC IMPULSE (SEC)	340.	500.

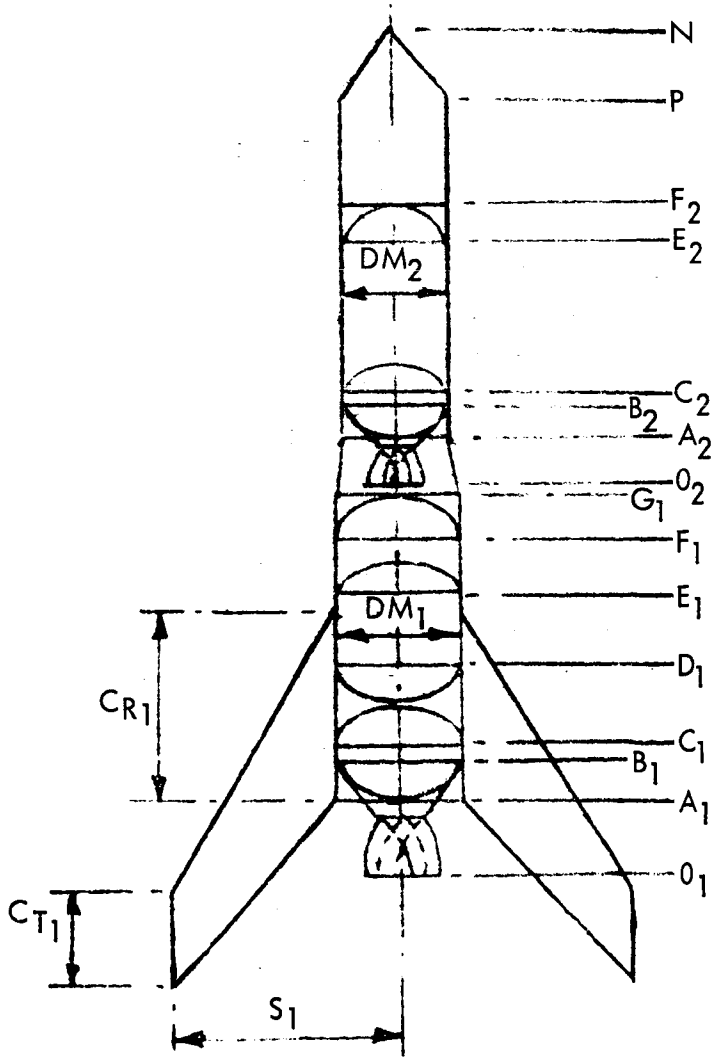

Station	Stage 1*	Stage 2*
N	—	2075.8
P	—	1918.7
C_T	213.0	—
C_R	473.0	—
S	516.0	—
DM	260.0	220.0
G	889.5	—
F	759.5	1808.7
E	667.6	1730.9
D	515.1	—
C	315.6	1175.3
B	265.3	1106.8
A	173.4	1029.0
0	0	1007.6

*Dimensions in inches

TABLE 34. - PERFORMANCE CHARACTERISTICS FOR 1.9 X 10^6-POUND VEHICLE, NEAR-TERM I_{sp}

WEIGHT PERFORMANCE CHARACTERISTICS

STAGE	1	2
WEIGHT (LB)		
PAYLOAD	499852.	88023.
BURN-OUT	189155.	43153.
STRUCTURE/SUBSYSTEMS	157746.	33514.
ENGINES	31409.	9639.
PROPELLANT	1210993.	368675.
STAGE	1400148.	411829.
RATIOS		
PERFORMANCE	0.63736	0.73757
MASS FRACTION	0.86490	0.89522
DELTA VELOCITY (FPS)	10060.	19815.
SPECIFIC IMPULSE (SEC)	308.	460.

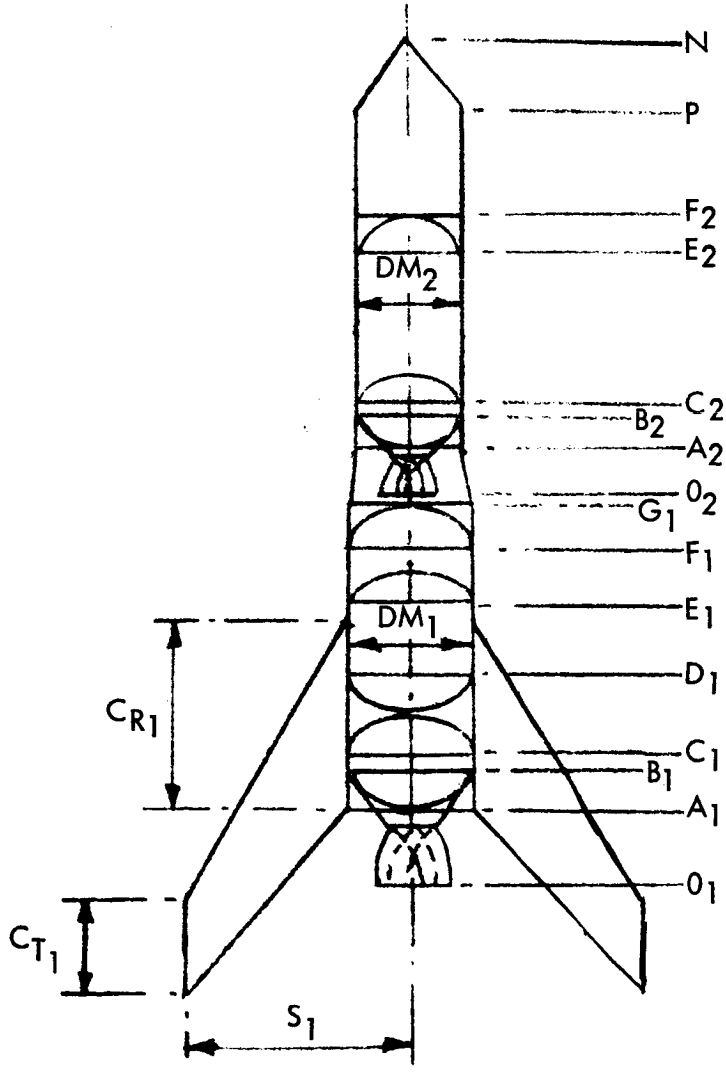

Station	Stage 1*	Stage 2*
N	—	2232.7
P	—	2047.1
C_T	258.0	—
C_R	573.0	—
S	617.0	—
DM	300.0	260.0
G	1001.7	—
F	851.7	1917.1
E	780.5	1825.1
D	602.7	—
C	372.6	1293.3
B	313.3	1250.9
A	207.2	1159.0
0	0	1134.9

*Dimensions in inches

TABLE 35. - PERFORMANCE CHARACTERISTICS FOR 1.9 X 10^6-POUND VEHICLE, FUTURE I_{sp}

WEIGHT PERFORMANCE CHARACTERISTICS

STAGE	1	2
WEIGHT (LB)		
PAYLOAD	572358.	120232.
BURN-OUT	185669.	46939.
STRUCTURE/SUBSYSTEMS	154260.	36263.
ENGINES	31409.	10676.
PROPELLANT	1141972.	405187.
STAGE	1327642.	452126.
RATIOS		
PERFORMANCE	0.60104	0.70793
MASS FRACTION	0.86015	0.89618
DELTA VELOCITY (FPS)	10060.	19815.
SPECIFIC IMPULSE (SEC)	340.	500.

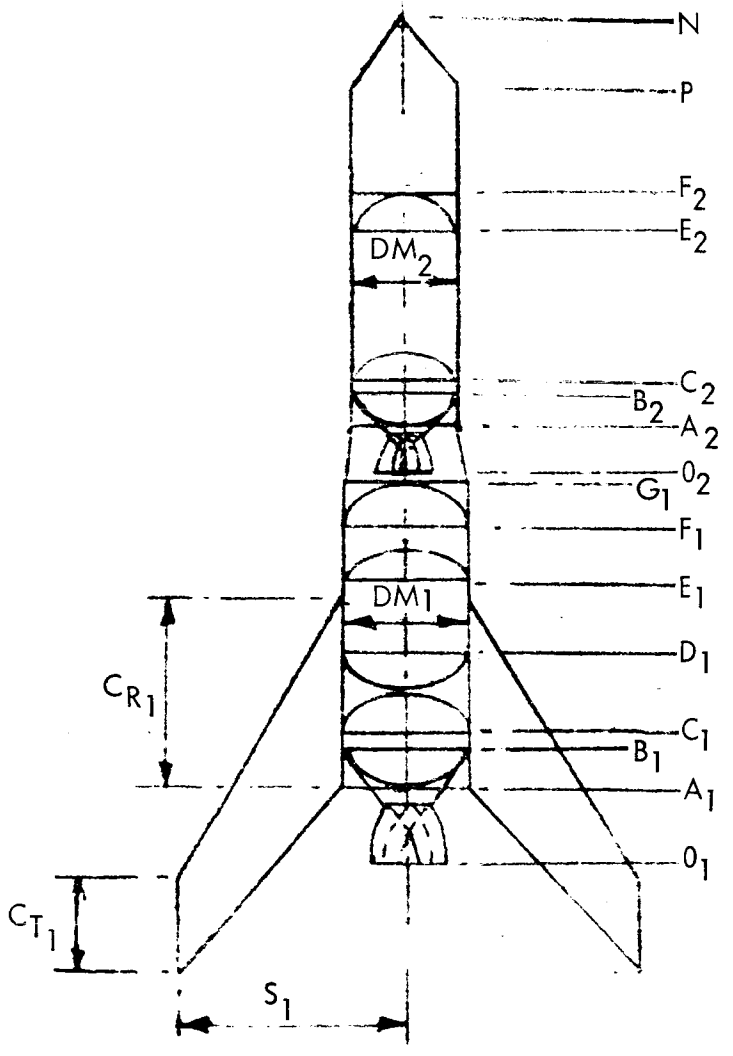

Station	Stage 1*	Stage 2*
N	—	2283.4
P	—	2097.7
C_T	255.0	—
C_R	567.0	—
S	612.0	—
DM	300.0	260.0
G	972.9	—
F	822.9	1967.7
E	751.7	1875.8
D	592.2	—
C	362.0	1383.2
B	314.2	1232.6
A	208.1	1140.6
0	0	1114.8

*Dimensions in inches

TABLE 36. - PERFORMANCE CHARACTERISTICS FOR 2.5 X 10^6-POUND VEHICLE, NEAR-TERM I_{sp}

WEIGHT PERFORMANCE CHARACTERISTICS

STAGE	1	2
WEIGHT (LB)		
PAYLOAD	663651.	117696.
BURN-OUT	242936.	56467.
STRUCTURE/SUBSYSTEMS	202083.	44530.
ENGINES	40854.	11936.
PROPELLANT	1593412.	489489.
STAGE	1836349.	545955.
RATIOS		
PERFORMANCE	0.63736	0.73757
MASS FRACTION	0.86771	0.89657
DELTA VELOCITY (FPS)	10060.	19815.
SPECIFIC IMPULSE (SEC)	308.	460.

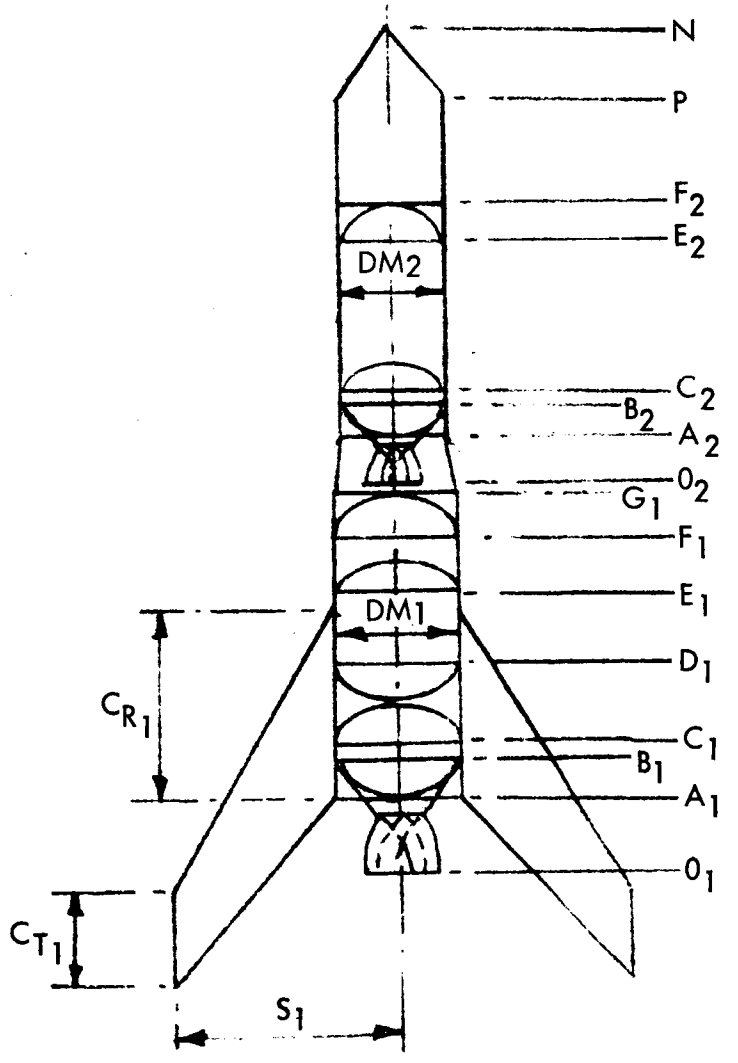

Station	Stage 1*	Stage 2*
N	—	2429.0
P	—	2214.8
C_T	295.0	—
C_R	655.0	—
S	694.0	—
DM	320.0	300.0
G	1118.7	—
F	958.7	2064.8
E	895.0	1958.7
D	676.7	—
C	431.2	1428.3
B	350.0	1405.3
A	236.8	1299.2
0	0	1271.6

*Dimensions in inches

TABLE 37. - PERFORMANCE CHARACTERISTICS FOR 2.5 X 10^6-POUND VEHICLE, FUTURE I_{sp}

WEIGHT PERFORMANCE CHARACTERISTICS

STAGE	1	2
WEIGHT (LB)		
PAYLOAD	758655.	160220.
BURN-OUT	238750.	61364.
STRUCTURE/SUBSYSTEMS	197896.	48161.
ENGINES	40854.	13203.
PROPELLANT	1502595.	537071.
STAGE	1741345.	598435.
RATIOS		
PERFORMANCE	0.60104	0.70793
MASS FRACTION	0.86289	0.89746
DELTA VELOCITY (FPS)	10060.	19815.
SPECIFIC IMPULSE (SEC)	340.	500.

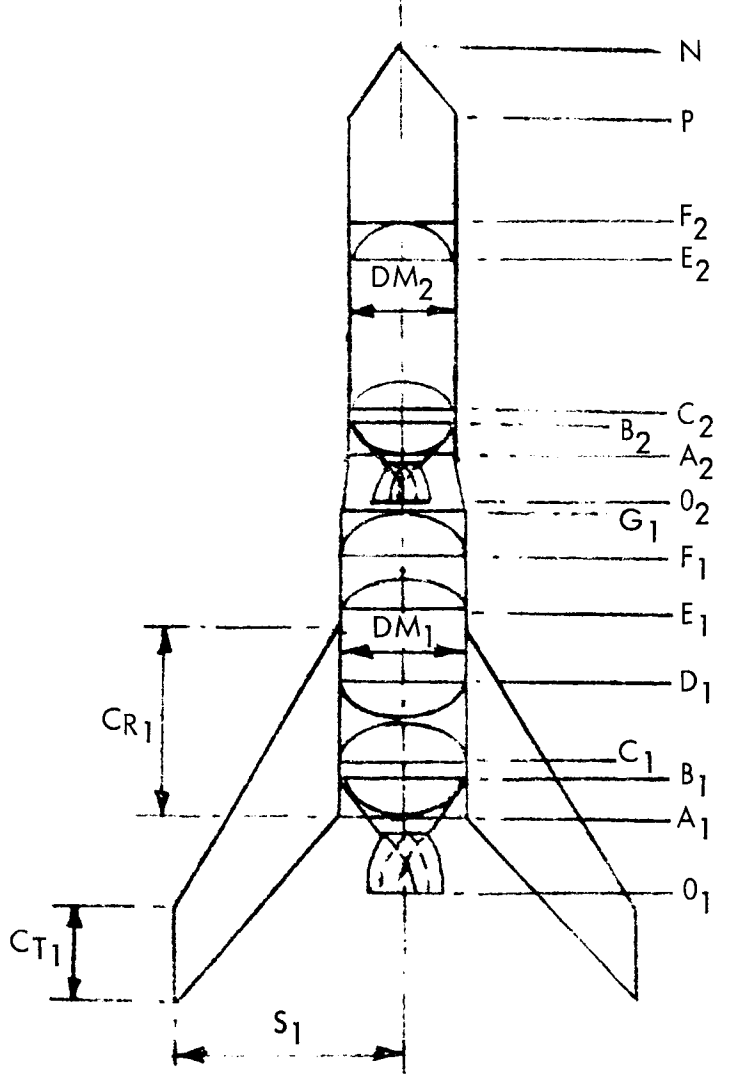

Station	Stage 1*	Stage 2*
N	—	2475.1
P	—	2260.8
C_T	292.0	—
C_R	648.0	—
S	689.0	—
DM	320.0	300.0
G	1085.4	—
F	925.4	2110.8
E	861.7	2004.7
D	664.4	—
C	418.9	1422.8
B	350.9	1383.7
A	237.8	1277.7
0	0	1248.1

*Dimensions in inches

TABLE 38. - WEIGHT AND LOADING FOR 1.3 X 10^6-POUND VEHICLE, NEAR-TERM I_{sp}

Weight Distribution

STATION	DIA	PRELAUNCH WEIGHT	PRELAUNCH STATION	MAX Q ALPHA WEIGHT	MAX Q ALPHA STATION	END BOOST WEIGHT	END BOOST STATION
173.	260.	24669.	121.	24669.	121.	24669.	121.
265.	260.	138021.	219.	138021.	219.	13415.	219.
325.	260.	91270.	295.	50071.	295.	8871.	295.
525.	260.	305759.	425.	170582.	425.	35405.	425.
694.	260.	245436.	609.	130857.	609.	16278.	609.
786.	260.	133457.	740.	8851.	740.	8851.	740.
916.	260.	15516.	851.	15516.	851.	15516.	851.
1046.	220.	19776.	994.	19776.	994.	19776.	994.
1124.	220.	29800.	1085.	29800.	1085.	29800.	1085.
1177.	220.	20148.	1151.	20148.	1151.	20148.	1151.
1255.	220.	29800.	1216.	29800.	1216.	29800.	1216.
1681.	220.	163307.	1468.	163307.	1468.	163307.	1468.
1759.	220.	29800.	1720.	29800.	1720.	29800.	1720.
1759.	220.	0.	1720.	0.	1720.	0.	1720.
2026.	220.	58528.	1861.	58528.	1861.	58528.	1861.
TOTAL WEIGHT		1305285.		911623.		496062.	
CENTER OF GRAVITY		739.		805.		1142.	

Loads Matrix

STATION	PRELAUNCH MOMENT	PRELAUNCH SHEAR	PRELAUNCH AXIAL	MAX Q ALPHA MOMENT	MAX Q ALPHA SHEAR	MAX Q ALPHA AXIAL	END BOOST MOMENT	END BOOST SHEAR	END BOOST AXIAL
173.	20353643.	41116.	1280616.	-1331087.	28080.	1632786.		8368.	1626279.
265.	16781123.	36600.	1142596.	-4025944.	30543.	1372673.	-374738.	6873.	1577743.
325.	14704884.	31701.	1051325.	-5531863.	18996.	1262760.	-764381.	5945.	1545648.
525.	9994618.	15525.	745566.	-6424.	-74396.	820737.	-1622420.	2658.	1417553.
694.	7468299.	14358.	500130.	9034704.	-32549.	623514.	-1966865.	1417.	1358659.
786.	6225824.	12671.	366673.	11897095.	-29719.	610174.	-2070856.	846.	1326635.
916.	4683638.	11055.	351157.	15438018.	-24757.	586790.	-2125819.	-0.	1270498.
1046.	3298506.	10146.	331382.	18834883.	-25973.	549445.	-2082826.	-823.	1198950.
1124.	2533534.	9520.	301582.	20484723.	-16443.	504532.	-1980147.	-1817.	1091133.
1177.	2057432.	8583.	281434.	21180135.	-10000.	474166.	-1869990.	-2371.	1018238.
1255.	1593035.	3356.	251634.	21587395.	-470.	429253.	-1660423.	-3016.	910421.
1681.	386000.	2307.	88327.	10655852.	51754.	183124.	-411567.	-2843.	319572.
1759.	206550.	2307.	58528.	6259079.	61283.	138211.	-217985.	-2134.	211755.
1759.	206550.	2307.	58528.	6259079.	61283.	138211.	-217985.	-2134.	211755.

TABLE 39. - WEIGHT AND LOADING FOR 1.3 X 10^6-POUND VEHICLE, FUTURE I_{sp}

Weight Distribution

		PRELAUNCH		MAX Q ALPHA		END BOOST	
STATION	DIA	WEIGHT	STATION	WEIGHT	STATION	WEIGHT	STATION
173.	260.	24668.	121.	24668.	121.	24668.	121.
265.	260.	136242.	219.	136242.	219.	13313.	219.
316.	260.	74614.	290.	40952.	290.	7291.	290.
515.	260.	302035.	415.	168677.	415.	35318.	415.
668.	260.	218464.	591.	116536.	591.	14609.	591.
760.	260.	131739.	714.	8809.	714.	8809.	714.
890.	260.	15457.	825.	15457.	825.	15457.	825.
1029.	220.	21351.	973.	21351.	973.	21351.	973.
1107.	220.	29979.	1068.	29979.	1068.	29979.	1068.
1175.	220.	26411.	1141.	26411.	1141.	26411.	1141.
1253.	220.	29979.	1214.	29979.	1214.	29979.	1214.
1731.	220.	184105.	1492.	184105.	1492.	184105.	1492.
1809.	220.	29979.	1770.	29979.	1770.	29979.	1770.
1809.	220.	0.	1770.	0.	1770.	0.	1770.
2076.	220.	80351.	1911.	80351.	1911.	80351.	1911.
TOTAL WEIGHT		1305372.		935395.		543519.	
CENTER OF GRAVITY		780.		861.		1202.	

Loads Matrix

	PRELAUNCH			MAX Q ALPHA			END BOOST		
STATION	MOMENT	SHEAR	AXIAL	MOMENT	SHEAR	AXIAL	MOMENT	SHEAR	AXIAL
173.	20943155.	41170.	1280704.	-1245785.	42770.	1634341.		8579.	1641102.
265.	17358012.	36820.	1144462.	-5093868.	40940.	1381778.	-407192.	7147.	1597138.
316.	15615412.	32399.	1069848.	-6885400.	30223.	1293152.	-748360.	6405.	1573061.
515.	10743136.	16452.	767813.	-3001216.	-69157.	859259.	-1704451.	3181.	1456429.
668.	8323225.	15292.	549349.	4980043.	-35532.	687027.	-2104073.	2061.	1408186.
760.	6994350.	13616.	417610.	8129916.	-32990.	574022.	-2266682.	1476.	1379094.
890.	5335684.	11902.	402154.	12128604.	-28529.	651205.	-2401089.	592.	1328051.
1029.	3738735.	10997.	380803.	16289696.	-29906.	512147.	-2430245.	-365.	1257544.
1107.	2914839.	10185.	350824.	18279652.	-21254.	567892.	-2358784.	-1472.	1158544.
1175.	2248930.	9248.	324414.	19475089.	-13631.	528004.	-2229987.	-2286.	1071326.
1253.	1757278.	3392.	294435.	20198968.	-4979.	484549.	-2033270.	-3028.	972326.
1731.	390124.	2331.	110330.	9884965.	48157.	212871.	-526532.	-3322.	364348.
1809.	208754.	2331.	80351.	5802123.	56809.	168515.	-273254.	-2676.	265347.
1809.	208754.	2331.	80351.	5802123.	56809.	168515.	-273254.	-2676.	265347.

TABLE 40. - WEIGHT AND LOADING FOR 1.9 X 10^6-POUND VEHICLE, NEAR-TERM I_{sp}

Weight Distribution

		PRELAUNCH		MAX Q ALPHA		END BOOST	
STATION	DIA	WEIGHT	STATION	WEIGHT	STATION	WEIGHT	STATION
207.	300.	35711.	145.	35711.	145.	35711.	145.
313.	300.	208778.	260.	208778.	260.	19677.	260.
373.	300.	116621.	343.	63806.	343.	10992.	343.
603.	300.	463774.	488.	258631.	488.	53487.	488.
780.	300.	339018.	692.	180580.	692.	22142.	692.
887.	300.	202314.	834.	13213.	834.	13213.	834.
1002.	300.	17336.	944.	17336.	944.	17336.	944.
1159.	260.	29232.	1096.	29232.	1096.	29232.	1096.
1251.	260.	48651.	1205.	48651.	1205.	48651.	1205.
1293.	260.	22412.	1272.	22412.	1272.	22412.	1272.
1385.	260.	48651.	1339.	48651.	1339.	48651.	1339.
1825.	260.	232794.	1605.	232794.	1605.	232794.	1605.
1917.	260.	48651.	1871.	48651.	1871.	48651.	1871.
1917.	260.	0.	1871.	0.	1871.	0.	1871.
2233.	260.	88023.	2038.	88023.	2038.	88023.	2038.
TOTAL WEIGHT		1901965.		1327877.		722380.	
CENTER OF GRAVITY		829.		898.		1267.	

Loads Matrix

	PRELAUNCH			MAX Q ALPHA			END BOOST		
STATION	MOMENT	SHEAR	AXIAL	MOMENT	SHEAR	AXIAL	MOMENT	SHEAR	AXIAL
207.	30229704.	56483.	1866254.	-1699669.	91134.	2378590.		12120.	2372211.
313.	24561915.	50374.	1657476.	-11023377.	84649.	1986816.	-596327.	9898.	2300974.
373.	21759646.	44208.	1540855.	-15549847.	68127.	1848908.	-1148352.	8734.	2261181.
603.	14330214.	20350.	1077081.	-13105303.	-89369.	1176757.	-2581346.	3718.	2067545.
780.	10853774.	18763.	738063.	-1138532.	-45269.	900035.	-3091531.	2022.	1987387.
887.	8957003.	16997.	535750.	3492525.	-42042.	879786.	-3260680.	1167.	1939552.
1002.	7133913.	14682.	518414.	8087759.	-37808.	853220.	-3339765.	207.	1876791.
1159.	4926962.	13379.	489182.	14277530.	-39466.	799629.	-3293975.	-1038.	1770965.
1251.	3725130.	12766.	440531.	17359766.	-27585.	725076.	-3123702.	-2666.	1594836.
1293.	3212941.	11422.	418120.	18412132.	-22111.	690732.	-2997609.	-3289.	1513700.
1385.	2464734.	4855.	369469.	19898825.	-10230.	616178.	-2645692.	-4367.	1337571.
1825.	661474.	3343.	136674.	11894025.	46622.	259442.	-735279.	-4319.	494796.
1917.	354103.	3343.	88023.	7061532.	58503.	184888.	-388720.	-3220.	318667.
1917.	354103.	3343.	88023.	7061532.	58503.	184888.	-388720.	-3220.	318667.

TABLE 41. - WEIGHT AND LOADING FOR 1.9×10^6-POUND VEHICLE, FUTURE I_{sp}

Weight Distribution

STATION	DIA	PRELAUNCH WEIGHT	PRELAUNCH STATION	MAX Q ALPHA WEIGHT	MAX Q ALPHA STATION	END BOOST WEIGHT	END BOOST STATION
208.	300.	35724.	146.	35724.	146.	35724.	146.
314.	300.	206041.	261.	206041.	261.	19589.	261.
362.	300.	92887.	338.	50859.	338.	8831.	338.
592.	300.	458033.	477.	255763.	477.	53493.	477.
752.	300.	300327.	672.	160091.	672.	19855.	672.
858.	300.	199651.	805.	13199.	805.	13199.	805.
973.	300.	17320.	915.	17320.	915.	17320.	915.
1141.	260.	31542.	1074.	31542.	1074.	31542.	1074.
1233.	260.	48949.	1187.	48949.	1187.	48949.	1187.
1291.	260.	31241.	1262.	31241.	1262.	31241.	1262.
1383.	260.	48949.	1337.	48949.	1337.	48949.	1337.
1876.	260.	262265.	1629.	262265.	1629.	262265.	1629.
1968.	260.	48949.	1922.	48949.	1922.	48949.	1922.
1968.	260.	0.	1922.	0.	1922.	0.	1922.
2283.	260.	120232.	2088.	120232.	2088.	120232.	2088.
TOTAL WEIGHT		1902112.		1362534.		791548.	
CENTER OF GRAVITY		873.		958.		1329.	

Loads Matrix

STATION	PRELAUNCH MOMENT	PRELAUNCH SHEAR	PRELAUNCH AXIAL	MAX Q ALPHA MOMENT	MAX Q ALPHA SHEAR	MAX Q ALPHA AXIAL	END BOOST MOMENT	END BOOST SHEAR	END BOOST AXIAL
208.	31007353.	56552.	1866388.	-1582057.	108216.	2330964.		12437.	2393585.
314.	25321206.	50651.	1660347.	-12443831.	96555.	2000308.	-652924.	10303.	2328860.
362.	23031441.	45108.	1567460.	-16715841.	82091.	1892597.	-1123922.	9394.	2299680.
592.	15363180.	21525.	1109426.	-16616632.	-82953.	1232598.	-2719070.	4467.	2122932.
752.	12054016.	19949.	809099.	-6182097.	-47826.	932524.	-3309994.	2939.	2057329.
858.	10030778.	18195.	609449.	-1262259.	-44930.	977781.	-3575186.	2060.	2013718.
973.	8077636.	15744.	592128.	3690262.	-41129.	946757.	-3754537.	1056.	1956488.
1141.	5546129.	14446.	560586.	10861172.	-43005.	896561.	-3835038.	-384.	1852268.
1233.	4256884.	13600.	511637.	14321191.	-32264.	817259.	-3716777.	-2188.	1690532.
1291.	3498293.	12257.	480396.	16013237.	-25403.	772417.	-3558959.	-3157.	1587308.
1383.	2709305.	4907.	431447.	17855575.	-14654.	697332.	-3213175.	-4387.	1425571.
1876.	668517.	3379.	169182.	19907743.	42878.	333729.	-898885.	-5009.	559004.
1968.	357868.	3379.	120232.	6471913.	53614.	83802.	-484201.	-4012.	397267.
1968.	357868.	3379.	120232.	6471913.	53614.	83802.	-484201.	-4012.	397267.

TABLE 42. - WEIGHT AND LOADING FOR 2.5 X 10^6-POUND VEHICLE, NEAR-TERM I_{sp}

Weight Distribution

		PRELAUNCH		MAX Q ALPHA		END BOOST	
STATION	DIA	WEIGHT	STATION	WEIGHT	STATION	WEIGHT	STATION
237.	320.	46461.	166.	46461.	166.	46461.	166.
350.	320.	257871.	293.	257871.	293.	24107.	293.
431.	320.	185088.	391.	101196.	391.	17303.	391.
677.	320.	574751.	554.	321155.	554.	67559.	554.
895.	320.	481913.	786.	256459.	786.	31005.	786.
1008.	320.	249838.	952.	16074.	952.	16074.	952.
1119.	320.	18704.	1063.	18704.	1063.	18704.	1063.
1299.	300.	37577.	1227.	37577.	1227.	37577.	1227.
1405.	300.	73778.	1352.	73778.	1352.	73778.	1352.
1428.	300.	16034.	1417.	16034.	1417.	16034.	1417.
1534.	300.	73778.	1481.	73778.	1481.	73778.	1481.
1959.	300.	295102.	1747.	295102.	1747.	295102.	1747.
2065.	300.	73778.	2012.	73778.	2012.	73778.	2012.
2065.	300.	0.	2012.	0.	2012.	0.	2012.
2429.	300.	117696.	2204.	117696.	2204.	117696.	2204.
TOTAL WEIGHT		2502370.		1746517.		949811.	
CENTER OF GRAVITY		926.		999.		1395.	

Loads Matrix

	PRELAUNCH			MAX Q ALPHA			END BOOST		
STATION	MOMENT	SHEAR	AXIAL	MOMENT	SHEAR	AXIAL	MOMENT	SHEAR	AXIAL
237.	42397077.	72488.	2455908.	-2030694.	160257.	3129650.		15699.	3124453.
350.	34630541.	64785.	2198038.	-19102184.	141482.	2642049.	-741707.	12890.	3037123.
431.	29711011.	56360.	2012949.	-29367695.	111310.	2423449.	-1712191.	11009.	2974442.
677.	19722739.	25008.	1438198.	-29532410.	-109968.	1569937.	-3621711.	4547.	2729703.
895.	14466907.	23152.	956285.	-11100534.	-58927.	1173041.	-4353363.	2157.	2617384.
1008.	11952486.	21290.	706447.	-4613653.	-55728.	1148165.	-4539441.	1132.	2559155.
1119.	9766003.	18267.	687743.	1341182.	-52006.	1113213.	-4607837.	106.	2491400.
1299.	6630439.	16476.	650167.	10627761.	-49397.	1066195.	-4513552.	-1463.	2355275.
1405.	4903831.	16077.	576388.	15089045.	-34713.	942917.	-4234297.	-3804.	2088008.
1428.	4554457.	14232.	560354.	15852560.	-31523.	917203.	-4141699.	-4229.	2029924.
1534.	3445470.	6676.	486576.	18417681.	-16333.	838224.	-3809363.	-5807.	1762657.
1959.	1051933.	4606.	191474.	13102372.	41843.	466825.	-1136197.	-5850.	693630.
2065.	563352.	4606.	117696.	7873428.	55575.	341145.	-598105.	-4294.	426363.
2065.	563352.	4606.	117696.	7873428.	55575.	341145.	-598105.	-4294.	426363.

TABLE 43. - WEIGHT AND LOADING FOR 2.5 X 10^6-POUND VEHICLE, FUTURE I_{sp}

Weight Distribution

		PRELAUNCH		MAX Q ALPHA		END BOOST	
STATION	DIA	WEIGHT	STATION	WEIGHT	STATION	WEIGHT	STATION
238.	320.	46492.	166.	46492.	166.	46492.	166.
351.	320.	254729.	294.	254729.	294.	24044.	294.
419.	320.	153070.	385.	83759.	385.	14448.	385.
664.	320.	568242.	542.	317986.	542.	67730.	542.
862.	320.	430151.	763.	229105.	763.	28059.	763.
975.	320.	246783.	918.	16098.	918.	16098.	918.
1085.	320.	18727.	1030.	18727.	1030.	18727.	1030.
1278.	300.	40558.	1201.	40558.	1201.	40558.	1201.
1384.	300.	74305.	1331.	74305.	1331.	74305.	1331.
1423.	300.	27341.	1403.	27341.	1403.	27341.	1403.
1529.	300.	74305.	1476.	74305.	1476.	74305.	1476.
2005.	300.	333325.	1767.	333325.	1767.	333325.	1767.
2111.	300.	74305.	2058.	74305.	2058.	74305.	2058.
2111.	300.	0.	2058.	0.	2058.	0.	2058.
2475.	300.	160220.	2250.	160220.	2250.	160220.	2250.
TOTAL WEIGHT		2502554.		1792110.		1040813.	
CENTER OF GRAVITY		970.		1060.		1457.	

Loads Matrix

	PRELAUNCH			MAX Q ALPHA			END BOOST		
STATION	MOMENT	SHEAR	AXIAL	MOMENT	SHEAR	AXIAL	MOMENT	SHEAR	AXIAL
238.	43249452.	72482.	2456062.	-1887099.	177896.	3132783.		16107.	3152239.
351.	35469319.	65032.	2201333.	-20665135.	154006.	2660389.	-820615.	13401.	3072749.
419.	31305431.	57443.	2048263.	-30227808.	127266.	2481452.	-1679857.	11872.	3024981.
664.	21015171.	26385.	1480022.	-33276318.	-102432.	1641324.	-3812365.	5500.	2801062.
862.	15992742.	24544.	1049871.	-17110389.	-61497.	1295556.	-4682444.	3323.	2708295.
975.	13320010.	22696.	803088.	-10314505.	-58620.	1270585.	-4998376.	2261.	2655074.
1085.	10987592.	19501.	784361.	-4019140.	-55274.	1242333.	-5138649.	1181.	2593160.
1278.	7409269.	17718.	743802.	6519918.	-52837.	1176362.	-5275749.	-640.	2459072.
1384.	5565330.	17046.	669497.	11427180.	-39621.	1048569.	-5369125.	-3256.	2213412.
1423.	4935912.	15204.	642156.	12878399.	-34736.	1020176.	-4926141.	-4070.	2123019.
1529.	3771985.	6740.	567850.	15859043.	-21459.	939983.	-4398229.	-5882.	1877359.
2005.	1061930.	4650.	234525.	11909442.	-8037.	605554.	-1388375.	-5768.	775359.
2111.	568697.	4650.	160220.	7154873.	51373.	342961.	-745455.	-5353.	529700.
2111.	568697.	4650.	160220.	7154873.	51373.	342961.	-745455.	-5353.	529700.

TABLE 44. - PRESSURES AND APPLIED LOADS FOR 1.3 X 10^6-POUND VEHICLE, NEAR-TERM I_{sp}

Pressure Matrix, psi

	PRELAUNCH	MAX Q ALPHA	END BOOST
STAGE 1			
AFT TANK	6.3	39.0	39.0
FWD TANK	7.6	39.0	39.0
AFT BULKHEAD		45.8	
FWD BULKHEAD		39.0	39.0
AFT TANK FWD BULKHEAD		39.0	39.0
FWD TANK AFT BULKHEAD		43.8	
STAGE 2			
AFT TANK	5.4	45.7	55.5
FWD TANK	1.5	38.7	41.4
AFT BULKHEAD			61.2
FWD BULKHEAD		36.0	36.0
AFT TANK FWD BULKHEAD		36.0	36.0
FWD TANK AFT BULKHEAD			0.0

Applied Loads Matrix

NX IN LB/IN
NX/R IN LB/IN/IN
NUMBER OF STAGES = 2

STATION	PRELAUNCH NX	MAX Q ALPHA NX	END BOOST NX	MAX NX/R
173.	2732.	2834.	3058.	23.5239
265.	2401.	-76.	179.	18.4683
325.	2190.	2310.	2920.	22.4585
525.	1541.	-1128.	-63.	11.8571
694.	1054.	1307.	2604.	20.0288
786.	793.	1360.	2547.	19.5901
916.	725.	1413.	2443.	18.7928
1046.	793.	1807.	2740.	24.9107
1124.	704.	-204.	303.	6.4018
1177.	646.	1741.	2331.	21.1931
1255.	568.	-315.	-75.	5.1671
1681.	193.	763.	725.	6.9398
1759.	126.	510.	478.	4.6407
1759.	126.	510.	478.	4.6407

TABLE 45. - PRESSURES AND APPLIED LOADS FOR 1.3 X 10^6-POUND VEHICLE, FUTURE I_{sp}

Pressure Matrix, psi

	PRELAUNCH	MAX Q ALPHA	END BOOST
STAGE 1			
AFT TANK	5.9	39.0	39.0
FWD TANK	7.1	39.0	39.0
AFT BULKHEAD		45.5	
FWD BULKHEAD		39.0	39.0
AFT TANK FWD BULKHEAD		39.0	39.0
FWD TANK AFT BULKHEAD		43.6	
STAGE 2			
AFT TANK	6.0	46.4	56.0
FWD TANK	1.6	38.8	41.4
AFT BULKHEAD			61.5
FWD BULKHEAD		36.0	36.0
AFT TANK FWD BULKHEAD		36.0	36.0
FWD TANK AFT BULKHEAD			0.0

Applied Loads Matrix

NX IN LB/IN
NX/R IN LB/IN/IN
NUMBER OF STAGES = 2

STATION	PRELAUNCH NX	MAX Q ALPHA NX	END BOOST NX	MAX NX/R
173.	2747.	2834.	3086.	23.7355
265.	2419.	-32.	213.	18.6099
316.	2245.	2398.	2971.	22.8503
515.	1599.	-983.	6.	12.3023
668.	1161.	1309.	2701.	20.7735
760.	900.	1370.	2651.	20.3900
890.	830.	1436.	2559.	19.6838
1029.	909.	1840.	2884.	26.2181
1107.	818.	-156.	454.	7.4362
1175.	740.	1789.	2463.	22.3941
1253.	661.	-254.	64.	6.0102
1731.	238.	795.	828.	7.5238
1809.	170.	555.	599.	5.4444
1809.	170.	555.	599.	5.4444

TABLE 46. - PRESSURES AND APPLIED LOADS FOR 1.9 X 10^6-POUND VEHICLE, NEAR-TERM I_{sp}

Pressure Matrix, psi

	PRELAUNCH	MAX Q ALPHA	END BOOST
STAGE 1			
AFT TANK	6.8	39.0	39.0
FWD TANK	8.3	39.0	39.0
AFT BULKHEAD		46.9	
FWD BULKHEAD		39.0	39.0
AFT TANK FWD BULKHEAD		39.0	39.0
FWD TANK AFT BULKHEAD		44.6	
STAGE 2			
AFT TANK	5.5	46.0	56.1
FWD TANK	1.6	38.9	41.8
AFT BULKHEAD			62.9
FWD BULKHEAD		36.0	36.0
AFT TANK FWD BULKHEAD		36.0	36.0
FWD TANK AFT BULKHEAD			0.0

Applied Loads Matrix

NX IN LB/IN
NX/R IN LB/IN/IN
NUMBER OF STAGES = 2

STATION	PRELAUNCH NX	MAX Q ALPHA NX	END BOOST NX	MAX NX/R
207.	3371.	3567.	3867.	25.7768
313.	2949.	245.	505.	19.6570
373.	2720.	3054.	3699.	24.6575
603.	1884.	-917.	197.	12.5584
780.	1311.	1359.	3296.	21.9726
887.	973.	1376.	3222.	21.4789
1002.	911.	1428.	3122.	20.8105
1159.	968.	1747.	3415.	26.2689
1251.	853.	-639.	476.	6.5637
1293.	801.	1669.	2924.	22.4932
1385.	698.	-759.	22.	5.3712
1825.	252.	758.	949.	7.2983
1917.	160.	503.	609.	4.6816
1917.	160.	503.	609.	4.6816

TABLE 47. - PRESSURES AND APPLIED LOADS FOR 1.9 X 10^6-POUND VEHICLE, FUTURE I_{sp}

Pressure Matrix, psi

	PRELAUNCH	MAX Q ALPHA	END BOOST
STAGE 1			
AFT TANK	6.4	39.0	39.0
FWD TANK	7.8	39.0	39.0
AFT BULKHEAD		46.6	
FWD BULKHEAD		39.0	39.0
AFT TANK FWD BULKHEAD		39.0	39.0
FWD TANK AFT BULKHEAD		44.3	
STAGE 2			
AFT TANK	6.2	46.7	56.6
FWD TANK	1.7	39.0	41.7
AFT BULKHEAD			63.1
FWD BULKHEAD		36.0	36.0
AFT TANK FWD BULKHEAD		36.0	36.0
FWD TANK AFT BULKHEAD			0.0

Applied Loads Matrix

NX IN LB/IN
NX/R IN LB/IN/IN
NUMBER OF STAGES = 2

STATION	PRELAUNCH NX	MAX Q ALPHA NX	END BOOST NX	MAX NX/R
208.	3387.	3568.	3901.	26.0057
314.	2968.	294.	547.	19.7857
362.	2785.	3142.	3761.	25.0710
592.	1952.	-765.	282.	13.0151
752.	1441.	1597.	3414.	22.7617
858.	1104.	1470.	3349.	22.3276
973.	1040.	1479.	3260.	21.7336
1141.	1107.	1813.	3583.	27.5613
1233.	989.	-562.	656.	7.6091
1291.	916.	1743.	3078.	23.6795
1383.	811.	-675.	188.	6.2379
1876.	308.	808.	1074.	8.2605
1968.	216.	565.	759.	5.8362
1968.	216.	565.	759.	5.8362

TABLE 48. - PRESSURES AND APPLIED LOADS FOR 2.5 X 10^6-POUND VEHICLE, NEAR-TERM I_{sp}

Pressure Matrix, psi

	PRELAUNCH	MAX Q ALPHA	END BOOST
STAGE 1			
AFT TANK	8.0	39.0	39.0
FWD TANK	9.7	39.0	39.0
AFT BULKHEAD		47.4	
FWD BULKHEAD		39.0	39.0
AFT TANK FWD BULKHEAD		39.0	39.0
FWD TANK AFT BULKHEAD		44.9	
STAGE 2			
AFT TANK	5.3	45.6	55.3
FWD TANK	1.6	38.9	41.9
AFT BULKHEAD			63.2
FWD BULKHEAD		36.0	36.0
AFT TANK FWD BULKHEAD		36.0	36.0
FWD TANK AFT BULKHEAD			0.0

Applied Loads Matrix

NX IN LB/IN
NX/R IN LB/IN/IN
NUMBER OF STAGES = 2

STATION	PRELAUNCH NX	MAX Q ALPHA NX	END BOOST NX	MAX NX/R
237.	4158.	4394.	4776.	29.8482
350.	3664.	893.	1122.	22.8989
431.	3320.	3886.	4563.	28.5197
677.	2346.	-420.	744.	14.6635
895.	1584.	1827.	4070.	25.4349
1008.	1192.	1679.	3984.	24.9027
1119.	1128.	1582.	3883.	24.2658
1299.	1097.	1779.	3924.	26.1627
1405.	953.	-1002.	485.	6.3554
1428.	923.	1676.	3388.	22.5850
1534.	791.	-1142.	-10.	5.2735
1959.	305.	774.	1152.	7.6770
2065.	186.	501.	706.	4.7045
2065.	186.	501.	706.	4.7045

TABLE 49. - PRESSURES AND APPLIED LOADS FOR 2.5 X 10^6-POUND VEHICLE, FUTURE I_{sp}

Pressure Matrix, psi

	PRELAUNCH	MAX Q ALPHA	END BOOST
STAGE 1			
AFT TANK	7.5	39.0	39.0
FWD TANK	9.1	39.0	39.0
AFT BULKHEAD		47.1	
FWD BULKHEAD		39.0	39.0
AFT TANK FWD BULKHEAD		39.0	39.0
FWD TANK AFT BULKHEAD		44.7	
STAGE 2			
AFT TANK	6.0	46.3	55.8
FWD TANK	1.8	39.0	41.8
AFT BULKHEAD			63.4
FWD BULKHEAD		36.0	36.0
AFT TANK FWD BULKHEAD		36.0	36.0
FWD TANK AFT BULKHEAD			0.0

Applied Loads Matrix

NX IN LB/IN
NX/R IN LB/IN/IN
NUMBER OF STAGES = 2

STATION	PRELAUNCH NX	MAX Q ALPHA NX	END BOOST NX	MAX NX/R
238.	4173.	4396.	4818.	30.1095
351.	3683.	945.	1173.	23.0188
419.	3397.	3982.	4640.	28.9969
664.	2427.	-254.	847.	15.1681
862.	1740.	2101.	4214.	26.3395
975.	1350.	1949.	4139.	25.8704
1085.	1284.	1800.	4049.	25.3037
1278.	1252.	1876.	4110.	27.3970
1384.	1105.	-894.	688.	7.3648
1423.	1052.	1773.	3556.	23.7066
1529.	918.	-1035.	176.	6.1214
2005.	369.	837.	1290.	8.5987
2111.	249.	576.	877.	5.8450
2111.	249.	576.	877.	5.8450

TABLE 50. - WING SIZE AND INSULATION FOR 1.3 X 10^6-POUND VEHICLE, NEAR-TERM I_{sp}

Wing Dimensions, Angles, and Weights

STAGE	1
DIMENSIONS (IN)	
ROOT	479.
TIP	216.
SPAN	782.
SWEEP ANGLES (DEGREES)	
LEADING EDGE	60.
FRONT SPAR	58.
AFT SPAR	50.
TRAILING EDGE	47.
FIFTY PERCENT CHORD	54.
WEIGHT (LB)	
COVER PLATES	5808.
SHEAR WEBS	3172.
LEADING EDGE	1085.
TRAILING EDGE	1809.
FINS	1208.
CARRY-THROUGH	620.
TOTAL WING	13702.
WING AREA (SQ FT)	1885.
WING LOADING (LB SQ FT)	115.20000
VERTICAL SURFACES	
HEIGHT (IN)	50.
ROOT CHORD (IN)	216.
TOTAL FIN AREA (SQ FT)	151.

Component Insulation Weight

COMPONENT	WEIGHT (LB)	UNIT WEIGHT	DESIGN TEMP (R)
CREW COMPT	705.9212	0.0066	1923.9818
FWD SKIRT	491.6116	0.0065	1873.2104
FWD TANKWALL	889.6578	0.0064	1820.9094
CENTER SECTION	1037.4919	0.0064	1783.7641
AFT TANKWALL	315.3426	0.0064	1775.0453
AFT SKIRT	475.1135	0.0063	1763.3644
TOTAL BODY INS	3915.1386		
LEADING EDGE	357.0118	0.0069	2026.6322
WING BOX	1092.7211	0.0065	1866.0703
TRAILING EDGE	334.6101	0.0064	1811.6187
FIN	141.8630	0.0065	1866.0703
TOTAL WING INS	1926.2060		

TABLE 51. - WING SIZE AND INSULATION FOR 1.3 X 10^6-POUND VEHICLE, FUTURE I_{sp}

Wing Dimensions, Angles, and Weights

STAGE	1
DIMENSIONS (IN)	
ROOT	473.
TIP	213.
SPAN	772.
SWEEP ANGLES (DEGREES)	
LEADING EDGE	60.
FRONT SPAR	58.
AFT SPAR	50.
TRAILING EDGE	47.
FIFTY PERCENT CHORD	54.
WEIGHT (LB)	
COVER PLATES	5618.
SHEAR WEBS	3054.
LEADING EDGE	1071.
TRAILING EDGE	1786.
FINS	1177.
CARRY-THROUGH	605.
TOTAL WING	13312.
WING AREA (SQ FT)	1838.
WING LOADING (LB SQ FT)	115.20000
VERTICAL SURFACES	
HEIGHT (IN)	50.
ROOT CHORD (IN)	213.
TOTAL FIN AREA (SQ FT)	147.

Component Insulation Weight

COMPONENT	WEIGHT (LB)	UNIT WEIGHT	DESIGN TEMP (R)
CREW COMPT	705.9212	0.0066	1923.9818
FWD SKIRT	491.6116	0.0065	1873.2104
FWD TANKWALL	803.2042	0.0064	1824.8577
CENTER SECTION	1038.3222	0.0064	1786.3118
AFT TANKWALL	261.4697	0.0064	1778.8162
AFT SKIRT	475.6052	0.0063	1766.6379
TOTAL BODY INS	3776.1340		
LEADING EDGE	352.5324	0.0069	2026.6322
WING BOX	1057.4225	0.0065	1867.2487
TRAILING EDGE	330.5421	0.0064	1812.8851
FIN	138.3754	0.0065	1867.2487
TOTAL WING INS	1878.8724		

TABLE 52. - WING SIZE AND INSULATION FOR 1.9 X 10^6-POUND VEHICLE, NEAR-TERM I_{sp}

Wing Dimensions, Angles, and Weights

STAGE	1
DIMENSIONS (IN)	
ROOT	573.
TIP	258.
SPAN	934.
SWEEP ANGLES (DEGREES)	
LEADING EDGE	60.
FRONT SPAR	58.
AFT SPAR	50.
TRAILING EDGE	47.
FIFTY PERCENT CHORD	54.
WEIGHT (LB)	
COVER PLATES	8476.
SHEAR WEBS	5416.
LEADING EDGE	1496.
TRAILING EDGE	2494.
FINS	1725.
CARRY-THROUGH	1022.
TOTAL WING	20629.
WING AREA (SQ FT)	2693.
WING LOADING (LB SQ FT)	115.20000
VERTICAL SURFACES	
HEIGHT (IN)	60.
ROOT CHORD (IN)	258.
TOTAL FIN AREA (SQ FT)	215.

Component Insulation Weight

COMPONENT	WEIGHT (LB)	UNIT WEIGHT	DESIGN TEMP
CREW COMPT	723.6933	0.0067	1935.7312
FWD SKIRT	654.5766	0.0065	1873.5315
FWD TANKWALL	1078.6323	0.0064	1819.0839
CENTER SECTION	1378.8292	0.0064	1778.1238
AFT TANKWALL	354.0910	0.0063	1770.1388
AFT SKIRT	631.3747	0.0063	1757.4986
TOTAL BODY INS	4821.1970		
LEADING EDGE	490.2680	0.0068	2012.1833
WING BOX	1586.4847	0.0065	1849.5075
TRAILING EDGE	459.0929	0.0064	1795.2102
FIN	201.6219	0.0065	1849.5075
TOTAL WING INS	2737.4675		

TABLE 53. - WING SIZE AND INSULATION FOR 1.9 X 10^6-POUND VEHICLE, FUTURE I_{sp}

Wing Dimensions, Angles, and Weights

STAGE	1
DIMENSIONS (IN)	
ROOT	567.
TIP	255.
SPAN	924.
SWEEP ANGLES (DEGREES)	
LEADING EDGE	60.
FRONT SPAR	58.
AFT SPAR	50.
TRAILING EDGE	47.
FIFTY PERCENT CHORD	54.
WEIGHT (LB)	
COVER PLATES	8243.
SHEAR WEBS	5245.
LEADING EDGE	1480.
TRAILING EDGE	2468.
FINS	1688.
CARRY-THROUGH	1001.
TOTAL WING	20125.
WING AREA (SQ FT)	2636.
WING LOADING (LB SQ FT)	115.20000
VERTICAL SURFACES	
HEIGHT (IN)	60.
ROOT CHORD (IN)	255.
TOTAL FIN AREA (SQ FT)	211.

Component Insulation Weight

COMPONENT	WEIGHT (LB)	UNIT WEIGHT	DESIGN TEMP (R)
CREW COMPT	723.6933	0.0067	1935.7312
FWD SKIRT	654.5766	0.0065	1873.5315
FWD TANKWALL	969.5561	0.0064	1823.3327
CENTER SECTION	1379.9615	0.0064	1780.7337
AFT TANKWALL	286.1267	0.0063	1774.0358
AFT SKIRT	632.0429	0.0063	1760.8407
TOTAL BODY INS	4645.9571		
LEADING EDGE	485.0435	0.0068	2012.1833
WING BOX	1543.4784	0.0065	1850.4985
TRAILING EDGE	454.3515	0.0064	1796.2709
FIN	197.4079	0.0065	1850.4985
TOTAL WING INS	2680.2812		

TABLE 54. - WING SIZE AND INSULATION FOR 2.5 X 10^6-POUND VEHICLE, NEAR-TERM I_{sp}

Wing Dimensions, Angles, and Weights

STAGE	1
DIMENSIONS (IN)	
ROOT	655.
TIP	295.
SPAN	1068.
SWEEP ANGLES (DEGREES)	
LEADING EDGE	60.
FRONT SPAR	58.
AFT SPAR	50.
TRAILING EDGE	47.
FIFTY PERCENT CHORD	54.
WEIGHT (LB)	
COVER PLATES	11519.
SHEAR WEBS	8096.
LEADING EDGE	1825.
TRAILING EDGE	3042.
FINS	2255.
CARRY-THROUGH	1426.
TOTAL WING	28163.
WING AREA (SQ FT)	3521.
WING LOADING (LB SQ FT)	115.20000
VERTICAL SURFACES	
HEIGHT (IN)	69.
ROOT CHORD (IN)	295.
TOTAL FIN AREA (SQ FT)	282.

Component Insulation Weight

COMPONENT	WEIGHT (LB)	UNIT WEIGHT	DESIGN TEMP (R)
CREW COMPT	742.2954	0.0067	1939.6385
FWD SKIRT	744.5211	0.0065	1872.4694
FWD TANKWALL	1408.6055	0.0064	1809.7923
CENTER SECTION	1564.9160	0.0063	1770.2530
AFT TANKWALL	516.0834	0.0063	1760.3968
AFT SKIRT	716.2828	0.0063	1748.3506
TOTAL BODY INS	5692.7043		
LEADING EDGE	596.8180	0.0068	2005.7006
WING BOX	2147.9365	0.0065	1837.1550
TRAILING EDGE	557.7237	0.0064	1782.6117
FIN	262.6000	0.0065	1837.1550
TOTAL WING INS	3565.0783		

TABLE 55. - WING SIZE AND INSULATION FOR 2.5 X 10^6-POUND VEHICLE, FUTURE I_{sp}

Wing Dimensions, Angles, and Weights

STAGE	1
DIMENSIONS (IN)	
ROOT	648.
TIP	292.
SPAN	1058.
SWEEP ANGLES (DEGREES)	
LEADING EDGE	60.
FRONT SPAR	58.
AFT SPAR	50.
TRAILING EDGE	47.
FIFTY PERCENT CHORD	54.
WEIGHT (LB)	
COVER PLATES	11233.
SHEAR WEBS	7858.
LEADING EDGE	1807.
TRAILING EDGE	3012.
FINS	2211.
CARRY-THROUGH	1398.
TOTAL WING	27519.
WING AREA (SQ FT)	3452.
WING LOADING (LB SQ FT)	115.20000
VERTICAL SURFACES	
HEIGHT (IN)	68.
ROOT CHORD (IN)	292.
TOTAL FIN AREA (SQ FT)	276.

Component Insulation Weight

COMPONENT	WEIGHT (LB)	UNIT WEIGHT	DESIGN TEMP (R)
CREW COMPT	742.2954	0.0067	1939.6385
FWD SKIRT	744.5211	0.0065	1872.4694
FWD TANKWALL	1274.6223	0.0064	1814.2097
CENTER SECTION	1566.2746	0.0063	1773.0053
AFT TANKWALL	432.6207	0.0063	1764.4136
AFT SKIRT	717.0715	0.0063	1751.8173
TOTAL BODY INS	5477.4056		
LEADING EDGE	590.9167	0.0068	2005.7006
WING BOX	2095.1523	0.0065	1838.0681
TRAILING EDGE	552.3773	0.0064	1783.5818
FIN	257.5052	0.0065	1838.0681
TOTAL WING INS	3495.9515		

TABLE 56. - WEIGHT STATEMENT FOR 1.3 X 10^6-POUND VEHICLE, NEAR-TERM I_{sp}

CASE 4 REC/EXP 1,630,000 THRUST

VEHICLE AND STAGE WEIGHTS (LB)

STAGE	1	2
SHELL STRUCTURES		
CREW COMPARTMENT	2513.	0.
INTERSTAGE	2495.	0.
FWD SKIRT	1787.	818.
FWD BULKHEAD	910.	509.
FWD TANKWALL	2783.	4833.
INTER BULKHEAD	1893.	916.
CENTER SECTION	4001.	0.
INTER AFT BULKHEAD	910.	0.
AFT TANKWALL	1234.	698.
AFT BULKHEAD	1980.	1603.
AFT SKIRT	1869.	1075.
THRUST STRUCTURE	5913.	1554.
SHELL INSULATION	3915.	0.
SUBSYSTEMS		
ENGINES	21900.	7196.
PROPELLANT/PRESS SYSTEM	7439.	2581.
ULLAGE SYSTEM	0.	1076.
SEPARATION SYSTEM	1064.	280.
TVC SYSTEM	2944.	535.
FIXED EQUIPMENT	3203.	2492.
RESIDUAL PROP/GASES	12766.	3130.
CONTINGENCY	3324.	1251.
RECOVERY PROVISIONS		
CREW SYSTEMS	3000.	0.
WING	13702.	0.
FLYBACK ENGINES	10080.	0.
WING INSULATION	1926.	0.
LANDING GEAR	4599.	0.
FLYBACK FUEL	15340.	0.
BURNOUT	133492.	30548.
PROPELLANT	831124.	250192.
STAGE GROSS	964616.	280740.
PAYLOAD	339268.	58528.
VEHICLE GROSS	1303884.	339268.
LANDING CONDITION	118152.	0.
STAGE MASS FRACTION	0.8616	0.8912
PERFORMANCE RATIO	0.6374	0.7376
STAGE VELOCITY	10060.0000	19815.0000

TABLE 57. - WEIGHT STATEMENT FOR 1.3×10^6-POUND VEHICLE, FUTURE I_{sp}

VEHICLE AND STAGE WEIGHTS (LB)		
STAGE	1	2
SHELL STRUCTURES		
CREW COMPARTMENT	2539.	0.
INTERSTAGE	2706.	0.
FWD SKIRT	1805.	831.
FWD BULKHEAD	910.	509.
FWD TANKWALL	2546.	5364.
INTER BULKHEAD	1885.	916.
CENTER SECTION	4021.	0.
INTER AFT BULKHEAD	910.	0.
AFT TANKWALL	1066.	856.
AFT BULKHEAD	1968.	1610.
AFT SKIRT	1874.	1093.
THRUST STRUCTURE	5913.	1725.
SHELL INSULATION	3776.	0.
SUBSYSTEMS		
ENGINES	21900.	7986.
PROPELLANT/PRESS SYSTEM	7224.	2709.
ULLAGE SYSTEM	0.	1186.
SEPARATION SYSTEM	1003.	309.
TVC SYSTEM	2818.	576.
FIXED EQUIPMENT	3432.	2920.
RESIDUAL PROP/GASES	12038.	3449.
CONTINGENCY	3135.	1379.
RECOVERY PROVISIONS		
CREW SYSTEMS	3000.	0.
WING	13312.	0.
FLYBACK ENGINES	9862.	0.
WING INSULATION	1879.	0.
LANDING GEAR	4517.	0.
FLYBACK FUEL	15008.	0.
BURNOUT	131049.	33417.
PROPELLANT	783754.	275715.
STAGE GROSS	914802.	309131.
PAYLOAD	389483.	80351.
VEHICLE GROSS	1304285.	389483.
LANDING CONDITION	116040.	0.
STAGE MASS FRACTION	0.8567	0.8919
PERFORMANCE RATIO	0.6010	0.7079
STAGE VELOCITY	10060.0000	19815.0000

TABLE 58. - WEIGHT STATEMENT FOR 1.9 X 10^6-POUND VEHICLE, NEAR-TERM I_{sp}

VEHICLE AND STAGE WEIGHTS (LB)		
STAGE	1	2
SHELL STRUCTURES		
CREW COMPARTMENT	3035.	0.
INTERSTAGE	4110.	0.
FWD SKIRT	2815.	1363.
FWD BULKHEAD	1398.	840.
FWD TANKWALL	3866.	7080.
INTER BULKHEAD	2958.	1513.
CENTER SECTION	6318.	0.
INTER AFT BULKHEAD	1398.	0.
AFT TANKWALL	1584.	798.
AFT BULKHEAD	3111.	2718.
AFT SKIRT	2952.	1805.
THRUST STRUCTURE	8480.	2082.
SHELL INSULATION	4821.	0.
SUBSYSTEMS		
ENGINES	31409.	9639.
PROPELLANT/PRESS SYSTEM	8980.	3133.
ULLAGE SYSTEM	0.	1585.
SEPARATION SYSTEM	1550.	413.
TVC SYSTEM	3905.	716.
FIXED EQUIPMENT	3889.	3056.
RESIDUAL PROP/GASES	18601.	4612.
CONTINGENCY	4844.	1843.
RECOVERY PROVISIONS		
CREW SYSTEMS	3000.	0.
WING	20629.	0.
FLYBACK ENGINES	14264.	0.
WING INSULATION	2737.	0.
LANDING GEAR	6507.	0.
FLYBACK FUEL	21708.	0.
BURNOUT	188872.	43196.
PROPELLANT	1210993.	368675.
STAGE GROSS	1399866.	411871.
PAYLOAD	499895.	88023.
VEHICLE GROSS	1899760.	499895.
LANDING CONDITION	167164.	0.
STAGE MASS FRACTION	0.8651	0.8951
PERFORMANCE RATIO	0.6374	0.7376
STAGE VELOCITY	10060.0000	19815.0000

TABLE 59. - WEIGHT STATEMENT FOR 1.9 X 10^6-POUND VEHICLE, FUTURE I_{sp}

VEHICLE AND STAGE WEIGHTS (LB)		
STAGE	1	2
SHELL STRUCTURES		
CREW COMPARTMENT	3069.	0.
INTERSTAGE	4451.	0.
FWD SKIRT	2844.	1398.
FWD BULKHEAD	1398.	840.
FWD TANKWALL	3518.	7847.
INTER BULKHEAD	2943.	1513.
CENTER SECTION	6351.	0.
INTER AFT BULKHEAD	1398.	0.
AFT TANKWALL	1335.	1023.
AFT BULKHEAD	3090.	2726.
AFT SKIRT	2961.	1833.
THRUST STRUCTURE	8480.	2306.
SHELL INSULATION	4646.	0.
SUBSYSTEMS		
ENGINES	31409.	10676.
PROPELLANT/PRESS SYSTEM	8720.	3285.
ULLAGE SYSTEM	0.	1742.
SEPARATION SYSTEM	1462.	454.
TVC SYSTEM	3737.	769.
FIXED EQUIPMENT	4161.	3571.
RESIDUAL PROP/GASES	17541.	5069.
CONTINGENCY	4568.	2026.
RECOVERY PROVISIONS		
CREW SYSTEMS	3000.	0.
WING	20125.	0.
FLYBACK ENGINES	14001.	0.
WING INSULATION	2680.	0.
LANDING GEAR	6394.	0.
FLYBACK FUEL	21308.	0.
BURNOUT	185590.	47077.
PROPELLANT	1141972.	405187.
STAGE GROSS	1327563.	452264.
PAYLOAD	572497.	120232.
VEHICLE GROSS	1900059.	572497.
LANDING CONDITION	164282.	0.
STAGE MASS FRACTION	0.8602	0.8959
PERFORMANCE RATIO	0.6010	0.7079
STAGE VELOCITY	10060.0000	19815.0000

TABLE 60. - WEIGHT STATEMENT FOR 2.5 X 10^6-POUND VEHICLE, NEAR-TERM I_{sp}

VEHICLE AND STAGE WEIGHTS (LB)		
STAGE	1	2
SHELL STRUCTURES		
CREW COMPARTMENT	3463.	0.
INTERSTAGE	5563.	0.
FWD SKIRT	3568.	2115.
FWD BULKHEAD	1697.	1291.
FWD TANKWALL	5441.	9345.
INTER BULKHEAD	3619.	2324.
CENTER SECTION	8034.	0.
INTER AFT BULKHEAD	1697.	0.
AFT TANKWALL	2419.	683.
AFT BULKHEAD	3817.	4194.
AFT SKIRT	3761.	2769.
THRUST STRUCTURE	11031.	2578.
SHELL INSULATION	5693.	0.
SUBSYSTEMS		
ENGINES	40854.	11936.
PROPELLANT/PRESS SYSTEM	10300.	3610.
ULLAGE SYSTEM	0.	2105.
SEPARATION SYSTEM	2040.	548.
TVC SYSTEM	4797.	886.
FIXED EQUIPMENT	4481.	3534.
RESIDUAL PROP/GASES	24475.	6124.
CONTINGENCY	6374.	2447.
RECOVERY PROVISIONS		
CREW SYSTEMS	3000.	0.
WING	28163.	0.
FLYBACK ENGINES	18320.	0.
WING INSULATION	3565.	0.
LANDING GEAR	8350.	0.
FLYBACK FUEL	27880.	0.
BURNOUT	242402.	56487.
PROPELLANT	1593412.	489489.
STAGE GROSS	1835815.	545976.
PAYLOAD	663672.	117696.
VEHICLE GROSS	2499486.	663672.
LANDING CONDITION	214522.	0.
STAGE MASS FRACTION	0.8680	0.8965
PERFORMANCE RATIO	0.6374	0.7376
STAGE VELOCITY	10060.0000	19815.0000

TABLE 61. - WEIGHT STATEMENT FOR 2.5 X 10^6-POUND VEHICLE, FUTURE I_{sp}

VEHICLE AND STAGE WEIGHTS (LB)		
STAGE	1	2
SHELL STRUCTURES		
CREW COMPARTMENT	3505.	0.
INTERSTAGE	6015.	0.
FWD SKIRT	3608.	2167.
FWD BULKHEAD	1697.	1291.
FWD TANKWALL	4975.	10343.
INTER BULKHEAD	3601.	2324.
CENTER SECTION	8079.	0.
INTER AFT BULKHEAD	1697.	0.
AFT TANKWALL	2077.	969.
AFT BULKHEAD	3791.	4206.
AFT SKIRT	3772.	2810.
THRUST STRUCTURE	11031.	2852.
SHELL INSULATION	5477.	0.
SUBSYSTEMS		
ENGINES	40854.	13203.
PROPELLANT/PRESS SYSTEM	10003.	3782.
ULLAGE SYSTEM	0.	2309.
SEPARATION SYSTEM	1923.	602.
TVC SYSTEM	4591.	949.
FIXED EQUIPMENT	4791.	4123.
RESIDUAL PROP/GASES	23080.	6719.
CONTINGENCY	6010.	2685.
RECOVERY PROVISIONS		
CREW SYSTEMS	3000.	0.
WING	27519.	0.
FLYBACK ENGINES	18004.	0.
WING INSULATION	3496.	0.
LANDING GEAR	8205.	0.
FLYBACK FUEL	27400.	0.
BURNOUT	238198.	61334.
PROPELLANT	1502595.	537071.
STAGE GROSS	1740794.	598405.
PAYLOAD	758624.	160220.
VEHICLE GROSS	2499418.	758624.
LANDING CONDITION	210799.	0.
STAGE MASS FRACTION	0.8632	0.8975
PERFORMANCE RATIO	0.6010	0.7079
STAGE VELOCITY	10060.0000	19815.0000

It should be realized that the synthesis outputs are usually summary statements, and various factors have been lumped together to produce a concise format. In table 43 the loading intensity quoted was derived from the axial load and bending moments on the appropriate flight regime. At end boost, the value of N_x quoted has been temperature corrected, based upon the stability criteria.

$$N_{x_{quoted}} = N_{x_{temp}} \cdot \left(\frac{E_{RT}}{E_{temp}}\right)$$

for end boost only.

Stage and component weights have various structural elements combined. The tankage shell weights include the load-carrying structure, closeout and secondary structure factors, and ground-hold insulation weights. The aft bulkhead includes additional weight penalties for the compression stiffness near the equator of both the forward end aft bulkheads and the bulkhead-shell junction. Insulation weights quoted in the weight statement table refer to the additional insulation required for the thermal protection during entry only.

Vehicle Sensitivities

The base line vehicles defined in the previous section were synthesized for a series of fixed parameters and basic assumptions. It is important to determine the sensitivity of the vehicle design and payload capability to various vehicle parameters in order (1) to gain a better insight into the realism of the vehicles synthesized for the purposes of this study and (2) to obtain an understanding of the relative effectiveness of structural changes and other system changes. Therefore, a sensitivity study was conducted on two base line vehicles of 1.3×10^6 pounds and 2.5×10^6 pounds lift-off weight, respectively, with the near-term propulsion characteristics. The investigation was broken down into four different parameter areas: propulsion system, flyback requirements, landing characteristics, and weights-inert, structures, and subsystems.

The propulsion system changes considered were the propellant mixture ratios and specific impulses. Figure 86 shows the effect of changing first stage mixture ratio (MR) from 2.25 to 2.0 and second stage MR from 5.0 to 7.0; the specific impulses were held constant. It is realized that this would not be true; in fact, MR changes could affect impulse, expansion ratio, chamber pressure, thrust levels, etc., and as such should all be considered simultaneously. The current program has the ability to synthesize such a vehicle system, but all the interconnected parameter changes have to be

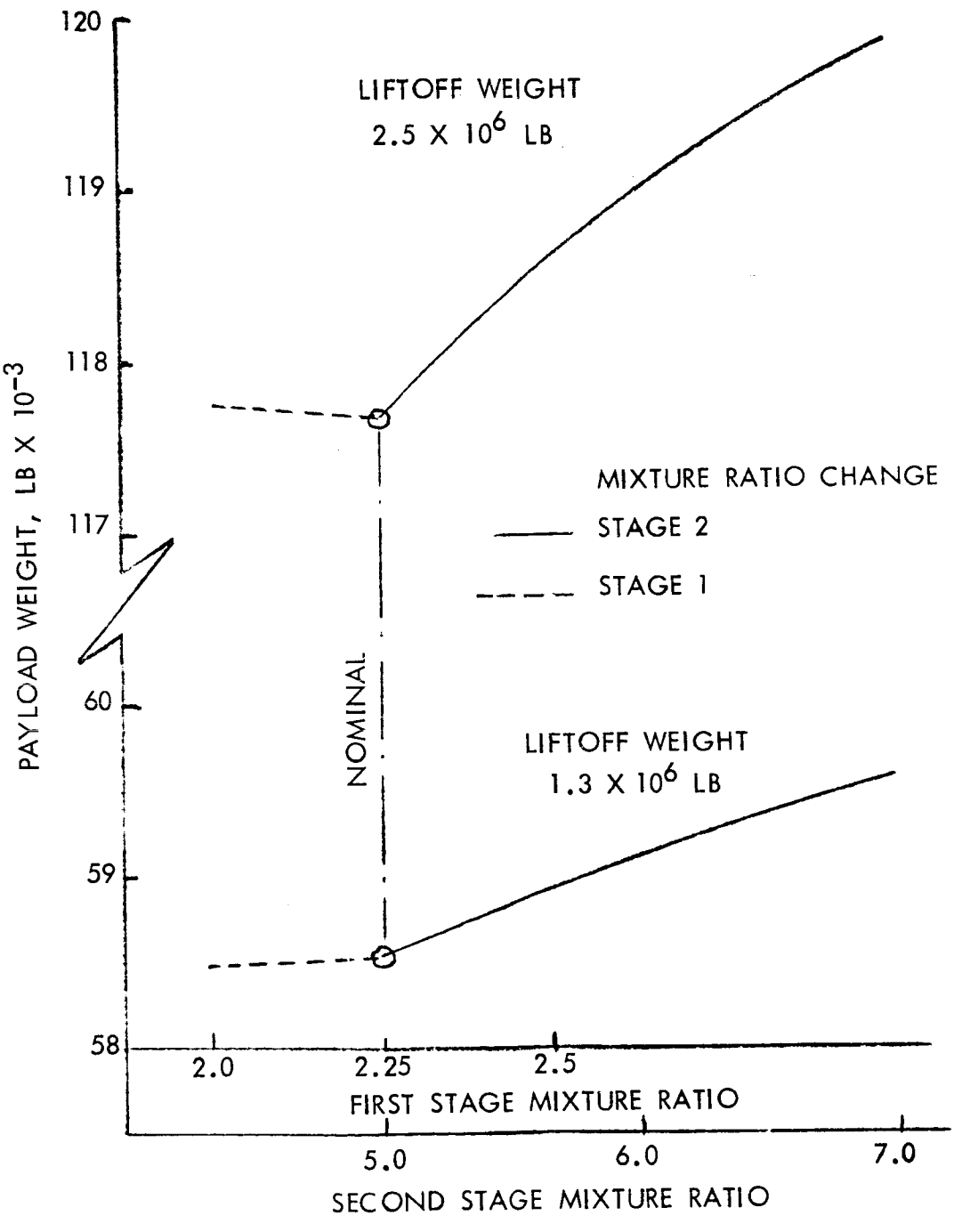

Figure 86. - Propellant Mixture Ratio Sensitivity

supplied as input data. Small parameter changes can be considered separately and their interconnected effect determined by the combination of the sensitivity partials.

Figure 86 shows that there is a payload gain with higher mixture ratio changes since the second-stage tank volumes are decreased. If the second-stage MR is changed from 5.0 to 6.0, a payload increase of 600 pounds is achieved for the smaller vehicle. If this MR change degrades the specific impulse by more than 2.5 seconds, this payload improvement will be offset. Payload sensitivities to specific impulse changes are indicated in figure 87 for both the first and second stages. Each vehicle system was completely resized to the parameter variation, and as such did not perform on off-loading design condition from the base line system.

Flyback requirements were imposed upon the vehicle system; then relative sensitivities were found which are shown in figures 88 and 89. Figure 88 shows the effect of changes in the flyback cruise range requirements, the additional fuel, structural weight and, hence, system weights. The flyback engine performance and installation parameter selected for the base-line vehicles were re-assessed to determine their relative importance. Figure 89 shows the payload changes to specific fuel consumption, flyback cruise velocity, and cruise maximum lift-to-drag ratio of the vehicle system. Effect of additional installed weights for the engines, etc., are discussed in the inert weight sensitivity chart.

The wing shape, size, and weight, and the wing effects on the fuselage bending moments during boost are all influenced by the landing characteristics desired for the vehicle system. The three basic design parameters that affect the wing sizing are stall velocity desired, touch-down angle, and attainable landing lift coefficient.

The payload sensitivity to these three parameters is indicated in figure 90. The final sensitivity shown, figure 91, was the effect of inert weights carried by the first stage vehicle system. This inert weight can reflect contingencies in structural weights, engine systems, fixed equipment, etc.

Other design parameters were exercised through the parametric vehicle program, but it appears that the synthesis subroutine for wing weight was fairly insensitive to wing loading and shape parameters. The wing weight analysis is applicable to large-aspect-ratio wings with wing loadings producing large loads in the wing cover plates and shear webs. For the base line configurations with low-aspect-ratio wings and minimum lift flight

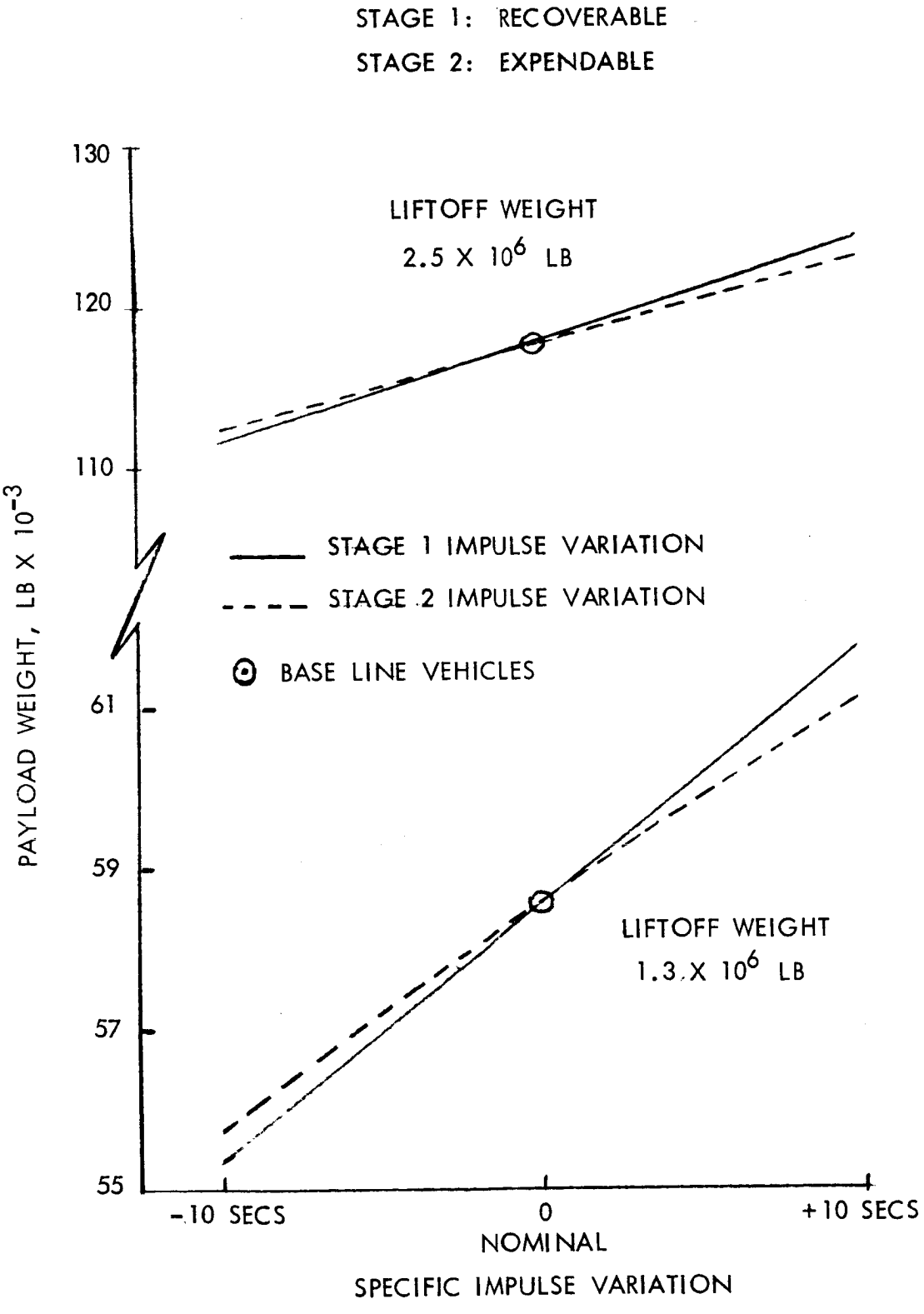

Figure 87. - Specific Impulse Sensitivity

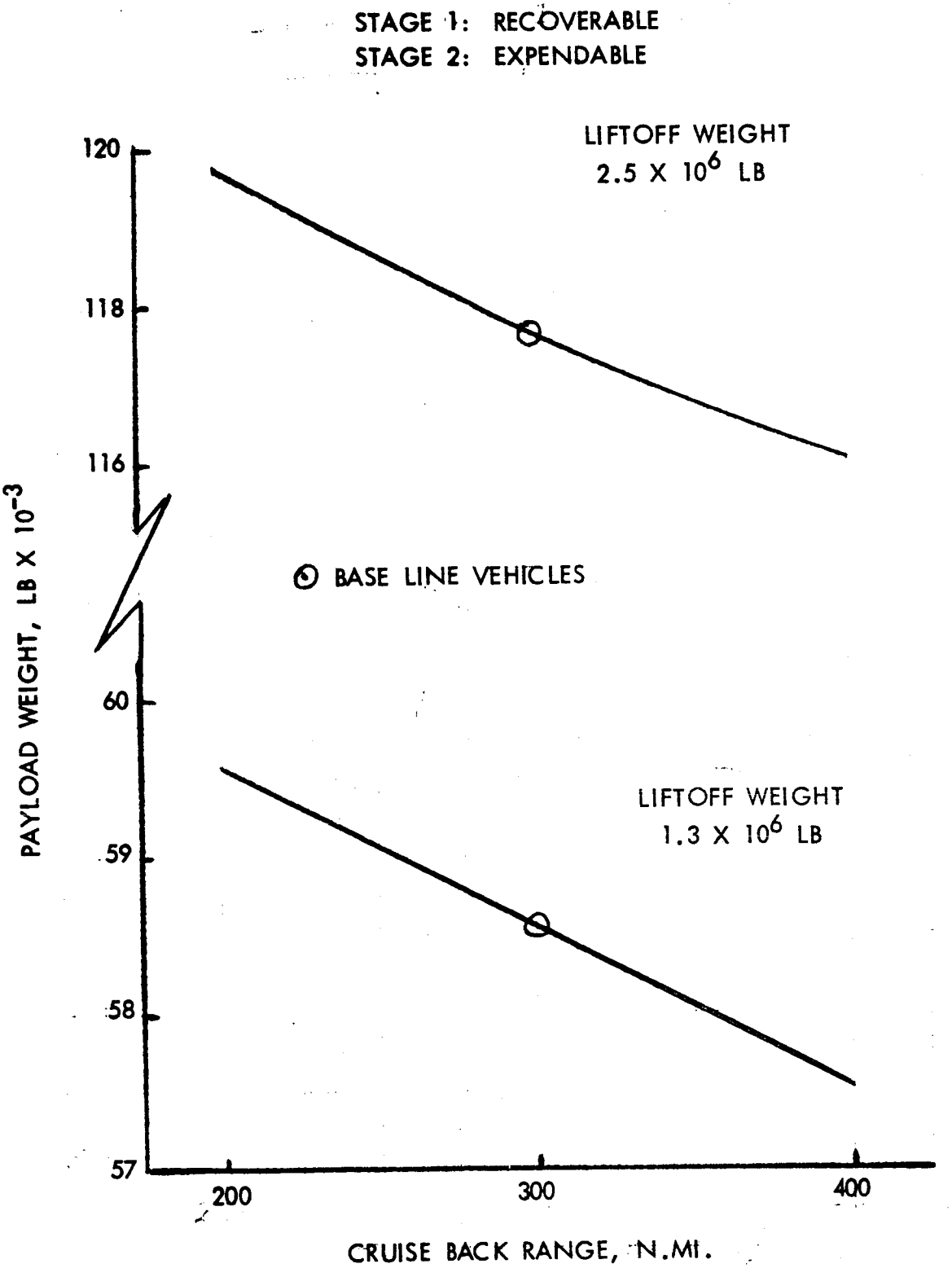

Figure 88. Cruise-Back Range Sensitivity

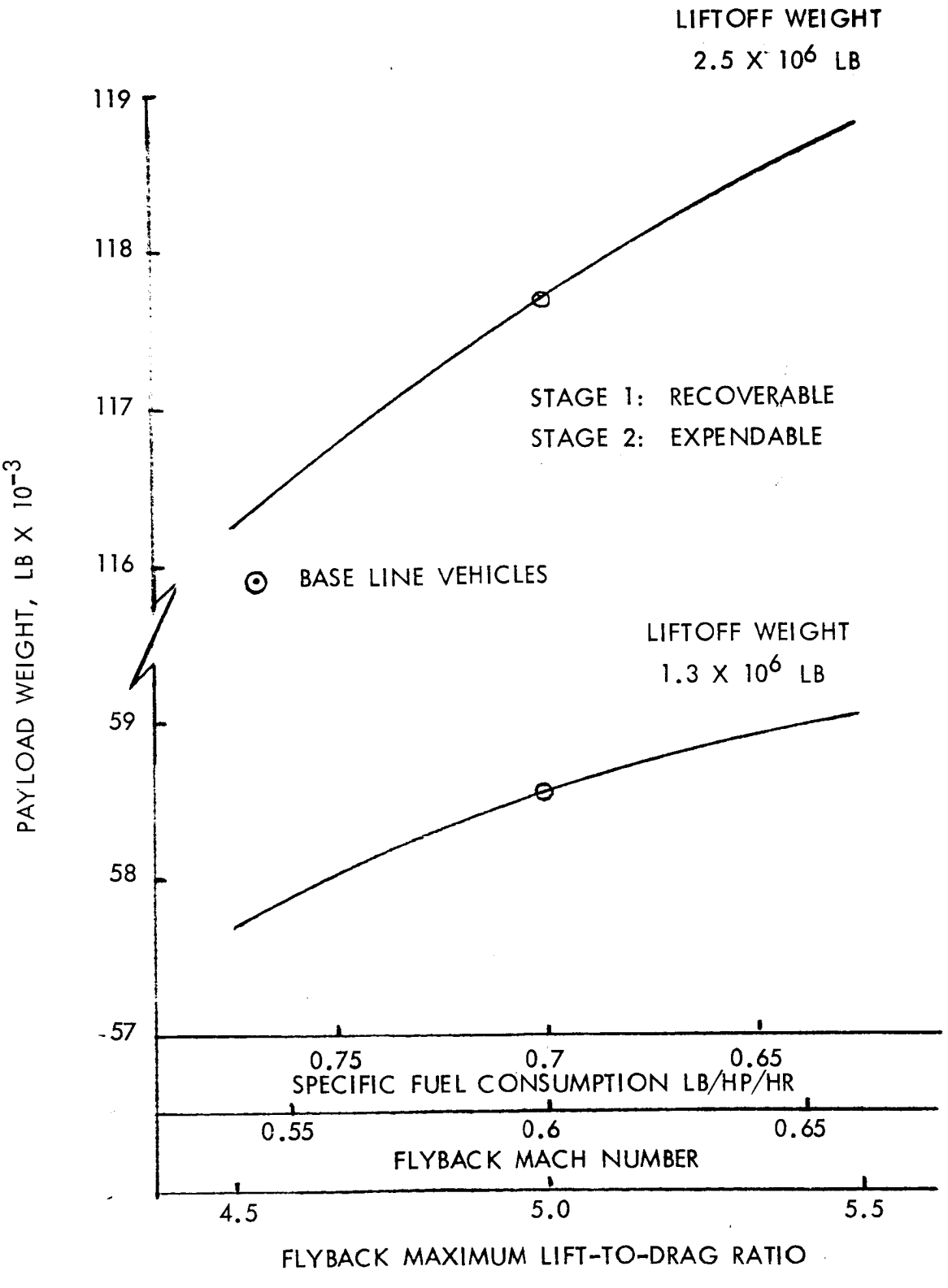

Figure 89. Flyback Parameter Sensitivity

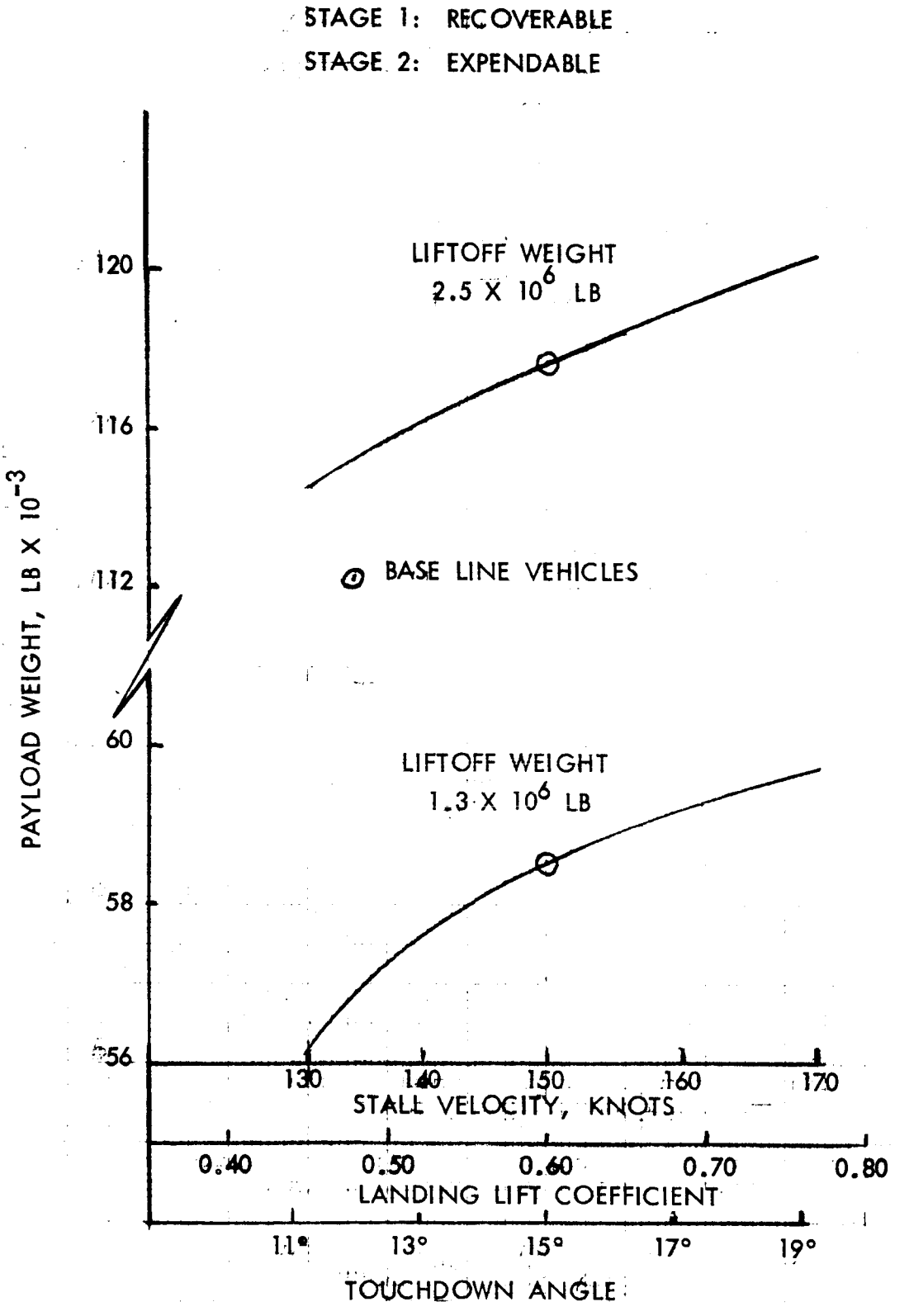

Figure 90. Landing Characteristics Sensitivity

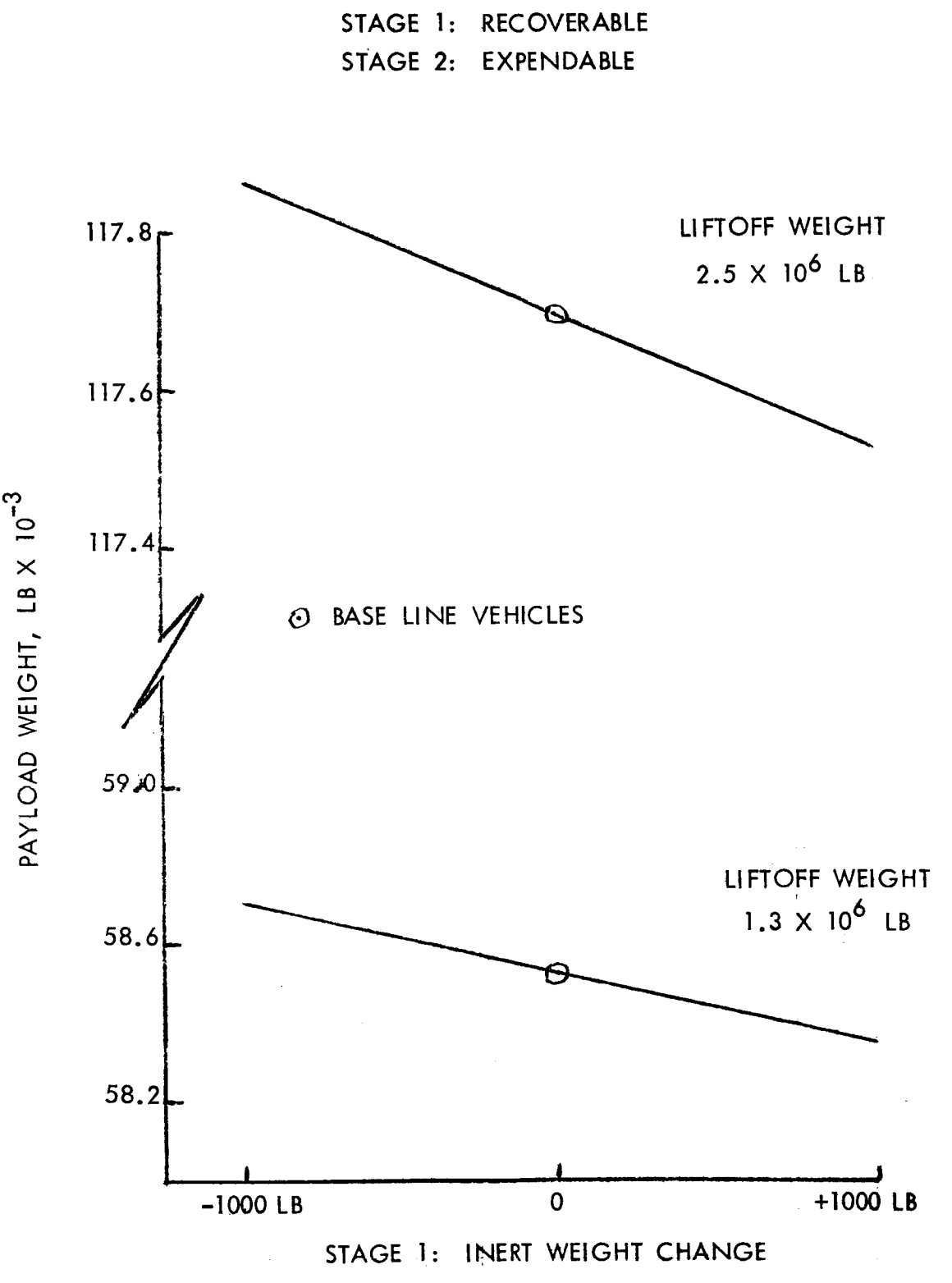

Figure 91. Inert Weight Sensitivities

profile, the design loadings are extremely low and as such are not recognized by the wing weight synthesis routine. In order to handle the lightly loaded wings, a realistic minimum unit weight limit of 5 pounds per square foot was built into the computer subroutine. Even though the wing weight values were frequently established from the minimum weight constraint, the program correctly parametrically sized the wing and determined its affects on the loading envelope of the fuselage.

The weight partials for the synthesized vehicle systems were compared with previous in-depth point-design studies conducted on recoverable vehicle systems to determine their relative validity. Table 62 lists the 1.3×10^6-pound vehicle of this study (PAID synthesis) with three other base vehicle systems, two are of NAA and the third is the Lockheed/General Dynamics Reusable Orbital Transport (ref. 18). The weight partials were referenced to the stage's propellant weight unless otherwise noted. It can be seen that PAID vehicles synthesized herein were in good agreement with the three comparison vehicles—particularly in view of the broad differences in configuration and design requirements. Differences occur for the R. O. T. where the vehicle is a piggy-back arrangement and a lifting body concept, which results in high weight partials for shell structure, due to body shape, flyback engines which are buried with long inlet and outlets, and flyback fuel due to low (L/D) max. Also, the wings of the first two vehicles were sized for a horizontal launch mode; therefore, their wing weight partials are considerably higher than the PAID vehicles.

The results shown in figures 87 through 91 have been considered linearized in the neighborhood of the base-line vehicles, and a summary listing is given in table 63.

The vehicle design load envelope and applied load intensity changes for the condition of an expendable upper stage or winged recoverable upper stage are shown in tables 64 and 65. Whereas the upper stage wing changes the bending moments at prelaunch, and bending moment distribution at maximum dynamic pressure (table 64) the average design loading intensities of most fuselage elements remain unchanged (table 65). This is due to the major portion of the loading arising from axial force due to engine thrust, and for these particular vehicle systems, the end boost conditions give rise to the maximum applied loads.

TABLE 62. - WEIGHT PARTIALS FOR RECOVERABLE FIRST STAGES

Vehicle System	Lockheed/GD Reusable Orbital Transports	NAA 10-Ton Reusable Orbital Carrier	NAA 50-Ton Reusable Orbital Carrier	PAID Synthesis
Shell structures	0.0397	(0.0246)	(0.0345)	(0.0240)
Bulkheads	0.0059			
Thrust structures	0.0077	0.0042	0.0054	0.0071
Crew compartment	0.0013	0.0014	0.0016	0.0030
Wing and Fins & In.	0.0439	0.0936	0.0110	0.0188
Landing gear	0.0455*	0.0298*	0.0136*	0.0389*
Engines	0.0346	0.0248	0.0657	0.0263
TVC	0.0041	0.0033	0.0021	0.0035
Contingency				0.004
Flyback engine	0.2044*	0.1314*	0.0565*	0.0853*
Prop/press system	0.0142	0.0007	0.0066	0.0090
Separation system	0.0026		0.0025	0.0013
Fixed equipment	0.0067	0.0040	0.0020	0.0038
Flyback fuel	0.2155*	0.1115*	0.0387*	0.1300*
Residuals	0.0167	0.0277	0.0189	0.0154
Protection body	0.0039		0.0020	0.0047
Stage propellant weight, lb	1.07×10^6	0.73×10^6	4.06×10^6	0.83×10^6
Vehicle Design	Lifting Body	Winged Body	Winged Body	Winged Body

*Partial based on landed weight

TABLE 63. - PAYLOAD SENSITIVITY RATIOS*

Design Parameter	1.3×10^6-Pound Vehicle	2.5×10^6-Pound Vehicle
Mixture ratio, Stage 1, lb/MR	0	-400
Mixture ratio, Stage 2, lb/MR	600	1420
Specific impulse, Stage 1, lb/sec	310	635
Specific impulse, Stage 2, lb/sec	250	535
Cruise-back range, lb/n. mi.	-11	-15.5
Specific fuel consumption, lb/(lb/hp/hr)	-12 000	-20 000
Flyback Mach number, lb/M	7600	18 000
(Lift/Drag) max, lb/~	1000	2300
Stall velocity, lb/knots	85	210
Landing lift coefficient, lb/~	2000	17 000
Touch-down angle, lb/degree	30	65
Inert weight, Stage 1, lb/lb	0.17	0.175

*Payload sensitivity ratio = $\frac{\text{Payload increase}}{\text{1-unit increase of design parameter}}$

TABLE 64. - EFFECTS OF RECOVERABLE UPPER STAGE ON DESIGN LOADS MATRIX

Expendable Upper Stage

STATION	PRELAUNCH MOMENT	PRELAUNCH SHEAR	PRELAUNCH AXIAL	MAX Q ALPHA MOMENT	MAX Q ALPHA SHEAR	MAX Q ALPHA AXIAL	END BOOST MOMENT	END BOOST SHEAR	END BOOST AXIAL
173.	20353643.	41116.	1280616.	-1331087.	28080.	1632766.	325856.	8368.	1626279.
265.	16781123.	36600.	1142596.	-4025944.	30543.	1372673.	-374738.	6873.	1577743.
325.	14704884.	31701.	1051325.	-5531863.	18996.	1262760.	-764381.	5945.	1545648.
525.	5994618.	15525.	745566.	-6424.	-74396.	820737.	-1622420.	2658.	1417553.
694.	7468299.	14358.	500130.	9034704.	-32549.	623514.	-1966865.	1417.	1356659.
786.	6225824.	12671.	366673.	11897096.	-29719.	610174.	-2070856.	846.	1326635.
916.	4683638.	11055.	351157.	15438018.	-24757.	586790.	-2125819.	-0.	1270498.
1046.	3298506.	10146.	331382.	18834883.	-25973.	549445.	-2082826.	-823.	1198950.
1124.	2533534.	9520.	301582.	20484723.	-16443.	504532.	-1980147.	-1817.	1091133.
1177.	2057432.	8583.	281434.	21180135.	-10000.	474166.	-1869990.	-2371.	1018238.
1255.	1593035.	3356.	251634.	21587396.	-470.	429253.	-1660423.	-3016.	910421.
1681.	386000.	2307.	88327.	10655852.	51754.	183124.	-411567.	-2843.	319572.
1759.	206550.	2307.	58528.	6259079.	61283.	138211.	-217985.	-2134.	211755.
1759.	206550.	2307.	58528.	6259079.	61283.	138211.	-217985.	-2134.	211755.

Recoverable Upper Stage

STATION	PRELAUNCH MOMENT	PRELAUNCH SHEAR	PRELAUNCH AXIAL	MAX Q ALPHA MOMENT	MAX Q ALPHA SHEAR	MAX Q ALPHA AXIAL	END BOOST MOMENT	END BOOST SHEAR	END BOOST AXIAL
173.	393C2455.	57972.	1280067.	-1998080.	-55053.	1639651.	328002.	8315.	1625385.
265.	3418C53C.	53449.	1142001.	1469697.	-20384.	1401848.	-367144.	6807.	1576651.
325.	31C8CC71.	48546.	1050700.	2705321.	-20264.	1299982.	-752573.	5873.	1544425.
525.	23C16293.	32303.	744784.	12146084.	-74392.	884652.	-1594819.	2572.	1415675.
694.	17653253.	21136.	499280.	18597735.	-1923.	708644.	-1925203.	1336.	1356496.
786.	14868239.	29449.	365786.	18548359.	2997.	696695.	-2022111.	772.	1324318.
916.	11144845.	27834.	350219.	17598656.	11614.	675767.	-2068761.	-54.	1267956.
1046.	7569377.	26925.	330405.	16001457.	15041.	641591.	-2020549.	-841.	1196222.
1124.	5614058.	23344.	296968.	15122161.	7565.	564157.	-1914496.	-1885.	1075161.
1177.	4468633.	20379.	274447.	14857730.	2529.	512005.	-1800888.	-2451.	993625.
1254.	3425998.	6426.	238183.	16775743.	-51840.	370202.	-1583281.	-3143.	862334.
1680.	913712.	5378.	63511.	18264300.	44846.	135381.	-409457.	-2372.	229938.
1758.	554042.	3869.	31588.	14088311.	62515.	92465.	-259556.	-1482.	114363.
1868.	211384.	2361.	22083.	6922253.	67777.	79687.	-115739.	-1133.	79951.

AXIAL LOAD (LB), SHEAR (LB), MOMENT (IN. LB.)

TABLE 65. - EFFECTS OF RECOVERABLE UPPER STAGE ON APPLIED LOADING INTENSITIES (LB/IN.)

Expendable Upper Stage

STATION	PRELAUNCH NX	MAX Q ALPHA NX	END BOOST NX	MAX NX/R
173.	2732.	2834.	3058.	23.5239
265.	2401.	-76.	179.	18.4683
325.	2190.	2310.	2920.	22.4585
525.	1541.	-1128.	-63.	11.8571
694.	1054.	1307.	2604.	20.0288
786.	793.	1360.	2547.	19.5901
916.	725.	1413.	2443.	18.7928
1046.	793.	1807.	2740.	24.9107
1124.	704.	-204.	303.	6.4018
1177.	646.	1741.	2331.	21.1931
1255.	568.	-315.	-75.	5.1671
1681.	193.	763.	725.	6.9398
1759.	126.	510.	478.	4.6407
1759.	126.	510.	478.	4.6407

Recoverable Upper Stage

STATION	PRELAUNCH NX	MAX Q ALPHA NX	END BOOST NX	MAX NX/R
173.	3230.	2863.	3056.	24.8489
265.	2859.	-94.	177.	21.9897
325.	2620.	2299.	2917.	22.4382
525.	1883.	-698.	-67.	14.4881
694.	1321.	1705.	2598.	19.9884
786.	1019.	1683.	2541.	19.5459
916.	894.	1622.	2437.	18.7434
1046.	948.	1889.	2732.	24.8330
1124.	808.	-280.	268.	7.3482
1177.	720.	1584.	2274.	20.6720
1254.	609.	-612.	-175.	5.5331
1680.	162.	947.	526.	8.6081
1758.	84.	706.	264.	6.4196
1868.	53.	416.	182.	3.7851

PROGRAM TURNOVER

Effort under this task included formulating an orderly process for the release of computer programs to the NASA/OART. These programs include the parametric synthesis and design synthesis subroutines from Phase I, as shown in figure 92. Actual turnover of the subroutines has been planned with representatives of NASA/ERC, Cambridge, Massachusetts, and is scheduled during the planned Phase III follow-on. Although NAA has recently implemented IBM 360 computer systems using FORTRAN G, H, and E programming languages, the "Programmed Assistance" subroutines have been, and are being, executed in an emulation mode using FORTRAN IV, Version 13, language. This has been done to keep the subroutines compatible with computer hardware and software systems at NASA/ERC and other NASA centers. It is felt that these subroutines will find use at many of the NASA centers in the future.

The actual turnover of these subroutines will be accomplished at a period to be mutually agreed upon between NASA and NAA during the latter half of the planned Phase III effort. If required, an NAA representative will be made available at NASA/ERC for a one- to two-week period to assist in running test cases on NASA equipment. Preparation and documentation of the digital computer decks will follow the preliminary draft guidelines transmitted to North American by NASA/ERC in December 1966. The only difficulties that might be encountered involve the limitations on COMMON data transference between the following program subdivisions:

Input

Output

Control

Calculations

Bulk data

Since some of these subroutines are fairly large and occupy much of the available core, allowances should be made to print some design information directly from the subroutine in which it is calculated. Print data transferred to the output region should be limited to primary study parameters and assessments.

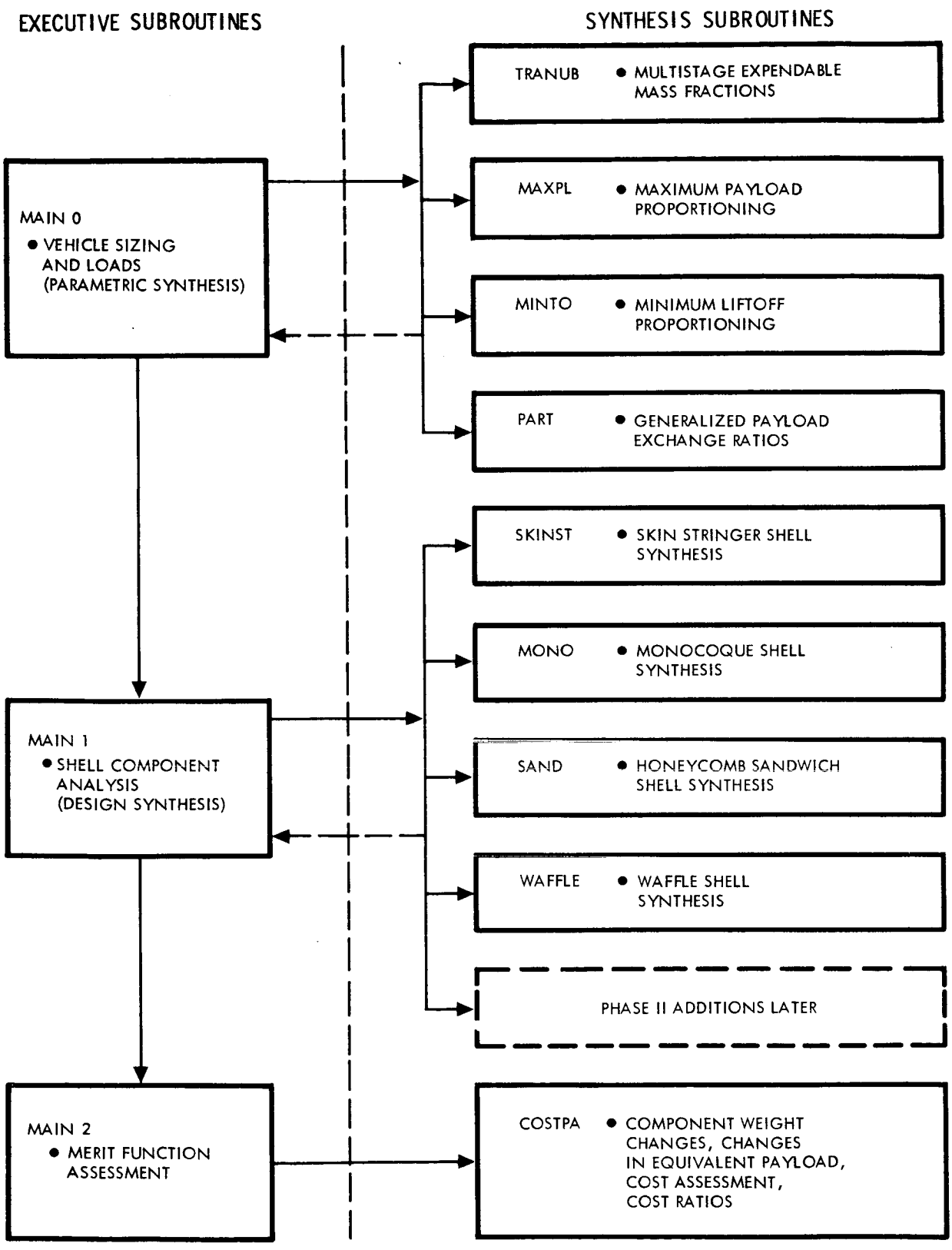

Figure 92. - Executive and Synthesis Subroutines (Phase I Only)

Synthesis and evaluation programs are, of necessity, unique in their operations and are difficult to treat in the same fashion as mathematical analyses. The basic synthesis process involves assuming initial design indices, calculating new indices, comparing with the previously initialized indices, and iterating this process to some controlled tolerance. This means that all pertinent subroutines must be included in the iteration loop with answers resulting from the last cycle through this loop. Hundreds of pieces of data are re-cycled in this loop, and the most efficient place to output data is from this loop. Also, it is more efficient to transfer data through COMMON than in complex argument lists; this latter approach will greatly increase the program running time.

Three separate operations are illustrated in figure 92. The three executive subroutines (MAIN 0, MAIN 1, and MAIN 2) provide partial cycling capability so that the parametric synthesis, design synthesis, and merit function assessment can be executed singly or in conjunction with each other. This procedure provides a series of checkpoints. Input, output, and program control are handled by subroutines which transfer commands and data to the executive subroutines.

For example, the mass fraction subroutine (TRANUB) contains a parametric assessment of vehicle design loads for maximum dynamic pressure and maximum acceleration conditions. The program may be halted after executing MAIN 0 to input the vehicle data to a more sophisticated external loads program, if desired, to determine if any correction coefficients in the TRANUB input array require changing. In a similar manner, the MAIN 1 executive program could be used to provide structural designs for an array of applied loads rather than a selected set of values. Linkage of these program packages will be flexible and versatile so that NASA may apply the programs to various types of problems by treating them as "black boxes" within their master executive logic.

At the present time, the subroutines are being used as independent packages to accomplish trade-off studies. Further effort during Phase III will provide the proper linkage for a complete automatic operational mode.

Program documentation will include a summary of the programming approach, primary equations, flow logic diagrams, input format, typical output, program listings, and test cases. Table 66 presents a preliminary outline of the user's manual to be submitted along with the program source decks.

TABLE 66.- PRELIMINARY USER'S MANUAL OUTLINE

- Abstract
- Theory
  - Introduction
  - Nomenclature
  - Scope and Limitations
  - Coordinate System
  - Input Requirements
  - Sizing Equations
  - Loading Equations
  - Weight Equations
  - Stage Proportioning
  - Payload Exchange Ratios
  - Structural Synthesis
    - Design Criteria
    - Shell Equations
    - Bulkhead Equations
  - Merit Function Assessment
    - Weight Complexity Factors
    - Cost Complexity Factors
    - Starter Package
    - Cost Assessment
- General Description of the Computer Programs
  - Introduction
  - Program Capabilities and Limitations
  - Sign Conventions and Dimensions
  - Geometry
  - Indicators (Cycling)
  - Compilation Time
  - Output Indicators
- Detailed Use of the Programs
  - Introduction
  - Deck Setup
  - Data Deck Setup
  - Function Subroutines
  - Utility Subroutines
  - Sample Problem No. 1
    - Description/Setup
    - Data Sheets
    - Subprograms Used
    - Execution Time
    - Output
  - Sample Problem No. 2
    - Description/Setup
    - Data Sheets
    - Subprograms Used
    - Execution Time
    - Output
  - Error Indications
  - Logic Diagrams
  - Program Listings
  - Nomenclature

REENTRY VEHICLE SYNTHESIS

The recoverable Launch Vehicle Parametric Synthesis program described in Appendix B of this report was compiled with some of the main program logic capable of synthesizing winged body upper stages. However, specific subroutines for this task were not included in the program because they are outside of the present study's scope. The principal differences involve the geometric shape of the vehicle stage, the loads and thermal environments encountered during reentry, and the means of adequately assessing the thermal-protection system. For entry vehicle stages, the structural system represents up to 18 percent of the stage gross weight, and the construction material thermal-protection choice is a major item for stage performance and vehicle design feasibility. Previous studies of upper stages (refs. 26 through 28)indicate that future primary study requirements will involve definition of a reasonable development path from expendable stages to winged entry to other concepts. Hand-in-hand with this problem is one of construction and material.

A logical approach is to first consider recovering the upper stage of a tandem-staged vehicle with a winged body configuration before considering parallel staging and lifting bodies shapes; that is, to consider the reentry and recovery of modified expendable upper stages.

Parametric synthesis of reentry vehicles can encompass a range of hypersonic lift-to-drag ratios from approximately zero to three. The size of the vehicle is primarily dependent upon the number of crew and/or passengers, mission payload, and operational modes. The synthesis of semiballistic vehicles of the Apollo shape is relatively straightforward; however, in the future, there will be growing interest in complex shape vehicles and vehicles with $L/D > 1.0$. Essentially, this interest of spacecraft with $L/D > 1.0$ derives from their extended longitudinal and lateral range, and their ability to make horizontal land landings. The capability for aerodynamic maneuver during entry can minimize waiting time in orbit, allow choice of landing sites, etc. Little, however, has been accomplished in determining the weight penalty paid for this maneuverability. Current studies indicate that the penalty in total spacecraft weight alone could be approximately 100 percent when comparing a vehicle with a $L/D = 0$ to one with $L/D \approx 3$. In addition, the weight increase, vehicle length, lift coefficient, and projected area would have a marked effect on booster payload bending moment constraints (ref. 27). A NASA study (ref. 28) shows the weight of a $L/D = 3$ vehicle to a $L/D = 1$ vehicle at about 1.5. This means a 50 percent increase in weight for an

increased lateral range capability of up to 500 percent; most of the weight penalty is for added aerodynamic and thermal protection structures.

From the standpoint of structures and materials research direction, it appears logical to start with a winged-body configuration and concentrate the parametric synthesis effort in structural and thermal protection areas, considering ablators, and cooled and high-temperature structures and heat shields. In a parametric sense, the specific subroutines (illustrated as (A) through (G) in figure 93 should be added to the parametric program.

It must be remembered that upper-stage design considerations become more complex as basic mission requirements are increased. For example, a typical mission from ref. 4 includes an integral payload in the stage, and the capability of returning cargo or personnel from an orbit operation. This vehicle is more than a booster stage and, therefore, all mission phases must be considered, as well as all mission subsystems.

For the launch vehicle systems (expendable/recoverable), the synthesis approach dealt with simple cylindrical shapes, experiencing easily evaluated symmetrical design load envelopes. For these configurations, load and thermal environments and major structural shell weights are assessed, and with the other subsystem weights, the vehicle mass fractions are evaluated and the vehicle performance defined. When considering entry vehicle shapes other than the simple winged-body concept (i.e., cylindrical shells and tanks and with wings), the automatic synthesis program must be far more complex. High lift-to-drag and lifting body shapes present a considerable problem in the systematic packaging of all the required subsystems into a geometric envelope while retaining required aerodynamic and inertial characteristics. Therefore, the usual techniques of maximizing a structural mass fraction, ν B, are interchanged with maximizing a packaging efficiency factor. For lifting body configurations, there are several candidates, e.g., M-2 and HL-10; each with its own unique design arrangement. Individual parametric synthesis programs will be required for each lifting body concept, each program unique to the design configuration.

Due to the complex structural shapes, the structural elements are no longer symmetric and additional design considerations are warranted. For shapes with flat sides or surfaces, the pressurized propellant tanks may be internal nonintegral spheres or tapered tanks, depending on the packaging criteria. Stability frames and internal bracing have been required for several design concepts suggested to withstand external pressures resulting from air loads. The weight estimation of any of these structural elements is comparatively difficult, even parametrically. Additionally, it is necessary to define the design-loading envelope at various stations throughout the vehicle and the load and temperature history to determine the critical design

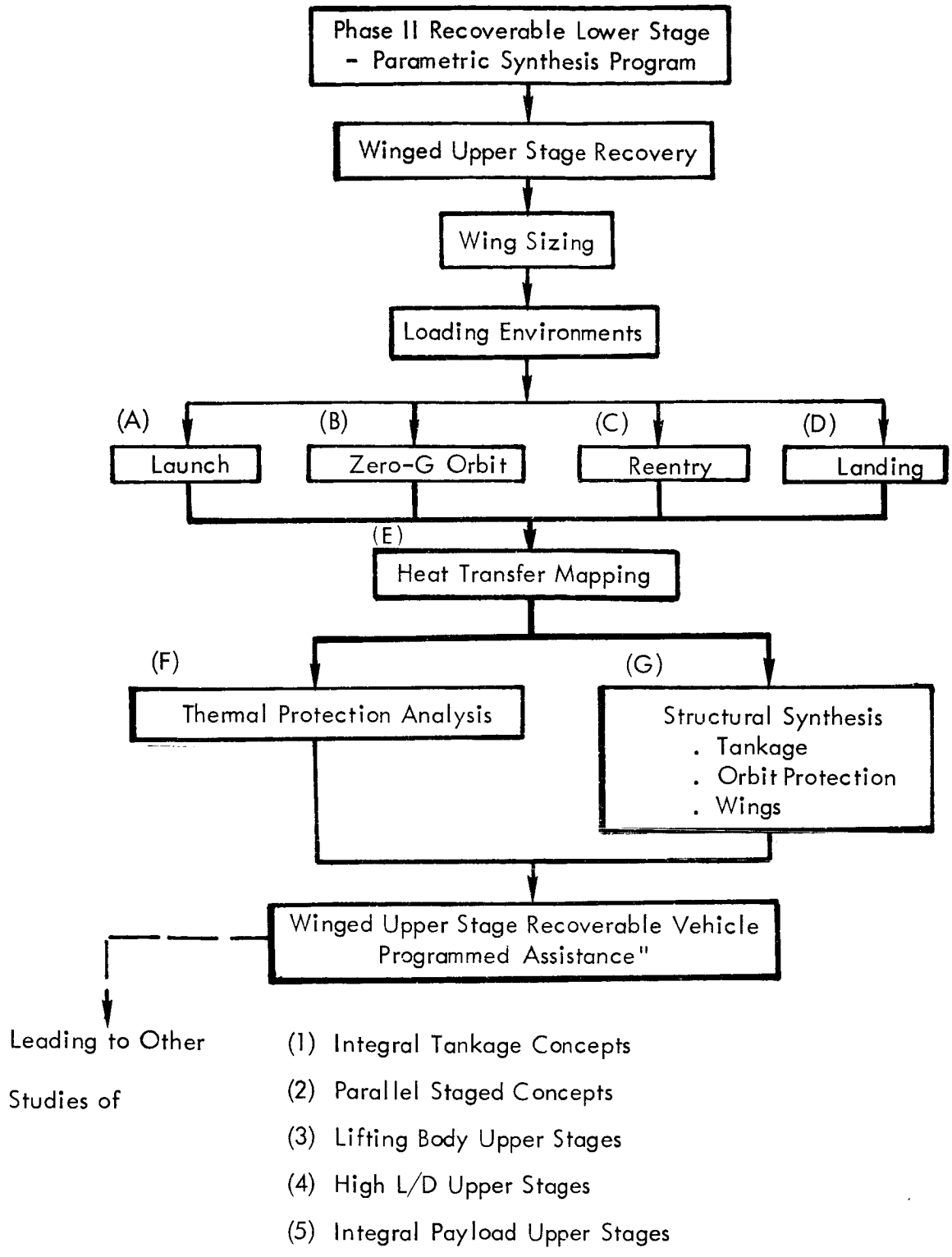

Figure 93. -Winged Upper-Stage Synthesis

conditions. The design condition could be at maximum load and low-temperature, maximum temperature and low load, or somewhere in between. Added to the load-carrying structure is the thermal protection system—whether it is reradiative, transpiration-cooled, ablative, or combinations thereof. The weights associated with the design of thermal-protection systems are of equal importance to the load-carrying structures and must be realistically evaluated.

A solution to the parametric synthesis problem for complex vehicle and structural shapes appears to be in developing mathematical and empirical scaling relationships for the various subsystems (including structures, thermal protection, etc.) to handle the initial parametric sensitivity studies. The results of these parametric studies can be evaluated in further detail outside of the synthesis program to determine the vehicle system design environments for the various structural components. Separate synthesis subroutines are then developed for the major structural elements for each vehicle design and are exercised individually to synthesize the components weight for ranges of design parameters and sizes. These results are summarized in updated empirical relationships for inclusion into the overall reentry vehicle synthesis programs. This would perform a boot-strap operation of continually improving the synthesis program with its own study results.

The required parametric vehicle-scaling approach is indicated in figure 94. A list of the typical parameters considered for vehicle subsystems definition is seen in figure 95. This figure shows that any vehicle-sizing consideration has to have the range, time, and mission profile defined in detail for the subsystem weights evaluation to be compatible with mission requirements.

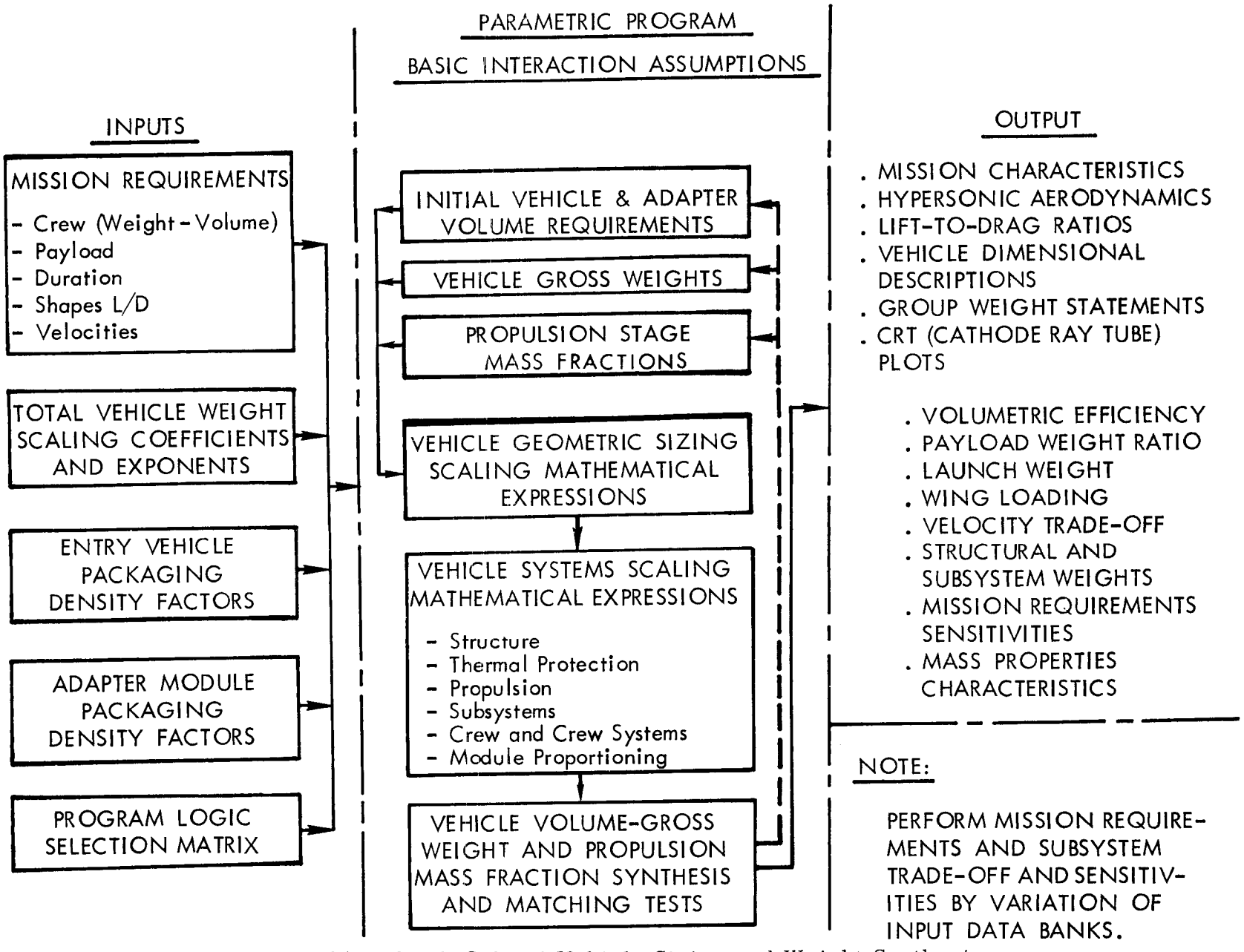

Figure 94. - Earth Orbital Vehicle Sizing and Weight Synthesis

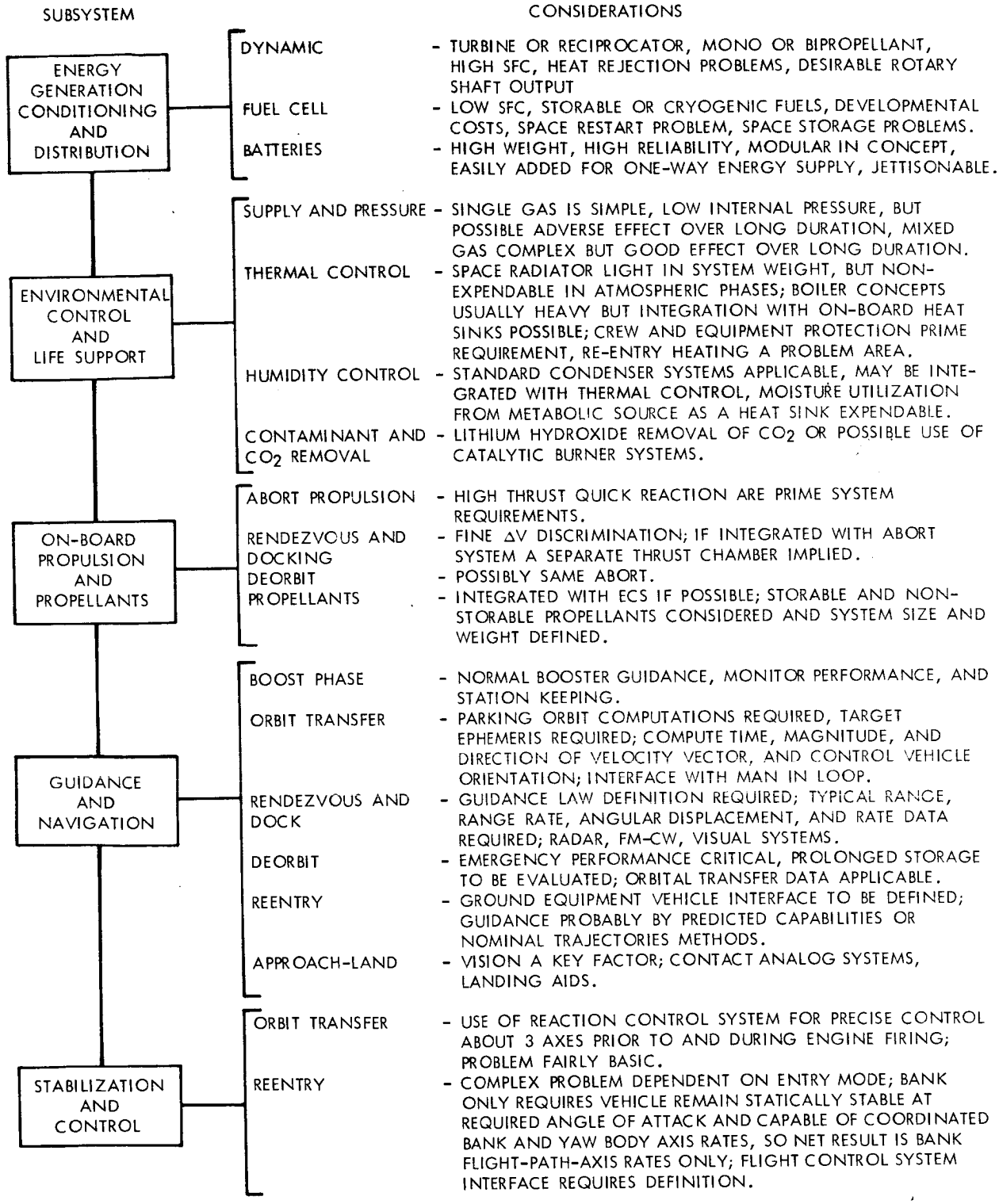

Figure 95. Subsystem Considerations

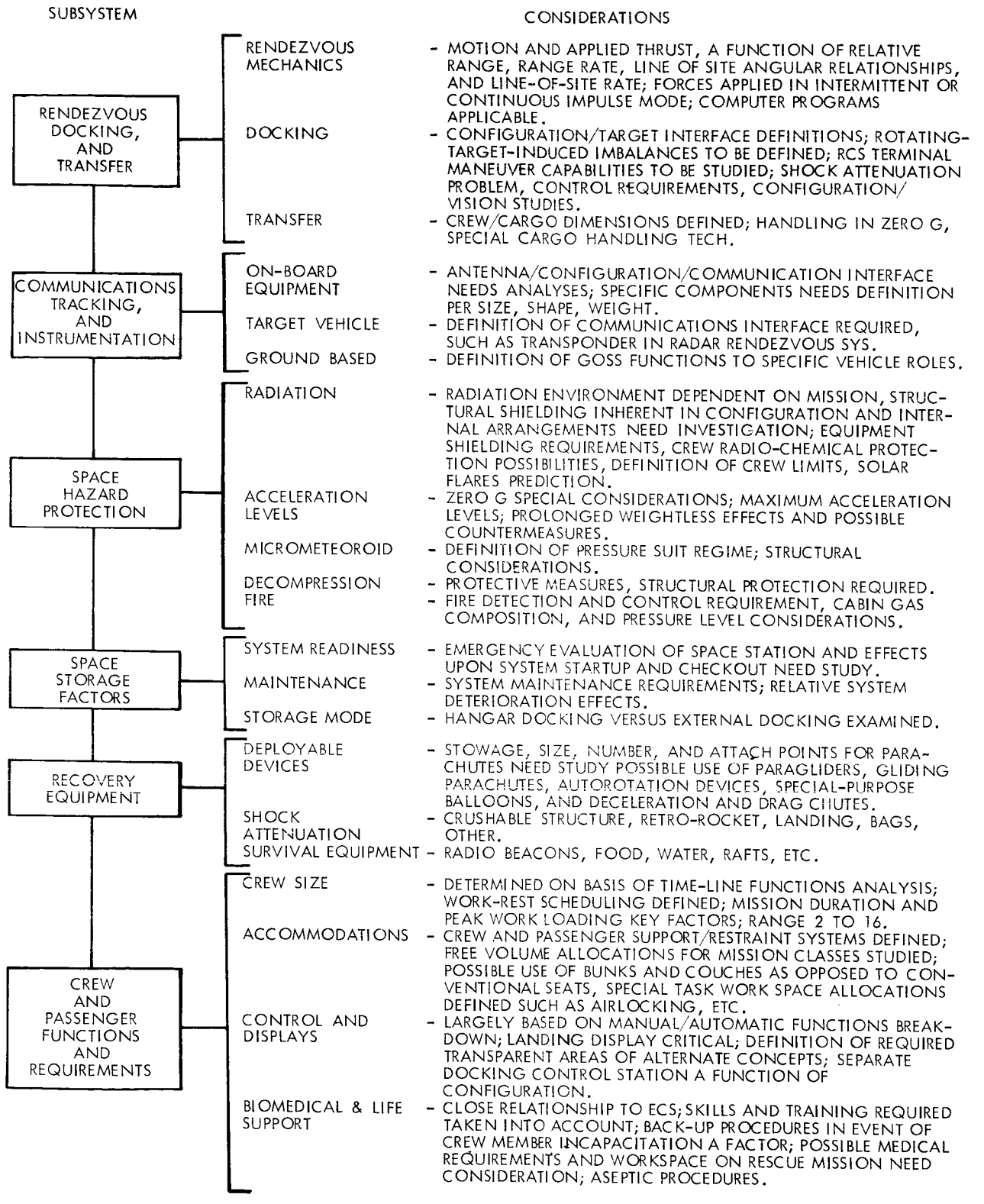

Figure 95. - Subsystem Considerations - Concluded

CONCLUSIONS

The study objectives were to develop and apply analytical techniques for determining areas wherein research and development in the structural sciences will yield significant improvements in future space vehicle systems. Both the method employed and the results obtained are products of constraints and design criteria imposed upon the baseline vehicle systems. These constraints have been defined elsewhere in this report. Statements which follow apply only within this context. Material and structural assessment pertained to expendable launch vehicles, whose generic categories were defined during Phase 1. The following general conclusions and directions can be made from the results obtained for the vehicle systems and structural concepts considered during this study.

Construction Concepts

Multiwall and double-wall concepts offer distinct weight advantages for unpressurized shells over integrally stiffened, single-sheet designs. The multiwall construction with corrugated face sheets offers the lightest weight concept in aluminum rather than in titanium. From a weight loading standpoint, the advanced structural concepts using either aluminum or titanium offer effective weight reductions, but they are not competitive weight-wise with single-wall concepts using beryllium. Advanced concepts offer payload increases from the baseline construction of approximately 1 percent for first-stage designs, 2.5 percent for medium- and Saturn-class upper stages, and 10 percent for post-Saturn-class upper stages. The payload increase in the latter vehicle is due to large diameter, moderate compressive load intensity tank walls using double-wall skin stringer design. Medium- and Saturn-class payload improvements with advanced structural concepts are comparable to unrestricted sandwich honeycomb designs using deep core construction. For pressurized shells (propellant tanks) the multiwall concept for the lightly loaded, small-diameter upper stages is inferior to conventional waffle or skin stringer. Multiwall and double-wall concepts for large vehicle systems offer good weight and relative cost advantages and should be considered when beryllium structures are excluded due to high cost, availability criteria, etc.

Application of double-wall and multiwall concepts to tank walls offers weight advantages, but presents design problems in trapped propellant, tank volume degradation, leakage and insulation. The major surface areas of the boost vehicle systems are the tank walls, and as such they represent potential research areas for weight saving.

Honeycomb sandwich is an overall light-weight design with a moderate structural cost (costs greater than skin stringer but appreciably less than structures fabricated with beryllium). The aluminum honeycomb sandwich is one of the lightest design concepts with the exception of beryllium constructions. It is competitive cost-wise with skin-stringer concepts for use in upper-stage components and is appreciably lighter. It offers a potential payload improvement from four percent for the medium class vehicle to nine percent with the post-Saturn class when compared to the integrally stiffened baseline vehicles. Large radii and load intensities result in potential weight and cost advantages only with deep core sandwich. Analysis and "knock-down" factors on both general instability and core shear properties tend to dictate deep core as a requirement for optimum weight designs. With no factors required, optimum designs have one- to two-inch core heights. If experimental verification justifies these factors and deep core is required, then design could present fabrication difficulties. Large height restrictions could impose severe weight penalties and result in honeycomb sandwich being inferior to other types of double-wall and multiwall designs. Therefore, honeycomb sandwich should be considered as a light-weight design concept for all vehicle systems, but with large size components. The "knock down" factors and manufacturing feasibility require verification.

The most attractive weight-to-cost design is an aluminum skin-stiffened concept using Z-section or top-hat stringers. Although other designs exist which are lighter, their structural costs are appreciably higher. A relative payload "worth index" must be assigned to the vehicle system before the best choice is defined. If a structural worth index of 300 dollars per pound of payload is assigned, then it is best to use the skin-stiffened concept for the first stages, while for the upper stage the honeycomb sandwich should be used, i.e., more potential weight reduction and within the assigned worth index.

Although designs fabricated from beryllium offer the greatest weight advantages, their present structural costs do not justify their general application to large structural components for the boost stages considered. The major disadvantage investigated for the beryllium designs was an extremely high structural cost index, this being due to both the high cost of material and its fabrication difficulties. If demand and application increases, these two costs will decrease and with complexity factors reduced by 50 percent from those assigned for this study, the beryllium designs are effective, structural

cost-wise, with light weight aluminum concepts. It is recognized that other design problems will still exist due to the present brittleness of materials, etc.

Simplified construction (ring-stiffened) when used for the first stage results in moderate payload decreases. If a simplified design for cost or schedule reasons is considered, then the payload degradation is less noticeable when the design is applied to the first stage. With the ring-stiffened concepts using close-pitch rings, the payloads were only decreased by 2 percent with first-stage application and from 5 to 15 percent when used in the upper stage. The justification of using this design concept for any structural component has been made upon the basis of required payload capability and the "worth index" associated with the payload.

Material Strength Improvement

Application of improved-strength material should be to multiwall and sandwich construction concepts. Improvement in the material's compressive yield and ultimate tensile stress is beneficial and should be applied to constructions having very thin facing sheets which are highly loaded. An ordering of constructions which most benefit by material improvements is as follows:

Aluminum: Honeycomb sandwich, multiwall corrugated, and double-wall skin stiffened.

Titanium: Honeycomb sandwich and multiwall corrugated.

Beryllium: Honeycomb sandwich, multiwall corrugated, double-wall skin stiffened, corrugated sandwich, skin-stringer, and waffle.

Percentage increases in the material properties do not correspond to identical percentage weight reductions. At best, the effect of a 10-percent compressive-yield increase results in an 8-percent weight reduction if the designs considered are both optimum concepts (minimum weight). Large-radius tank walls whose shell's skin thickness is dictated solely by the burst pressure requirements will benefit slightly. A 10-percent material property improvement could reduce the shell's unit weight by approximately two-percent for the lightly loaded 270-inch-radius shell.

Experimental verification. - General instability "knock down" factors influence the choice of optimum weight construction concept and its relative

configuration details. The small-deflection theoretical critical buckling load for all constructions is multiplied by a stability correction factor to obtain an effective design load. Theoretical upper-bound stability stresses have been attained with carefully controlled test specimens and testing conditions. As a result of this, the correction factor is believed to include the effects of initial imperfections, differences in boundary conditions, etc. However, these influences with deep sections (double-wall, multiwall, and deep-core honeycomb) may be appreciably less, and the concepts are being unfairly penalized. Relaxing of these factors would decrease the unit weight slightly for optimum designs and greatly influence the detail element design. The core and substructure depths for honeycomb and multiwall concepts respectively are controlled by these factors. Justification of applying these "knock down" factors to advanced construction concepts and to large diameter shells is required.

Experimental verification is required of core shear stiffness for double-wall and multiwall concepts which are competitive as light-weight attractive structural cost designs. The general instability analysis for the double-wall and corrugated concepts is based, to a large extent, on theoretical shear stiffnesses of the substructure and core. This shear stiffness is believed to represent an upper bound. Hence, additional investigations, primarily of an experimental nature, are required to define the percentage of the theoretical shear stiffness that can be obtained with the sine-wave substructure and to determine the most efficient substructure arrangement and the weight penalties incurred, if any.

The evaluation of candidate structural concepts is highly dependent on the analytical techniques utilized. For the advanced structural concepts, the unknowns associated with inaccurate assessment of the shear stiffnesses may result in the interchange of the ordering of two structural concepts on the structural evaluation curve. With the present synthesis evaluation, the multi-wall and double-wall concepts are lighter than single-wall construction and slightly heavier than sandwich honeycomb for the same material.

Longitudinal stiffeners should be positioned externally for most beryllium designs; aluminum and titanium designs require individual assessment for small changes if any; eccentricity effects diminish with increased shell diameter. The effects of the positioning of the longitudinal stiffeners, either internally or externally, indicated weight benefits either way depending upon the loading, size, and material. All circumferential rings were considered internal. Greatest benefits from external stiffeners were achieved with beryllium shells of small diameter which were moderately loaded. Titanium structures appeared not to notice the effects of stiffener eccentricity. Aluminum structures with the synthesized light-weight design configurations considered could benefit from either position, depending upon the individual designs.

Manufacturing Development

The above discussions consistently allude to the fact that research would be highly beneficial when devoted to increasing "know-how" in manufacturing of new and advanced structural concepts and in the development of the manufacturing technology to fabricate structures from highly advanced materials or from new materials with radically different properties. Such efforts would undoubtedly lead to reduced structures and materials costs and make the advanced structural concepts much more competitive cost-wise than presently. From the study results, it appears that research in improvement of the strength properties of current material does not offer significant advantages. Improvement of the material properties which influence the fabrication process, while not analyzed in detail in this study, will effectively reduce construction costs and save weight of the secondary structure, such as weld lands, attachment points, etc.

Recoverable Vehicles

Recoverable vehicle systems with their small payload-to-launch-weight ratios will greatly benefit from structural weight reduction of the upper stages. With a fully recoverable vehicle system, the payload-to-launch-weight ratio is one to two percent; therefore, structural weight reduction is important. Any structural weight saving in recoverable vehicles is compounded by additional savings in the flyback recovery features. Lighter shell structures for the boost vehicle result in smaller burnout weight requiring recovery and, therefore, smaller wings, less flyback fuel, etc.

APPENDIX A. STRUCTURAL DESIGN SYNTHESIS

Introduction

The structural design synthesis for Phase II is an extension of the synthesis programs initiated in Phase 1. The general procedures used to evaluate the structural integrity are based upon the design strength and stability requirements when the structural concept is subjected to a series of prescribed design loading and thermal environments.

The principal structural components discussed in this appendix are cylindrical and conical shells and membrane bulkheads. The shell configurations analyzed are:

Longitudinally Corrugated Core Sandwich Shells - This type of construction consists of two face skins separated by a corrugated core, the corrugation being oriented parallel to the axis of the cylinder.

Multiwalled Corrugated Sandwich Cylinder - Each face panel of this configuration consists of two thin sheets stabilized by a corrugated core to form a facing panel sandwich, the corrugation being oriented parallel to the axis of the cylinders. The face panels are separated by a sine-wave substructure.

Double-Wall Skin Stringer - This composite shell structure, similar to the multiwalled corrugated sandwich shell, consists of two face panels separated by a sine wave substructure. Each face panel is a single face skin stiffened with integral, Z, hat, or I section stringers attached to its outer face.

Ring-Stiffened Cylindrical Shell - This configuration consists of a single skin shell with circumferential stabilizing ring frames attached.

Eccentrically Stiffened Shells - This configuration consists of a shell with longitudinal stiffeners placed either inside or outside the shell skin.

Membrane Bulkheads - Various types of bulkhead shapes, including elliptical, oblate spheroidal, and a modified semitoroidal, are synthesized for their design weight and cost assessment. The cross-section of the modified semitoroidal bulkhead may be elliptical or hemispherical.

Structural Analysis Criteria

The structural analysis criteria used during this phase of the study were identical to those employed during Phase I. As such, the principal failure modes considered in the structural analysis and design synthesis of the structural components are material failure, general instability, and local instability of the structural elements.

Material failure. - The classes of loads used for design are defined as

AL - limit axial load
BM - limit bending moment
P - propellant tank pressures

and the safety factors are

FSY = yield factor of safety
FSU = ultimate factor of safety

The following strength criteria were used to analyze the shell structures for material failure:

A tensile stress resulting from ultimate pressure loads and/or inertia loads will not exceed the tensile ultimate stress, F_{t_u}, of the material. If the inertia loads are added to the tensile stresses, ultimate inertia loads are used. Limit inertia loads are used if the inertia loads are subtracted from the tensile stresses.

$$F_{t_u} \geq \frac{1}{\bar{t}} \left[\left(\frac{BM}{\pi R^2} + \frac{PR}{2} \right) FSU - \frac{AL}{2\pi R} \right]$$

$\bar{t}$ is the equivalent shell longitudinal extensional thickness.

A tensile stress caused by yield pressure and/or limit inertia loads will not exceed the tensile yield stress F_{t_y} of the material. If the

inertia loads are added to the tensile stresses, yield inertia loads are used. Limit inertia loads are used when the inertia loads are subtracted from the tensile stress.

$$F_{t_y} \geq \frac{1}{t}\left[\left(\frac{BM}{\pi R^2} + \frac{PR}{2}\right) FSY - \frac{AL}{2\pi R}\right]$$

A compressive stress resulting from ultimate inertia loads and pressure will not exceed the allowable compressive strength, F_{c_u}, of the material. If the pressure is added to the compressive stresses, ultimate pressure is used. Minimum pressure is used when the pressure is subtracted from the compressive stresses.

$$F_{c_u} \geq \frac{1}{t}\left[\left(\frac{BM}{\pi R^2} + \frac{AL}{2\pi R}\right) FSU - \frac{P_{MIN}R}{2}\right]$$

or for collapsing pressures

$$F_{c_u} \geq \frac{1}{t}\left[\left(\frac{BM}{\pi R^2} + \frac{AL}{2\pi R} + \frac{PR}{2}\right) FSU\right]$$

A compressive stress resulting from yield inertia loads and pressure will not exceed the yield compressive strength F_{c_y} of the material. If the pressure is added to the compressive stresses, yield pressure is used. Minimum pressure is used when the pressure is subtracted from the compressive stresses.

$$F_{c_y} \geq \frac{1}{t}\left[\left(\frac{BM}{\pi R^2} + \frac{AL}{2\pi R}\right) FSY - \frac{P_{MIN}R}{2}\right]$$

General instability. - A primary mode of structural failure considered is general instability of the shell. A compressive stress resulting from ultimate inertia loads and/or pressure will not exceed the critical general instability stress of the structure. If the pressure is added to the compressive stresses, ultimate pressure is used. Minimum pressure is used when the pressure subtracts from the compressive stresses. If the shell structure is stabilized by internal pressure, the minimum internal pressure is used in the analysis. The general instability considered orthotropic and isotropic shells for column buckling and small-deflection theory modified with appropriate correction factors based on available experimental data.

Local instability. - Another mode of structural failure considered in this program is local instability. A compressive stress resulting from ultimate inertia loads and/or pressure will not exceed the critical local stability stress of the structural component. If the pressure is added to the compressive stresses, ultimate pressure is used. If the pressure is subtracted from the compressive stresses, minimum pressure is used. Local instability was concerned with skin panel buckling and stiffened element panel buckling as plates with simply supported edges or one edge simply supported and the other edge free.

Analysis and synthesis. - General design analysis procedures are used to evaluate the structural integrity of selected structural concepts when they are subjected to prescribed loading conditions and environments. The procedures used in the evaluation are primarily influenced by the requirement to consider a large spectrum of component sizes, applied loads, and temperature regimes. As such, they were selected on the basis of the computational (computer) time required to obtain an answer and the influence of this answer on the resulting weight of the structure. For instance, if the internal dimensions of a structural component are related such that a trial and error procedure is required to determine the optimum combination, and if at the same time the weight penalty associated with a non-optimum allocation of materials is less than an arbitrary percentage of the total component weight then the internal dimensions are selected in an arbitrary manner. Similarly, if the equation which describes the structural behavior of a component when subject to a given load environment contains several unknowns, and some of these unknowns appear in terms which have a small influence on the resulting answer as compared with other terms, then a simplified expression consisting of only the primary terms will generally be used.

Whereas the program does not always guarantee an absolute minimum weight design, it will develop an extremely efficient light-weight practical design which is within a small percentage of the absolute minimum weight. It is felt that the extensive additional searching and computational time required to identify the absolute minimum weight design does not warrant the improvement or reduction in the weight of the design concept. The use of these synthesis procedures, i.e., the sacrifice of accuracy for speed, is justified because the resulting computer programs are intended to assess the potential of selected structural concepts and not to furnish final design values. The primary factors which influence this assessment are the weight of the structural component, its relative ease of manufacture, and its resulting cost. Only the first two parameters are considered in formulating the design analytical procedures for the design synthesis.

Corrugated Core Sandwich Cylinder

This section presents the analytical procedure used to synthesize a minimum weight design of a corrugated core sandwich cylinder. The composite cylindrical structure (fig. A-1) consists of two thin face sheets, separated and stabilized by a thin corrugated core which is oriented parallel to the axis of the cylinder. The principal failure modes considered are material failure, local instability of the skin and core elements, and general instability of the overall cylinder.

Material failure. - The design criteria presented in the preceding section are used to determine the minimum equivalent shell thickness required to prevent material failure. This minimum equivalent thickness, $\bar{t}$, assumes that the longitudinally oriented core is fully effective in resisting the equivalent axial loads. The general form of the thickness equations are:

$$\bar{t} = 2t_{skin} + \frac{t_{web}}{\cos \theta}$$

$$t_{skin} = \max (N_{x_1}/f_1, \text{ min gauges})$$

$$t_{skin} = \max (N_{x_2}/f_2, \text{ min gauges})$$

where

N_{x_1}, N_{x_2} = load intensity functions of the design loads or pressures

f_1, f_2 = material or stability allowable stresses

$\bar{t}$ = the equivalent skin thickness

t_{skin} = the face skin thickness

t_{web} = the core material thickness

θ = the angle between the core and the face sheet

Local instability. - The local instability analysis assumes that the principal dimensions of the structural elements of a cross-section of the shell

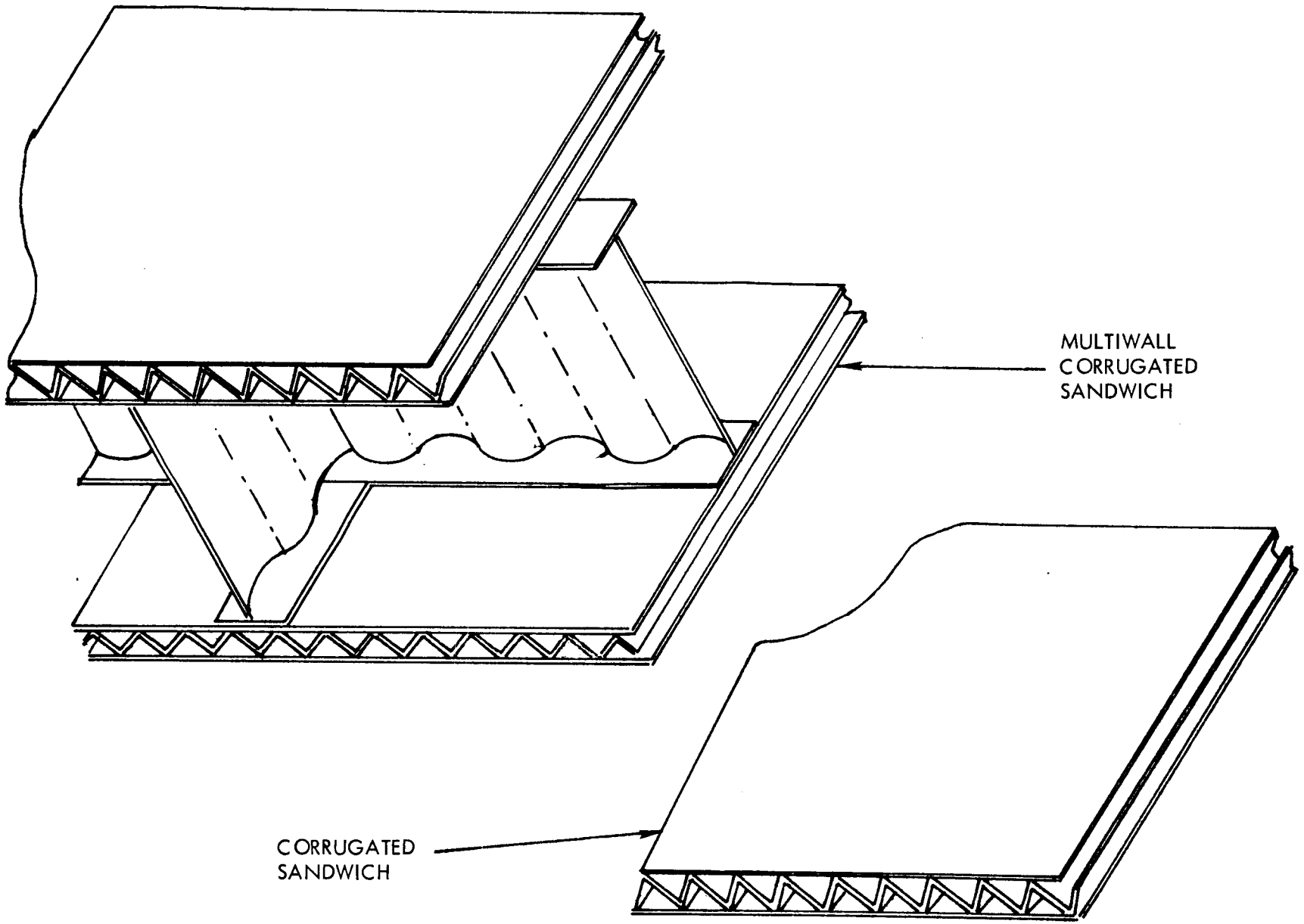

Figure A-1. - Corrugated Design Concepts

wall are sufficiently small when compared with the radius of the cylinder that the influence of shell curvature is negligible. Then the structural response of the idealized shell is treated as a series of flat plates and evaluated with the method presented by Anderson (ref. A-1) for truss core sandwich panels.

For the purpose of the local instability analysis, the core is assumed to consist of straight line elements. Buckling is assumed to occur with rotation of the joints but with no deflection of the joints, and the angles between the various elements are maintained during buckling. The idealized sandwich plate is assumed to be of sufficient length and width that the end effects are negligible. Anderson's analysis includes the influences of the interaction of the relative orientation and material gauges of the face sheets and web. He considers four primary local instability buckling modes for the idealized single truss core sandwich panel (ref. A-1). The minimum value of the buckling coefficient, k_x, that satisfies the appropriate stability equation for the four failure modes has been calculated, and the results are given in figure A-2 for the single-truss-core sandwich for a range of typical design parameters. The buckling coefficients are presented as carpet plots which permit linear horizontal interpolation for both of the independent variables θ and t_c/t_s.

The critical local instability stress for the idealized structure is given by

$$\frac{\sigma_{cr}}{\eta} = \frac{k_x \pi^2 E}{12\,(1 - \nu^2)} \left(\frac{t_s}{b_f}\right)^2$$

where

k_x = local buckling coefficient

η = plasticity factor

ν = Poisson's ratio

E = modulus of elasticity

t_s = skin thickness

b_f = distance between face sheet supports

Figure A-2 shows that the local instability characteristics of the shell can be divided into two regions. They are (1) face sheet is the unstable element and is restrained by the core, and (2) core is unstable and is

$$\sigma_{CR} = \frac{k_x \pi^2 \eta E}{12(1-\mu^2)} \left(\frac{t_s}{b_f}\right)^2$$

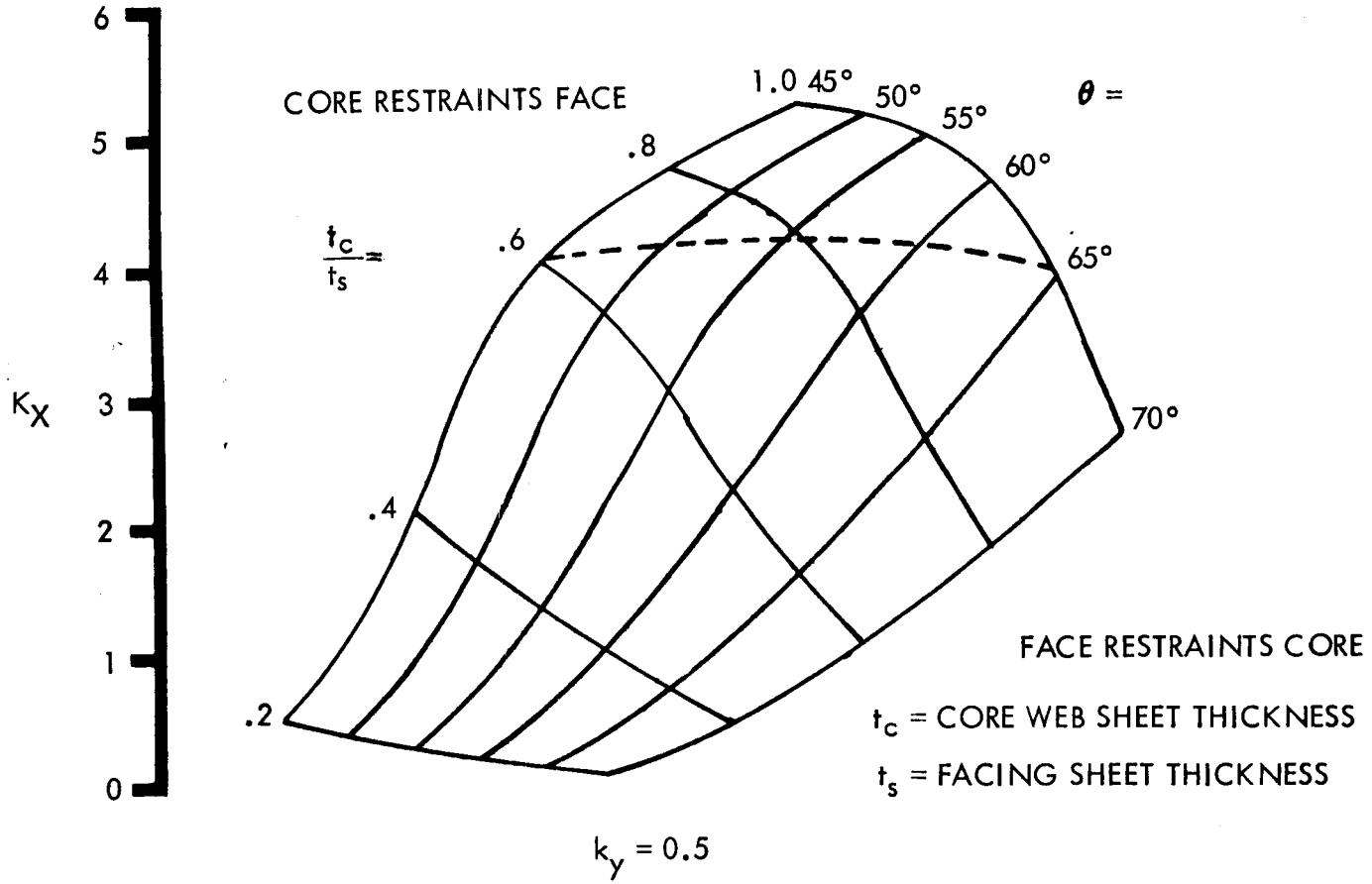

Figure A-2. - Local Buckling Coefficient for Single-Truss-Core Sandwich Plate

restrained by the face sheet. When designing corrugated sandwich cylinder, it is preferable to have the face sheet restrain the core in order to prevent the coupling of the local and general instability failure modes and the premature failure of the cylinder.

General instability. - The general instability analysis is the method presented by Baker and Harris in reference A-2 . Their analysis is based on the small-deflection theory for curved sandwich plates of Stein and Mayer (ref. A-3) and includes the effect of shear distortion of the core.

The idealized corrugated core sandwich cylinder is considered to have relatively thin face sheets which have negligible flexural rigidity about their centroidal axis. The shear distortions of the orthotropic core are restricted to the plane perpendicular to the corrugation. In addition, the core is assumed to have negligible bending rigidity in the transverse direction.

The resulting differential equations for the idealized structure is solved with Galerkin's method to obtain the critical buckling coefficient. The theoretical critical general instability stress resultant for the longitudinally corrugated core sandwich cylinder is given by

$$N_x = \frac{K_c \pi^2 D}{L^2}$$

where

K_c = general instability coefficient

D = flexural stiffness of the cylinder

L = length of the cylinder

The buckling coefficient, K_c, for the truss core sandwich cylinders under axial compression is shown in figure A-3.

Reference A-4 states "while this [small-deflection] theory is known to be inaccurate for monocoque cylinder design, it appears reasonable in this case. Test of monocoque cylinder generally indicates that the thicker the cylinder wall, the closer the correlation between test and small-deflection theory, even though the size of the average imperfection, to which deviation is attributed, remains approximately constant; thus a sandwich cylinder should be predictable by small-deflection theory in view of its equivalent wall thickness compared to a monocoque wall thickness of similar load carrying ability."

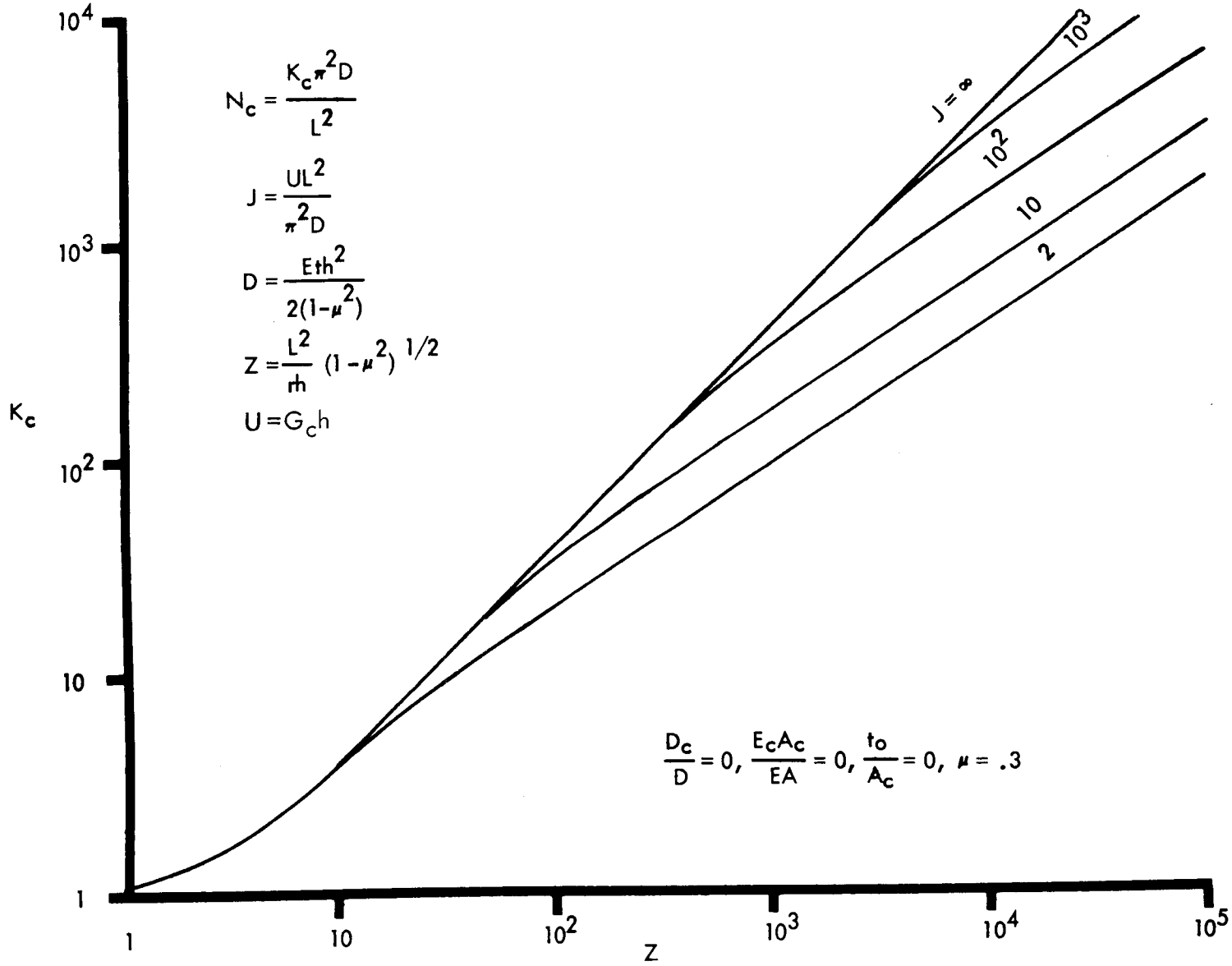

Figure A-3. - Buckling Stress Coefficient for Axial Compression

However, the test results contained in reference A-5 for a ten-foot-diameter Rene 41 cylinder did not substantiate this conjecture. The critical buckling load for the cylinder is approximately equal to the product of the theoretical small-deflection stress and the ratio of the experimental buckling stress for a monocoque cylindrical shell with an equivalent value of the parameter

$$\gamma = \frac{R}{\sqrt[4]{\frac{D_x D_y}{E_x E_y}}}$$

where

$D_{x(y)}$ = the flexural stiffness in the x(y) direction

$E_{x(y)}$ = the extensional stiffness in the x(y) direction

R = the radius of the cylinder

Although only one specimen was tested (ref. A-5),for this study the critical general instability buckling stress is obtained by multiplying the theoretical small-deflection buckling stress by the ratio of the experimental design to the theoretical buckling stress for a monocoque shell, γ, the correlation factor.

Multiwall Corrugated Sandwich Shell

This section contains the principal equations used to synthesize minimum weight multiwall corrugated sandwich shells. This composite cylindrical structure consists of corrugated sandwich face panels separated by a stabilizing sine wave substructure. Each face panel consists of two relatively thin face skins and a corrugated core with the corrugations parallel to the axis of the cylinder (fig. A-1). The principal failure modes analyzed are material failure and local and general instability.

Material failure. - The design criteria presented early in this appendix are used to determine the minimum skin thickness to prevent material failure. This minimum equivalent skin thickness $\bar{t}$ assumes that the face sheets and the longitudinally oriented cores of the sandwich face panels resist all the applied equivalent axial load. The contribution of the sine wave

substructure for carrying the axial load is considered negligible. The resulting equations have the general form as shown in the preceding section for corrugated core sandwich cylinder.

Local instability. - Cylindrical corrugated sandwich face panel is analyzed with the method presented by Anderson (ref. A-1) for truss core sandwich panels and discussed in the preceding section.

The critical local instability stress is given by

$$\frac{\sigma_{cr}}{\eta} = \frac{K_x \pi^2 E}{12\,(1 - \mu^2)} \left(\frac{t_s}{b_f}\right)^2$$

where

t_s = the facing sheet skin thickness

b_f = the distance between the face sheet supports

Figure A-2 shows that the local instability characteristics of the shell can be divided into two regions. They are (1) the core restrains the face sheets, and (2) the face sheets restrain the core.

The geometric proportions of the corrugated sandwich panels are selected such that the face sheets restrain the core in the local instability mode. If the core were restraining the face sheets, the eccentricities of the face could precipitate an interaction between the local and general instability failure modes and result in premature structural failure.

General instability. - The general instability stress analysis is based on small-deflection theory for a sandwich cylinder with an orthotropic core. The analysis assumes that each corrugated sandwich face panel may be replaced by an equivalent homogeneous face sheet. In addition, it is assumed that the principal dimensions of the sine wave substructure are sufficiently small that this substructure may be replaced by an equivalent orthotropic layer. The resultant homogeneous face sheets and orthotropic core comprise the idealized sandwich shell which is analyzed for the general instability failure mode. Stability of the cylindrical shell wall requires sufficient bending and shear stiffness to prevent the formation of the buckles characteristic of this failure mode.

The critical general instability stress for sandwich shells consisting of homogeneous face sheets and orthotropic core is given (ref. A-6) by

$$\sigma_{cr} = KE\frac{h}{R}\frac{2\sqrt{t_1 t_2}}{\sqrt{(1 - \nu^2)}\,(t_1 + t_2)}$$

where

σ_{cr} = critical buckling stress
K = buckling coefficient
E = modulus of elasticity
h = distance between cover panels, centroids
t_1 = equivalent thickness of outer panel
t_2 = equivalent thickness of inner panel
R = mean radius of cylinder
ν = Poisson's ratio

The buckling coefficient, K, is found by minimizing the equation

$$K = \frac{\eta}{(1 + \xi)^2} + \frac{(1 + \xi)^2}{4\eta} \cdot \frac{1 + \frac{1 - \nu}{2}(\xi + \theta)\frac{V_x}{\eta}}{1 + \frac{1 - \nu}{2}(\xi + \theta)\frac{V_x}{\eta} + (1 + \xi\theta)\frac{V_x}{\eta} + \frac{1 - \nu}{2}(1 + \xi)^2\,\theta\,\frac{V_x^2}{\eta^2}}$$

where

$$V_x = \frac{Et_c\sqrt{t_1 t_2}}{2\sqrt{1 - \nu^2}hRG_{xz}}$$

G_{xz} = longitudinal core shear modulus, lb/in.^{2}
G_{yz} = circumferential core shear modulus, lb/in.^{2}
a = length of cylinder, in.

$$\theta = \frac{G_{xz}}{G_{yz}}$$

$$\zeta = \left(\frac{na}{m\pi R}\right)^2$$

$$\eta = \frac{a^2\sqrt{1-\nu^2}\,(t_1 + t_2)}{2m^2\pi^2 Rh\sqrt{t_1 t_2}}$$

m = number of half-waves in axial direction

n = number of waves in circumferential direction

The results of these minimization processes, showing K plotted versus V_x for various values of θ, are presented in figure A-4.

The preceding procedure defines the theoretical general instability stress for the cylindrical sandwich shell. As explained in the preceding section for corrugated core sandwich cylinder, such a structure should be sufficiently stiff that the preceding equations will accurately describe the response of the structure. However, test data are not available to substantiate the conjecture, and the analytical procedures used previously (Phase I) always contained a general instability correction factor. In order to be consistent, a corrective factor, based on test data for homogeneous isotropic monocoque cylindrical shells, is also used for this construction. The general instability correction factor C_1, given by figure A-5 as a function of the parameter

$$\gamma = \frac{R}{\sqrt[4]{\frac{D_x}{E_x}\frac{D_y}{E_y}}}$$

where for sandwich shells

$$\gamma = \frac{R\,(t_1 + t_2)}{\sqrt{t_1 t_2 h^2}}$$

Hence, for this study, the critical general instability stress is given by

$$\sigma_{cr} = C_1 K E \frac{h}{R} \frac{2\sqrt{t_1 t_2}}{\sqrt{(1 - \nu^2)}\,(t_1 + t_2)}$$

The sine wave substructure is treated as core material that requires a certain shear rigidity to stabilize the facing panels. Sufficient material is allocated to develop the shear stiffness in the form of an "egg crate" grid. Since the grid can be of reasonal dimensions the substructure wide thicknesses are not subject to local instability.

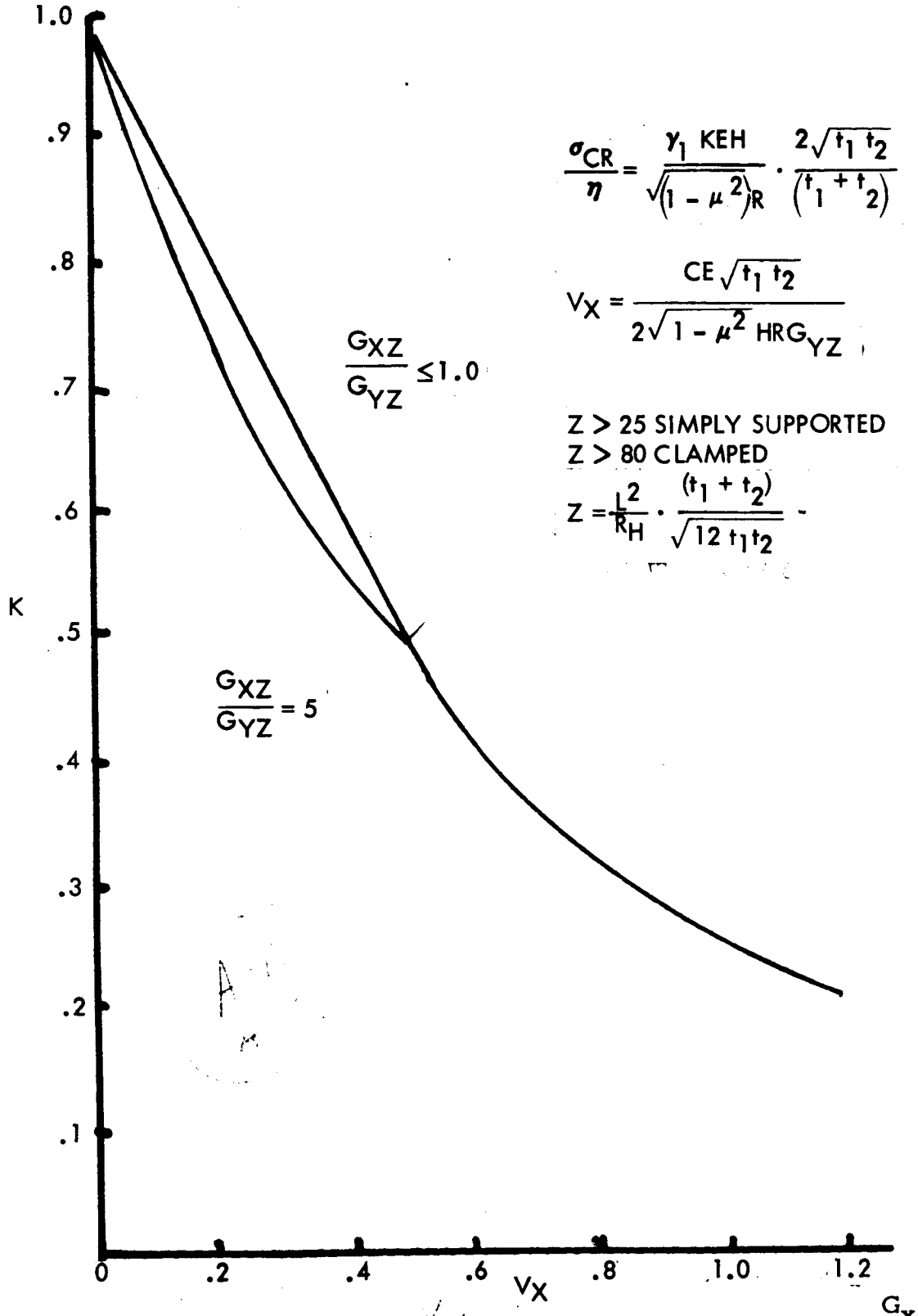

Figure A-4. - Buckling Coefficient V_x for Various Values of $\frac{G_{xz}}{G_{yz}}$

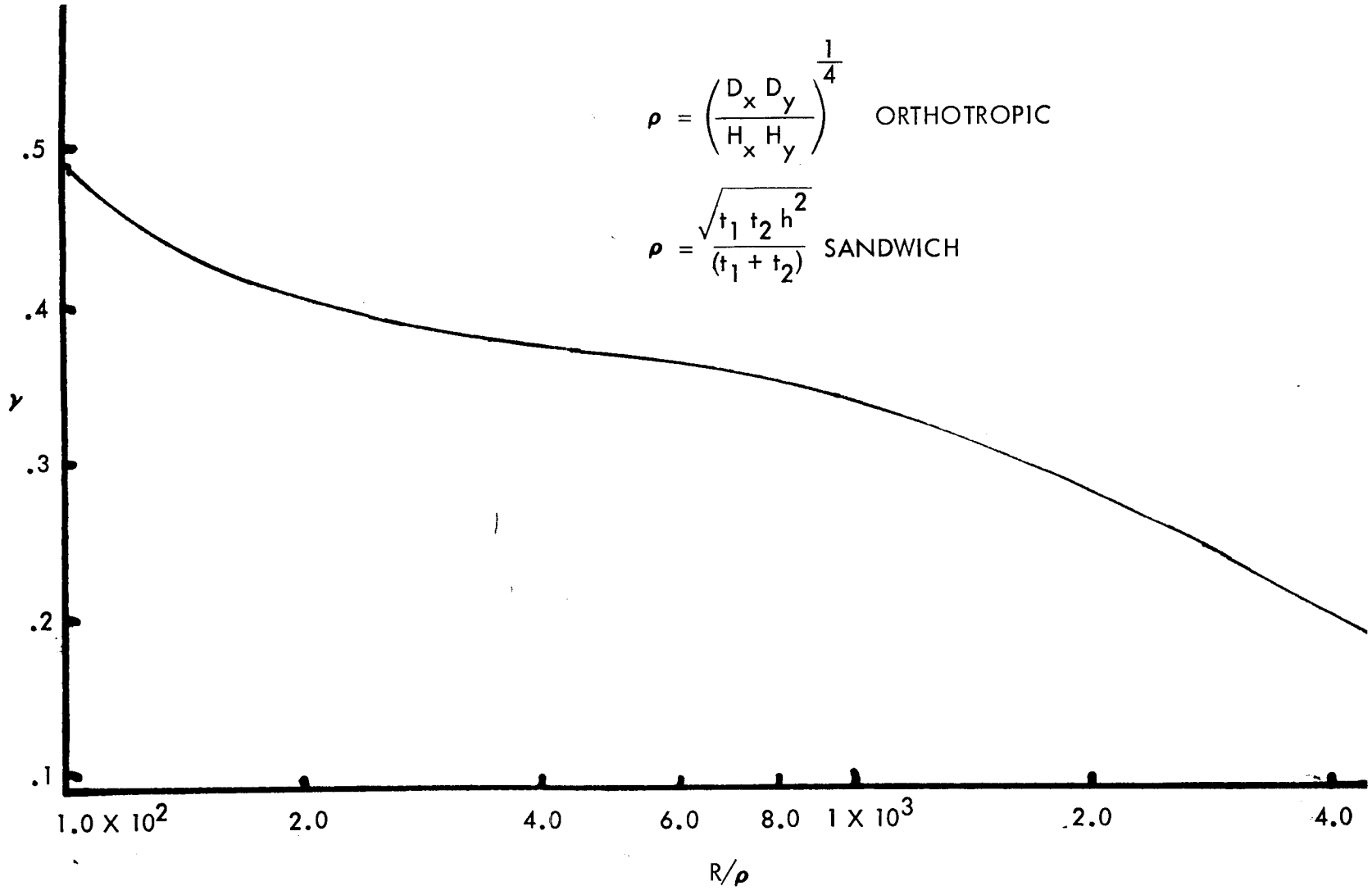

Figure A-5. - Stability Correction Coefficient

Double-Wall Skin Stringer

This double-wall structure (fig. 2, p. 18), consists of two face sheet panels and a deep sine wave substructure. The face panels are relatively thin isotropic sheets with longitudinal stringer elements attached to the outer faces. The stringers may be a hat section, integral, Z, or I cross-section. The principal failure modes considered are material failure of the face panel skin and stringer elements, local instability of the face panel skin and stringers, and general instability of the overall composite structure.

Material failure. - The criteria presented in the Structural Analysis Criteria section of this Appendix are used to determine the minimum equivalent skin thickness to prevent material failure in the double-wall stringer cylindrical shell. The face panel skins and longitudinal stringer elements are assumed to be fully effective in resisting the applied equivalent axial load. Pressure loads are resisted entirely by the face sheets. The contribution of the sine-wave substructure to carry the axial load is assumed to be negligible. The general forms of the relevant equations for material failures are

$$\bar{t} = 2\left(t_{skin} + \frac{A_{str}}{b}\right)$$

$$t_{skin} = \max\,(N_x/f_1,\ \text{min gauges})$$

where

t_{skin} = face panel skin thickness

A_{str} = area of face panel stringer element

b = spacing of face panel stringer element

Local instability. - The local instability failure modes for this design concept are panel instability of the face sheets and local crippling of the stringer element. If a stiffened-skin structure has a sufficiently stiff substructure, the first failure mode generally encountered is panel instability. In this failure mode, the substructure and stringers effectively divide the shell skin into small panels, whose principal dimensions are the spacings of the circumferential substructure and longitudinal stringers.

The critical buckling stress for the plate element is

$$\frac{\sigma_{cr}}{\eta} = KE\left(\frac{t}{b}\right)^2$$

where

K = a buckling coefficient which includes the influence of end fixity

b = the stringer spacing

η = plasticity correction factor

The stiffener elements of the facing panels are considered for their buckling stress which is a combination of the column buckling and the crippling stress of the stringer element. The ultimate element crippling stress, F_{cc_i}, is defined as follows:

$$F_{cc_i} = c_{e_i} \sqrt{F_{cy_i} E_{c_i}} \left(\frac{t}{b}\right)_i \quad 0.75$$

where

c_e = material and shape constant derived from crippling tests

F_{cy} = compressive yield stress of the element

E_{c_i} = compressive modulus of the element

Note: Subscript i denotes the i^{th} element of the stiffener

Any given stiffener section can be broken up into straight elements with either one edge free or no free edges. Therefore, to evaluate the ultimate crippling stress of a stringer section, a weighted average of the individual elements crippling stresses is used.

$$F_{cc} = \frac{\sum_{i=1}^{N} A_i F_{cc_i}}{\sum_{i=1}^{N} A_i}$$

where

A_i = area of the i^{th} element

N = total number of elements of one stiffener

The critical Euler buckling stress F_{c_e}, for stringer column instability is given by

$$F_{c_e} = \frac{\pi^2 E}{(L^1/\rho)^2}$$

where

L^1 = the effective length of the stringer

ρ = the radius of gyration of the stringer

E = the modulus of elasticity of the stringer material

When the critical stress F_{c_e} obtained from the preceding equation is greater than approximately 50 percent of the crippling stress, F_{c_e}, the stringer column instability stress F_c is determined by the Johnson-Euler equation

$$F_c = F_{cc} - \frac{F_{cc}^2}{4 F_{c_e}}$$

General instability. - The general instability stress analysis is based on representing the actual double-wall skin stringer cylindrical shell with an equivalent three-layer sandwich cylinder consisting of homogeneous face sheets, which represent the skin stringer face panels, and an orthotropic core, which represents the sine wave substructure. The resulting structure is analyzed with small deflection theory to determine the critical general instability modes.

The critical general instability stress as explained in the preceding section for multiwall corrugated sandwich shell is given by

$$\sigma_{cr} = C_1 K E \frac{H}{R} \frac{2\sqrt{t_1 t_2}}{\sqrt{1 - \nu^2}\,(t_1 + t_2)}$$

where

σ_{cr} = the critical buckling stress

K = buckling coefficient (fig. A-5)

E = modulus of elasticity of shell material

H = distance between cover panel centroids

t_1 = equivalent thickness of outer cover panel

t_2 = equivalent thickness of inner cover panel

R = mean radius of cylinder

ν = Poisson's ratio

C_1 = general instability correction factor-f (R/ρ) (fig. A-6)

The buckling coefficient, K, is a function of the design properties, V_x, where

$$V_x = \frac{EC\sqrt{t_1 t_2}}{2\sqrt{1 - \nu^2}\, HRG_{xy}}$$

The general instability correction factor, C_1, is dependent on equivalent radius of gyration of the section, ρ.

$$\rho = \sqrt[4]{\frac{D_x}{E_x}\frac{D_y}{E_y}}$$

and for the double wall skin stringer concept

$$\rho = \frac{\sqrt{\bar{t}_1 \bar{t}_2 h^2}}{(\bar{t}_1 + \bar{t}_2)}$$

Ring-Stiffened Cylindrical Shells

The ring-stiffened cylindrical shell is a homogeneous isotropic cylindrical shell with circumferential rings spaced periodically along its axis. The principal equations used to establish the structural integrity of the synthesized shells are presented in this section, and they consider failure due to stresses which exceed the material allowable and overall instability of the cylinders, face skin, and rings.

Material failure. - The face sheet thickness required to prevent material failure is based on the design criteria presented early in this appendix. The general form of the equations are

$$t_{skin} = \max\,(N_x/f_1,\ \text{min gauges})$$

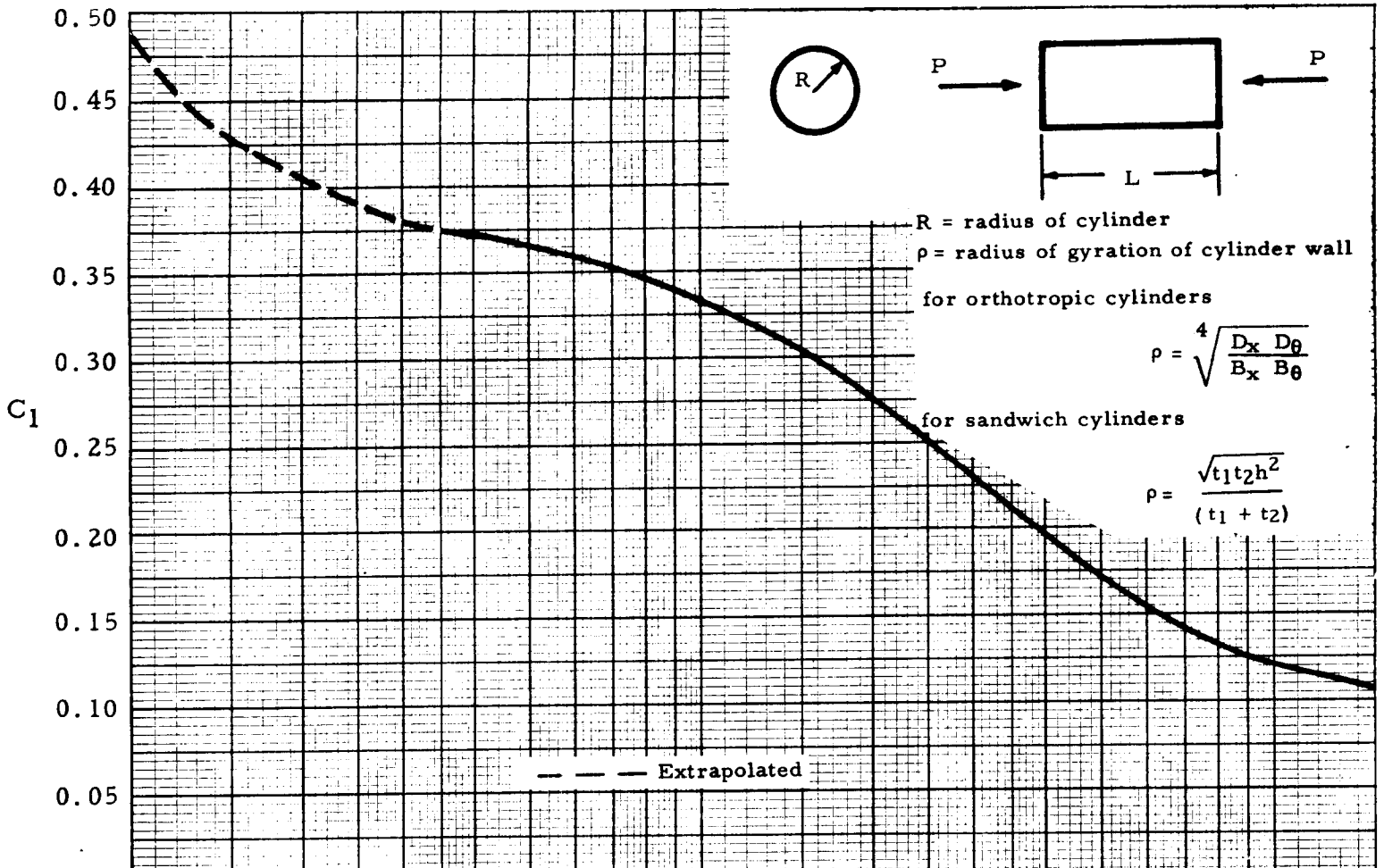

Figure A-6. Design Correction Coefficient for Cylinders Subjected to Axial Compression

General instability. -

$$\frac{\sigma_{cr}}{\eta} = KE\, t/R$$

where

σ_{cr} = critical buckling stress

E = modulus of elasticity of the shell material

t = material gauge of the cylinder

R = radius of the cylinder

η = a plasticity correction factor

K = stability coefficient

With the ring-stiffened concept, the rings are positioned close together to break up the length of the monocoque shell. This reduces the effective length of the shell and helps to reduce the required skin thickness. Therefore, the stability coefficient, K, is a function of the length-to-radius ratio, L/R, and the radius-to-skin-thickness ratio, R/t, of the cylinder. Reference A-6 derives this variation for the stability coefficient which is reproduced in figure A-7.

The stabilizing ring frames are sized as a function of the stresses in the face sheet, the radius and length of the cylinder, and the ring frame spacing. Shanley (ref. A-7) determines the required ring frame stiffness to prevent general instability as

$$(EI)_f = \frac{MD^2}{16000L}$$

where

E_f = modulus of elasticity of the frame material

I_f = moment of inertia of the frame material

D = diameter of the cylinder

L = ring frame spacing

M = equivalent bending moment applied to the cylinder

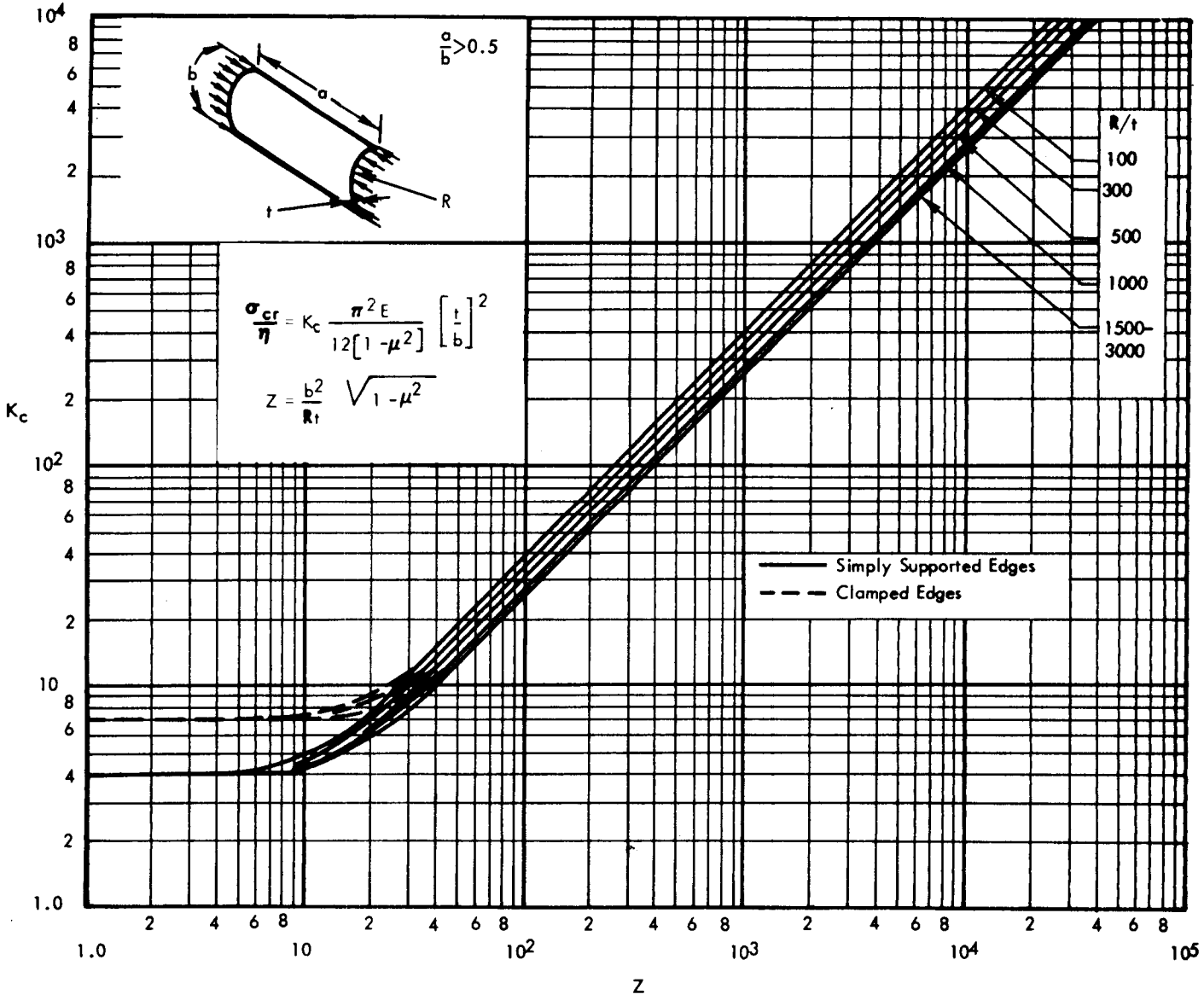

Figure A-7. - Stability Coefficient Versus Z

This equation determines the stiffness required to force nodes to occur at the ring frames. When the skin thickness is determined using this equation with K, a function of the ratio of the ring frame spacing to the radius of the cylinder, a balanced design is achieved.

Hess and Garber (ref. A- 7) presented a method for determining the required skin thickness and ring frame sizes for shells subjected to lateral pressure and axial load. Their method assumes the cylinder to be simply-supported at the ring frames. The skin thickness is determined from design curves for a cylindrical shell with a length that equals the ring frame spacing; then the ring frame moment of inertia required to prevent general instability is determined. This ring frame moment of inertia is based on the ring frame participating in the general instability deformation pattern, and usually results in smaller ring frame requirements than those predicted by Shanley's equation.

The synthesis approach adopted was to determine the critical buckling stress of the cylindrical shell as a monocoque short cylinder, using figure A- 7, and to evaluate the required ring properties utilizing Hess and Garber's method (ref. A- 7). The frame spacing and strain parameters are given by

$$K_1 = R/L$$

$$\phi = \frac{\sigma}{E}(1 - \nu^2)$$

where

L = effective length of the frame spacing

σ = actual stress in the shell in axial direction

Reference A- 8 has developed the interaction curves to be used in the determination of the required effective moment of inertia of the ring frames and are reproduced in figure A- 8 . The required moment of inertia of the ring and shell combination, I_e, is obtained from

$$\alpha_1 = \frac{I_e (1 - \nu^2)}{LtR^2}$$

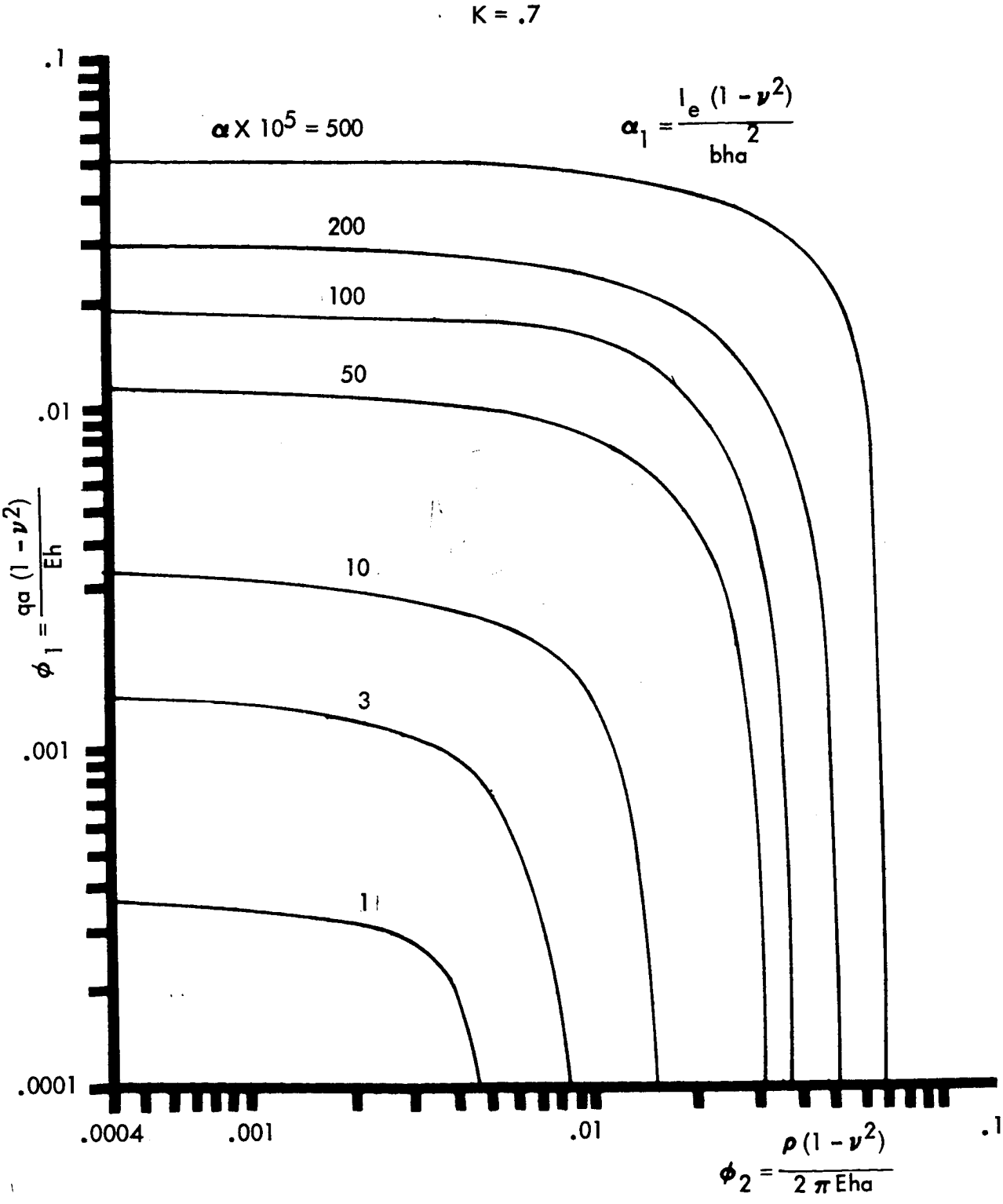

Figure A-8. - Interaction Curves for Effective Moment of Inertia

Eccentrically Stiffened Orthotropic Cylinders

The theory developed for the stiffened cylinder shown in figure A-9 is given in reference A-9 and has been used for this study to determine the relative load carrying efficiency of typical large shell structures. The small-deflection theory for buckling of an orthotropic cylinder stiffened by both stringers and rings includes stiffener eccentricity effects and represents a generalization of the work by Baruch and Singer (ref. A-10) for ring-and-stringer-stiffened isotropic shells. The theory is a classical buckling theory in that the effect of prebuckling deformations is neglected and only small deflections are considered. The buckling equations and boundary conditions are derived in a consistent manner from the potential energy of the loaded stiffened shell. Solutions to the equations corresponding to boundary conditions analogous to classical simple support in isotropic shell theory are obtained for cylinders subjected to any combination of axial and circumferential loading. Several basic assumptions are made in the theory, these being: (1) the stiffened cylinder is considered to be composed of an orthotropic shell uniformly stiffened by equally spaced rings and stiffeners, all having elastic material properties, (2) transverse shearing stiffnesses of the shell are assumed to be infinitely large, (3) rings and stiffeners elastic properties are averaged over the stiffener spacing, and (4) effects of joints in the stiffener framework are ignored.

The usual Donnell-type assumptions are used to specify buckling displacements in the shell, whereas the stiffeners are treated as beam elements with stiffened twisting accounted for in an appropriate manner.

A stability equation valid for compressive buckling of an unstiffened orthotropic cylinder can be obtained from reference A-9.

$$\overline{N}_x = \left(\frac{m\pi}{a}\right)^2 \left[\frac{D_x}{1 - \mu_x\mu_y} + \left(\frac{2\mu_y D_x}{1 - \mu_x\mu_y} + 2D_{xy}\right)\left(\frac{na}{m\pi R}\right)^2 + \frac{D_y}{1 - \mu_x\mu_y}\left(\frac{na}{m\pi R}\right)^4\right] + \frac{E_x E_y}{\left(\frac{m\pi}{a}\right)^2 R^2 \left[E_x - \left(2\mu_y' E_x - \frac{E_x E_y}{G_{xy}}\right)\left(\frac{na}{m\pi R}\right)^2 + E_y\left(\frac{na}{m\pi R}\right)^4\right]} \tag{A-1}$$

This equation is identical to that obtained by Stein and Mayers (ref. A-11) when the transverse shearing stiffnesses of the referenced equation are taken to be infinitely large. Equation (A-1), or forms comparable to it, have been used in many contemporary compressive buckling analyses of

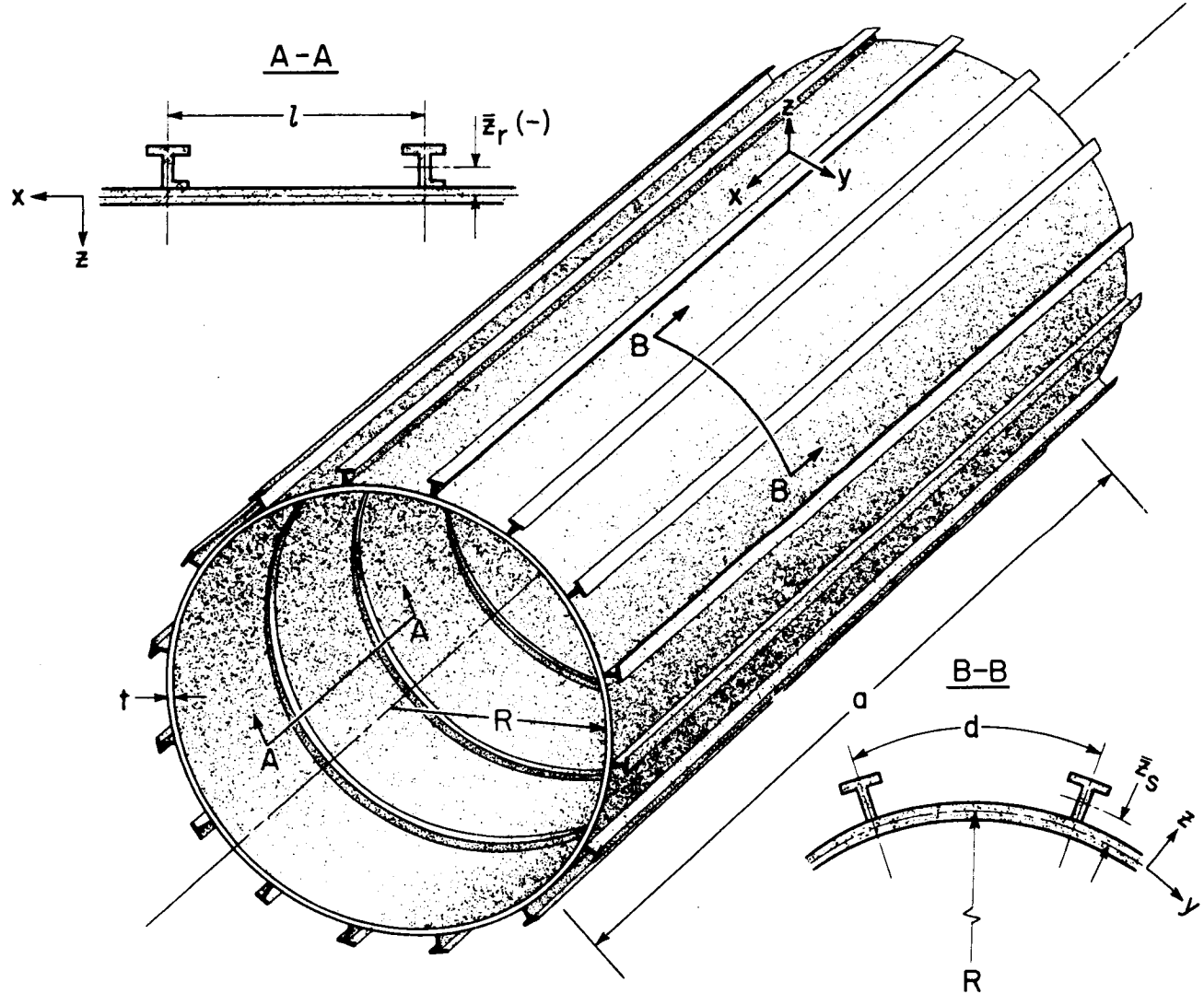

Figure A-9. - Geometry of Stiffened Cylinder

stiffened isotropic cylinders. In such analyses, effective orthotropic constants are defined to approximate the total bending and extensional stiffnesses of the composite wall of shell and stiffeners. Such approximations neglect eccentricity effects and effect predictions even in large-diameter stiffened cylinders.

This orthotropic cylinder theory was used for ring-and-stringer-stiffened cylinders to determine its differences with the isotropic theory. The following values were assigned to the orthotropic constants:

$$\left.\begin{aligned}
&\mu_x = \mu_y = \mu_x' = \mu_y' = 0 \\
&D_x = \frac{E_s I_s}{d}\left[1 + \frac{(\bar{z}_s/\rho_s)^2}{1 + \frac{A_s}{dt}}\right] \\
&D_{xy} = \frac{G}{2}\left(\frac{J_s}{d} + \frac{J_r}{\ell} + \frac{t^3}{3}\right) \\
&D_y = \frac{E_r I_r}{\ell}\left[1 + \frac{(\bar{z}_r/\rho_r)^2}{1 + \frac{A_r}{\ell t}}\right] \\
&E_x = E\left(\frac{A_s}{d} + t\right) \\
&G_{xy} = Gt \\
&E_y = E\left(\frac{A_r}{\ell} + t\right)
\end{aligned}\right\} \qquad (A\text{-}2)$$

where ρ_s and ρ_r are the radii of gyration of a stringer and ring, respectively, about the centroid of the stiffener.

Equation (A-1) has to be minimized with respect to the buckling pattern of the cylinder half waves in longitudinal direction, m, and full waves in circumferential direction, n. This minimization was performed by a computer program and, in order to reduce computational time, equations (A-1) and (A-2) were rearranged to be more amenable to automatic search procedures. The program steps n searching for a minimum solution for a fixed m; then m is stepped, and the procedure is repeated to obtain the answer. The rearranged equation (A-1) is given by:

$$\frac{\bar{N}_x a^2}{\pi^2 D} = C_1\alpha^2 + C_2\alpha^2\beta^2 + C_3\alpha^2\beta^4 + \frac{C_4}{\left[C_5\alpha^2 + C_6\alpha^2\beta^2 + C_7\alpha^2\beta^4\right]} \qquad \text{(A-3)}$$

where

$$\left.\begin{aligned}
C_1 &= \left(\frac{a}{\pi R}\right)^2 \frac{D_x}{D} & C_2 &= 2\left(\frac{a}{\pi R}\right)^2 \frac{D_{xy}}{D} \\
C_3 &= \left(\frac{a}{\pi R}\right)^2 \frac{D_y}{D} & C_4 &= 12Z^2\left(\frac{R}{\pi a}\right)^2 C_5 C_7 \\
C_5 &= \frac{E_x}{E_t} & C_6 &= \frac{C_5 C_7}{\frac{G_{xy}}{Et}} \\
C_7 &= \frac{E_y}{Et} & Z^2 &= \frac{a^4(1-\mu^2)}{R^2 t^2} \\
\alpha &= \frac{m\pi R}{a} & \beta &= \frac{na}{m\pi R}
\end{aligned}\right\} \qquad \text{(A-3a)}$$

A buckling equation for stiffened isotropic cylinders subjected to combinations of axial and circumferential loading is obtained from reference A-11 and is as follows:

$$(\bar{N}_x + \bar{N}_y\beta^2)\frac{a^2}{\pi^2 D} = m^2(1+\beta^2)^2 + m^2\frac{E_s I_s}{dD} + m^2\beta^4\frac{E_r I_r}{\ell D} + \left(\frac{G_s J_s}{dD} + \frac{G_r J_r}{\ell D}\right)m^2\beta^2 + \frac{12Z^2}{m^2\pi^4}\left(\frac{1 + \bar{S}\Lambda_s + \bar{R}\Lambda_r + \bar{S}\bar{R}\Lambda_{rs}}{\Lambda}\right) \qquad \text{(A-4)}$$

where

$$\left.\begin{aligned}
\Lambda_r &= 1 + 2\alpha^2\beta^2(1-\beta^2\mu)\frac{\bar{z}_r}{R} + \alpha^4\beta^4(1+\beta^2)\left(\frac{\bar{z}_r}{R}\right)^2 \\
\Lambda_s &= 1 + 2\alpha^2(\beta^2-\mu)\frac{\bar{z}_s}{R} + \alpha^4(1+\beta^2)^2\left(\frac{\bar{z}_s}{R}\right)^2
\end{aligned}\right\} \qquad \text{(A-4a)}$$

$$\Lambda_{rs} = 1 - \mu^2 + 2\alpha^2\beta^2(1-\mu^2)\left(\frac{\bar{z}_r}{R} + \frac{\bar{z}_s}{R}\right) + \alpha^4\beta^4\left[1 - \mu^2 + 2\beta^2(1+\mu)\right]\left(\frac{\bar{z}_r}{R}\right)^2 + 2\alpha^4\beta^4(1+\mu)^2\frac{\bar{z}_r\bar{z}_s}{R^2} + \alpha^4\beta^2\left[2(1+\mu) + \beta^2(1-\mu^2)\right]\left(\frac{\bar{z}_s}{R}\right)^2 \quad \text{(A-4a)}$$

$$\Lambda = (1+\beta^2)^2 + 2\beta^2(1+\mu)(\bar{R}+\bar{S}) + 1 - \mu^2)\left[\bar{S} + 2\beta^2\bar{R}\bar{S}(1+\mu) + \beta^4\bar{R}\right]$$

with

$$Z^2 = \frac{a^4(1-\mu^2)}{R^2t^2} \qquad D = \frac{Et^3}{12(1-\mu^2)}$$

$$\bar{S} = \frac{E_sA_s}{Etd} \qquad \bar{R} = \frac{E_rA_r}{Et\ell}$$

$$\alpha = \frac{m\pi R}{a} \qquad \beta = \frac{na}{m\pi R}$$

In equation (4) I_s and I_r are the moments of inertia of the stringer and ring, respectively, about their centroids.

The effect of locating the stiffeners on the internal or external surface of the cylinder shell is reflected in the quantities Λ_r, Λ_s, and Λ_{rs} by the terms linear in $\bar{z}_r$ or $\bar{z}_s$. (The eccentricities $\bar{z}_r$ and $\bar{z}_s$ are positive when the stiffeners are located on the external surface of the cylinder and negative when the stiffeners are on the internal surface.) The eccentricities are weighted by functions of m and n and therefore will effect the prediction of whether external or internal stiffening of a specified cylinder will be more effective.

If it is assumed that the stringer and ring eccentricities do not affect the buckling mode shape, a generalized form of the Becker equation can be used (ref. A-12). It was found by evaluating equation (A-4)'s solution that the buckling mode shape does change between internal and external stiffeners. Sometimes the buckling modes for external stiffeners were greater by two than those for internal stiffeners, both in the longitudinal and circumferential

directions. Since there was no consistency among the changes of buckling modes for external as opposed to internal, it was considered that any further approximation to the mode shape would cause errors in excess of the differences arising from the eccentricity effect. Therefore, equation (A-4) was minimized by search procedure of the buckling patterns.

To ease computation procedure, equation (A-4) was rearranged into terms of ascending powers of β^2 and α^2 in the following:

$$\bar{\lambda} \triangleq 1 + \bar{S}\lambda_s + \bar{R}\lambda_r + \bar{S}\bar{R}\lambda_{rs}$$

$$\bar{\lambda} = K_1\beta^0 + K_2\beta^2 + K_3\beta^4 + K_4\beta^6 + K_5\beta^8$$

and

$$\lambda = K_6\beta^0 + K_7\beta^2 + K_8\beta^4$$

where the coefficients are given by ascending powers of α^2

$$K_1 = C_1 + C_2\alpha^2 + C_3\alpha^4$$

$$K_2 = C_4\alpha^2 + C_5\alpha^4$$

$$K_3 = C_6\alpha^2 + C_7\alpha^4$$

$$K_4 = C_8\alpha^4$$

$$K_5 = C_9\alpha^4$$

and the section constants are as follows:

$$C_1 = 1 + \bar{S} + \bar{R} + \bar{S}\bar{R}\,(1 - \mu^2)$$

$$C_2 = -\,2\bar{S}\mu\left(\frac{\bar{z}_s}{R}\right)$$

$$C_3 = \bar{S}\left(\frac{\bar{z}_s}{R}\right)^2$$

$$C_4 = 2\bar{S}\left(\frac{\bar{z}_s}{R}\right) + 2\bar{R}\left(\frac{\bar{z}_s}{R}\right) + 2\bar{S}\bar{R}\,(1 - \mu^2)\left(\frac{\bar{z}_r}{R} + \frac{\bar{z}_s}{R}\right)$$

$$C_5 = 2\bar{S}\left(\frac{\bar{z}_s}{R}\right)^2 + 2\bar{S}\bar{R}\,(1 + \mu)\left(\frac{\bar{z}_s}{R}\right)^2$$

$$C_6 = -2\bar{R}\mu\left(\frac{\bar{z}_r}{R}\right)$$

$$C_7 = \bar{S}\left(\frac{\bar{z}_s}{R}\right)^2 + \bar{R}\left(\frac{\bar{z}_r}{R}\right)^2 + \bar{S}\bar{R}\left[(1-\mu^2)\left(\frac{\bar{z}_r}{R}\right)^2 + 2(1+\mu)^2\left(\frac{\bar{z}_r\,\bar{z}_s}{R^2}\right) + (1-\mu^2)\left(\frac{\bar{z}_s}{R}\right)^2\right]$$

$$C_8 = 2\bar{R}\left(\frac{\bar{z}_r}{R}\right)^2 + 2\bar{S}\bar{R}(1+\mu)\left(\frac{\bar{z}_r}{R}\right)^2$$

$$C_9 = \bar{R}\left(\frac{\bar{z}_r}{R}\right)^2$$

The torsional stiffness terms in equation (A-4) were originally neglected for the initial program, but as was indicated in reference A-13 it is possible to arrive at an erroneous conclusion regarding the relative efficiencies of internal or external stiffeners if the torsional stiffness is neglected. A subsequent version of the computer program now includes the two torsional effects of the stiffeners.

Bulkheads

Monocoque Ellipsoidal Bulkheads. - This section presents the methods used to verify the structural integrity of monocoque ellipsoidal bulkheads. The principal failure modes considered are material failure due to pressure stresses that exceed the material allowables and buckling due to internal or external pressure.

Material failure: The Von Mises criteria are used to determine the minimum skin thickness required to prevent material failure. This minimum skin thickness is given by

$$t_i = \frac{\sqrt{N_{\theta_i}^2 - N_{\theta_i} N_{\phi_i} + N_{\phi_i}^2}}{\sigma}$$

where

t_i = the membrane thickness at select points of the bulkhead

t_{min} = minimum membrane thickness based on constraints imposed by available material gauges, fabrication considerations, etc.

σ = allowable material stress, including safety factors

N_{θ_i} = circumferential stress resultant at the ith station

N_{ϕ_i} = meridional stress resultant at the ith station

The circumferential and meridional stress resultants are given

$$N_{\theta_i} = Pr_2\left(1 - \frac{r_2}{2r_1}\right)$$

$$N_{\phi_i} = \frac{Pr_2}{2}$$

where

$$r_1 = a^2 b^2/(a^2\sin^2\phi + b^2\cos^2\phi)^{3/2}$$

$$r_2 = a^2/(a^2\sin^2\phi + b^2\cos^2\phi)^{1/2}$$

P = the bulkhead pressure

a = major semi-axis of bulkhead

b = minor semi-axis of bulkhead

Stability analysis: The critical buckling stress for an elliptical isotropic monocoque bulkhead subjected to external pressure is evaluated by converting the elliptical bulkhead into an equivalent hemispherical dome and using the classic Von Karmen-Tsien formula to predict buckling of the monocoque spherical shells. This buckling equation is given by

$$\sigma_{cr} = \frac{0.606CEt}{R(\sin\beta)^{1/3}}$$

where

C = 0.25, the buckling correction factor required to correlate theoretical with experimented results.

R = radius of the equivalent spherical shell

In order to convert the ellipsoidal bulkhead to the equivalent spherical bulkhead, the following equations are used (fig. A-10):

$$\beta = \pi - 2 \arctan \frac{a}{b}$$

$$R_1 = a/\sin \beta$$

For equivalent stresses at the apex of the elliptical and spherical bulkhead, the pressure in the spherical bulkhead is given by

$$p_{eq} = \frac{pa \sin \beta}{b}$$

Hence, the buckling equation may be rewritten

$$\frac{\sigma_{cr}}{\eta} = \frac{p_{eq} R_i}{2t\eta} = 0.15E\left(\frac{t}{a}\right) \sin^{2/3} \beta$$

Therefore, the minimum skin thickness required to prevent buckling due to external pressure is given by

$$t = \left[\frac{pa^3}{0.36E (\sin \beta)^{2/3} \eta}\right]^{1/2}$$

To determine the true weight, in pounds per square foot, of any ellipsoidal shell of monocoque construction, the following is used.

$$\omega = \left(\frac{\rho t}{12}\right) F_b$$

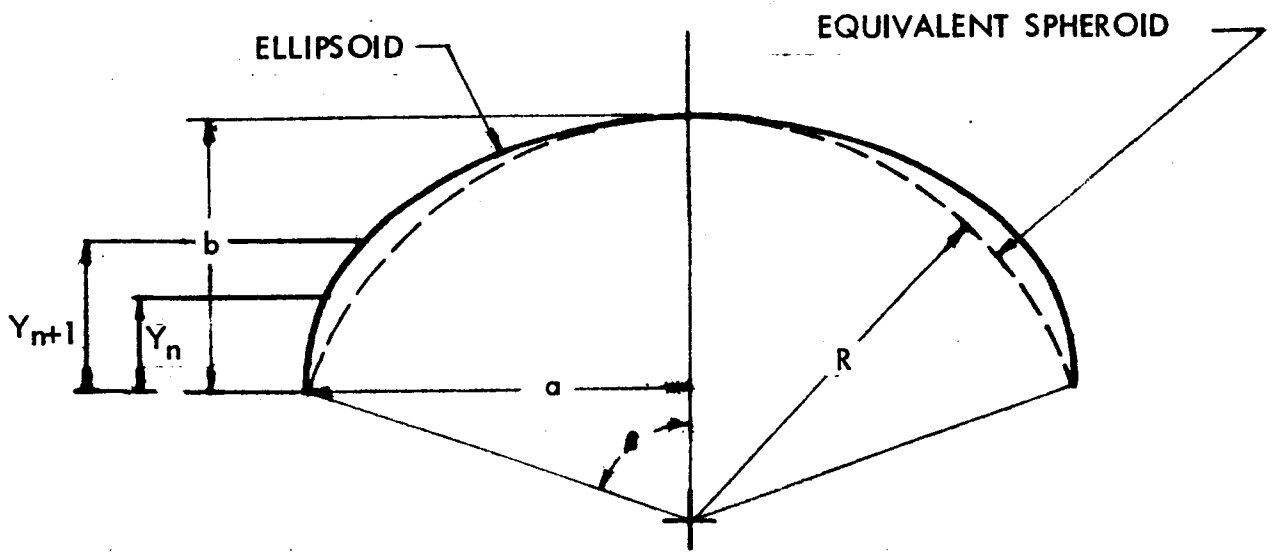

Figure A-10. Ellipsoid-to-Spheroid Conversion for Bulkheads

where F_b is a fabrication factor which accounts for non-calculated items. The total weight is calculated as ω times the surface area, where the surface area is

$$\text{surface area} = \frac{\pi a}{144 b^2} \left\{ y\sqrt{(a^2 - b^2)\, y^2 + b^4} + \frac{b^4}{\sqrt{a^2 - b^2}} \ln \left[y\sqrt{a - b^2} + \sqrt{(a^2 - b^2)\, y^2 + b^4} \right] \right\}_{y_n}^{y_{n+1}}$$

Ellipsoidal domes with an aspect ratio greater than $\sqrt{2}$ are subject to buckling stresses near the lower edges of the bulkhead when there is an internal pressure. The actual stress resultant can be obtained from the previous equations, and the shell stability is checked as an equivalent cylindrical shell. The buckling stress is approximated by

$$\sigma_{cr} = \frac{CEt}{a}$$

The stability coefficient C is given by

$$C = C_c + \Delta C_p$$

where

C_c = the stability coefficient for cylindrical shell with equivalent radius-to-thickness ratio

ΔC_p = the increase in the cylindrical shell stability coefficient due to internal pressure

The stability coefficients C_c and ΔC_p are derived from reference A-14 and are shown in figures A-11 and A-12.

Hence, the minimum skin thickness required to prevent buckling due to internal pressure is given by

$$t_{stab} = \left[\frac{N_{\theta c}\, a}{CE} \right]^{1/2}$$

where $N_{\theta c}$ = circumferential stress resultant at the equator of the elliptical bulkhead.

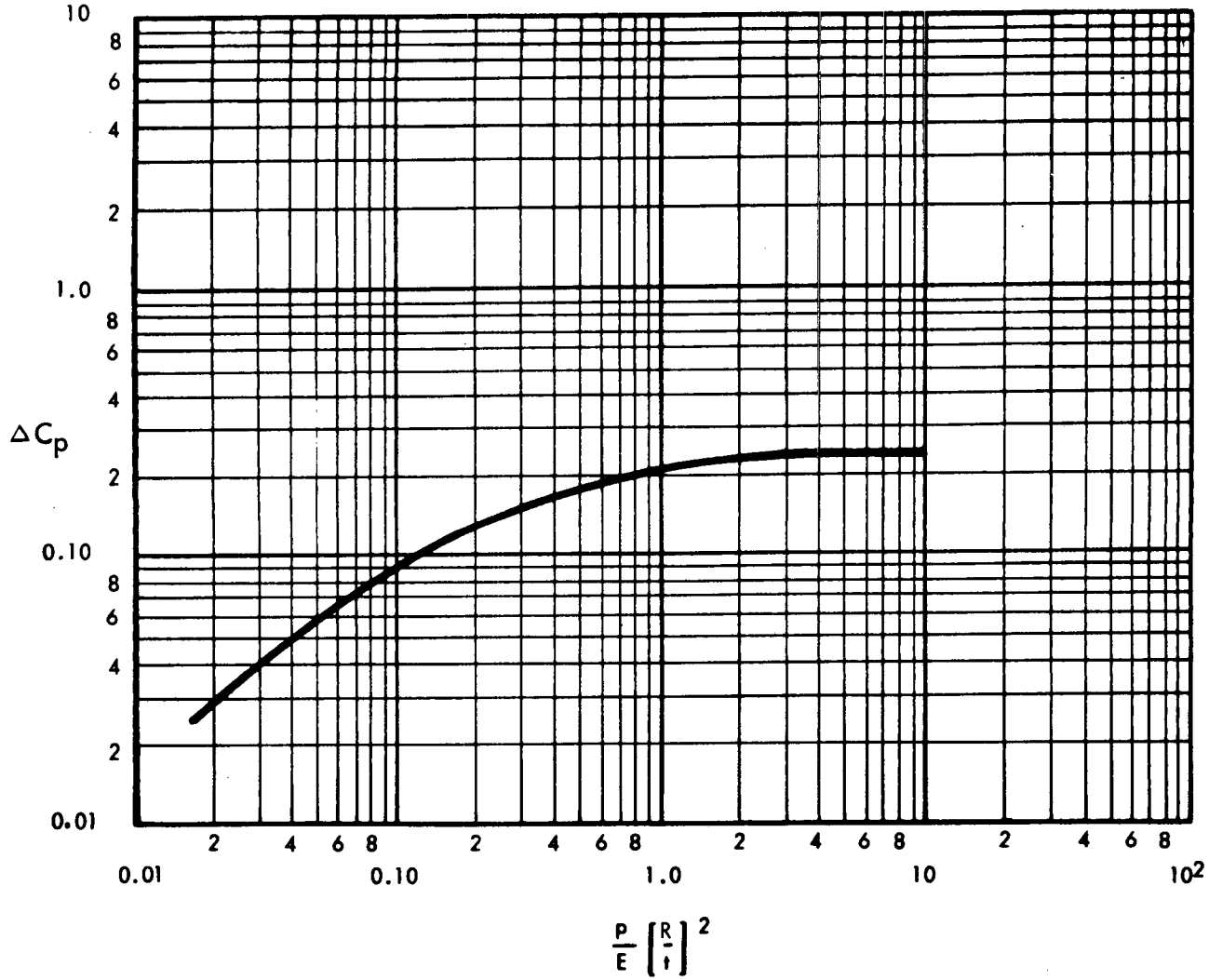

Figure A-11. Increase in Axial-Compressive Buckling-Stress Coefficient of Cylinders Due to Internal Pressure

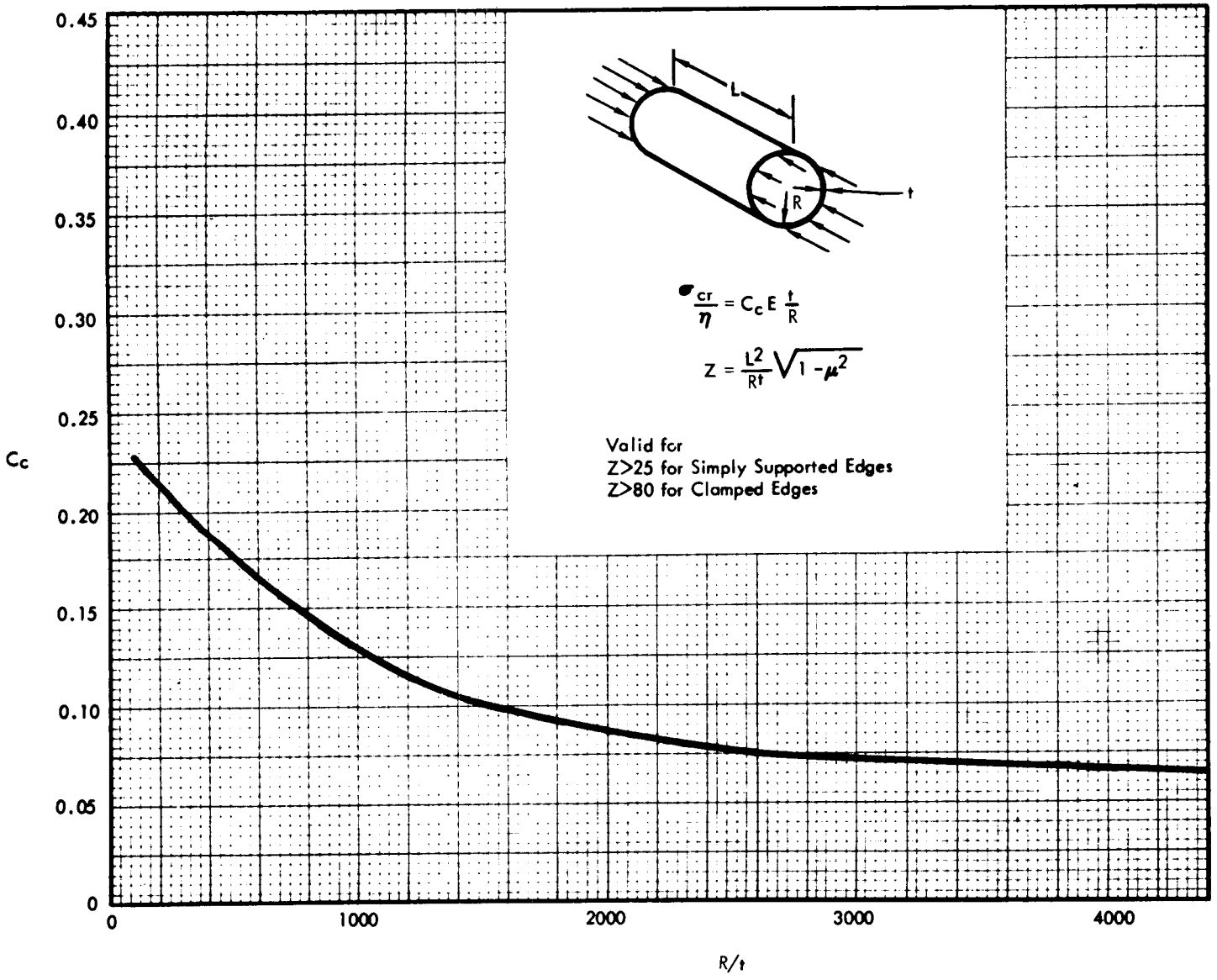

Figure A-12. - Buckling Stress Coefficient, C_c, for Unstiffened, Unpressurized Circular Cylinders in Axial Compression

Oblate spheroidal bulkhead. - This section presents the equations used in the synthesis of minimum-weight oblate spheroidal bulkheads (fig. A-13). The only failure modes considered in this analysis are material failures due to stresses that exceed the materials allowable.

Material failure: The Von Mises criteria are used to determine the minimum equivalent skin thickness required to prevent material failure. This theoretical minimum skin thickness is compared with the minimum skin gauges dictated by fabrication requirements in order to determine the minimum weight structure.

$$t_i = \frac{\sqrt{N_{\phi_i}^2 - N_{\phi_i} N_{\theta_i} + N_{\theta_i}^2}}{\sigma}$$

$$t_i = \max (t_i, t_{min})$$

where

t_i = material thickness at selected locations of the bulkhead

t_{min} = minimum skin thickness based on restraints imposed by available material gauges, fabrication consideration, etc.

σ = allowable stresses, including safety factor

N_{θ_i} = circumferential stress resultant

N_{ϕ_i} = meridional stress resultant

The stress resultants N_{θ_i} and N_{ϕ_i} are given by

$$N_{\theta_i} = pa\left[\frac{r_2}{a} - \left(\frac{a}{r_2}\right)^n\right]$$

$$N_{\phi_i} = \frac{pa}{2}\left(\frac{r_2}{a}\right)$$

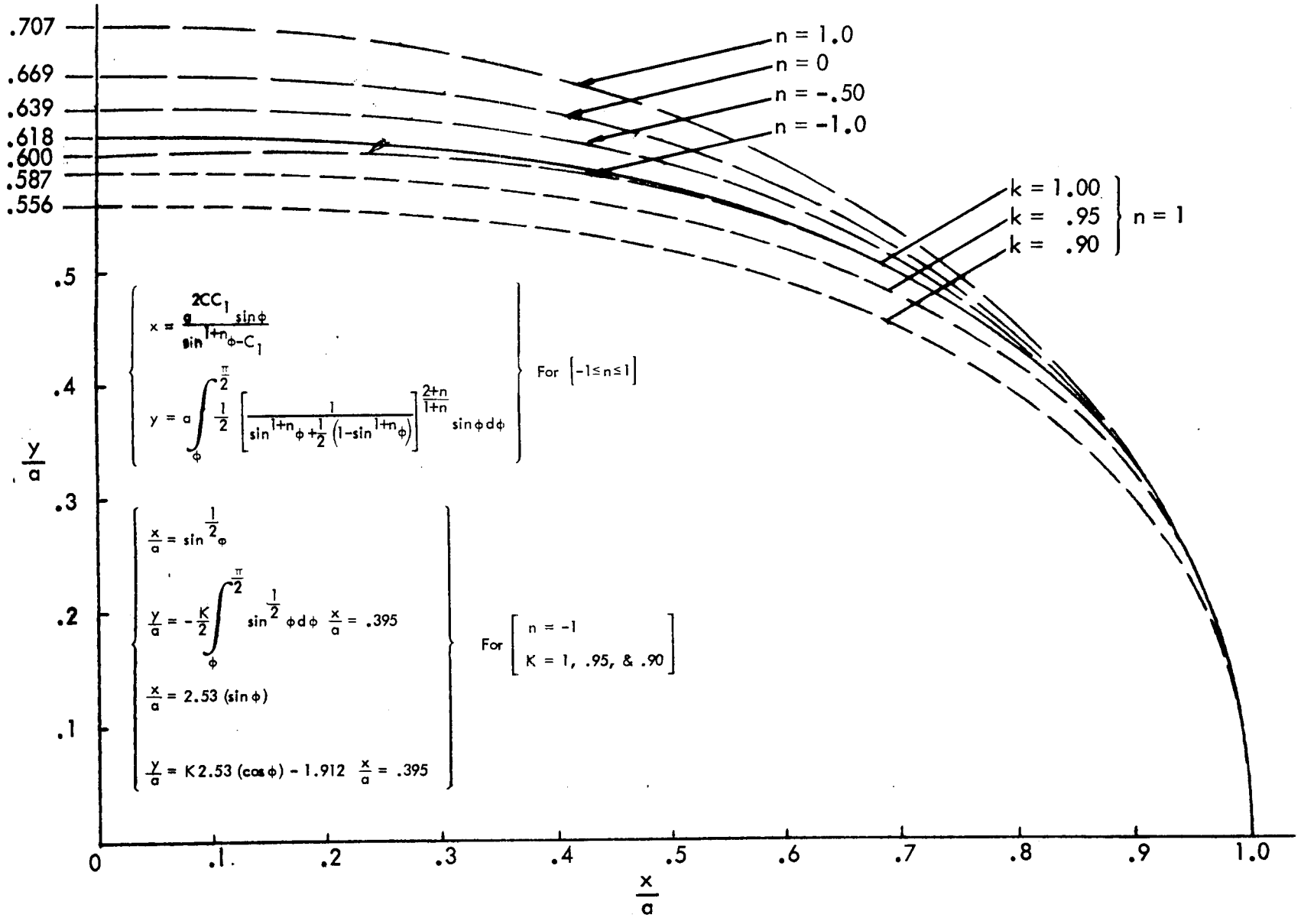

Figure A- 13. - Oblate Spheroid Bulkhead Shape for Various n and k Values

where

p = the pressure in the bulkhead

a = the major semi-axis of the bulkhead

r_2 = tangential radius of curvature at any point on bulkhead

n = bulkhead shape factor

The equation defining the curvatures of the oblate spheroid bulkheads are given by

$$x = \frac{a\,(2CC_i)\,\sin\theta}{\sin\phi^{(1+n)} - C_1}$$

$$y = a\int_{\phi}^{\pi/2} \frac{1}{2}\left\{\frac{1}{(\sin\phi)^{(1+n)} + \frac{1}{2}\left[1 - (\sin\phi)^{(1+n)}\right]}\right\}^{\left(\frac{2+n}{1+n}\right)} \cdot \sin\phi \cdot d\phi$$

where

C_1 = constant of integration

C = geometrical constant having units of $(\text{length})^{n+1}$

Modified semitoroidal bulkhead. - The advanced modified semitoroidal bulkhead (fig. A-14) is a light-weight bulkhead design which, by reason of its low profile, can effectively reduce a vehicle's length and, therefore, produce an effective design concept (ref. A-15). The principal failure modes considered are material failure due to stresses which exceed the material allowables and buckling due to internal or external pressure.

Material failure: The Von Mises criteria is used to determine the minimum skin thickness required to prevent material failure. This minimum skin thickness is given by

$$t_i = \frac{\sqrt{N_{\theta_i}^2 - N_{\theta_i} N_{\phi_i} + N_{\phi_i}^2}}{\sigma}$$

$$t = \max (t_i, t_{min})$$

where

t_i = the required membrane thickness at selected locations on the bulkhead

t_{min} = minimum membrane thickness based on constraints imposed by available material gauges, fabrication considerations, etc.

σ = allowable material stress including safety factors

N_{θ_i} = circumferential stress resultant at the i^{th} location

N_{ϕ_i} = meridional stress resultant at the i^{th} location

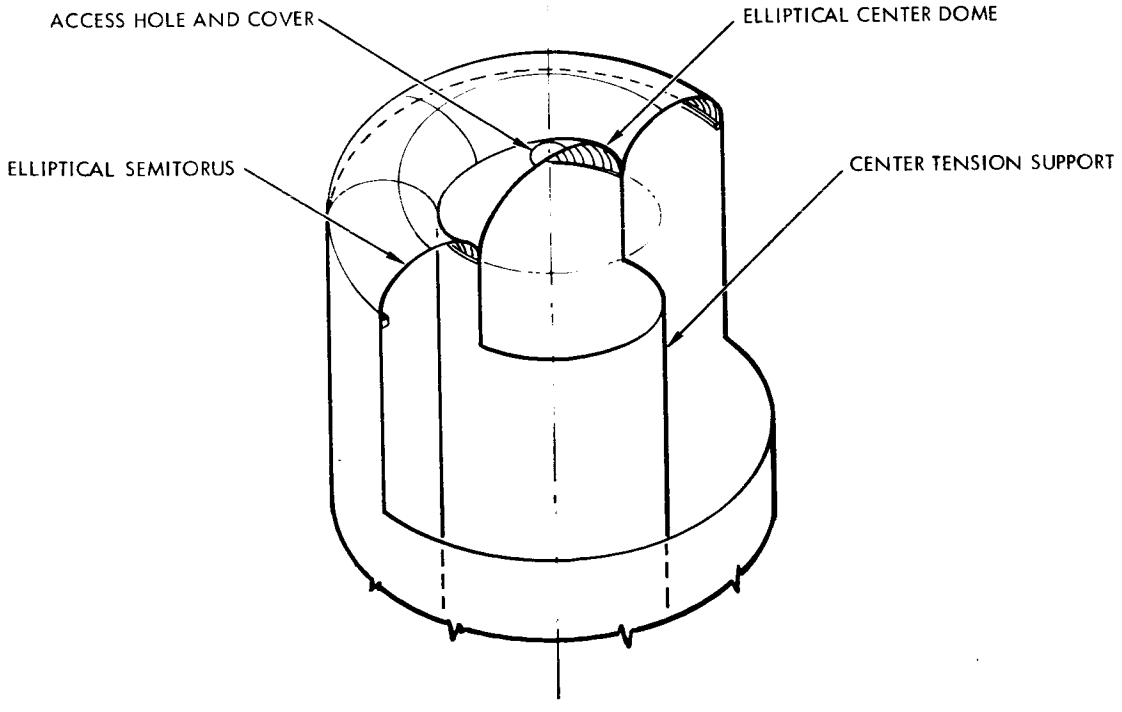

Figure A-14. - Modified Semitoroidal Bulkhead

The circumferential and meridional stress resultants for the toroidal segments, the outer membrane of the shell, are given (ref. A-16) by:

$$N_{\theta_i} = pa \frac{e^2 \sin\zeta (1 + \lambda \sin\zeta) + \lambda/2 \left(\frac{b}{c}\right)^2}{(1 - e^2 \cos 2\zeta)^{1/2}}$$

$$N_{\phi_i} = pb \frac{1 + \lambda/2 \sin\zeta (1 - e^2 \cos^2\zeta)^{1/2}}{1 + \lambda \sin\zeta}$$

where

p = applied pressure

a = radial distance from the axis of rotation to the midpoint of the elliptical cross-section

r = radial distance from the axis of rotation to a point on the elliptical shell

b = radial semi-axis of the elliptical cross-section

c = vertical semi-axis of the elliptical cross-section

$e^2 = 1 - \left(\frac{b}{c}\right)$ = eccentricity factor

z = vertical distance of a point on the shell from the equatorial plane

$$\sin\zeta = \frac{r - a}{b}$$

$$\cos\zeta = -\frac{z}{c}$$

The stress resultants for the elliptical segments, the inner membrane of the bulkhead, are given by

$$N_{\theta_i} = pr_2 \left(1 - \frac{r_2}{2r_1}\right)$$

$$N_{\phi_i} = \frac{pr_2}{2}$$

where

$$r_1 = a^2b^2/(a^2 \sin^2 \phi + b^2 \cos^2 \phi)^{3/2}$$

$$r_2 = a^2/(a^2 \sin^2 \phi + b^2 \cos^2 \phi)^{1/2}$$

p = bulkhead pressure

a = major semi-axis of the elliptical segment of the bulkhead = a - b

b = minor semi-axis of the elliptical segment of bulkhead

Stability analysis: The stability analysis for the complex membrane shape of the outer toroidal membrane coupled to an inner ellipsoidal membrane is beyond the current synthesis capability of the program. Therefore, the stability of the total membrane was considered as two separate membrane shapes, and their load interaction at the intersection was not considered. The inner dome, ellipsoidal, was converted to an equivalent spherical cross section, and its stability analysis was identical to that given for monocoque ellipsoidal bulkheads in this appendix. The outer membrane was analyzed as a toroidal shell under uniform external pressure. The stability analysis was the method used by Sobel and Flügge (ref. A-17), and a copy of their buckling curve used for the synthesis program was reproduced in figure A-15.

Joint Discontinuity

Determination of additional weight necessary to assure structural integrity for the joint region is required for the weight synthesis. The joint being considered consists of the intersection of two cylindrical shells and one bulkhead. An IBM 7094 computer program has been written to determine the additional weights to account for the joint discontinuity shears and stresses.

The method for analyzing the joint discontinuity shears and bending moments is that treated in references A-18 and A-19 by considering a symmetrically loaded shell with respect to the longitudinal axis. The joint shears and moments for each of the shells (i.e., skirt, bulkhead, and tank) are determined by assuring conditions of equilibrium and the conditions of compatibility at the joint. Hence conditions of equilibrium (ref. A-19) fig. A-16) give

$$Q_1 + Q_2 + Q_3 = 0 \qquad \text{(A-5)}$$

$$M_1 + M_2 - M_3 = -\frac{PR}{2}d \qquad \text{(A-6)}$$

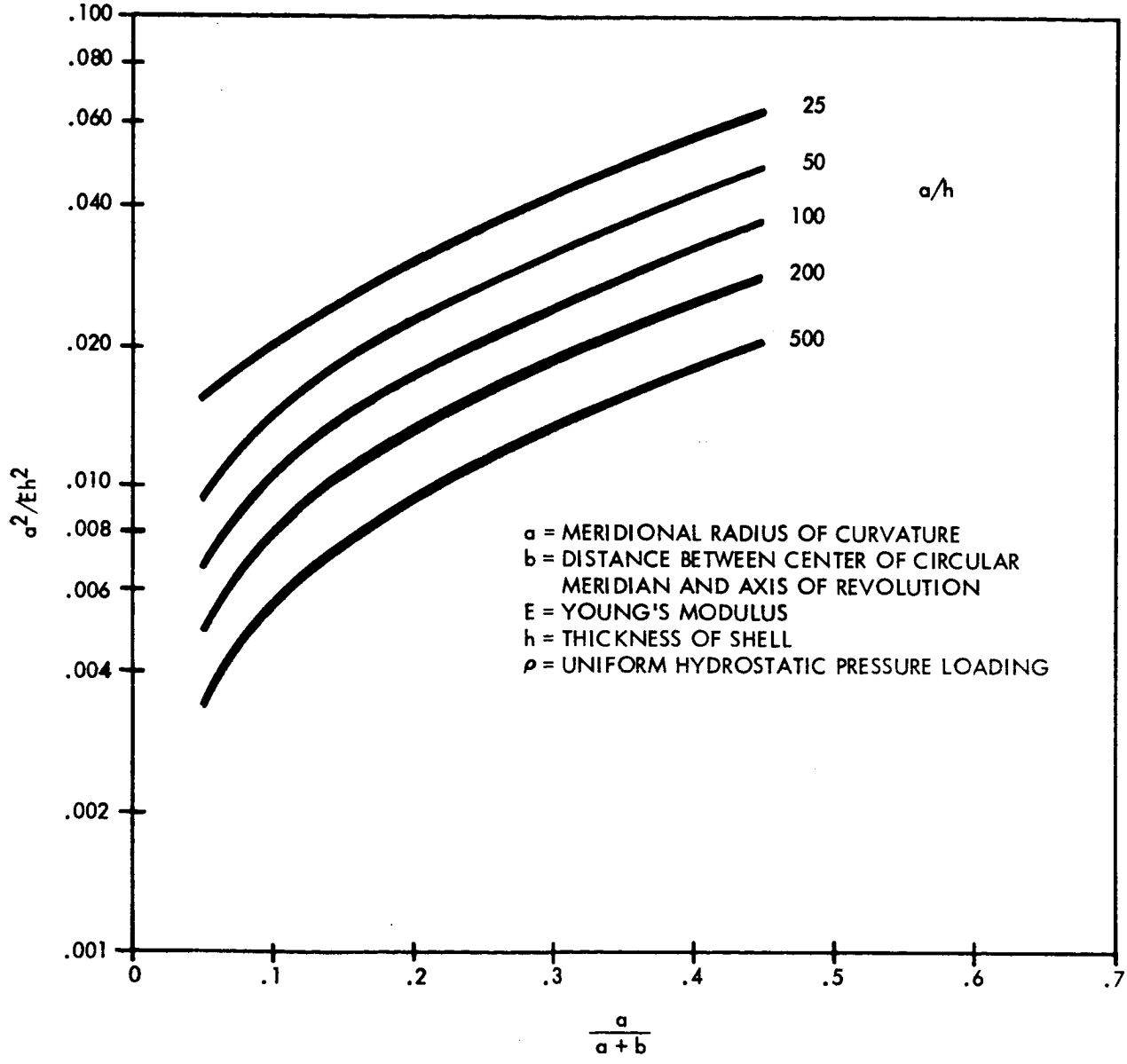

Figure A-15. - Buckling Curve

and the conditions of compatibility give the following relationships (ref. A-19)

$$w_{o_3} + \delta_3 = w_{o_2} + \delta_2 \tag{A-7}$$

$$w_{o_3} + \delta_3 = w_{o_1} \tag{A-8}$$

$$\theta_2 = -\theta_3 \tag{A-9}$$

$$\theta_1 = -\theta_3 \tag{A-10}$$

where

1, 2, 3 = subscripts associated with skirt, bulkhead, tank, i.e., sections 1, 2, 3 (fig. A-16)

Q = shear force at edge of shell, lb/in.

M = bending moment of edge of shell, in.-lb/in.

p = internal pressure, psi

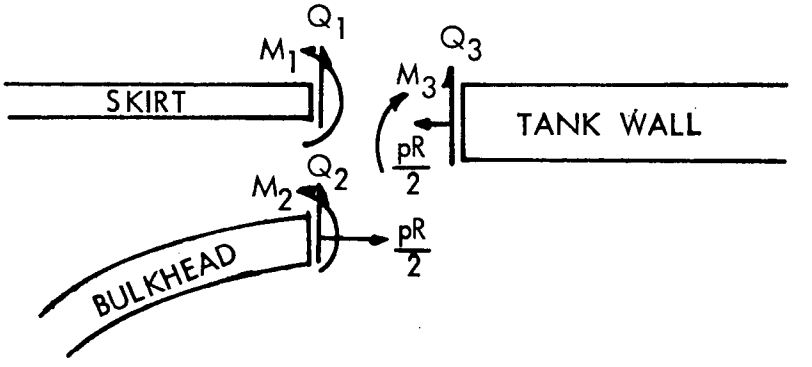

Figure A-16. - Compatability Conditions at Bulkhead Junction

R = radius of cylinder, in.

d = distance between the centroid of section 2 and section 3, in.

w_o = radial deflection of shell at edge due to M and Q (eq. (A-11)), in.

θ = rotation at edge of shell due to M and Q (eq. (A-12)), radians

δ = radial deflection of shell due to membrane forces

The differential equation that is to be satisfied (ref. A-19) is

$$\frac{d^4w}{dx^4} - \frac{E_y}{D_{Q_x}R^2}\frac{d^2w}{dx^2} + \frac{E_y(1 - \mu_x\mu_y)}{D_xR^2}w = 0$$

where the general solution to the above is

$$w = C_1e^{m_1x} + C_2e^{m_2x} + C_3e^{m_3x} + C_4e^{m_4x}$$

where

$$m_1 = -m_3 = \sqrt{2\alpha^2 - 2\sqrt{\alpha^4 - \beta^4}}$$

$$m_2 = -m_4 = \sqrt{2\alpha^2 + 2\sqrt{\alpha^4 - \beta^4}}$$

$$\alpha^2 = \frac{E_y}{4D_{Q_x}R^2}$$

$$\beta^4 = \frac{E_y(1 - \mu_x\mu_y)}{4D_xR^2}$$

and C_1, C_2, C_3, C_4 are constants.

The deflections w_o and rotations θ_o (ref. A-19) at the joint due to joint discontinuity shears Q_o and bending moments M_o are as follows

$$w_o = \frac{-Q_o (\beta^2 + \alpha^2)^{1/2} - M_o \beta^2}{\alpha \beta^4 D_x} \tag{A-11}$$

$$\theta_o = \frac{Q_o (2\alpha^2 + \beta^2) + M_o 2\beta^2 (\alpha^2 + \beta^2)^{1/2}}{2 D_x \beta^4} \tag{A-12}$$

where

$$Q_o = Q_x\Big|_{x=0} \tag{A-13}$$

$$M_o = M_x\Big|_{x=0} \tag{A-14}$$

D_{Q_x} = the beam shear stiffness in xz plane per inch of width

D_x = the beam flexural stiffness per width

μ_x, μ_y = the Poisson's ratios associated with bending in longitudinal and circumferential direction, respectively

E_y = the extensional stiffness in the circumferential direction

These conditions were made for very long shells; i.e., the edge influence to the opposite end of the joint is negligible. The analysis is based on the assumption that the outside tank wall and outside skirt wall are attached.

An existing computer program, 6J-138, was modified to determine the discontinuity shears, moments stresses, and the increase in weight, if necessary, due to the localized joint behavior. The joint discontinuity stresses σ_θ, σ_x, and τ are determined from elementary structural mechanics as

$$\sigma_{\theta_{max}} = \left| \frac{pR}{E_x/E} + \nu \frac{p}{2\pi R\left(\frac{E_x}{E}\right)} \right| + \left| \frac{\nu M_x x}{\left(D_x/E\right)} \right| \quad , \text{psi} \tag{A-15}$$

where

$$\frac{p}{2\pi R\left(\frac{E_x}{E}\right)} = \frac{N_x}{\left(\frac{E_x}{E}\right)} - \frac{pR}{2\left(\frac{E_x}{E}\right)}, \text{ psi} \qquad \text{(A-16)}$$

and N_x is the inplane load, including the effect of the pressure in pounds per inch.

The longitudinal or meridional stress is determined from

$$\sigma_{x_{max}} = \left| \frac{N_x}{\left(E_x/E\right)} \right| + \left| \frac{M_x \bar{X}}{\left(D_x/E\right)} \right|, \text{ psi} \qquad \text{(A-17)}$$

The shear stress in the core is computed by

$$\tau = \frac{Q_x}{h}, \text{ psi} \qquad \text{(A-18)}$$

where Q_x is the joint discontinuity shear in pounds per inch and h is the core height in inches.

The additional core weight necessary is determined as follows: First, the shear stress is checked to see if it exceeds the material allowable in shear. If not, then no increase in weight is needed; however, no decrease is made since the structure was originally designed without the effect of the joint discontinuity. If the shearing stress is larger than the material design allowable in shear, then an additional core weight is added as follows:

$$\Delta w = \left(\frac{\tau - \tau_{allow}}{\tau_{allow}} \right) w_c \ell \qquad \text{(A-19)}$$

where w_c is the core weight per running inch of length and where the length, ℓ, is determined from the condition where the influence of the discontinuity shears and moments are very small. Figure A-17 shows a typical decay of the discontinuity shears and moments.

Since the governing differential equation used is of the type similar to the beams on elastic foundation, it is well known (ref. A-20 and A-21) that the influence of the edge loads, i.e., discontinuity shears and moments, are very small (less than 1 percent) for

$$\beta L \geq 6$$

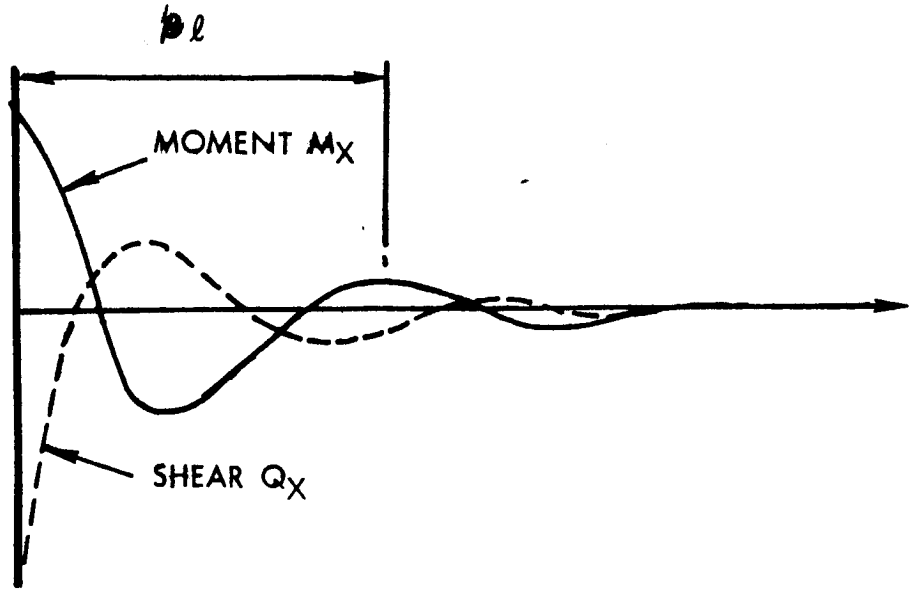

Figure A-17. - Typical Shear and Moment Decay

The length condition used in equation (A-19) was $\beta L = \pi$. The justification of using π is twofold: (1) the value of w was selected to account for approximately one complete cycle of the discontinuity shears and moments, and (2) the shearing stress is somewhat proportional to the core depth. It is noted that the discontinuity shears and moments decay exponentially. Equation (A-19) is used and, in effect, for weight

$$\beta L \geq 2\pi$$

or

$$L \geq \frac{2\pi}{\beta}$$

To assure conservativeness, the exponential decay was selected as a triangular decay (fig. A-18) for the purpose of establishing the additional needed weight of core. Since $\beta L > 2\pi > 6$, it has been assured that the edge condition is fully accounted for. Change in skin thickness for the discontinuity effects results in a stiffer joint than initially assumed (this is a second-order effect on discontinuity stresses).

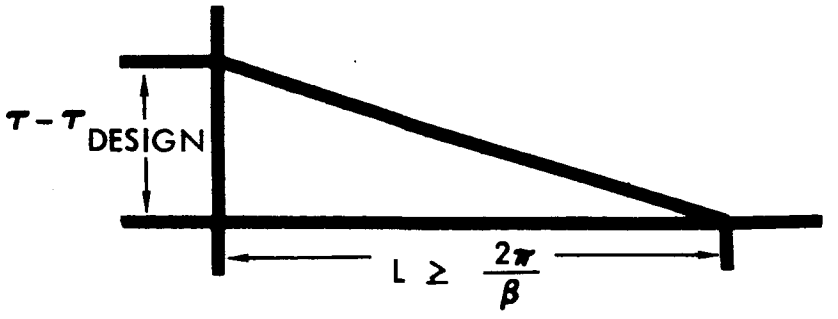

Figure A-18. - Idealized Triangular Stress Level Decay

Similar analysis was made for the skin portion of the composite structure. Here the longitudinal (or meridional) and circumferential stresses were calculated. The greater of these two stresses was checked to see if the calculated stress, σ, is greater than the material design allowable, σ_{design}. If $\sigma < \sigma_{design}$, then $\Delta w_{skin} = 0$, i.e., no additional weight is required. No reduction in weight exists, since this structure was originally designed not considering the influence of the discontinuity stresses. If $\sigma > \sigma_{design}$, then

$$\Delta w_{skin} = \left(\frac{\sigma - \sigma_{design}}{\sigma_{design}} \right) w_{skin} \ell$$

where ℓ is as defined before and w_{skin} is the weight of the skin per running inch of length. A flow diagram of the computer program written to determine these weights (i.e., core weight and total weight) for each of the joining shells is given in figure A-19.

Computer Programs

The equations presented in the preceding sections of this Appendix are used in computer programs to synthesize the major structural components. In order to facilitate the synthesis, the forms of the equations are generally adjusted to be more amenable to automatic computation. In addition, various iteration and systematic search procedures are used for the optimization process.

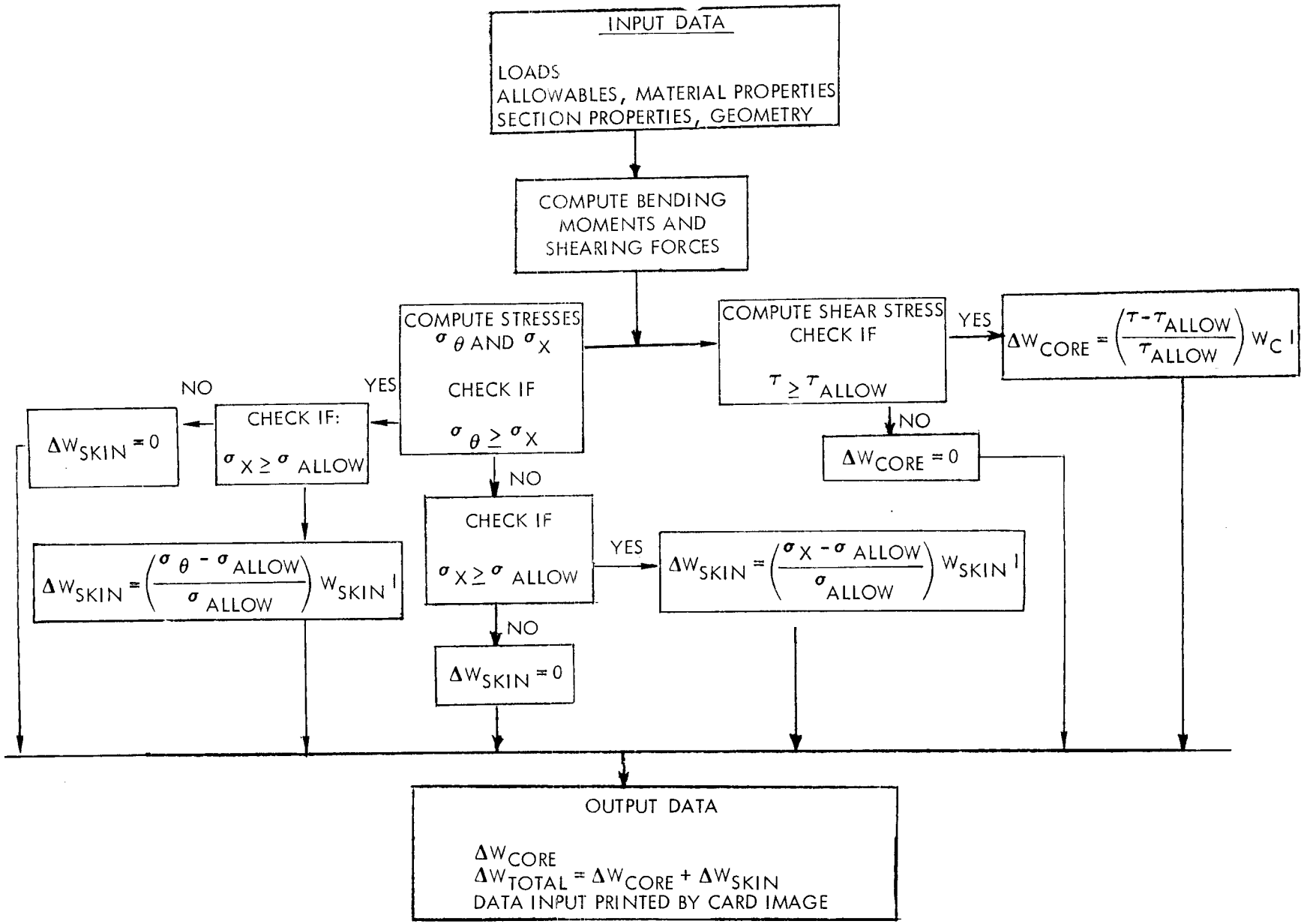

Figure A-19. - Computer Diagram—Discontinuity Stresses

The stress subroutines have been written completely in Fortran IV and are compatible with the IBM 7094 and IBM 360 with 7094 emulation systems. The programs are linked together by a main executive routine which calls the particular structural design analysis requested by the input information. The program currently uses an in-house input data-read routine (DECRD), which shortens the input data requirements for the additional design test cases. The read routine only requires data which are altered from the previous data run; all other input data remain unchanged.

The general stress routine program resolves the force and moments applied to the structural component into normal components of loading intensities on the structural shells. The program also considers external applied forces (wind pressures) and internal forces (gravity, ullage pressure, and hydrostatic pressures). All forces and moments are resolved stationwise into stress resultants perpendicular, N_θ, and parallel, N_x, to the structure's axis of revolution. The structural analysis considers both the load intensity and its associated temperature regime for various points along a flight path, and will develop a structural design with both strength and stability capability for the complete design envelope.

The types of structures which the program can consider are composed of cylinders, frustums, cones, and sections of ellipses of revolution. Various construction concepts are included in the over-all program. In addition to Phase I synthesis routines, these consist of corrugated sandwich, multiwall corrugated sandwich, double-wall skin stringer, ring stiffened cylindrical shell, and membrane bulkheads (ellipsoidal, oblate spheroidal, and modified semitoroidal). Also, coupled to an existing skin stringer subroutine, it includes an additional analysis to determine the stiffener eccentricity effects.

The computer input data required to synthesize the structural components are presented in table A-1. In general, these data consist of the radius, applied loads, material properties, and manufacturing constraints. A concise summary of the computer individual programs is presented in the following paragraphs, together with sample output formats and design options. A description of the data symbols and requirements shown in table A-1 is given in table A-2.

TABLE A- 1. - REQUIRED INPUT DATA FOR VARIOUS STRUCTURAL DESIGN CONCEPTS

Subroutine		Design Concept - Program Code							
No.	Title	MØNØ	SKINST	SAND	WAFFLE	CØRRUG	CØRRMW	SKINDW	RINGS
1	CØNS	1	2	3	4	5	6	7	8
2	XMAT	X	X	X	X	X	X	X	X
3	FSY	X	X	X	X	X	X	X	X
4	FSU	X	X	X	X	X	X	X	X
5	R	X	X	X	X	X	X	X	X
6	PMAX	X	X	X	X	X	X	X	X
7	PMIN	X	X	X	X	X	X	X	X
8	PULL	X	X	X	X	X	X	X	X
9	TMIN	X	X	X	X	X	X	X	X
10	RF	X	X	X	X	X	X	X	X
11	BMMIN	X	X	X	X	X	X	X	X
12	BMMAX	X	X	X	X	X	X	X	X
13	ALMIN	X	X	X	X	X	X	X	X
14	ALMAX	X	X	X	X	X	X	X	X
15	CØLUMN	X	X	X	X	X	X	X	X
16	HMAX			X				X	
17	XIND			X		X			X
18	CCO			X					
* 19	XMATC			X					
20	ANGLE	X	X	X	X	X	X	X	X
21	TWMIN				X				
22	BSMIN				X				
23	HTSMAX				X				
24	BØ		X					X	X
25	XK		X					X	
26	FFØRMO		X						X
27	HT		X					X	
28	XLG		X			X		X	X
29	TMINST		X					X	
30	BL		X					X	
31									
32									
33	CC1							X	
34	CGX							X	
35	TWIMIN						X	X	

TABLE A-2. - DESCRIPTION OF DATA SYMBOLS AND REQUIREMENTS

Subroutine		Description
No.	Title	
1	CØNS	type of construction (1 to 8)
2	XMAT	material indicator (1 to 20)
3	FSY	yield factor of safety
4	FSU	ultimate factor of safety
5	RO	average radius, in.
6	PMAX	maximum pressure (ullage + hydraulic), psi
7	PMIN	minimum pressure (vapor), psi
8	PULL	ullage pressure, psi
9	TMIN	minimum skin thickness, in.
10	RF	bending moment relief factor
11	BMMIN	minimum limit bending moment, in-lbs
12	BMMAX	maximum limit bending moment, in-lbs
13	ALMIN	minimum limit axial load, lbs.
14	ALMAX	maximum limit axial load, lbs.
15	CØLUMN	column indicator (1 to 200) If CØLUMN is 0.0, only one load will be run, using BMMIN (11) and ALMIN (13)

Note: Data marked X are used for that construction. In some cases, as noted, a 0.0 may be loaded and the program will compute a value. Otherwise, the data marked X must be loaded.

TABLE A-2. - DESCRIPTION OF DATA SYMBOLS AND REQUIREMENTS - Continued

Subroutine		Description
No.	Title	
16	HMAX	maximum sandwich height in SAND, in. maximum core height in SKINDW, in.
17	XIND	sand { 1 - no sandwich height correction 0 - compute factor (FEGCI) from curve } sand
	CØRRUG	1 - ENC from curves 0 - ENC from equations rings { 0 - inertia from formula -1 - ALPHA from curve, ≥1 +1 - ALPHA from curve, no limit } rings
18	CCO	axial buckling coefficient (if 0, program will compute)
19	XMATC	core material indicator (1 to 4) When IN-ØUT version of SKINST is used, DA(19) is used as an indicator of what will be run: 1 - isotropic and inside orthotropic 2 - isotropic and outside orthotropic 3 - isotropic and inside and outside orthotropic 4 - inside and outside orthotropic
20	ANGLE	angle between cylinder wall and horizontal, degrees
21	TWMIN	minimum waffle thickness, in.
22	BSMIN	minimum waffle spacing, in.
23	HTSMAX	maximum ratio of waffle height/skin thickness
24	BØ	stringer spacing for SKINST and SKINDW, in. ring spacing for RINGS, in.

Note: Data marked X are used for that construction. In some cases, as noted, a 0.0 may be loaded and the program will compute a value. Otherwise, the data marked X must be loaded.

TABLE A-2. - DESCRIPTION OF DATA SYMBOLS AND REQUIREMENTS - Continued

Subroutine		Description
No.	Title	
25	XK	stringer shape indicator (1 = ⊓, 2 = Z, 3 = I, 4 = ⊥)
26	FFØRMO	frame form factor (if 0, program will compute)
27	HT	stringer height (if 0, program will compute)
28	XLG	frame pitch for SKINST and SKINDW, in. (if 0, program will compute) cylinder length for CØRRUG and RINGS, in.
29	TMINST	minimum stringer leg thickness, in.
30	BL	buckling load (must be 100.0 for SKINDW), percent
31		
32		
33	CC1	buckling coefficient (if 0, program will compute)
34	CGX	buckling coefficient
35	TWIMIN	minimum thickness of corrugation material, in.

Note: Data marked X are used for that construction. In some cases, as noted, a 0.0 may be loaded and the program will compute a value. Otherwise, the data marked X must be loaded.

Corrugated sandwich cylinder. - The computer input data required to synthesize longitudinally corrugated core sandwich cylinders are presented in table A-1. These data include the axial load, bending moment, internal pressure, shell radius, material properties, safety factors, and minimum skin thickness. The computer program iterates with these data to obtain the face panel thickness and core material gauges, the depth of the composite wall, and the angle between the corrugated web and the face sheets. The resultant configuration is a minimum-weight structure consistent with the fabrication constraints. These fabrication constraints can be altered to investigate their weight sensitivity effects.

A representative computer printout is shown in table A- 3. The first segment of this printout consists of the invariant input data. The first column contains the minimum allowable skin thickness, the burst and relief pressures, the material density, and the component's length. The second column contains the yield and ultimate material stresses, the elastic and shear modulus, and the temperature corresponding to these property values. The third column contains the limit and ultimate load factors. The bottom part of the printout consists of the variable input data and the output results of the computer. The first three columns of the second segment consist of the component radius, the axial loads, and the bending moment applied to the component. The fourth column contains the compressive load intensity. The unit shell weight is contained in the fifth column. The equivalent skin thickness and the skin and web thickness are presented in columns six through eight. Column nine contains the composite wall height, and column ten presents the corrugation angle. The last three columns consist of the resultant skin stresses, the loading index, and the weight-to-radius ratio, respectively.

This program allows the user to specify the design environment, axial load, bending moment, pressures and temperatures, the shell radius and length, and the type of material to be used. The program has two different correlation factors to account for the discrepancy between buckling theory and experiment. The first correlation factor was the same as that used for honeycomb structures in Phase I of the study and is based on reference A-14. The other factor was obtained from the NASA space vehicle design criteria, reference A-22.

Multiwall corrugated sandwich. - The computer input data required to define the optimum multiwall corrugated sandwich cylinder are presented in table A- 1. These data include the axial load, bending moment, internal pressure, and material allowables. In addition, manufacturing constraints such as minimum skin or web gauge may be prescribed. These two manufacturing constraints have a secondary constraint effect by allowing the program user to impose a height restriction by selecting an artificial minimum skin thickness to effectively reduce the design optimum height.

The computer iterates to determine the stress intensity for the composite cylinder, the percentage of material in the face sheets and core of the corrugated face panel, and the corrugation angle. The resultant configuration is a minimum-weight structure that satisfies the design criteria without violating manufacturing constraints.

A representative computer printout for the multiwall corrugated sandwich cylinder is presented in table A- 5. The first part of the printout consists of the invariant input data for this construction and material. The

TABLE A-3. - CORRUGATED SANDWICH PRINTOUT

CONSTRUCTION - CORRUGATED SANDWICH

MATERIAL - TITANIUM A

MIN SKIN THICKNESS =	0.0100 INS	YIELD STRESS =	100000. PSI	LIMIT LOAD FACTOR =	1.1
BURST PRESSURE =	0.0000 PSI	ULTIMATE STRESS =	115000. PSI	ULTIMATE LOAD FACTOR =	1.4
RELIEF PRESSURE =	0.0000 PSI	YOUNGS MODULUS =	14000000. PSI	ANGLE (WITH HORIZ.) =	90.0
MATERIAL DENSITY =	0.1600 PCI	SHEAR MODULUS =	5263158. PSI		
CYLINDER LENGTH =	260.0000 INS	TEMPERATURE =	300. DEGF		

COMP. RADIUS INS	AXIAL LOAD LBS	BENDING MOMENT IN-LBS	COMP.LOAD INTENSITY LBS/IN	UNIT WEIGHT LB/FT2	TBAR INS	SKIN THICK INS	WEB THICK INS	SAND HEIGHT INS	CORR. ANGLE DEGREES	STRESS PSI	NX/R PSI	WT/R PCI
130.	1166876.	0.	2000.	1.75	0.076	0.022	0.022	0.59	45.00	26266.	15.385	0.0000937
130.	2333751.	0.	4000.	2.74	0.119	0.035	0.035	0.82	45.00	33688.	30.769	0.0001461
130.	3500627.	0.	6000.	3.53	0.153	0.045	0.045	0.98	45.00	39180.	46.154	0.0001885
130.	4667503.	0.	8000.	4.19	0.182	0.053	0.053	1.10	45.00	43960.	61.538	0.0002240
130.	5834379.	0.	10000.	4.86	0.211	0.062	0.062	1.23	45.00	47408.	76.923	0.0002596
130.	7001254.	0.	12000.	5.41	0.235	0.069	0.069	1.33	45.00	51126.	92.308	0.0002889
130.	8168130.	0.	14000.	5.95	0.258	0.076	0.076	1.42	45.00	54255.	107.692	0.0003176
130.	9335006.	0.	16000.	6.43	0.279	0.082	0.082	1.49	45.00	57364.	123.077	0.0003433
130.	10501881.	0.	18000.	6.95	0.302	0.088	0.088	1.58	45.00	59681.	138.461	0.0003712
130.	11668757.	0.	20000.	7.45	0.323	0.095	0.095	1.67	45.00	61863.	153.846	0.0003979
130.	12835633.	0.	22000.	7.88	0.342	0.100	0.100	1.73	45.00	64362.	169.231	0.0004207
130.	14002509.	0.	24000.	8.26	0.358	0.105	0.105	1.78	45.00	66962.	184.615	0.0004411
130.	15169384.	0.	26000.	8.63	0.375	0.110	0.110	1.83	45.00	69410.	200.000	0.0004610
130.	16336260.	0.	28000.	9.11	0.395	0.116	0.116	1.91	45.00	70798.	215.385	0.0004868
130.	17503136.	0.	30000.	9.57	0.415	0.122	0.122	1.99	45.00	72214.	230.769	0.0005113
130.	18670011.	0.	32000.	9.85	0.427	0.125	0.125	2.00	45.00	74854.	246.154	0.0005262
130.	19836887.	0.	34000.	10.26	0.445	0.130	0.130	2.06	45.00	76351.	261.538	0.0005481
130.	21003763.	0.	36000.	10.65	0.462	0.135	0.135	2.10	45.00	77878.	276.923	0.0005689
130.	22170638.	0.	38000.	11.02	0.478	0.140	0.140	2.14	45.00	79435.	292.308	0.0005888
130.	23337514.	0.	40000.	11.60	0.504	0.147	0.147	2.25	45.00	79435.	307.692	0.0006198

TABLE A-4 . - MULTIWALL CORRUGATED SANDWICH PRINTOUT

CONSTRUCTION - MULTI-WALL CORRUGATED SANDWICH

MATERIAL - TITANIUM B

MIN SKIN THICKNESS	= 0.0100 INS	YIELD STRESS	= 105000. PSI	LIMIT LOAD FACTOR	= 1.1
BURST PRESSURE	= 0.0000 PSI	ULTIMATE STRESS	= 120000. PSI	ULTIMATE LOAD FACTOR	= 1.4
RELIEF PRESSURE	= 0.0000 PSI	YOUNGS MODULUS	= 14000000. PSI	ANGLE (WITH HORIZ.)	= 90.0
MATERIAL DENSITY	= 0.1600 PCI	SHEAR MODULUS	= 5263158. PSI		
MIN CORE THICKNESS	= 0.0100 INS	TEMPERATURE	= 300. DEGF		

COMP. RADIUS INS	AXIAL LOAD LBS	BENDING MOMENT IN-LBS	COMP.LOAD INTENSITY LBS/IN	UNIT WEIGHT LB/FT2	TBAR INS	SKIN THICK INS	WEB THICK INS	SAND HEIGHT INS	CORR. ANGLE DEGREES	STRESS PSI	NX/R PSI	WT/R PCI
270.	2423511.	0.	2000.	1.59	0.061	0.010	0.006	0.25	57.00	33023.	7.407	0.0000409
270.	4847022.	0.	4000.	1.94	0.066	0.010	0.007	0.22	57.00	60878.	14.815	0.0000498
270.	7270533.	0.	6000.	2.28	0.076	0.010	0.009	0.24	61.00	78634.	22.222	0.0000587
270.	9694044.	0.	8000.	2.70	0.095	0.012	0.012	0.28	61.00	84357.	29.630	0.0000694
270.	12117555.	0.	10000.	3.14	0.115	0.014	0.014	0.32	61.00	86913.	37.037	0.0000809
270.	14541066.	0.	12000.	3.61	0.135	0.017	0.016	0.36	61.00	88660.	44.444	0.0000929
270.	16964577.	0.	14000.	4.09	0.155	0.019	0.019	0.40	61.00	90442.	51.852	0.0001053
270.	19388088.	0.	16000.	4.60	0.175	0.022	0.021	0.43	61.00	91346.	59.259	0.0001182
270.	21811599.	0.	18000.	5.13	0.195	0.027	0.021	0.45	61.00	92260.	66.667	0.0001320
270.	24235110.	0.	20000.	5.66	0.213	0.034	0.019	0.41	61.00	94114.	74.074	0.0001457
270.	26658621.	0.	22000.	6.21	0.236	0.036	0.022	0.50	61.00	93182.	81.481	0.0001597
270.	29082132.	0.	24000.	6.76	0.255	0.039	0.020	0.46	66.00	94114.	88.889	0.0001738
270.	31505643.	0.	26000.	7.30	0.276	0.045	0.023	0.52	61.00	94114.	96.296	0.0001878
270.	33929154.	0.	28000.	7.86	0.298	0.048	0.026	0.57	61.00	94114.	103.704	0.0002022
270.	36352665.	0.	30000.	8.42	0.316	0.047	0.024	0.53	68.00	95055.	111.111	0.0002164
270.	38776176.	0.	32000.	8.66	0.347	0.044	0.042	0.83	61.00	92260.	118.518	0.0002227
270.	41199687.	0.	34000.	9.11	0.369	0.046	0.044	0.89	61.00	92260.	125.926	0.0002344
270.	43623198.	0.	36000.	9.53	0.386	0.049	0.047	0.90	61.00	93182.	133.333	0.0002452
270.	46046709.	0.	38000.	10.02	0.408	0.051	0.049	0.95	61.00	93182.	140.741	0.0002578
270.	48470220.	0.	40000.	10.43	0.425	0.053	0.051	0.95	61.00	94114.	148.148	0.0002682

second part consists of the variable input data and the results of the computer computation. The input data are similar to the corrugated sandwich printout but with the addition of a minimum core thickness of the substructure in the first column.

The first three columns of the second part consist of the component's radius and the applied loads. The fourth column is the resultant stress intensity. The fifth column is the unit shell weight of the synthesized component. The sixth through tenth columns define the principal geometric parameters of the shell's wall, equivalent thickness (TBAR), facing skin panel and corrugated web thickness, the sandwich panel thickness, and the corrugation angle of the stiffener webs in the facing sheets.

Double-wall skin stringer. - The computer input data required to define the optimum double-wall skin stringer construction are presented in table A-1. These data include the axial loads, bending moment, shell radius, safety factors, type of stringer (integral, Z, or hat section) and the stringer spacing. With these data, the computer iterates to define the optimum stress level for the shell component, the distribution of material between the face sheets and stringers, the required substructure material gauge, and the substructure spacing.

A typical computer printout for the double-wall skin stringer construction is presented in table A-5. The input data print format is similar to Phase I skin stringer except for a difference in maximum core height in column one. The output data have the design loading and the principal dimensions of the optimized sections. Table A-5 shows the effect of internal pressures of 0 and 40 pounds per square inch on the unit shell weight and the weight changes due to decreasing of stiffeners pitch 8 inches to 4.0 inches. These printouts were for a top-hat section stiffener for the facing sheets. The program has the ability to synthesize using integral, Z, and I section stiffeners.

Ring stiffened cylindrical shell. - The computer input data required for synthesis of ring stiffened cylindrical shells are presented in table A-1. These data include the applied loads, the shell radius and ring spacing, material properties, safety factors, and minimum skin gauges. The computer iterates with the data to obtain the stress level in the face sheet and the required frame area. The resultant configuration is a minimum-weight structure that will satisfy the design criteria without violating the fabrication constraints.

A representative printout for ring stiffened cylindrical shell is shown in table A-6. The invariant input data are present in the first part of the printout. They consist of the minimum allowable skin thickness, the burst

TABLE A- 5. - DOUBLE-WALL SKIN STRINGER PRINTOUT

CONSTRUCTION - DOUBLE WALL SKIN STRINGER

MATERIAL - ALUMINUM A
STRINGER SHAPE - HAT SECTION

MIN SKIN THICKNESS	= 0.0100 INS	YIELD STRESS	= 50000. PSI	BUCKLING COEFFICIENT	= 0.0
STRINGER SPACING	= 8.0000 INS	ULTIMATE STRESS	= 55000. PSI	LIMIT LOAD FACTOR	= 1.100
MAX CORE HT	= 6.0000 INS	YOUNGS MODULUS	= 10000000. PSI	ULTIMATE LOAD FACTOR	= 1.400
BURST PRESSURE	= 0.0000 PSI	TEMPERATURE	= 300. DEGF	BM RELIEF FACTOR	= 0.714
RELIEF PRESSURE	= 0.0000 PSI	MATERIAL DENSITY	= 0.1000 PCI	ANGLE (WITH HORIZ.)	= 90.0

COMP. RADIUS INS	AXIAL LOAD LB	BENDING MOMENT IN-LBS	COMP. LOAD INTENSITY LBS/IN	UNIT WEIGHT LB/FT2		THICK OR AREA	PITCH INS	STRESS PSI		STGR THICK	STGR ELEMENT LENGTH	NX/R PSI	WT/R PCI
198.	1777242.	0.	2000.	3.96	SK	0.072	1.33	7500.	UP	0.058	2.15	10.101	0.0001384
					ST	0.47	8.0		BL	0.058	0.86		
					CORE	0.010	10.51		OE	0.058	2.15		
198.	3554483.	0.	4000.	5.03	SK	0.091	2.60	12000.	UP	0.073	2.19	20.202	0.0001765
					ST	0.61	8.0		BL	0.073	0.87		
					CORE	0.010	8.29		OE	0.073	2.19		
198.	5331725.	0.	6000.	5.69	SK	0.105	3.27	16000.	UP	0.084	2.06	30.303	0.0001996
					ST	0.66	8.0		BL	0.084	0.82		
					CORE	0.010	7.37		OE	0.084	2.06		
198.	7108966.	0.	8000.	6.35	SK	0.115	3.81	19200.	UP	0.092	2.13	40.404	0.0002229
					ST	0.75	8.0		BL	0.092	0.85		
					CORE	0.010	6.63		OE	0.092	2.13		
198.	8886208.	0.	10000.	6.94	SK	0.124	4.35	22400.	UP	0.100	2.09	50.505	0.0002398
					ST	0.79	8.0		BL	0.100	0.84		
					CORE	0.010	6.19		OE	0.100	2.09		
198.	10663449.	0.	12000.	7.21	SK	0.133	4.89	25600.	UP	0.106	2.01	60.606	0.0002529
					ST	0.81	8.0		BL	0.106	0.80		
					CORE	0.010	5.90		OE	0.106	2.01		

TABLE A-5. - DOUBLE-WALL SKIN STRINGER PRINTOUT - Continued

CONSTRUCTION - DOUBLE WALL SKIN STRINGER

MATERIAL - ALUMINUM A
STRINGER SHAPE - HAT SECTION

MIN SKIN THICKNESS	=	0.0100 INS	YIELD STRESS	=	50000. PSI	BUCKLING COEFFICIENT	=	0.0
STRINGER SPACING	=	3.0000 INS	ULTIMATE STRESS	=	55000. PSI	LIMIT LOAD FACTOR	=	1.100
MAX CORE HT	=	5.0000 INS	YOUNGS MODULUS	=	10000000. PSI	ULTIMATE LOAD FACTOR	=	1.400
BURST PRESSURE	=	47.0000 PSI	TEMPERATURE	=	300. DEGF	BM RELIEF FACTOR	=	0.714
RELIEF PRESSURE	=	0.0000 PSI	MATERIAL DENSITY	=	0.1000 PCI	ANGLE (WITH HORIZ.)	=	90.0

COMP. RADIUS INS	AXIAL LOAD LB	BENDING MOMENT IN-LBS	COMP. LOAD INTENSITY LBS/IN	UNIT WEIGHT LB/FT2		THICK OR AREA	PITCH INS	STRESS PSI		STGR THICK	STGR ELEMENT LENGTH	NX/R PSI	WT/R PCI
198.	1777242.	0.	2000.	3.95	SK	0.101	1.83	7500.	UP	0.081	0.80	10.101	0.0001384
					ST	0.25	8.0		BL	0.081	0.32		
					CORE	0.010	10.51		DE	0.081	0.80		
198.	3554483.	0.	4000.	5.93	SK	0.101	2.60	12000.	UP	0.081	1.72	20.202	0.0001765
					ST	0.53	8.0		BL	0.081	0.69		
					CORE	0.010	8.29		DE	0.081	1.72		
198.	5331725.	0.	6000.	8.69	SK	0.105	3.27	16000.	UP	0.084	2.06	30.303	0.0001996
					ST	0.66	8.0		BL	0.084	0.82		
					CORE	0.010	7.37		DE	0.084	2.06		
198.	7108966.	0.	8000.	6.35	SK	0.115	3.31	19200.	UP	0.092	2.13	40.404	0.0002228
					ST	0.75	8.0		BL	0.092	0.85		
					CORE	0.010	6.63		DE	0.092	2.13		
198.	8886208.	0.	10000.	6.84	SK	0.124	4.35	22400.	UP	0.100	2.09	50.505	0.0002398
					ST	0.79	8.0		BL	0.100	0.84		
					CORE	0.010	6.19		DE	0.100	2.09		
198.	10663449.	0.	12000.	7.21	SK	0.133	4.39	25600.	UP	0.106	2.21	60.606	0.0002529
					ST	0.81	8.0		BL	0.106	0.80		
					CORE	0.010	5.90		DE	0.106	2.21		

TABLE A-5. - DOUBLE-WALL SKIN STRINGER PRINTOUT - Continued

CONSTRUCTION - DOUBLE WALL SKIN STRINGER

MATERIAL - ALUMINUM A
STRINGER SHAPE - HAT SECTION

MIN SKIN THICKNESS	=	0.0100 INS	YIELD STRESS	=	50000. PSI	BUCKLING COEFFICIENT	= 0.0
STRINGER SPACING	=	4.0000 INS	ULTIMATE STRESS	=	55000. PSI	LIMIT LOAD FACTOR	= 1.100
MAX CORE HT	=	5.0000 INS	YOUNGS MODULUS	=	10000000. PSI	ULTIMATE LOAD FACTOR	= 1.400
BURST PRESSURE	=	0.0000 PSI	TEMPERATURE	=	300. DEGF	BM RELIEF FACTOR	= 0.714
RELIEF PRESSURE	=	0.0000 PSI	MATERIAL DENSITY	=	0.1000 PCI	ANGLE (WITH HORIZ.)	= 90.0

COMP. RADIUS INS	AXIAL LOAD LB	BENDING MOMENT IN-LBS	COMP. LOAD INTENSITY LBS/IN	UNIT WEIGHT LB/FT2		THICK OR AREA	PITCH INS	STRESS PSI		STGR THICK	STGR ELEMENT LENGTH	NX/R PSI	WT/R PCI
198.	1777242.	0.	2000.	2.52	SK	0.044	2.60	12000.	UP	0.035	1.19	10.101	0.0000882
					ST	0.16	4.0		BL	0.035	0.48		
					CORE	0.010	16.59		OE	0.035	1.19		
198.	3554483.	0.	4000.	3.18	SK	0.055	3.81	19200.	UP	0.044	1.16	20.202	0.0001114
					ST	0.20	4.0		BL	0.044	0.47		
					CORE	0.010	13.27		OE	0.044	1.16		
198.	5331725.	0.	6000.	3.61	SK	0.064	4.89	25600.	UP	0.051	1.10	30.303	0.0001265
					ST	0.21	4.0		BL	0.051	0.44		
					CORE	0.010	11.80		OE	0.051	1.10		
198.	7108966.	0.	8000.	4.03	SK	0.070	5.77	30800.	UP	0.056	1.12	40.404	0.0001412
					ST	0.24	4.0		BL	0.056	0.45		
					CORE	0.010	10.64		OE	0.056	1.12		
198.	8886208.	0.	10000.	4.29	SK	0.076	5.66	35600.	UP	0.061	1.12	50.505	0.0001540
					ST	0.26	4.0		BL	0.061	0.45		
					CORE	0.012	9.84		OE	0.061	1.12		
198.	10663449.	0.	12000.	4.80	SK	0.082	5.59	39600.	UP	0.065	1.12	60.606	0.0001682
					ST	0.28	4.0		BL	0.065	0.45		
					CORE	0.014	9.12		OE	0.065	1.12		

TABLE A-5 . - DOUBLE-WALL SKIN STRINGER PRINTOUT - Continued

Nomenclature

①	Skin thickness
②	Pitch between two face skins, i.e., section core height
③	Stringer cross-sectional area
④	Stringer pitch
⑤	Substructure core thickness
⑥	Substructure core pitch

TABLE A-6. - RING STIFFENED CYLINDRICAL SHELL PRINTOUT

CONSTRUCTION - RING STIFFENED SHELL

MATERIAL - ALUMINUM A

MIN SKIN THICKNESS	=	0.0100 INS	YIELD STRESS	=	50000. PSI	LIMIT LOAD FACTOR	=	1.1
BURST PRESSURE	=	0.0000 PSI	ULTIMATE STRESS	=	55000. PSI	ULTIMATE LOAD FACTOR	=	1.4
RELIEF PRESSURE	=	0.0000 PSI	YOUNGS MODULUS	=	10000000. PSI	ANGLE (WITH HORIZ.)	=	90.0
MATERIAL DENSITY	=	0.1000 PCI	TEMPERATURE	=	300. DEGF	FRAME SHAPE FACTOR	=	4.00
RING SPACING	=	50.0000 INS	CYLINDER LENGTH	=	350. INS	BM RELIEF FACTOR	=	0.714

COMPONENT RADIUS INS	AXIAL LOAD LBS	BENDING MOMENT IN-LBS	COMP. LOAD INTENSITY LB/IN	UNIT WEIGHT LB/FT2	SKIN THICKNESS INS	RING AREA	STRESS PSI	NX/R PSI	WT/R PCI
200.	1795196.	0.	2000.	5.93	0.3784	1.46	5286.	10.000	0.0002058
200.	3590392.	0.	4000.	7.72	0.4977	1.67	8037.	20.000	0.0002680
200.	5385587.	0.	6000.	9.02	0.5851	1.81	10255.	30.000	0.0003133
200.	7180783.	0.	8000.	10.07	0.6555	1.92	12205.	40.000	0.0003496
200.	8975979.	0.	10000.	10.98	0.7168	2.01	13951.	50.000	0.0003813
200.	10771175.	0.	12000.	11.77	0.7702	2.08	15581.	60.000	0.0004088
200.	12566370.	0.	14000.	12.49	0.8185	2.14	17104.	70.000	0.0004338
200.	14361566.	0.	16000.	13.15	0.8629	2.20	18542.	80.000	0.0004566
200.	16156762.	0.	18000.	13.76	0.9043	2.25	19906.	90.000	0.0004779
200.	17951958.	0.	20000.	14.35	0.9436	2.30	21195.	100.000	0.0004981
200.	19747154.	0.	22000.	14.88	0.9800	2.34	22449.	110.000	0.0005168
200.	21542349.	0.	24000.	15.39	1.0144	2.39	23661.	120.000	0.0005344
200.	23337545.	0.	26000.	15.87	1.0467	2.42	24841.	130.000	0.0005511
200.	25132741.	0.	28000.	16.33	1.0781	2.46	25975.	140.000	0.0005672
200.	26927937.	0.	30000.	16.78	1.1085	2.49	27072.	150.000	0.0005827
200.	28723132.	0.	32000.	17.20	1.1368	2.53	28162.	160.000	0.0005973
200.	30518328.	0.	34000.	17.62	1.1652	2.56	29202.	170.000	0.0006118
200.	32313524.	0.	36000.	18.01	1.1915	2.59	30251.	180.000	0.0006253
200.	34108720.	0.	38000.	18.40	1.2179	2.61	31264.	190.000	0.0006388
200.	35903915.	0.	40000.	18.77	1.2433	2.64	32275.	200.000	0.0006519

TABLE A-6. - RING STIFFENED CYLINDRICAL SHELL PRINTOUT - Continued

CONSTRUCTION - RING STIFFENED SHELL

MATERIAL - ALUMINUM A

MIN SKIN THICKNESS =	0.0100 INS	YIELD STRESS	= 50000. PSI	LIMIT LOAD FACTOR	= 1.1
BURST PRESSURE =	0.0000 PSI	ULTIMATE STRESS	= 55000. PSI	ULTIMATE LOAD FACTOR	= 1.4
RELIEF PRESSURE =	0.0000 PSI	YOUNGS MODULUS	= 10000000. PSI	ANGLE (WITH HORIZ.)	= 90.0
MATERIAL DENSITY =	0.1000 PCI	TEMPERATURE	= 300. DEGF	FRAME SHAPE FACTOR	= 4.00
RING SPACING =	25.0100 INS	CYLINDER LENGTH	= 325. INS	BM RELIEF FACTOR	= 0.714

COMPONENT RADIUS INS	AXIAL LOAD LBS	BENDING MOMENT IN-LBS	COMP. LOAD INTENSITY LB/IN	UNIT WEIGHT LB/FT2	SKIN THICKNESS INS	RING AREA	STRESS PSI	NX/R PSI	WT/R PCI
200.	1795196.	0.	2000.	5.29	0.3264	0.96	6128.	10.000	0.0001838
200.	3590392.	0.	4000.	6.91	0.4327	1.10	9244.	20.000	0.0002401
200.	5385587.	0.	6000.	8.09	0.5101	1.20	11763.	30.000	0.0002808
200.	7180783.	0.	8000.	9.04	0.5735	1.27	13951.	40.000	0.0003140
200.	8975979.	0.	10000.	9.88	0.6288	1.33	15903.	50.000	0.0003430
200.	10771175.	0.	12000.	10.61	0.6772	1.38	17721.	60.000	0.0003683
200.	12566370.	0.	14000.	11.26	0.7205	1.42	19430.	70.000	0.0003909
200.	14361566.	0.	16000.	11.86	0.7609	1.46	21028.	80.000	0.0004119
200.	16156762.	0.	18000.	12.42	0.7983	1.50	22549.	90.000	0.0004314
200.	17951958.	0.	20000.	12.94	0.8326	1.53	24021.	100.000	0.0004492
200.	19747154.	0.	22000.	13.44	0.8660	1.56	25407.	110.000	0.0004666
200.	21542349.	0.	24000.	13.91	0.8974	1.59	26751.	120.000	0.0004829
200.	23337545.	0.	26000.	14.34	0.9267	1.61	28068.	130.000	0.0004981
200.	25132741.	0.	28000.	14.77	0.9551	1.64	29341.	140.000	0.0005128
200.	26927937.	0.	30000.	15.18	0.9825	1.66	30581.	150.000	0.0005270
200.	28723132.	0.	32000.	15.57	1.0088	1.68	31802.	160.000	0.0005406
200.	30518328.	0.	34000.	15.96	1.0352	1.70	32985.	170.000	0.0005543
200.	32313524.	0.	36000.	16.34	1.0605	1.73	34179.	180.000	0.0005674
200.	34108720.	0.	38000.	16.72	1.0859	1.75	35368.	190.000	0.0005805
200.	35903915.	0.	40000.	17.10	1.1113	1.77	36569.	200.000	0.0005937

TABLE A-6. - RING STIFFENED CYLINDRICAL SHELL PRINTOUT - Continued

CONSTRUCTION - RING STIFFENED SHELL

MATERIAL - ALUMINUM A

MIN SKIN THICKNESS =	0.0100 INS	YIELD STRESS =	50000. PSI	LIMIT LOAD FACTOR =	1.1
BURST PRESSURE =	0.0000 PSI	ULTIMATE STRESS =	55000. PSI	ULTIMATE LOAD FACTOR =	1.4
RELIEF PRESSURE =	0.0000 PSI	YOUNGS MODULUS =	10000000. PSI	ANGLE (WITH HORIZ.) =	90.0
MATERIAL DENSITY =	0.1000 PCI	TEMPERATURE =	300. DEGF	FRAME SHAPE FACTOR =	4.00
RING SPACING =	25.0100 INS	CYLINDER LENGTH =	200. INS	BM RELIEF FACTOR =	0.714

COMPONENT RADIUS INS	AXIAL LOAD LBS	BENDING MOMENT IN-LBS	COMP. LOAD INTENSITY LB/IN	UNIT WEIGHT LB/FT2	SKIN THICKNESS INS	RING AREA	STRESS PSI	NX/R PSI	WT/R PCI
200.	89760.	0.	100.	1.73	0.0970	0.52	1031.	0.500	0.0000602
200.	179520.	0.	200.	2.23	0.1280	0.60	1563.	1.000	0.0000775
200.	269279.	0.	300.	2.60	0.1510	0.65	1987.	1.500	0.0000901
200.	359039.	0.	400.	2.90	0.1700	0.69	2353.	2.000	0.0001005
200.	448799.	0.	500.	3.15	0.1860	0.72	2688.	2.500	0.0001093
200.	538559.	0.	600.	3.38	0.2009	0.75	2986.	3.000	0.0001173
200.	628318.	0.	700.	3.58	0.2137	0.77	3275.	3.500	0.0001243
200.	718078.	0.	800.	3.76	0.2255	0.80	3547.	4.000	0.0001307
200.	807838.	0.	900.	3.93	0.2364	0.81	3808.	4.500	0.0001365
200.	897598.	0.	1000.	4.08	0.2462	0.83	4062.	5.000	0.0001418
200.	987357.	0.	1100.	4.24	0.2560	0.85	4297.	5.500	0.0001471
200.	1077117.	0.	1200.	4.39	0.2658	0.86	4514.	6.000	0.0001523
200.	1166877.	0.	1300.	4.52	0.2746	0.88	4734.	6.500	0.0001571
200.	1256637.	0.	1400.	4.64	0.2825	0.89	4957.	7.000	0.0001613
200.	1346396.	0.	1500.	4.78	0.2913	0.90	5150.	7.500	0.0001660
200.	1436156.	0.	1600.	4.89	0.2981	0.91	5367.	8.000	0.0001696
200.	1525916.	0.	1700.	5.01	0.3059	0.93	5557.	8.500	0.0001738
200.	1615676.	0.	1800.	5.11	0.3127	0.94	5756.	9.000	0.0001774
200.	1705435.	0.	1900.	5.23	0.3205	0.95	5927.	9.500	0.0001816
200.	1795195.	0.	2000.	5.32	0.3264	0.96	6128.	10.000	0.0001847

and relief pressures, the material density, ring frame spacing, yield and ultimate allowable material stresses, the materials's modulus of elasticity, and the design temperature. In addition, the data contain the cylinder length, the limit and ultimate load factors, the ring frame shape factor, and the bending moment relief factor. The data output indicates the shell unit weight, the required skin thickness, and the ring frame area to meet the strength and stability requirements. Table A-6 also shows the effect of changing the ring spacing and the cylinder length.

Eccentrically stiffened shells. - The computer input data are identical to the skin-stringer program of Phase I of this study. An additional indicator data bit (DA19) allows the eccentricity effect to be evaluated and indicates whether the stiffeners are inside or outside.

The typical printout for the eccentricity effects is shown in table A-7 . The orthotropic and isotropic load intensities quoted are the theoretical values and their corresponding buckling pattern both longitudinal and circumferential. Table A-7 shows the weight changes when the stiffener pitch is constrained from 5 inches to 8 inches and when the stiffener section is modified from hat section to Z section.

Membrane bulkheads. - The computer input data required to synthesize membrane bulkheads are presented in table A-1 . These data include the internal and/or external pressure, the major and minor semi-axis, material properties, and safety factors. An iteration procedure is not required to synthesize the membrane bulkheads, because the only loading condition analyzed is internal or external pressure.

Typical computer printouts for the membrane bulkheads are presented in table A-8 . The first part of these printouts consists of the yield and ultimate material allowable stresses, the material elastic modulus, and its density. In addition, the minimum membrane thickness and the limit and ultimate factors of safety are presented. The second part of the printout contains the components radii and the resulting skin thickness of several points along the bulkhead. The membrane thickness is assumed to taper linearily between the points where the thickness is computed. For the semitoroidal bulkheads, seven thicknesses are given; their relative positions along the bulkhead are indicated in the table.

TABLE A-7. - ECCENTRICITY EFFECTS

CONSTRUCTION - SKIN STRINGER

MATERIAL - ALUMINUM A
STRINGER SHAPE - HAT SECTION

MIN SKIN THICKNESS	=	0.0100	INS	YIELD STRESS	=	50000.	PSI	BUCKLING LOAD(POINT)	=	100.0
STRINGER SPACING	=	5.0000	INS	ULTIMATE STRESS	=	55000.	PSI	LIMIT LOAD FACTOR	=	1.100
FRAME PITCH	=	20.0000	INS	YOUNGS MODULUS	=	10000000.	PSI	ULTIMATE LOAD FACTOR	=	1.400
BURST PRESSURE	=	0.0000	PSI	TEMPERATURE	=	300.	DEGF	BM RELIEF FACTOR	=	0.714
RELIEF PRESSURE	=	0.0000	PSI	MATERIAL DENSITY	=	0.1000	PCI	FRAME SHAPE FACTOR	=	0.000
CYLINDER LENGTH	=	360.0000	INS	MAX FRAME STRESS	=	25000.	PSI	ANGLE (WITH HORIZ)	=	90.0
STRINGER HEIGHT	=	0.0000	INS							

COMP. RADIUS INS	AXIAL LOAD LB	BENDING MOMENT IN-LBS	COMP. LOAD INTENSITY LBS/IN	UNIT WEIGHT LB/FT2		THICK OR AREA	PITCH INS	STRESS PSI		STIFF THICK	STIFF ELEMENT LENGTH	NX/E PSI	WT/E PCI
130.	2917189.	0.	5000.	3.21	SK	0.081		26605.	JP	0.065	2.16	38.462	0.0001715
					ST	0.53	5.0		BL	0.065	0.96		
					ER	1.06	30.2		DE	0.065	2.16		

(1) (2) (3)

(ORTHO 13854. ISO 12883. 11790.)

0.5000E 01 0.5000E 01 0.5000E 01 0.6000E 01 0.4000E 01 0.6000E 01

(4) (5) (6) (7) (8) (9)

COMP. RADIUS INS	AXIAL LOAD LB	BENDING MOMENT IN-LBS	COMP. LOAD INTENSITY LBS/IN	UNIT WEIGHT LB/FT2		THICK OR AREA	PITCH INS	STRESS PSI		STIFF THICK	STIFF ELEMENT LENGTH	NX/E PSI	WT/E PCI
130.	5834379.	0.	10000.	4.33	SK	0.123		42322.	JP	0.082	2.38	76.223	0.0002312
					ST	0.74	5.0		BL	0.082	0.95		
					ER	1.49	30.3		DE	0.082	2.38		

REDUCE TO :

(1) (2) (3)

(ORTHO 20730. ISO 18858. 17462.)

0.4000E 01 0.5000E 01 0.5000E 01 0.6000E 01 0.4000E 01 0.6000E 01

(4) (5) (6) (7) (8) (9)

TABLE A-7. - ECCENTRICITY EFFECTS - Continued

CONSTRUCTION - SKIN STRINGER

MATERIAL - ALUMINUM A
STRINGER SHAPE - HAT SECTION

MIN SKIN THICKNESS	=	0.0100	INS	YIELD STRESS	=	50000.	PSI	BUCKLING LOAD(PCNT)	=	100.0
STRINGER SPACING	=	8.0000	INS	ULTIMATE STRESS	=	55000.	PSI	LIMIT LOAD FACTOR	=	1.100
FRAME PITCH	=	0.0000	INS	YOUNGS MODULUS	=	10000000.	PSI	ULTIMATE LOAD FACTOR	=	1.400
BURST PRESSURE	=	0.0000	PSI	TEMPERATURE	=	300.	DEGF	BM RELIEF FACTOR	=	0.714
RELIEF PRESSURE	=	0.0000	PSI	MATERIAL DENSITY	=	0.1000	PCI	FRAME SHAPE FACTOR	=	0.000
CYLINDER LENGTH	=	260.0000	INS	MAX FRAME STRESS	=	25000.	PSI	ANGLE (WITH HORIZ)	=	90.0
STRINGER HEIGHT	=	0.0000	INS							

COMP. RADIUS INS	AXIAL LOAD LB	BENDING MOMENT IN-LBS	COMP. LOAD INTENSITY LBS/IN	UNIT WEIGHT LB/FT2		THICK OR AREA	PITCH INS	STRESS PSI		STGR THICK	STGR ELEMENT LENGTH	NX/R PSI	WT/R PCI
130.	11668757.	0.	22000.	7.17	SK	0.193		53965.	JP	0.154	3.54	153.946	0.0003931
					ST	2.08	8.0		BL	0.154	1.41		
					FR	1.83	40.2		DE	0.154	3.54		

(1) (2) (3)

(ORTHO 43093. ISO 46277. 36657.)

0.3000E 01 0.5000E 01 0.3000E 01 0.6000E 01 0.3000E 01 0.6000E 01

(4) (5) (6) (7) (8) (9)

TABLE A- 7. - ECCENTRICITY EFFECTS - Continued

CONSTRUCTION - SKIN STRINGER

MATERIAL - BERYLLIUM A
STRINGER SHAPE - ZEE SECTION

MIN SKIN THICKNESS	=	0.0100	INS	YIELD STRESS	=	48000.	PSI	BUCKLING LOAD(PCNT)	=	100.0
STRINGER SPACING	=	8.0000	INS	ULTIMATE STRESS	=	63000.	PSI	LIMIT LOAD FACTOR	=	1.100
FRAME PITCH	=	0.0000	INS	YOUNGS MODULUS	=	43000000.	PSI	ULTIMATE LOAD FACTOR	=	1.400
BURST PRESSURE	=	0.0000	PSI	TEMPERATURE	=	300.	DEGF	BM RELIEF FACTOR	=	0.714
RELIEF PRESSURE	=	0.0000	PSI	MATERIAL DENSITY	=	0.0660	PCI	FRAME SHAPE FACTOR	=	0.000
CYLINDER LENGTH	=	540.0000	INS	MAX FRAME STRESS	=	25000.	PSI	ANGLE (WITH HORIZ)	=	90.0
STRINGER HEIGHT	=	0.0000	INS							

COMP. RADIUS INS	AXIAL LOAD LB	BENDING MOMENT IN-LBS	COMP. LOAD INTENSITY LBS/IN	UNIT WEIGHT LB/FT2		THICK OR AREA	PITCH INS	STRESS PSI		STGR THICK	STGR ELEMENT LENGTH	NX/R PSI	WT/R PCI
270.	5834379.	0.	4815.	1.65	SK	0.112		30400.	UP	0.089	2.31	17.833	0.0000425
					ST	0.37	8.0		BL	0.089	0.93		
					FR	1.01	65.8		DE	0.089	0.93		

(ORTHO 23420. ISO 23652. 21597.)

0.8000E 01 0.1000E 02 0.9000E 01 0.1100E 02 0.7000E 01 0.1100E 02

TABLE A-7 . - ECCENTRICITY EFFECTS — Continued

Nomenclature

① Orthotropic analysis, theoretical load capability, lb/in.

② Isotropic analysis, outside stiffeners, theoretical load capability, lb/in.

③ Isotropic analysis, inside stiffeners, theoretical load capability, lb/in.

④ Longitudinal buckle half-waves, orthotropic analysis

⑤ Circumferential buckle half-waves, orthotropic analysis

⑥ Longitudinal buckle half-waves, isotropic analysis, outside stiffeners

⑦ Circumferential buckle half-waves, isotropic analysis, outside stiffeners

⑧ Longitudinal buckle half-waves, isotropic analysis, inside stiffeners

⑨ Circumferential buckle half-waves, isotropic analysis, inside stiffeners

TABLE A-8. - MEMBRANE BULKHEAD PRINTOUT

CONSTRUCTION - ELLIPTICAL DOME BULKHEAD

MATERIAL - ALUMINUM A

YIELD STRESS	65000.0	MATERIAL DENSITY	0.1000	LIMIT LOAD FACTOR	1.1
ULTIMATE STRESS	75000.0	TEMPERATURE	-300.0000	ULT LOAD FACTOR	1.4
YOUNGS MODULUS	10600000.0	MIN SKIN THICKNESS	0.0100		

MAJOR RADIUS	MINOR RADIUS	NET PRESSURE	BULKHEAD SKIN THICKNESS EQUATOR	MID-POINT	APEX	WEIGHT
110.0	77.9	35.0	0.0508	0.0374	0.0359	250.4
110.0	77.8	50.0	0.0726	0.0534	0.0513	357.7
110.0	77.8	80.0	0.1161	0.0855	0.0821	572.3
130.0	91.9	35.0	0.0600	0.0442	0.0425	413.3
130.0	91.9	50.0	0.0858	0.0631	0.0606	590.4
130.0	91.9	80.0	0.1372	0.1010	0.0970	944.7
160.0	113.1	35.0	0.0739	0.0544	0.0523	770.6
160.0	113.1	50.0	0.1056	0.0777	0.0746	1100.8
160.0	113.1	80.0	0.1689	0.1243	0.1194	1761.3
198.0	140.0	35.0	0.0915	0.0673	0.0647	1460.2
198.0	140.0	50.0	0.1307	0.0962	0.0924	2086.0
198.0	140.0	80.0	0.2090	0.1539	0.1478	3337.7
270.0	191.0	35.0	0.1247	0.0918	0.0882	3702.7
270.0	191.0	50.0	0.1782	0.1311	0.1260	5289.5
270.0	191.0	80.0	0.2851	0.2098	0.2015	8463.3
320.0	226.3	35.0	0.1478	0.1088	0.1045	6164.2
320.0	226.3	50.0	0.2112	0.1554	0.1493	8806.0
320.0	226.3	80.0	0.3378	0.2487	0.2389	14099.6
324.0	229.1	35.0	0.1497	0.1102	0.1058	6398.2
324.0	229.1	50.0	0.2138	0.1574	0.1512	9140.3
324.0	229.1	80.0	0.3421	0.2518	0.2418	14624.5

TABLE A-8. - MEMBRANE BULKHEAD PRINTOUT - Continued

CONSTRUCTION - OBLATE SPHEROIDAL BULKHEAD

MATERIAL - ALUMINUM A

YIELD STRESS	65000.0	MATERIAL DENSITY	0.1000	LIMIT LOAD FACTOR	1.1
ULTIMATE STRESS	75000.0	TEMPERATURE	-300.0000	ULT LOAD FACTOR	1.4
YOUNGS MODULUS	10600000.0	MIN SKIN THICKNESS	0.0100		

MAJOR RADIUS	DOME INDEX	INTERNAL PRESSURE	BULKHEAD SKIN THICKNESS EQUATOR	MID-POINT	APEX	WEIGHT
110.0	1.0	35.0	0.0359	0.0463	0.0512	278.7
110.0	1.0	50.0	0.0513	0.0662	0.0732	398.1
110.0	1.0	80.0	0.0821	0.1059	0.1171	637.0
130.0	1.0	35.0	0.0425	0.0548	0.0605	460.0
130.0	1.0	50.0	0.0607	0.0782	0.0865	657.1
130.0	1.0	80.0	0.0971	0.1251	0.1384	1051.4
160.0	1.0	35.0	0.0523	0.0674	0.0745	857.6
160.0	1.0	50.0	0.0747	0.0963	0.1065	1225.1
160.0	1.0	80.0	0.1195	0.1540	0.1703	1960.2
198.0	1.0	35.0	0.0647	0.0834	0.0922	1625.2
198.0	1.0	50.0	0.0924	0.1191	0.1317	2321.7
198.0	1.0	80.0	0.1478	0.1906	0.2108	3714.7
270.0	1.0	35.0	0.0882	0.1137	0.1258	4121.0
270.0	1.0	50.0	0.1260	0.1625	0.1797	5887.1
270.0	1.0	80.0	0.2016	0.2599	0.2874	9419.4
320.0	1.0	35.0	0.1045	0.1348	0.1490	6860.6
320.0	1.0	50.0	0.1493	0.1925	0.2129	9800.8
320.0	1.0	80.0	0.2389	0.3081	0.3407	15681.3
324.0	1.0	35.0	0.1058	0.1365	0.1509	7121.1
324.0	1.0	50.0	0.1512	0.1949	0.2156	10173.0
324.0	1.0	80.0	0.2419	0.3119	0.3449	16276.8

TABLE A-8. - MEMBRANE BULKHEAD PRINTOUT - Continued

CONSTRUCTION - SEMI-TOROIDAL BULKHEAD

MATERIAL - ALUMINUM B

YIELD STRESS	70000.0	MATERIAL DENSITY	0.1000	LIMIT LOAD FACTOR	1.1
ULTIMATE STRESS	80000.0	TEMPERATURE	-300.0000	ULT LOAD FACTOR	1.4
YOUNGS MODULUS	10600000.0	MIN SKIN THICKNESS	0.0100		

MAJOR RADIUS	MAJOR SEMI-AXIS	MINOR SEMI-AXIS	NET PRESSURE	BULKHEAD SKIN THICKNESSES INNER EQUATOR	INNER MID-POINT	APEX	OUTER MID-POINT	OUTER EQUATOR	WEB	WEIGHT
70.7	39.3	27.8	35.0	0.0414	0.0394	0.0295	0.0714	0.1551	0.0167	343.2
70.7	39.3	27.8	50.0	0.0591	0.0563	0.0421	0.0836	0.1827	0.0238	424.0
70.7	39.3	27.8	80.0	0.0946	0.0900	0.0674	0.1121	0.2302	0.0381	581.1
83.6	46.4	32.8	35.0	0.0489	0.0465	0.0348	0.0843	0.1833	0.0197	566.5
83.6	46.4	32.8	50.0	0.0699	0.0665	0.0498	0.0988	0.2159	0.0281	700.0
83.6	46.4	32.8	80.0	0.1118	0.1064	0.0796	0.1325	0.2721	0.0450	959.3
102.9	57.1	40.4	35.0	0.0602	0.0573	0.0429	0.1038	0.2256	0.0242	1056.1
102.9	57.1	40.4	50.0	0.0860	0.0818	0.0612	0.1216	0.2657	0.0346	1304.9
102.9	57.1	40.4	80.0	0.1376	0.1310	0.0980	0.1630	0.3349	0.0554	1788.4
127.3	70.7	50.0	35.0	0.0745	0.0709	0.0531	0.1284	0.2792	0.0300	2001.4
127.3	70.7	50.0	50.0	0.1064	0.1013	0.0758	0.1504	0.3288	0.0428	2473.0
127.3	70.7	50.0	80.0	0.1702	0.1620	0.1213	0.2017	0.4144	0.0685	3389.2
173.6	96.4	68.2	35.0	0.1016	0.0967	0.0723	0.1751	0.3807	0.0409	5075.1
173.6	96.4	68.2	50.0	0.1451	0.1381	0.1034	0.2052	0.4484	0.0584	6270.8
173.6	96.4	68.2	80.0	0.2322	0.2210	0.1654	0.2751	0.5651	0.0934	8594.0
205.7	114.3	80.8	35.0	0.1204	0.1146	0.0857	0.2076	0.4512	0.0484	8448.9
205.7	114.3	80.8	50.0	0.1720	0.1637	0.1225	0.2431	0.5314	0.0692	10439.5
205.7	114.3	80.8	80.0	0.2751	0.2619	0.1960	0.3261	0.6697	0.1107	14307.1
208.3	115.7	81.8	35.0	0.1219	0.1160	0.0868	0.2102	0.4568	0.0490	8769.6
208.3	115.7	81.8	50.0	0.1741	0.1657	0.1240	0.2462	0.5380	0.0701	10835.8
208.3	115.7	81.8	80.0	0.2786	0.2652	0.1984	0.3301	0.6781	0.1121	14850.2

APPENDIX B. PARAMETRIC VEHICLE SYNTHESIS

Overall Synthesis Logic

The computer program for the parametric synthesis of multistage vehicles with recoverable lower stages contains 11 basic subroutines in addition to a main program. Figure B-1 illustrates the simple overlay of these subroutines as compiled in FORTRAN IV on the IBM 7094 computer. Input data are handled by an NAA data-read subroutine (DECRD) to facilitate ease of varying input parameters. The vehicle sizing is similar to that performed in the previous study phase for expendable vehicles (ref. B-1); however, additional analyses are included for the landing phase and for the new thermal regimes encountered by the launch vehicle and recovered stage.

The main program contains an iteration loop that provides convergence of the stage mass fractions for lower and upper stages alike. When a combination of recoverable-expendable stages is considered, the option is provided to iterate on the recoverable stage, this being the more difficult to converge. All subroutines are included in this looping operation, if required for analysis. Execution time for each cycle is approximately one to six seconds. Controls can be inserted to suppress data printout until a vehicle has converged, or each iteration may be printed out. The following paragraphs summarize the principal features of each basic subroutine.

MAIN. - The MAIN subroutine is the principal link in the overlay and includes the data read logic. Input data are read in two blocks: the first (invariant) is reserved for data and coefficients that are typical for a series of program runs; the second (variant) includes all basic sizing and design parameters that bear investigation. Control indicators are set to provide the proper call-up of synthesis subroutines, the printing of desired formats, and the cycling of the iteration loop. This program section contains diagnostic formats which are printed if an error is encountered during execution of any of the subsequent subroutines. This subroutine satisfies the NASA-ERC physical structuring requirement of containing input, bulk data, and control in specific program regions. Due to the complexity of the vehicle being synthesized and the storage limitations of the 7094 system, output formats and print steps are presently positioned as the last item in each synthesis subroutine. Output and common blocks can be readily adapted to NASA standards, if required at some future date.

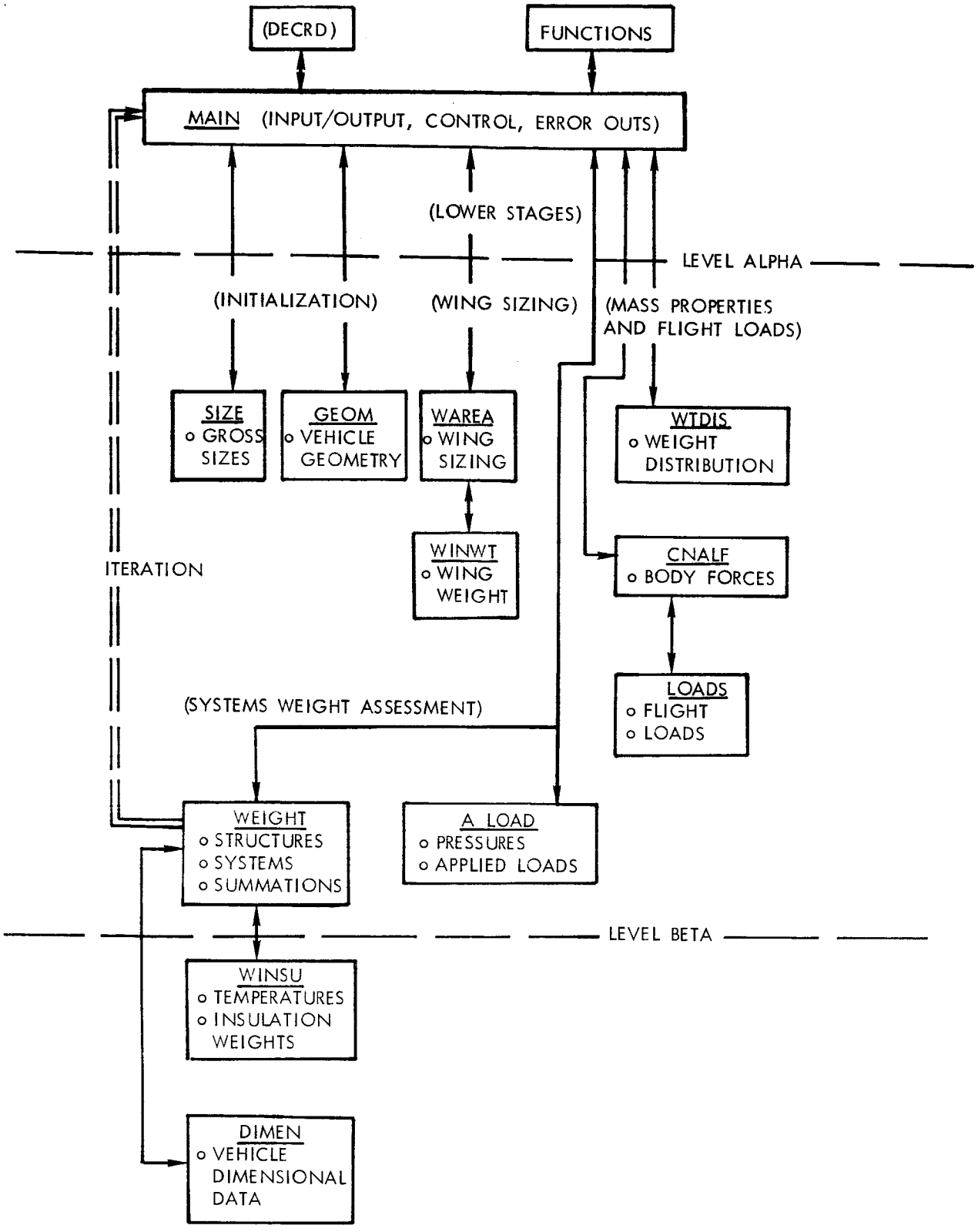

Figure B-1. - Parametric Synthesis Program for Recoverable Lower Stages

SIZE. - The SIZE subroutine contains basic vehicle sizing logic similar to that described in Appendix B of reference B-1. The stage mass fraction is again used as the stage performance index. This mass fraction, which includes the recoverable systems, can be defined as the weight of the launch phase performance propellant divided by the stage weight at burnout during launch plus the launch-phase propellant. In this manner, the same parameter is used for sizing both recoverable and expendable stages. This basic sizing operation is represented as follows:

$$W_{BO} = W_{ST} + W_{SYS} + W_{FUEL}$$

$$W_G = W_{BO} + W_P$$

$$\nu_B = \frac{W_P}{W_G}$$

$$\nu = 1 - \frac{1}{\exp\left(\frac{\Delta V + \Delta V_L}{Ig}\right)}$$

$$\frac{W_{PL}}{W_O} = \left(1 - \frac{\nu}{\nu_B}\right)$$

where

W_{ST} = stage structure weight, including wings and fins

W_{SYS} = stage system weights, including flyback engines and landing gear

W_{FUEL} = fuel for the flyback phase

W_P = stage launch propellant

ΔV = stage performance velocity

ΔV_L = stage velocity losses

I = delivered specific impulse

g = gravity constant

ν = performance mass ratio

ν_B = stage mass fraction

W_{PL} = stage payload weight

W_O = vehicle gross weight at stage ignition

It can be seen from the preceding that sizing can be accomplished in two ways: (1) by inputting a payload weight to minimize lift-off weight, and (2) by inputting gross vehicle weight to maximize payload weight. The above logic is used in a multistage process for a vehicle containing up to four stages. Velocity losses are discussed in the final section of this Appendix.

The SIZE subroutine performs two other basic tasks in using propellant mixture ratio, ullage factor, and density inputs to identify propellant volumes and stage thrust-to-weight ratios, and in using propellant type to estimate main propulsion engine weight. These data are later used to provide a weight distribution for the loads calculation. Table B-1 is a weight performance printout from this subroutine.

GEOM. - The GEOM subroutine defines the basic stage dimensions without the wing and considers each stage independently. Indicators are provided in the main input array to identify basic stage geometry parameters such as fixed stage diameters, bulkhead aspect ratios, and engine parameters. The synthesis operation can establish a stage diameter if none is given as input. Bulkheads can be varied from ellipsoidal to hemispherical. Tankage models can contain a common bulkhead between the two cylindrical tanks or separate bulkheads. Engine geometries are sized using inputs of chamber pressure, number of engines, expansion ratio, and type. A fitting process is utilized to insure that the stage diameters are compatible with the outside diameter of the engine clusters.

Figure B-2 presents a summary diagram of the GEOM subroutine. The crew compartment for the recoverable stage is assumed to be a hemisphere unless the input required volume exceeds this section; in such a case, a cylindrical section is added to the hemisphere to provide room for the additional crew systems. Another option is provided to permit adjustment of the stage fineness ratio to a desired input. The payload is also geometrically sized from input factors for controlling the cylindrical-to-conical-section ratio, and for the half-angle of the conical section. All stages are then added up to provide a total vehicle length.

TABLE B-1. - WEIGHT-PERFORMANCE PRINTOUT FORMAT

CASE 4 REC/EXP 1,63C,CCC THRUST

WEIGHT PERFORMANCE CHARACTERISTICS

STAGE	1	2
WEIGHT (LB)		
PAYLOAD	339212.	58528.
BURN-OUT	133664.	30492.
STRUCTURE/SUBSYSTEMS	111764.	23296.
ENGINES	21900.	7196.
PROPELLANT	831124.	250192.
STAGE	964788.	280684.
RATIOS		
PERFORMANCE	0.63736	0.73757
MASS FRACTION	0.86146	0.89137
DELTA VELOCITY (FPS)	10060.	19815.
SPECIFIC IMPULSE (SEC)	308.	460.

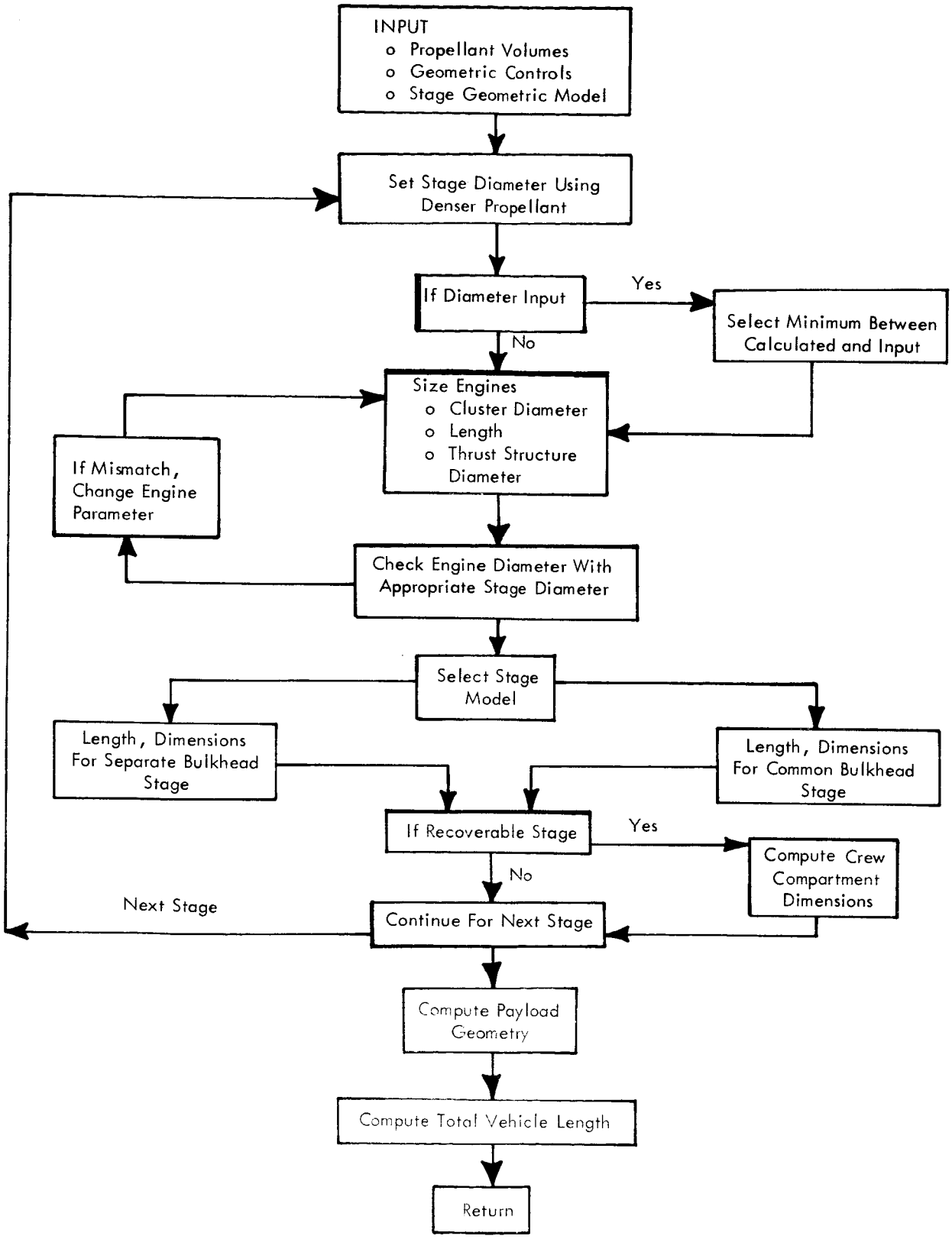

Figure B-2. - GEOM Subroutine Logic Diagram

WAREA. - The next step in the synthesis process applies only to recoverable vehicles and is by-passed for expendable stages. This region includes two steps: the first, to size the wing to launch-entry-landing environments, and the second, to weigh the wing in the WINWT subroutine. The wing sizing is discussed in detail in the Wing Sizing Aerodynamics of this Appendix.

The WAREA subroutine uses stage burnout weight and input range, lift-to-drag, and specific fuel consumption values to determine the amount of fuel required for flyback. Lift-to-drag and flyback engine thrust-to-weight ratio are used to weigh the flyback engines. Centers of gravity are then determined for the flyback condition with the flyback fuel aboard. The next step calculates both required wing area and exposed wing area, using V_{STALL}, $C_{L\alpha}$, L, and α_{TD} parameters (see Wing Sizing Aerodynamics, this Appendix).

This wing area is used, along with aspect ratios and sweep angles, to calculate the root and tip chord dimensions for the wing. The program assumes that the trailing edge of the wing joins the tank fuselage at the aft ring on the aft skirt. Root dimensions are checked against stage length center of pressure, and checked with stage center of gravity. If resizing is required, the subroutine, depending upon input options, can alter sweep angle and aspect ratio to design a better wing geometry. Stops are provided in the subroutine to print suggestions as to input changes required to make the wing acceptable if internal variations are not effective.

Table B-2 shows the basic wing sizing options that are available. In all conditions, a maximum sweep angle and aspect ratio are input to provide stops in the logic. Output data from this subroutine are illustrated in table B-3.

WINWT. - The wing weight subroutine, WINWT, is called from the wing sizing subroutine (WAREA). This subroutine first refines the wing geometry, checking the fuselage geometry for feasible attachment points for the forward and aft spar. The main wing box is not permitted to cycle below 50 percent of the root chord. Both inboard and outboard stations are set, and the sweep angles for the spars, fifty-percent chord, and trailing edge are computed. Figure B-3 presents a summary diagram of the logic contained in this subroutine. The wing is weighed for both the launch and entry loading conditions, with the critical design weights saved. Input material allowables are associated with an insulation subroutine (WINSU) which can be called later, if required. A sample output format from WINWT is shown in table B-4.

TABLE B-2. - WING SIZING OPTIONS

Condition	Sizing Options		
	Free	Fixed 1	Fixed 2
INPUT			
V_{Stall}	X	X	X
α_{TD}	X	X	X
$C_{L\alpha}$	X	X	X
Aspect ratio		X	X
Sweep angle		X	-
Maximums			
Aspect ratio	X	X	X
Sweep angle	X	X	X
Taper ratio	-	-	X
OUTPUT			
Sweep angle	-	-	X
Taper ratio	X	X	-

WTDIS. - The weight distribution subroutine, WTDIS, per figure B-1, is used to define loads stations on the vehicle and distributed weights for these stations for prelaunch, maximum dynamic pressure, and stage-one end boost flight regimes. Figure B-4 illustrates the basic loads stations (seven per stage for a recoverable stage, six per stage for an expendable vehicle). The weight of the element above the station is considered for each flight condition. Structural shell and bulkhead weights are distributed in a linear fashion, with the wing sections being assigned to their respective elements. Propellant in the first stage for the maximum dynamic pressure condition is

TABLE B-3. - WING AND FLYBACK SIZING PARAMETERS OUTPUT FORMAT

CASE 4 REC/EXP 1,63C,CCC THRLST

WING AND FLYBACK SIZING PARAMETERS

STAGE	1
WEIGHT (LB)	
FLYBACK FUEL	15340.
FLYBACK ENGINES	10080.
LANDING VEHICLE	118324.
CENTERS OF GRAVITY (IN FROM NOSE)	
BURNOUT STAGE	359.
ENGINE	815.
BURNOUT STAGE LESS ENGINE	270.
LIFT CURVE SLOPE	
WING	0.02667
LANDING	0.04000
WING PRIME	0.04796
ASPECT RATIO	2.25000
TAPER RATIO	0.45000
WING SPAN (IN)	782.
WING ROOT CHORD (IN)	479.
WING THICK/CHORD RATIO	0.08000
STAGE LENGTH (IN)	916.
TOUCH DOWN ANGLE (DEG)	15.
TOUCH DOWN SPEED (KNOTS)	150.

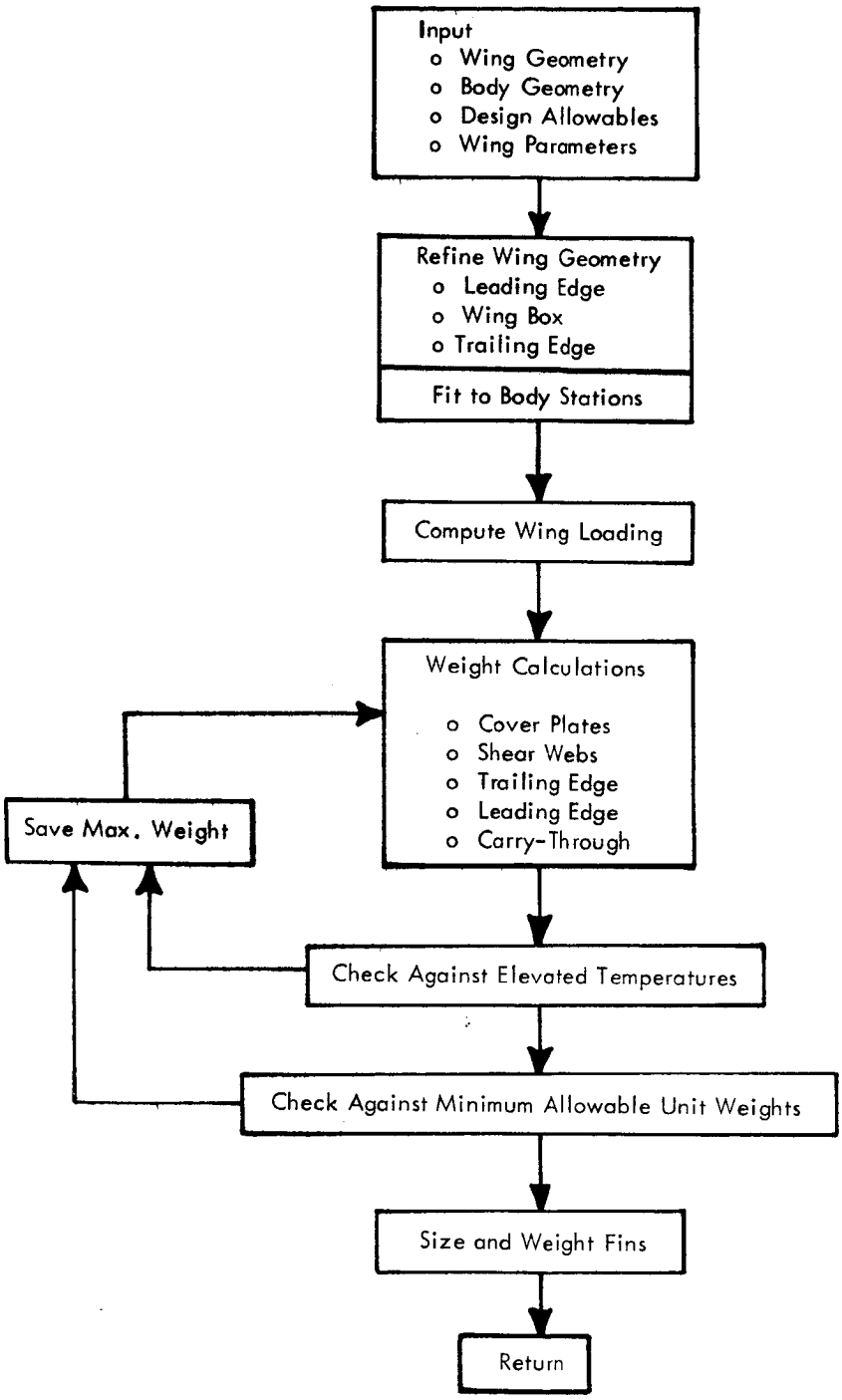

Figure B-3. - WINWT Subroutine Logic Diagram

TABLE B-4. - WING WEIGHT PRINTOUT FORMAT

CASE 4 REC/EXP 1,63C,COC THRUST

WING DIMENSIONS, ANGLES, AND WEIGHTS

STAGE	1
DIMENSIONS (IN)	
ROOT	479.
TIP	216.
SPAN	782.
SWEEP ANGLES (DEGREES)	
LEADING EDGE	60.
FRONT SPAR	58.
AFT SPAR	50.
TRAILING EDGE	47.
FIFTY PERCENT CHORD	54.
WEIGHT (LB)	
COVER PLATES	58C8.
SHEAR WEBS	3172.
LEADING EDGE	1085.
TRAILING EDGE	1809.
FINS	12C8.
CARRY-THROUGH	620.
TOTAL WING	13702.
WING AREA (SQ FT)	1885.
WING LOADING (LB SQ FT)	115.20000
VERTICAL SURFACES	
HEIGHT (IN)	50.
ROOT CHORD (IN)	216.
TOTAL FIN AREA (SQ FT)	151.
AREAS (SQ FT)	
LEADING EDGE	362.
WING BOX	1162.
TRAILING EDGE	362.

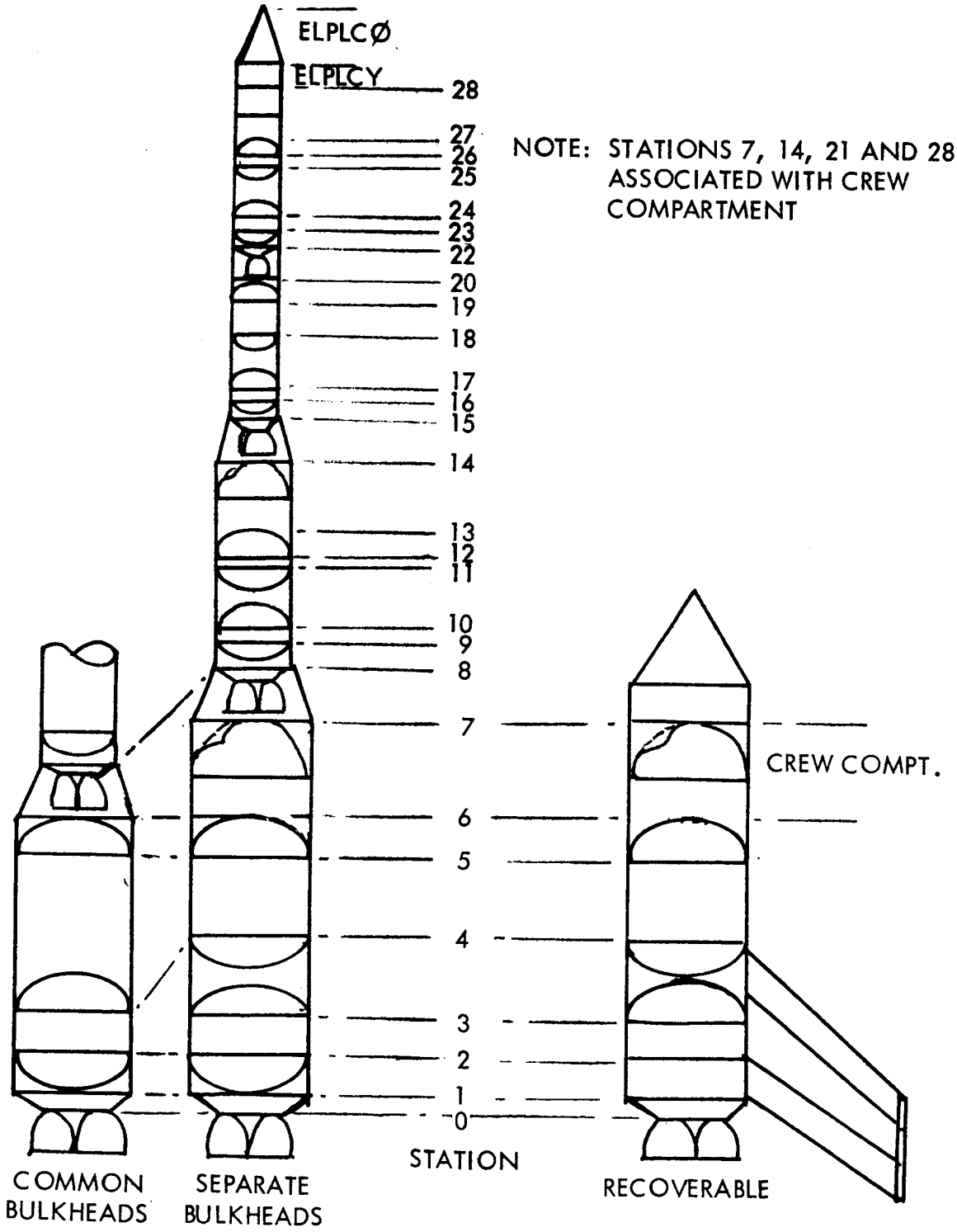

Figure B-4. - Basic Loads Stations

analyzed for each element. Table B-5 presents a typical printout from this subroutine. It should be noted that weights are carried in pounds per section rather than pounds per inch, and that this section weight is identified with a lower and upper station and with the center of gravity of the section mass at the particular flight condition.

CNALF. - A rather simple subroutine, CNALF, is provided to compute normal forces on the body elements using inputs of α, $C_{N\alpha}$ and q, and the vehicle geometry and exposed area. This subroutine, at a later date, will be used for a more complete assessment of body forces (see Loading Environment section of this Appendix).

LOADS. - The LOADS subroutine is called from the CNALF subroutine and is used to compute external loads at all body stations for the prelaunch, maximum dynamic pressure, and end boost flight conditions. A complete description of this technique may be found in the loading environment section. The subroutine is separated into sections to compute prelaunch wind velocities at the body stations; wind forces on the body and wings; forces on the payload; and body station shear, bending moment, and axial load values for all three flight conditions, using distributions from WTDIS. Included in these analyses are calculations of in-flight center of pressure, pitch moments of inertia, lateral acceleration distribution, total vehicle drag, and axial forces producing acceleration. The loads matrix is printed out as in Table B-6 and transferred to COMMON for use later on.

ALOAD. - The applied load subroutine, ALOAD, also includes an analysis of the vehicle pressure schedule using input ullage pressures. Figure B-5 presents a diagram of the logic contained in this subroutine. A typical pressure schedule printout is shown in table B-7. This subroutine computes hoop tension, tension, and compression loads for each pertinent station and for each of the three trajectory points, then searches the N_x matrix and identifies the maximum ultimate applied load for each body station, identifying these for both pressurized and unpressurized components. Final selected applied load values are stored in COMMON as more generalized values by dividing each by its station radius (N_x/R).

WEIGHT. - The WEIGHT subroutine evaluates the vehicle shell, bulkhead, and subsystem weights, organizes weight statements for the synthesized vehicle, calls in the insulation subroutine WINSU, if required, and calls in a subroutine which itemizes and prints out all vehicle dimensions.

Generalized curves for unit weight per radius (N_x/R) versus applied load per radius are stored in the variant bulk data section of the program. These curves cover the basepoint structure for both pressurized and

TABLE B-5. - WEIGHT DISTRIBUTION PRINTOUT

CASE 4 REC/EXP 1,63C,CCC THRLST

WEIGHT DISTRIBUTION
WEIGHT IN LB -- STATION IN INCHES FROM STAGE ONE ENGINE EXIT
NUMBER OF STAGES = 2

		PRELAUNCH		MAX Q ALPHA		END BOOST	
STATION	DIA	WEIGHT	STATION	WEIGHT	STATION	WEIGHT	STATION
173.	26C.	24669.	121.	24669.	121.	24669.	121.
265.	26C.	138C21.	219.	138021.	219.	13415.	219.
325.	26C.	91270.	295.	50071.	295.	8871.	295.
525.	26C.	3C5759.	425.	170582.	425.	35405.	425.
694.	26C.	245436.	609.	130857.	6C9.	16278.	6C9.
786.	26C.	133457.	740.	8851.	740.	8851.	740.
916.	26C.	15516.	851.	15516.	851.	15516.	851.
1C46.	22C.	19776.	994.	19776.	994.	19776.	994.
1124.	22C.	29800.	1085.	29800.	1085.	29800.	1085.
1177.	22C.	20148.	1151.	20148.	1151.	20148.	1151.
1255.	22C.	29800.	1216.	29800.	1216.	29800.	1216.
1681.	22C.	163307.	1468.	163307.	1468.	163307.	1468.
1759.	22C.	29800.	1720.	29800.	1720.	29800.	1720.
1759.	22C.	0.	1720.	0.	1720.	C.	1720.
2C26.	22C.	58528.	1861.	58528.	1861.	58528.	1861.
TOTAL WEIGHT		13C5285.		911623.		496C62.	
CENTER OF GRAVITY		739.		805.		1142.	

TABLE B-6. - LOADS MATRIX PRINTOUT

CASE 4 REC/EXP 1,630,000 THRUST

LOADS MATRIX
BENDING MOMENT IN IN/LB
SHEAR IN IN/LB
AXIAL LOAD IN LB
NUMBER OF STAGES = 2

	PRELAUNCH			MAX Q ALPHA			END BOOST		
STATION	MOMENT	SHEAR	AXIAL	MOMENT	SHEAR	AXIAL	MOMENT	SHEAR	AXIAL
173.	20353643.	41116.	1280616.	-1331087.	28080.	1632786.	-325856.	8368.	1626279.
265.	16781123.	36600.	1142596.	-4025944.	30543.	1372673.	-374738.	6873.	1577743.
325.	14704884.	31701.	1051325.	-5531863.	18996.	1262760.	-764381.	5945.	1545648.
525.	9994618.	15525.	745566.	-6424.	-74396.	820737.	-1622420.	2658.	1417553.
694.	7468299.	14358.	500130.	9034704.	-32549.	623514.	-1966865.	1417.	1358659.
786.	6225824.	12671.	366673.	11897096.	-29719.	610174.	-2070856.	846.	1326635.
916.	4683638.	11055.	351157.	15438018.	-24757.	586790.	-2125819.	-0.	1270498.
1046.	3298506.	10146.	331382.	18834883.	-25973.	549445.	-2082826.	-823.	1198950.
1124.	2533534.	9520.	301582.	20484723.	-16443.	504532.	-1980147.	-1817.	1091133.
1177.	2057432.	8583.	281434.	21180135.	-10000.	474166.	-1869990.	-2371.	1018238.
1255.	1593035.	3356.	251634.	21587396.	-470.	429253.	-1660423.	-3016.	910421.
1681.	386000.	2307.	88327.	10655852.	51754.	183124.	-411567.	-2843.	319572.
1759.	206550.	2307.	58528.	6259079.	61283.	138211.	-217985.	-2134.	211755.
1759.	206550.	2307.	58528.	6259079.	61283.	138211.	-217985.	-2134.	211755.

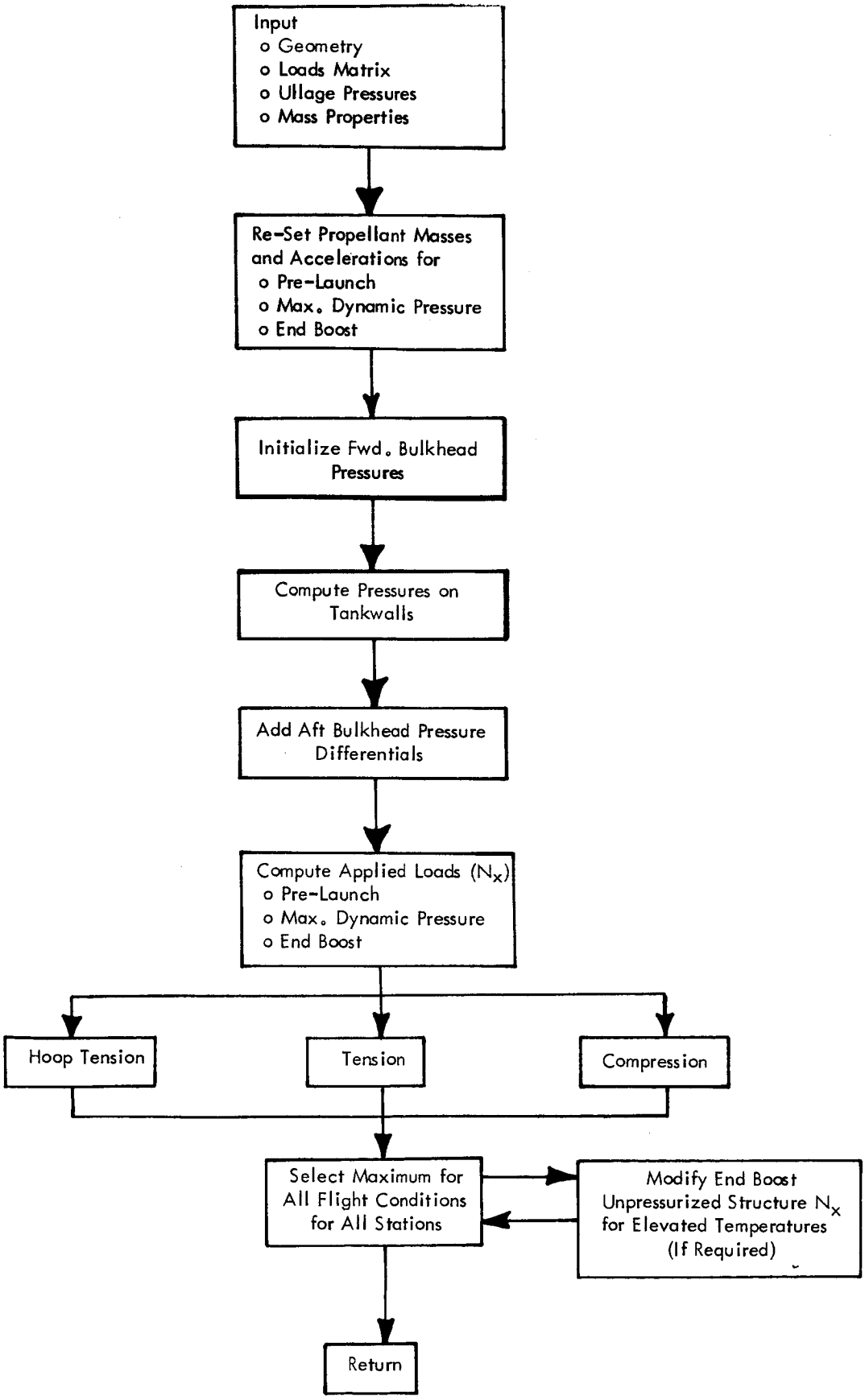

Figure B-5. - ALOAD Subroutine Logic Diagram

TABLE B-7. - PRESSURE MATRIX PRINTOUT

CASE 4 REC/EXP 1,63C,0C0 THRUST
PRESSURE MATRIX (PSI)

	PRELAUNCH	MAX Q ALPHA	END BOOST
STAGE 1			
AFT TANK	6.3	39.0	39.0
FWD TANK	7.6	39.0	39.0
AFT BULKHEAD		45.8	
FWD BULKHEAD		39.0	39.0
AFT TANK FWD BULKHEAD		39.0	39.0
FWD TANK AFT BULKHEAD		43.8	
STAGE 2			
AFT TANK	5.4	45.7	55.5
FWD TANK	1.5	38.7	41.4
AFT BULKHEAD			61.2
FWD BULKHEAD		36.0	36.0
AFT TANK FWD BULKHEAD		36.0	36.0
FWD TANK AFT BULKHEAD			0.0

shells. Specific thermal properties and pressure loads are considered in these curves. Vehicle sizing is efficiently accomplished by inserting the proper curve for the case in question. The curves are scanned, and the proper weights are selected for each body station. Shell areas are then computed for all shell sections and structural component weights identified. Special additional weight assessments are included for frustums. End attachment rings are included in the tank wall weights.

Bulkhead weights are computed in a similar manner to that used in reference B-1. Using input weight and area coefficients (figs. B-6 and B-7), the bulkheads are weighted as follows:

$$\text{Weight Forward Bulkhead} = \frac{\rho P_u C_{10} \pi r^3 K_8 F_s}{F_{t_u}}$$

$$\text{Weight Aft Bulkhead} = \frac{1.5\, P_T r^2}{2h\, F_{t_u}} \rho C_{11} r^2 K_8 F_s$$

where

ρ = material density

P_u = ullage pressure

C_{10} = weight coefficient (see fig. B-6)

r = tank radius

F_{t_u} = ultimate tensile strength

P_T = maximum average pressure on aft bulkhead

h = aft bulkhead height

C_{11} = aft bulkhead area coefficient (see fig. B-7)

K_8 = adjustment factor

F_s = safety factor

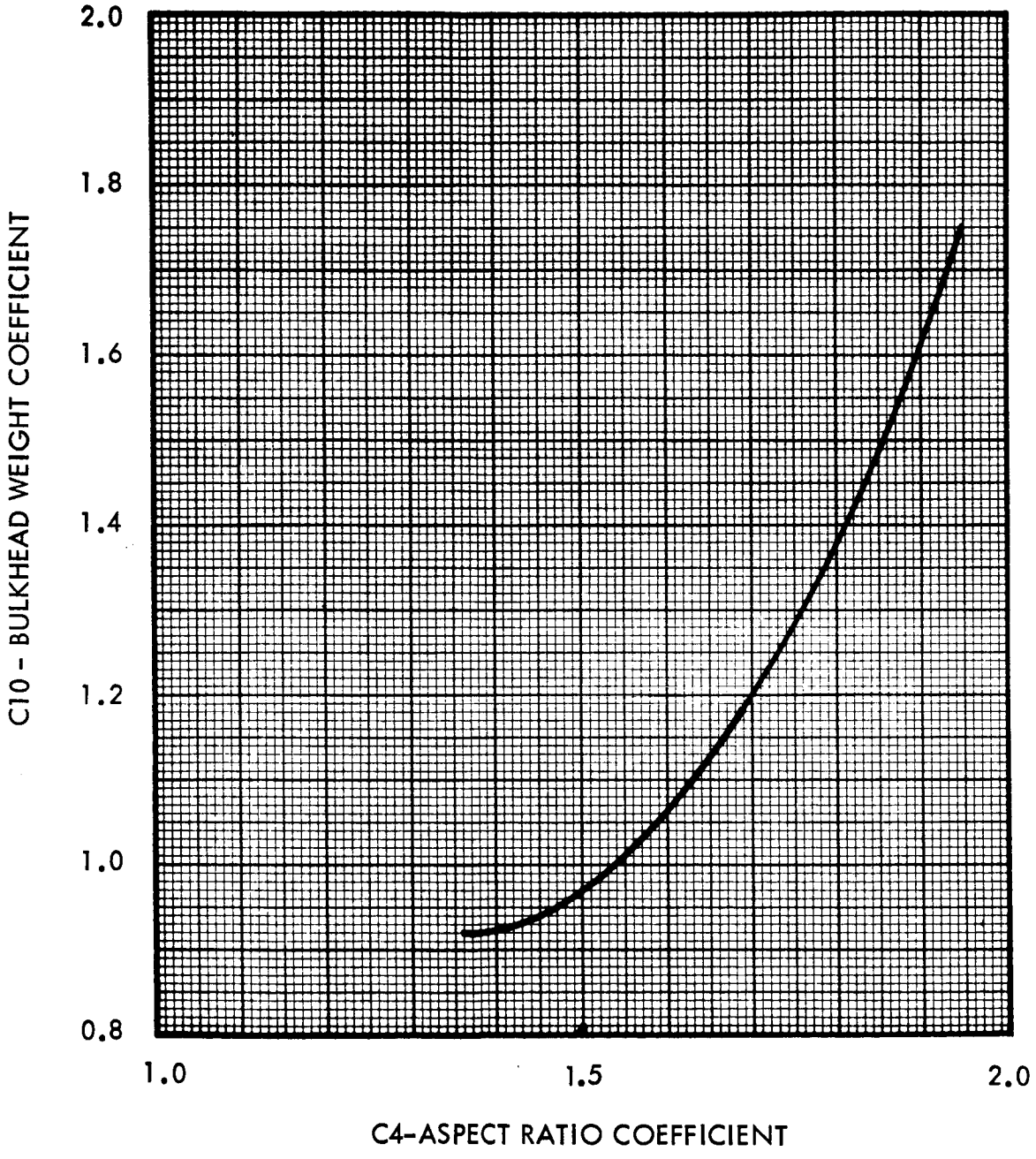

Figure B-6. - Bulkhead Weight Coefficients

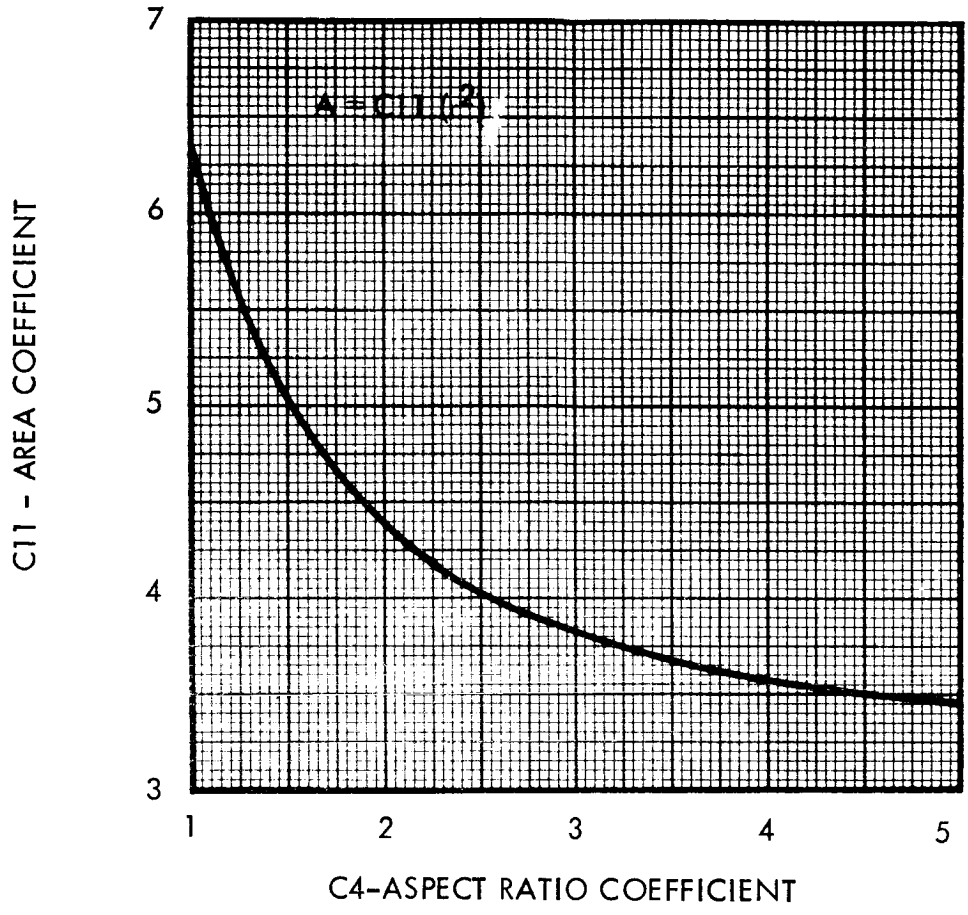

Figure B-7. - Bulkhead Area Coefficients

In the case of a common bulkhead tankage configuration, the common bulkhead weight results from a differential pressure design and an adjustment which separates the bulkhead into two membrane faces and inserts a sandwich between the membranes.

Generalized equations are included in the subroutine to weigh thrust structures, separation systems, thrust vector control systems, ullage systems, propellant feed and pressurization systems, fixed equipment, residual and reserve propellants, and to include stage weight contingencies. If the lower stage is recoverable, the subroutine calls WINSU which provides insulation weights for both body and wing. Landing gear for the recoverable stage is assessed at approximately 3-1/2 percent of the launched weight. All weight-scaling equations contain adjustment factors which are stowed in the invariant bulk data section of the program.

When the vehicle has been completely weighed out, mass fractions are determined for the designed stages. These stage indices are transferred to the main program to compare against initial sizing values, and the program is iterated until convergence is reached. When convergence of the stage mass fraction is achieved, a print indicator is set, and the program is recycled to print all formats. Figure B-8 summarizes the steps included in the WEIGHT subroutine, and table B-8 shows output format.

WINSU. - The WINSU subroutine provides a thermal map and insulation weight assessment based upon input stagnation temperatures, insulation unit weight curves, and the geometry of the recoverable stage. A maximum allowable temperature for both the body and wing are input to the program; if these values are exceeded, a diagnostic is printed. The maximum temperature that the body and wing material can take without insulation is defined in the program. If body or wing temperatures are below this value, no insulation is provided. Body and wing section temperatures, insulation unit weights, and component insulations are printed in a format (see table B-9). A complete discussion of this thermal analysis technique can be found in the Structural Weight of Shells section of this Appendix.

DIMEN. - The dimensional subroutine, DIMEN, is called up only after complete convergence, and it is included in the program to more completely define the total vehicle geometry. The previous phase of this study used a similar subroutine, but without the crew compartment or wing dimensions. In reference B-1, automated graphics illustrations were output by calling up NAA Computer Aided Design graphics packages from this region. This capability for recoverable stages is in work at NAA, but is not included as a part of this study. Profile sketches were drawn from the type of data shown in table B-10.

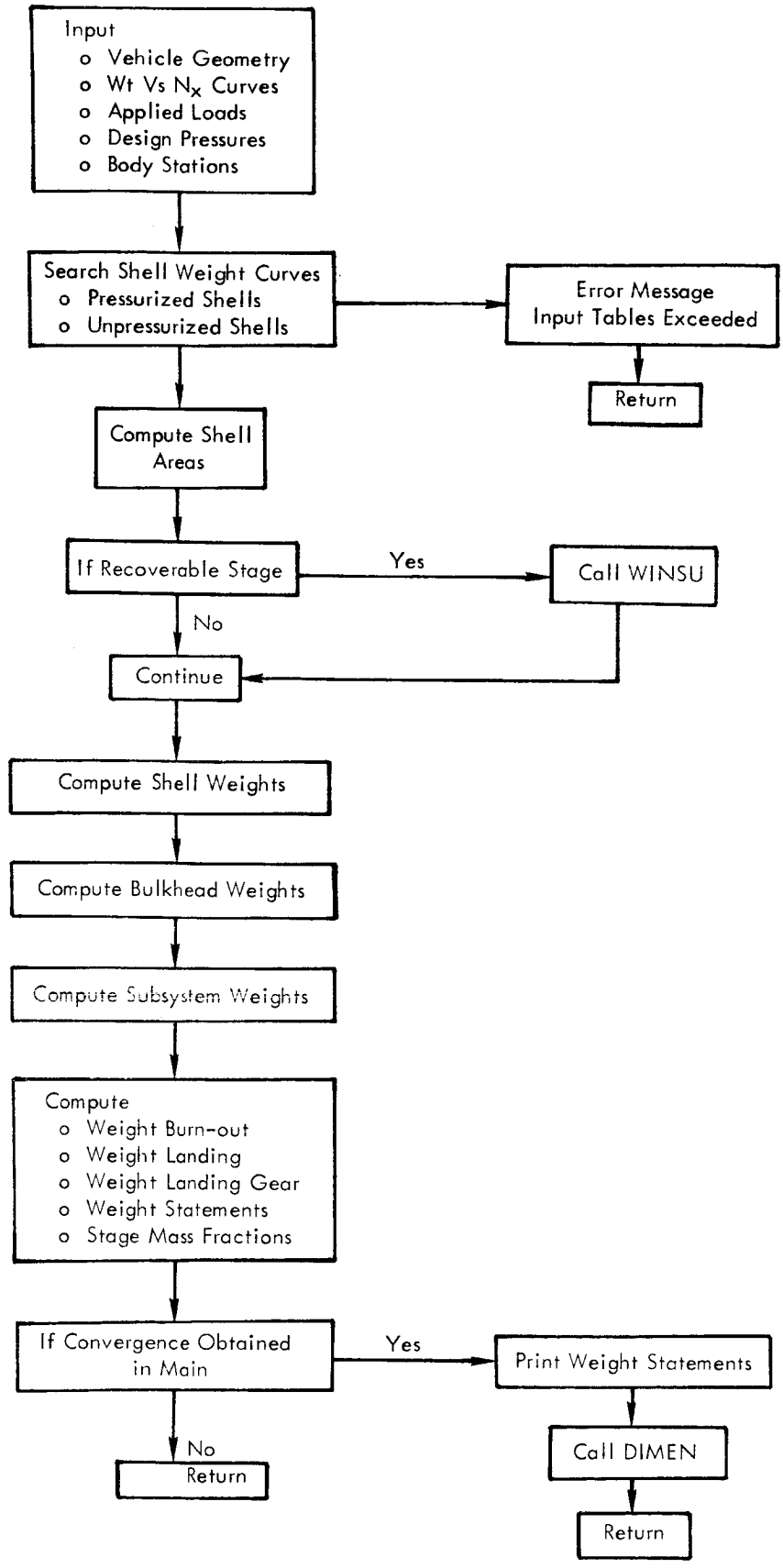

Figure B-8. - WEIGHT Subroutine Logic Diagram

TABLE B-8. - VEHICLE AND STAGE WEIGHTS PRINTOUT

CASE 4 REC/EXP 1,63C,CCC THRUST

VEHICLE AND STAGE WEIGHTS (LB)

STAGE	1	2
SHELL STRUCTURES		
CREW COMPARTMENT	2513.	0.
INTERSTAGE	2495.	0.
FWD SKIRT	1787.	818.
FWD BULKHEAD	910.	509.
FWD TANKWALL	2783.	4833.
INTER BULKHEAD	1893.	916.
CENTER SECTION	4001.	0.
INTER AFT BULKHEAD	910.	0.
AFT TANKWALL	1234.	698.
AFT BULKHEAD	1980.	1603.
AFT SKIRT	1869.	1075.
THRUST STRUCTURE	5913.	1554.
SHELL INSULATION	3915.	0.
SUBSYSTEMS		
ENGINES	21900.	7196.
PROPELLANT/PRESS SYSTEM	7439.	2581.
ULLAGE SYSTEM	0.	1076.
SEPARATION SYSTEM	1064.	280.
TVC SYSTEM	2944.	535.
FIXED EQUIPMENT	3203.	2492.
RESIDUAL PROP/GASES	12766.	3130.
CONTINGENCY	3324.	1251.
RECOVERY PROVISIONS		
CREW SYSTEMS	3000.	0.
WING	13702.	0.
FLYBACK ENGINES	10080.	0.
WING INSULATION	1926.	0.
LANDING GEAR	4599.	0.
FLYBACK FUEL	15340.	0.
BURNOUT	133492.	30548.
PROPELLANT	831124.	250192.
STAGE GROSS	964616.	280740.
PAYLOAD	339268.	58528.
VEHICLE GROSS	1303884.	339268.
LANDING CONDITION	118152.	0.
STAGE MASS FRACTION	0.8616	0.8912
PERFORMANCE RATIO	0.6374	0.7376
STAGE VELOCITY	10060.0000	19815.0000

TABLE B-9. - INSULATION DATA PRINTOUT

CASE 4 REC/EXP 1',63C,CCC THRLST

INSULATION DATA FOR RECOVERABLE STAGE 1

UNIT WEIGHT ON BODY (LB/SC IN)

COMPONENT	UNIT WEIGHT	DESIGN TEMP (R)
CREW COMPT	C.CC66	1923.9818
FWD SKIRT	C.C065	1873.2104
FWD TANKWALL	C.CC64	1820.9094
CENTER SECTION	C.CC64	1783.7641
AFT TANKWALL	C.CC64	1775.0453
AFT SKIRT	C.CC63	1763.3644

UNIT WEIGHT ON WING (LB/SC IN)

COMPONENT	UNIT WEIGHT	DESIGN TEMP (R)
LEADING EDGE	C.CC69	2026.6322
WING BOX	C.CC65	1866.0703
TRAILING EDGE	C.CC64	1811.6187
FIN	C.C065	1866.0703

COMPONENT INS WEIGHT

COMPONENT	WEIGHT (LB)
CREW COMPT	7C5.9212
FWD SKIRT	491.6116
FWD TANKWALL	889.6578
CENTER SECTION	1C37.4919
AFT TANKWALL	315.3426
AFT SKIRT	475.1135
TOTAL BODY INS	3915.1386
LEADING EDGE	357.C118
WING BOX	1C92.7211
TRAILING EDGE	334.61C1
FIN	141.863C
TOTAL WING INS	1926.2C6C

TABLE B-10. - VEHICLE GEOMETRY DATA FOR PROFILE DRAWINGS

PAYLOAD		VEHICLE GEOMETRY STAGE 4		STAGE 3		STAGE 2		STAGE 1	
DIAMETERS (INCHES)									
D5C5	22C.	D5C5	22C.	D405	0.	D305	0.	D205	22C.
D52C	C.	D425	C.	D325	0.	D225	220.	D125	26C.
D525	22C.	D415	0.	D315	0.	D215	220.	D115	26C.
		D414	C.	D314	0.	D214	0.	D114	1042.
		D412	C.	D312	0.	D212	0.	D112	1042.
		D41C	0.	D310	0.	D210	92.	D110	135.
		D4C5	C.	D305	0.	D205	220.	D105	26C.
		D4C1	0.	D301	0.	D201	260.	D101	26C.
		DEC4	C.	DEC3	0.	DEC2	138.	DEC1	204.
BODY STATIONS (INCHES FROM X1C1)									
X55C	2C25.9	X5C5	1758.8	X405	0.0	X305	0.0	X205	1046.5
		X455	C.C	X355	0.0	X255	0.0	X155	915.8
X525	1868.8	X45C	C.C	X350	0.0	X250	1758.8	X150	785.8
X5C5	1758.8	X445	C.C	X345	0.0	X245	1681.0	X145	693.9
		X44C	C.0	X340	0.0	X240	1681.0	X140	693.9
				X339	0.0	X239	0.0	X139	C.0
				X338	0.0	X238	0.0	X138	C.0
		X437	C.C	X337	0.0	X237	0.0	X137	651.7
		X436	C.C	X336	0.0	X236	1254.7	X136	C.0
		X435	C.C	X335	0.0	X235	1176.9	X135	C.0
		X434	C.0	X334	0.0	X234	0.0	X134	524.8
		X433	0.0	X333	0.0	X233	0.0	X133	432.9
		X432	C.C	X332	0.0	X232	0.0	X132	417.3
		X431	C.0	X331	0.0	X231	0.0	X131	325.3
		X43C	C.C	X330	0.0	X230	0.0	X130	C.0
		X426	C.0	X326	C.0	X226	0.0	X126	C.0
		X425	C.0	X325	0.0	X225	1124.3	X125	264.5
		X42C	C.C	X320	0.0	X220	1124.3	X120	264.5
		X415	C.C	X315	0.0	X215	1085.4	X115	218.6
		X414	C.C	X314	0.0	X214	0.0	X114	-25.0
		X413	C.C	X313	0.0	X213	0.0	X113	172.6
		X412	C.C	X312	0.0	X212	0.0	X112	-240.6
		X411	C.C	X311	0.0	X211	1046.5	X111	172.6
		X41C	0.C	X310	0.0	X210	1026.5	X11C	143.8
		X4C5	C.0	X305	0.0	X205	1046.5	X105	172.6
		X4C1	C.0	X301	0.0	X201	926.8	X101	0.0

Flyback Propulsion System Requirements and Weights

One of the smaller subroutines in the parametric synthesis for recoverable vehicle systems assessed and evaluated the weight penalties associated with the propellant weight for the flyback cruise portion of the recovery mode.

In order to conduct a meaningful comparison between expendable and recoverable orbital launching systems, it was essential to evaluate the weight associated with the first stage flyback system. The flyback system is defined as encompassing the weight of the flyback fuel and installed engines required to cruise the vehicle a fixed number of miles. The need for this added flyback system results from the fact that, normally, the first stage burns out at suborbital altitudes and velocities and does not have the range capability from these altitudes for a power-off glide to the specified landing site. If flyback to a particular site is not mandatory, this system may not be required.

For purposes of this study, an evaluation of flyback system weights was limited to a consideration of the independent systems required by rocket-propelled, vertically launched vehicles and a specified flyback range. The weight of the wings and associated recovery equipment was excluded from the flyback system, since this weight is required to provide recovery capability independent of flyback range. The wing and recovery weights are calculated in the synthesis program by additional subroutines.

The weights used for fuel and engines are representative of propulsion systems burning specified fuel for the state of the art during various time periods. The weights given for the engines include engine-installation weight and inlet weight for both supersonic and subsonic cruise. For the type of designs being considered, it appears because of practical handling purposes that a subsonic cruise is favored. The developed approach is meaningful for both subsonic and supersonic cruise fuel requirements.

The lift-to-drag ratios selected as a function of Mach number are obtainable for the particular configuration, and are values which should be obtainable with reasonable aerodynamic design techniques. For vehicles using the storable propellant combination, this assumption is not valid, since flyback engines would not utilize these propellants. However, the effect on establishing vehicle propellant fractions and mass ratios is small; hence, the error introduced by making this assumption for this case is not considered to be significant.

Flyback system weights were determined for two different types of fueled engines. The fuels are (1) JP (RP-1), and (2) LH_2. These two fuels were selected on the basis that most boost vehicles will probably use these fuels, and no special tankage will be required for the flyback fuel. In order to optimize the weight-to-thrust ratios, a detailed analysis should be made so that the engine thrust values used for determining the weight-to-thrust ratios could reflect the exact thrust value which corresponds to the altitude associated with the optimum lift-to-drag ratio. This analysis was beyond the scope of this study; hence, engine and lift-to-drag ratio optimization estimates will be made for both engine operating limits, thrust and weight. The synthesis program used a predetermined flyback cruise subsonic Mach number, typical engine systems weights, and specific fuel consumption.

The flyback engine weight as used in the weight scaling methodology is designated as W_{ENG} = flyback engines weight. In addition, the thrust required for flyback is a function of vehicle drag, and the lift is a function of vehicle weight. Therefore, $T \propto D$ and $L \propto W$.

For level flight with no acceleration and the vehicle operating at its maximum lift-to-drag ratio

$$\frac{L}{D} = \frac{W}{T} \tag{B-1}$$

This equation can be rewritten as

$$\frac{W}{L/D} = \left(\frac{T}{W}\right)_{ENG} \cdot W_{ENG} \tag{B-2}$$

where W is the vehicle flight weight. This weight is dependent upon where level flight without altitude loss is required. This is at least the landing weight, which is the empty vehicle plus engine weight. Thus, the engine weight can be expressed by the following relationship:

$$W_{ENG} = \frac{W}{\left(\frac{L}{D}\right)\left(\frac{T}{W}\right)_{ENG}} = \frac{W_{(empty\ Stage\ I)} + W_{ENG}}{\left(\frac{L}{D}\right)\left(\frac{T}{W}\right)_{ENG}}$$

From the above equation, the engine weight can be expressed as a percentage of the stage empty weight,

$$\frac{W_{ENG}}{W_{EMPTY}} = \frac{100}{\left[\left(\frac{L}{D}\right)\left(\frac{T}{W}\right)_{ENG} - 1\right]} \tag{B-3}$$

The weight-to-thrust ratio of an engine can easily be converted to engine weight in percent of vehicle weight without flyback fuel as a function of lift-to-drag ratio by the conversion chart shown in figure B-9 . When using figure B-9 for a given existing engine, the percent of engine weight for a given vehicle must be either increased or decreased to reflect a whole number of engines. This conversion chart is for steady-state flight. For a final engine weight analysis, some consideration must be given to the acceleration required, as well as to the complete speed-and-altitude operating regime and the possibility of first stage plus second stage ferry applications.

The flyback propulsion systems to be considered employ podded turbojet engines of which advanced, high-bypass-ratio turbofans in the CF-6 (General Electric C-5A power plant) and the STF-200 (P&W) are considered representative for the 1970-to-1980 time period. Space Division studies of reusable launch vehicles have indicated that such systems represent a significant portion of the inert vehicle weight. Such studies have also concluded that during the recovery flyback mode, a subsonic cruise at approximately Mach 0.6 to 0.8 is desirable. As an example, for a recoverable vehicle exhibiting a lift-to-drag ratio of 5 and flyback at Mach 0.8, the propulsion system weight (including engine, nacelle inlet, fuel systems, and inlet covers) is approximately 10 percent of the empty vehicle weight.

For the parametric synthesis program, the critical empty weight (W_{EMPTY}) is not defined prior to the engine weight; therefore, equation (B-3) can be modified for the synthesis technique as:

$$W_{ENG} = \frac{W_{BO} - W_{FUEL}}{\left(\frac{L}{D}\right)\left(\frac{T}{W}\right)_{ENG}} \qquad \text{(B-4)}$$

Where W_{BO} = weight of stage at burnout prior to start of recovery mode.

The weight of the flyback propellant required, W_{FUEL}, to return to the launch site, is a function of range, specific fuel consumption, flyback velocity (Mach number), and L/D ratio. Range is a function of the vehicle burnout condition and therefore must be determined as a function of staging velocity, burnout flight path angle, L/D, and engine parameters. Using the Breguet equation,

$$R = \left(\frac{L}{D}\right)\left(\frac{V}{C}\right) \ln \mu \qquad \text{(B-5)}$$

To maximize this expression for range it is required to operate at an optimum flyback velocity such that $\left(\frac{L}{D}\right)\left(\frac{V}{C}\right)$ is a maximum. This is

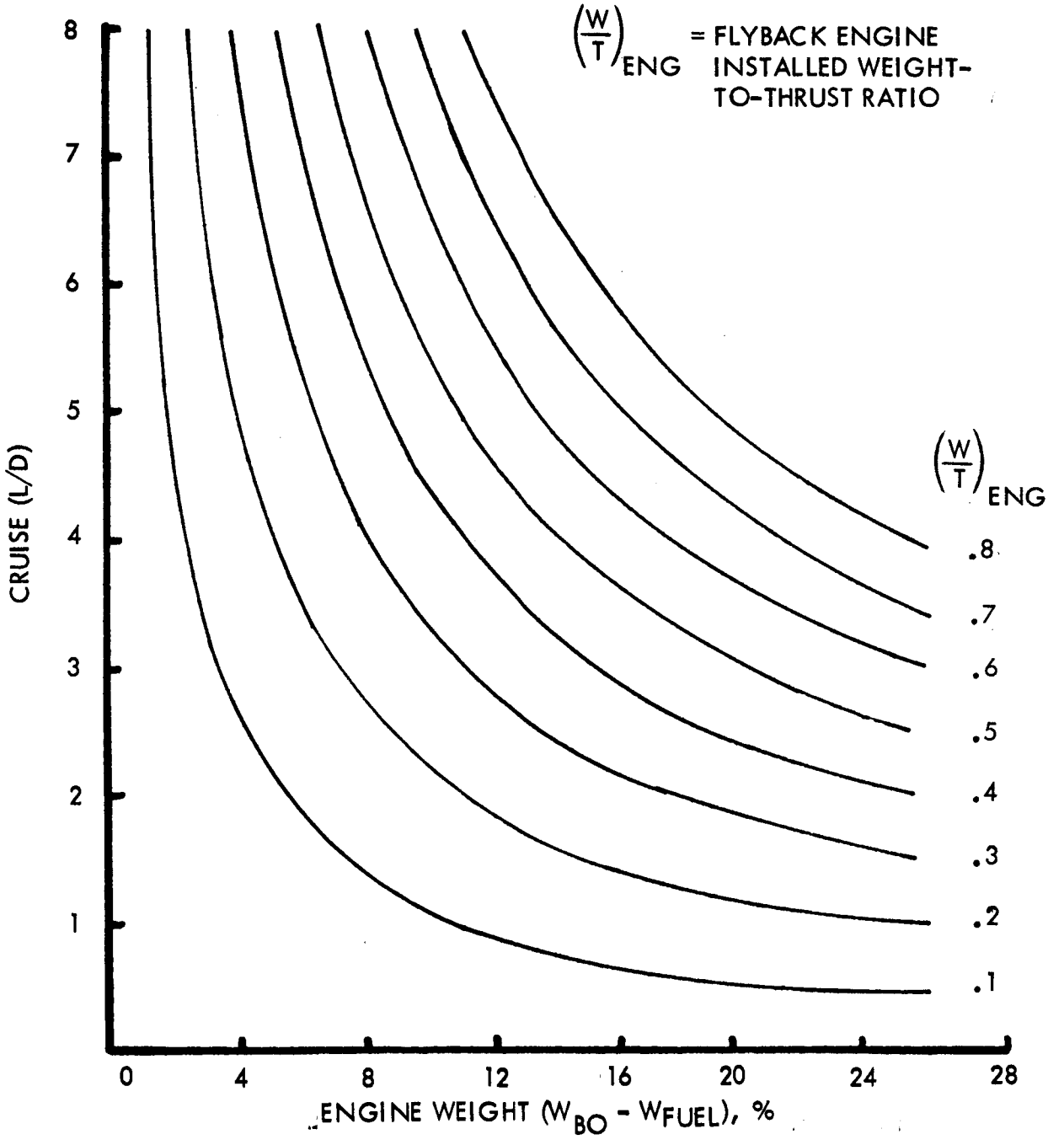

Figure B-9. - Installed Weight of Flyback Engines

dependent upon the flyback engine system being considered and upon its specific fuel consumption, C. From equation (B-5), the required fuel weight for a specified range can be expressed in terms of the burnout weight of the stage

$$W_{FUEL} = W_{BO}\left(1 - e^{-\frac{R}{(L/D)(V/C)}}\right) \qquad \text{(B-6)}$$

Combining the engines weight required for cruise at the respective Mach number and lift-to-drag ratio with the fuel weight results in the total flyback system weights. Data indicate that both JP (RP-1) and LH_2 fueled rocket vehicles should fly back at subsonic Mach numbers. The exact subsonic Mach number for the JP (RP-1) rocket vehicle is not clearly indicated; however, for weight scaling purposes the following conditions are assumed: (1) $0.60 < M < 0.8$, and (2) (L/D) = maximum.

Figure B-10 presents a parametric representation of flyback propulsion fuel weight as a function of range for various vehicle lift-to-drag ratios when a podded flyback propulsion system using JP-4 (RP-1) turbofan engines. cruise speed, $M = 0.8$, and specific fuel consumption is employed. The fuel requirement for a 250-mile return leg is approximately nine percent of the empty vehicle weight. A 10-percent engine installation weight results in a 19-percent addition to the landed weight of an unpowered recoverable stage. For a 400-nautical-mile flyback, this percentage increases to 24 percent. The significance of the flyback system on launch vehicle mass fraction is readily apparent. The mechanization of the flyback propulsion system weight for the synthesis program is shown in figure B-11.

Wing Sizing

Synthesis techniques and evaluation methodology have been extended to encompass the parametric synthesis of winged, vertically launched, first stages that employ a powered, horizontal flyback-and-recovery flight mode. Wing sizing relationships for touchdown condition and subsonic longitudinal stability during flyback are discussed in this section. The preliminary subroutine logic and the equations required to compile the wing sizing program are included.

Wing size and geometry for recoverable boosters. - The wing size and shape for the recoverable first stage is based upon the required aerodynamic characteristics associated with stage touchdown, subsonic longitudinal

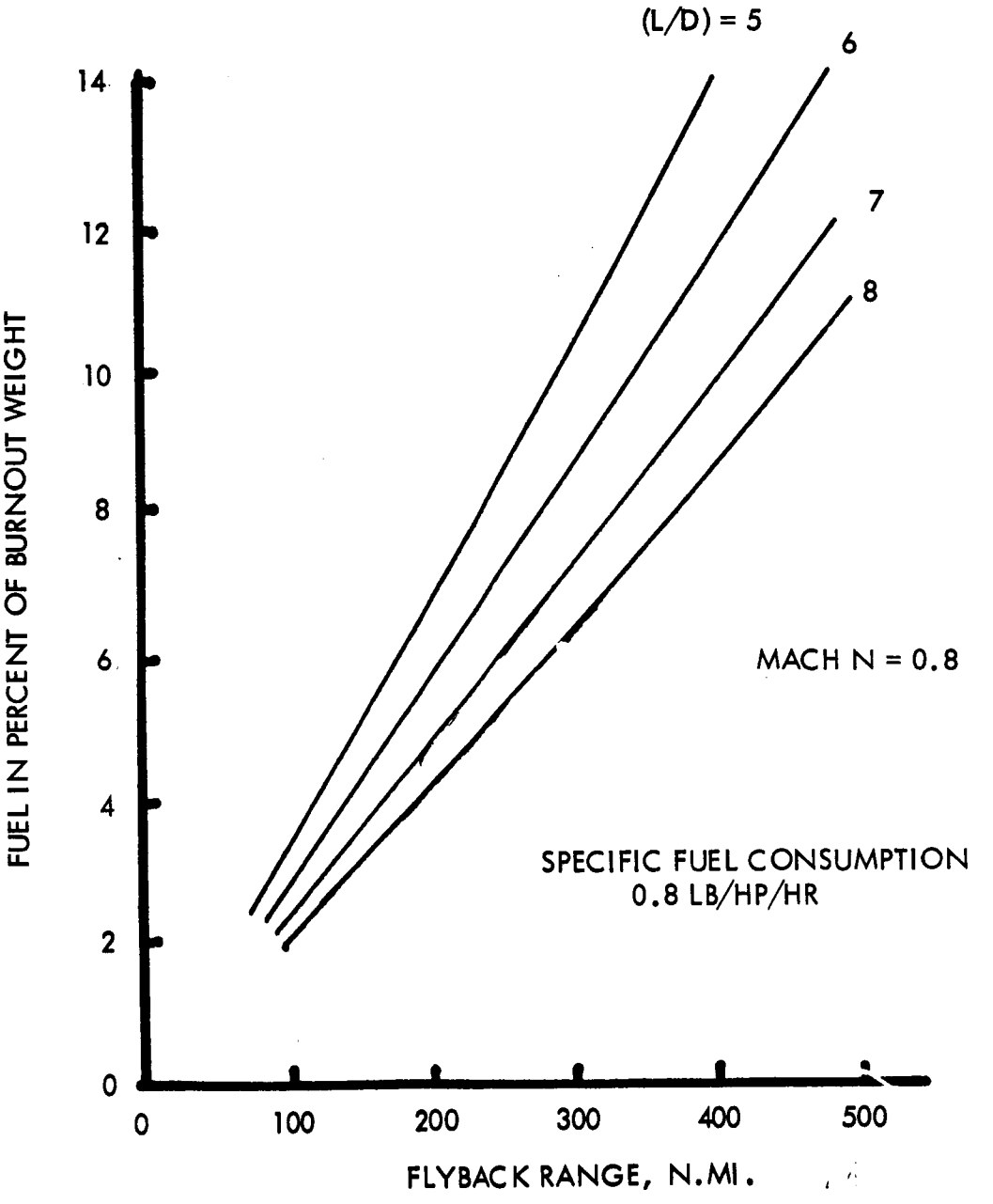

Figure B-10. - Flyback Fuel Requirements

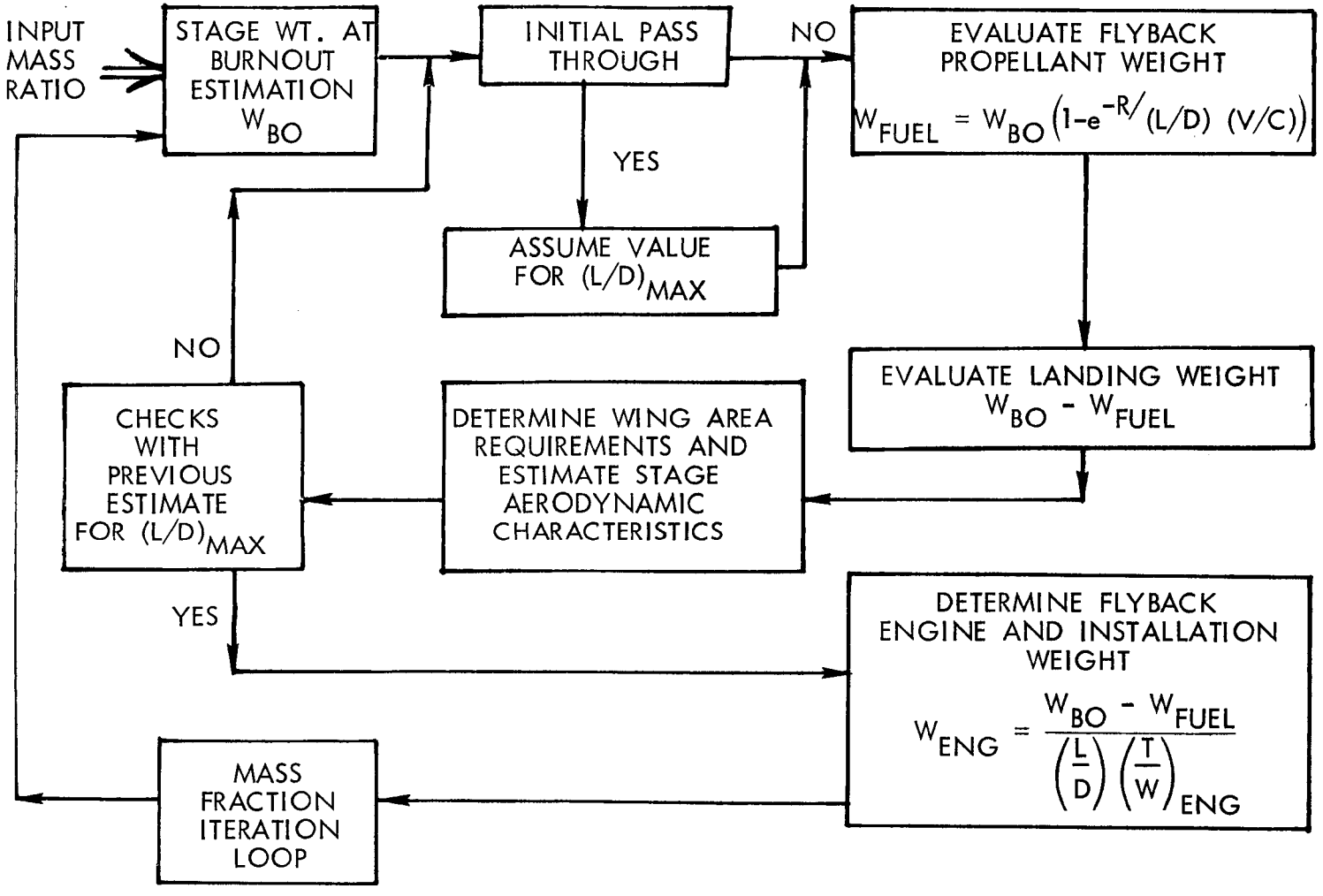

Figure B-11. - Program Synthesis for Flyback Propulsion System

stability, and hypersonic wing loading constraints. Because of heating of the spent first stage during reentry, it is advisable to restrain the wing loading during the initial entry phase of the trajectory. It has been suggested that $40\ lb/ft^2 \leq (W/S) \leq 60\ lb/ft^2$ would be an acceptable range. The program does not automatically optimize this parameter, but does accept (W/S) as input data, performing several synthesis runs to find the effect of (W/S) on vehicle performance if sufficient thermal data, as a function of wing loading, are available. The basic input to the wing sizing routine will therefore be the wing loading, stall speed, and touchdown angle.

To define the wing shape and position relative to the basic launch vehicle, the following four parameters are needed (fig. B-12).

Span, b
Root chord, C_R
Tip chord, C_T or taper ratio, $\lambda = C_R/C_T$
Leading edge sweep, Λ_{LE}

For the loading requirement, the vehicle lift must equal the empty weight just prior to touchdown at the stall velocity

$$W = \frac{1}{2}\,\rho_{sl}\,V_{STALL}^2\,S_{REF}\,C_{L_\alpha}\,\alpha_{TD} \tag{B-7}$$

where, for example

ρ_{sl} = density at sea level = 2.377×10^{-3} slug/ft^2

$V_{STALL} = 0.8\ V_{touchdown} = 150$ knots

α_{TD} = touchdown angle of attack = 15°

C_{L_α} = lift curve slope of vehicle

S_{REF} = planform area = $\frac{C_R b}{2}(1 + \lambda)$

W = Stage 1 burnout weight at end of boost flyback propellant

The vehicle's velocity prior to touchdown is about 150 knots, and the subsonic lift curve slope of a wing body, using the standard methods of references B-2 and B-3 is given by

$$C_{L_\alpha} = C_{L_{\alpha_{FOREBODY}}} + \left(K_{B_W} + K_{W_B}\right) C_{L_{\alpha_{WING}}} \tag{B-8}$$

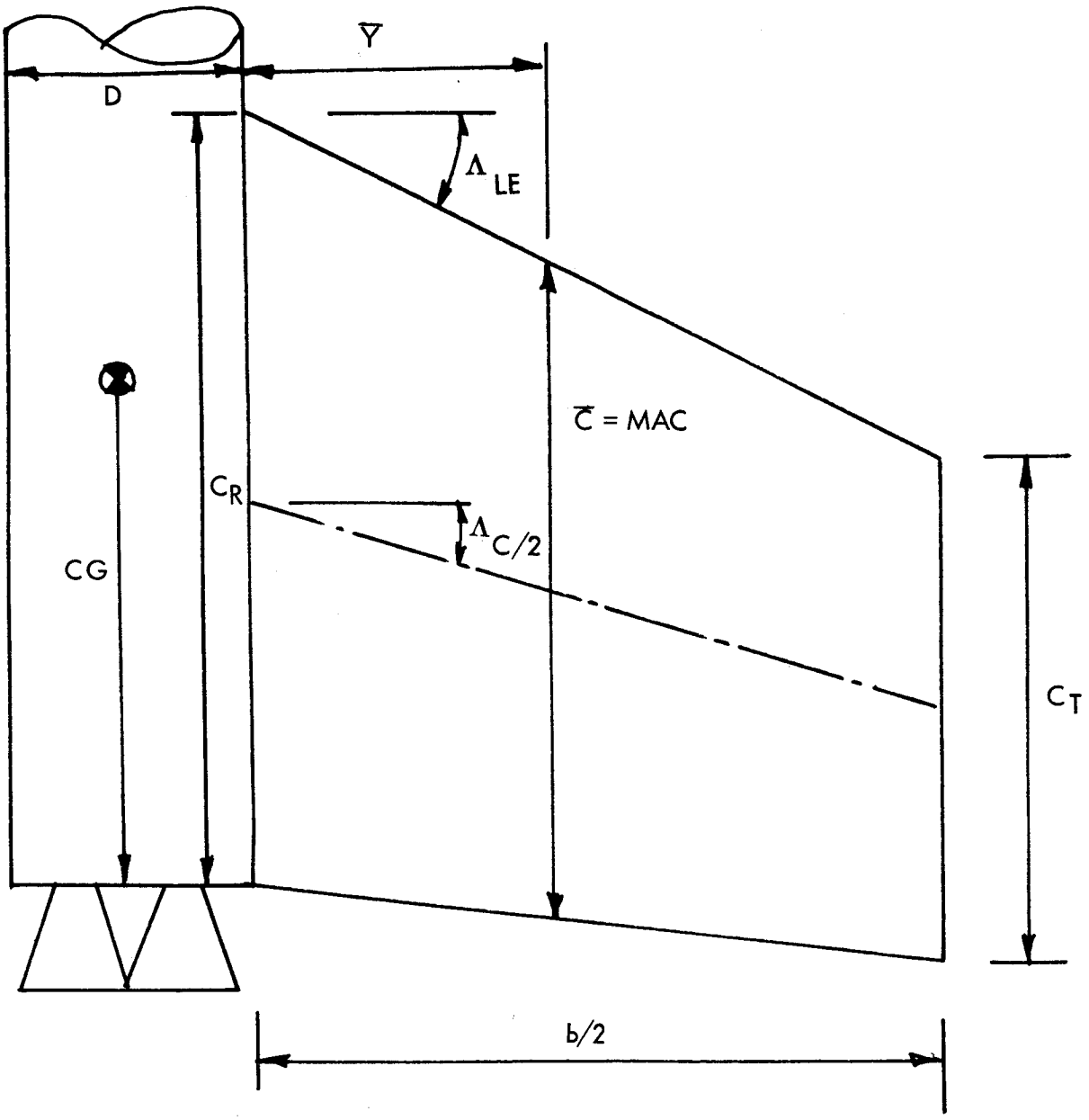

$AR = b^2/S$ = ASPECT RATIO

$\lambda = C_T/C_R$ = TAPER RATIO

$$S_{WING} = C_R \frac{b}{2} (1 + \lambda)$$

$$\bar{C} = \frac{2 C_R (1 + \lambda + \lambda^2)}{3 (1 + \lambda)}$$

$$\bar{Y} = \frac{b (1 + 2\lambda)}{6 (1 + \lambda)}$$

Figure B-12. - Wing Geometry

where

$$C_{L_{\alpha_{FOREBODY}}} = \left(\frac{2}{rad}\right)\frac{(\pi d^2/4)}{S_{WING}}$$

d = diameter of basic booster, ft.

The lift-curve slope for the wing alone for subsonic flight is given in reference B-2 and can be empirically expressed as

$$C_{L_{\alpha_{WING}}} = \frac{\pi^2/90\,AR}{2 + \left[(AR\ \beta)^2\left(1 + \frac{TAN^2\Lambda_{c/2}}{\beta^2}\right) + 4\right]^{1/2}} \qquad (B\text{-}9)$$

where

$\Lambda_{c/2}$ = sweep of half chord

$\beta^2 = 1 - M_{TD}^2$

M_{TD} = touchdown or stall Mach number

AR = wing aspect ratio = b^2/S_{WING}

From figure B-12, the half chord can be represented by

$$\Lambda_{c/2} = \arctan\left[\tan\Lambda_{LE} - \frac{(1-\lambda)\,C_R}{b}\right] \qquad (B\text{-}10)$$

The synthesis program is initiated with a wing loading requirement for the hypersonic flight conditions or the landing requirements. During the initial entry phase, the vehicle weight is W_{BO} and an estimate for the required wing area for the hypersonic flight regime is given by:

$$S_{WING_{HYP}} = \frac{W_{BO}}{(W/S)_{hyp}} - d\ell \qquad (B\text{-}11a)$$

where

$(W/S)_{hyp}$ = desired hypersonic wing loading

d = stage diameter

ℓ = stage length

For the selection of an appropriate wing planform, there are several program options which allow the user to define several of the wing's design parameters. Design requirements for the landing must be specified for each vehicle test condition in order to synthesize the wing area required for landing. The total lift support area is defined by

$$S_{WING_{TOTAL}} = S_{WING} + S_{WING_{FUSELAGE}} \qquad \text{(B-11b)}$$

where

$$S_{WING_{FUSELAGE}} \approx d \times \text{root chord}$$

But, since the root chord and geometric shape and size of the wing are not completely defined, average values are assumed in order to arrive at an estimate. If the taper ratio, λ, is assumed to be 0.8, then the exposed wing area is

$$S_{WING} = \frac{C_R b}{2}(1 + \lambda) \qquad \text{(B-11c)}$$

Therefore, the root chord is given by

$$C_R = \frac{S_{WING}}{0.9\, b} \qquad \text{(B-12a)}$$

Also, the wing span can be expressed as

$$b = (S_{WING}\, AR)^{1/2} \qquad \text{(B-12b)}$$

The subroutine input for the synthesis program includes the aspect ratio required for the vehicle. If this has not been defined, the subroutine itself initializes a minimum aspect ratio to perform its evaluation and systematically increases its estimate for aspect ratio until it obtains an "acceptable" value. This value will be such that the vehicle constitutes a stable configuration prior to touchdown. Therefore, in either mode the

subroutine has available a value for the vehicle's aspect ratio to proceed through the subroutine's logic. Therefore, equation (B-11b) can be rewritten as

$$S_{WING_{TOTAL}} = S_{WING} + \frac{d}{0.9}\left(\frac{S_{WING}}{AR}\right)^{1/2} \qquad \text{(B-13a)}$$

The above equation can now be solved for the required wing area, since the remainder of the parameters are defined. Therefore,

$$S_{WING} = S_{WING_{TOTAL}} + \frac{d^2}{1.62\,AR} - \left[\frac{S_{WING_{TOTAL}}\, d^2}{0.81\,AR} + \left(\frac{d^2}{1.62\,AR}\right)^2\right]^{1/2} \qquad \text{(B-13b)}$$

The lift coefficient can be separated into the lift coefficient dependent upon the stage's aerodynamic characteristics and the remainder dependent only upon the wing area, already defined by equation (B-13b).

$$C_{L_\alpha}{}' = C_{L_\alpha} - \frac{\pi^2 d^2}{360\, S_{WING}} \qquad \text{(B-14)}$$

This assumes that the C_{L_α} from the forebody is 2/radian. The wing and body interference factors K_{W_B} and K_{B_W} are obtained from reference B-3 and are shown in figure B-13. For the particular range of interest for a vehicle system, these factors can be represented by a straight line, therefore

$$K_{B_W} + K_{W_B} \approx 0.8 + \frac{3d}{b + d} \qquad \text{(B-15)}$$

When equations (B-14) and (B-15) are used, the lift curve slope requirement for the wing along is approximated by

$$C_{L_{\alpha_{WING}}} = \frac{C_{L_\alpha}{}'}{\left(0.8 + \frac{3d}{b + d}\right)} \qquad \text{(B-16)}$$

The subroutine now has sufficient parameters to evaluate the wing lift curve slope, equation (B-16), and, thence, the root chord. Equation (B-9) is now rearranged to obtain

$$\tan \Lambda_{c/2} = \left\{\frac{4}{AR^2}\left[\left(\frac{\pi^2 AR}{180\, C_{L_{\alpha WING}}} - 1\right)^2 - 1\right] - \beta^2\right\}^{1/2} \qquad \text{(B-17)}$$

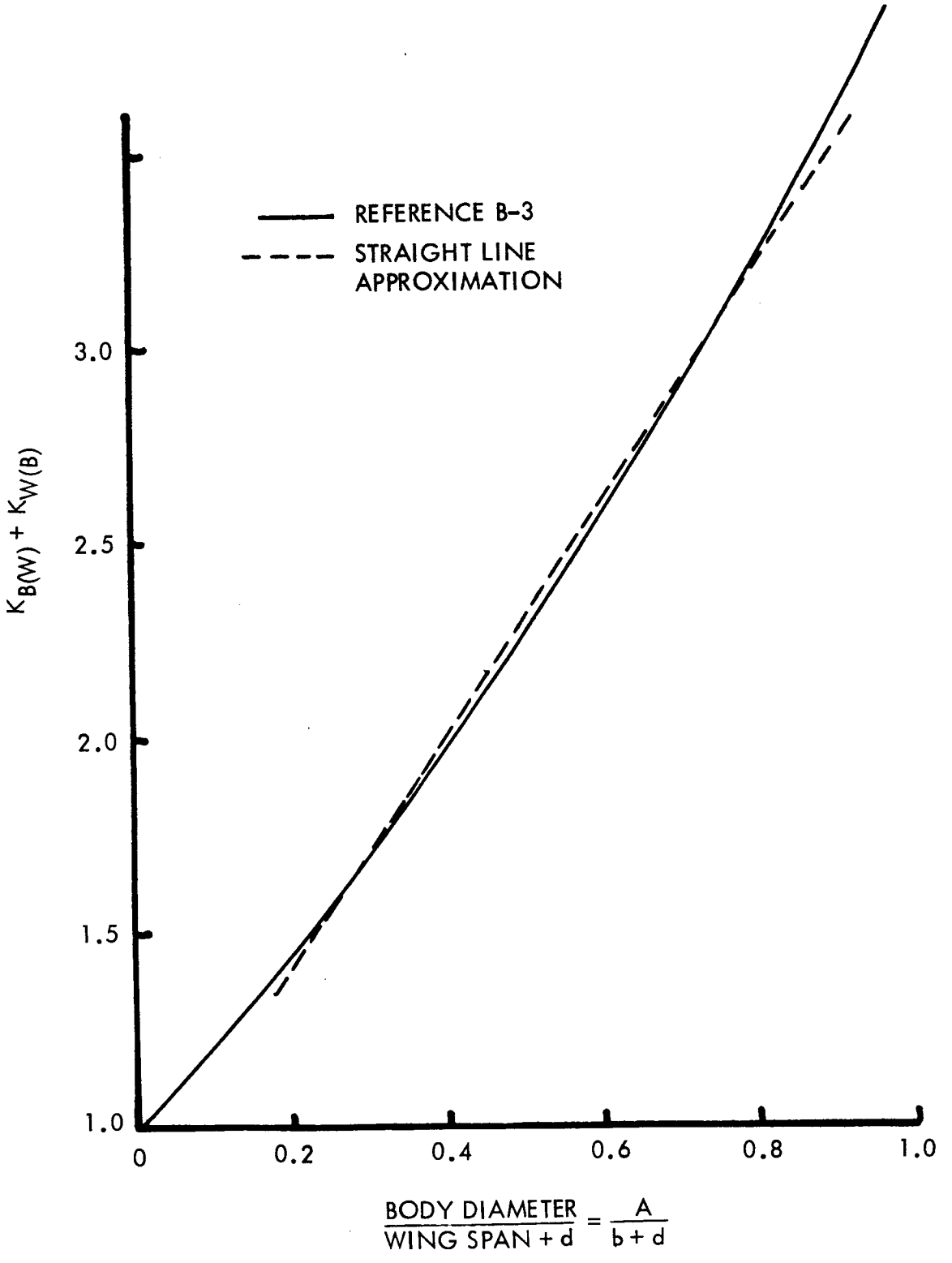

Figure B-13. - Wing-Body Interference Parameter

and from this above equation, the root chord is

$$C_R = (\tan \Lambda_{LE} - \tan \Lambda_{c/2}) \frac{b}{2} + \frac{S_{WING}}{b} \qquad \text{(B-18)}$$

and the taper ratio is

$$\lambda = \frac{2\, S_{WING}}{C_R b} - 1 \qquad \text{(B-19)}$$

This completely defines the geometric shape of the wing whose lift coefficients are consistent with the loading requirements. This portion of the sizing program does not guarantee a longitudinally stable vehicle. This can be achieved perhaps by increasing the leading edge sweepback and/or the aspect ratio. For the condition where the vehicle's aspect ratio is a fixed input and stability is required, the stability can only be achieved by positioning of the wing and varying of the leading edge sweepback. Since the center of gravity of the empty stage is toward the rear, the wing is automatically positioned as far aft as possible (fig. B-12).

The center of pressure for the subsonic flight is assumed to be located at the geometric quarter-mean aerodynamic chord ($0.25\overline{c}$), and its position forward of the aft body station is given by

$$\text{c.p.} = C_R - \overline{y} \tan \Lambda_{LE} - \frac{1}{4} \overline{c} \qquad \text{(B-20)}$$

For a stable vehicle, the c.p. should be behind the stage center of gravity.

Program logic for wing sizing. - The first part of this section dealt with the relationships associated with the wing sizing and geometric definition to achieve a required lift coefficient for the stage touchdown. In the following paragraphs, the procedure for the synthesis subroutine is indicated and the multipath selection is discussed.

The wing sizing program subroutine logic and its associated steps are shown in figure B-14. The initial routine is required to define the total wing area required consistent with the hypersonic wing loading input data, equation (B-11a), and the landing requirement, equations (B-13a) and (B-13b). The maximum wing area from the two evaluated areas is selected, and the program proceeds to the four-way option selector.

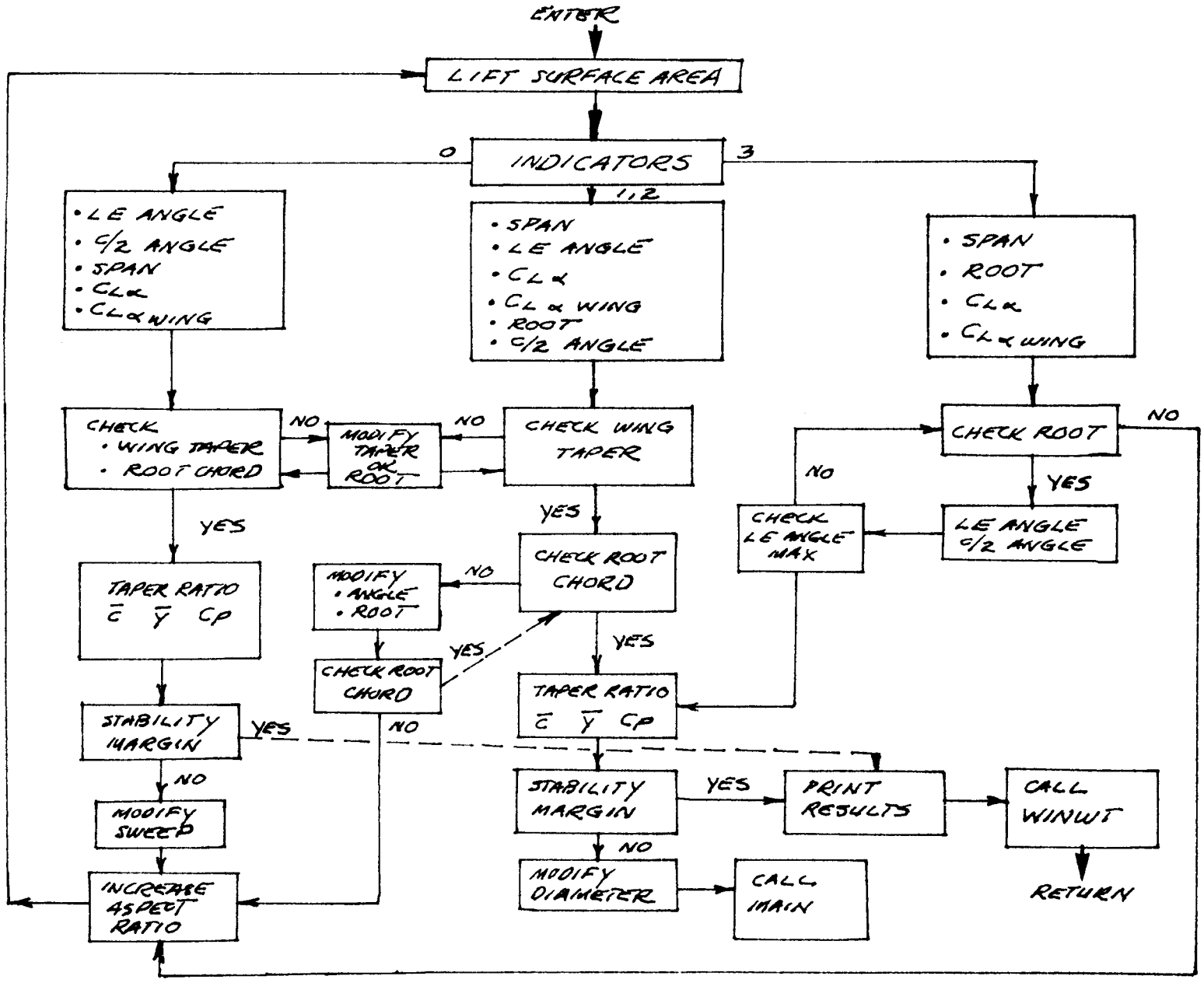

Figure B-14. - Wing Sizing Logic

For option, O, with no fixed AR, the machine itself selects a minimum AR to initialize the subroutine. This AR is obtained by considering a maximum root chord of 0.85 body length and a taper ratio of 0.80. With the AR minimum determined, the lift curve slope for the wing and wing span are found by means of equations (B-12b), (B-14), (B-15), and (B-16). Then the remaining wing geometry for the required wing lift is found from equations (B-17) through (B-19) and the stability margin is evaluated with equations (B-20) and (B-21); positive is defined as a stable vehicle.

If this margin is positive, the user is to exit from this subroutine; if negative, it must be determined whether stability is required for this vehicle. To achieve stability, the wing leading edge angle has to be successively increased and iterated through the subroutine until the stability margin produces a stable system or the maximum geometric parameters of the wing planform are reached. If this latter event occurs, the program will exit with final wing design but an unstable vehicle statement, which the program user can accept or rectify at his discretion.

For an unstable vehicle and geometry parameters not at a maximum, there are two choices, either increase the AR or sweep the leading edge and iterate through the subroutine. In order to retain a realistic vehicle, there should be a defined range of sensible AR and leading-edge angles for the program to iterate on. If stability is not achieved within these ranges, the subroutine accepts a negative margin and proceeds with the remainder of the synthesis. The preference order for iteration should result in the lightest wing structure. Intuitively, this appears to be the wing with the smallest aspect ratio irrespective of the wing sweepback. Therefore, the preference order will be to increase the sweep angle to achieve stability. This increase is to continue until $\Lambda_{LE_{MAX}}$ is attained or the wing tip edge is a specified maximum distance aft of the rear face of the engine system. This would constitute a vertical launch constraint which would prevent the vehicle from sitting on its launch pad without ground interference.

Options 1, 2, and 3 have several of the wing-shape-parameters as fixed input data, such as the aspect ratio, taper ratio, or sweepback. The synthesis subroutine systematically evalutes the remainder of the geometric parameters, sizes the wing, and tries to achieve a stable vehicle by continually increasing design parameters until a design constraint value is attained. If the program search for stability is unsuccessful, then we will select maximum design values, compute wing size, print statement of unstable vehicle, exit from subroutine, and return to main program.

Wing Weights

The weight of the wings and their associated carry-through structure for the parametric synthesis is broken down into several elements. The wing weight is considered to be the weight arising from the load-carrying structure as well as weight from insulation and its attachment, if required.

The structural elements considered in this synthesis are:

Main wing structural box

- Wing covers
- Shear webs

Leading and trailing edge structures

- Cover panels
- Shear ribs

Vertical stabilizers

Carry-through structure

The structural elements are considered to be either bending material or shear material. Bending moments due to the main air loads are assumed to be reacted by the cover panels of the wing structural box by differential bending. The bending material towards the root chord can either be considered to be the cover plates or the spar caps where the loading will be concentrated prior to its transmittal to the carry-through structure. The synthesized weight associated with the wing cover will not differentiate between the surface panels and the spar cap material; instead the program will quote a "lumped mass" material required to react the bending moments. Any additional detail description is not available for the parametric vehicle synthesis because of the preliminary description of the tankage shell-wing attachment design, in particular with regard to the number of spars and the type of carry-through structure. It is to be appreciated that the wing synthesis is required only to furnish a realistic parametric weight description for the stage mass fraction determination.

The wing structural box width is quoted as a percentage of the local chord, K. The width of the leading and trailing edge are therefore assumed

equal to $\frac{C}{2}(1-K)$. This assumes equal disposition between leading and trailing edge members.

The wing loading for the structural design can arise from the ascent trajectory phase at maximum dynamic pressure and a superimposed wind speed plus gust velocity. This produces a pressure over the wing surface which is treated as a uniform pressure. A second condition will be during entry and a maneuver causing a normal inertial loading.

If W_o is the weight of the vehicle and n the normal G-loading for a specific design condition, the lift on the wing is

$$L_W = k_L n W_o$$

where

k_L = the percentage lift on the vehicle developed by the wing

If S_W = the exposed wing area, then the loading per unit area of exposed wing is

$$\omega = \frac{L_W}{S_W} = \frac{k_L\, n\, W_o}{S_W}$$

This loading is assumed constant over the wing.

The main wing structural box reacts the bending and shear from the wing surface loading. Chord length at any point, X, from the wing tip, the chord length y_{S_1} quoted being normal to the 50-percent chord line, is given by

$$y_{S_1} \approx C_R \cos \Lambda_{50} \left[\lambda + (1 - \lambda) \frac{X_1}{b/2} \right]$$

where

C_R = root chord

λ = taper ratio = tip chord/root chord

Λ_{50} = sweepback angle of the 50-percent chord line

If distances along the chord line are considered, then

$$X_1 = S_1 \cos \Lambda_{50}$$

and the chord can be rewritten as

$$y_{S_1} = C_R \cos \Lambda_{50} \left[\lambda + (1 - \lambda) \frac{S_1 \cos \Lambda_{50}}{b/2} \right]$$

Therefore the bending moment at any station due to an assumed uniform wing loading, ω, is given by

$$M_S = \int_o^S \omega y_{Si} (S - S_i) \, dS_i$$

which, on integrating, produces

$$M_S = \omega C_R \cos^2 \Lambda_{50} \left[\frac{\lambda S^2}{2} + (1 - \lambda) \frac{\cos \Lambda_{50}}{b/2} \frac{S^3}{6} \right]$$

This result assumes that the wing has a constant taper ratio and sweep angle.

The wing depth at any section for a constant thickness/chord wing can be expressed as

$$H_S = H_R \left[\lambda + (1 - \lambda) \frac{S \cos \Lambda_{50}}{b/2} \right]$$

With the bending moments taken as differential end loads in the cover plates, this end load is

$$N_S \approx \pm M_S / H_S$$

Required cross-sectional area of the cover panel at any section is expressed as

$$A_S = \frac{2N_S}{\sigma_a}$$

where

σ_a = allowable stress level of cover panels

This stress level is a function of the type of construction and its stability capability. Therefore, the cross-sectional area is given approximately as

$$A_S = \frac{2\omega C_R \cos \Lambda_{50} \left[\lambda S^2/2 + (1 - \lambda) \cos \Lambda_{50} S^3/3b \right]}{\sigma_a H_R \left[\lambda + (1 - \lambda) 2 \cos \Lambda_{50} \cdot S/b \right]}$$

If this cross-sectional area is integrated along the 50-percent chord line, the material volume required for the wing covers is produced.

$$V_S = 2 \int_o^S A_S dS$$

Therefore, the wing cover weight is given by:

$$W_c = V_s \times \rho_m$$

where

ρ_m = density of cover material

When the required integration is performed, the wing cover weight expression is reduced to

$$W_c = \frac{2\omega\rho_m}{\sigma_a} \left[\frac{(b/2)^3}{t_c \left(\frac{1}{\lambda} - 1 \right)^3 \cos^2 \Lambda_{50}} \right] \left[\frac{8}{9} + \frac{1}{9} \left(\frac{1}{\lambda} \right)^3 - \left(\frac{1}{\lambda} \right) + \frac{2}{3} \ell n \frac{1}{\lambda} \right]$$

This expression for cover weight is used for tapered wings, but does not apply for delta or rectangular platforms because of the singularities present in the expression for W_c when $\lambda = 1.0$ $\lambda = 0$. When $\lambda \geq 0.9$, the above expression presents large errors. Therefore, the formula for the wing cover volume is initially expanded into a convergent series and then integrated term by term. Then the cover weight is rewritten as

$$W_c = \frac{4\omega\rho_m C_R \cos \Lambda_{50}}{\sigma_a t_c \lambda} \int_o^S \left[\frac{\lambda S^2}{2} + \frac{(1 - \lambda) S^3 \cos \Lambda_{50}}{3b} \right] \cdot \left(\frac{1}{\lambda} \right)$$

$$\cdot \left[1 + \frac{2 (1 - \lambda) \cos \Lambda_{50} S}{\lambda b} \right]^{-1} dS$$

The general solution for this integration and expansion can be represented by

$$W_c = \frac{\rho_m \omega C_R b^3}{2\sigma_a H_R \cos^2 \Lambda_{50}} \left[\frac{1}{3} - \sum_{i=1}^{\infty} \left(\frac{1 - \lambda}{\lambda} \right)^i \frac{1}{3\,(3 + i)} \right]$$

An allowable compressive stress level associated with the wing design has to be assumed for the program generation. This stress level can be based upon structural design experience of typical stability stresses allowed for a given material.

The shear material required is defined along the 50-percent chord line and the shear force Q_S at any station, S is

$$Q_S = \int_o \omega C_R \cos \Lambda_{50} \left[\lambda + 2\,(1 - \lambda) \frac{S_1 \cos \Lambda_{50}}{b} \right] dS_1$$

which reduces to

$$Q_S = \omega C_R \cos \Lambda_{50} \left[\lambda S + (1 - \lambda) \frac{S^2}{b} \cos \Lambda_{50} \right]$$

The shear cross-sectional area at Station, S, is

$$A_{SS} = \frac{Q_S}{\sigma_S}$$

where

σ_S = allowable shear stress

Integrating along the chord line produces the shear web material volume

$$V_{SS} = 2 \int_o^{b/2} A_{SS} dS$$

and for a given web material, the weight of the shear web can be represented by

$$W_{S_{WEB}} = \left(\frac{\omega \rho_m}{6\sigma_s} \right) \left(\frac{b}{2} \right)^2 \frac{C_R}{\cos \Lambda_{50}} \left(\frac{5}{\lambda} - 1 \right)$$

If the web is considered to be single sheet with vertical stiffeners to subdivide the panels, the buckling stresses of the panels can be evaluated as

$$\sigma_{SHEAR} = K_S E \left(\frac{t}{H_S}\right)^2$$

This can be translated into the shear carrying capability at any station by assuming a constant thickness and a knowledge of the height at any section

$$Q_s = K_S E t^3 / H_S$$

Therefore, the required thickness at any section can be expressed as a function of the total shear force on the two spars at this section

$$t = \left(\frac{H_S Q_S}{K_S E^2}\right)^{1/3}$$

Toward the wing tip where the shear force, and/or the tip-chord are small compared to the root values, the required skin thickness will be less than the minimum practical gauges. Also, toward the root chord, the total web weights formula with the assumed allowable shear stress might be inconsistent with the actual thickness derived from the formula. In order to produce reasonable web weights, the web is considered to be constant thickness along a portion of the span in a series of four steps at 0 to 25 percent, 25 to 50 percent, 50 to 75 percent and 75 to 100 percent. An average height at these four sections is evaluated together with its corresponding shear force.

$$H_{x_i} = \lambda C_R + C_R (1 - \lambda) \frac{2x_i}{b}$$

$$Q_{s_{x_i}} = \omega C_R \left[\lambda (x_i + 0.125\, b/2) + \frac{(1 - \lambda)}{b} (x_i + 0.125\, b/2)^2\right]$$

The required thicknesses for checking allowable stability stresses and maximum input shear stresses are given by

$$t_{i_Q} = \left(\frac{H_{x_i} Q_{s_{x_i}} FSU}{9.24\, E}\right)^{1/3}$$

$$t_{i_\sigma} = \left(\frac{Q_{s_{x_i}} \, FSU}{2H_{x_i} \sigma S_{MAX}} \right)$$

where FSU = ultimate safety factor. The thickness is then selected as the maximum required or the minimum manufacturing gauge permissible.

$$t_l = \max \left(t_{i_Q}, \, t_{i_\sigma}, \, t_{min} \right)$$

and the total shear web weight, including 25 percent weight allowable for web stiffeners, etc., for both wings can be given as

$$W_{S_{WEB}} \approx \frac{0.625 \, b \rho_m}{\cos \Lambda_{50}} \left(\sum_{i=1}^{4} H_{x_i} t_i \right) SF \cdot NOF$$

where

SF = weight factor to account for shear web stiffener and attachment

NOF = non-optimum weight factors

The leading and trailing edge structures are sized by bending and shear. The chord length of each is assumed equal to $\frac{C}{2}$ (1 - K). The air loads imposed on the leading and trailing edges are taken in bending by the skins and considered normal to the fore and aft spars. This bending is transmitted to the spar caps via the skin panels, and the shear force is taken by ribs normal to the spars and sheared into these spars.

The bending moment along a strip dS normal to the forward spar is given by

$$M_{LS} = \int_o^{y_L} \omega dS \, (y_L - y_{Ll}) \, dy_L$$

which, upon integration, yields

$$M_{LS} = \frac{\omega dS y_L^2}{2}$$

The leading edge chord normal to the forward spar, y_{L_S}, at any point, X, is

$$y_{L_S} = \frac{\lambda C_R}{2}\left[1 + 2\left(\frac{1}{\lambda} - 1\right)\frac{S \cos \Lambda_{FS}}{b}\right](1 - k) \cos \Lambda_{FS}$$

The depth at any section S along the chord normal to the forward spar is

$$H_{SL} = 2y_L \tan \theta_{LS}$$

where

$$\theta_{LS} = \tan^{-1}\left[\frac{t_L}{(1 - k) \cos \Lambda_{FS}}\right]$$

It is assumed for this included angle θ_{LS} that the leading edge box can be represented by a triangular-shaped structural box normal to the front spar. Therefore, the edge load due to bending within the plane of the front-box cover panel is

$$N_{S\theta} = \frac{\omega y_L}{4 \sin \theta_{LS}}$$

with the cross-sectional area required at any section being

$$a_\theta = \frac{\omega y_L}{2 \sin \theta_L \sigma_a}$$

Double-integrating this cross-sectional area along the front box chord and then along the wing span results in the required weight of the leading edge bending material being approximated by

$$W_L = \left(\frac{\omega \rho_m}{8\sigma_a}\right)\frac{\frac{b}{2}\lambda^2 C_R^2 (1 - k)^2}{3}\left[\left(\frac{1}{\lambda}\right)^2 + \left(\frac{1}{\lambda}\right) + 1\right]\frac{\cos \Lambda_{FS}}{\sin \theta_{LS}}$$

and similarly the weight of bending material for the trailing edge

$$W_T = \left(\frac{\omega \rho_m}{8\sigma_a}\right)\frac{\frac{b}{2}\lambda^2 C_R^2 (1 - k)^2}{3}\left[\left(\frac{1}{\lambda}\right)^2 + \left(\frac{1}{\lambda}\right) + 1\right]\frac{\cos \Lambda_{RS}}{\sin \theta_{TS}}$$

Shear material is required in the leading edge wing box in the form of nose ribs. There is a shear relief due to the leading edge tapered box section which is given by:

$$N_{Z_{y_L}} = 2N_S \tan \theta_L$$

The applied shear at any station, y_L, is

$$N_{Z_A} = \int_a^{y_L} \omega dy$$

which gives the net shear as

$$N_{Z_N} = \frac{\omega y_L}{2}$$

Cross-sectional area of the nose ribs to react the net shear is

$$a_S = \frac{\omega y_L}{2\sigma_S}$$

so that the material volume at that section will be

$$AV_S = \int_o^{y_{L_S}} \frac{\omega y_L}{2\sigma_S} dy = \frac{\omega y_{L_S}^2}{4\sigma_S}$$

Thus, the total material volume of the leading edge

$$V_{S_L} = \frac{2\omega}{4\sigma_S} \int_o^S y_{LS}^2 \, dS$$

$$= \frac{\omega}{8\sigma_S} \frac{\lambda^2 C_R^2 (1 - k)^2 \cos \Lambda_{FS} \frac{b}{2}}{3} \left[\left(\frac{1}{\lambda}\right)^2 + \left(\frac{1}{\lambda}\right) + 1 \right]$$

and, therefore, the weight of the leading edge is

$$W_{L_S} = \left(\frac{\omega \rho_m}{8\sigma_S}\right) \frac{\lambda^2 C_R^2 (1 - k)^2 \, b/2}{3} \left[\left(\frac{1}{\lambda}\right)^2 + \left(\frac{1}{\lambda}\right) + 1 \right] \cos \Lambda_{FS}$$

Similarly, the weight of the trailing edge is

$$W_{T_S} = \left(\frac{\omega \rho_m}{8\sigma_S}\right) \frac{\lambda^2 C_R^2 (1 - k)^2 \, b/2}{3} \left[\left(\frac{1}{\lambda}\right)^2 + \frac{1}{\lambda} + 1\right] \cos \Lambda_{RS}$$

The carry-through structure is assumed to consist of a beam to transfer the bending across for balance, and a frame to react the shear into the fuselage skins.

The bending moment at the root rib is

$$M_R = \frac{\omega C_R b^2 \lambda}{24} \left(2 + \frac{1}{\lambda}\right)$$

and the root thickness is $t_c \, C_R$.

Therefore, the load in the beam caps:

$$N_{SR} = \frac{\omega b^2 \lambda}{24 \, t_c} \left(2 + \frac{1}{\lambda}\right)$$

The total cross-sectional area required to resist the bending moment is

$$A_R = \frac{\omega b^2 \lambda}{12 \, t_c \sigma_a} \left(2 + \frac{1}{\lambda}\right)$$

Thus, the beam weight will be

$$W_B = \frac{\omega b^2 \lambda D \rho_m}{12 \, t_c \sigma_a} \left(2 + \frac{1}{\lambda}\right)$$

The wing shear is reacted via the circular ring frame and sheared out into the fuselage skins. Required cross-sectional area of the frame can be subdivided into areas required for axial load, A_A, for bending A_B, and for shear A_S. Total weight for the attachment frames is approximated by

$$W_F = \rho_m \pi D \left(1 - \frac{d_f}{D}\right) (2A_B + A_A + A_S)$$

where

d_f = depth of frame.

The required areas are based upon an average value of the load or moment around the ring frame.

$$A_B = \frac{M_{AV}}{d_f \sigma_a} = \frac{0.00506\,\omega A\,(D - d_f)}{d_f \sigma_a}$$

$$A_A = \frac{P_{AV}}{\sigma_a} = \frac{0.083\,\omega A}{\sigma_a}$$

$$A_S = \frac{Q_{AV}}{\sigma_S} = \frac{0.02525\,\omega A}{\sigma_S}$$

If the ratio of frame depth to frame diameter is assumed to be 0.1, then the frame weight is simplified to

$$W_F = 0.9\,\pi \rho_m D_w A \left(\frac{0.1741}{\sigma_a} + \frac{0.02525}{\sigma_S} \right)$$

Derivation of Aerodynamic Coefficients for Recoverable Booster

The vehicle design and the subsystem weights for the parametric synthesis program are strongly influenced by the external loads induced during the vertical boost phase. The regime of maximum dynamic pressure and its associated load will provide the design criteria for several of the major structural components of the stages. Of prime interest are the normal force coefficients, C_N, and center of pressure, c.p., for the various sublements of the booster and a gross estimate of the vehicle drag.

The estimation of C_N and c.p. are based on references B-4 and B-5 and this section describes the methods being used to determine the normal force coefficient and the center of pressure. The data presented, which are based primarily on theoretical analyses, have been substantiated with experimental data by various governmental agencies. The analyses are limited for the Mach range of 1.2 to 1.8, which corresponds to the region of high dynamic pressure and, therefore, maximum aerodynamic loads. This region will be adequate for vertically launched vehicles with a moderate T/W at liftoff.

The approach taken was to divide the vehicle into components of simple geometric shapes and to analyze each component separately with respect to both initial slope and center of pressure. For each component, the normal force coefficient can be expressed as

$$C_N = C_{N_\alpha} \alpha + \eta C_D \frac{A_P}{A} \sin^2 \alpha \qquad \text{(B-22)}$$

The first term is the initial slope or linear term, and the second is the cross-flow term.

Figure B-15 indicates the geometric elements that make up the vehicle system. The C_{N_α} and c.p. estimation for each element are discussed in the following sections.

Cone - cylinder ($\alpha \neq 0°$). - The vehicle's payload and top stage can be represented as a cone cylinder. During the maximum dynamic pressure regimes the vehicle's Mach number is approximately 1.5, therefore, data for the normal force coefficient and center of pressure for supersonic bodies are modified from reference B-4 . These data are only applicable where laminar flow is expected, but the non-linear cross-flow drag contribution to normal force has been included.

For the parametric studies, the value of $\beta = \sqrt{M^2 - 1}$ ranges from 0.6 to 1.5, with an angle of attack approximately 10 degrees. For most practical vehicles, the ratio of cylinder length to cone length is greater than 1. With these ranges of parameters, the value of βC_N can be considered to be independent of the cylinder-to-cone-length ratio. Therefore, the normal force coefficient can be empirically expressed as follows

$$C_N = 0.00313 \beta\alpha^2 \text{ X } 0.0125 \alpha + \frac{0.10}{\beta} \qquad \text{(B-23)}$$

where

$\beta = \sqrt{M^2 - 1}$

α = angle of attack

M = Mach number

A representation of this is shown in figure B-16 for comparison with the original data from reference B-4 . The approximation gives close agreement for $l_a/l_n > 1.0$ and $4° > \beta\alpha > 16°$. The center of pressure for the cone

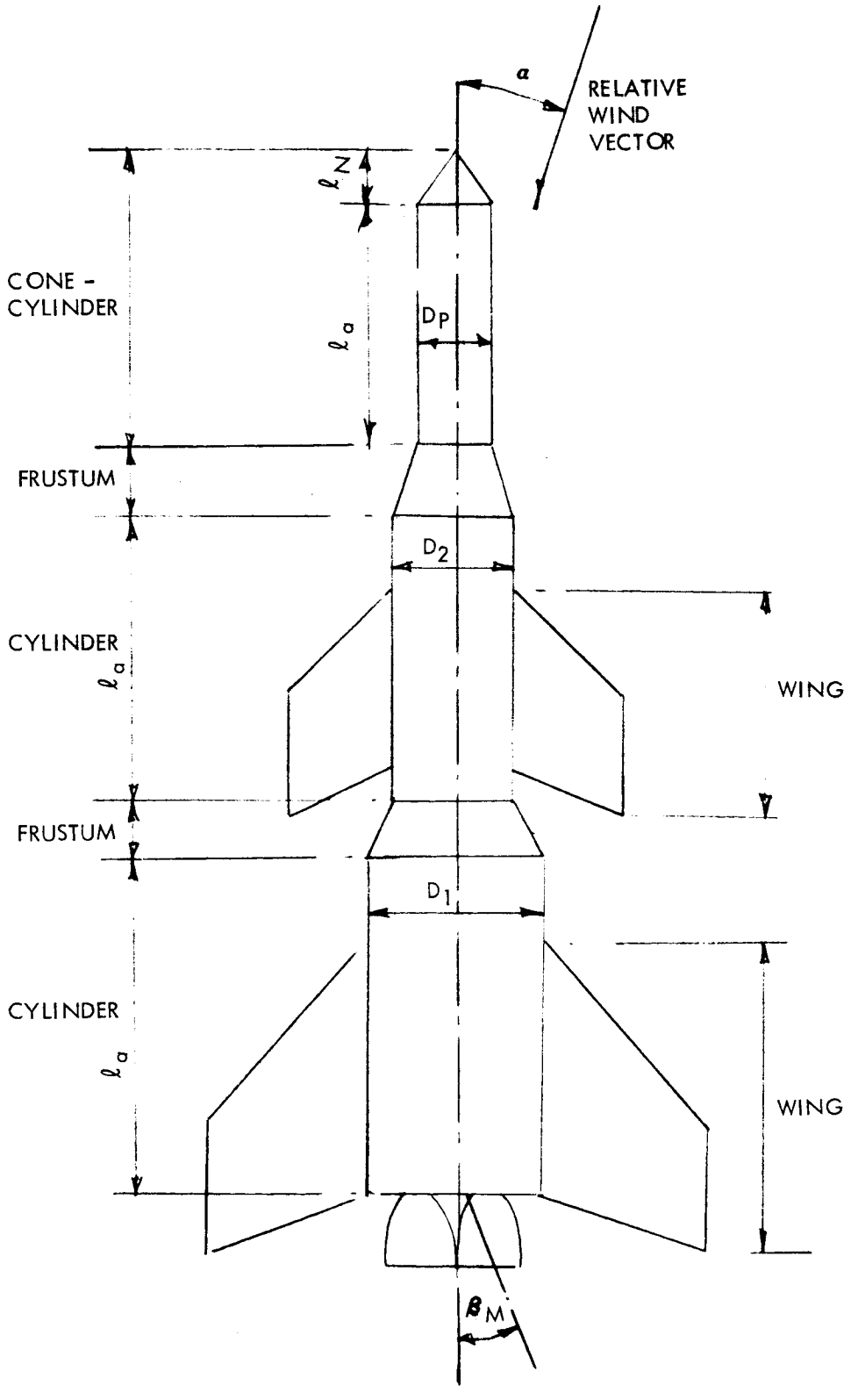

Figure B-15. - Basic Geometric Elements of Vehicle System

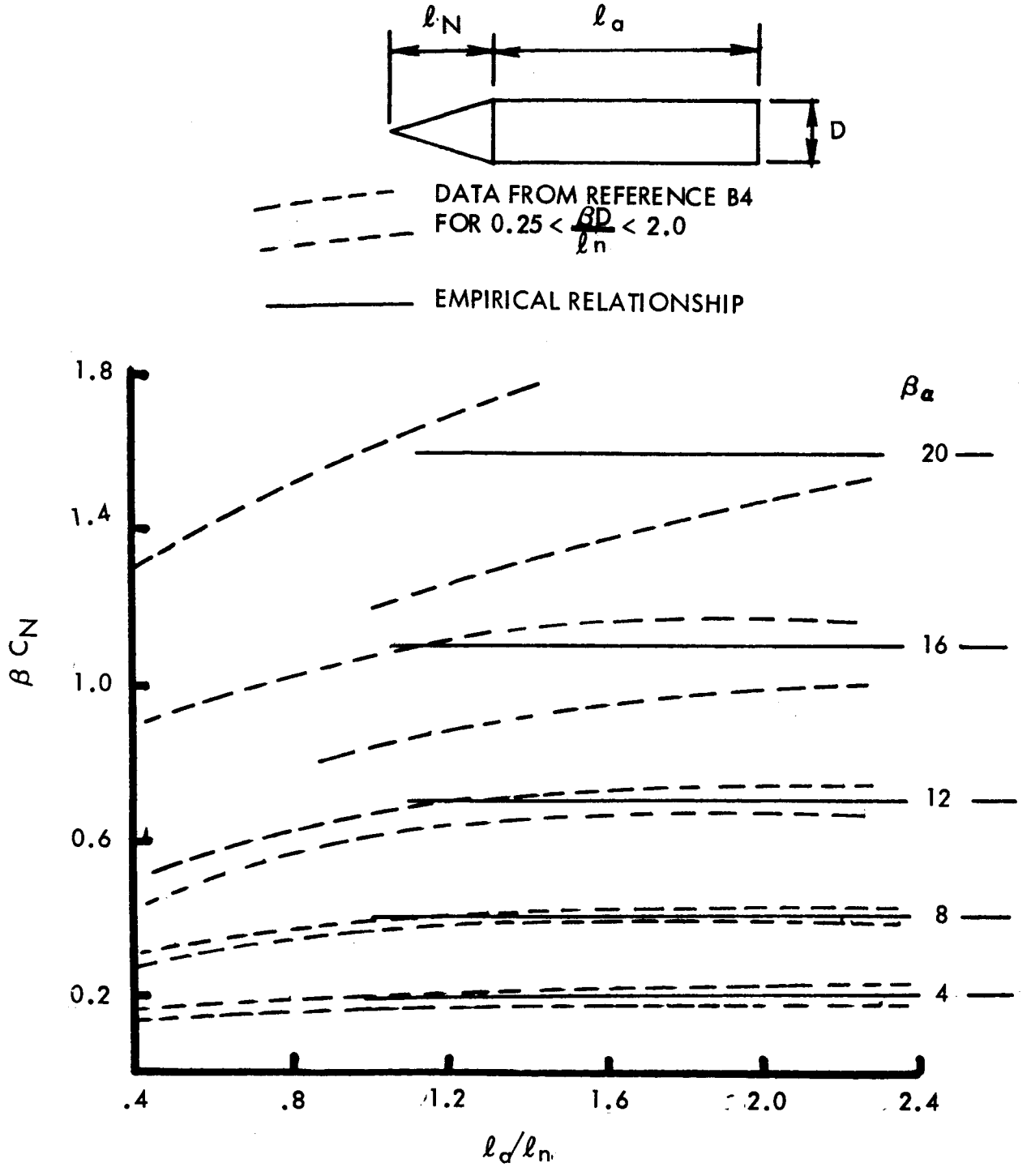

Figure B-16. - Cone-Cylinder Normal Force Coefficient

cylinder element is a function of (l_a/l_n) and $(\beta D/l_n)$. For the range of interest and since the c.p. estimation will only be used for the estimation of the bending moment throughout the vehicle's length, a reasonable error percent of c.p. position can be tolerated. This is reasonable when the element's C_N contribution is considered at a large distance away from that element. Therefore, the parametric estimate of the c.p. will be assumed to be $0.80\ l_n$.

Cylindrical section. - The initial normal slope for cylindrical sections is based on data contained in reference B-2 for configurations with conical forebodies and cylindrical afterbodies. In order to isolate the carry-over on the cylinder, the contribution of the conical forebody was subtracted from the cone-cylinder combination. The data presented in reference B-2 are reported to agree fairly well with the experimental test results; however, the lowest Mach number shown was 2.0. For the purpose of this analysis it was necessary to extrapolate the Mach number down to 1.2. The initial normal slope for cylindrical section versus Mach number is expressed empirically by

$$C_N = 0.0108\ (\text{Mach number}) - 0.0024 \tag{B-24}$$

Since the normal force contribution from cylinders is small compared to cones and frustums, this approximation will be acceptable for a range of cylindrical fineness ratio from 1 to 5.

The c.p. for the cylinder was taken from reference B-2 and expressed as

$$\frac{\text{c.p.}}{D} = \min(Y,\ Z) \tag{B-25}$$

where

$$Y = A\ (\text{Mach number} - 1.2) + B$$

$$Z = 0.4\left(\frac{\ell_a}{D}\right) - 0.08\left(\frac{\ell_a}{D} - 1\right)^{3/2}$$

$$A = \min\left(1.9,\ -0.275 + 0.625\left(\frac{\ell_a}{D}\right)\right)$$

$$B = 0.14 + 0.14\left(\frac{\ell_a}{D}\right)$$

This relationship for c.p. is compared with the original data in figure B-17. The center of pressure for the cylindrical section is based on the assumption that the load distribution has the same shape as the

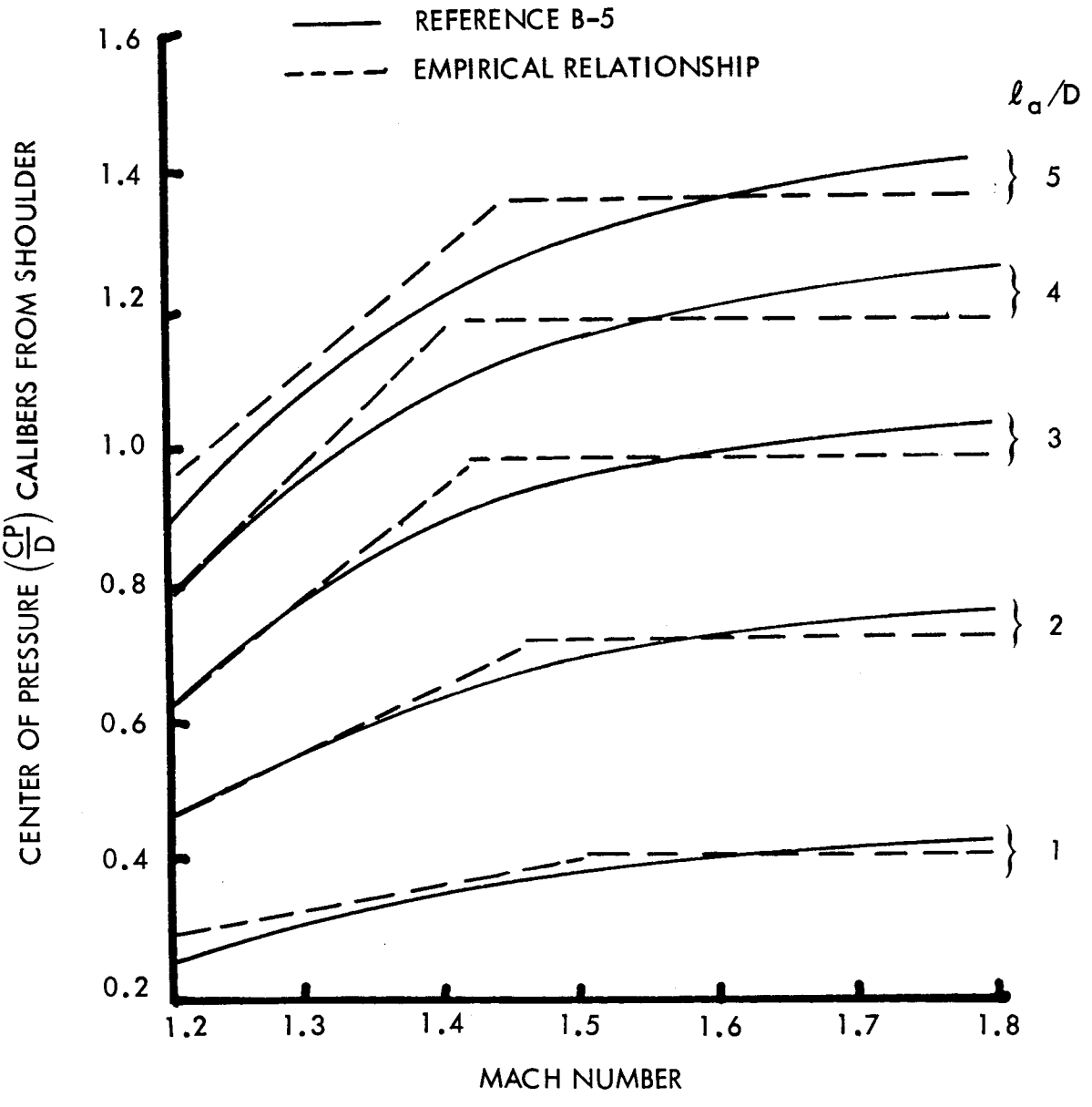

Figure B-17. - Center of Pressure for Cylindrical Sections

corresponding zero-angle-of-attack pressure distribution (ref. B-5). Figure B-17 is reproduced from reference B-2 to show the effects of Mach number and fineness ratio on the center of pressure for a forebody cone angle of 15 degrees. In addition, reference B-2 contains similar plots for smaller forebody cone angles, but examination of the data indicates that the effects of cone angle on the center of pressure of the cylinder carry-over is negligible, especially for cone angles in the range anticipated for the booster vehicles.

Frustums. - Experimental data are available for both cone-cylinder and cone-cylinder-frustum configurations in reference B-2 . By subtracting the normal force coefficient for the cone-cylinder from the total normal force coefficient for cone-cylinder-frustum configurations, the normal force coefficient and its slope, which is contributed by the frustum alone, can be estimated. It is recognized that the normal force coefficient for the cone-cylinder would be larger if it had been considered in presence of the frustum afterbody. This is because of the additional pressure associated with flow separation. It is impossible to evaluate these effects without pressure distribution data; however, the small error introduced by neglecting these effects is well within the accuracy of the overall analysis. The normal force coefficients result from the initial slope and the amount attributed to flow separation. Measurement of the initial slope from experimental data for frustums with large vertex angles at low transonic Mach numbers would produce an extremely large initial slope, not valid above three-degree angle of attack (fig. B-18).

The cross-flow effects will amount to less than 5 percent and have been subtracted from the total moment force coefficient to determine the contribution of potential flow. At discrete angles of attack, this remaining normal force coefficient is divided by d to yield an effective initial slope that is valid at small angle of attack. The initial slope is then seen to decrease with α; for α's corresponding to high dynamic pressure, the effective initial slope is about half the actual initial slope. The C_{N_α} curves from reference B-2 have been parameterized for inclusion into the synthesis program and are given by:

$$C_N = A\alpha + B \qquad \text{(B-26)}$$

where

$$A = C_1 \left(\frac{D}{d}\right)^2 + C_2$$

$$B = C_3 \left(\frac{D}{d}\right)^2 + C_4$$

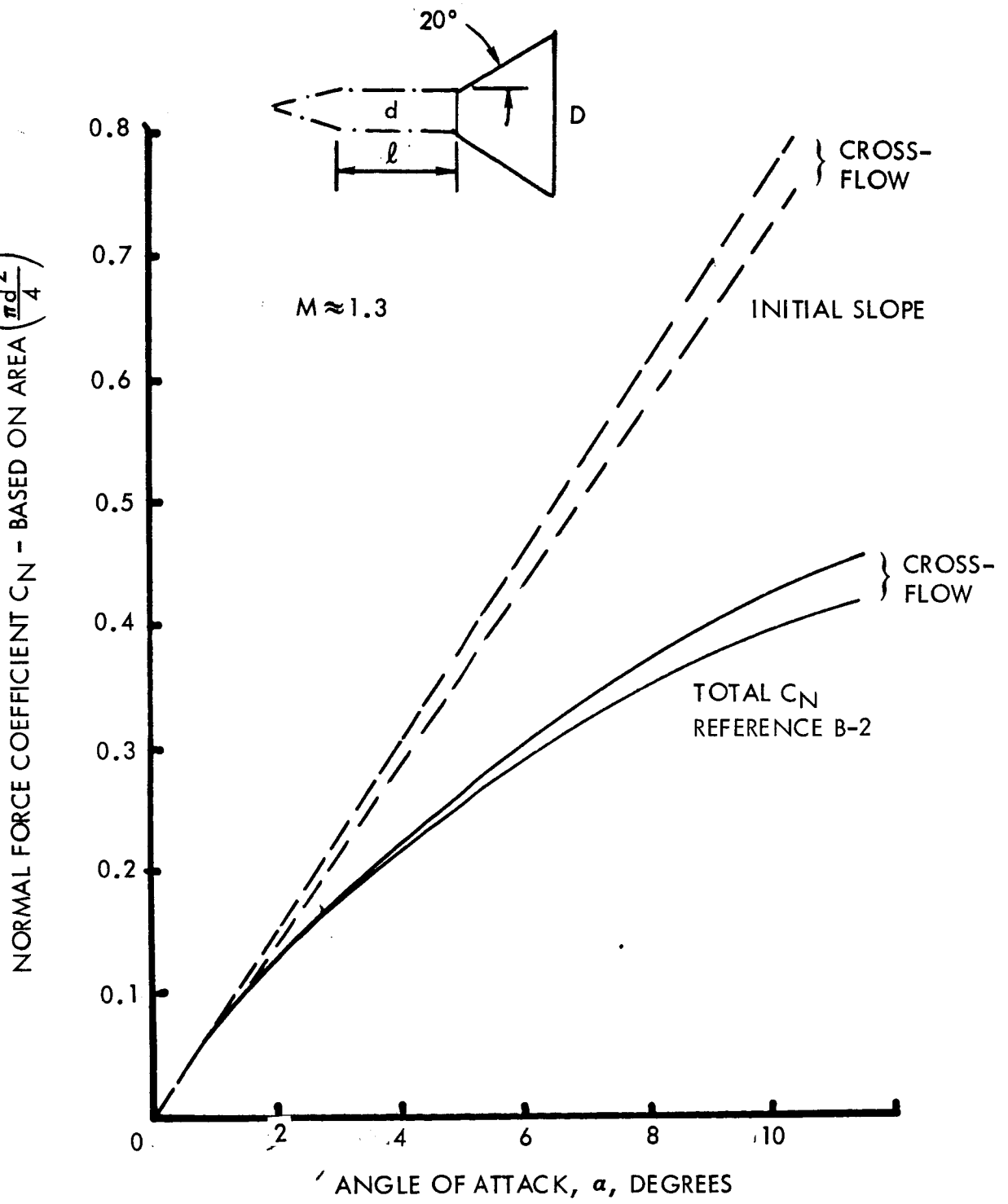

Figure B-18. - Normal Force Coefficients for 20-Degree Frustums

and where C_1 to C_4 are functions of the frustum angle θ and these values are shown in figure B-19. They give close agreement with reference B-2 for the angles of attack likely to be encountered at maximum dynamic pressure. The resulting empirical curves for C_N are shown in figure B-20. The total normal force, including cross-flow effects, is given by

$$C_N = 1.04\, C_{N_\alpha} \cdot \alpha \qquad \text{(B-27)}$$

The relationship for C_{N_α} has been assumed to be independent of the Mach number in the transonic region. The center of pressure for the frustum elements can be considered as 1/3 the frustum length forward of the rear shoulder without incurring any appreciable errors in the moment evaluation.

Wing alone. - A major design condition for the recoverable vehicles will occur during the maximum dynamic pressure regime. The lift contribution from the wings will contribute greatly to the over-all loading of the vehicle shell and tankage. It is anticipated that the vehicle velocity will be supersonic during this regime $1.2 < M < 1.5$. The lift curve slopes of unyawed symmetrical wings of hexagonal planform and with polygonal airfoil sections for supersonic Mach numbers were obtained from references B-2 and B-6 . The lift curve slope is expressed by 12

$$\beta \frac{dC_L}{d\alpha} = \beta \frac{dC_{L_o}}{d\alpha} + \beta \frac{d\Delta C_L}{d\alpha} \qquad \text{(B-28)}$$

where ΔC_L = incremental correction due to side edge effect. For the parametric synthesis program, the empirical relationship is subdivided into two portions, subsonic and supersonic leading edges.

Supersonic is defined by

$$m > 1.0 \qquad \text{(B-29)}$$

where

$m = \beta \tan \Lambda_{LE}$

$\beta = \sqrt{M^2 - 1}$

M = Mach number

Λ_{LE} = shape of the leading edge

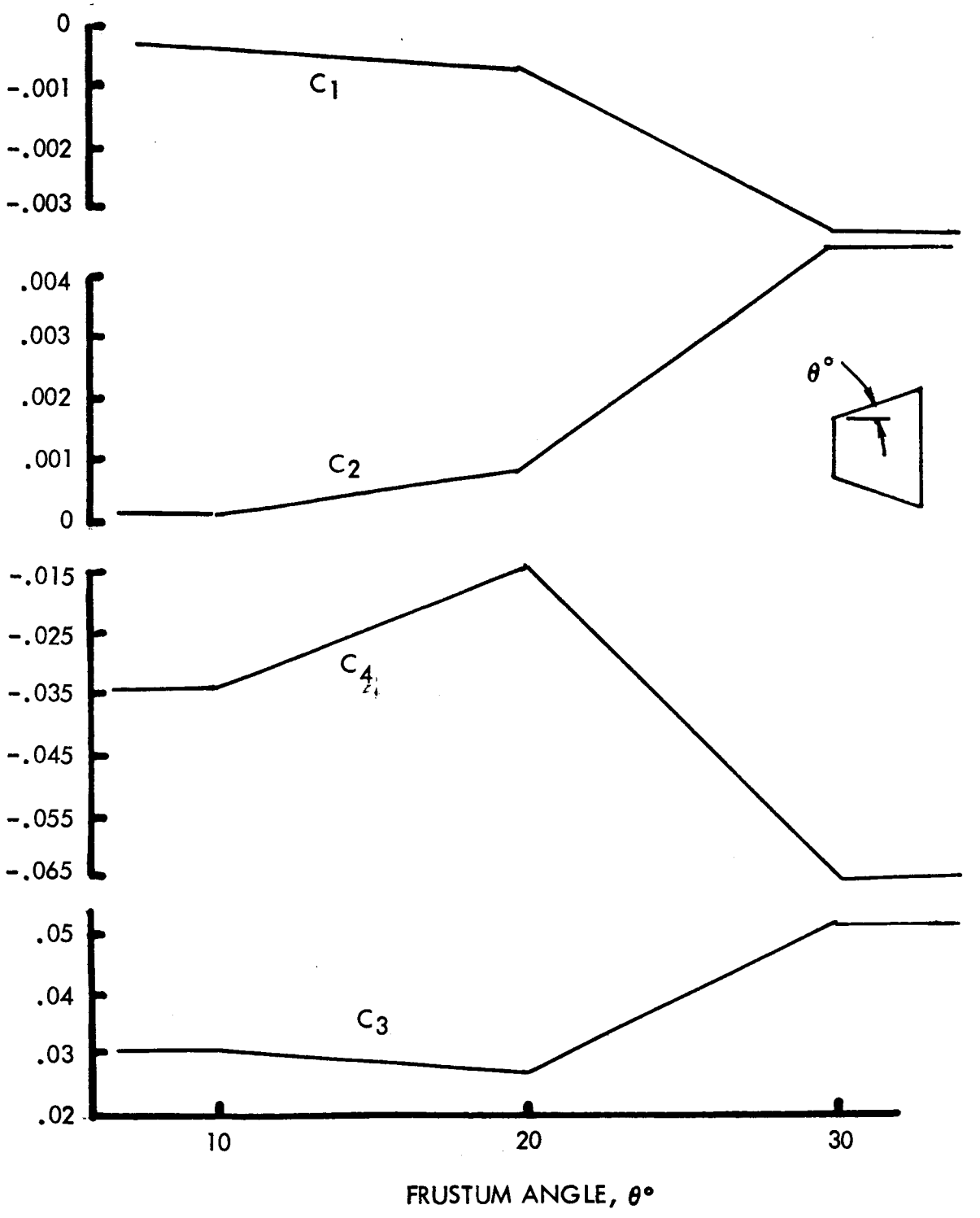

Figure B-19. - Empirical Coefficients for Frustum

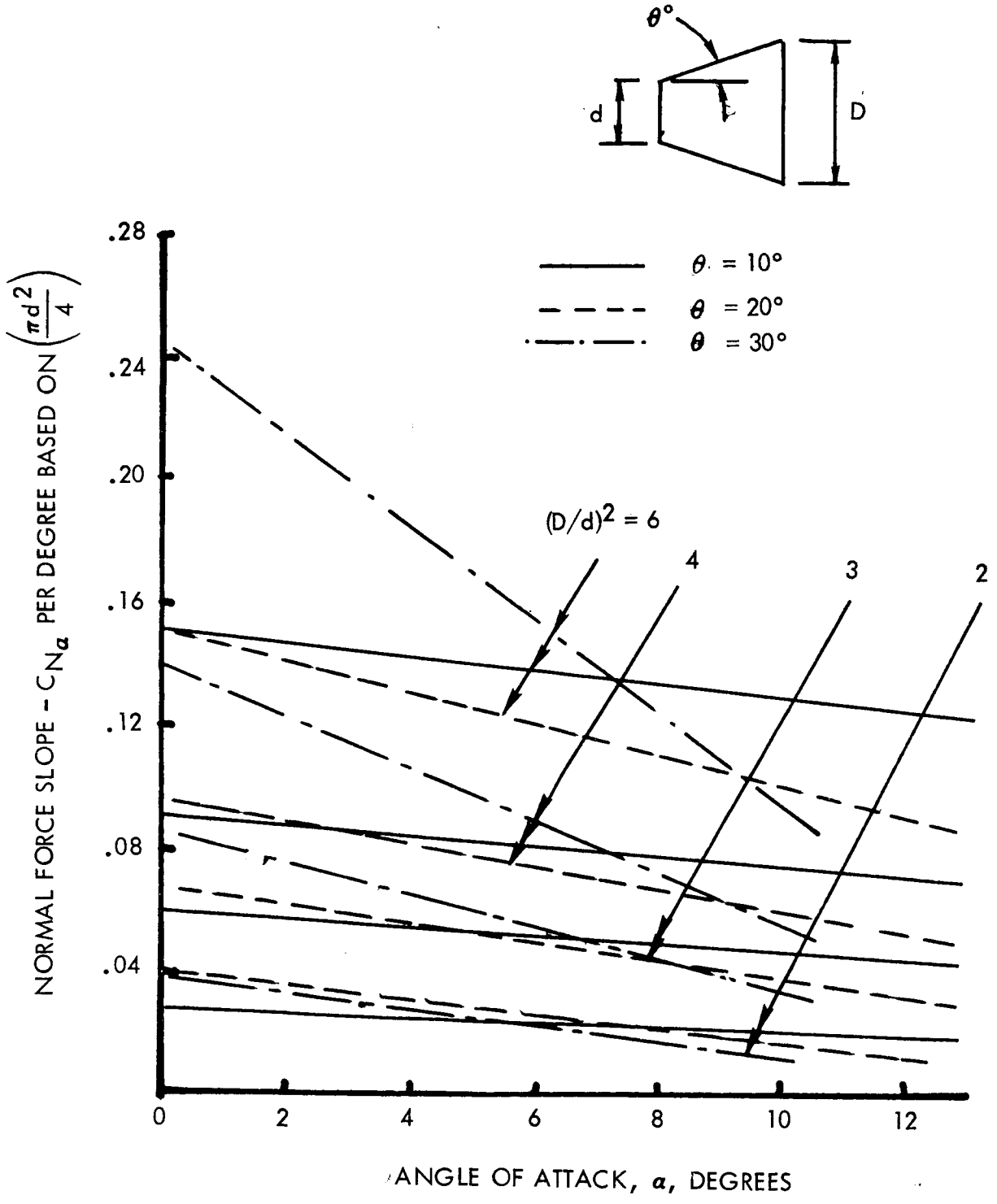

Figure B-20. - Normal Force Slope Versus Angle of Attack

The relationship can be expressed as follows

(Subsonic)

$$\beta \frac{dC_{L_o}}{d\alpha} = a\,(1 - m) + B - k\,(1 - m)^2 - 2.5 \left(\frac{a_t}{m}\right)^3 \left(1 - e^{1 - m_t/m}\right) m \tag{B-30}$$

(Supersonic)

$$\beta \frac{dC_{L_o}}{d\alpha} = 3.6 + \left(\frac{a_t}{m}\right) - \left[1.05 - 2.25 \left(\frac{a_t}{m}\right)^2\right] e^{0.7\,(1 - m)} \tag{B-31}$$

$$- 2.5 \left(\frac{a_t}{m}\right)^3 \left(1 - e^{1 - m_t/m}\right) \frac{1}{m}$$

(Subsonic)

$$\beta \frac{d\Delta C_L}{d\alpha} = -0.9 + 0.87 \;@\; (a_t/m \geq 0.4)^2 - 0.5\,(0.6 - a_t/m) \left(1 - e^{1 - m_t/m}\right) \tag{B-32}$$

(Supersonic)

$$\beta \frac{d\Delta C_L}{d\alpha} = \left(\beta \frac{d\Delta C_L}{d\alpha}\right)\Bigg|_{\text{subsonic}} \cdot e^{-C\,(m - 1)} \tag{B-33}$$

where

$$\begin{aligned} a &= -1.30 - a_t/m \\ B &= 2.55 + 3.0\,(a_t/m)^{1.5} \\ K &= 0.5 + a_t/2m \\ a_t &= \beta \tan \theta \\ m_t &= \beta \tan \lambda_{TE} \\ C &= 0.45 + 2\,(a_t/m - 0.4) \end{aligned} \tag{B-34}$$

A graphical representation of the empirical lift-curve slope for a typical range of parameters using equations (B-30) through (B-34) as shown in

figure B-21. For the purposes of the parametric synthesis, this accuracy is more than sufficient. Therefore the wing-lift-curve shape is given by

$$\left(\frac{dC_L}{d\alpha}\right)_W = \left(\beta \frac{dC_L}{d\alpha}\right) \cdot \frac{1}{\beta} \tag{B-35}$$

The wing-body and body-wing interference effects, respectively, can be considered by:

$$C_{L_{W(B)}} = \left[K_{W(B)}\alpha + k_{W(B)}\delta_W\right]\left(\frac{dC_L}{d\alpha}\right)_W \tag{B-36}$$

and

$$C_{L_{B(W)}} = \left[K_{B(W)}\alpha + k_{B(W)}\delta_W\right]\left(\frac{dC_L}{d\alpha}\right)_W \tag{B-37}$$

The lift ratio $K_{W(B)}$ is greater than unity because of body upwash and $k_{W(B)}$ is approximately one. The lift ratios $K_{W(B)}$, $K_{B(W)}$ and $k_{B(W)}$ have been determined from slender body theory and are given by

$$\begin{aligned} K_{W(B)} &= 1.0 + \left(\frac{D}{S}\right) \\ K_{B(W)} &= 1.6 \left(\frac{D}{S}\right) \\ k_{B(W)} &= 1.0 \left(\frac{D}{S}\right) \\ k_{W(B)} &\approx 1.0 \end{aligned} \tag{B-38}$$

where

D = body diameter

S = surface span including body diameter

For the c. p. of the wing shape to calculate the loading effect on the vehicle's fuselage, the program assumes c. p. is at the fifty-percent chord. This assumption is fairly good, since the velocity is supersonic at the design load condition of maximum dynamic pressure.

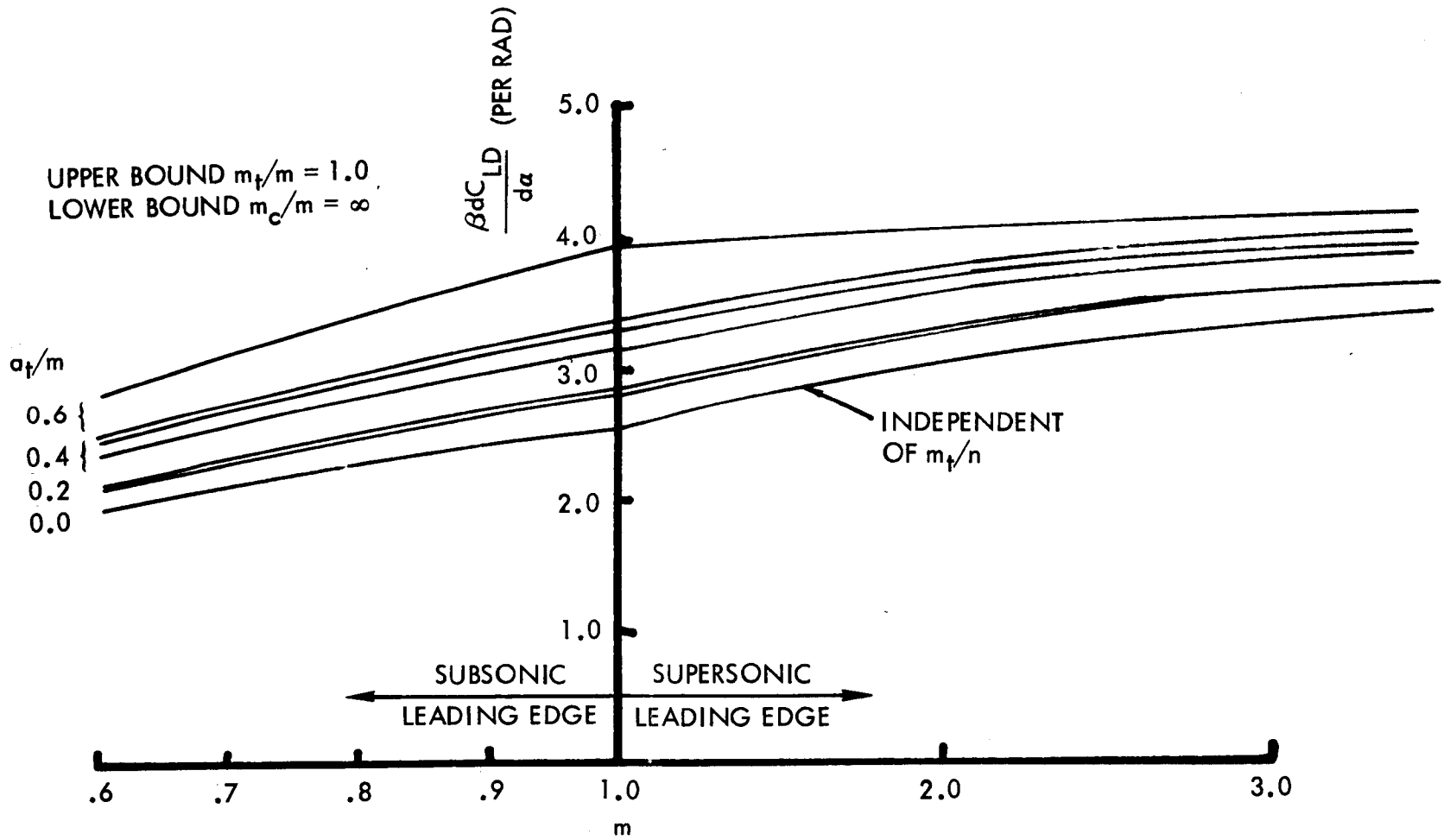

Figure B-21. - Supersonic Wing Lift Curve Slope

The synthesis of the aerodynamic characteristics for the various geometric elements of the vehicle system has been broken down into simple empirical relationship and should be included into a subroutine of the parametric vehicle synthesis program. This subroutine should consist of these empirical relationships plus the appropriate logic for the determination of the various geometric shapes of these elements to evaluate the system C_N and c.p. characteristics. The existing subroutine provides a more gross estimate by requiring C_N input data for the dummy subroutine.

Subsystem Weights

The Launch Vehicle Parametric Synthesis Program was developed as an evaluation tool principally for measuring the effects of changes in structures and materials upon vehicle weight, performance and cost. In order to accomplish this objective and to provide flexibility in the synthesis process, some analyses must be differentiated from the main parametric program. Analysis of the shell and bulkhead elements is handled in more detailed design synthesis subroutines; generalized curves from these subroutines are input to the variant bulk data section of the program. This technique removes all constraints on types of construction and types of material input to the program.

For each program run, a particular bulkhead type, shell construction, and material may be input. Two separate shell weight curves are read in as variable data (WT/R versus Nx/R). The first is for unpressurized shells subjected to no internal pressure and elevated flight temperatures. The second curve is for pressurized shells subjected to wetted propellant wall temperatures. Figure B-22 shows typical curves for an aluminum integral skin-stringer concept. These curves reflect a particular input minimum-gauge philosophy. The skin-stringer analysis technique was previously presented in reference B-1. In the invariant bulk data section of the program there are adjustment coefficients which permit alignment of results to particular designs and restrictions.

One factor that must be considered in assessing the weight-performance effects of structural shells and bulkheads is associated with non-optimum weights. This "weight-complexity factor" is included to account for material tolerances, miscellaneous attachments, etc. Tables B-11 and B-12 summarize the type of factors employed in this study.

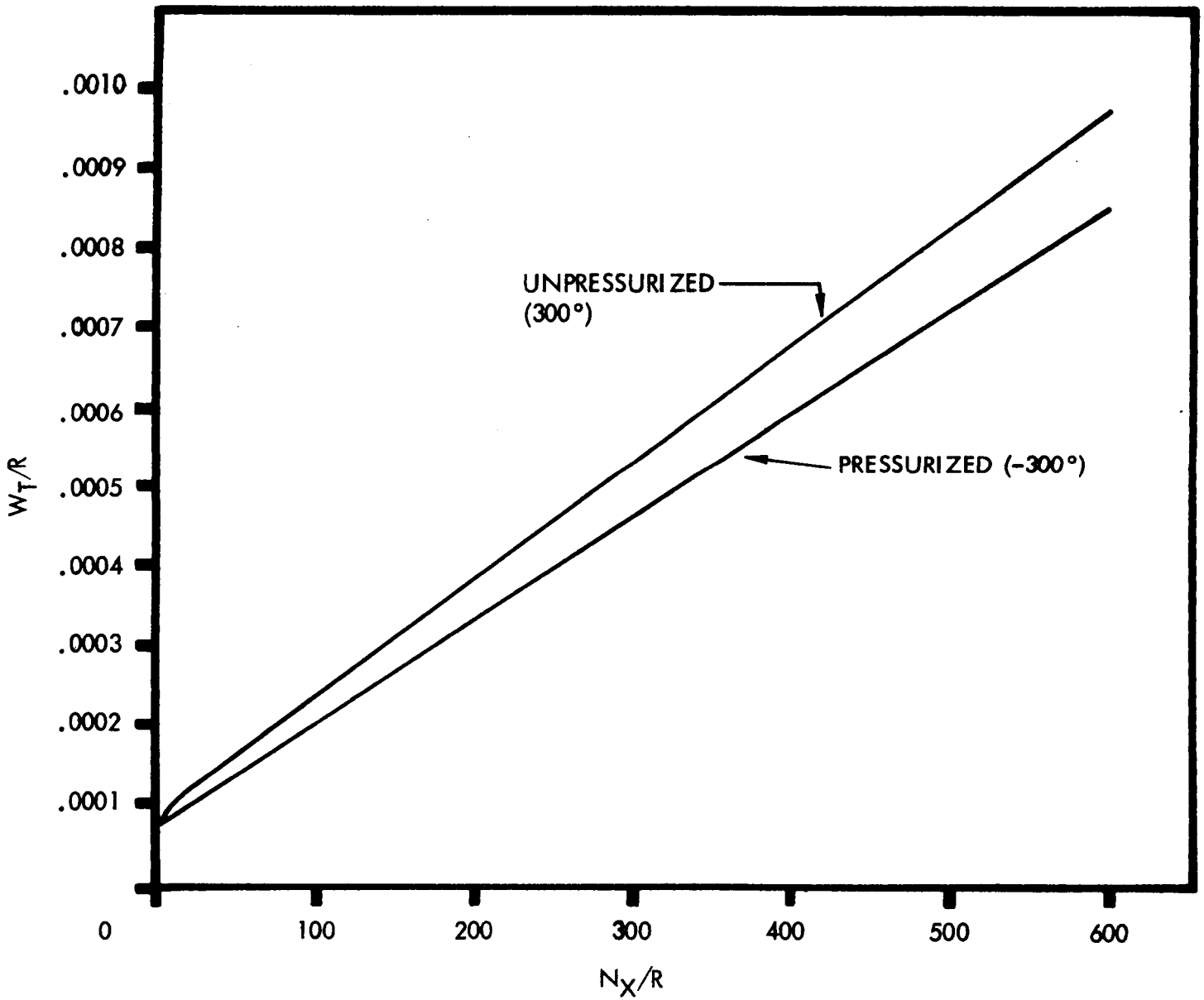

Figure B-22. - Weight-Versus-Load Curve

TABLE B-11. - SHELL WEIGHT COMPLEXITY FACTORS

Shell Structure	Complexity Factors (percent)	
	Stage 1	Upper Stages
Monocoque	8	7
Aluminum	10	10
Titanium	10	10
Beryllium	8	7
Steel		
Skin-Stringer		
Aluminum	10	8
Titanium	12	10
Beryllium	12	10
Steel	10	8
Waffle		
Aluminum	10	8
Titanium	12	10
Beryllium	12	10
Steel	10	8
Honeycomb Sandwich		
Aluminum	12	10
Titanium	12	10
Beryllium	14	12
Steel	12	10
Corrugated Sandwich		
Aluminum	12	11
Titanium	12	11
Beryllium	14	12
Steel	12	11
Double-Wall		
Aluminum	12	11
Titanium	12	11
Beryllium	14	12
Steel	12	11

TABLE B-12. - BULKHEAD WEIGHT COMPLEXITY FACTORS

Bulkhead Structure	Complexity Factors (percent)		
	Bulkhead Diameter (ft)		
	60	30	20
Forward			
Aluminum	9	8	9
Titanium	11	9	11
Beryllium	11	9	11
Steel	9	8	9
Aft			
Aluminum	10	9	10
Titanium	12	10	12
Beryllium	12	10	12
Steel	10	9	10
Common			
Aluminum	14	12	14
Titanium	16	14	16
Beryllium	16	14	16
Steel	14	12	14
Semitoroidal			
Aluminum	14	12	14
Titanium	18	15	18
Beryllium	18	15	18
Steel	14	12	14

Bulkhead design data, table B-13, were transferred into more generalized weight coefficients as described in the first section of this Appendix and figures B-6 and B-7. These coefficients are adjusted to account for joining and attachment.

An investigation of the subsystems weight scaling employed in references B-7 through B-9 indicated that many of the recoverable-stage subsystems could be scaled from adjusted equations for expendable vehicles. For example, main propulsion engine weight can be considered as a function of propellant weight and type of propellant as follows:

$$W_{ENG} = K_1 K_2 FST^{K_3}$$

TABLE B-13. - BULKHEAD DESIGN DATA PRINTOUT

CONSTRUCTION - ELLIPTICAL DOME BULKHEAD

MATERIAL - ALUMINUM B

YIELD STRESS	70000.0	MATERIAL DENSITY	0.1000	LIMIT LOAD FACTOR	1.1
ULTIMATE STRESS	80000.0	TEMPERATURE	-300.0000	ULT LOAD FACTOR	1.4
YOUNGS MODULUS	10600000.0	MIN SKIN THICKNESS	0.0100		

MAJOR RADIUS	MINOR RADIUS	NET PRESSURE	BULKHEAD SKIN THICKNESS EQUATOR	MID-POINT	APEX	WEIGHT
110.0	77.8	35.0	0.0476	0.0351	0.0337	240.3
110.0	77.8	50.0	0.0681	0.0501	0.0481	343.3
110.0	77.8	80.0	0.1089	0.0801	0.0770	549.4
130.0	91.9	35.0	0.0563	0.0414	0.0398	396.7
130.0	91.9	50.0	0.0804	0.0592	0.0569	566.7
130.0	91.9	80.0	0.1287	0.0947	0.0910	906.7
160.0	113.1	35.0	0.0693	0.0510	0.0490	739.6
160.0	113.1	50.0	0.0990	0.0729	0.0700	1056.6
160.0	113.1	80.0	0.1584	0.1166	0.1120	1690.6
198.0	140.0	35.0	0.0857	0.0631	0.0606	1401.6
198.0	140.0	50.0	0.1225	0.0902	0.0866	2002.3
198.0	140.0	80.0	0.1960	0.1443	0.1386	3203.6
270.0	191.0	35.0	0.1169	0.0861	0.0827	3554.0
270.0	191.0	50.0	0.1670	0.1229	0.1181	5077.1
270.0	191.0	80.0	0.2672	0.1967	0.1889	8123.4
320.0	226.3	35.0	0.1386	0.1020	0.0980	5916.7
320.0	226.3	50.0	0.1980	0.1457	0.1400	8452.4
320.0	226.3	80.0	0.3167	0.2331	0.2239	13523.9
324.0	229.1	35.0	0.1403	0.1033	0.0992	6141.3
324.0	229.1	50.0	0.2004	0.1475	0.1417	8773.3
324.0	229.1	80.0	0.3207	0.2361	0.2267	14037.3

where FST is total thrust, K_1, K_3 are scaling coefficients, and K_2 is a weighting parameter for the state of the art. Typical values are as follows:

Propulsion Type	K_1	K_2	K_3
$LO_2/RP1$	0.0427	1.073	0.895
LO_2/H_2	0.0245	1.041	0.958

The parametric program includes an additional adjustment factor to assist in measuring basic engine sizing parameters (expansion ratio, chamber pressure, etc.). The engine geometric sizing details were discussed in the opening section of this Appendix and are covered in more detail in reference B-7.

The flyback propulsion system is sized to range considerations and is discussed in the Flyback Requirements section of this Appendix, along with the effects of recovery range upon flyback fuel. Required insulation for both body and wing elements for recoverable stages is investigated in some detail in the parametric synthesis program. A discussion of the analysis technique is presented in the Thermal section of this Appendix.

Other subsystems weight scaling is handled in a parametric fashion, using the following primary weight relationships:

$$W_{\text{THRUST STRUCTURE}} = W_{ENG}\, K_4\, K_5$$

$$W_{\text{SEPARATION SYSTEM}} = W_p\, K_6\, K_7$$

$$W_{\text{THRUST VECTOR CONTROL}} = W_p\, 0.75\, K_8\, K_9$$

$$W_{\text{ULLAGE SYSTEM}} = W_p\, K_{10}\, K_{11}$$

$$W_{\text{PROP. FEED/PRESS. SYSTEM}} = W_p\, 0.5\, K_{12}\, K_{13}$$

$$W_{\text{FIXED EQUIPMENT}} = W_p\, 0.5\, K_{14}\, K_{15}$$

where

W_{ENG} = stage main propulsion engine weight

W_p = stage propellant weight

K_4, K_6, K_8, K_{10}, K_{12}, K_{14} = weight scaling coefficients

K_5, K_7, K_9, K_{11}, K_{13}, K_{15} = invariant data bank adjustment factors to align scaling equations to a particular system.

Items such as residual propellants and gases and the weight contingencies that should be included for each stage are handled as percentages of the stage propellant weight. The program provides a technique for quickly scaling all subsystem weights, and also provides a technique for adjusting weight details to approach a particular system design. For studies, such as described in this report, the ability to include similar system concepts in all vehicles provides a more effective comparison, even though slight adjustments to the subsystems might be required if the vehicles are subjected to a more detailed analysis.

Design Loading Criteria of Recoverable Boosters for Parametric Synthesis

During a parametric synthesis of any vehicle system, the weight estimation for the structural components is dependent upon the types and magnitudes of the loads imposed upon them. Therefore, the load-time history for the vehicle mission requires definition of details to adequately describe the resulting load conditions. The following four loading conditions are estimated for the parametric synthesis:

Prelaunch-unpressurized condition
Maximum dynamic pressure
End boost of stage one
Maximum heating during entry

These four conditions are simplified for their incorporation into the synthesis subroutines. The various techniques for their estimation are based upon experience with the Saturn V loading conditions and existing detail studies dealing with recoverable boosters (ref. B-7).

Each of the trajectory loading conditions and its associated thermal environment has to be scanned by the synthesis subroutine to derive the maximum design load envelope. This envelope is the maximum tension load for design of the skins for the pressure tanks, and the maximum compression due to axial load and bending moment for the unpressurized shells and the

tank stiffener elements. Since the material properties are dependent upon the design thermal environment, the N_x lb/in. compression has to consider the associated temperatures to define the design maximum envelope.

Prelaunch loads. - When the vehicle is fully fueled and sitting upon the launch pad, it is subjected to ground winds which exert a static drag force normal to the longitudinal or thrust axis.

$$D = \frac{1}{2} \rho V_W^2 C_D A_P \tag{B-39}$$

where

V_W = wind velocity, ft/sec

A_P = reference area, ft^2

The drag coefficient, C_D, is a function of Reynolds number. For most vehicles of the IRBM and larger classes, the Reynolds number is supercritical, and the $C_D \approx 0.7$ for a cylindrical vehicle. Steady winds of constant speed and direction create unsymmetrical, alternate vortex shedding (Von Karmen vortex), and these produce an oscillating force normal to the drag force. On top of the steady condition there is imposed a wing gust velocity. The vectorial sum of these drag forces produces a total design condition

$$\Delta F = \left\{ \begin{array}{l} \left[F_{SS_B} (1 + GF_S) + F_{SS_W} (1 + GF_W) \right]^2 \\ + \left[F_{SS_B} VF_B + F_{SS_W} VF_W \right]^2 \end{array} \right\}^{\frac{1}{2}} \tag{B-40}$$

where

F_{SS} = force on element due to steady-state winds

GF = gust factor $\approx$ 1.54 for Saturn vehicle (ref. B-10)

VF = vortex factor $\approx$ 1.25 for Saturn vehicle (ref. B-10)

B = body element

W = wing element

Here the i^{th} element of the vehicle stack is considered (sketch), where station zero is at the payload apex.

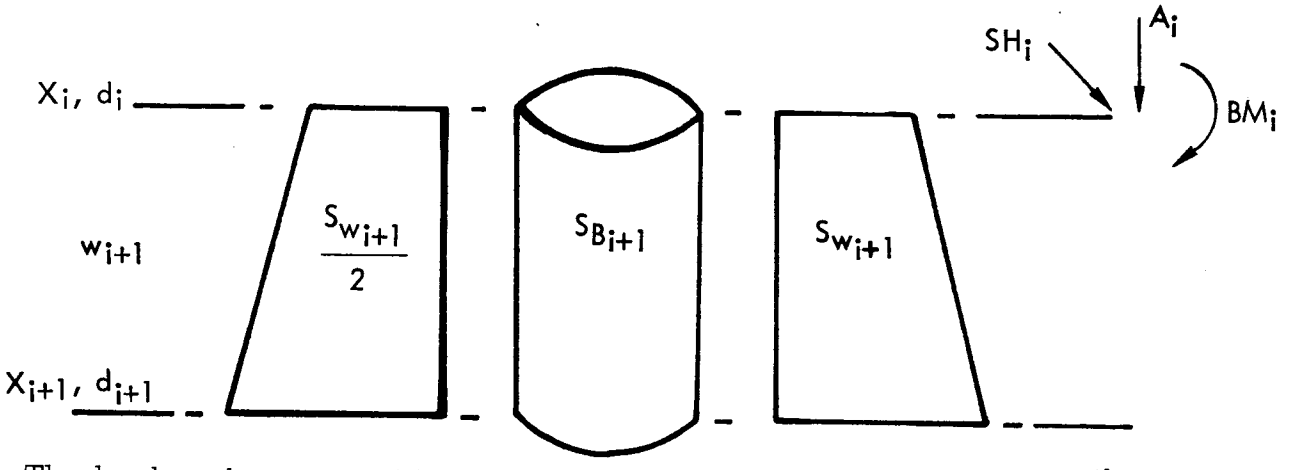

The loads, shears, and bending moments are required at the $i + 1^{th}$ station, assuming that they have been previously evaluated at the i^{th} station. The axial load is given by

$$A_{i+1} = A_i + W_{i+1} \tag{B-41}$$

The shear force and, hence, bending moments are due to the ground wind effects impinging on the vehicle. A linear wind velocity profile changing with altitude can be considered for the synthesis model. Therefore, the wind velocity affecting a particular structural component between station X_i and X_{i+1} is defined as

$$V_{W_{i+1}} = V_G - \frac{(V_G - V_H)}{H} (X - x_i) \tag{B-42}$$

where

V_H = wind velocity at altitude H

V_G = wind velocity at the ground

H = reference height ft

X = total vehicle length

The wind force on the body element is given by

$$L_{SS_{B_{i+1}}} = \frac{1}{2} \rho_{SL} V^2 W_{i+1} C_{D_B} \frac{(d_i + d_{i+1})}{2} (x_{i+1} - x_i)$$

and on the wings

$$L_{SS_{W_{i+1}}} = \frac{1}{2}\rho_{SL} V^2_{W_{i+1}} C_{D_W} S_{W_{i+1}} \tag{B-43}$$

The shear force is written as

$$SH_{i+1} = SH_i + \Delta F \tag{B-44}$$

Hence, the bending moment is

$$BM_{i+1} = BM_i + (x_{i+1} - x_i)\left(SH - \frac{\Delta F}{2}\right) \tag{B-45}$$

The axial loads and bending moments can be calculated for all stations of interest throughout the vehicle's length. This process will be undertaken the initial pass through the mass fraction subroutine. For subsequent passes where the vehicle's weight and size are varied by a moderate percentage, a quicker alternate-loads path is suggested where the previous loads are simply scaled as follows

$$A_i^{NEW} = \frac{W_o^{NEW}}{W_o^{OLD}} A_i^{OLD} \tag{B-46}$$

$$BM_i^{NEW} = \left(\frac{X^{NEW}}{X^{OLD}}\right)^2 BM_i^{OLD} \tag{B-47}$$

Maximum dynamic pressure region. - The maximum dynamic pressure region produces severe loading conditions which influence the design criteria for several structural components of the launch vehicle. A simplified model using a 3σ wind profile and a superimposed gust are a reasonable basis for the lift, control force, and bending moment evaluations. For preliminary design purposes, the vehicle's behavior is assessed for a steady wind shear with no angular rotation of vehicle, if sufficient engine control exists, or for maximum engine gimbal and a vehicular rotation. These loads do not consider the effects of gusts and transient angles of attack, but these can be included by the program operator with a dynamic response correction factor.

The relative angle of attack due to the vehicle's forward motion and the wind shear is given by

$$\alpha = \tan^{-1} \frac{V_{WIND}}{V_{FL\ SPEED}} \tag{B-48}$$

From experience (ref. B-4), it has been found that maximum dynamic pressure for a vertical launch vehicle occurs at altitudes between 30 000 and 35 000 feet. The burn time to maximum dynamic pressure is shown in figure B-23 and can be approximated by

$$t_{q_\alpha} = 42.1 \left(\frac{T}{W}\right)^2 - 175.2 \left(\frac{T}{W}\right) + 228 \tag{B-49}$$

This estimate of the burn time is required in the determination of fuel burned and the load distribution throughout the stage. The Mach number and the value of dynamic pressure are based upon numerous trajectory computations for ranges of initial T/W, and the average trends are shown in figure B-24. With a knowledge of α, q, and the reference areas, the normal and drag forces and center of pressure, c.p., for the total vehicle system can be assessed. The aerodynamic force coefficients for the major elements of the vehicle are described elsewhere.

The center of gravity, c.g., of the vehicle system at maximum dynamic pressure has to account for the amount of propellant burned since lift-off

$$W_{PROP}\Big|_{MAX\ q\alpha} \approx W_{PROP} - t_q \left(\frac{T}{I_{SP}}\right) \tag{B-50}$$

The remaining propellant can be proportioned between the tanks to produce the weight distribution for the c.g. position

$$c.g. = \frac{\sum W_i x_i}{\sum W_i} \tag{B-51}$$

and the center of pressure

$$c.p. = \frac{\sum D_i x_i}{\sum D_i} \tag{B-52}$$

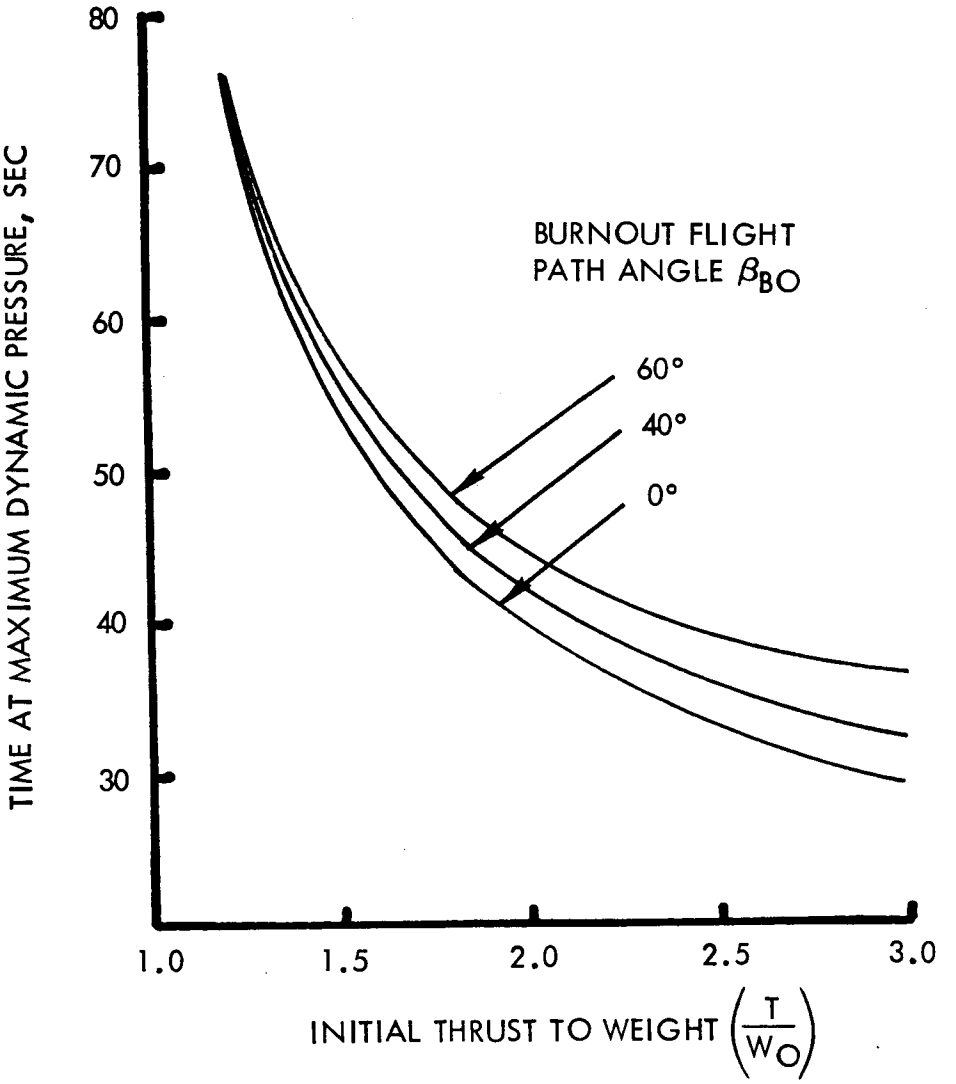

Figure B-23. - Time at Maximum Dynamic Pressure

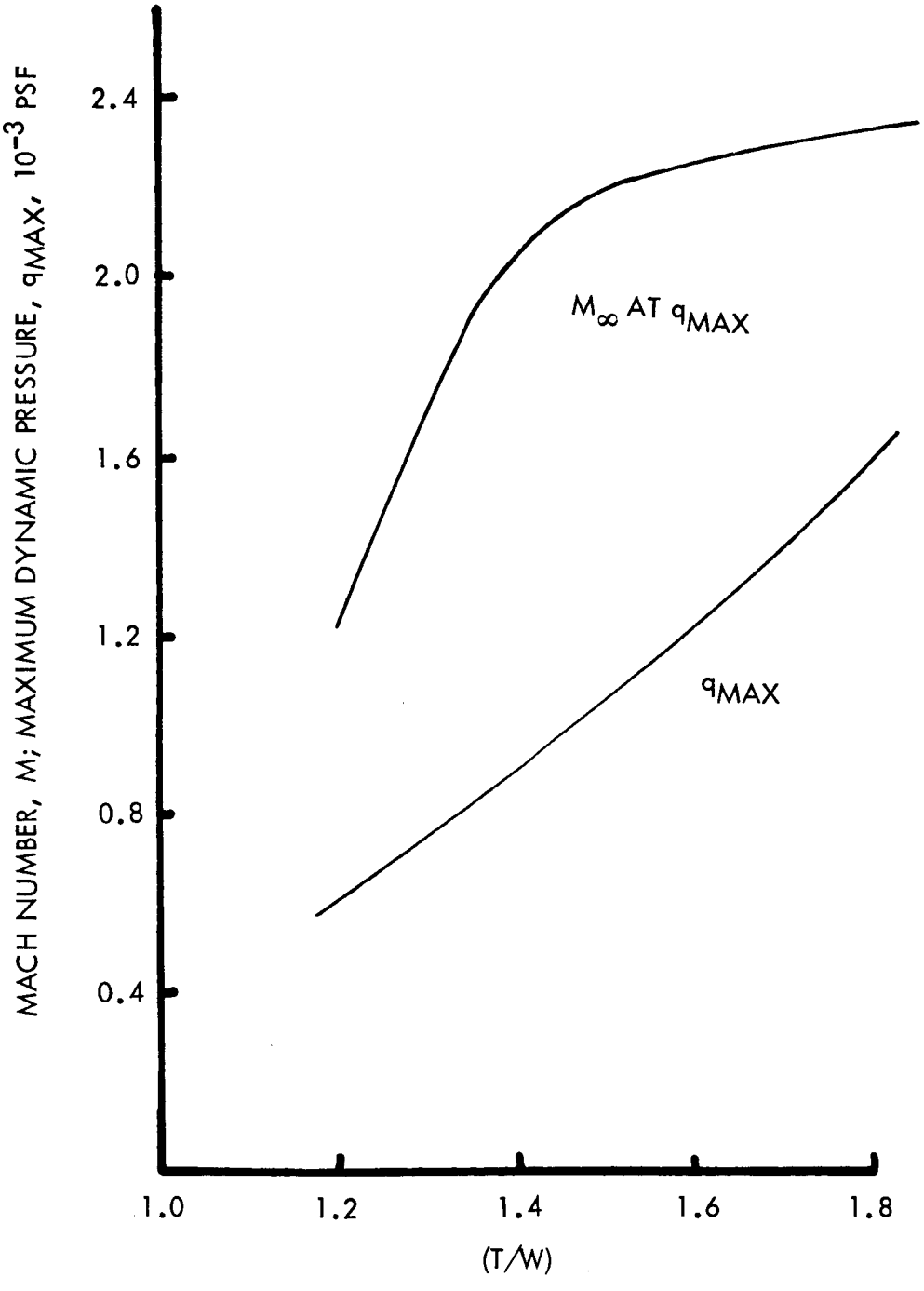

Figure B-24. - Velocity and Maximum Dynamic Pressures

where D_i is the normal force on the i^{th} element. These positions are measured relative to the payload so that, for stability, c.p. > c.g.. The effect of the aerodynamic moment about the center of gravity is

$$M_A = \sum D_i \text{ (c.g. - c.p.)} \tag{B-53}$$

To counteract this aerodynamic moment will be a control moment developed by the engine thrust. The gimbal thrust is given by

$$T_g = \frac{ng}{n} T \sin \beta \tag{B-54}$$

where

ng = number of gimbal engines of stage 1

n = total number of engines of stage 1

β = gimbal angle

The control force produces a control moment of

$$M_c = (\text{c.g.} - x_{ENG})\, T_g \tag{B-55}$$

For small angles of attack, the gimbal-engine-control moment will be sufficient to react the aerodynamic moment; therefore, the control force for the no-pitch condition will be

$$T_g = -\frac{M_a}{(\text{c.g.} - x_{ENG})} \tag{B-56}$$

When the maximum gimbal angle $\beta = \beta_{MAX}$ does not control, the vehicle will be subject to a pitching acceleration. The pitch inertia of the total vehicle is given by

$$I_P = \sum W_i x_i^2 - \sum W_i \text{c.g.}^2 \tag{B-57}$$

and the angular acceleration

$$\Omega_P = \frac{M_{C_{MAX}} + M_A}{I_P} \tag{B-58}$$

The vehicle is, therefore, subject to a lateral acceleration

$$\eta_y = \frac{\left(\sum D_i + T_g\right)}{\sum W_i} g, \text{ ft/sec}^2 \tag{B-59}$$

and lateral acceleration distribution

$$\eta_{y_i} = \eta_y + \Omega p(\text{c.g.} - x_i) \tag{B-60}$$

Therefore, the total equivalent shear force distribution is given by

$$F_{i+1} = F_i + D_{i+1} - \frac{\eta_{y_{i+1}}}{g} W_{i+1} \tag{B-61}$$

and the bending moment is

$$M_{i+1} = M_i + F_{i+1}\left(x_{i+1} - x_i\right) \tag{B-62}$$

The resulting axial engine thrust is

$$T_A = \frac{n_g}{n} T \cos \beta + \left(\frac{n - n_g}{n}\right) T \tag{B-63}$$

The total vehicle drag is given by

$$D = \sum D_i \tag{B-64}$$

The axial thrust minus the drag is the resultant axial force, producing an acceleration

$$\eta_x = \frac{(T_A - D)}{\sum W_i} g \tag{B-65}$$

from which the axial force distribution can be found to be

$$A_{i+1} = A_i + \eta_x W_{i+1} + D_{i+1} \tag{B-66}$$

End boost of stage one. - The final design load condition during the boost phase is just prior to staging, and it is assumed on the basis of past

experience that the dynamic pressure is negligible and will not contribute to the design load distribution. The maximum axial acceleration experienced by the vehicle is given by

$$\eta_x = \left(\frac{\text{THRUST}}{W_{BO}}\right) \tag{B-67}$$

If there has been a limit requested on the maximum acceleration by program input, the engine system is gradually shut down to fulfill this constraint. This early shutdown of an engine will increase the burning time and velocity losses of the first stage. The maximum axial force experienced by the structural components is given by

$$A_{i+1} = A_i + W_{i+1}\eta_x \tag{B-68}$$

Based upon a typical criterion used for the Saturn vehicle design, an engine thrust misalignment should be included to produce a vehicle bending moment. The lateral engine thrust due to misalignment can be expressed as

$$F_{LAT} = T \sin\left(\frac{1^\circ}{\sqrt{n}}\right) \tag{B-69}$$

where

n = number of engines

and the moment due to mismatch of thrust levels is

$$M_{LAT} = \frac{KD_E\Delta}{2} \tag{B-70}$$

where

K = 1.733 for the Saturn class vehicle

D_E = PCD of engines $\approx 0.6\, D_{STAGE}$

$$\Delta = \frac{\text{Maximum thrust - Minimum thrust}}{2}$$

These misalignments cause a lateral acceleration distribution along the vehicle center of gravity is given by

$$\text{c.g.} = \frac{\sum W_i x_i}{W_{BO}} \tag{B-71}$$

Pitching inertia is

$$I_{NA} = \sum W_i x_i^2 - W_{BO}\, c.g.^2 \tag{B-72}$$

and the lateral acceleration distribution is given by

$$\eta_{y_i} = \eta_y + \Omega\,(c.g. - x_i) \tag{B-73}$$

where

$$\eta_y = \frac{F_{LAT} \cdot g}{W_{BO}}$$

$$\Omega = \frac{\left[F_{LAT}\,(x_{ENG} - x_{c.g.}) + M_{LAT}\right] g}{I_{NA}} \tag{B-74}$$

The stationwise shear forces and bending moments at end boost can now be derived.

$$SH = SH + W_{i+1}\eta_{y_{i+1}}$$

$$BM_{i+1} = BM_i + (x_{i+1} - x_i)\left(SH - \frac{W_{i+1}}{2}\eta_{y_{i+1}}\right) \tag{B-75}$$

Maximum heating during entry. - For the initial mass fraction iteration, the condition of maximum heating during entry will not be required until the mass fraction estimate is consistent with the boost load design condition; i.e.:

$$W_{BO_{BOOST\ LOADS\ ONLY}} < W_{BO_{ESTIMATE}}$$

The discussion for the loads and thermal history for entry are explained in a subsequent section.

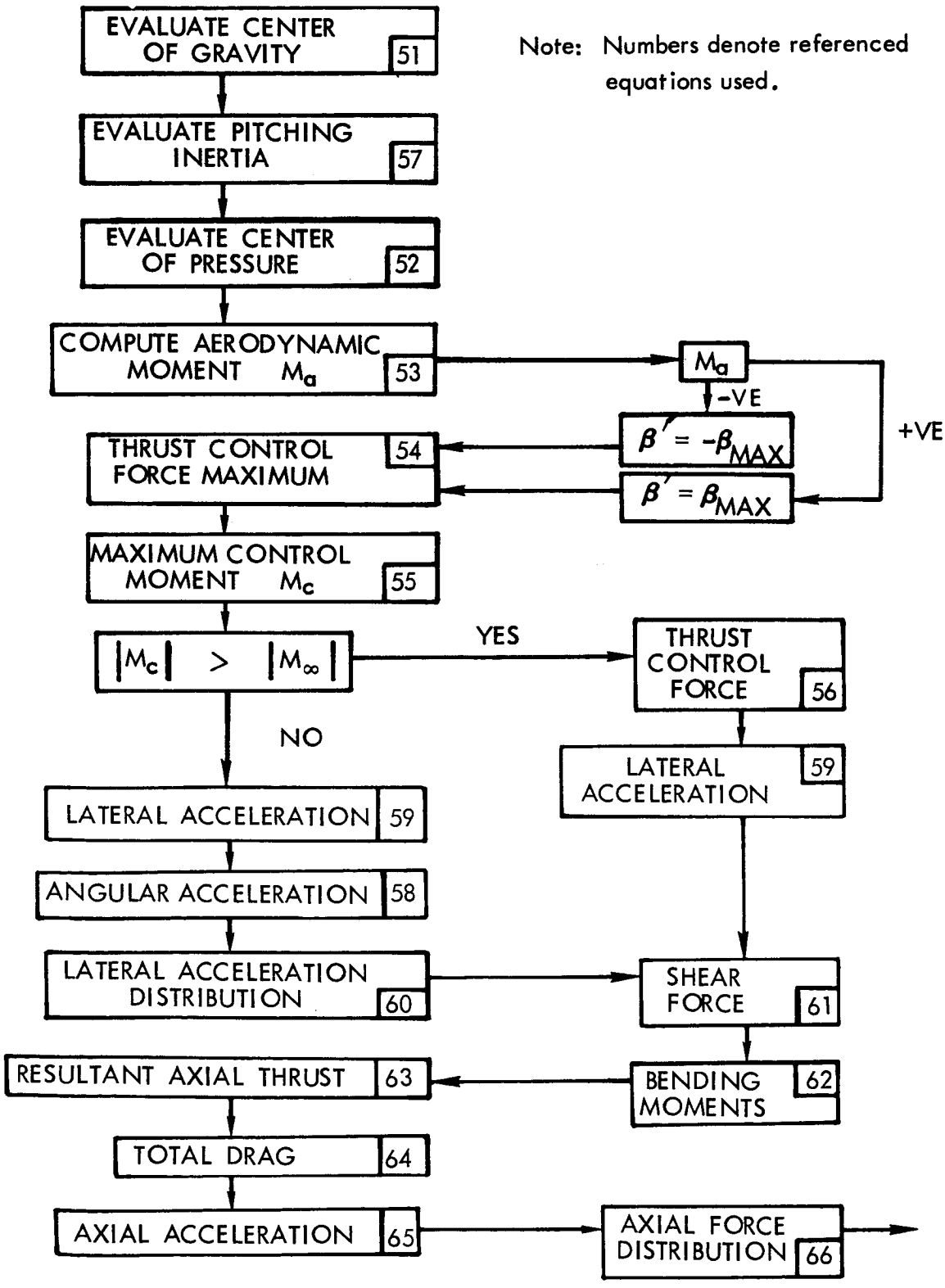

Figure B-25. - Maximum Dynamic Pressure Loads Subroutine

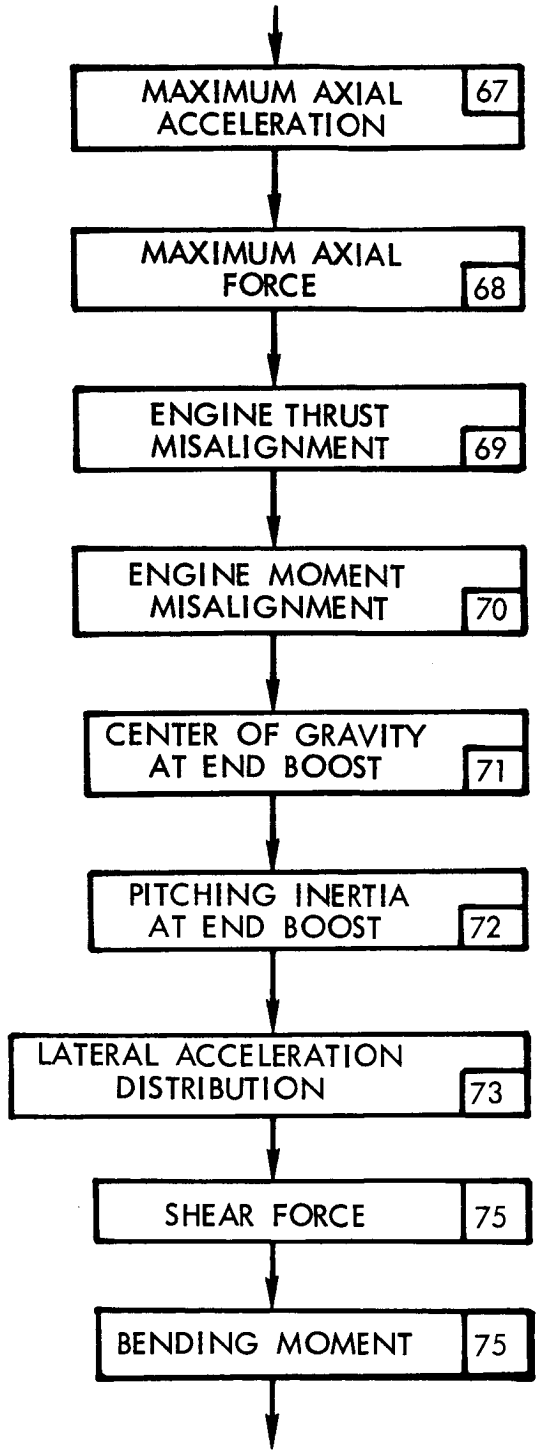

Note: Numbers denote referenced equations used.

Figure B-26. - End Boost Subroutine

Thermal Synthesis

The parametric synthesis program requires a simplified thermal mapping of the vehicle structures for the entry phase to assist in determining the weights of required insulation, if any, and the allowable stress levels to which the material can be worked at the elevated temperatures. Any completely automated entry-thermal synthesis is beyond the scope of this study and the allocated computer program running time. Therefore, the major portion of the thermal definition will be executed external to the synthesis program. For this study, the entry temperature is based upon previous studies; and the insulation weights, which have been developed by an additional structural synthesis routine, are systematically incorporated into the input data. This procedure allows the user to update or alter the temperature data and insulation weights to suit his own requirements. A short discussion of the parametric approach that has been adopted for this study indicates the type and quality of data that are employed in the program.

A first-stage entry trajectory is dependent upon the burnout conditions of the first-stage boost and the subsequent maneuver during entry. A typical altitude and velocity time history for this entry phase is shown in figure B-27. Various history profiles for the different vehicle systems should be considered to cover the range of staging velocities and attitudes.

The hypersonic velocity entry produces high temperatures over the vehicle surfaces. The aerodynamic heating rates for the body and wing of the first stage have been evaluated using an in-house IBM 7094 program which computes the heating rates through application of E. R. Van Driest's theory for a turbulent boundary layer for flat-plate flow. The equilibrium stagnation temperature for a one-foot-radius hemisphere as a function of velocity and its corresponding altitude are indicated in figure B-28.

Since the parametric synthesis is principally concerned with the total system weight, the program is not so much concerned with the temperatures at the stagnation point, but rather with a thermal mapping of the major portion of the vehicle. Therefore, equilibrium skin temperature five feet aft of the stagnation point have been plotted for a flat plate at an angle of attack of 20 degrees in figure B-29. The trajectory profile from figure B-27 can now be superimposed upon the temperature profiles to produce the skin temperature pattern. An example of this overlay mapping is shown in figure B-30, which shows an example of the equilibrium temperatures due to turbulent flows as the stage enters through the atmosphere with a 40-degree flight angle. These temperatures-altitude histories, coupled with attitude-time data given in

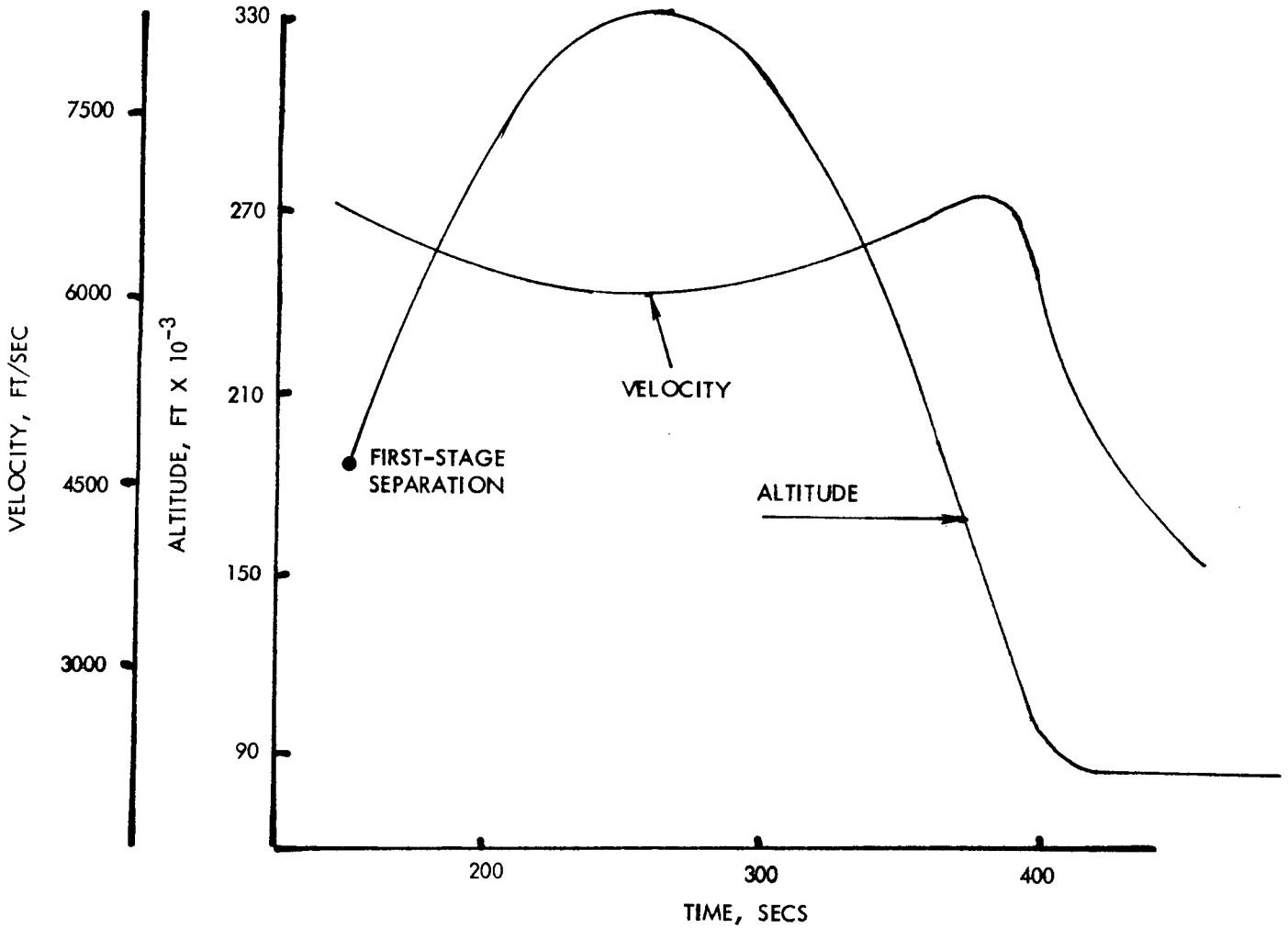

Figure B-27. - Entry Phase Trajectory

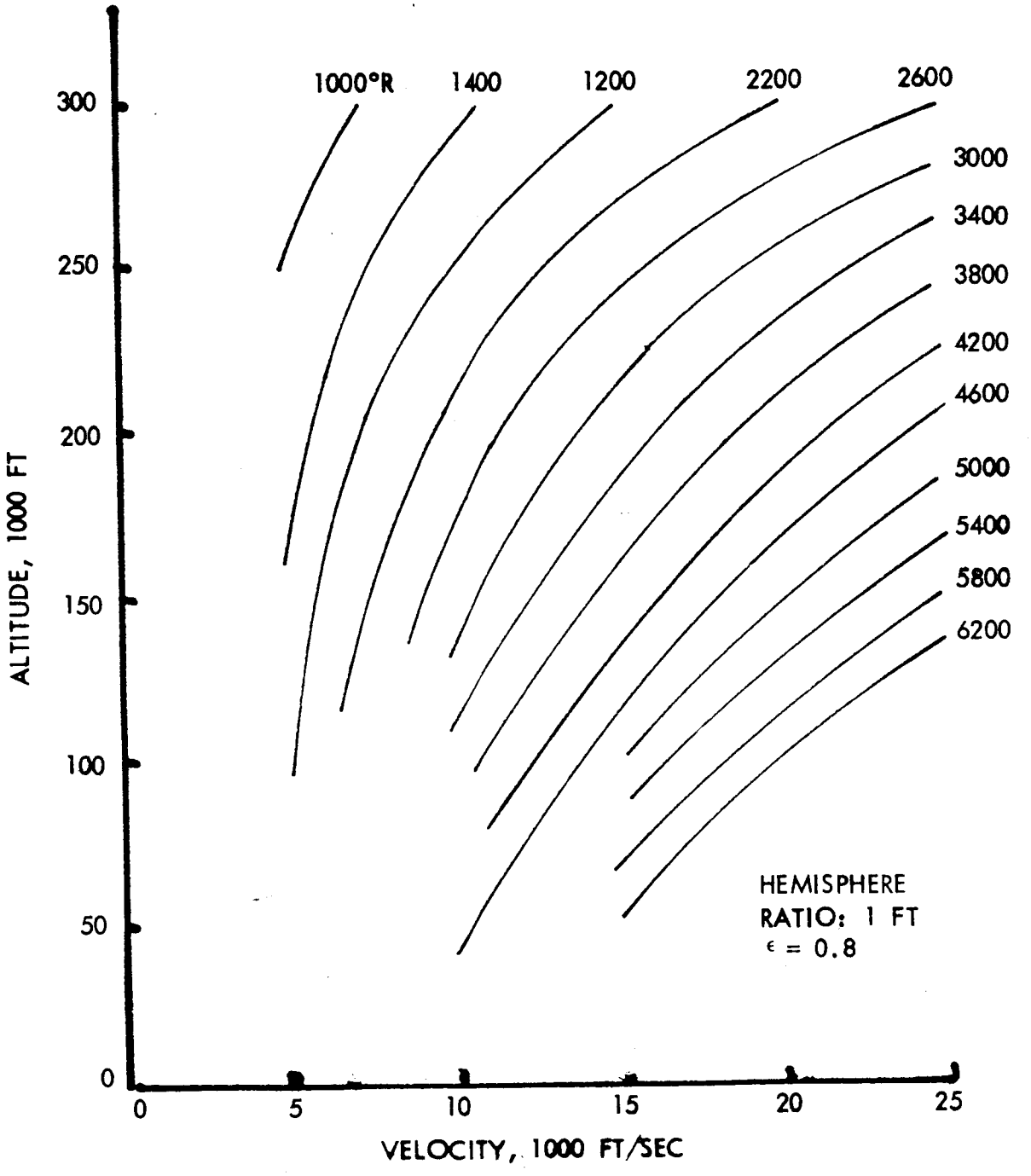

Figure B-28. - Equilibrium Stagnation Temperature

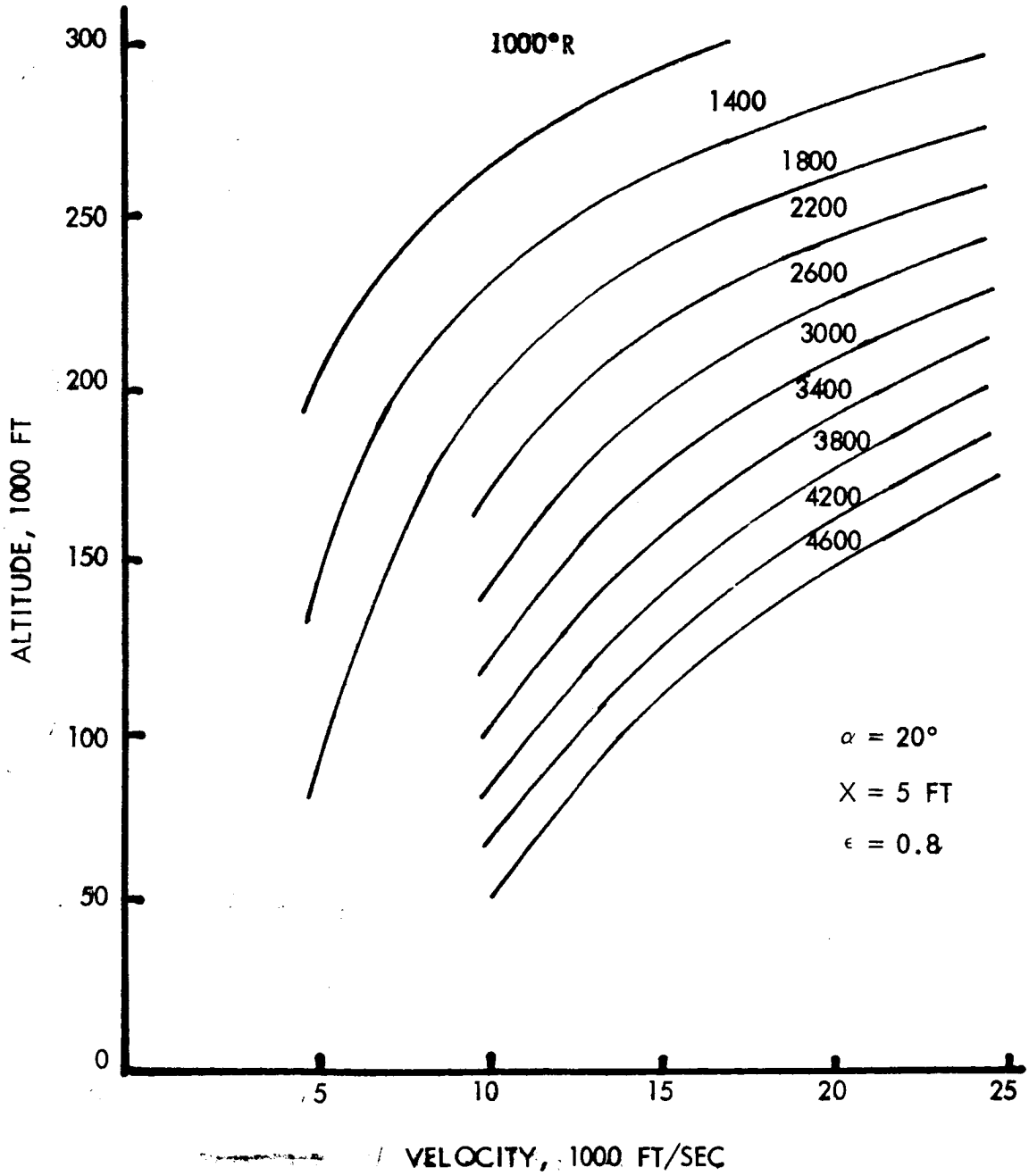

Figure B-29. Equilibrium Skin Temperature - Turbulent Flow

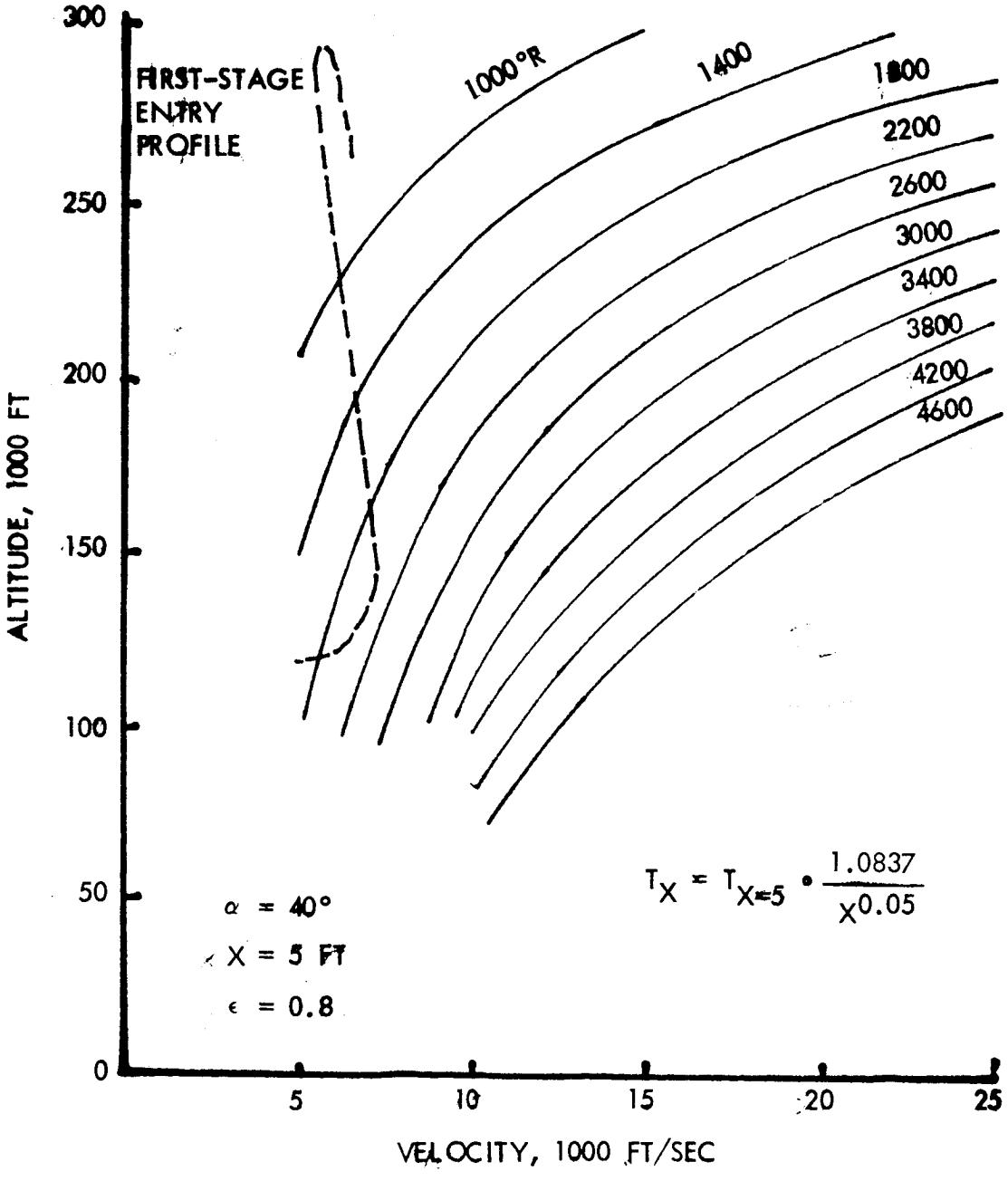

Figure B-30. Thermal Profile Overlay

figure B-27, develop a temperature-time history for heating input to estimate insulation requirements. These temperatures can be translated to other positions over the vehicle by a simplified empirical relationship.

$$T_x = T_{x=5} \cdot \left(\frac{1.0837}{X^{0.05}} \right)$$

where T_x is temperature at Station "x" feet aft of the stagnation point. The maximum equilibrium temperatures for a range of vehicle-staging velocities, altitudes, and flight path angles have been developed from previous studies and are represented in parametric form by figure B-31. The equilibrium temperature from this figure is required as input data for the synthesis program when sizing a particular vehicle system with known stage separation conditions. The synthesis routine automatically defines the temperatures that the various structural elements of the vehicle stage experience as given by the preceding empirical relationship. The fuselage elements are considered aft of the stage-one nose, and the wing and vertical surfaces are considered aft of the wing leading edge.

The required amount of insulation and its heatshield have been evaluated and are inputted into the synthesis program in table look-up form. The thermal analysis and insulation evaluation is based upon reference B-11. A solution was developed with appropriate boundary conditions for an infinite slab of insulation with finite thermal conductivity, in contact at one surface with a slab of metal of infinite thermal conductivity and in contact at the other surface with the hot, free air stream. Additional assumptions include (a) conduction of heat is only in the direction normal to the plane, (b) temperature is initially uniform throughout, (c) only conduction heat transfer occurs from insulation to metal slab, (d) no thermal resistance exists at metal/insulation interface, and (e) thermal diffusivity of the insulation is invariant with temperature.

The basic heat conduction equation is

$$\frac{K\partial^2 T}{\partial x^2} = \rho c \frac{\partial T}{\partial \theta}$$

A solution of this basic equation was developed using Laplace transforms with the boundary conditions

$$T = T_o \text{ at } \theta = 0$$

$$T \rightarrow T' \text{ as } \theta \rightarrow \infty$$

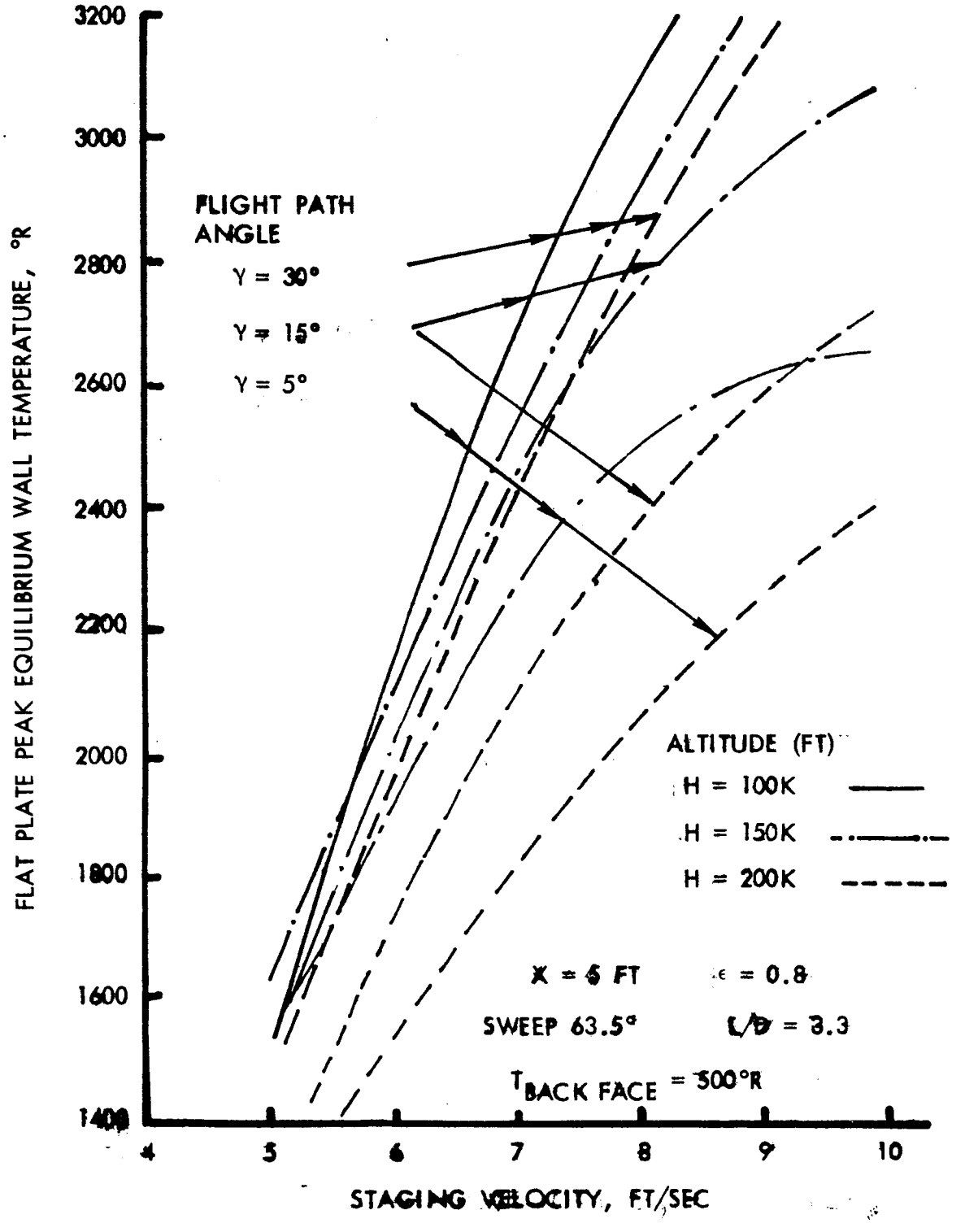

Figure B-31. - Peak Wall Temperature Versus Staging Velocity

$$-K\frac{\partial T}{\partial x} = h\,(T' - T) \text{ at } x = 0$$

$$-K\frac{\partial T}{\partial x} = \rho_m c_m \ell_m \frac{\partial T}{\partial \theta} \text{ at } x = \ell.$$

A nondimensionial parameter for the temperature of the metal slab is given by:

$$y = \sum_{i=1}^{\infty} \frac{2e^{-x\beta_i^2}\,(1 + m^2\beta_i^2)\,(1 + n^2\beta_i^2)\cos\beta_i}{\beta_i^2\,(m+n)\left[(1 + m^2\beta_i^2)\,(1 + n^2\beta_i^2) + n\,(1 + m^2\beta_i^2) + m\,(1 + m^2\beta_i^2)\right]}$$

where

$$m = \frac{k}{hl}$$

$$n = \frac{\rho_m c_m \ell_m}{\rho c \ell}$$

$$X = \frac{\alpha\theta}{\ell^2}$$

$$y = \frac{T' - T_m}{T' - T_o}$$

β_i = positive roots of $\tan\beta_i = \dfrac{1 - mn\beta_i^2}{(m+n)\,\beta_i}$

A graphical representation of this solution is given by figure B-32. For the purposes of an insulated structure where the temperature rise of the load carrying structure is small compared to the gas temperature, the parameter $y \approx 1.0$, and as seen from figure B-32 the determination of insulation requirements becomes extremely difficult using graphical interpolation. Therefore, the analytical solutions were used for an in-house synthesis program to develop parametric weights for the insulation requirements.

For the parametric vehicle synthesis, one of the baseline vehicles was assumed to have an aluminum load carrying structure, and the thermal protection system used micro-quartz with a three-pounds-per-cubic-foot density. The equilibrium temperature for the heat input side was considered

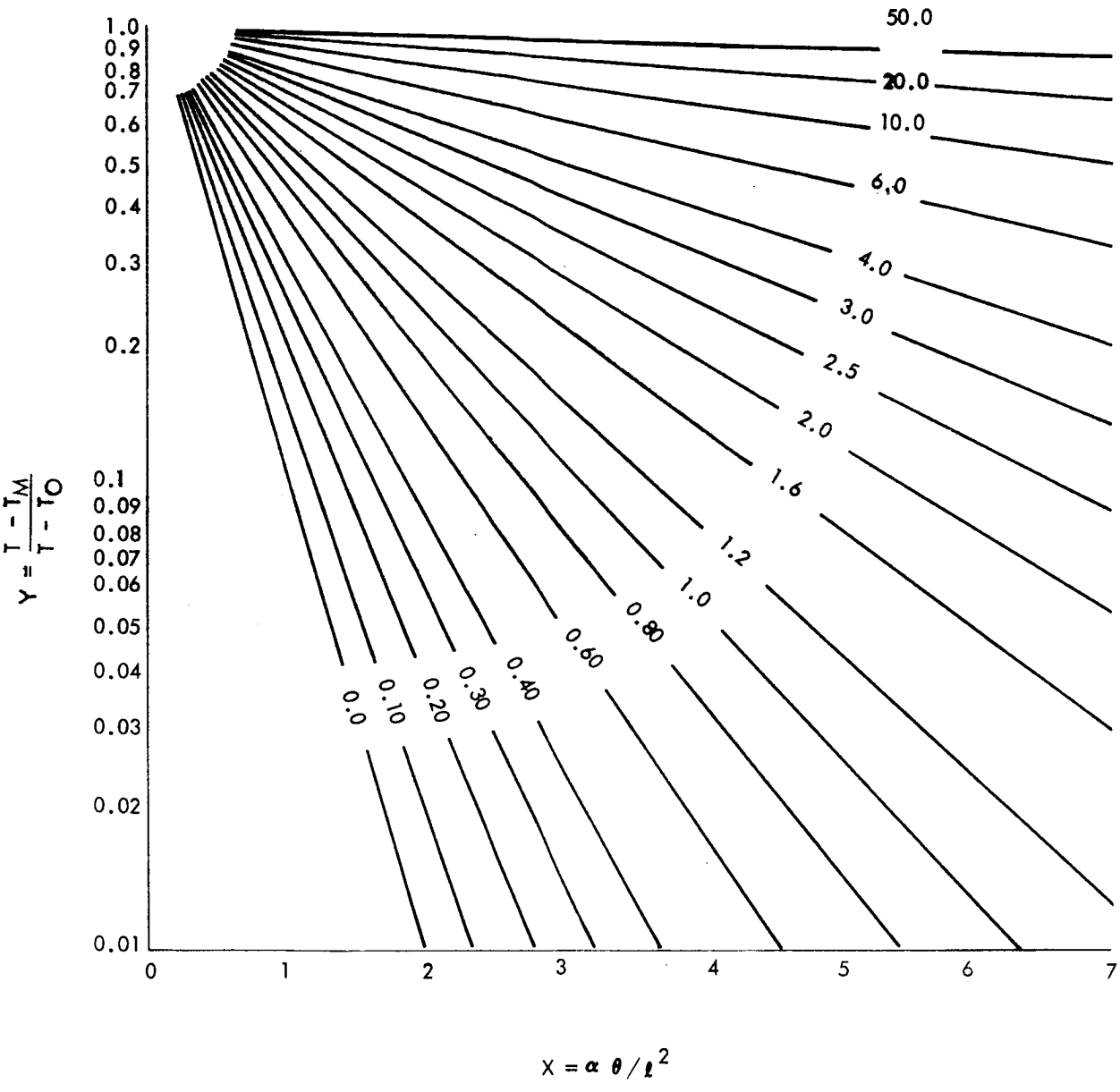

Figure B-32. Dimensionless Plot of Temperature Rise Vs. Heating Time for an Insulated Infinite Metal Slab

to be 1500°F for a duration of 600 seconds, and a range of material back-face temperatures was considered to evaluate the insulation thickness required. Figure B-33 shows this insulator thickness for a range of metal sink thicknesses and the relative structural index (a structural efficiency factor). For an optimum arrangement of high efficiency figure B-33 indicates that the metal temperature should be fairly low. For this vehicle synthesis, the metal temperature is assumed to be a constant 300°F and with the appropriate insulator thickness. A heatshield and attachment mechanism is required to retain the insulation and to take any air loads and transmit them to the main load-carrying structure. In order to make a weight allowance for these elements, a weight penalty of 1/2 pound per square foot has been assessed. The total weights per square foot for the insulator and its attachment are shown in figures 83 and 84 (pp. 162 and 166).

Velocity Losses Associated With Parametric Synthesis of Recoverable Vehicles

In the synthesis program for vehicles with recoverable stage(s), the initial subroutine is involved with the determination of the performance mass ratio for either the first or second stage. To be able to define the mass ratio, the vehicle's performance characteristics and velocity requirements must be specified. None of these data are completely defined prior to the main parametric stage synthesis program. The velocity to be attained by the stage is known, but the velocity losses incurred during stage burn are dependent upon burning time, i.e., weight of propellant. This propellant weight is also a function of the ideal velocity, which is composed of velocity gained by the stage plus stage-velocity loss. In order to assess the propellant and, hence, stage weight, it is required to define an estimate of the stage mass fraction. If this estimate is in error, then the total velocity required and the resulting mass ratio will be in error. This analysis evaluates the magnitude of errors incurred in total velocity requirements for a percentage error in the mass fraction estimate.

The ideal velocity gained for a specific mass ratio, μ, is given by

$$V_{IDEAL} = I_{SP}\, g \ln \mu \qquad \text{(B-76)}$$

$$\mu = \frac{W_O}{W_{BO}}$$

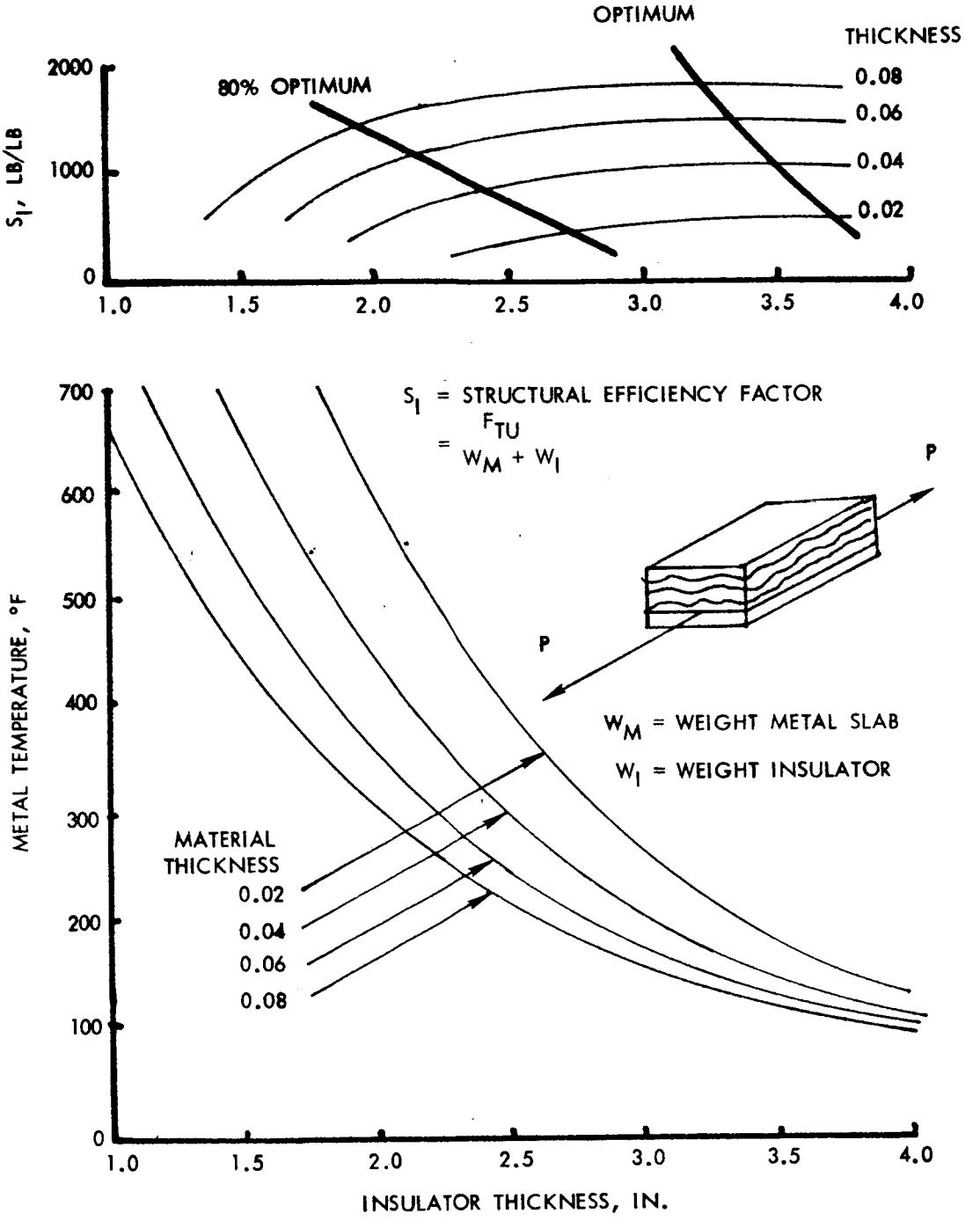

Figure B-33. - Insulator Thickness

where

V_{IDEAL} = ideal velocity gained = $V_{GAIN} + V_{LOSS}$

I_{sp} = specific impulse of the stage

W_O = initial weight of system at stage burn

W_{BO} = burnout weight of system

If the structural mass fraction is defined to be

$$\nu_B = \frac{W_P}{W_O - W_{PL}} \tag{B-77}$$

where

W_P = weight of stage propellant

W_{PL} = stage payload

then equation (B-76) can be rewritten to

$$V_{IDEAL} = I_{sp}\, g\, \ln \left[\frac{W_{PL} + W_P/\nu_B}{\frac{1 - \nu_B}{\nu_B} W_P + W_{PL}} \right] \tag{B-78}$$

The burning rate of propellant is defined as

$$\dot{\omega} = \frac{\text{THRUST}}{I_{sp}}$$

Hence, the burning time is given by

$$t = \frac{W_P}{\dot{\omega}} \tag{B-79}$$

When equations (B-77), (B-78), and (B-79) are combined, the burning time is rewritten as

$$t = \frac{1}{\left(\frac{T}{W_O}\right)\left[\frac{W_{PL}}{W_P} + \frac{1}{\nu_B}\right]} \tag{B-80}$$

In equation (B-80) the thrust-to-initial-weight ratio, T/W_O, is assumed to be constant irrespective of the vehicle size for the stage synthesis. This implies that a rubberized engine system is being considered. It will be shown by keeping the T/W_O constant that the velocity-loss estimation is independent of the mass fraction.

The velocity losses associated with the second stage can be defined (ref. B-4) by

$$V_{LOSS_{II}} \approx g\, t \cos \overline{\beta} \tag{B-81}$$

where $\overline{\beta}$ is the weighted average flight path angle dependent on the initial and final flight path angle of the second stage. By rearrangment of equations (B-76) and (B-77), the propellant-to-payload ratio is expressed in terms of the mass ratio and mass fraction

$$\frac{W_P}{W_{PL}} = \frac{\nu}{(1 - \nu/\nu_B)} \tag{B-82}$$

where

ν = performance mass fraction = $1 - \frac{1}{\mu}$

Therefore, using equation (B-81), the second stage velocity loss is redefined as

$$V_{LOSS_{II}} = \frac{g \cos \beta}{T/W_O}\left(1 - \frac{1}{\mu}\right) \tag{B-82}$$

This relationship clearly shows that for fixed initial flight path angle, as prepared in the synthesis program, the velocity loss is a function of the performance mass ratio, μ, and, consequently, V_{IDEAL}. Therefore, for the second stage, velocity loss is independent of the stage mass fraction.

Reference B-4 indicates the form of the velocity losses for the first stage as:

$$V_{LOSS} = V_{LOSS_{GRAVITY}} + V_{LOSS_{DRAG}} + V_{LOSS_{THRUST}} \quad \text{(B-83)}$$

Considering each contribution of velocity loss the portion due to gravity and thrust are independent of the mass fraction.

$$V_{LOSS_{GRAVITY}} = f\left(t,\ I_{SP},\ \frac{T}{W_O},\ \mu,\ \beta\right) \quad \text{(B-84)}$$

and

$$V_{LOSS_{THRUST}} = f\left(I_{SP},\ \frac{T}{W_O}\right)$$

The contribution due to drag can be described by

$$V_{LOSS_{DRAG}} = f\left(I_{sp},\ \frac{T}{W_O},\ \beta,\ C_D,\ A,\ W_O\right) \quad \text{(B-85)}$$

Unfortunately, the vehicle initial weight, W_O, is strongly dependent upon the stage mass fraction.

$$W_O = \frac{\nu_B W_{PL}}{\nu_B - \left(1 - \frac{1}{\mu}\right)} \quad \text{(B-86)}$$

The rate of change of velocity loss due to drag with respect to the stage mass fraction is defined as

$$\frac{dV_{LOSS_{DRAG}}}{d\nu_B} = \frac{dV_{LOSS_{DRAG}}}{dW_O} \cdot \frac{dW_O}{d\nu_B} \quad \text{(B-87)}$$

where

$$\frac{dV_{LOSS_{DRAG}}}{dW_O} = \frac{-V_{LOSS_{DRAG}}}{W_O} \quad \text{(B-88)}$$

and from equation (B-86) the other differential is obtained. Therefore, equation (B-87) can be rewritten as:

$$\frac{dV_{LOSS_{DRAG}}}{d\nu_B} = - V_{LOSS_{DRAG}} \left[\frac{1}{\nu_B} - \frac{1}{\nu_B - \left(1 - \frac{1}{\mu}\right)} \right] \qquad \text{(B-89)}$$

This assumes that the mass ratio μ is not affected by changes in stage mass fraction. Equation (B-89) can be expressed as the percentage change in the velocity loss due to drag as a function of mass fraction change.

$$\% \ \Delta V_{LOSS_{DRAG}} = - 100 \left[\frac{1}{\nu_B} - \frac{1}{\nu_B - \left(1 - \frac{1}{\mu}\right)} \right] \Delta\nu_B \qquad \text{(B-90)}$$

This percentage error for a range of mass fractions and mass ratios is shown in figure B-34 to vary between 10 and 50 percent. The magnitude of the velocity loss due to drag will be less than 500 feet per second for the recoverable first stage, while the total velocity requirements are 5000 feet per second gained and approximately 3000 feet per second total losses. Therefore, it can be deduced that the maximum likely error of velocity requirements will be 3 percent, for a 5-percent error of mass fraction estimate. This is well within the acceptable accuracy for the parametric synthesis program. Although the velocity is assessed on an estimated mass fraction, the actual stage weight finally evaluated in the synthesis program is based upon a consistent mass fraction.

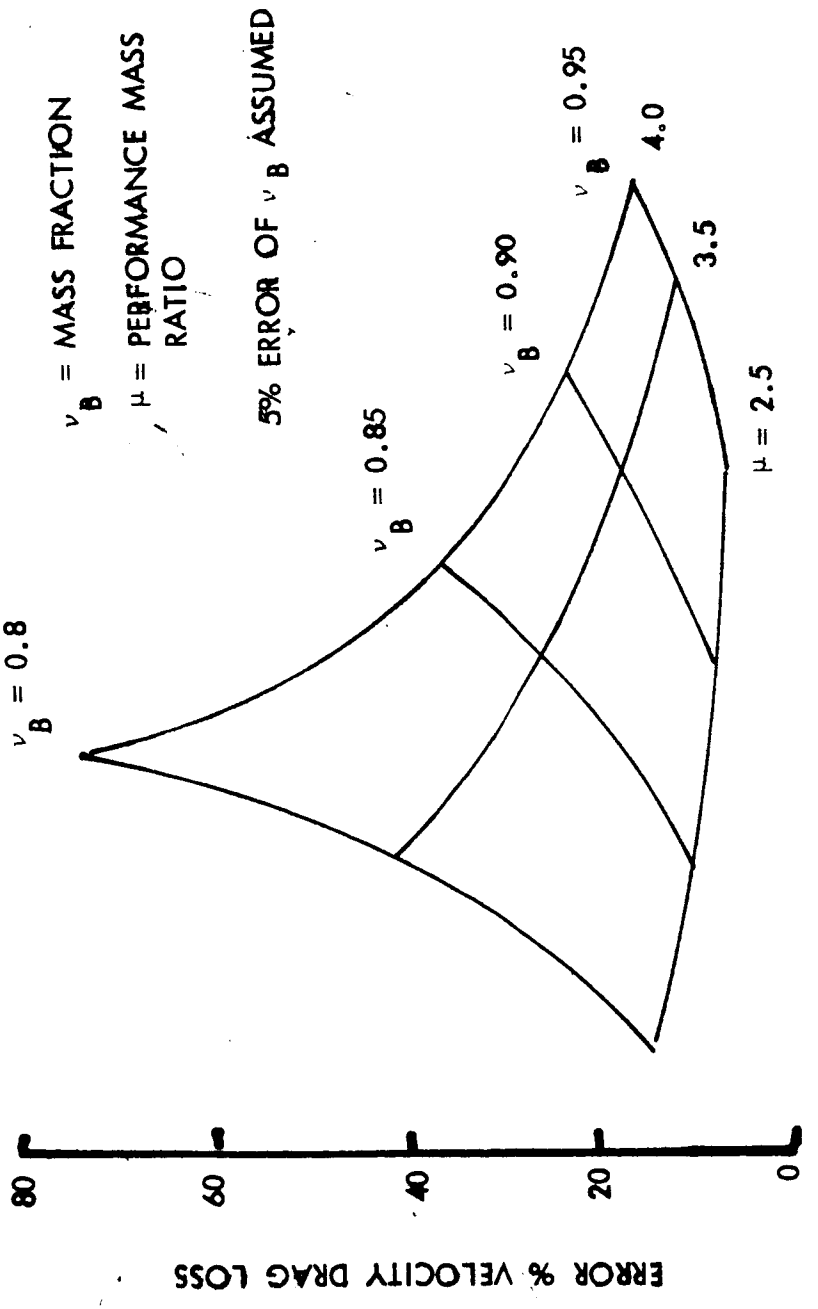

Figure B-34. - Drag Loss Error

APPENDIX C. COSTING MODEL

The first phase of this study program (ref. C-1) used three basic merit functions for assessment: component weight, change in equivalent payload weight, and cost ratio. The cost ratio (cost index) compared all components to a basepoint design, assuming that development and testing costs were identical for both the improved component and the basepoint design. Therefore, the only cost differences considered were production costs. This technique had been utilized in references C-2 and C-3.

The basic costing premise in the aerospace industry for structural components is that the cost of an item to be built can be determined by an analysis of the cost of analogous items that have been built. However, when proposed systems differ greatly in basic vehicle characteristics (vehicle size, weight, type of construction, etc.) difficulties arise because of a lack of identical historical data. In the aerospace industry, as in the Phase I study, weight has been used as the basis for cost estimating. This approach uses cost-per-pound, or hours-per-pound, as the relationship between cost and the stage structural weight. Values of cost-per-pound are not constant for all vehicle systems and have a scaling factor introduced to account for the relative sizes and weights of components (ref. C-4).

An array of complexity factors for fabrication, tooling and equipment was introduced into the following relationship, these factors being in agreement with those contained in reference C-3.

$$y = CF\ 4619\ (X)^{-0.322}$$

where

y = first unit airframe cost in dollars per pound of weight adjusted for complexity

CF = total complexity factor of structural component

X = component weight

Added to this cost is the material cost which, as in the case of beryllium, can be significant. Material costs such as the following tend to influence the cost ratios in favor of the cheaper material:

Material	Cost (dollars/lb)
Aluminum	0.9
Titanium	30.0
Beryllium	200.0

Also of some significance is the experience (percent learning) used to determine construction costs. Cost dependency is placed upon the number of consecutively produced production units and the slope of this learning curve. Reference C-6 defines the experience curve by

$$K_{EXP} = A\,X^{-B}$$

where

A, B = constants, values of which are selected to express appropriately the relation for a specific situation

K_{EXP} = adjustment factor based upon experience

X = consecutive number of a specific production unit

The unit cost decreases for the experience curve by a constant factor as the number of consecutive production units is doubled. This factor was assumed as 85 percent in the Phase I Study (ref. C-1) and changed from recently-gained experience to 87 percent for the Phase II assessments.

The cost assessment is dependent upon production learning, weight and cost of stock material purchased, production cost of a basepoint material/construction component, and the production complexity of the alternate component. This production complexity must include material, structural type, shape of item being constructed, and its size characteristic. The Phase II study included an attempt to assign complexities to the alternate materials and constructions using in-house historical data and data from references C-2 and C-3. This matrix of complexities factors, as illustrated in table C-1, used a reference value of 1.0 for an aluminum attached-skin-stringer construction with a flat-plate shape. Labor costs tend to increase as dimensions increase and as the component shape becomes more complex. The cost complexity factors are illustrated in table C-1 for the following factors: material: aluminum, titanium, and beryllium; construction: monocoque,

TABLE C-1. - COMPLEXITY FACTORS

Material	Construction	Shape and Diameter											
		Flat Plate	Cylindrical				Conical				Spherical			
			10 ft	20 ft	30 ft	60 ft	10 ft	20 ft	30 ft	60 ft	10 ft	20 ft	30 ft	60 ft
Aluminum	Monocoque	.9	1.0	1.0	1.0	1.0	1.1	1.1	1.1	1.2	2.8	2.9	3.1	3.5
	Integral skin-stringer	1.2	1.8	1.6	1.4	1.4	2.1	2.0	2.0	1.8	6.4	6.8	7.2	8.2
	Attached skin-stringer	1.0*	1.6	1.4	1.2	1.2	2.0	1.9	1.8	1.6	6.0	6.5	7.0	8.0
	Waffle	1.4	2.0	1.7	1.5	1.5	2.2	2.1	2.1	1.9	6.6	6.9	7.4	8.4
	Honey sandwich	2.8	3.4	3.2	3.0	3.0	4.0	3.9	3.8	3.6	10.0	10.4	11.4	12.4
	Corrugations	3.0	3.6	3.4	3.2	3.2	4.3	4.2	4.1	4.0	10.2	10.6	11.6	12.6
	Double-wall/ multiwall	3.4	4.0	3.8	3.6	3.6	4.6	4.5	4.4	4.3	10.6	11.0	12.0	13.2
Titanium	Monocoque	1.4	1.5	1.4	1.3	1.5	1.6	1.6	1.6	1.7	3.4	3.5	3.7	4.1
	Integral skin-stringer	4.2	4.8	4.6	4.4	4.4	5.0	4.9	4.8	4.8	13.2	13.6	14.0	15.0
	Attached skin-stringer	4.0	4.6	4.4	4.2	4.2	4.8	4.7	4.6	4.6	13.0	13.5	14.0	15.0
	Waffle	4.4	5.0	4.7	4.5	4.5	5.1	5.0	4.9	4.9	13.3	13.7	14.3	15.2
	Honey sandwich	8.0	9.0	8.8	8.6	8.6	9.5	9.3	9.2	9.2	18.0	18.4	19.0	20.0
	Corrugations	8.4	9.4	9.2	9.0	9.0	9.8	9.6	9.4	9.4	18.4	18.8	19.2	20.2
	Double-wall/ multiwall	9.0	10.0	9.8	9.6	9.6	10.4	10.2	10.0	10.0	19.0	19.4	19.8	20.8
Beryllium	Monocoque	1.8	1.8	1.7	1.6	1.8	1.9	1.9	1.9	2.0	4.6	4.7	4.9	5.3
	Integral skin-stringer	6.0	6.6	6.4	6.2	6.2	6.8	6.7	6.6	6.6	16.4	16.8	17.2	18.2
	Attached skin-stringer	5.0	5.6	5.4	5.2	5.2	6.0	5.9	5.8	5.8	16.0	16.5	17.0	18.0
	Waffle	6.2	6.8	6.5	6.3	6.3	6.9	6.8	6.7	6.7	16.5	16.9	17.4	18.4
	Honey sandwich	10.0	10.8	10.6	10.2	10.2	11.0	10.9	10.8	10.8	20.0	20.4	21.0	22.0
	Corrugations	12.0	12.6	12.4	12.2	12.2	13.0	12.9	12.8	12.8	22.0	22.4	22.8	23.8
	Double-wall/ multiwall	13.0	13.6	13.4	13.2	13.2	14.0	13.9	13.8	13.8	23.0	23.4	23.8	24.8

*Basepoint

integral skin-stringer, attached skin-stringer, waffle, honeycomb sandwich, corrugations, double-wall and multiwall; diameter: 10, 20, 30, and 60 feet; and shape: flat plate, cylindrical, conical, and spherical.

Figure C-1 presents a summary of the costing program which contains two basic subroutines (START, COSTPA), a main program (MAIN), and a stored data bank (see tables B-11 and B-12 for shell and bulkhead weight complexity factors and table C-1 for cost complexity factors).

In the "programmed assistance" concept, data may be generated as an integral part of the program, or specific designs may be input to the program. To ensure a like assessment of basepoint structures with alternative structures, the same matrix of weight adjustment factors are used (see tables B-11 and B-12 for weight complexity factors). The weight adjustment process involves three basic steps. First, a test case is run through the design synthesis programs using the same geometry and loads that the basepoint design was subjected to. Next, unit weights for the test case are compared with unit weights for the basepoint vehicle, the basepoint unit weights previously being divided by their weight complexity factors. The resulting coefficient is then multiplied by the proper alternative-concept weight complexity factor, and then by the alternative basic unit weight to determine an adjusted alternative component weight. The basepoint weights and the adjusted alternate weights are then used in the evaluation process. This technique is illustrated in the START subroutine diagram (fig. C-2). Figures C-3 and C-4 present two typical printouts from the START subroutine.

The cost subroutine (COSTPA) is called from the main subroutine using data stored in COMMON from the START subroutine. This subroutine essentially accomplishes the task outlined in figure C-5. Fabrication costs are based upon a dollars-per-pound input for the basepoint flat plate construction (CF = 1.0) and upon the slope of the learning curve. These costs for the basepoint are saved for comparison with alternative components. If the material is machined, the material costs are based upon the thickness of the stock material required; if not machined, material cost is based upon component-design adjusted weight from the START subroutine. For the Phase II study, fabrication cost of the flat plate basepoint was set at 10 dollars per pound. Material cost curves for titanium and beryllium are illustrated in figure C-6.

Aluminum A cost/pound was set at a constant 90 cents, Aluminum B at a constant $1.00/pound, and Aluminum C at a constant $1.05/pound. Performance exchange ratios for the basepoint expendable vehicles were as given in table C-2.

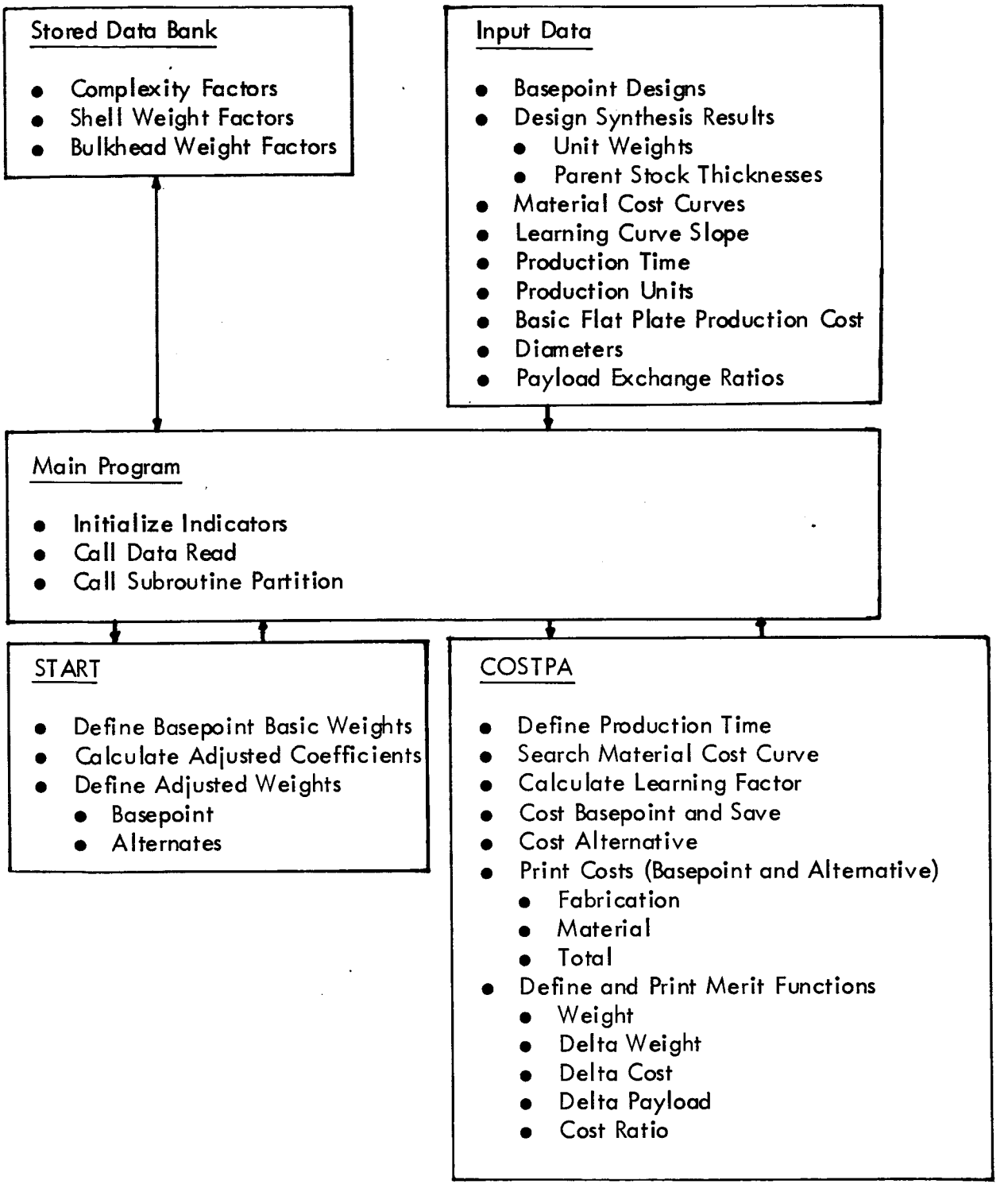

Figure C-1. - Costing Program

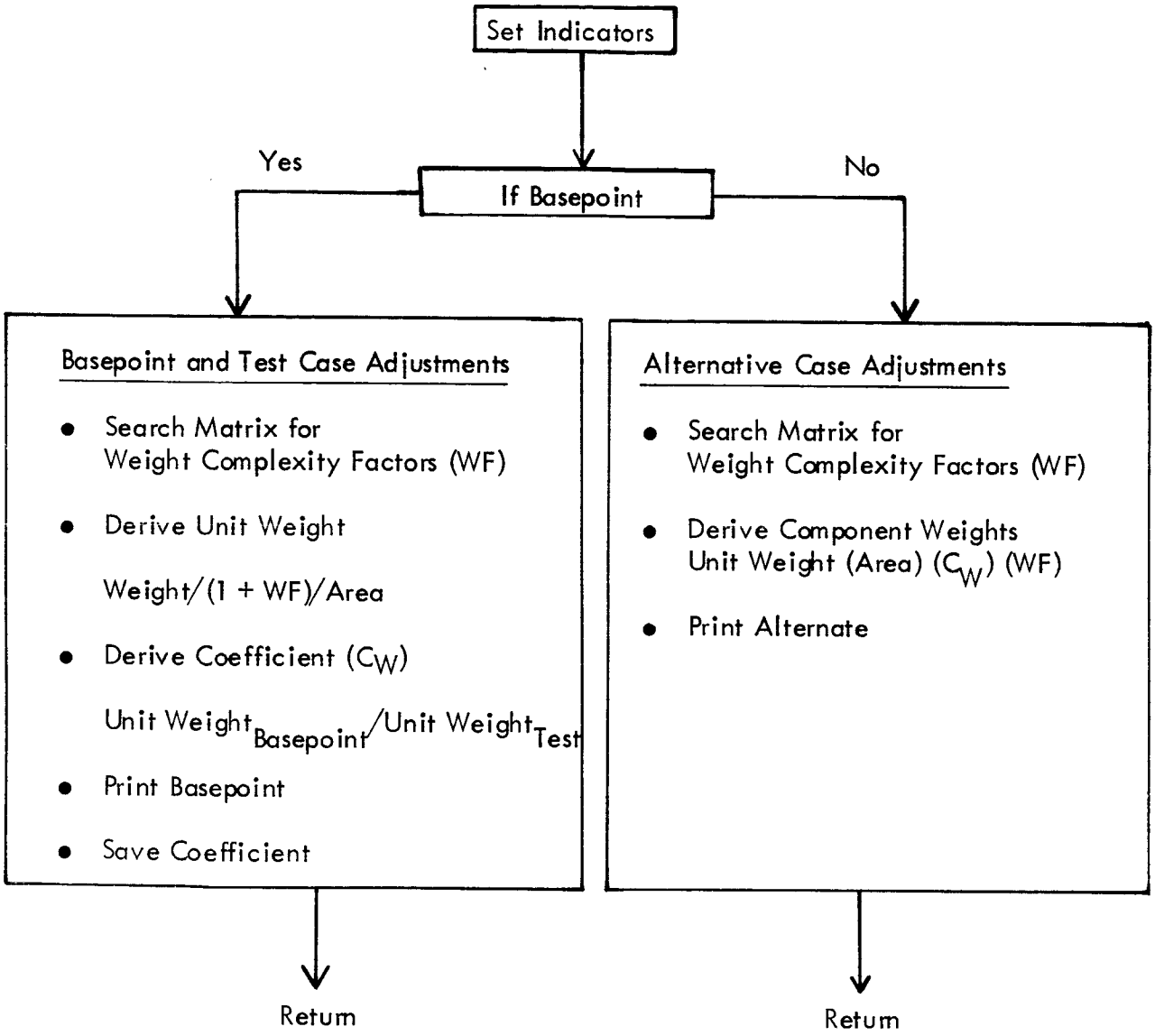

Figure C-2. - START Subroutines

VEHICLE — CURRENT ISP AND THRUST — ORBITAL PAYLOAD 240000 LBS
MATERIAL — ALUMINUM A PROPERTIES — 4 UNITS/TOOL/YEAR
CONSTRUCTION — INTEGRAL SKIN STRINGER BASEPOINT

STAGE	COMPONENT	AREA	NX (P)	UNIT WT BASEPOINT (NOTE)	CORR COEF	UNIT WT ALTERNATE (NOTE)	WEIGHT ALTERNATE
1							
	INTERSTAGE	0.1931E 04	0.7965E 04	0.5380E 01	0.1029E 01	0.5380E 01	0.1069E 05
	FWD SKIRT	0.1210E 04	0.8005E 04	0.5420E 01	0.1012E 01	0.5420E 01	0.6638E 04
	FWD TANKWALL	0.3456E 04	0.7400E 04	0.5240E 01	0.1084E 01	0.5240E 01	0.1962E 05
	CENTER SECTION	0.2625E 04	0.8365E 04	0.5560E 01	0.9855E 00	0.5550E 01	0.1438E 05
	AFT TANKWALL	0.1682E 04	0.9700E 04	0.5980E 01	0.8977E 00	0.5980E 01	0.9029E 04
	AFT SKIRT	0.1210E 04	0.6965E 04	0.5050E 01	0.1091E 01	0.5050E 01	0.6668E 04
	FWD BULKHEAD	0.1000E 01	0.3500E 02	0.1495E 04	0.1655E 01	0.1495E 04	0.2474E 04
	INT BULKHEAD	0.1000E 01	0.5000E 02	0.2136E 04	0.3499E 01	0.2136E 04	0.7473E 04
	INT AFT BULK	0.1000E 01	0.3500E 02	0.1495E 04	0.1655E 01	0.1495E 04	0.2474E 04
	AFT BULKHEAD	0.1000E 01	0.8000E 02	0.3417E 04	0.2152E 01	0.3417E 04	0.7355E 04
2							
	FWD SKIRT	0.1210E 04	0.2750E 04	0.2930E 01	0.1415E 01	0.2930E 01	0.5017E 04
	FWD TANKWALL	0.5813E 04	0.3070E 04	0.3040E 01	0.1360E 01	0.3040E 01	0.2404E 05
	AFT TANKWALL	0.1890E 03	0.6300E 04	0.4450E 01	0.1039E 01	0.4450E 01	0.8740E 03
	AFT SKIRT	0.1210E 04	0.6765E 04	0.4650E 01	0.1014E 01	0.4650E 01	0.5703E 04
	FWD BULKHEAD	0.1000E 01	0.3500E 02	0.1495E 04	0.1655E 01	0.1495E 04	0.2474E 04
	INT BULKHEAD	0.1000E 01	0.3500E 02	0.1495E 04	0.2979E 01	0.1495E 04	0.4453E 04
	AFT BULKHEAD	0.1000E 01	0.8000E 02	0.3417E 04	0.3186E 01	0.3417E 04	0.1089E 05

NOTE-UNIT WT FOR SHELLS-TOTAL WT FOR BULKHEADS

Figure C-3. Basepoint Printout (START)

VEHICLE — CURRENT ISP AND THRUST — ORBITAL PAYLOAD 240000 LBS
MATERIAL — ALUMINUM A PROPERTIES — 4 UNITS/TOOL/YEAR
CONSTRUCTION — INTEGRAL SKIN-STR BASEPOINT — TOP-HAT SKIN-STR ALTERNATE

STAGE	COMPONENT	AREA	NX (P)	UNIT WT BASEPOINT (NOTE)	CORR COEF	UNIT WT ALTERNATE (NOTE)	WEIGHT ALTERNATE
1							
	INTERSTAGE	0.1931E 04	0.7965E 04	0.5380E 01	0.1019E 01	0.4760E 01	0.9370E 04
	FWD SKIRT	0.1210E 04	0.8005E 04	0.5420E 01	0.1003E 01	0.4780E 01	0.5801E 04
	FWD TANKWALL	0.3456E 04	0.7400E 04	0.5240E 01	0.1074E 01	0.4650E 01	0.1726E 05
	CENTER SECTION	0.2625E 04	0.8365E 04	0.5560E 01	0.9766E 00	0.4920E 01	0.1261E 05
	AFT TANKWALL	0.1682E 04	0.9700E 04	0.5980E 01	0.8895E 00	0.5350E 01	0.8004E 04
	AFT SKIRT	0.1210E 04	0.6965E 04	0.5050E 01	0.1081E 01	0.4460E 01	0.5835E 04
2							
	FWD SKIRT	0.1210E 04	0.2750E 04	0.2930E 01	0.1402E 01	0.2550E 01	0.4326E 04
	FWD TANKWALL	0.5813E 04	0.3070E 04	0.3040E 01	0.1348E 01	0.2680E 01	0.2100E 05
	AFT TANKWALL	0.1890E 03	0.6300E 04	0.4450E 01	0.1030E 01	0.4080E 01	0.7939E 03
	AFT SKIRT	0.1210E 04	0.6765E 04	0.4650E 01	0.1004E 01	0.4220E 01	0.5128E 04

NOTE-UNIT WT FOR SHELLS-TOTAL WT FOR BULKHEADS

Figure C-4. - Alternative Printout (START)

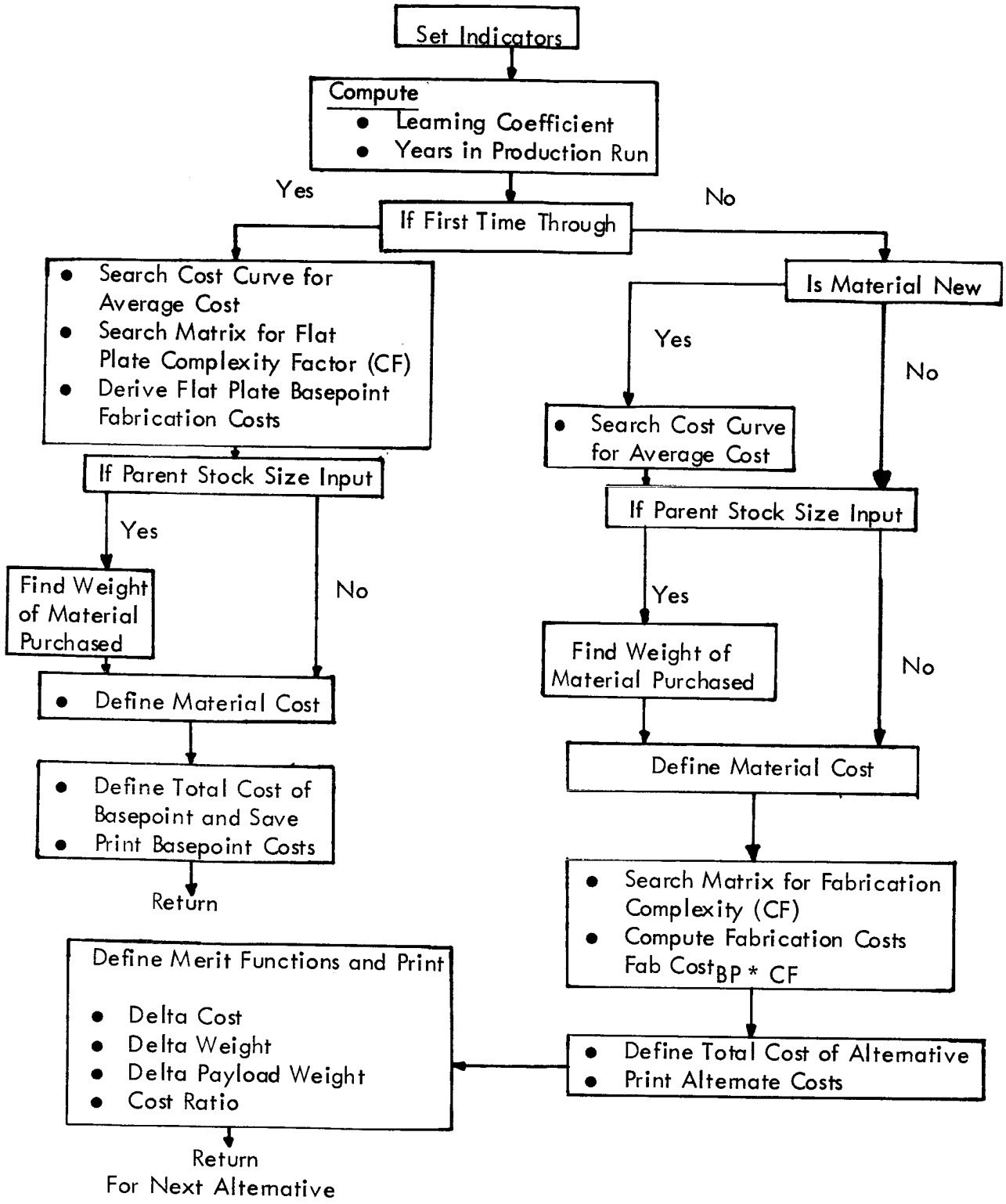

Figure C-5. - COSTPA Subroutine

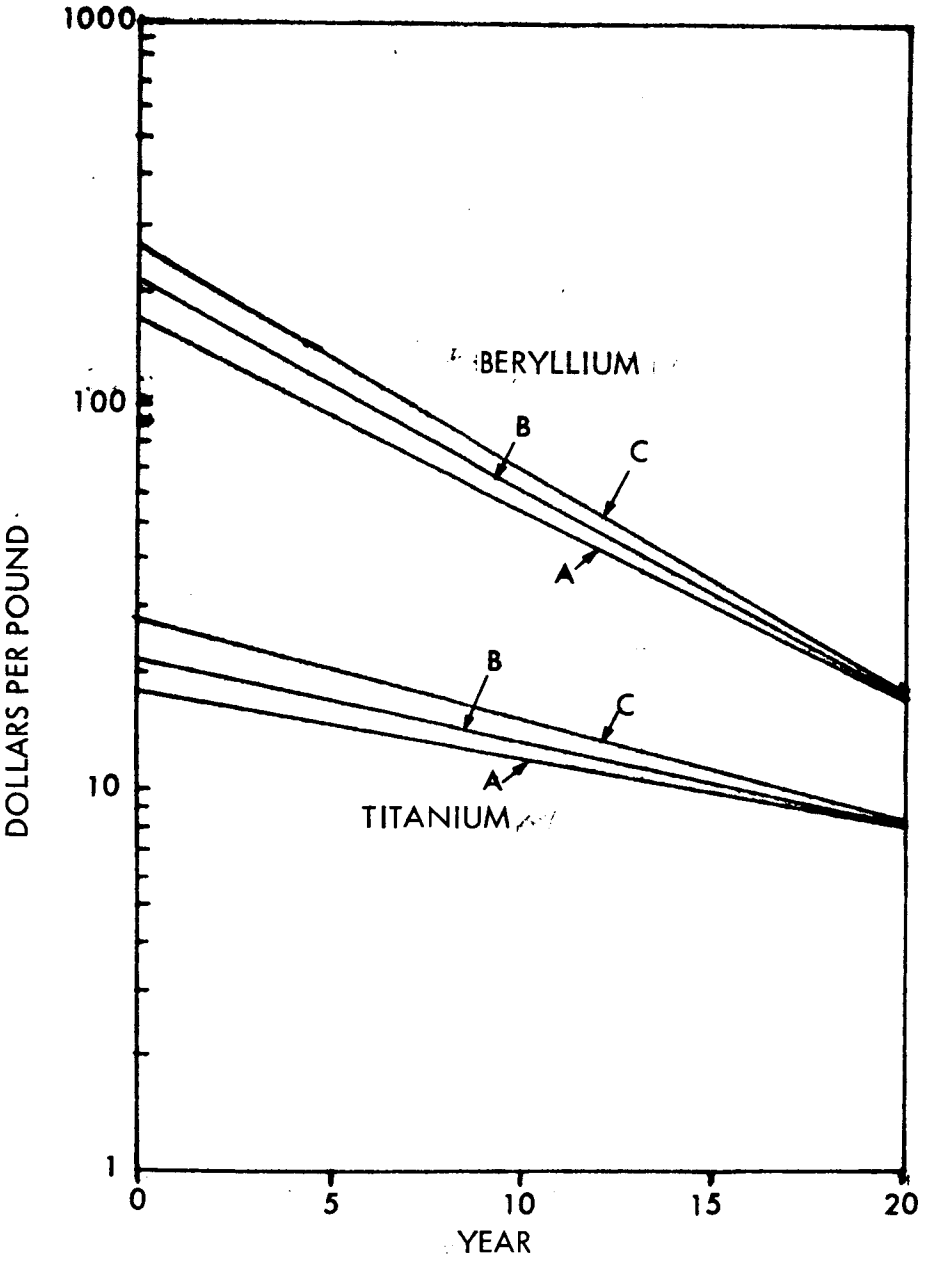

Figure C-6. - Material Cost With Year

TABLE C-2. - PERFORMANCE EXCHANGE RATIOS FOR BASEPOINT EXPENDABLE VEHICLES

Parameter	Vehicle					
	1	2	3	4	5	6
Payload, lb	30 000	10 000	240 000	445 000	1×10^6	2×10^6
Exchange ratios						
Stage 1	.09	.12	.11	.15	.11	.13
Stage 2	1.00	1.00	1.00	1.00	1.00	1.00
(See reference C-1 for derivations)						

Typical printouts from the COSTPA subroutine are illustrated for the basepoint and an alternative construction in figures C-7 and C-8. The merit function assessment for the shell construction changes is shown in Appendix D (printed as a separate volume).

VEHICLE	CURRENT ISP AND THRUST		ORBITAL PAYLOAD 240000 LBS
MATERIAL	ALUMINUM A PROPERTIES		4 UNITS/TOOL/YEAR
CONSTRUCTION	INTEGRAL SKIN STRINGER BASEPOINT		
LAUNCH RATE	4.	NUMBER OF UNITS	20.
NUMBER OF TEST VEHICLES	2.	NUMBER OF TOOLS	1.
YEARS IN PRODUCTION RUN	5.		

STAGE	COMPONENT	WEIGHT PER UNIT	FABRICATION COST PER UNIT	MATERIAL COST PER UNIT	TOTAL COST PER UNIT
1					
	INTERSTAGE	10688.	81961.	51493.	133454.
	FWD SKIRT	6638.	50903.	31745.	82648.
	FWD TANKWALL	19625.	150494.	97076.	247570.
	CENTER SECTION	14384.	110303.	67056.	177360.
	AFT TANKWALL	9029.	69239.	39136.	108374.
	AFT SKIRT	6658.	51133.	34225.	85358.
	FWD BULKHEAD	2474.	111120.	2227.	113347.
	INT BULKHEAD	7473.	335652.	6726.	342378.
	INT AFT BULK	2474.	111120.	2227.	113347.
	AFT BULKHEAD	7355.	330352.	6619.	336972.
2					
	INTERSTAGE	0.	0.	0.	0.
	FWD SKIRT	5017.	38473.	44382.	82855.
	FWD TANKWALL	24041.	184358.	204981.	389339.
	CENTER SECTION	0.	0.	0.	0.
	AFT TANKWALL	874.	6702.	5091.	11793.
	AFT SKIRT	5703.	43733.	31790.	75523.
	FWD BULKHEAD	2474.	111120.	2227.	113347.
	INT BULKHEAD	4453.	200008.	4008.	204016.
	INT AFT BULK	0.	0.	0.	0.
	AFT BULKHEAD	10887.	488993.	9798.	498791.

VEHICLE	CURRENT ISP AND THRUST		ORBITAL PAYLOAD 240000 LBS
MATERIAL	ALUMINUM A PROPERTIES		4 UNITS/TOOL/YEAR
CONSTRUCTION	INTEGRAL SKIN-STR BASEPOINT		TOP-HAT SKIN-STR ALTERNATE
LAUNCH RATE	4.	NUMBER OF UNITS	20.
NUMBER OF TEST VEHICLES	2.	NUMBER OF TOOLS	1.
YEARS IN PRODUCTION RUN	5.		

STAGE	COMPONENT	WEIGHT PER UNIT	FABRICATION COST PER UNIT	MATERIAL COST PER UNIT	TOTAL COST PER UNIT
1					
	INTERSTAGE	9370.	70252.	8433.	78685.
	FWD SKIRT	5801.	43631.	5221.	48852.
	FWD TANKWALL	17257.	128995.	15531.	144526.
	CENTER SECTION	12613.	94546.	11351.	105897.
	AFT TANKWALL	8004.	59347.	7204.	66551.
	AFT SKIRT	5835.	43829.	5252.	49080.
2					
	INTERSTAGE	0.	0.	0.	0.
	FWD SKIRT	4326.	32977.	3893.	36870.
	FWD TANKWALL	20998.	158021.	18898.	176919.
	CENTER SECTION	0.	0.	0.	0.
	AFT TANKWALL	794.	5745.	715.	6459.
	AFT SKIRT	5128.	37486.	4615.	42101.

DIVIDE CHECK AT 22461

DIVIDE CHECK AT 22461

Figure C-7. - Basepoint and Alternate Costs

VEHICLE		CURRENT ISP AND THRUST			ORBITAL PAYLOAD 240000 LBS	
MATERIAL		ALUMINUM A PROPERTIES			4 UNITS/TOOL/YEAR	
CONSTRUCTION		INTEGRAL SKIN-STR BASEPOINT			TOP-HAT SKIN-STR ALTERNATE	
LAUNCH RATE		4.	NUMBER OF UNITS		20.	
NUMBER OF TEST VEHICLES		2.	NUMBER OF TOOLS		1.	
YEARS IN PRODUCTION RUN		5.				
STAGE	COMPONENT	WEIGHT PER UNIT	DELTA DOLLARS PER UNIT	DELTA WEIGHT PER UNIT	DELTA PAYLOAD PER UNIT	COST RATIO
1						
	INTERSTAGE	9370.	-54768.	-1318.	145.	-378.
	FWD SKIRT	5801.	-33796.	-837.	92.	-367.
	FWD TANKWALL	17257.	-103044.	-2368.	260.	-396.
	CENTER SECTION	12613.	-71463.	-1771.	195.	-367.
	AFT TANKWALL	8004.	-41823.	-1025.	113.	-371.
	AFT SKIRT	5835.	-36278.	-833.	92.	-396.
2						
	INTERSTAGE	0.	0.	0.	-0.	0.
	FWD SKIRT	4326.	-45985.	-691.	691.	-67.
	FWD TANKWALL	20998.	-212420.	-3043.	3043.	-70.
	CENTER SECTION	0.	0.	0.	-0.	0.
	AFT TANKWALL	794.	-5334.	-80.	80.	-67.
	AFT SKIRT	5128.	-33422.	-575.	575.	-58.

Figure C-8. - Cost Printout

REFERENCES

1. Boddy, J. A., and Mitchell, J. C.: Development of Programmed Assistance in Directing Structures Research. Interim Rept; NAA/SD SID 66-408, June 1966.

2. Propulsion Evaluation. Lockheed, Calif. Co., LR 18650, Jan. 15, 1965.

3. Reusable Orbital Transport First Stage. Lockheed, Calif. Co., LR18790, May 21, 1965.

4. Reusable Orbital Transport - Final Presentation. General Dynamics - Convair, GD/C-DCB-65-022, May 4, 1965.

5. Reusable Orbital Transport - Baseline Vehicle - First Stage Definition. Lockheed Calif. Co., LR 18387, Dec. 2, 1964.

6. Design Investigation of Cylindrical Structures Other Than Honeycomb. Final Rept., NAA/LAD NA65-1026, Nov. 1965.

7. Van der Neut, A.: The General Instability of Stiffened Cylindrical Shells Under Axial Compression. Report S 314, Nat. Aeron. Res. Inst. (Amsterdam), 1957.

8. Block, David L.; Cord, Michael F.; and Mihulor, Monten M., Jr.: Buckling of Eccentrically Stiffened Orthotropic Cylinders. NASA TND 2960, August 1965.

9. Hedgepath, John M.; and Hall, David B.: Stability of Stiffened Cylinders. AIAA J., vol. 3, no. 12, Dec. 1965, pp. 2275-2286.

10. Crawford, R. F.: Effects of Asymetric Stiffening on Buckling of Shells. AIAA Paper no. 65-371, Am. Inst. Aeron. Astronaut., July 1965.

11. Card, Michael F.; and Jones, Robert M.: Experimental and Theoretical Results for Buckling of Eccentrically Stiffened Cylinders. NASA TND 3639, October 1966.

12. Hutchingson, John W.; and Amajigo, John C.: Imperfection Sensitivity of Eccentrically Stiffened Cylindrical Shells. AIAA J., vol. 5, no. 3, March 1967.

13. Structural Systems and Program Decisions. vol. 1, NASA SP 6008.

14. Buckling of Thin Walled Circular Cylinders. NASA Space Vehicle Design Criteria, NASA SP 8007.

15. Sobel, S. H.; and Flügge, W.: Stability of Toroidal Shells Under Uniform External Pressure. AIAA J., vol. 5, no. 3, March 1967.

16. White, Frederick J.: Flight Performance Handbook for Powered Flight Operations. Space Tech. Lab., Inc., March 1962.

17. Conceptual Design Study of Ten-Ton Reusable Orbital Carrier. NAA/SD SID 63-158, Final Rept., February 22, 1963.

18. Reusable Orbital Transport. CR 7138L, Lockheed Calif, Co., Dec. 1964.

19. Reusable Orbital Transport Second Stage Research and Technology Implications. GD/C DCB 65-018 Vol. V, April 1965.

20. Proposal for Development of Programmed Assistance in Directing Structures Research. Phase II, NAA/SD SID 66-63, Jan. 1966.

21. CSM Technical Specification Block II. NAA/SD SID 64-13444, Nov. 22, 1966.

22. Apollo Technical Manuals, Structural Loads and Criteria. ARM-6, Jan 31, 1964.

23. Saturn S-II, Structural Design Loads Manual. NAA/SD SID 62-1184, May 1, 1963.

24. Proposal for Reusable Aerospace Passenger Transport System. NAA/SD SID 65-1211, Sept. 15, 1965.

25. Preliminary Draft, Preparation and Documentating of Digital Computer Decks. Transmitted from Dr. Stanley Ross, NASA/ERC, to J. C. Mitchell, NAA/SD, Dec. 20, 1966.

26. ROT Second Stage Summary Technical Report. GD/C DCB-65-018 vol. I, April 1956.

27. Xenakis, George; Estepp, Gerald W.; Henkener, Billy J.; and McCarthy, James P.: An Investigation of Reentry Configurations Having Large Lateral Range Capability. TDR No. ASD-TDR-63, August 1963.

28. Alelyunas, Paul: L > D Spacecraft. Space/Aeronautics, February 1967.

A-1. Anderson, Melvin S.: Local Instability of the Elements of a Truss-Core Sandwich Plate. NASA TR R-30, 1959.

A-2. Baker, Edward H; and Harris, Leonard A.: The Stability of Longitudinally Corrugated Sandwich Cylinders Under Combined Loads. NAA/SD STR 72, Oct. 1960.

A-3. Stein, M.; and Mayers, J.: A Small Deflection Theory for Curved Sandwich Plates. NACA TN 2017.

A-4. Crawford, R. F. and Burns: Strength Efficiency and Design Data for Beryllium Structures. ASD TR-61-692, Feb. 1962.

A-5. Peterson, J. P.; and Anderson, J. K.: Test of a Truss-Core Sandwich Cylinder Loaded to Failure in Bending. NASA TN D3157, Dec. 1965.

A-6. Harris, L. A., Skeene, W. J.; and Benjamin, Seuver: The Stability of Thin Walled Unstiffened Circular Cylinders Under Axial Compression. Aero Sciences vol. 24, August 1957.

A-7. Hess, T. F.; and Garber, A. M.: Stability of Ring Stiffened Conical Shells Under Simultaneous Lateral Pressure and Axial Compression. General Electric Rept. R58SD226, Apr. 1958.

A-8. Shanley, F. R.: Weight Strength Analysis of Aircraft Structures. McGraw-Hill Book Co. Inc., 1952.

A-9. Block, David L.; Card, Michael F.; and Mikulas, Martin M., Jr.: Buckling of Eccentrically Stiffened Orthotropic Cylinders. NASA TND-2960, 1965.

A-10. Baruch, M.; and Singer, J.: Effect of Eccentricity of Stiffeners on the General Instability of Stiffened Cylindrical Shells under Hydrostatic Pressure. J. Mech. Eng. Sci., vol. 5, no. 1, 1963, pp. 23-27.

A-11. Stein, Manuel; and Mayers, J.: Compressive Buckling of Simply Supported Curved Plates and Cylinders of Sandwich Construction. NACA TN 2601, 1952.

A-12. Becker, H.: General Instability of Stiffened Cylinders. NACA TN 4237, July 1958.

A-13. Card, Michael F.; and Jones, R.M.: Experimental and Theoretical Results for Buckling of Eccentrically Stiffened Cylinders. NASA TN D-3639, October 1966.

A-14. Structures Manual. NAA/SD AL-1444, Revised, Jan. 1967.

A-15. Advanced Bulkhead Concept Development (ABCD) Conceptual Design and Parametric Analysis. NAA/SD SID 66-1530, Oct. 15, 1966.

A-16. Jordan, P.F.: Analytical and Experimental Investigation of Pressurized Toroidal Shells. NASA CR-261, July 1965.

A-17. Jobel, S.H.; and Flügge, W.: Stability of Toroidal Shells Under Uniform External Pressure. AIAA J., vol. 5, no. 3, March 1967.

A-18. Baker, E.H.: The Analysis of a Symmetrically Loaded Sandwich Cylinder Including Axial Forces. NAA/SD STR 95, September 1963.

A-19. Baker, E.H.: On the Analysis of a Sandwich Cylinder Loaded Symmetrically with Respect to the Longitudinal Axis. STR 87, NAA/SD November 1962.

A-20. Novozhilov, V.V.: Thin Shell Theory. P. Noordhoff Ltd., The Netherlands, 1964.

A-21. Hetenyi, Beams on Elastic Foundations. Ann Arbor, The University of Michigan Press, 1961.

A-22. Buckling of Thin-Walled Circular Cylinders, NASA Space Vehicle Design Criteria. NASA SP-8007, Sept. 1965.

B-1. Boddy, J.A.; and Mitchell, J.C.: Development of Programmed Assistance in Directing Structures Research. Interim Rept., NAA/SD SID 66-408, June 1966.

B-2. USAF Stability and Control Handbook (DATCOM).

B-3. Olsen, D. C.; and Webb, H. G.: Stability and Control Manual. NAA/SD SID 61-236, August 1961.

B-4. White, J. F.: Flight Performance Handbook for Power Flight Operations. Space Tech. Lab. Inc., March 1962.

B-5. Saturn S-II, Structural Design Loads Manual. NAA/SD 62-1184, May 1, 1963.

B-6. Omitted.

B-7. Conceptual Design Study of Ten-Ton Reusable Orbital Carrier. Final Rept., NAA/SD SID 63-158, February 22, 1963.

B-8. Reusable Orbital Transport. CR 71382 Lockheed Calif. Co., Dec. 1964.

B-9. Reusable Orbital Transport, Second Stage, Research and Technology Implications. GD/C DCB 65-018, vol. V, April 1965.

B-10. Apollo Technical Manuals, Structural Loads and Criteria. ARM-6 January 31, 1964.

B-11. Graver, J. A., and Holter, W. H.: Solution of the Transient Heat Conduction Equation for an Insulated Infinite Metal Lab. J. of Jet Propulsion, Dec. 1957.

C-1. Boddy, J. A. and Mitchell, J. C.: Development of Programmed Assistance in Directing Structures Research. Interim Rept., NAA/SD SID 66-408, June 1966.

C-2. Large, J. P.: Concepts and Procedures of Cost Analysis, The RAND Corp., Memo, RM3589PR, June 1963.

C-3. Launch Vehicle Components Cost Study. Lockheed Missiles and Space Co., LMSC 895424, June 30, 1965.

C-4. Koelle, H. H.: Handbook of Astronautical Engineering. McGraw-Hill Book Co.; 1961, pp. 3-2 to 11-26.